UNIVERSITÀ DEGLI STUDI DI MILANO

Dipartimento di Chimica

Doctorate School of Chemical Sciences and Technologies

Pseudo-glycodendrimers containing a molecular rod core: synthesis, characterization and DC-SIGN antagonism.

Stefania Ordanini

Matricola n° R09678

Tutor: Prof. Anna Bernardi

Coordinator: Prof. Emanuela Licandro

Summary

List of abbreviations

Ar: aromatic

Ax: axial

Boc: *tert*-butoxycarbonyl

BSA: Bovine serum albumin

CRD: carbohydrate recognition domain

DC: dendritic cell

DC-SIGN: Dendritic Cell-Specific ICAM-3 Grabbing Nonintegrin

DHB: 2,5-dihydroxybenzoic acid

DIPEA: diisopropylethylamine

DMA: N,N'-dimethylacetamide

DMF: N,N'-dimethylformamide

DMF: N,N'-dimethylformamid

DMSO: dimethylsulfoxide

ECD: extracellular domain

EDC: *N*-(3-Dimethylaminopropyl)-N′-ethylcarbodiimide hydrochloride

ELISA: Enzyme-Linked ImmunoSorbent Assay

ELLA: Enzyme-linked lectin assay

Eq: equatorial

ESI-MS electronspray ionization mass spectroscopy

HCCA: α-cyano-4-hydroxycinnamic acid

Hex: hexane

HRMS: high resolution mass spectroscopy

IC_{50}: median inhibition concentration

ICAM-3: Intercellular Adhesión Molecule 3

J: coupling constant

MALDI: matrix-assisted laser desorption/ionization spectrometry

Man: D-mannose

NMR nuclear magnetic resonance

PAMAM poly(amido amine)

PAMPs pathogen-Associated Molecular Patterns

PG protecting group

RT: room temperature

SPR: surface Plasmon resonance

STD: saturation transfer difference

TBAF: tetrabutylammonium fluoride

TBTA: tris[(1-benzyl-1H-1,2,3-triazol-4-yl)methyl]amine

tBu: $tert$-butyl

TFA: trifluoroacetic acid

THF: tetrahydrofurane

TLC: thin layer chromatography

TMSOTf: trimethylsilyl trifluoromethanesulfonate

Aim of the thesis

The main scope of the PhD research project described in this thesis was the synthesis and the characterization of pseudo-glycodendrimers as potential ligands of the receptor DC-SIGN. DC-SIGN is a lectin expressed at the surface of immature Dendritic Cells (DCs), and it is the first target of several pathogens that attack the human body following the mucosal-entry pathway. HIV virus belongs to this category; therefore, constructs able to antagonize the interaction between the receptor and the virus, such as the ones here envisaged, may in principle act as anti-adhesive pharmaceutical drugs.

In **Chapter 1**, the immunobiology of DCs will be introduced. The DC-SIGN receptor and its immunological activity will be presented, as well as its deficient role in HIV infection. Natural DC-SIGN ligands will be shown, since mimicking natural compounds able to bind to DC-SIGN is a way to produce active ligands. The state of the art related to known artificial DC-SIGN ligands will be described. Also the topic of multivalency will be explained; a brief thermodynamic overview will underline how multivalent ligands are involved in strong binding events with their target receptors. Few examples of compounds that exploit the chelating-multivalent effect will be described. The possibility of producing multivalent compounds able to chelate DC-SIGN was indeed the main goal of my thesis. The distance between DC-SIGN binding sites is known to be about 4 nm.

In **Chapter 2**, the design of multivalent compounds potentially able to bridge two DC-SIGN binding sites will be presented. My project started from the results obtained by N. Varga in his PhD thesis (2012): he developed multivalent constructs active towards DC-SIGN but not able to chelate it. The library of hexavalent and divalent glycodendrimers that I've produced with the aim to chelate DC-SIGN will be here present, together with the synthetic pathways followed to achieve it. Our approach envisaged to control the relative disposition of active ligands using molecular rods. Active ligands, overall valency, rod length and system flexibility are all parameters that we varied in order to dissect their relative contribution in affecting compounds performances. The ability of these glycodendrimers to effectively chelate DC-SIGN was first confirmed through computational models. Two biological tests were performed in order to evaluate their activity as DC-SIGN ligands and as inhibitors of the DC-SIGN-mediated HIV infection. Former tests were performed through SPR inhibition assays, evaluating the ability of compounds to inhibit the DC-SIGN binding to a high mannosylated surface. *Trans*-infection inhibition assays were conducted *in vitro* on a cellular model of HIV infections. Biological assays revealed that a good combination of active monovalent ligands, medium valency and appropriate size of the rod can lead to efficient DC-SIGN ligands. The rational design that we've tried

to implement led to one of the most potent inhibitors of the DC-SIGN-mediated HIV adhesion, up to date. Remarkably, cytotoxicity of these glycodendrimers was excluded.

Since DC-SIGN is able to internalize bound antigens and route them to intracellular compartments to start generating an immunological response, the behavior of glycodendrimers once interacting with DC-SIGN and DCs was investigated and it will be presented in **Chapter 3**. Exploiting the intrinsic fluorescence of the rods, the most active compound was chosen to perform confocal microscopy experiments. The compound was demonstrated to bind selectively to the Carbohydrate Recognition Domain of DC-SIGN, as expected, and not to its neck. Internalization studies on tested compounds will also be described, showing that they are internalized inside DCs and, particularly, that they are routed to lysosomes.

In **Chapter 4**, the morphological behavior of the glycodendrimers in water will be evaluated. Their amphiphilic structure suggested that they could in principle self-assemble as aggregates in aqueous solution. Several analytical techniques were used, in collaboration with other groups. Results demonstrated that all compounds are mainly monomers in solution, but that a small amount of the sample (< 10 %) generally fails to dissolve and it gives rise to large aggregates of hundred nm-sized diameters. We realized that these aggregates can be almost totally removed through centrifugation and that, once pelleted, they do not form anymore. If this holds true, biological performances described in **Chapter 3** naturally arise only from monomers.

Finally, in **Chapter 5**, slight modifications of the monovalent ligands in order to improve their activity but also selectivity towards DC-SIGN will be described. In particular, a previous PhD thesis (N. Varga, 2012) suggested that the presence of an amino group, normally protonated at physiological pH, should lead to less active species towards Langerin. Langerin is another lectin expressed on Denditic Cells, still able to perform an efficient action against HIV virus; it presents two Lysine residues in its active site, that should generate electrostatic repulsions with positively-charged compounds. Pursuing this issue, a monovalent ligand totally selective for DC-SIGN (i.e. not binding Langerin) was produced. Multivalent constructs bearing multiple –NH_2 groups were synthesised. The evaluation of their biological behavior is still ongoing.

To go along with the habits of the different disciplines, the experimental parts describing synthesis will be at the end of each related chapter (Chapter 2 and Chapter 3). On the contrary, experimental details describing biological and physical investigations have been inserted before corresponding results (Chaper 2.6, Chapter 3, Chapter 4).

Chapter 1

Introduction

1.1 Immunobiology of Dendritic Cells

The body's answer to danger and disease is the immune system, which is constituted by two subsystems: the innate (non-specific) and the adaptive (specific) ones. The former, through inflammatory and phagocytic barriers, recognizes pathogens and/or tissue injuries and signals the presence of danger to cells of the adaptive immune system that, in turn, activates to produce antibodies specifically against a particular antigen[a] and to establish an immunological memory - meaning that there will be a quicker answer to the antigen during a second exposure.[1,2] The adaptive immune system is driven by lymphocytes; in particular, B lymphocytes (or B cells) are involved in the so-called humoral response, whilst T lymphocytes (or T cells) are involved in the cell-mediated response. Both classes of lymphocytes recognize antigens through surface receptors. Surface antibodies on B cells are specific for recognizing a certain antigen; this recognition process mediates the activation of B cells, that start producing a large quantity of antibodies to block the harmful effects of that specific antigen. T cells don't recognize a free antigen, but they need it to have been processed (i.e. divided in short peptides) by other cells. T cell receptors (TCRs) mediate the interaction between T cells and antigens presented at the surface of Antigen Presenting Cells (APCs) as Major Hystocompatibility (MHC) complexes. Every nucleated cell, when altered (e.g. tumoral or infected), can present its endogenous antigen as MHC type I complex to $CD8^+$ Cytotoxic T cells (CTLs), that are therefore activated to destroy them. In contrast, the role of the so-called professional APCs is to process exogenous captured antigens as MHC type II complexes and to present them to $CD4^+$ T helper cells (T_h). Once activated, T_h cells can trigger the activities of macrophages (MF)[b] and natural killer (NK) cells,[c] secrete cytokines and help B cells to make the appropriate antibodies.[3] T helper cells can also contribute to stimulate the CTL response.[4]

Dendritic Cells (DCs) are Antigen Presenting Cells, whose major role is to present antigens to the lymphocytes. Being located on human skin and mucosal tissues, they are sentinels for the human body. After pathogen uptake, immature Dendritic Cells (iDCs) process it and complex its fragments on the MHC, and start migrating from the periphery into the T cell area of the lymphoid organs, releasing chemokynes[d] to attract T and B cells.[5] They therefore evolve from immature antigen capturing cells to proper mature antigen presenting cells. Interestingly, MHC complexes on DCs are 10-100 times higher than on other APCs.[6] Antigens processed on MHC are then presented

---

[a] Antigen: any substance that is capable, under appropriate conditions, of inducing the formation of antibodies and reacting specifically with the antibodies so produced.

[b] Macrophage: a type of white blood cell that recognizes, engulfs and destroys target cells.

[c] Natural killer Cell: a type of lymphocyte that can react against and destroy another cell without prior sensitization to it.

[d] Chemokynes: small protein molecules that act as chemoattractants, leading to the migration of immune cells to an infection site so they can target and destroy pathogens.

to select T cells, stimulating a strong immune response (Figure **1.1**). Immature DCs accumulate MHC class II molecules in lysosome-related intracellular compartments and MHC class I in the endoplasmatic reticulum. The interaction between dendritic and T cells is mediated by several adhesion proteins, like ICAM3 (which stands for intracellular adhesion molecule 3).
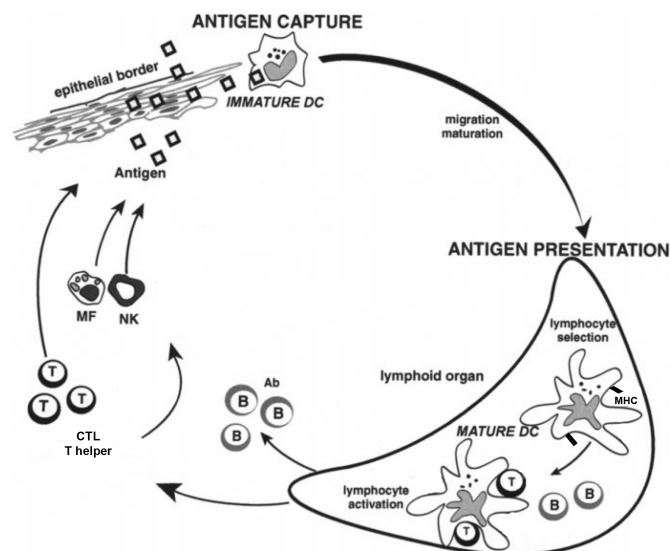
Figure 1.1 The life cycle of DCs. Immature Dendritic Cells bind antigens and present their fragments to T-lymphocytes, after a maturation process. Once activated, T cells can stimulate the activities of macrophages (MF), natural killer (NK) cells and Cytotoxic T cells (CTL) and help B cells to produce the appropriate antibodies (ab).[4]

DCs can uptake pathogens by macropinocytosis[7] - in which the uptake of extracellular fluid and solutes is mediated by membrane ruffling- and phagocytosis,[8] and through surface pathogen recognition receptors (PRR)[7] that trigger adsorptive endocytosis. Macropinocytosis and receptor-mediated antigen uptake are so efficient that nano- and picomolar concentrations of antigen suffice; remarkably, other APCs typically need micromolar antigen concentrations.

C-type lectins are a subset of DCs surface receptors that specifically interact with carbohydrate moieties.[9] They possess a carbohydrate recognition domain (CRD) that includes Ca^{++} ions involved both in ligand binding and in the maintenance of the active folding of the CRD itself.[10] Besides the metal ion coordination by hydroxyl groups on the sugar, the interaction between the lectin and the sugars is driven also by hydrogen bonds and ionic and hydrophobic interactions.[11] C-type lectins specificity arises from their ability to recognize even slight differences in the arrangement, spacing and branching of the carbohydrate residues of their ligands. Several pathogens present carbohydrate residues at their surface that differ significantly from the glycans of mammalians; therefore humans lectin can interact with them and recognize them as non-self signals. Once recognized a pathogen, lectins internalize it to lysosomes where it is are processed for presentation to T lymphocytes.

Toll-like receptors (TLR) are another class of DCs receptors, which recognize specific pathogen-derived components, such as lipoproteins, lipopolysaccharide, and bacterial DNA. After the recognition process, they activate intracellular signalling cascades ending in the production of proinflammatory cytokines that activate T cells.[12]

1.2 The C-type lectin DC-SIGN and its role in HIV-1 infection.

Dendritic cell-specific ICAM-3 grabbing non-integrin, known as DC-SIGN, is a tetrameric transmembrane C-type lectin expressed at the surface of DCs present in dermal and submucosal tissues and in the blood too.[13] DC-SIGN presents a CRD that is selective for fucose- and mannose-based carbohydrates. The CRD is separated from the transmembrane region (TM) by a neck domain, which is made by seven complete and one incomplete tandem repeats. Finally, a cytoplasmatic tail is present, which contains also the di-leucine (LL) motif and the tri-acidic (EEE) clusters designated for the internalization processes (Figure **1.2**). Interestingly, the neck domain is needed by the receptor to oligomerize and form tetramers,[14] which increases the affinity but also the selectivity of the receptor towards its binding partner (see Paragraph 1.5).
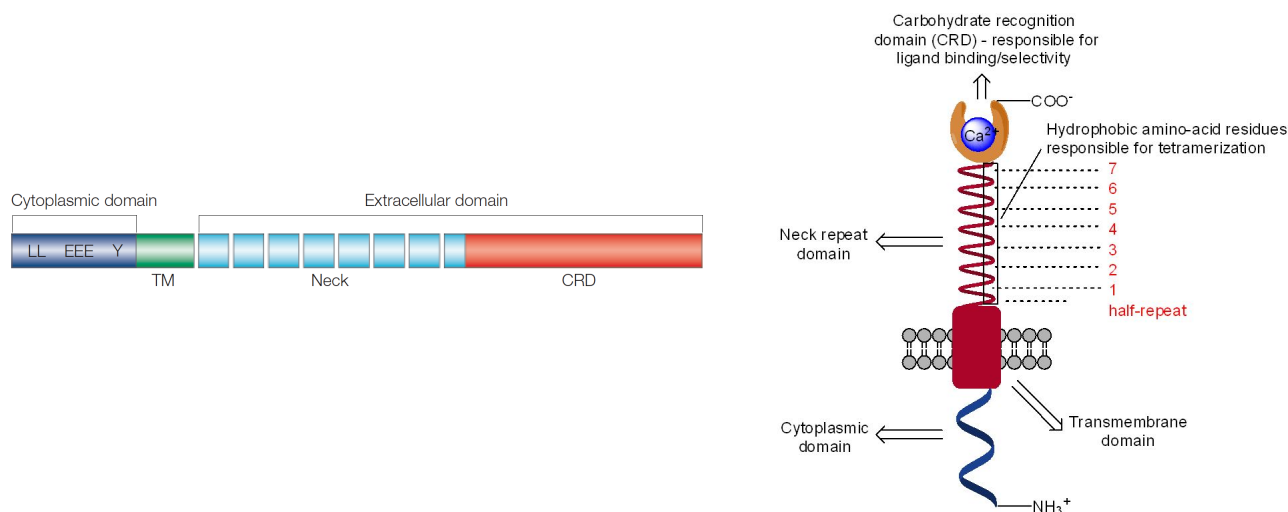
Figure 1.2 Two ways of representing the monomeric DC-SIGN structure.

Interacting with the adhesion receptors ICAM-3 on T-lymphocytes and ICAM-2 on both blood and lymphatic vessels, DC-SIGN mediates DCs-T cells interactions and trans-endothelial migration of DCs, respectively; both ICAM2 and ICAM3 are heavily glycosylated glycoproteins. DC-SIGN is also responsible for the recognition of several pathogens, like viruses (Hepatitis C, Ebola, Cytomegalovirus, Dengue, SARS), bacteria (*Mycobacterium tuberculosis*, *Klebsiella pneumonae*, *Helicobacter pylori*), yiest (*Candida albicans*), and parasites (*Leishmania spp*, *Schistosoma mansoni*).[15] Instead of being processed as MHC complexes and stimulate an immunological

response,[16] some of these pathogens hijack the DCs to disseminate the infection in the human body. Human Immunodeficiency Virus type I (HIV-1) belongs to this category, leading to the severe disease known as the Acquired Immune Deficiency Syndrome (AIDS).[17] The interaction between DC-SIGN and HIV-1 is mediated by the virus highly-mannosylated glycoprotein gp120.[18,19]After the recognition process, HIV-1 is internalized into acidic non-lysosomal organelles of DCs,[20] where it remains stable and is somehow protected. Indeed, instead of being degraded, the virus is presented to CD4^{+} T cells in the lymphoid tissues, resulting in a productive infection of T cells. CD4, together with the CCR5, represents a receptor complex on T cells needed for the virus entry. If the infection occurs fast and independently of *de novo* virus synthesis, it is referred to as *trans* infection (Figure **1.3a**). It can also be possible that, several days after HIV-1 infection, progeny virions produced in DCs infect target cells. In that case, DCs would be infected in *cis*, after the interaction between the virus and CD4 and co-receptors expressed on them (Figure **1.3b**).[21] Betts and co-workers demonstrated the presence of HIV-1-specific CD4^{+} and CD8^{+} T cells in twenty-three HIV-1 infected patients, suggesting that DCs should also be able to process the virus as MHCI and MHCII complexes. However, this immunological response can only be able to delay the progression of the AIDS, but not to inhibit the replication of the virus itself.[22]
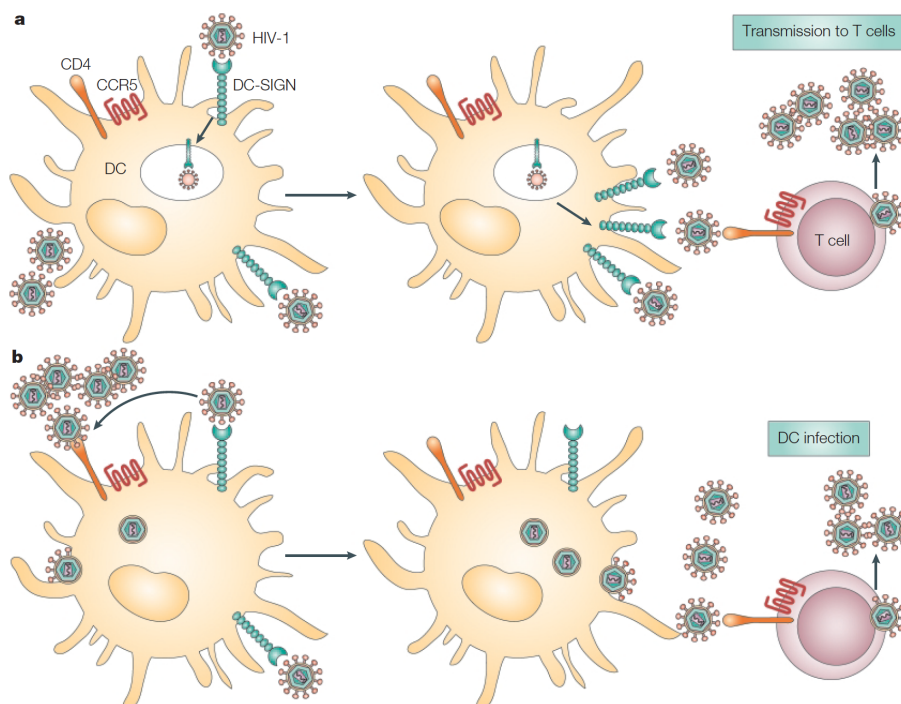
Figure 1.3 *Trans* (a) and *cis* (b) infections of T cells mediated by DC-SIGN.[23]

At low virus titre, which should mimic the *in vivo* HIV-1 levels, T cells are not infected in the absence of DC-SIGN[+] DCs, thus underlying that DC-SIGN not only transmits HIV-1 to T cells, but

it also enhances the infection.[18] The mechanism of DC-SIGN mediated enhancement of HIV-1 infectivity is still not totally clear. It can be possible that, after binding to DC-SIGN, gp120 undergoes conformational changes that enhance its efficiency in interacting with T-cells. It might also be that internalized HIV-1, exposed to low pH media, increases its infectivity.[20] Finally, it can be a matter of concentration of virus particles at the interface between Dendritic and T cells.[24] Remarkably, HIV-1 is able to retain its infectivity 4 days after having interacted with DCs *in vitro*.

1.2.1 DC-SIGN natural ligands

Glycan array is a common technology used to evaluate the binding of a fluorescently-tagged receptor to glycans immobilized on a plate.[25] Van Liempt *et al.* performed this assay to evaluate the interaction between DC-SIGN and a library of mannosylated and fucosylated compounds.[26] Concerning mannose ligands, DC-SIGN was found to have the highest affinity for the structure $(Man)_9(GlcNAc)_2$ (Scheme **1.1**) and lower affinities as the number of mannose units decreases (Figure **1.4** bottom). Among the fucosylated compounds, Lewis B (Fucα1-2Galβ1-3(Fucα1-4)GlcNAcβ; Le^b) was the best ligand; interestingly, diantennary N-glycans as Bi-LDN and Bi-LeX doubled their affinity compared to the individual ones (Figure **1.4**). These results were obtained by using chimeric DC-SIGN/Fc, which has as a dimeric carbohydrate-binding domain assembled on the Fc domain of human IgG1. However, they are comparable to the ones obtained by Guo *et al.* using a renatured tetramer of DC-SIGN.[27]
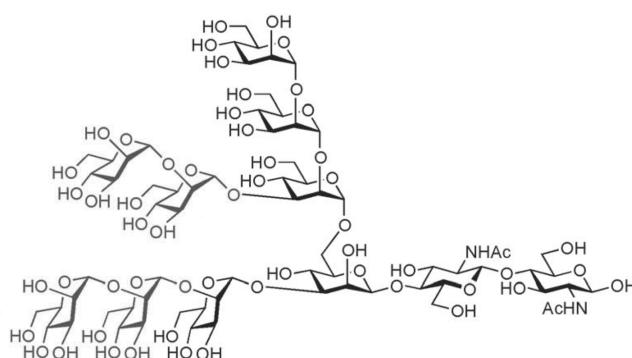
Scheme 1.1 Structure of $(Man)_9(GlcNAc)_2$.[27]

Name (#number)	Lewis B (#24)	Lewis Y (#88)	Lewis A (#29)	LDNF (#26)	Lewis X (#25)	Blood group B (#77)	Sulfo Lewis X (#79)	H-type 2 (#87)	alpha-L-Fuc (#12)	alpha-D-Man (#10)
Structure							3-O-Su			
S/N	6,53	6,15	4,73	3,76	2,98	2,69	2,40	2,06	1,89	1,37
Relative binding	47%	45%	34%	27%	22%	20%	17%	15%	14%	10%

Name (#number)	Bi-LDNF (#185)	Bi-LeX	Man-9 (#132)	Man-8 (#131)	Man-7 (#130)	Man-6 (#129)	Man-5 (#114)	As-Tf-GP	Man-3 core α6Fuc (#186)
Structure									
S/N	13,79	10,24	9,89	8,10	4,41	3,75	1,50	1,96	1,55
Relative binding	100%	74%	72%	59%	32%	27%	11%	14%	11%

Explanation of glycan symbols: ● mannose; ○ galactose; □ GalNAc; ■ GlcNAc; △ fucose.

Figure 1.4 Data obtained from the glycan array; carbohydrate structures are schematically represented. Affinity is expressed as S/N = $\frac{signal\ (fluorescence)}{noise}$. Relative binding is calculated respect of the highest one (Bi-LDNF).[27]

Remarkably, also simpler fragments of Man$_9$ where found to be active DC-SIGN ligands (Scheme 1.2).[28] In particular, above all, linear trivalent and tetravalent mannose derivatives **4** and **5** approached the binding affinity of Man$_9$ itself. This suggests the importance of the Manα1-2Man residue in binding the DC-SIGN CRD (over e.g. the 3,6-branched Man or Manα1-6Man residue, see compounds **3** and **7**). Also Mannose alone (compound **6**) had a remarkable ability to bind the lectin in this surface assay. The lower activity of the branched trisaccharide **3** compared to mannose **6** was probably due to steric constraints.[29]
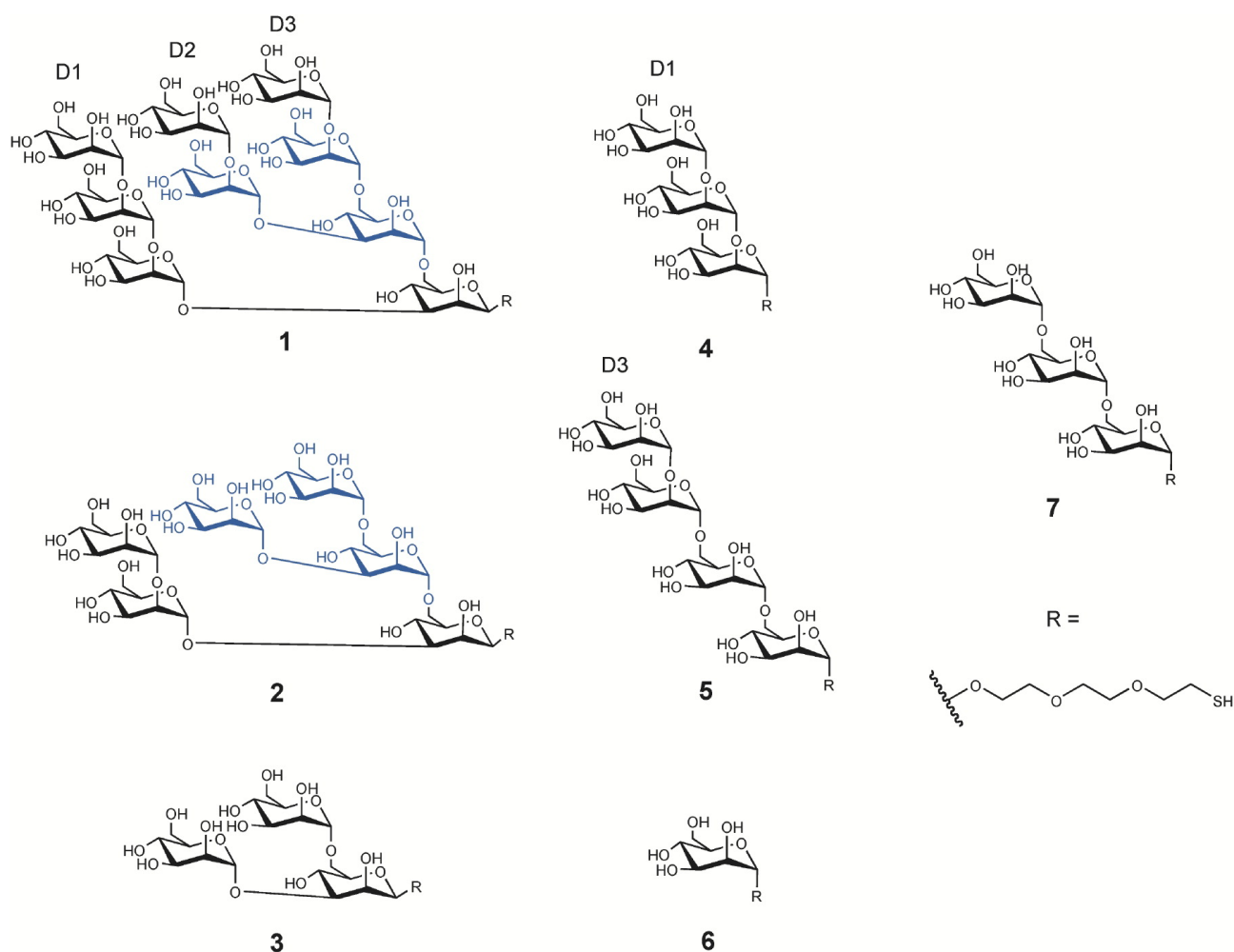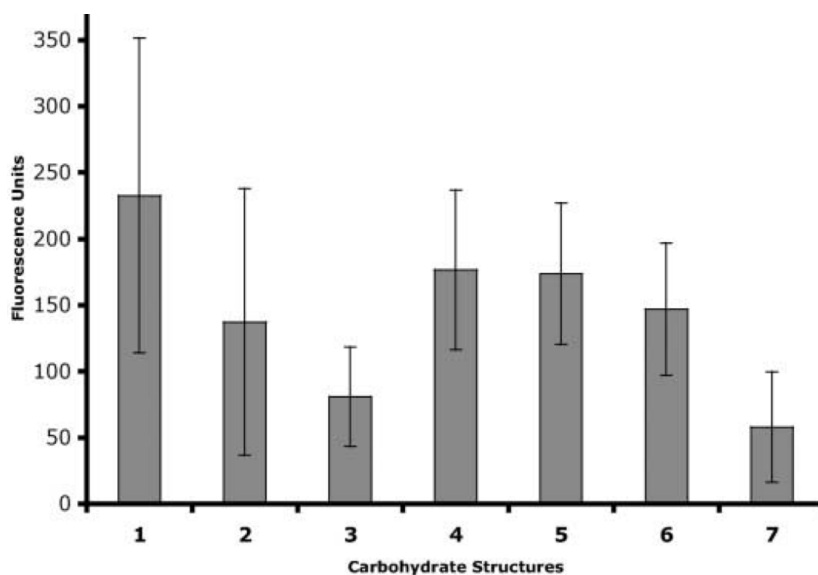
Scheme 1.2 Evaluation of the interaction between DC-SIGN and Man$_9$ or its fragments (compounds **1-7**). The amount of (fluorescently tagged) bound protein on the oligosaccharide is measured as fluorescence units.[28]

Lewis$^{\text{X}}$ is known to be expressed, for instance, at the surface of the Gram-negative bacterium *H. pylori*, which induces peptic ulcers and gastric carcinoma; Le$^{\text{x}}$, Le$^{\text{y}}$, Le$^{\text{a}}$, Le$^{\text{b}}$ are also blood group epitopes.[30] High mannose type glycans are found on the HIV-1 glycoprotein gp120,[19] on the

Mycobacterium tuberculosis and the yeast *Candida albicans*.[23] In 2011, Sabatte *et al.* demonstrated that semen clusterin, and not serum one, is a natural potent DC-SIGN ligand (K_D = 76 nM). Clusterin is a protein involved in a variety of physiological and pathological processes (e.g. inflammation, atherosclerosis, cancer), and semen clusterin contains highly fucosylated glycans in high concentration, as demonstrated by MALDI-MS analysis.[31]

1.3 The role of other proteins in HIV infection

DC-SIGN seems to be the major HIV-1 receptor located on DCs, responsible for sequestering the virus and transferring it to CD4$^+$ T cells. However, other proteins and receptors are involved in the virus-cell attachment process. First of all, virus accumulation on cell surfaces can be driven by an interaction between positively charged regions on the virus envelope and negatively charged proteoglycans on the cell membrane.[32] Other DC receptors, like CD4, glycospingholipid galactosyl ceramide[33] and the mannose receptor[34], might be involved in HIV-1 capture.

As already stated above (see Paragraph 1.2), also receptors located on T cells (CD4, CCR5 and CXR4 coreceptors) are essentials for the binding between HIV-1 and the target T cells. This binding induces conformational modifications in the virus gp41 envelope glycoprotein, which forces its amino-terminal fusion peptides into the target cell membrane, thus leading the virus-cell fusion process to occur.[35]

1.3.1 Langerin

Langerin is a C-type lectin specific for mannose exclusively expressed on Langheran Cells (LCs), which are a subset of immature Dendritic Cells (iDCs). Found in the epidermis of the skin and in mucosal stratified epithelia, LCs are the first Dendritic Cells encountered by external pathogens, as HIV virus (Figure **1.5**).[36] Langerin has an extracellular region consisting of a carbohydrate recognition domain and a neck, which stabilizes the formation of rigid trimers where the three CRDs are in fixed positions and the sugar binding sites are separated by a distance of 41.5 Å (Figure **1.6**).[37]
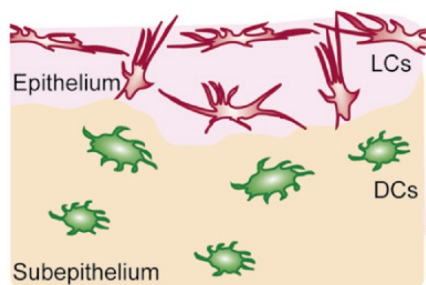
Figure 1.5 Specific localization of the Langheran Cells and the DC-SIGN[+] Dendritic Cells.

Figure 1.6 Side view of Langerin in its trimeric arrangement.

As DC-SIGN, also Lagerin possesses a CRD that recognizes fucose and high mannose structures; therefore, it is able to bind gp120 on HIV-1 surface. Langerin was found to be a natural barrier against HIV-1, serving as a sort of scavenger receptor that mediates virus degradation inside Langheran Cells.[38] Indeed, LCs where not able to transfer HIV-1 to T cells, except when using high concentrations of the virus (i.e. 10000 Tissue Culture Infective Doses, whereas *in vivo* HIV-1 levels are lower). The virus clearance probably happens after its internalization inside Birbeck granules, which are pentalamellar cytoplasmatic organelles.[39] Even if it is not known if Birbeck granules promote antigen processing, it is possible that they route captured HIV-1 to lysosomes for degradation.

The main difference between the carbohydrate recognition domains of DC-SIGN and Langerin is that Langerin CRD presents two lysine residues (Lys299 and Lys313) in its sugar binding site, close to the Ca^{++} ion.[40] This is the reason why Langerin accommodates positively charged sulfated sugars in its CRD (see Chapter 5).

1.4 DC-SIGN as a therapeutic target

Since AIDS curative treatments or preventive vaccines against HIV-1 virus are still a challenge, avoiding virus-body attachment is a way of preventing HIV-1 infection.[41] In this field, DC-SIGN is a suitable target; indeed, synthesising artificial molecules that mimic the cluster presentation of gp120 on HIV-1 and can occupy DC-SIGN binding sites antagonizing the virus is a way of producing anti-adhesive drugs. From a biological point of view, these molecules should be strong

and selective DC-SIGN binders. Non-selective compounds can be detrimental for the curative purpose if they bind other receptors that are able to contrast HIV-1, like Lingerin (see Paragraph 1.3.1).[38] From a pharmaceutical point of view, they could be formulated as a topic gel, possibly colourless and odourless, which confers sustained protection from HIV after a single dose.

In principle, HIV infection can be blocked also antagonizing the other receptors involved in the virus dissemination (see Paragraph 1.3).[42,43] Indeed, HIV-1 infection of T cells can be prohibited by blocking the interaction between the virus and either the CD4 receptor or the CCR5 and CXCR4 coreceptors. Also the fusion process between HIV-1 and target cell occurring after membranes coalescence mediated by gp41 on the virus can be prevented. However, interaction with DC-SIGN is the first adhesion event and blocking it may be more efficient in reducing viral load.

Beside HIV, DC-SIGN ligands can prevent the adhesion of other pathogens that use this receptor to attack the human body, like Ebola and Dengue viruses.[23]

1.4.1 Artificial DC-SIGN ligands

Artificial glycomimetic compounds, which imitate the structure of natural DC-SIGN ligands (e.g. Le^X and (Man)$_9$(GlcNac)$_2$, see paragraph 1.2.1), can be active DC-SIGN binders, thus antagonists of HIV-1 attachment on DCs. The use of glycomimetics instead of complex oligosaccharides should lead to compounds more easily synthesised, as well as more metabolically stable. Glycomimetic compounds should maintain the anchoring moieties that allow their main binding with the receptor, but can also present other elements that favour their accommodation in the binding sites thanks to further non-covalent interactions. In that way, it may also be possible to tune their selectivity towards DC-SIGN relative to other C-type lectins.

In the following paragraphs, a number of artificial carbohydate and non-carbohydrate molecules synthesised as DC-SIGN ligands will be presented; their affinity towards the target receptor will be expressed as *IC$_{50}$* and/or *K$_D$*.

1.4.1.1 Fucose based

Fucosed-based ligands where designed and synthesised as mimics of the natural DC-SIGN binder Lewis X (compound **1.1** in Scheme **1.3**). Unless differently stated, all fucose-based compounds here presented were tested as DC-SIGN inhibitors thorough an SPR inhibition assay, by evaluating their ability to inhibit binding of DC-SIGN to Man-BSA (Manα1-3[Manα1-6]Man, 15 trimannose residues, on average). The fucose moiety was maintained as the chelator of Ca^{2+} ions on the receptor binding site. Compound **1.2** was obtained by replacing the galactose sub-unit with a

cyclohexyl mimic and the central N-acetyl-glucosamine (Glc-NAc) with a 2-amino-cyclohexanecarboxylic acid (Scheme **1.3**).[44]
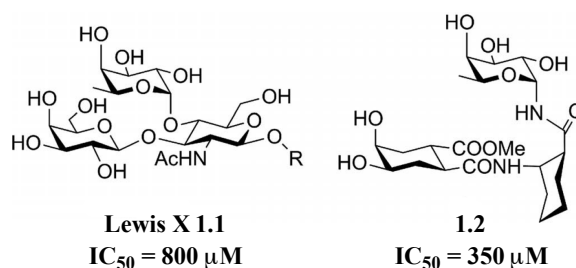
Scheme 1.3 First Lewis X mimic **1.2**. *IC$_{50}$* values were obtained through SPR inhibition assays, using BSA-mannotriose as competitor.[44]

No further affinity improvements were obtained by replacing the galactose mimic with aromatic systems –which, on the contrary, were expected given its interaction with lipophilic protein areas suggested by docking studies-, nor varying the configuration of the 2-amino-cyclohexanecarboxylic acid to find the most efficient one. Within the synthesised library of compounds with the general structures depicted in Scheme **1.4**, **1.3** was the most active ligand. Compound **1.4** was produced by using the commercially available β-alanine as the central building block and, despite its simplicity, proved to have an affinity similar to that of Le^{X} (Scheme **1.4**).
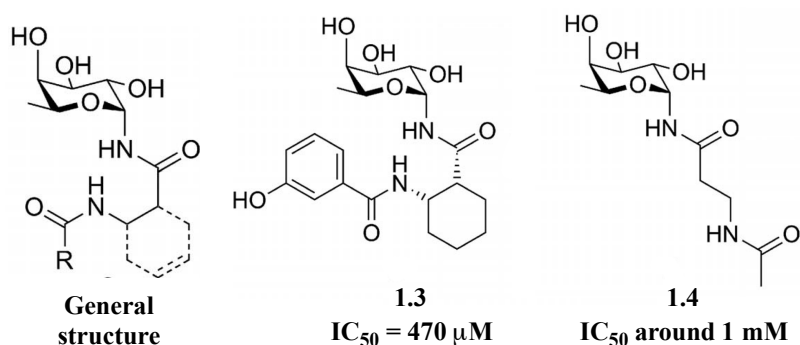
Scheme 1.4 The most interesting compounds within a new library of fucose based glycomimetics whose general structure is indicated in the left. *IC$_{50}$* values were obtained through SPR inhibition assays, using BSA-mannotriose as competitor.[44]

Compounds **1.3** and **1.4** were selected to build multivalent derivatives; thus, they were functionalized with linkers or functional groups suitable for the conjugation on a multivalent scaffold. The tetravalent presentations **1.5** and **1.6** of the weak carbohydrate DC-SIGN antagonists on a pentaerythritol-based core improved their affinity up to one order of magnitude (Scheme **1.5**).[45] *IC$_{50}$* were evaluated through SPR inhibition assays, using Man-BSA as competitor.
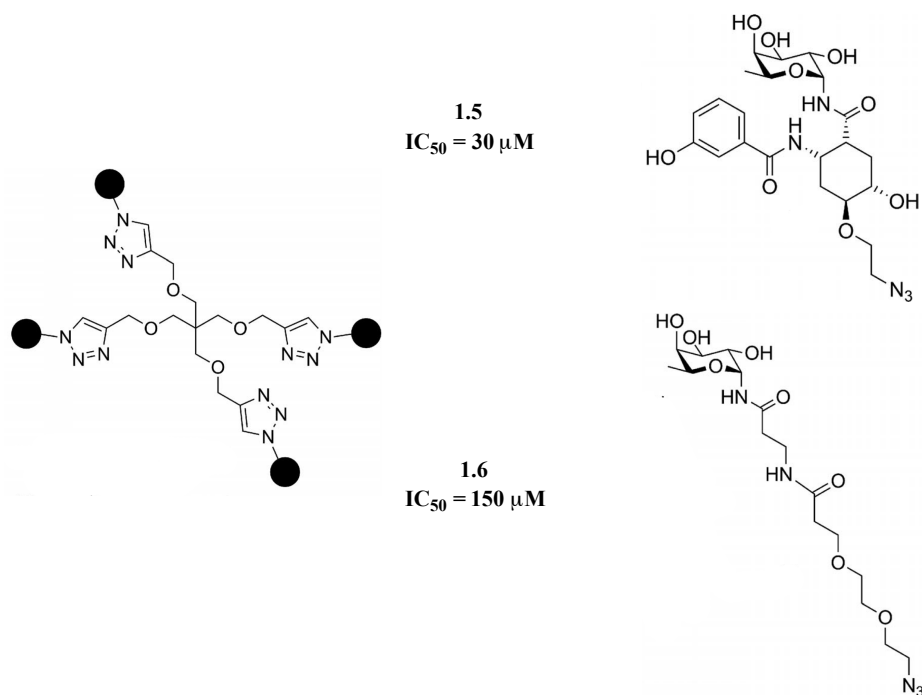
Scheme 1.5 Tetravalent presentations of selected fucose based ligands. *IC$_{50}$* values were obtained through SPR inhibition assays, using BSA-mannotriose as competitor.[45]

Compound **1.4** was used also to decorate gold nanoparticles. Particles containing 50 % of fucosylated amide had a similar behaviour of gold nanoparticles bearing Lewis X (10 % LeX-loading). They both displayed *IC$_{50}$* values around 12 ng/mL, measured by inhibiting the binding of fluorescent gp120 to DC-SIGN.[46]

1.4.1.2 Mannose based

In the Bernardi group, compound **1.7** (Scheme **1.6**) was synthesis to mimic the Manα1-2Man residue of (Man)$_9$(GlcNAc)$_2$; authors demonstrated that the two compounds share the same three-dimensional structure and conformational behaviour (NMR and docking studies), but **1.7** is more stable to hydrolysis mediated by jack-bean mannosidase and also less cytotoxic.[47] Compound **1.7** consists of one mannose residue, involved in the direct chelation of Ca^{2+} in the receptor binding site,[48] and one conformationally locked cyclohexyl moiety (i.e. a pseudo mannose) substituted with two methyl ester groups (Scheme **1.6**); it allowed an increase of affinity towards DC-SIGN by almost a factor of two with respect to mannose (*IC$_{50}$* = 1.0 mM *vs* 1.8 mM, obtained through SPR inhibition assays, using ManBSA as competitor). This suggests an additional and positive interaction of the substituted cyclohexyl in the DC-SIGN CRD.

1.7
IC$_{50}$ = 1.0 mM
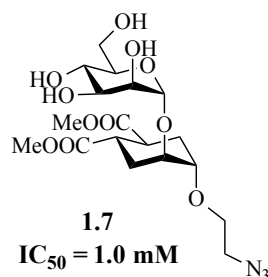
Scheme 1.6 Structure of the pseudo-dimannoside **1.7**. *IC$_{50}$* values were obtained through SPR inhibition assays, using BSA-Mannotriose as competitor.[47]

The same research group, by adding a third mannose moiety to compound **1.7**, obtained the pseudo-trimannoside **1.8** (Scheme **1.7**).[49] The presence of another mannose unite in the DC-SIGN binding site allowed to increase the affinity toward the receptor by about one order of magnitude, as measured in the inhibition assay.

1.8
IC$_{50}$ = 125 μM
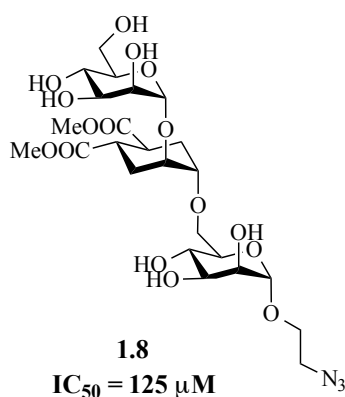
Scheme 1.7 Structure of the pseudo-trimannoside **1.8**. *IC$_{50}$* values were obtained through SPR inhibition assays, using BSA-mannotriose as competitor.[49]

However, the synthesis of **1.8** is rather long and complicated. Additionally, later studies showed that the high affinity measured by SPR inhibition study for **1.8** depended on the format of the assay (i.e. protein soluble in solution) and derived mostly by dimerization of the DC-SIGN tetramer. These results were confirmed by calculating the stoichiometry associated to the interaction through Isothermal Titration Calorimetry and by detecting the dimer through Analytical Ultracentrifugation.[50] Therefore, other type of modifications of compound **1.7** is desirable. In order to gain additional positive contacts between the artificial compounds and the DC-SIGN binding site, the methyl esters groups in **1.7** were replaced by aromatic amides and benzyl amides, obtaining two new different libraries of DC-SIGN ligands.[51,52] Among all, compound **1.9** was found to be the most interesting one: having an *IC$_{50}$* = 325 μM (SPR inhibition assay using Man-BSA as competitor, Scheme **1.8**), it approaches the activity of the pseudo-trimannoside. It is equipped with

two additional hydroxyl groups that help improving its solubility in water. Remarkably, **1.9** has also a good selectivity *vs* Langerin.

1.9
IC$_{50}$ = 325 μM
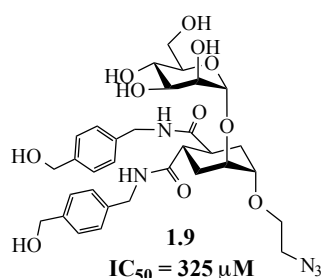
Scheme 1.8 Structure of the bisamide **1.9**. *IC$_{50}$* values were obtained through SPR inhibition assays, using BSA-mannotriose as competitor.[52]

Compounds **1.8**, **1.7** and **1.9** were used to decorate multivalent polyalkyne scaffolds, thus obtaining multivalent ligands with an improved affinity toward DC-SIGN relative to their monovalent counterparts (Scheme **1.9**).[53,54,55] Compound **1.9** gave the best affinity improvements, even if, increasing its valency up to 9, it showed a rather low solubility in water (< 300 μM).[55]

Remarkably, a 32-valent presentation of **1.8** on a 3rd generation of Boltorn type dendrimer **(G3-(ps-tri)$_{32}$**, Scheme **1.10**)[54] was just 4 times as active as a 4-times presentation on a tetravalent dendron[53] (**Polyman2**, Scheme **1.10**). All *IC$_{50}$* values were obtained through SPR inhibition assays *vs* Man-BSA.

= **1.7**, IC$_{50}$ = 136 μM

= **1.8**, IC$_{50}$ = 112 μM

= **1.9**, IC$_{50}$ = 12 μM

= **1.7**, IC$_{50}$ = 39 μM

= **1.8**, IC$_{50}$ = 51 μM

= **1.9**, IC$_{50}$ = 5.7 μM

= **1.7**, IC$_{50}$ = 14 μM

= **1.9**, not soluble
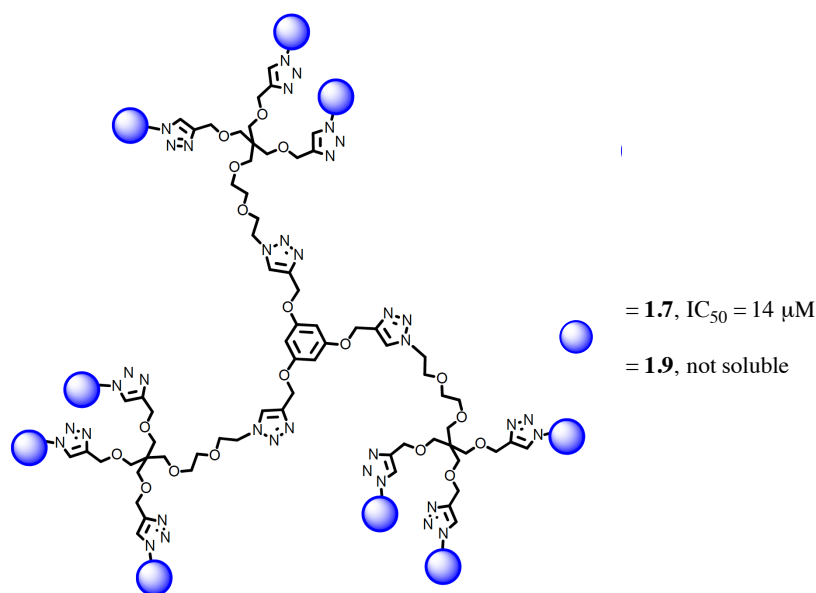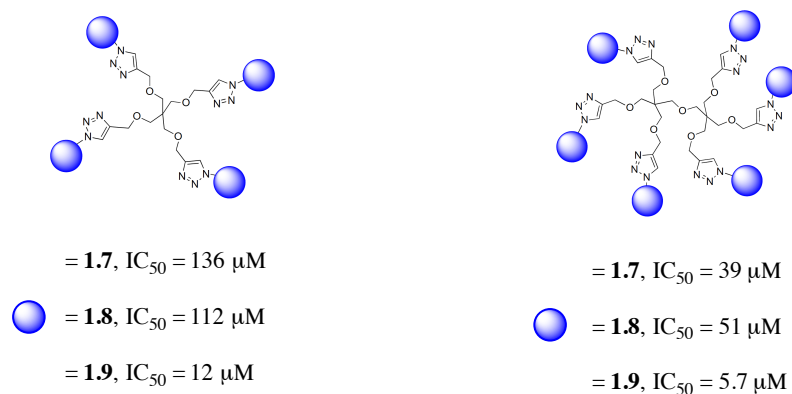
Scheme 1.9 Multivalent presentations of compounds **1.7**, **1.8** and **1.9**. *IC$_{50}$* values were obtained through SPR inhibition assays, using BSA-mannotriose as competitor.[55]

G3-(ps-tri)$_{32}$
IC$_{50}$ = 5 μM

Polyman2
IC$_{50}$ = 1.25 μM
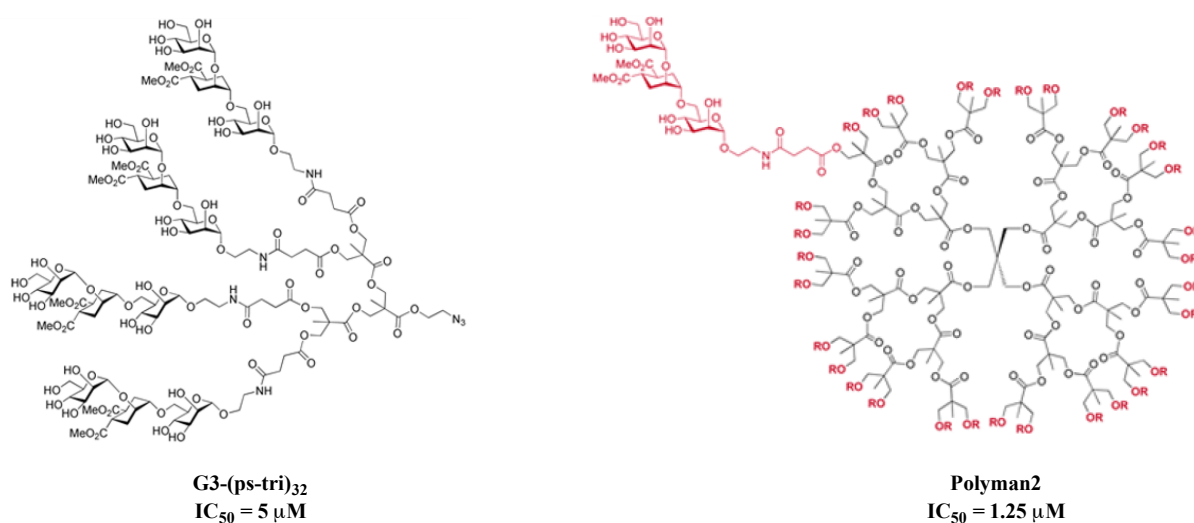
Scheme 1.10 4-valent (**G3-(ps-tri)$_{32}$**, left) and 32-valent (**Polyman2**, right) presentations of compound **1.8**. *IC$_{50}$* values were obtained through SPR inhibition assays, using BSA-mannotriose as competitor.[53,54]

The group of Kiessling used a library of Shikimic acid derivatives to discover glycomimetic DC-SIGN antagonists.[56] Shikimic acid is a mannose mimic, since it presents three hydroxyl groups that match the configuration of the mannose hydroxyl groups in positions 2, 3 and 4. In has three points of variations where different substituents can be used to modulate final affinity and selectivity toward DC-SIGN (Scheme **1.11**).

Mannose   **Shikimic acid**   **Mannose-mimetic**
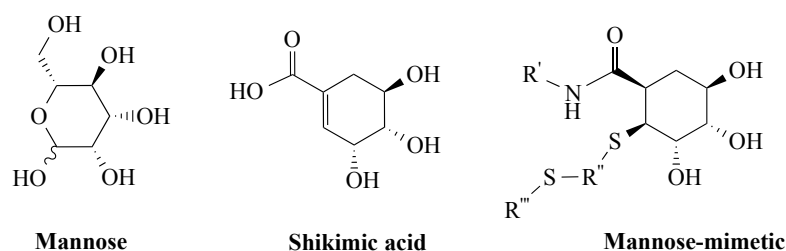
Scheme 1.11 Shikimic acid and its derivatives are mannose-mimetics. *IC$_{50}$* values were obtained through inhibition assays, using Man-BSA as competitor.[56]

Compound **1.10** (Scheme **1.12 A**) was found to be the most active towards DC-SIGN (*IC$_{50}$* = 3.2 mM, evaluating its ability to inhibit binding of fluorescent Man-BSA bearing 20-25 copies of mannose to DC-SIGN). It didn't show any affinity improvement relative to mannose itself but, interestingly, it was selective against Mannose Binding Protein-A. Through ^{1}H-^{15}N HSQC NMR experiments, the authors demonstrated that compound **1.10**, besides having a binding mode analogous to that of saccharide ligands (ManNAc and Fuc were tested), is also involved in the recognition of adjacent secondary sites.[57]

By decorating a ROMP-generated polymeric backbone with compound **1.10**, a powerful multivalent ligand **1.11** was obtained (*IC$_{50}$* = 2.9 μM, inhibition assay *vs* Man-BSA, Scheme **1.12 B**). The degree of polymerization (29) was chosen to generate a multivalent structure able to bind simultaneously more that one binding site on the tetrameric DC-SIGN CRD, knowing that each extended monomer within a ROMP-derived polymer spans approximately 5 Å and that the width of the DC-SIGN CRD is about 40 Å. Each polymer displays about 7 glycomimetic units and should be able also to cluster multiple copies of DC-SIGN on the cell surface.

A

B

1.10
IC$_{50}$ = 3.2 mM

1.11
IC$_{50}$ = 2.9 μM

R^1 =

R^2 =
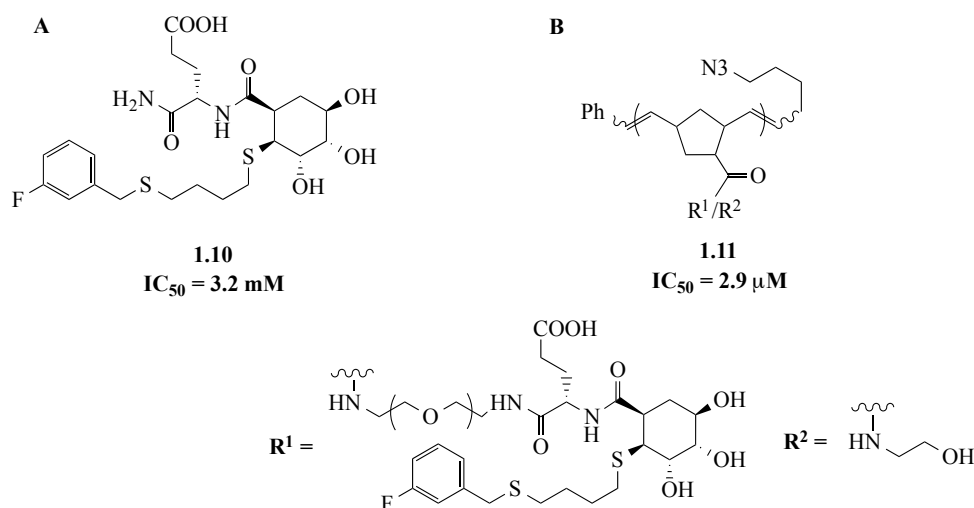
Scheme 1.12 A) Shikimic acid derivative **1.10**; B) its multivalent polymeric presentation **1.11**. The ratio R^2/R^1 is about 1:3. *IC$_{50}$* values were obtained through inhibition assays, using Man-BSA as competitor.[56]

Several research groups, with the aim of synthesising powerful multivalent DC-SIGN ligands, used directly mannose or the Manα1-2Man disaccharide as monovalent substrates.

The mannose containing glyco-polymer **1.12**, with a degree of polymerization of ca. 58, was a potent DC-SIGN ligand, showing *IC$_{50}$* = 37 nM (SPR inhibition assay performed using gp120 immobilized on the chip, as competitor, Scheme **1.13**). It was obtained by coupling a suitable azide-functionalised mannose on a polymer backbone synthesized by copper-mediated living radical polymerization of trimethylsilyl propargyl methacrylate. The azide-alkyne Huisgen cycloaddition was performed after removal of the trimethylsilyl groups on the polymer.[58]

1.12
IC$_{50}$ = 37 nM
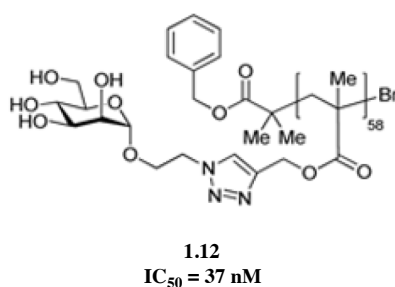
Scheme 1.13 Structure of the mannose containing glycopolymer **1.12**. *IC$_{50}$* values were obtained through SPR inhibition assays, using gp120 as competitor.[58]

A library of mannosylated gold-glyconanoparticles (GNPs) was obtained by decorating a 2 nm gold core with mannose or oligomannoses functionalised with linkers ending in a thiol group, thus suitable to be attached on the gold surface.[59] The nature of the glyco-moieties as well of the linkers was varied in order to find the most active sugar and to modulate the solubility and the flexibility of the NP, respectively. Linker lengths modulate also the accessibility of the sugar epitope to the

receptor. Among all synthesised compounds, GNPs **1.13** and **1.14** presenting different densities of the Manα1-2Manα residue were the most active species, with IC_{50} values in the low nM range (obtained thorugh SPR assays, evaluating the ability of compounds to inhibit the binding of DC-SIGN on gp120, Scheme **1.14**). Given the similarity of their binding levels towards DC-SIGN (SPR inhibition assays), the authors concluded that, above a certain threshold, higher density of glycoconjugates does not improve the efficacy of the GNPs.

1.13
Man$_2$ 66%
Avarage Man$_2$ copy number = 25
IC_{50} = 15 nM

1.14
Man$_2$ 100%
Avarage Man$_2$ copy number = 59
IC_{50} = 8 nM
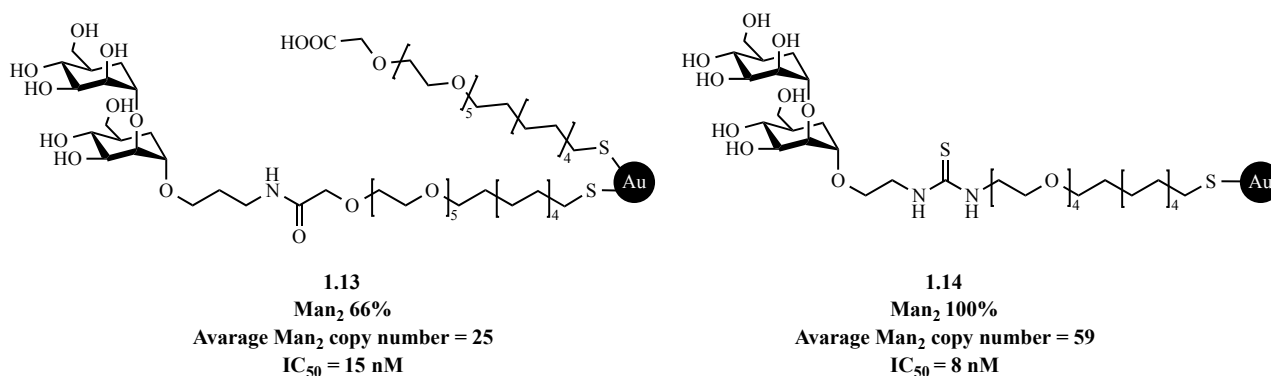
Scheme 1.14 Mannosylated gold-nanoparticles **1.13** and **1.14**. *IC$_{50}$* values were obtained through SPR inhibition assays, using gp120 as competitor.[59]

The group of Wagner synthesised a small library of ampiphilic manno-lipids made by a polar mannose residue (the epitope), a hydrophilic linker (to improve solubility in water) and a hydrophobic saturated lipid chain of variable length.[60] Among these compounds, **1.15** and **1.16** displayed the highest K_D towards DC-SIGN (Scheme **1.15**). K_D values were obtained through SPR direct assays, by evaluating the ability of compounds to bind to a surface were DC-SIGN is immobilized. Due to their amphiphilic structure, these compounds are able to form micelles in water, thus assuming a self-organized multivalent presentation without the need to synthetically create it. Interestingly, HIV-1 *trans*-infection inhibition assays revealed that **1.16** is active already under its Critical Micelle Concentration (IC_{50} = 500 nM, CMC = 109 μM), meaning that it is a good DC-SIGN binder also in its monovalent presentation. This can be explained by the formation of strong additional interactions of the lipid chain in DC-SIGN binding site or by the formation of other self-assembled multivalent structures that are not micelles.

1.15
CMC = 97 μM
K_D = 320 nM
IC$_{50}$ = 120 μM

1.16
CMC = 109 μM
K_D = 3.19 μM
IC$_{50}$ = 500 nM
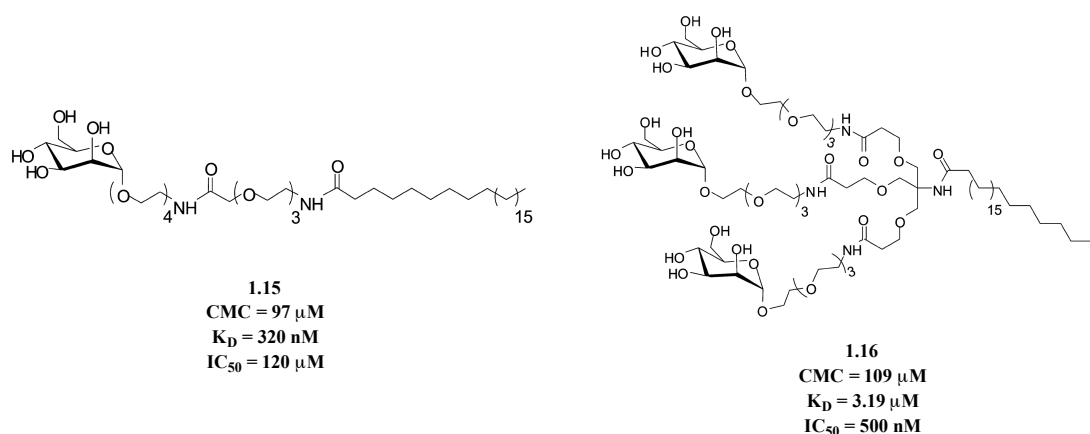
Scheme 1.15 Glycolipids **1.15** and **1.16**. K_D values were obtained through SPR direct assays, immobilizing DC-SIGN on the chip; *IC$_{50}$* were calculated on the ability of compounds to inhibit the DC-SIGN mediated infection from DCs to T lymphocytes.[60]

1.4.1.3 Non-carbohydrate based

Trying to obtain monovalent compounds with a low-micromolar affinity towards DC-SIGN, in 2007 the group of Kiessling developed a high-throughput assay to screen a library of 36000 small molecules and find potential DC-SIGN ligands.[61] Compounds were tested in a competition assay with Mannosylated BSA, bearing 20-25 copies of Man/BSA. In Scheme **1.16** the structures of identified DC-SIGN ligands are reported, together with the obtained *IC$_{50}$*; compounds **1.17** and **1.19** belong to the quinaxolinone derivatives, whereas compounds **1.18** and **1.20** contain a pyrazolone scaffold. They all revealed to have an affinity towards DC-SIGN higher than the one displayed by sugar-derived monovalent ligands. Remarkably, they don't bear any hydroxyl group, meaning that either they coordinate Ca^{2+} in DC-SIGN binding sites with other functional groups (i.e. amides) or they can even bind the receptor at a site which is different from the one used by oligosaccharides, leading to an allosteric effect.
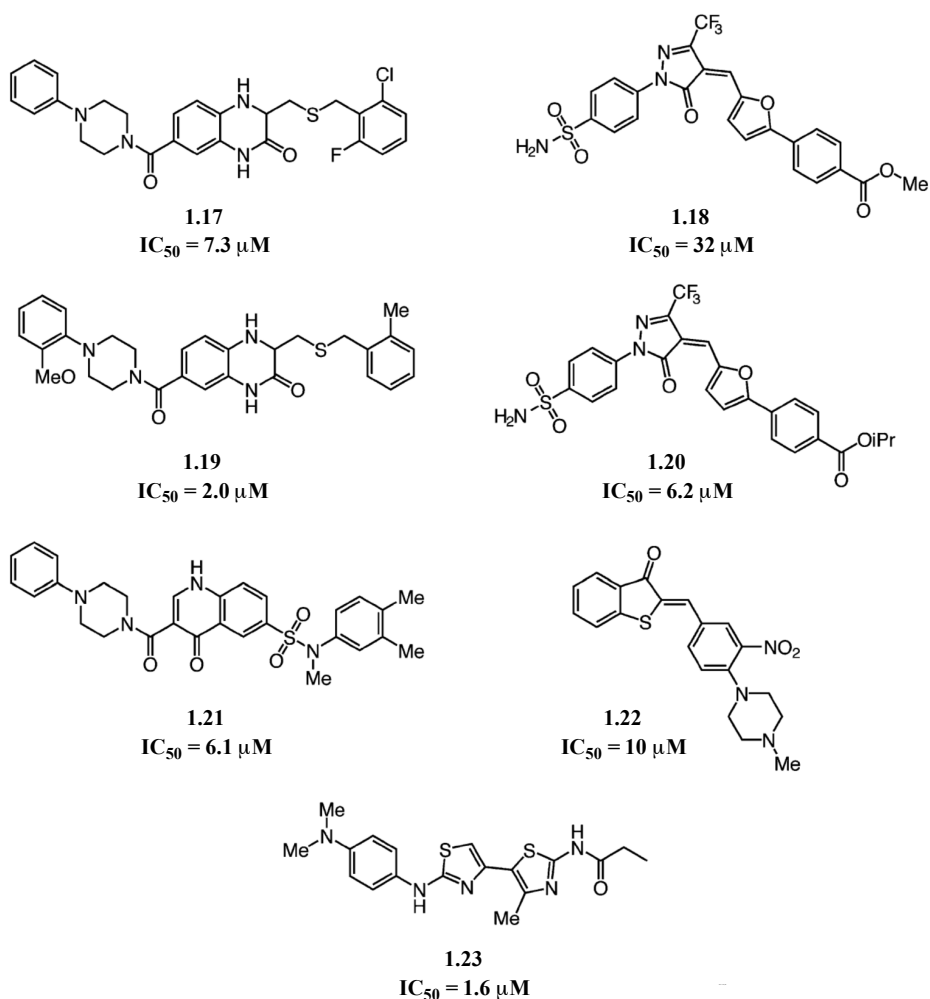
Scheme 1.16 Structure and activities of non-carbohydrate DC-SIGN ligands. IC_{50} values were obtained through inhibition assays, using Man-BSA as competitor.[61]

Given the electrophilic behaviour of pyrazolone-containing compounds, they are not suitable for cell-based assays.[62] On the contrary, the drawback of quinoxalinone-bearing molecules is the liability of the thioether group; indeed, they are not stable in air at room temperature and they undergo degradation and inactivation within few weeks. For this reason, the selected compound **1.17** was modified by firstly substituting the thioether group with a methylene one, and then by varying three other positions (Scheme **1.17 left**).[63] The activity of synthesised compounds was assessed again in a competition experiment with the fluorescein mannosylated BSA. Compound **1.24** (Scheme **1.17 right**) revealed to be the most active one, with IC_{50} = 0.3 μM. This result underlines the importance of having aromatic groups to increase the affinity of artificial ligands by increasing lyophilic (hydrophobic) interactions with the lectin surface.

General structure

1.24
$IC_{50} = 0.3 \ \mu M$
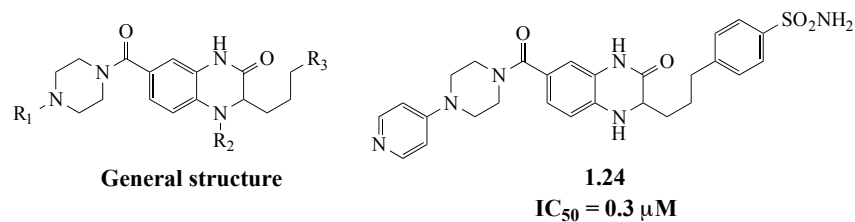
Scheme 1.17 1.24 is the lead compound obtained by varying R_1, R_2 and R_3 positions depicted in the general structure (left). *IC_{50}* values were obtained through inhibition assays, using Man-BSA as competitor.[63]

1.5 Multivalency

The strength of the interaction between two materials can be dramatically increased by exploiting multivalency, meaning that multiple interactions occurring at the same time often lead to stronger binding. Nature has taken deep advantage of this concept and made the weak interactions between proteins and carbohydrates biological relevant by using multivalent binding partners.

The valency of a material is defined as the number of separate, identical connections that it can make with its binding counterpart.[64] There are several mechanisms, often occurring synergistically, that can lead to multiple connections.[65] In this thesis, multivalency will always be referred to multivalent carbohydrate-based ligands interacting with a multivalent protein.[66]

One mechanism that can enhance binding affinity is *chelation*, occurring when a ligand is able to bind simultaneously more than one binding site on the same multivalent receptor (Figure **1.7A**). Also a ligand with two non-identical subunits can chelate two non-identical binding sites on the protein.

When the linker separating ligand subunits is not long enough to allow chelation, or when the receptor has only one binding site, the presence of proximal additional sub-ligands that can easily replace the first one after it is released enhances the overall binding potency. This mechanism is called *statistical rebinding* (Figure **1.7B**) and it has been interpreted as resulting from increased local concentration in the proximity of the binding site (see *C_{eff}* i.e. effective concentration in Paragraph 1.5.1).

Finally, multivalent ligands can bind more than one receptor, resulting in protein aggregation (Figure **1.7C**). This can occur with soluble receptors, but also receptors embedded in membranes can undergo a similar effect, due to membrane plasticity. In this case the effect is often referred to as "clustering" rather than aggregation.
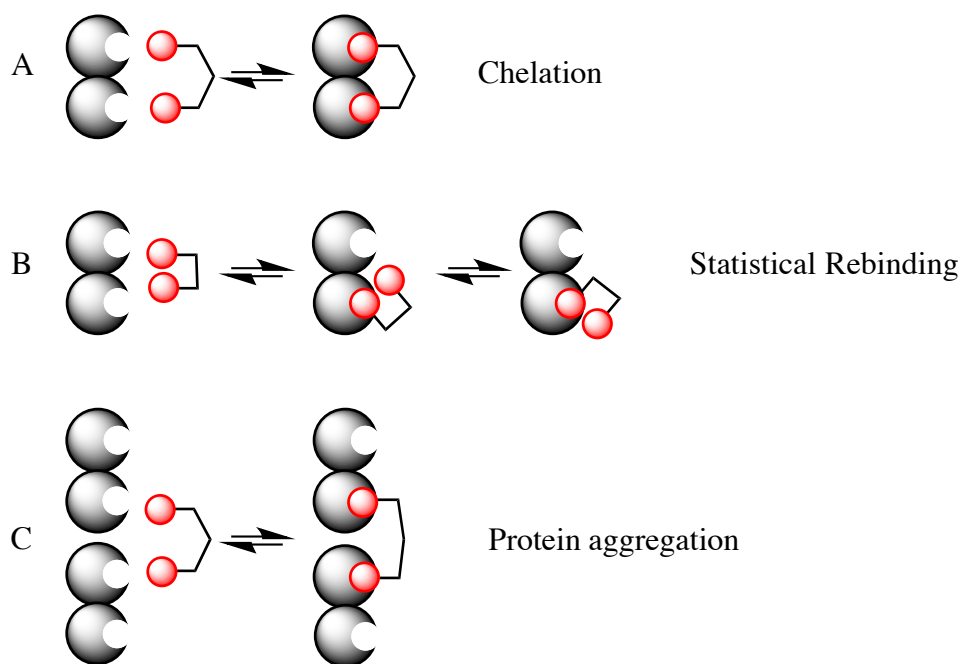
Figure 1.7 Schematic representation of the main polyvalent binding mechanisms that can occur between a divalent ligand (red) and one ore more divalent protein (grey).

Besides these binding mechanisms, simple statistical considerations can explain the multivalence effect, given that a multivalent material (ligand or receptor) provides higher density of the binding partner.

1.5.1 On the thermodynamic principles of multivalency

The thermodynamic parameters describing a multivalent binding can't always be calculated from the ones of the corresponding monovalent interaction simply multiplying by the valency.[67,64] Indeed, when a multivalent ligand interacts with a receptor, sub-ligands don't operate individually, but they influence the following binding events in a way that depends on the nature of their presentation.

The enthalpic contribution $\Delta H^{multivalent}$ depends on the ΔH associated to the single interactions (Equation **1.1, term 1**) but also on the enthalpy variation associated to the linker and the environment. Indeed, if the linker has not the ideal length to chelate at least two binding sites, enthalpic penalties have to be paid by the linker (if it is too long) or by the receptor (if the linker is too short) in order to fit the one with the other (Equation **1.1, term 2**). In this case, a multiple interaction of the ligand with several separated receptor molecules instead of a chelating binding mode can be more beneficial for the system. Moreover, the breaking of old non-covalent interactions and the formation of new ones (e.g. ligand + receptor, linker + binding pocket, linker + water molecules) may affect the overall enthalpy (Equation **1.1, term 3**).

$$1 \qquad 2 \qquad 3$$

$$\Delta H^{mul} = n\Delta H^{mono} + (n-1)\Delta H^{mono}_{linker\ conf} + \Delta H_{linker,solution}$$

Equation 1.1 Contributions to the multivalent enthalpy change. *n* is the ligand valency.

Also the multivalent entropy change *(ΔS^multivalent)* is related to the entropy change experienced by each ligand after immobilization, but it has to be considered that the binding of one n-valent ligand to multivalent receptor is less entropically disfavoured than the binding of n monovalent ligands to the same receptor. This happens because, in a multivalent ligand, only the first subunit-receptor interaction pays the full entropic cost, whereas the other intramolecular interactions do not. The linker and water molecules play an important role also in entropic calculations. Indeed, the overall entropy will be affected by the reduction of linker degrees of freedom after binding, as well as by the disruption of water molecules organization around the binding pocket, the ligand and the linker (Equation **1.2**).

$$\Delta S^{mul} = n\Delta S^{mono'} + \Delta S_{linker\ conf} + \Delta S_{linker,solution}$$

Equation 1.2 Contributions to the multivalent entropy change. *ΔS^mono'* takes account of the lower energy penalty paid by the nth ligand in a multivalent system with respect to a single monovalent one.

These two parameters both contribute to the determination of the free energy released upon the formation of multiple interactions, as described by the well-known Equation **1.3**.

$$\Delta G^{mul} = \Delta H^{mul} - T\Delta S^{mul}$$

Equation 1.3 Enthalpic and entropic components of the multivalent free energy *ΔG^mul*.

From this brief thermodynamic overview, the importance of the linker clearly emerges. Indeed, the multivalent interaction will be more favoured if the linker has the ideal length not to pay enthalpic conformational penalties and is rigid enough to reduce also the entropic disfavouring components.

The effective concentration C_{eff} is another key parameter to model a multivalent interaction.[68,69] When the first sub-unit of a multivalent ligand interacts with a multiple receptor, the other available binding sites experiment a higher density of the free sub-ligands, which have approached. When the local concentration density of the ligand is higher than its bulk concentration, intramolecular multivalent bindings are favoured. Also according to this model, an

ideal linker length is required, since linkers that are too long separate the binding moiety from the receptor and make the effective concentration approaching to the bulk one.

It is common and useful to evaluate the potency of a multivalent ligand with respect to the corresponding monovalent one. The potency enhancement, indicated as β factor, can therefore be calculated according to Equation **1.4**, where K_N^{poly} is the association constant of the fully associated ligand-receptor complex, and K^{mono} is the association constant of the corresponding monovalent ligand-receptor complex. Since the concept of avidity refers to the association constant of a polyvalent interaction, $K_N^{poly} \equiv K^{avidity}$ (Figure **1.8B**), whereas $K^{mono} \equiv K^{affinity}$, being the affinity a qualitatively term that indicates a monovalent interaction (Figure **1.8A**).

$$\beta = \frac{K_N^{poly}}{K^{mono}} = \frac{K^{avidity}}{K^{affinity}}$$

Equation 1.4 β factor represents the benefit of having several ligands linked together and it is a measure of potency enhancement.
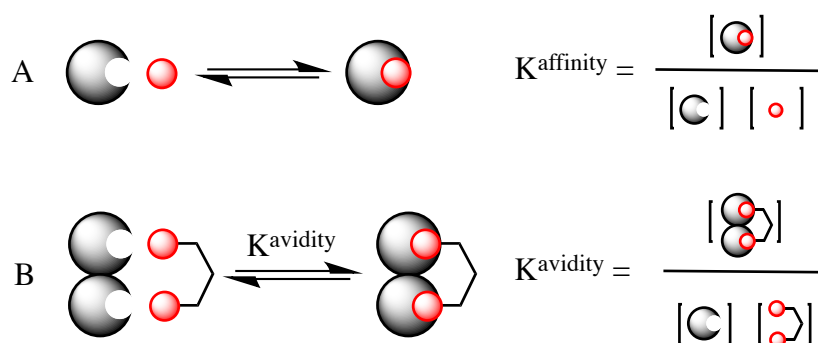
Figure 1.8 Thermodynamic equilibriums used for the definitions of affinity, avidity and enhancement.

When the β factor is divided by the valency of the ligand, the potency enhancement is corrected and evaluated per single ligand, obtaining the so called Relative Inhibitory Potency (*R.I.P*). *R.I.P* > 1 means that the whole multivalent interaction is stronger than the sum of its parts, and indicates a real multivalent effect. During this thesis, potency enhancements of multivalent compounds relative to the monovalent ones will be calculated as *R.I.P.* values.

1.5.2 Artificial ligands exploiting the chelation binding mode

Epitopes tethered to long flexible scaffolds have relatively high degrees of freedom and can adapt their conformation to match lectin binding sites. However, ligands separated by a linker that has the correct geometry to fit the distance between contiguous binding sites on the same receptor have less enthalpic and entropic costs to pay (see Paragraph 1.5.1) and give rise to a very strong

multivalent effect.[70] Moreover, exactly spanning the distance between the recognition sites on a protein leads to selective ligands that, in principle, can bridge only that specific distance. In this paragraph, some examples of carbohydrate-based ligands exploiting the chelation mechanism effect to bind lectins are presented.[71]

One of the first examples of artificial ligands that chelate a lectin is the so-called *Starfish* compound **1.25** (Scheme **1.18A**) designed by Bundle and co-workers to bind the Shiga-like toxin I (SLT-1).[72] SLT-1 belongs to the category of bacterial AB$_5$ toxins, which generally have a single toxic A-subunit associated with five nontoxic B-subunits (CTB). In SLT-1, each B subunit contains three binding sites, which are separated by 9 Å; however, distances up to 50 have to be taken into account when considering not contiguous binding sites. *Starfish* consists of a pentavalent glucose-based core decorated with five divalent arms bearing two globotriose units each. A crystal structure of the ligand-toxin complex demonstrated not only that the compound is able to bind simultaneously the five B-subunits (Scheme **1.18B**), but that if formed a sandwich like complex 2:1 in which two toxins bind one ligand; interestingly, each divalent arm of **1.25** shared the two globotriose units with the two toxins. This chelating binding mode led to an outstanding multivalency enhancement of 875500 (competitive ELISA assays *vs* BSA-glycoconjugate) with respect to globotriose.
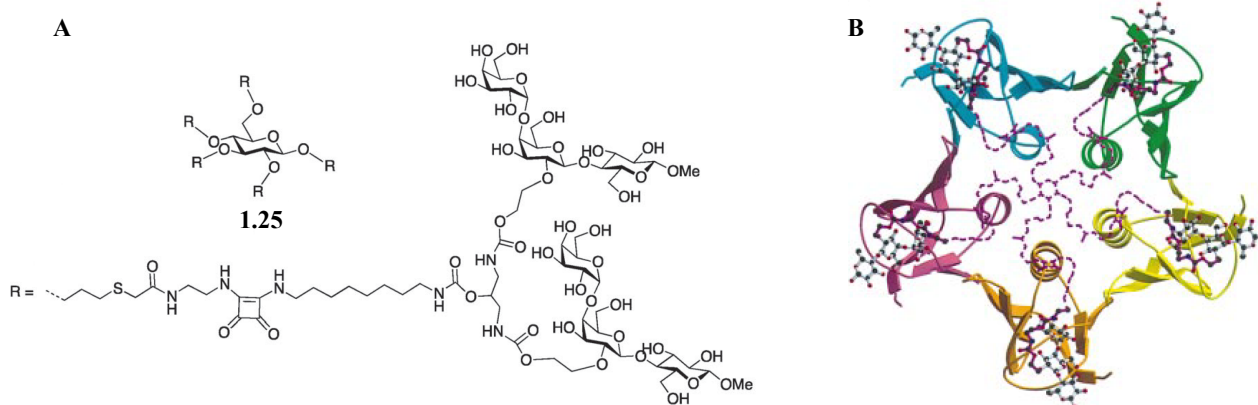
Scheme 1.18 A Structure of the SLT-I ligand **1.25**; B Diagram of half of the *Starfish*:SLT-1 B$_5$ sandwich obtained from crystallographic data; dashed magenta lines show a possible conformation for the central component of the linker, which could not be seen clearly in the electron density. Activity was measured through ELISA inhibitor assays, using glycosylated-BSA as competitor.[72]

After this initial example, many other multivalent constructs were designed as antagonists of various different lectins and they have extensively reviewed.[73,66] In this paragraph, I'm going to focus my attention on compounds that specifically exploit the chelating binding mode.

Very recently, Turnbull and co-workers published the most potent inhibitor of the bacterial AB_5 Cholera Toxin (CT), designed with the similar concept of binding simultaneously each toxin B-subunit.[74] In this case, the spacing between two binding sites is about 31 Å. Inhibitor **1.26** is a neoglycoprotein based on an inactive mutant CTB protein modified with GM1 oligosaccharides (GM1os) ligands, known to be CT ligands (Scheme **1.19**). In this way, the multivalent construct perfectly matches the size and the valency of the target CTB. This chelation-based interaction led to IC_{50} = 104 pM (competitive ELLA assays *vs* GM1 immobilized on a surface), corresponding to a potency enhancement of 5100 fold with respect to the monovalent GM1os. Dynamic Light Scattering and Analytical Ultracentrifugation assessed the formation of the 1:1 homodimer; on the contrary, Isothermal Titration Calorimetry showed a non-consistent K_D, probably because the high concentration of **1.26** needed for the assay (43 μM) led to the formation of random aggregates.
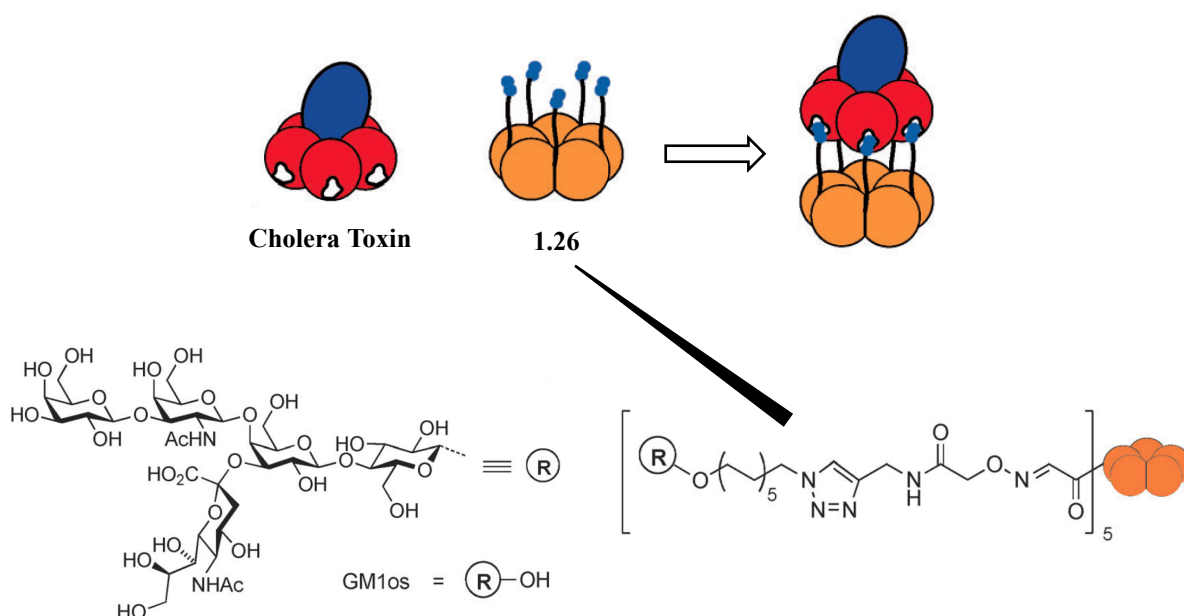
Scheme 1.19 1.26 binds CT forming a 1:1 homodimer. Activity was measured through ELLA inhibition assays, using GM1 as competitor.[74]

Lectin A is the adhesion protein and virulence factor of the pathogen *P. aeruginosa*; it is specific for galactose and it is a tetramer where two contiguous binding sites are separated by a distance of 26 Å. Pertici *et al*. modulated the length of a rigid linker to separate two galactose residues and chelate two binding sites on LecA.[75] Linker consists of glucose units connected via triazoles; variations in linker length led to very strong variations in the affinity towards LecA, thus demonstrating the need of the suitable length to chelate the receptor and to deeply increase ligands' potency. Among the small library of synthesised compounds, the most interesting were ligands **1.27** and **1.28** (Scheme **1.20**). Indeed, the first one didn't show any affinity improvement compared to

the reference compound **Ref(1.27)**, revealing to be too short, as confirmed by modeling. On the contrary, matching the distance between the two binding sites, compound **1.28** led to an activity improvement of 545-fold respect to the reference compound **Ref(1.28)** (IC_{50} = 220 nM, obtained through inhibition ELLA assays, using a galactoside functionalized surface as competitor). Remarkably, compound **1.28** presents a flexible C3 aliphatic chain between the galactose epitope and the linker that can allow the ligand to adjust its spatial disposition respect to the binding site, thus overcoming possible design imperfections.

Ref (1.27)   **1.27**

Ref (1.28)   **1.28**
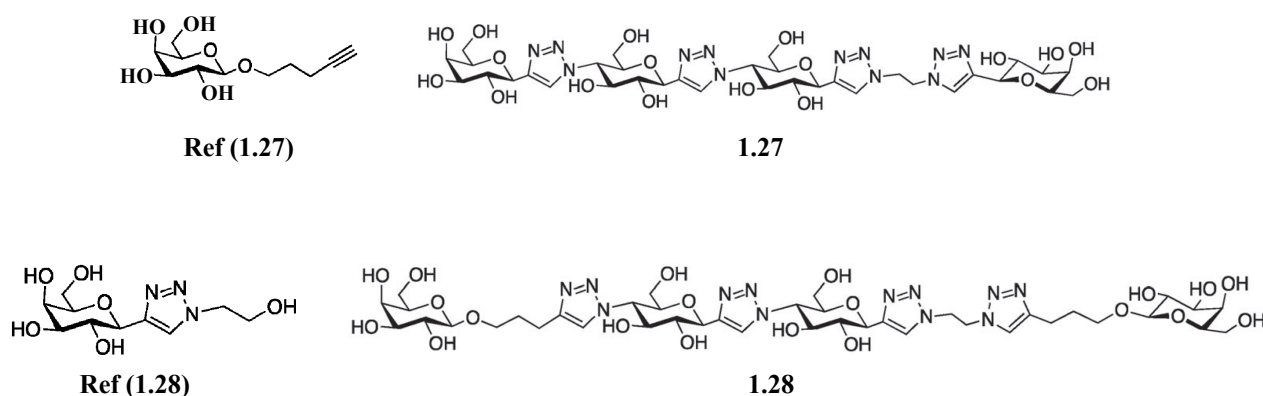
Scheme 1.20 Rigid Lec A ligands **1.27** and **1.28** and their corresponding monovalent units **Ref(1.27)** and **Ref(1.28)**. Activity was measured through ELLA inhibition assays *vs* a galactoside functionalized surface.[75]

A further improvement was obtained with compound **1.29**, which showed IC_{50} = 2.7 nM, thus representing a gain of 7555-fold (values were calculated through the ELLA inhibition assay *vs* galactosylated surface) with respect to the monovalent compound **Ref(1.29)** (Scheme **1.21**).[76] Molecular modeling confirmed that compound **1.29** had the "perfect length" (i.e. 26 Å) to chelate LecA.
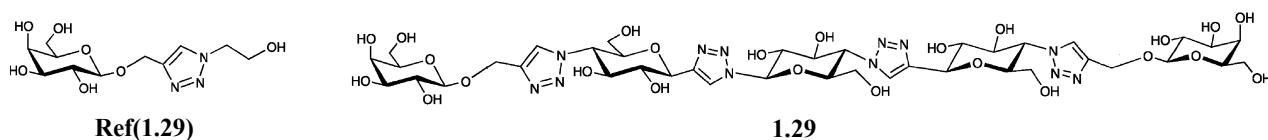
Ref(1.29)   **1.29**
Scheme 1.21 Ligands **1.28** and its corresponding monovalent unit **Ref(1.28)**.[76]

Divalent ligands using a rigid core constituted by phenylene-ethynylene units were synthesised in the groups of Pieters and Bernardi (Scheme **1.22**).[77] **1.30** is a divalent galactose-based compound and was tested as LecA ligand, revealing IC$_{50}$ = 900 nM (inhibition ELISA assay with respect to a galactosylated surface). Compound **1.31** was synthesised as potential DC-SIGN ligand, bearing one mannose unit at each scaffold end, but its activity was not evaluated. The interesting feature of this

family of scaffolds –also named rods- is their fluorescent behaviour and the possibility to easily tune their length by varying the number of phenylene units.

1.30

1.31
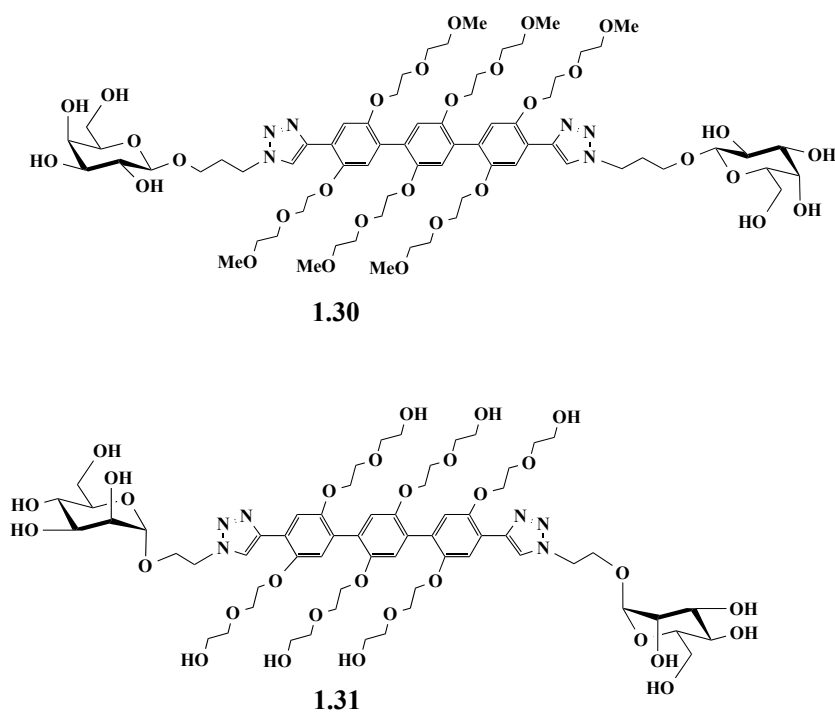
Scheme 1.22 Divalent rods derivatives **1.30** and **1.31**.[77]

1.6 References

[1] J. Banchereau; F. Briere; C. Caux; J. Davoust; S. Lebeque; Y. Liu, B.Pulendran; K. Palucka, Immunobiology of Dendritic Cells, *Annu. Rev. Immunol.* **2000**, 767.

[2] J. B. Zabriskie, Essential Clinical Immunology, Cambridge University Press: 2009.

[2] J. B. Zabriskie, Essential Clinical Immunology, Cambridge University Press: 2009.

[3] J. Bancherau; R. M. Steinman, Dendritic cells and the control of immunity, *Nature* **1998**, 245.

[4] G. Behrens; M. Li; C. M. Smith; G. T. Belz; J. Mintern; F. Carbone; W. R. Heath, Helper T cells, dendritic cells and CTL Immunity, *Immunology and Cell Biology* **2004**, 84.

[5] G. J. Adema; F. Hertger; R. Verstraten; E. de Vries; G. Marland; S. Menon; J. Foster; Y. Xu; P. Nooyen; T. McClanahan; K. B. Bacon; C. G. Figdor, A dendritic-cell-derived C-C chemokine that preferentially attracts naive T cells, *Nature* **1997**, 713.

[6] K. Inaba; M. Pack; M. Inaba; H. Sakuta; F. Isdell; R. M. Steinman, High levels of a major histocompatibility complex II–self peptide complex on dendritic cells from lymph node, *J. Exp. Med.* **1998**, 665.

[7] F. Sallusto; A. Lanzavecchia, Dendritic cells use macropinocytosis and the mannose receptor to concentrate antigen to the MHC class II compartment. Downregulation by cytokines and bacterial products, *J. Exp. Med.* **1995**, 389.

[8] K. Inaba; M. Inaba; M. Naito; R. M. Steinman, Dendritic cell progenitors phagocytose particulates, including Bacillus Calmette-Guerin organisms, and sensitize mice to mycobacterial antigens in vivo, *J. Exp. Med.* **1993**, 479.

[9] A. Cambi; M. Koopman; C. G. Figdor, How C-type lectins detect pathogens, *Cellular Microbiology* **2005**, 481.

[10] K. Drickamer, C-type lectin-like domains, *Curr. Opin. Struct. Biol.* **1999**, 585.

[11] W. Weis; K. Drickamer, Structural basis of lectin-carbohydrate recognition, *Annu. Rev. Biochem.* **1996**, 441.

[12] K. Takeda; T. Kaisho; S. Akira, Toll-like receptors, *Annu. Rev. Immunol.* **2003**, 335.

[13] T. B. Geijtenbeek; R. Torensma; S. J. van Vliet; G. C. van Duijnhoven; G. J. Adema; Y. van Kooyk; C. G. Figdor, Identification of DC-SIGN, a novel dendritic cell-specific ICAM-3 receptor that supports primary immune responses, *Cell* **2000**, 575.

[14] D. A. Mitchell; A. J. Fadden; K. Drickamer, A novel mechanism of carbohydrate recognition by the C-type lectins DC-SIGN and DC-SIGNR. Subunit organization and binding to multivalent ligands, *J. Biol. Chem.* **2001**, 28939.

[15] Y. van Kooyk; B. Appelmelk; T. B.H. Geijtenbeek, A fatal attraction: Mycobacterium tuberculosis and HIV-1 target DC-SIGN to escape immune surveillance, *Trends in Mol. Med.* **2003**, 153.

[16] A. Engering; T. B. H. Geijtenbeek; S. J. van Vliet; M. Wijers; E. van Liempt; N. Demaurex; A. Lanzavecchia; J. Fransen; C. G. Figdor; V. Piguet; Y. van Kooyk, The Dendritic Cell-Specific Adhesion Receptor DC-SIGN Internalizes Antigen for Presentation to T Cells, *The Journal of Immunology* **2002**, 2118.

[17] R. C. Gallo, A reflection on HIV/AIDS research after 25 years, *Retrovirology* **2006**, 72.

[18] T. B. Geijtenbeek; D. S. Kwon; R. Torensma; S. J. van Vliet; G. C. F. van Duijnhoven; J. Middel; I. L. M. H. A. Cornelissen; H. S. L. M. Nottet; V. N. KewalRamani; D. R. Littman; C. G. Figdor; Y. van Kooyk, DC-SIGN, a Dendritic Cell–Specific HIV-1 Binding Protein that Enhances trans-Infection of T Cells, *Cell* **2000**, 587.

[19] T. Mizuochi; T. J. Matthews; M. Kato; J. Hamako; K. Titani; J. Solomon; T. Feizi, Diversity of Oligossaccharide Structures on the Evelope Glycoprotein gp120 of Human Immunodeficiency Virus 1 from the Lymphoblastoid Cell Line H9, *The Journal of Biological Chemistry* **1990**, 8519.

[20] D. S. Kwon; G. Gregorio; N. Bitton; W. A. Hendrickson; D. R. Littman, DC-SIGN-mediated internalization of HIV is required for trans-enhancement of T cell infection, *Immunity* **2002**, 135.

[21] L. de Witte; A. Nabatov; T. B. H. Geijtenbeek, Distinct roles for DC-SIGN[+]-dendritic cells and Langerhans cells in HIV-1 transmission, *Trends in Mol. Med*. **2008**, 13.

[22] M. R. Betts; D. R. Ambrozak; D. C. Douek; S. Bonhoeffer; J. M. Brenchley; J. P. Casazza; R. A. Koup; L. J. Picker, Analysis of total human immunodeficiency virus (HIV)-specific CD4(+) and CD8(+) T-cell responses: relationship to viral load in untreated HIV infection, *J. Virol.* **2001**, 11983.

[23] Y. van Kooyk and T. B. H. Geijtenbeek, DC-SIGN: escape mechanism for pathogens, *Nature Reviews Immunology* **2003**, 697.

[24] D. McDonald; L. Wu; S. M. Bohks; V. N. KewalRamani; D. Unutmaz; T. J. Hope, Recruitment of HIV and Its Receptors to Dendritic Cell–T Cell Junctions, *Science* **2003**, 1295.

[25] D. M. Ratner; E. W. Adams; B. O'Keefe; M. Mrksich; P. H. Seeberger, Probing protein-carbohydrate interactions with microarrays of synthetic oligosaccharides, *Chembiochem* **2004**, 379.

[26] E. van Liempt; C. M.C. Bank; P. Mehta; J. J. Garcia-Vallejo; Z. S. Kawar; R. Geyer; R. A. Alvarez; R. D. Cummings; Y. van Kooyk; I. van Die, Specificity of DC-SIGN for mannose- and fucose-containing glycans, *FEBS Letters 580* **2006**, 6123.

[27] Y. Guo; H. Feinberg; E. Conroy; D. A. Mitchell; R. Alvarez; O. Blixt; M. E. Taylor; W. I. Weis; K. Drickamer, Structural basis for distinct ligand-binding and targeting properties of the receptors DC-SIGN and DC-SIGNR, *Nat. Struct. Mol. Biol.* **2004**, 591.

[28] E. W. Adams; D. M. Ratner; H. R. Bokesch; J. B. McMahon; B. R. O'Keefe; P. H. Seeberger, Oligosaccharide and Glycoprotein Microarrays as Tools in HIV Glycobiology: Glycan-Dependent gp120/Protein Interactions, *Chemistry & Biology* **2004**, 875.

[29] H. Feinberg; D. A. Mitchell; K. Drickamer; W. I. Weis, Structural basis for selective recognition of oligosaccharides by DC-SIGN and DC-SIGNR, *Science* **2001**, 2163**.**

[30] B. J. Appelmelk; I. van Die; S. J. van Vliet; C. M. Vandenbroucke-Grauls; T. B. Geijtenbeek; Y. van Kooyk, Cutting edge: carbohydrate profiling identifies new pathogens that interact with dendritic cellspecific ICAM-3-grabbing nonintegrin on dendritic cells, *J. Immunol.* **2003**, 1635.

[31] J. Sabatte; W. Faigle; A. Ceballos; W. Morelle; C. R. Rodrígue; F. R. Lenicov; M. Thépaut; F. Fieschi; E. Malchiodi; M. Fernàndez; F. Arenzana-Seisdedos; H. Lortat-Jacob; J. C. Michalski; J. Geffner; S. Amigorena, Semen Clusterin Is a Novel DC-SIGN Ligand, *J. Immunol.* **2011**, 5299.

[32] M. Moulard; H. Lortat-Jacob; I. Mondor; G. Roca; R. Wyatt; J. Sodroski; L. Zhao; W. Olson; P. D. Kwong; Q. J. Sattentau, Selective interactions of polyanions with basic surfaces on human immunodeficiency virus type 1 gp120, *J. Virol.* **2000**, 1948.

[33] A. Magerus-Chatinet, H. Yu; S. Garcia; E. Ducloux; B. Terris; M. Bomsel, Galactosyl ceramide expressed on dendritic cells can mediate HIV-1 transfer from monocyte derived dendritic cells to autologous T cells, *Virology* **2007**, 67.

[34] S. G. Turville; P. U. Cameron; A. Handley; G. Lin; S. Pöhlmann; R. W. Doms; A. L. Cunningham, Diversity of receptors binding HIV on dendritic cell subsets, *Nat. Immunol.* **2002**, 975.

[35] J. P. Moore; M. Stevenson, New targets for inhibitors of HIV-1 replication, *Nature Rev. Mol. Cell Biol.* **2000**, 40.

[36] J. Valladeau; O. Ravel; C. Dezutter-Dambuyant; K. Moore; M. Kleijmeer; Y. Liu; V. Duvert-Frances; C. Vincent; D. Schmitt; J. Davoust; C. Caux; S. Lebecque; S. Saeland, Langerin, a Novel C-Type Lectin Specific to Langerhans Cells, Is an Endocytic Receptor that Induces the Formation of Birbeck Granules, *Immunity* **2000**, 71.

[37] H. Feinberg; A. S. Powlesland; M. E. Taylor; W. I. Weis, Trimeric Structure of Langerin, *J. Biol. Chem.* **2010**, 13285.

[38] L. de Witte, A. Nabatov; M. Pion; D. Fluitsma; M. A. de Jong; T. de Gruijl; V. Piguet; Y. van Kooyk; T. B. Geijtenbeek, Langerin is a natural barrier to HIV-1 transmission by Langerhans cells, *Nat. Med.* **2007**, 367.

[39] M. S. Birbeck; A. S. Breathnach; J. D. Everall, An Electron Microscope Study of Basal Melanocytes and High-Level Clear Cells (Langerhans Cells) in Vitiligo, *The Journal of Investigative Dermatology* **1961**, 51.

[40] H. Feinberg; M. E. Taylor; N. Razi; R. McBride; Y. A. Knirel; S. A. Graham; K. Drickamer; W. I. Weis, Structural Basis for Langerin Recognition of Diverse Pathogen and Mammalian Glycans through a Single Binding Site, *J. Mol. Biol.* **2011**, 1027.

[41] M. M. Lederman; R. E. Offord; O. Hartley, Microbicides and other topical strategies to prevent vaginal transmission of HIV, *Nature Reviews Immunology* **2006**, 371.

[42] J. P.Moore; M. Stevenson, New Targets For Inhibitors of HIV-1 Replication, *Nat. Rev.* **2000**, 40.

[43] R. S. Veazey; P. J. Klasse; S. M. Schader; Q. Hu; T. J. Ketas; M. Lu; P. A. Marx; J. Dufour; R. J. Colonno; R. J. Shattock; M. S. Springer; J. P. Moore, Protection of macaques from vaginal SHIV challenge by vaginally delivered inhibitors of virus–cell fusion, *Nature* **2005**, 99.

[44] G. Timpano; G. Tabarani; M. Anderluh; D. Invernizzi; F. Vasile; D. Potenza; P. M. Nieto; J. Rojo; F. Fieschi; A. Bernardi, Synthesis of Novel DC-SIGN Ligands with an α-Fucosylamide Anchor, *ChemBioChem* **2008**, 1921.

[45] D. Doknic; M. Abramo; I. Sutkeviciute; A. Reinhardt; C. Guzzi; M. K. Schlegel; D. Potenza; P. M. Nieto; F. Fieschi; P. H. Seeberger; A. Bernardi, Synthesis and Characterization of Linker-Armed Fucose-Based Glycomimetics, *Eur. J. Org. Chem.* **2013**, 5303.

[46] D. Arosio; F. Chiodo; J. J. Reina; M. Marelli; S. Penadés; Y. van Kooyk; J. J. Garcia-Vallejo; A. Bernardi, Effective Targeting of DC-SIGN by α‐Fucosylamide Functionalized Gold Nanoparticles, *Bioconjugate Chem.* **2014**, 2244.

[47] J. J. Reina; S. Sattin; D. Invernizzi; S. Mari; L. Martínez-Prats; G. Tabarani; F. Fieschi; R. Delgado; P. M. Nieto; J. Rojo; A. Bernardi, 1,2-Mannobioside Mimic: Synthesis, DC-SIGN Interaction by NMR and Docking, and Antiviral Activity, *ChemMedChem* **2007**, 1030.

[48] M. Thépaut; C. Guzzi; I. Sutkeviciute; S. Sattin; R. Ribeiro-Viana; N. Varga; E. Chabrol; J. Rojo; A. Bernardi; J. Angulo; P. M. Nieto; F. Fieschi, Structure of a Glycomimetic Ligand in the Carbohydrate Recognition Domain of C‐type Lectin DC-SIGN. Structural Requirements for Selectivity and Ligand Design, *J. Am. Chem. Soc.* **2013**, 2518.

[49] S. Mari; I. Sanchez-Medina; P. Mereghetti; L. Belvisi; J. Jiménez-Barbero; A. Bernardi, Synthesis and conformational analysis of an α-D-mannopyranosyl-(1,2)-α-D-mannopyranosyl-(1,6)-α-D-mannopyranose mimic, *Carbohydr. Res.* **2007**, 1859.

[50] I. Sutkeviciute; M. Thépaut; S. Sattin; A. Berzi; J. McGeagh; S. Grudinin; J. Weiser; A. Le Roy; J. J. Reina; J. Rojo; M. Clerici; A. Bernardi; C. Ebel; F. Fieschi, Unique DC-SIGN Clustering Activity of a Small Glycomimetic: A Lesson for Ligand Design, *ACS Chem. Biol.* **2014**, 1377.

[51] N. Obermajer; S. Sattin; C. Colombo; M. Bruno; U. Svajger; M. Anderluh; A. Bernardi, Design, synthesis and activity evaluation of mannose-based DC-SIGN antagonists, *Mol. Divers.* **2011**, 347.

[52] N. Varga; I. Sutkeviciute; C. Guzzi; J. McGeagh; I. Petit-Haertlein; S. Gugliotta; J. Weiser; J. Angulo; F. Fieschi; A. Bernardi, Selective Targeting of Dendritic Cell-Specific Intercellular Adhesion Molecule-3-Grabbing Nonintegrin (DC-SIGN) with Mannose-Based Glycomimetics: Synthesis and Interaction Studies of Bis(benzylamide) Derivatives of a Pseudomannobioside, *Chem. Eur. J.* **2013**, 4786.

[53] S. Sattin; A. Daghetti; M. Thépaut; A. Berzi; M. Sánchez-Navarro; G. Tabarani; J. Rojo; F. Fieschi; M. Clerici; A. Bernardi, Inhibition of DC-SIGN-Mediated HIV Infection by a Linear Trimannoside Mimic in a Tetravalent Presentation, *Chemical Biology* **2010**, 301.

[54] J. Luczkowiak; S. Sattin; I. Sutkeviciute; J. J. Reina; M. Sanchez-Navarro; M. Thépaut; L. Martinez-Prats; A. Daghetti; F. Fieschi; R. Delgado; A. Bernardi; J. Rojo, Pseudosaccharide Functionalized Dendrimers as Potent Inhibitors of DC-SIGN Dependent Ebola Pseudotyped Viral Infection, *Bioconjugate Chem.* **2011**, 1354.

[55] N.Varga; I. Sutkeviciute; R. Ribeiro-Viana; A. Berzi; R. Ramdasi; A. Daghetti; G. Vettoretti; A. Amara; M. Clerici; J. Rojo; F. Fieschi; A. Bernardi, A multivalent inhibitor of the DC-SIGN dependent uptake of HIV-1 and Dengue virus, *Biomaterials* **2014**, 4175.

[56] K. C. A. Garber; K. Wangkanont; E. E. Carlsona; L. L. Kiessling, A general glycomimetic strategy yields non-carbohydrate inhibitors of DC-SIGN, *Chem. Commun.* **2010**, 6747.

[57] L. R. Prost; J. C. Grim; M. Tonelli; L. L. Kiessling, Noncarbohydrate Glycomimetics and Glycoprotein Surrogates as DC-SIGN Antagonists and Agonists, *ACS Chem. Biol.* **2012**, 1603.

[58] C. R. Becer; M. I. Gibson; J. Geng; R. Ilyas; R. Wallis; D. A. Mitchell; D. M. Haddleton, High-Affinity Glycopolymer Binding to Human DC-SIGN and Disruption of DC-SIGN Interactions with HIV Envelope Glycoprotein, *J. Am. Chem. Soc.* **2010**, 15130.

[59] O. Martínez-Ávila; K. Hijazi; M. Marradi; C. Clavel; C. Campion; C. Kelly; S. Penadés, *Chem. Eur. J.* **2009**, 9874.

[60] L. Dehuyser; E. Schaeffer; O. Chaloin; C. G. Mueller; R. Baati; A. Wagner, Synthesis of Novel Mannoside Glycolipid Conjugates for Inhibition of HIV‑1 Trans-Infection, *Bioconjugate Chem.* **2012**, 1731.

[61] M. J. Borrok; L. L. Kiessling, Non-carbohydrate Inhibitors of the Lectin DC-SIGN, *J. Am. Chem. Soc.* **2007**, 12780.

[62] E. E. Carlson; J. F. May; L. L. Kiessling, Chemical probes of UDP-galactopyranose mutase, *Chem. Biol.* **2006** 825.

[63] S. L. Mangold; L. R. Prostb; L. L. Kiessling, Quinoxalinone inhibitors of the lectin DC-SIGN, *Chem. Sci.* **2012**, 772.

[64] M. Reynolds; S. Pérez, Thermodynamics and chemical characterization of protein-carbohydrate interactions: The multivalency issue, *C. R. Chimie* **2011**, 74.

[65] R. J. Pieters, Maximising multivalency effects in protein–carbohydrate interactions, *Org. Biomol. Chem.*, **2009**, 2013.

[66] S. Cecioni; A. Imberty; S. Vidal, Glycomimetics versus Multivalent Glycoconjugates for the Design of High Affinity Lectin Ligands, *Chem. Soc. Rev.* **2014**, 525.

[67] M. Mammen; S. Choi; G. M. Whitesides, Polyvalent Interactions in Biological Systems: Implications for Design and Use of Multivalent Ligands and Inhibitors, *Angew. Chem. Int. Ed.* **1998**, 2754.

[68] R. H. Kramer; J.W. Karpen, Spanning binding sites on allosteric proteins with polymer-linked ligand dimers, *Nature* **1998**, 710.

[69] J. M. Gargano; T. Ngo; J. Y. Kim; D. W. Acheson; W. J. Lees, Thermodynamics of Multivalent Interactions: Influence of the Linker, *J. Am. Chem. Soc.* **2001**, 12909.

[70] D. Deniaud; K. Julienne; S. G. Gouin, Insights in the rational design of synthetic multivalent glycoconjugates as lectin ligands, *Org. Biomol. Chem.* **2011**, 966.

[71] V. Wittmann; R. J. Pieters, Bridging lectin binding sites by multivalent carbohydrates, *Chem. Soc. Rev.* **2013**, 4492.

[72] P. I. Kitov; J. M. Sadowska; G. Mulvey; G. D. Armstrong; H. Ling; N. S. Pannu; R. J. Read; D. R. Bundle, Shiga-like toxins are neutralized by tailored multivalent carbohydrate ligands, *Nature* **2000**, 669.

[73] A. Bernardi; J. Jiménez-Barbero; A. Casnati; C. De Castro; T. Darbre; F. Fieschi; J. Finne; H. Funken; K. E. Jaeger; M. Lahmann; T. K. Lindhorst; M. Marradi; P. Messner; A. Molinaro; P. V. Murphy; C. Nativi; S. Oscarson; S. Penadés; F. Peri; R. J. Pieters; O. Renaudet; J. L. Reymond; B. Richichi; J. Rojo; F. Sansone; C. Schäffer; W. B. Turnbull; T. Velasco-Torrijos; S. Vidal; S. Vincent; T. Wennekes; H. Zuilhof; A. Imberty, Multivalent glycoconjugates as anti-pathogenic agents, *Chem. Soc. Rev.* **2013**, 4709.

[74] T. R. Branson; T. E. McAllister; J. Garcia-Hartjes; M. A. Fascione; J. F. Ross; S. L. Warriner; T. Wennekes; H. Zuilhof; W. B. Turnbull, A Protein-Based Pentavalent Inhibitor of the Cholera Toxin B-Subunit, *Angew. Chem. Int. Ed.* **2014**, 8323.

[75] F. Pertici; R. J. Pieters, Potent divalent inhibitors with rigid glucose click spacers for Pseudomonas aeruginosa lectin LecA, *Chem. Commun.* **2012**, 4008.

[76] F. Pertici; N. J. de Mol; J. Kemmink; R. J. Pieters, Optimizing Divalent Inhibitors of Pseudomonas aeruginosa Lectin LecA by Using A Rigid Spacer, *Chem. Eur. J.* **2013**, 16923.

[77] F. Pertici; N. Varga; A. van Duijn; M. Rey-Carrizo; A. Bernardi; R. J. Pieters, Efficient synthesis of phenylene-ethynylene rods and their use as rigid spacers in divalent inhibitors, *Beilstein J. Org. Chem.* **2013**, 215.

Chapter 2

Designing nanomolar antagonists of DC-SIGN-mediated HIV infection: ligand presentation using molecular rods

2.1 Introduction

2.1.1 Designing DC-SIGN ligands

As seen in detail in Chapter 1.4, DC-SIGN is a tetrameric lectin (i.e. a carbohydrate-recognizing receptor) expressed at the surface of Dendritic Cells. Since the DC-SIGN-mediated anchoring of HIV virus on human cells represents the early stage of the infection,[1] DC-SIGN is a valid target to develop compounds with viral anti-adhesive properties. Active DC-SIGN ligands can be synthesised by mimicking HIV epitopes. The disaccharide Manα1-2Man and the trisaccharide Manα1-2Manα1-6Man (Figure **2.1**) are found in multiple copies of the HIV glycoprotein gp120 (through which the virus interacts with the receptor)[2] and they are known to bind to DC-SIGN.[3]
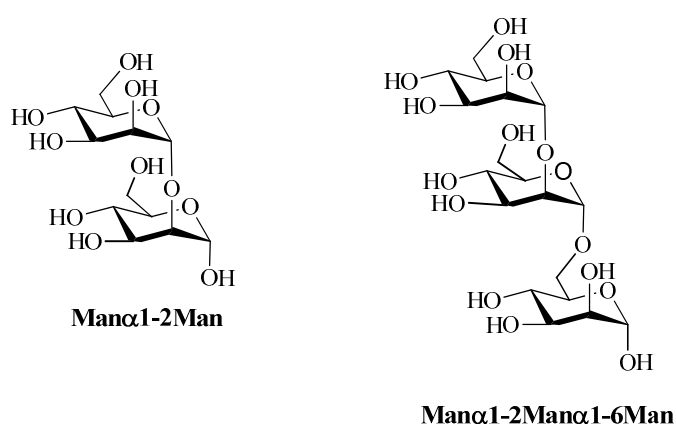

Manα1-2Man

Manα1-2Manα1-6Man

Figure 2.1 Structures of the disaccharide Manα1-2Man (left) and the trisaccharide Manα1-2Manα1-6Man (right).

These natural ligands can therefore be used as starting points to design artificial compounds, that would be more active and selective towards DC-SIGN with respect to other lectins (e.g. Langerin and the Mannose Receptor) once derivatized with functional groups able to participate in additional positive contacts with the target receptor. Activity can be improved also exploiting multivalency. Powerful DC-SIGN ligands could be used also against the plethora of other pathogens that infect humans through the mucosal entry pathway and that recognize DC-SIGN as their primary target.[4]

2.1.2 Multivalency

As stated in Chapter 1.5, multivalent interactions among binding partners lead to stronger binding.[5] Possible interactions between one divalent ligand (red) and one divalent receptor (blue) are reported as an example in Figure **2.2**. The presence of two proximal active ligands at one binding site increases their effective concentration C_{eff}. The possibility that one active ligand easily replaces the first one after it is released increases the overall potency of the interaction and it is referred to as *statistical rebinding effect*[5] (Figure **2.2 A**). It is also possible that the two active ligands are separate

by a distance which fits the one between two binding sites on the receptor. When a ligand is able to *chelate* (i.e. to bind simultaneously more than one subunit on) its binding partner (Figure **2.2B**), the resulting multivalent interaction is more probable and stronger. Indeed, from a thermodynamic point of view, only the first sub-ligand pays the full entropic costs associated with the interaction, thus favoring the binding of the second one. Finally, one multivalent ligand can *cluster* more than one receptor (Scheme **2.2 C**). This is possible when receptors are soluble, but also when they are embedded in membranes, since membranes are flexible and receptors can diffuse in them.
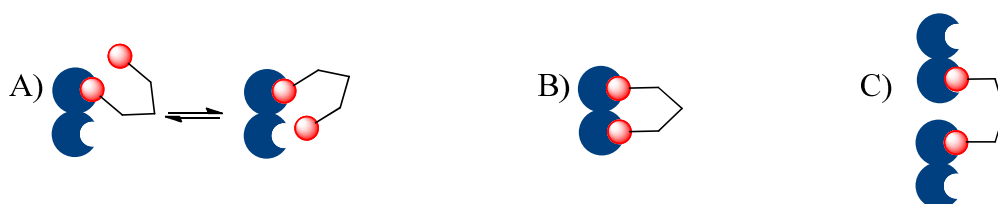
Figure 2.2 A) a multivalent ligand (red) binds to a protein (blue) exploiting the statistical rebinding (proximity) effect; B) a multivalent ligand chelates a divalent protein; C) a multivalent ligand clusters a soluble protein.

The efficiency of one multivalent compound with respect to its monovalent unit can be expressed in terms of β *factor*,[6] defined as in Equation **2.1**, or in terms of Relative Inhibitory Potency *R.I.P.*, which corresponds to the β factor corrected by valency (Equation **2.2**).

$$\beta = \frac{Activity_{multivalent}}{Activity_{monovalent}}$$

Equation 2.1 β *factor* represents the improvement obtained by using a multivalent presentation of a ligand with respect to the monovalent ligand itself.

$$R.I.P. = \frac{Acitivity_{multivalent}}{Acitivty_{monovalent} \times valency}$$

Equation 2.2 Relative Inhibitory Petency *R.I.P.* is the β *factor* corrected by valency.

Nature has taken deep advantage of these concepts to increase the strength of the interactions that would be too weak if involving only monovalent partners. Carbohydrates, that have a low affinity for proteins, bind tighter to their partners when they are presented in a multivalent way. Pathogens attack human body through multivalent interactions between multivalent presentations of epitopes and multiple receptor units.

In order to efficiently interfere with biological interactions, artificial ligands able to interact with a biological receptor in a multivalent fashion are suitable.[7]

2.2 State of the art

With the aim of mimicking the disaccharide Manα1-2Man, our laboratory has developed a series of mannosylated DC-SIGN ligands (see Chapter 1.4.1.2 for a broader overview). Among them, the pseudo-dimannosylated compounds **1.7**[8] and **1.9**[9] are the most promising ones (Figure **2.3**). They consist of one mannose residue, whose hydroxyl groups in position 3- and 4- are responsible for chelation of the calcium ion in the DC-SIGN binding pocket, and one conformationally locked cyclohexyl moiety, which is involved in additional Van der Waals contacts with the binding site.[10] Compound **1.7** bears methylesters on the cyclohexane moiety; their replacement with aromatic benzylamides in **1.9** provided more efficient interactions, thus leading to an affinity improvement.
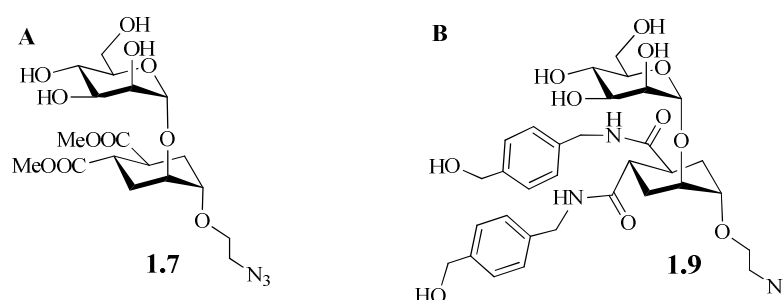
Figure 2.3 Structures of the lead compounds **1.7** (A) and **1.9** (B).

Through SPR inhibition assays, performed by evaluating the ability of artificial compounds to inhibit DC-SIGN binding to a mannosylated surface (Man-BSA), activity performances were calculated in terms of IC_{50} values, finding a value of 1 mM for **1.7** and 300 μM for **1.9**.[11] Compound **1.9** was the most active, thus identified as the lead for further modifications. Compound **1.7** was still worth an interest, since it has a high solubility in water and it is active despite its simplicity.

Multivalent presentations of **1.7** and **1.9** were prepared by coupling monovalent ligands to polyalkynes dendrimeric cores, obtaining dendrimers among which the most relevant are shown in Figure **2.4**.[12] These tetravalent, hexavalent and nonavalent compounds obtained from scaffolds IV, VI and IX, respectively (Figure **2.4**) were more chemically stable than previously synthesised Boltorn-type dendrons and dendrimers derived from 2,2-bis(hydroxymethyl) propionic acid.[13]
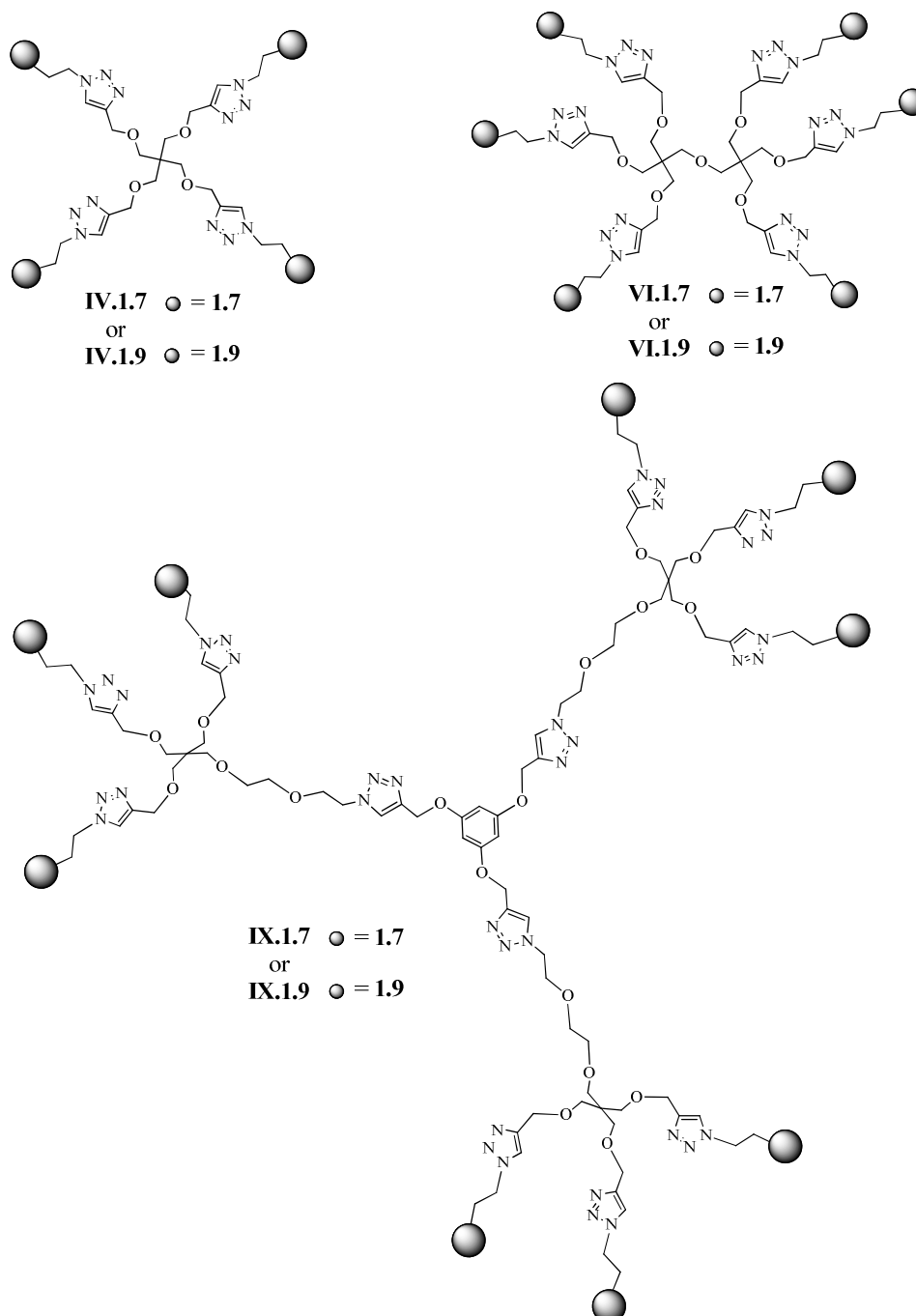
Figure 2.4 Structure of tetravalent (**IV**), hexavalent (**VI**) and nonavalent (**IX**) presentations of **1.7** and **1.9**.

Biological performances (SPR and inhibition studies) obtained for multivalent derivatives of **1.7** confirmed that multivalency helps in overcoming the low affinities associated to monovalent compounds. Moreover, multivalent compounds based on **1.7** had the advantage of having a rather high solubility in water ($\geq$ 5 mM). Still, the use of a more powerful monovalent ligand was demonstrated to be convenient, as shown by the best activities associated with the multivalent presentations of **1.9**. The drawback of these compounds was having a mediocre water solubility ($\leq$ 1 mM), which became limiting for the nonavalent derivative **IX.1.9**.

Their IC_{50} obtained again through SPR competition assays and associated *R.I.P.* values are reported in Table **2.1**. Among the complete series of compounds based on **1.7**, it was possible to observe how the IC_{50} values decrease and the *R.I.P.* values increase by increasing the valency of the system. Similar results were obtained for the **1.9** series, which found the hexavalent derivative **VI.1.9** to have the best *R.I.P.* values. No results were obtained for the nonavalent compound **IX.1.9**, because of solubility problems.

IC_{50} (μM) (*R.I.P.*)		
Scaffold	**Ligand 1.7**	**Ligand 1.9**
Mono	1018 (1)	308 (1)
Tetra (IV)	136 (1.9)	12 (6.4)
Hexa (VI)	39 (4)	5.7 (9)
Nona (IX)	14 (8)	not soluble

Table 2.1 IC_{50} values of tetravalent, hexavalent and nonavalent compounds **1.7**- or **1.9**-based. *R.I.P.* values with respect to corresponding monovalent ligands are in round brackets.[12]

The most active DC-SIGN ligands were tested also as inhibitors of the DC-SIGN-mediated HIV infection, using a cellular *in vitro* model. Compound **VI.1.9** was found to totally inhibit the infection already at a concentration of 10 μM (Figure **2.5**). This assay also confirms the powerful effect of a more powerful monovalent ligand (compare **IV.1.7** and **IV.1.9**) and of increased valency (compare **IV.1.9** and **VI.1.9**)
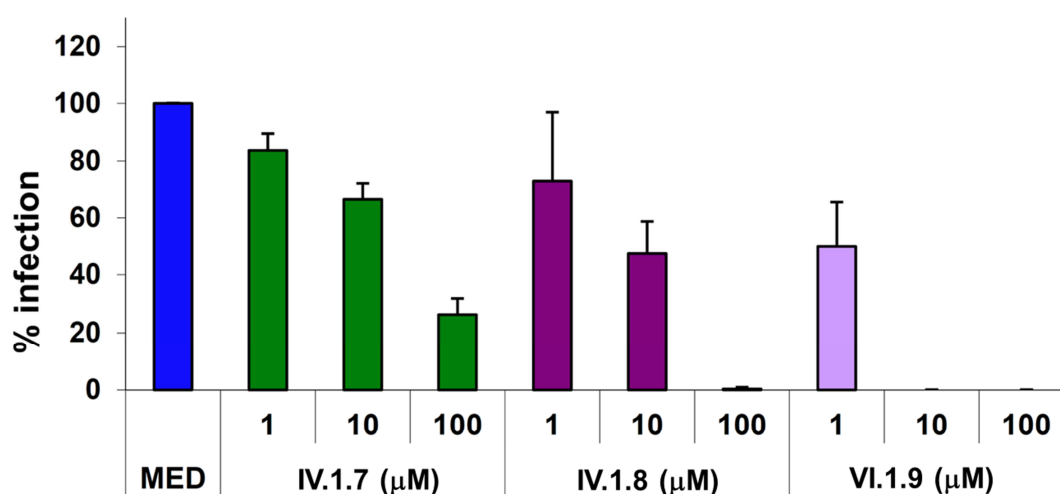

Figure 2.5 Percentage of DC-SIGN-mediated transmitted HIV infection, evaluated in a cellular *in vitro* infection model.[12]

In order to interpret the nature of the multivalent effect obtained with these multivalent compounds and to understand whether it derived from a statistical rebinding, chelating or clustering mechanism (or a combination of them), molecular dynamics simulations were used to estimate their average dimension. This was compared with the distance between two contiguous binding sites within one tetrameric DC-SIGN extracellular domain (ECD), which are separated by a distance ranging from 35.3 to 37.8 Å (Figure **2.6**).[14] Distances were calculated between calcium atoms, which are anchoring sites for DC-SIGN ligands.

Conformational analyses were conducted by Dr. G. Vettoretti and the undergraduate student A. Bertaglia under the supervision of Dr. L. Belvisi.
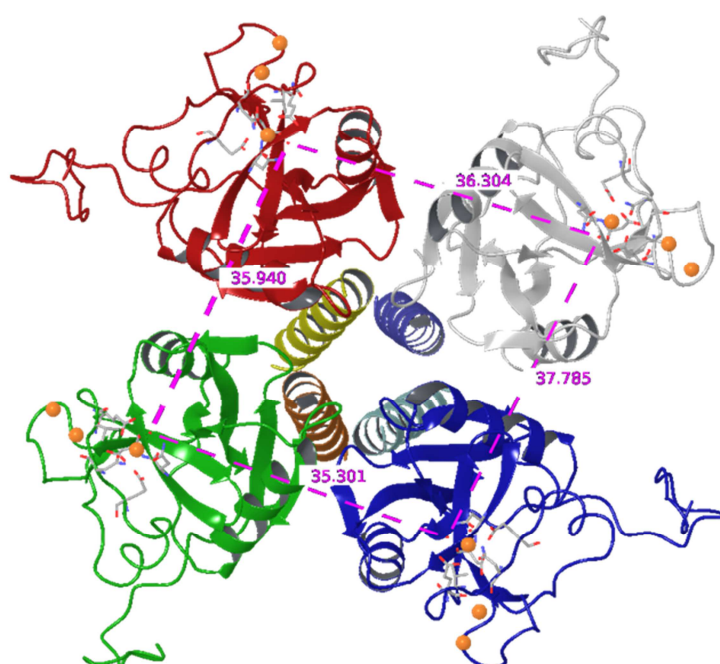
Figure 2.6 Structure of a tetrameric DC-SIGN extracellular domain. The four binding sites are here colored in red, green, grey and blue. Distances were evaluated between calcium ions (orange spheres) in two contiguous binding sites.

Compound **VI.1.7** was used as a model; in principle, it should have the same size and behavior of the corresponding **VI.1.9** derivative. The distance between oxygen atoms in 3- position of two different mannose residues was monitored, since mannose is known to chelate Calcium ions in DC-SIGN using O3 and O4. Results showed that the maximum extension of the compound (i.e. the maximum distance between two O3 atoms -*Max d_{O3-O3}*-), was 35.4 Å, which is not enough to bind simultaneously two DC-SIGN binding sites. In a similar way, also **IV.1.7** was demonstrated not to be able to reach across, as expected, given its smaller structure with respect to the hexavalent derivative. The nonavalent derivatives were not investigated, because **IX.1.9** is not soluble in water.

These assays revealed that the affinity improvement observed for the hexavalent and tetravalent dendrimers with respect to the monovalent ligand could be only due to the statistical rebinding effect or to protein clustering. The induction of DC-SIGN aggregation in the SPR assay can be easily understood, since DC-SIGN and the ligands flow free in solution; the induction of DC-SIGN clustering in the cellular inhibition assay could also be possible given DC-SIGN mobility on the membrane.[15]

2.3 Goal of the project

As stated in the previous paragraph, multivalent dendrimeric compounds based on tetravalent and hexavalent dendrimeric scaffolds are able to implement the multivalent mechanisms of statistical rebinding and/or protein clustering, leading to a gain in activity towards DC-SIGN receptor with respect to the corresponding monovalent compounds. We wanted to further improve the affinity of artificial ligands for DC-SIGN, with the aim to prepare potent inhibitors of DC-SIGN-mediated infections, especially the HIV one.

Starting from the results obtained with multivalent dendrimeric-based compounds, only derivatizations of the hexavalent compounds were investigated. Indeed, the low solubility of **IX.1.9** suggested a limit to an approach based only on increased valency for ligand **1.9**. Rather, we strived to find ways to efficiently exploit chelation mechanism and we therefore decided to separate two couples of trivalent materials with a rigid central spacer, obtaining compounds with the general structure shown in Scheme **2.1**.
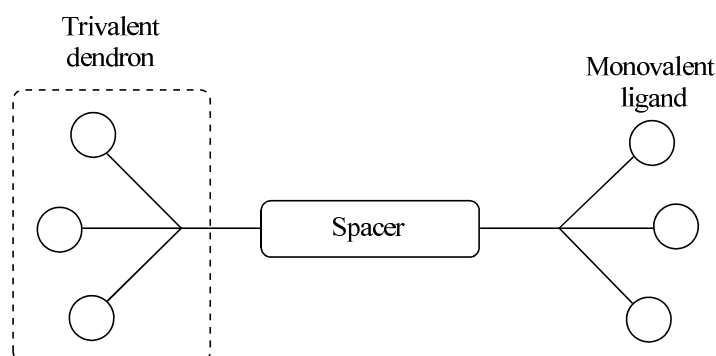
Scheme 2.1 Schematic representation of an hexavalent compound where two trivalent dendrons are separated by one central spacer. White circles represent monovalent ligands.

As monovalent ligand, the lead compound **1.9** was obviously employed. Compound **1.7** was used to build control molecules that were expected to be easier to synthesise and soluble in water and that would help in investigating the role of the monovalent ligand in determining the overall activity of the construct.

When designing a compound able to chelate a receptor, its rigidity is an important issue. When a ligand is equipped with a rigid linker, it has to pay less entropic costs to be fixed within the binding site, thus favoring the multivalent interaction. But ligands that do not fit the distance between contiguous binding sites demand for their bending or the receptor's to match their reciprocal shape; enthalpic costs increase when the ligand is too rigid. For these reasons, searching for a balance between rigidity and flexibility, we decided to use flexible dendrons connected to rigid spacers. This design should be able to add chelation mechanism while preserving a relatively high local concentration of the monovalent ligand in the vicinity of each binding site. Trivalent dendrons were designed by our group for the synthesis of **IX.1.9**[12] and they are characterized by flexible, PEG-based cores (Scheme **2.2**).
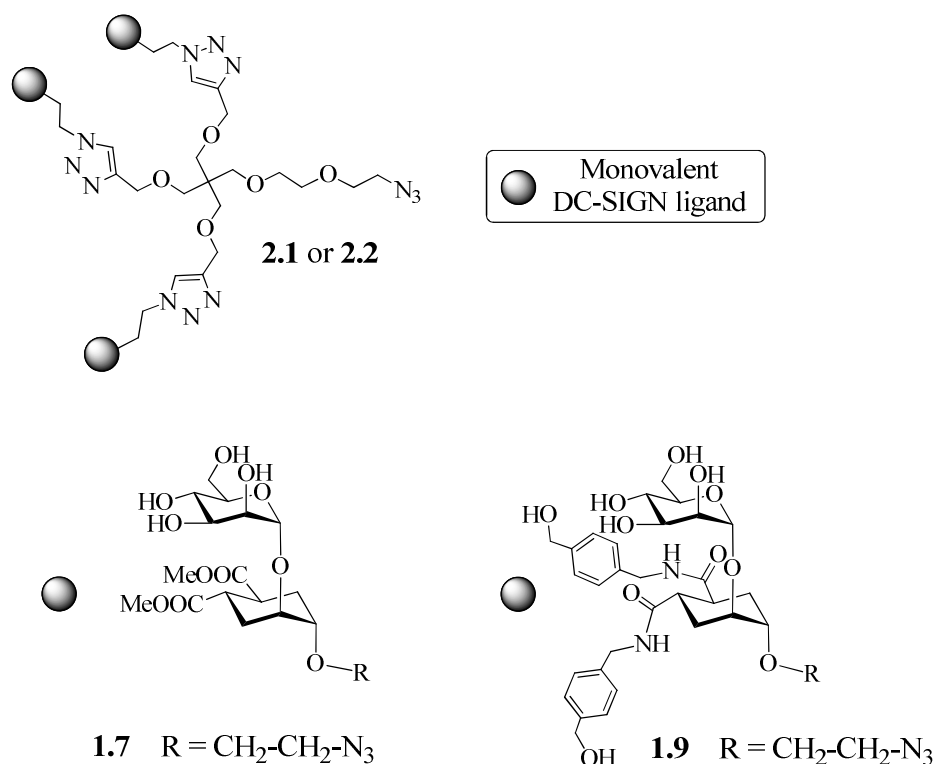
Scheme 2.2 Trivalent dendrimers presenting ligand **1.7** or **1.9** on a flexible scaffold.

As spacers, molecular rods made by aromatic rings connected via triple bonds (named *Rods*, Scheme **2.3**) were used. Three different Rods were generated by varying the number of phenylene-ethynylene units, thus producing compounds **2.3** (*Rod1*, one unit, 8 Å), **2.4** (*Rod2,* two units, 12 Å) or **2.5** (*Rod3*, three units, 24 Å). They were functionalized with PEG chains to improve their solubility in water. Their synthesis was published by the groups of Bernardi and Pieters, and divalent Rod-based galactose derivatives were investigated as ligands for *Pseudomonas aeruginosa* lectin LecA.[16]

Remarkably, derivatives **2.4** and **2.5** have an intrinsic fluorescence, which confers to their derivatives the important feature of being directly detectable through fluorescent microscopy, for instance within a cell, without the need of extra fluorescent tags.
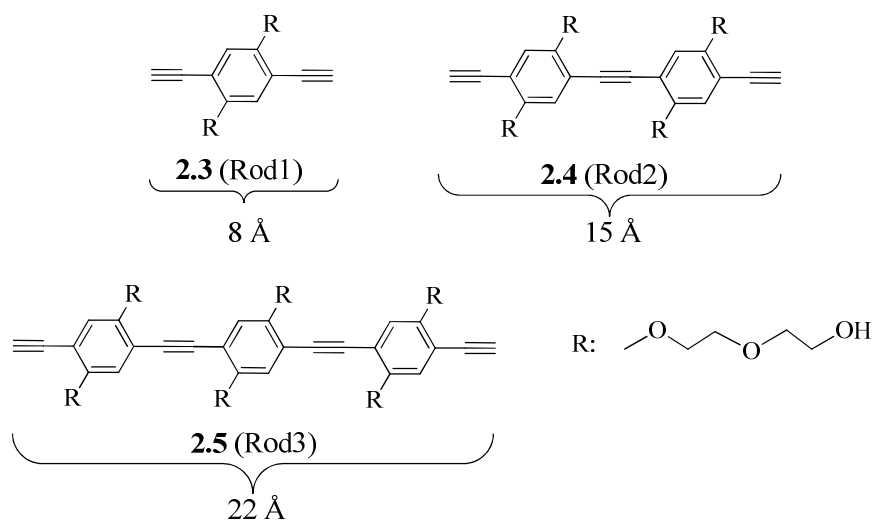
Scheme 2.3 Structure of phenylene-ethynylene Rods 1-3.

Since the fully extended conformation of **VI.1.7** (Figure **2.3**) was found to be only slightly shorter than the distance between two contiguous binding sites within the receptor, just adding the short Rod1 should result in a construct able to bridge two binding sites on the DC-SIGN tetramer. The synthesis of two series of compounds, characterized by three different lengths of the Rod (**2.35-2.37** and **2.43-2.45**, Table **2.2**), would allow to empirically assess which is the best ligand dimension to span the required distance for chelation. In order to investigate the effective role of valency in increasing compounds activity through the statistical rebinding effect, divalent compounds were also produced (**2.38-2.40** and **2.46-2.48**, Table **2.2**), by combining two monomeric ligands based on **1.7** or **1.9** to the Rods. To maintain the overall length of the molecules, **1.7** and **1.9** were first derivatized with an appropriate linker that matched the length of the dendrimeric core (Scheme **2.4**). Two other divalent molecules (**2.41** and **2.49**, Table **2.2**) were produced by directly linking **1.7** and **1.9** to the longest rod, Rod3.
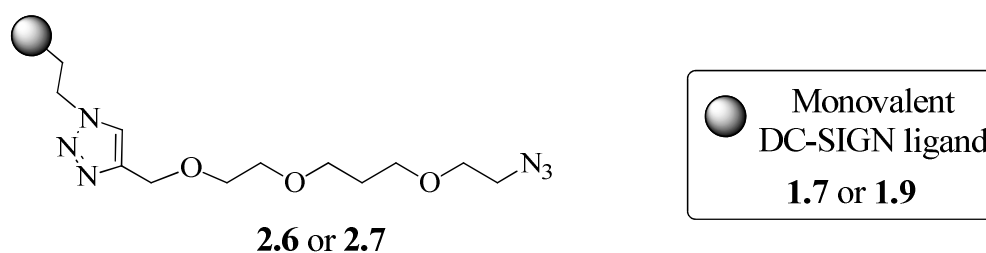
Scheme 2.4 Structure of the elongated monovalent derivatives of **1.7** and **1.9**.

All synthesised compounds are listed in Table **2.2**. They are characterized by a progressive number, together with a conventional lab name made by *PM* (which stands for Polyman) followed by a number.
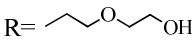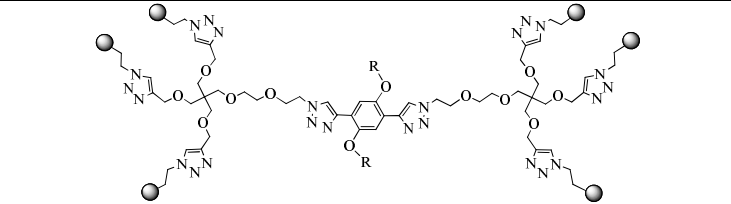
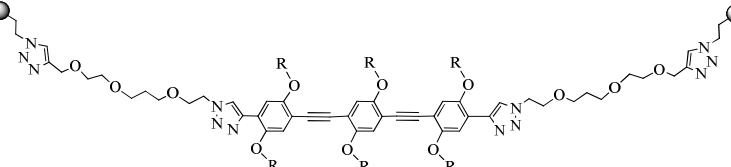| Structure	🔵 Ligand 1.7	🔴 Ligand 1.9
R= (structure shown)		
(tetravalent structure, benzene core)	2.35 *PM30*	2.43 *PM25*
(tetravalent structure, alkyne-bridged bis-benzene)	2.36 *PM32*	2.44 *PM33*
(tetravalent structure, bis-alkyne tris-benzene)	2.37 *PM31*	2.45 *PM26*
(divalent structure, benzene core)	2.38 *PM34*	2.46 *PM37*
(divalent structure, alkyne-bridged bis-benzene)	2.39 *PM35*	2.47 *PM38*
(divalent structure, bis-alkyne tris-benzene)	2.40 *PM36*	2.48 *PM39*
(divalent structure, short linkers, tris-benzene)	2.41 *PM41*	2.49 *PM40*
(hexavalent structure)	2.42 *PM09*	2.50 *PM19*

Table 2.2 General structure of synthesised compounds, together with identification numbers and conventional names. Grey spheres represent monovalent ligands **1.7** or **1.9**.

2.4 Synthesis

2.4.1 Synthesis of monovalent disaccharides 1.7 and 1.9

The synthesis of compounds **1.7** and **1.9** had already been accomplished by N. Varga during its PhD thesis (Scheme **2.5**).[17] Both compounds resulted from glycosylation of a cyclohexane derivative conveniently substituted (**2.9** or **2.10**) with a mannose donor activated as trichloroacetimidate at the anomeric position (**2.8**), yielding **2.11** and **2.12**. The *para*-nitrophenyl (PNP) ester in **2.12** was replaced with a benzylamine to achieve the desired functionalization to give **1.9**. Final products **1.7** and **1.9** were obtained after removal of benzoyl protecting groups (Scheme **2.5**).
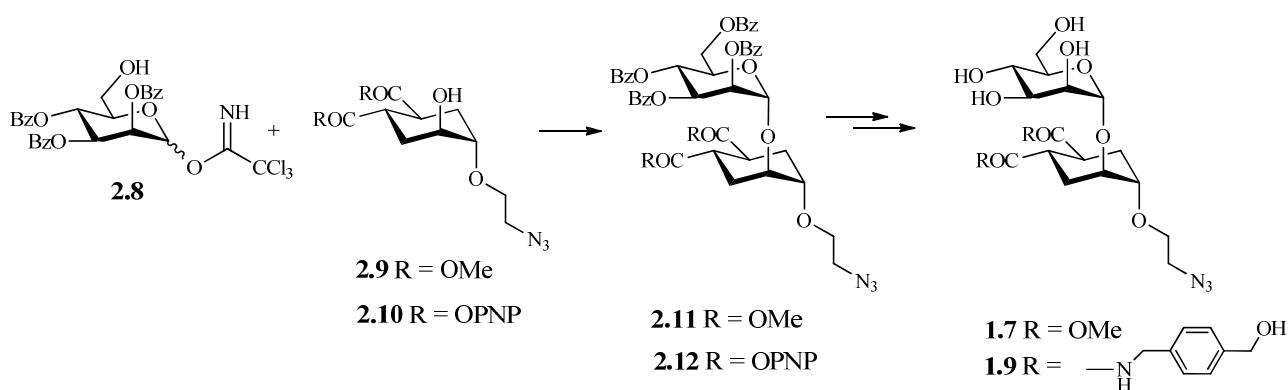
Scheme 2.5 A glycosylation reaction connects a trichloroacetimidate mannose derivative **2.8** and a cyclohexane conveniently substituted **2.9** or **2.10,** yielding **2.11** or **2.12** precursors, respectively, of disaccharides **1.7** and **1.9**.

Compounds were obtained with an overall yield of 64 % for **1.7** and 22 % for **1.9**, calculated based on **2.9** and **2.10**. Respectively, 2 g and 1 g of the two final products were obtained.

During my PhD thesis, I synthesised one batch of 100 mg of **1.9** (with 35 % yield, calculated based on **2.10**).

2.4.2 Synthesis of the Rods

The synthesis of the phenylene-ethynylene units made extensive use of the Pd-Cu catalysed reaction known as Sonogashira coupling. [18]

2.4.2.1 Sonogashira couplings

The catalytic cycle of Pd–Cu catalyzed cross-couplings of terminal acetylenes with sp^2-carbon halides is depicted in Scheme **2.6**. In this reaction, the active species Pd(0) undergoes first an oxidative addition with the aryl halide ArX. The resulting Pd(II) complex undergoes a ligand exchange reaction with the Cu acetylide formed *in situ*, to give the aryl-acetylide Pd species. A final reductive elimination leads to the formation of the new C-C bond.

As Pd(0) catalyst source ($\approx$ 0.04 eq.) we directly used $Pd^0(PPh_3)_4$ or, more conveniently because its higher air-stability, we reduced $Pd^{II}(PPh_3)_2Cl_2$ *in situ* with PPh_3 or NR_3. The amine, NEt_3 (TEA) or N,N'-diisopropylethylamine (DIPEA), was used as reducing agent and also as a base to deprotonate the terminal alkyne. Toluene or THF were used as solvents, conducting the reactions, respectively, at 50 °C or at room temperature. CuI ($\approx$ 0.04 eq.) was the source of Cu(I).
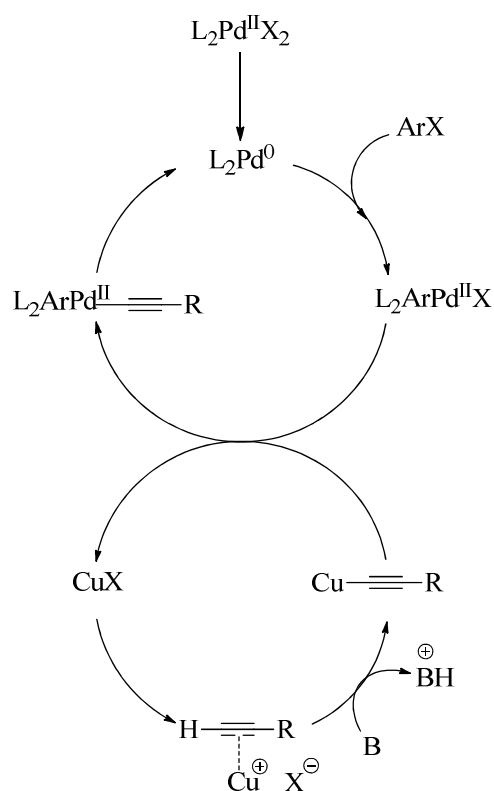
Scheme 2.6 Sonogashira coupling catalytic cycle.

Remarkably, Copper in the presence of an oxidant species catalyzes also the acetylene homocoupling, known as Glaser reaction.[19] A possible mechanism pathway is shown in Scheme **2.7**, where the Copper-acetylide dimerizes through a radical mechanism.

Even if Sonogashira reactions were performed in the complete absence of oxygen, the oxidant environment was unavoidably created by the I^-/I_2 equilibrium generated by activation of the aryl iodide (ArX, X = I) and by the presence of CuI.
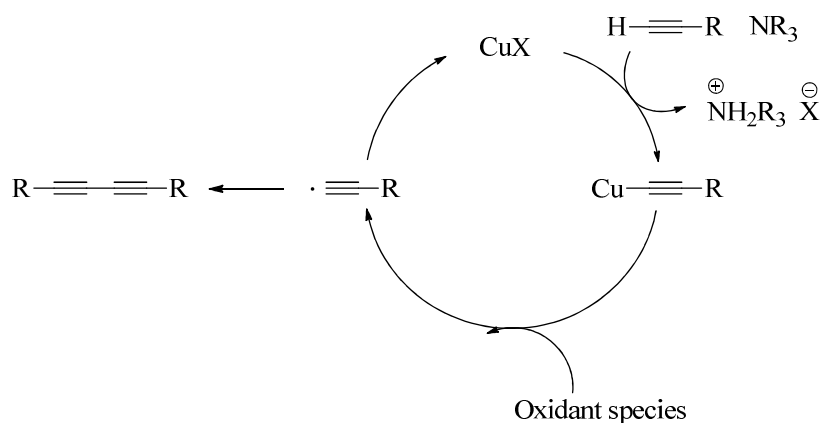
Scheme 2.7 Glaser homocoupling catalytic cycle.

For this reason, one should know that terminal alkynes can't be isolated as final products of Sonogashira couplings, since they would subsequently react with one another, at least in a certain amount. Moreover, given that the Glaser homocoupling competes with the Sonogashira one also for the terminal acetylene used as reagent, this last should be added in slight excess with respect to the halide.

2.4.2.2 Synthesis of the Rods

The synthesis of the three Rods started from the commercially available 1,4-dimethoxybenzene **2.13**, which was first transformed in the diiodide **2.15** by refluxing in methanol with iodine, in the presence of the periodic acid. The methyl ethers of **2.15** were first cleaved by treatment with BBr$_3$ at low temperature, yielding the bis-phenol **2.15**, and then replaced with short polyethyleneglycol chains (n = 2) by reacting with 2-(2-Chloroethoxy)ethanol in the presence of K$_2$CO$_3$ as the base, obtaining the diiodide **2.16** (Scheme **2.8**).
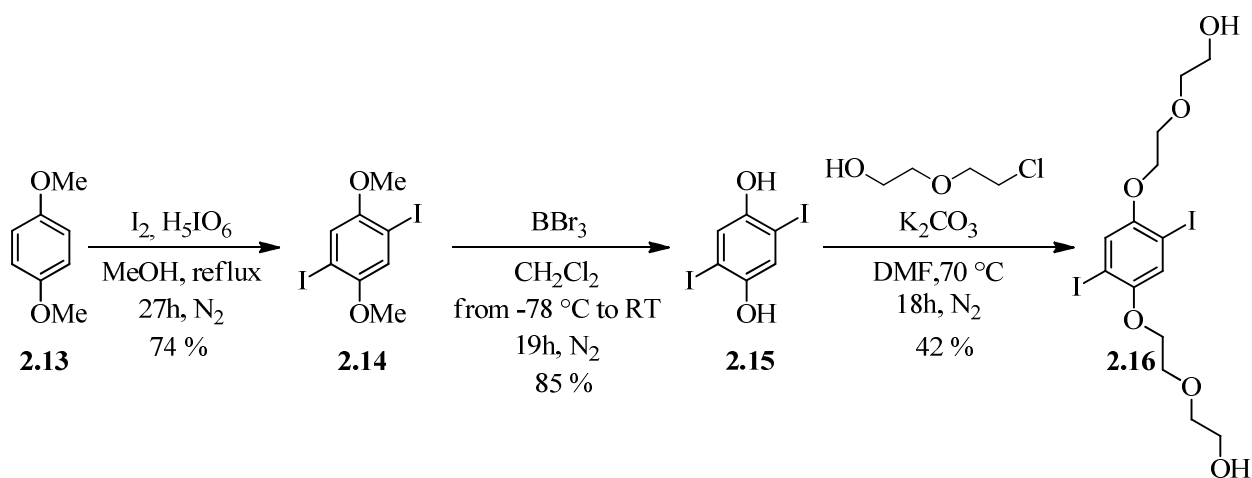
Scheme 2.8 Synthesis of the bis-PEGylated diiodide benzene **2.16**.

Compound **2.16** underwent a Sonogashira coupling with tri-isopropylsilylacetylene **2.17**, which was added in the proper amount (1.5 eq.) to allow the formation of both the mono-substituted product **2.18** and the di-substituted one **TIPS-2.3 (TIPS-Rod1)** (Scheme **2.9**). Both products were obtained in similar yields (≈ 40 %) and 20 % of the starting material was recovered; compounds were easily separated through flash chromatography on silica. Remarkably, the synthesis of only mono-substituted **2.18** was disfavoured; indeed, by adding 0.5 eq. of tri-isopropylsilylacetylene, both compounds **2.18** and **TIPS-2.23** were formed, thus increasing the amount of non-reacted **2.16** and decreasing the overall yield.
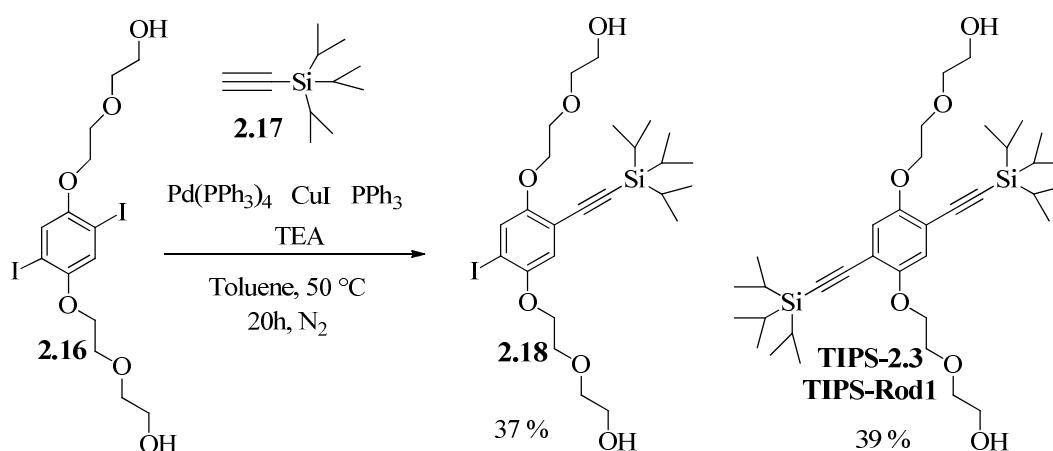
Scheme 2.9 Synthesis of mono-substituted **2.18** and di-substituted **TIPS-2.3** compounds.

Deprotection of compound **TIPS-2.3** with tetra-*n*-butylammonium fluoride (TBAF) gave **2.3** (**Rod1**) in high yields (Scheme **2.10**).
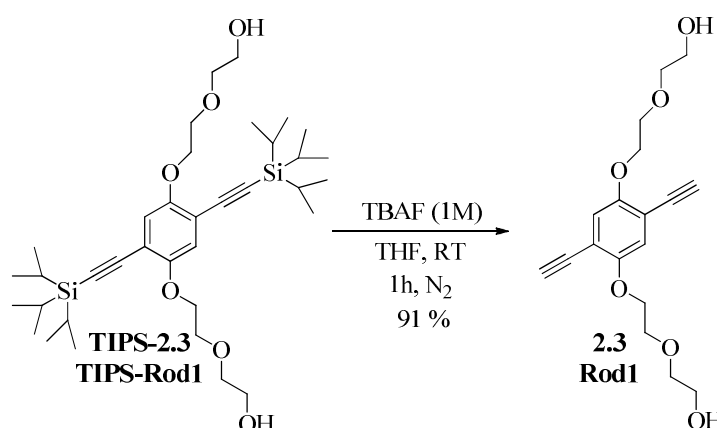
Scheme 2.10 Synthesis of compound **2.3** (i.e. **Rod1**).

We thought that another Sonogashira coupling reaction between compound **2.18** and **2.3** would provide the formation of both mono-protected **Rod2** (**2.19**, Scheme **2.11**) and **TIPS-Rod3 (TIPS-**

2.5 Scheme **2.11**), if using an excess of **2.3** (3:1). On the contrary, compound **2.19**, which should derive from a single coupling between **2.18** and **2.3**, couldn't be formed, due to several side reactions -mainly oligomerization ones- in which it was involved. The main one, a Glaser reaction (see Paragraph 2.4.1), gave the dimeric compound **2.20** (Scheme **2.11**).
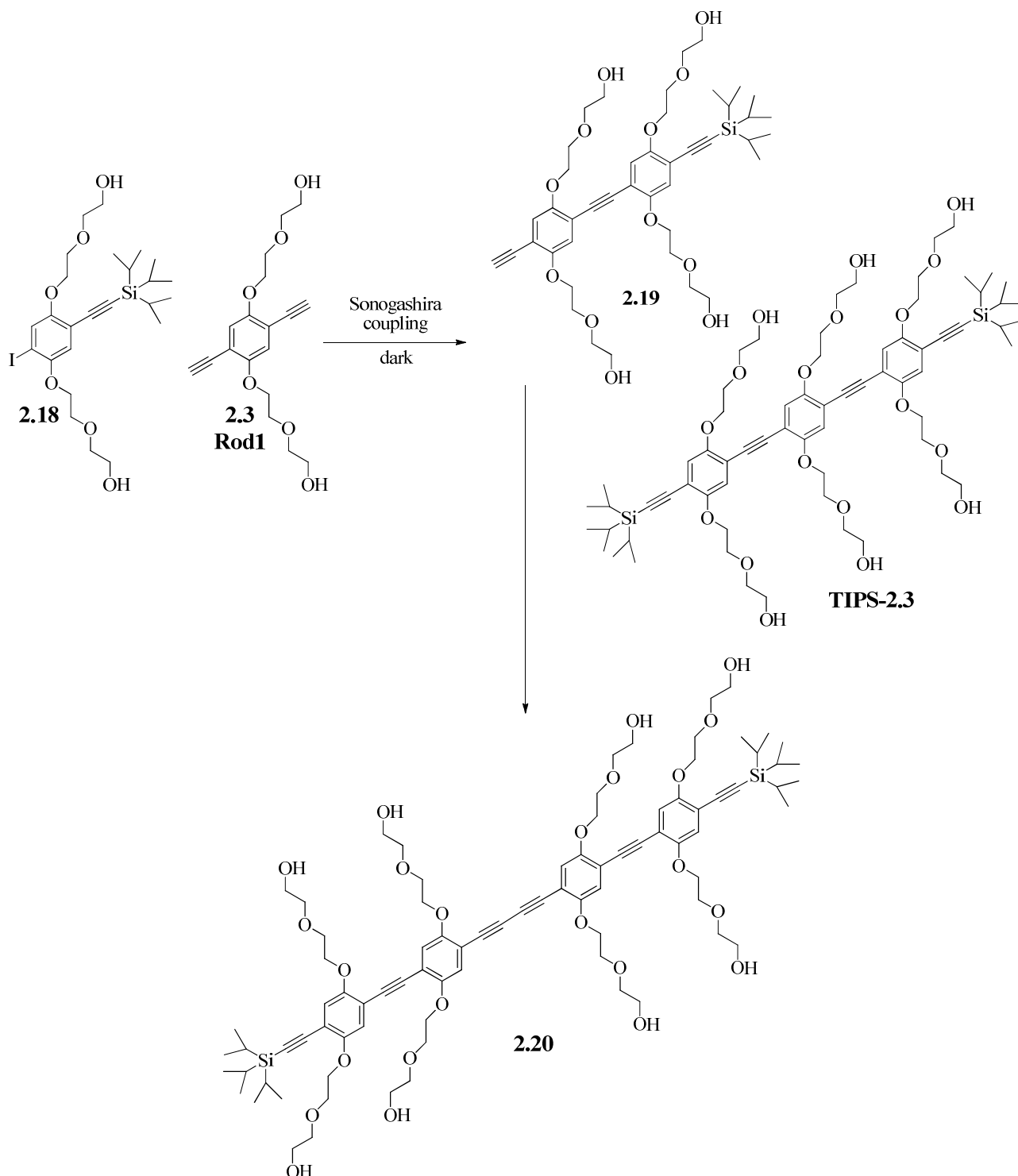
Scheme 2.11 A Sonogashira coupling between **2.18** and **2.3** (**Rod1**) afforded compound **TIPS-2.3** but not compound **2.19**, which underwent oligomerization reactions leading, for instance, to the dimer **2.20**.

In order to obtain **2.19**, solvent and reaction temperatures were varied. Also a Copper free Sonogashira reaction was tried, using [1,1′-Bis(diphenylphosphino)ferrocene]dichloropalladium as catalyst, but the desired product was never obtained. Apparently, the homocoupling reaction can be catalysed also by the Palladium species.[20] Tested reaction conditions are reported in Table **2.3**.

Table 2.3 Reaction condition tested to avoid Glaser homocoupling. Dppf = 1,1'-Bis(diphenylphosphino)ferrocene. [a] *vs* ArX, Reactions were performed in NEt$_3$ 10 eq. *vs* alkyne), at a concentration of 0.1-0.3 mM in the solvent.

Pd source	Cu source	Phosphine	Solvent	T (°C)	Time (h)
Pd(PPh$_3$)$_4$ 0.1 eq.[a]	CuI 0.1 eq.[a]	PPh$_3$ 0.2 eq.[a]	Toluene	50	24
Pd(PPh$_3$)$_4$ 0.1 eq.[a]	CuI 0.1 eq.[a]	PPh$_3$ 0.2 eq.[a]	DMF	20	44
Pd(dppf)$_2$Cl$_2$ 0.05 eq.[a]	Copper free	Dppf 0.1 eq.[a]	Toluene	50, then 20	3

We therefore realised that **Rod2** could be stably obtained only if protected on each terminal side. This double protection can be achieved through a Sonogashira reaction between the already known compound **2.18** and a monoprotected di-alkynyl substrate **2.21** (Scheme **2.12**).
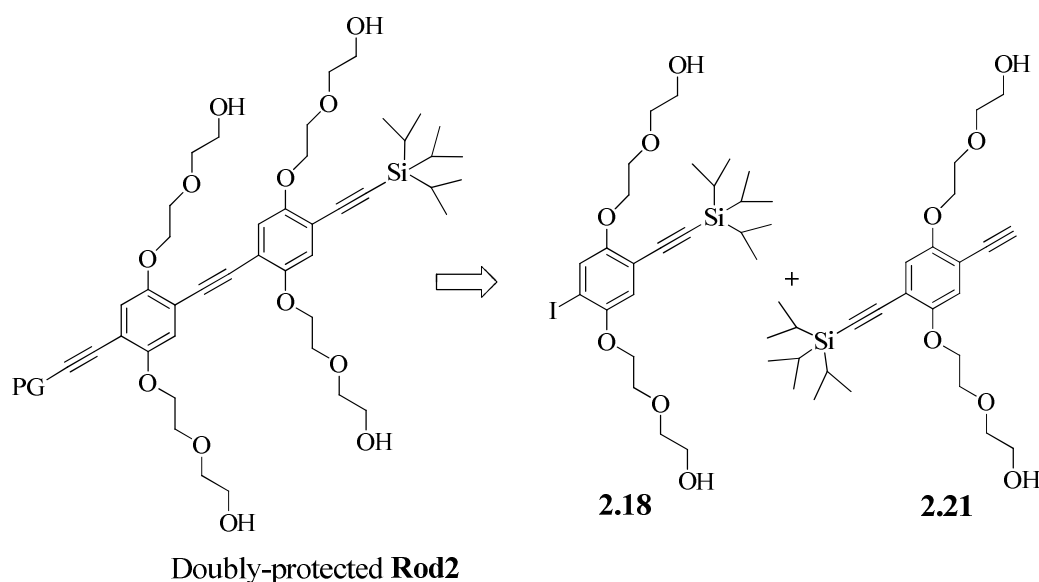
Scheme 2.12 Retrosynthetic route to di-protected **Rod2**.

Initial efforts to obtain **2.21** by selective monodeprotection of **TIPS-2.3** (Scheme **2.13**) with TBAF were unsuccessful, thus we envisaged to obtain **2.21** from the differentially protected analogue **2.22** (Scheme **2.13**).
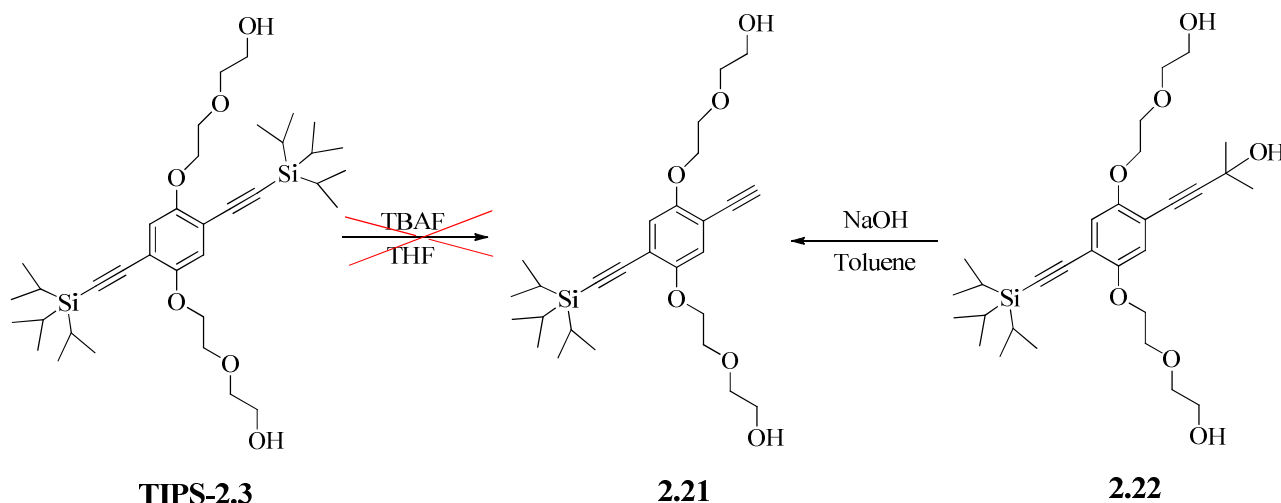
Scheme 2.13 Compound **2.22** is characterized by two orthogonal alkyne protecting groups.

As orthogonal alkyne protecting groups, TIPS and 2-propanol were used. Compound **2.21** was synthesised by a slight modification of a known procedure (Scheme 2.14).[21] Coupling of **2.18** with 2-Methyl-3-butyn-2-ol (MEBYNOL, **2.23**) under Sonogashira conditions afforded **2.22** in good yields. Removal of 2-propanol was achieved with NaOH under heterogeneous conditions. This reaction was rather critical because it didn't reach full conversion even in 18 h, but longer reaction times led to desilylation and decomposition of **2.21** to **2.3** (**Rod1**). Under optimized conditions, the reaction was stopped after 5 hours, once the formation of the side-product **2.3** (**Rod1**) was observed by TLC (Toluene:acetone 6:4). The reaction mixture was diluted with MeOH in order to protonate the acetylide intermediate species; the use of a drop of CH_3COOH for this purpose, led on the contrary to product degradation. **2.21** was isolated in 35% yields and 36% of **2.22** was recovered by silica chromatography (55% yield b.r.s.m.) (Scheme **2.14**).
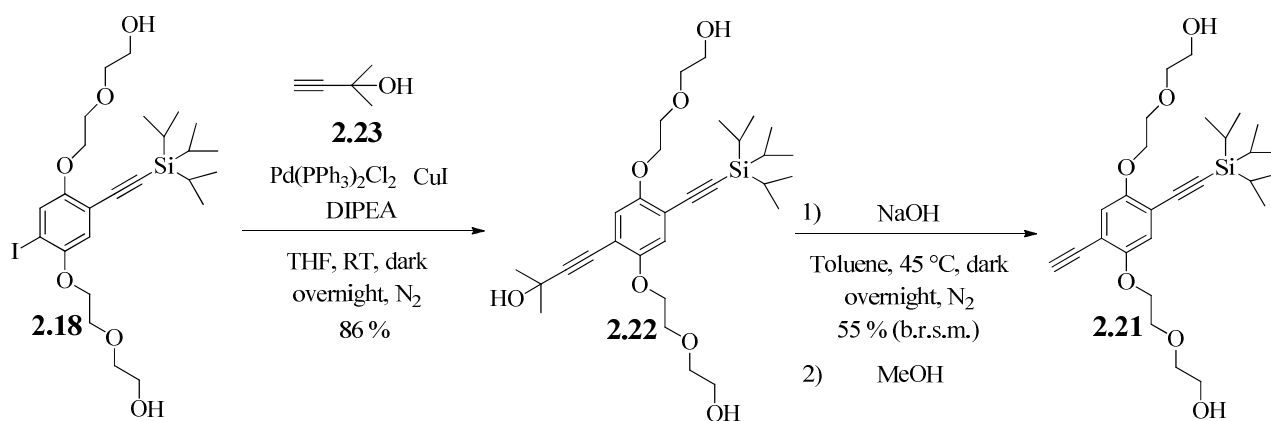
Scheme 2.14 Synthesis of the monoprotected di-alkynil benzene **2.21**.

A Sonogashira coupling reaction between compounds **2.18** and **2.21** conducted in the dark provided **TIPS-2.4** (**TIPS-Rod2**) in excellent yields (Scheme **2.15**).
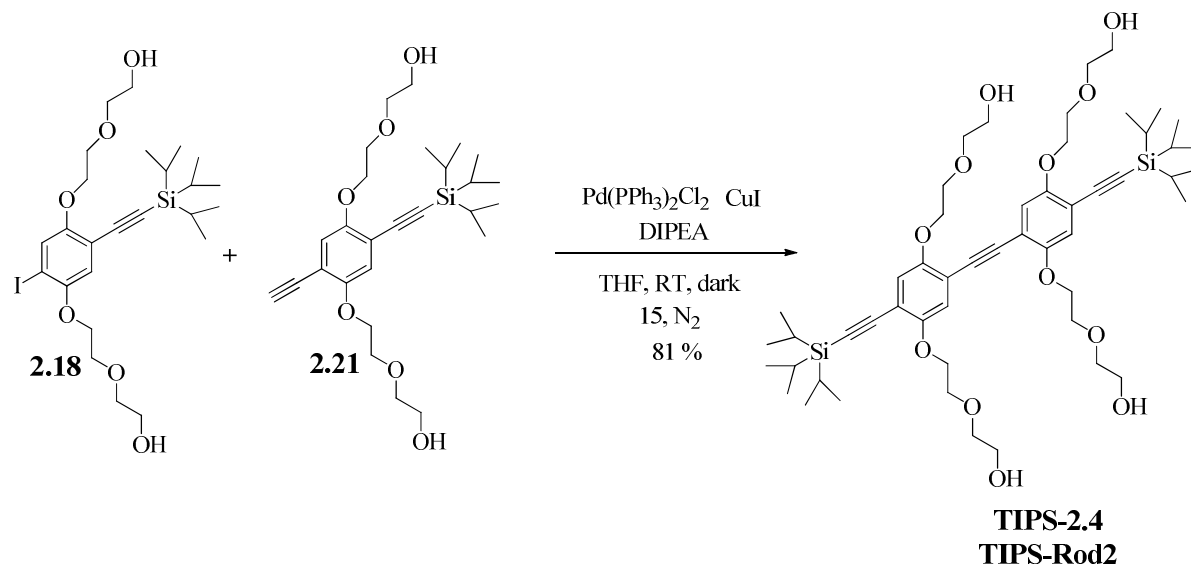
Scheme 2.15 Synthesis of **TIPS-2.4** (**TIPS-Rod2**).

Finally, compound **TIPS-2.5** (**TIPS-Rod3**) was synthesised in moderate yields with a Sonogashira coupling between **2.18** (2.2 eq.) and **2.3** (**Rod1**, 1 eq.), conducted again under dark (Scheme **2.16**). In the previously not optimized reaction, reported in Ref.[16], a ratio **2.25**:**2.26** = 1:3 had been used.
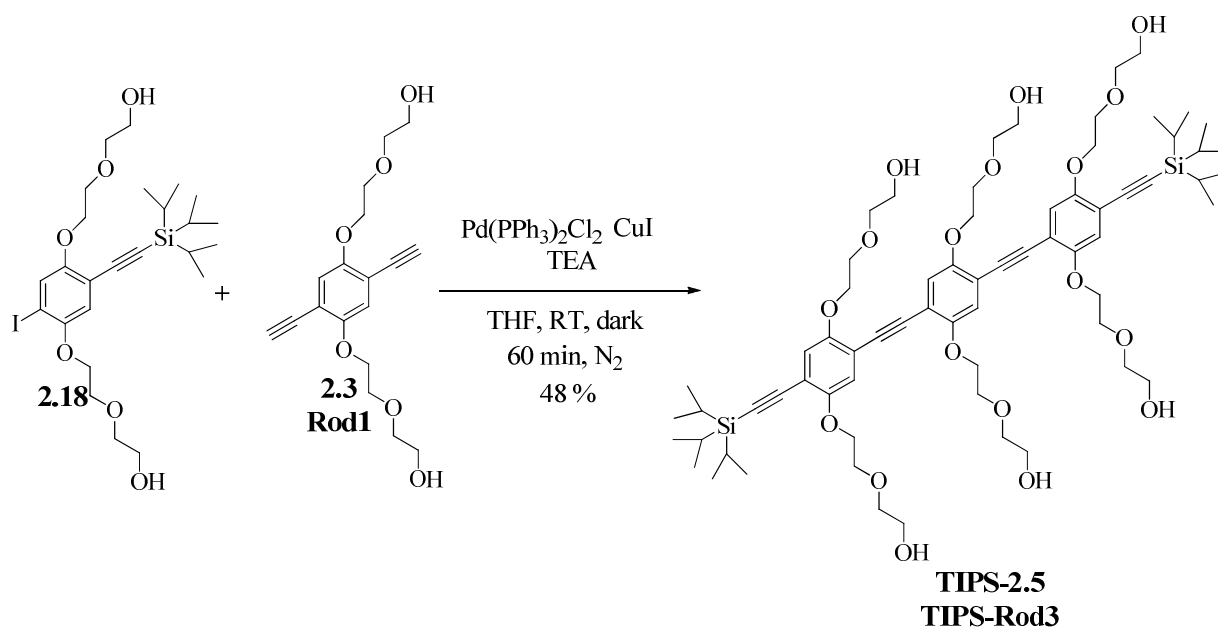
Scheme 2.16 Synthesis of **TIPS-2.5** (**TIPS-Rod3**).

2.4.3 Copper(I)-catalyzed Azide-Alkyne Cycloaddition

Copper(I)-catalyzed Azide-Alkyne Cycloaddition (CuAAC)[22] is the catalysed variation of a *Huisgen cycloaddition* between a terminal triple bond and an azide. It is referred to also as *click reaction*, and it regioselectively yields a 1,4-substituted triazole (Scheme **2.17**).
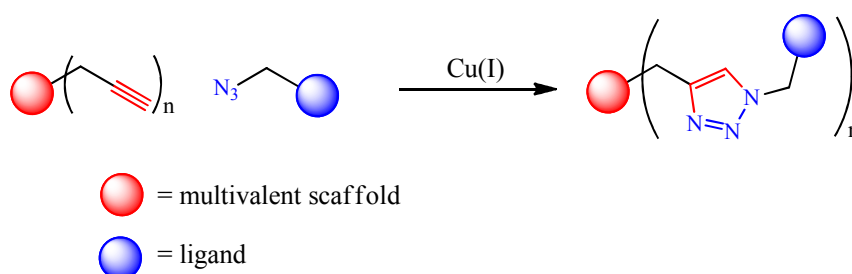
Scheme 2.17 General scheme of a Copper(I) catalyzed 1,3-dipolar cycloaddition (click reaction) between a terminal alkyne (red) and an alkyl azide (blue). Multivalent scaffolds can be decorated with multiple ligands.

A proposed mechanism of its catalytic cycle is depicted in Scheme **2.18**.[23] In the first step, the alkyne reacts with the cationic Cu(I) compound to give a Copper acetylide species, which then coordinates the nitrogen of the azide. The azido group and the Copper acetylide give a cycloaddition reaction that leads to an intermediate (I), which undergoes a rearrangement to give the triazole ring in a regioselective fashion. Finally, protonolysis of the Cu-C bond completes formation of the triazole.
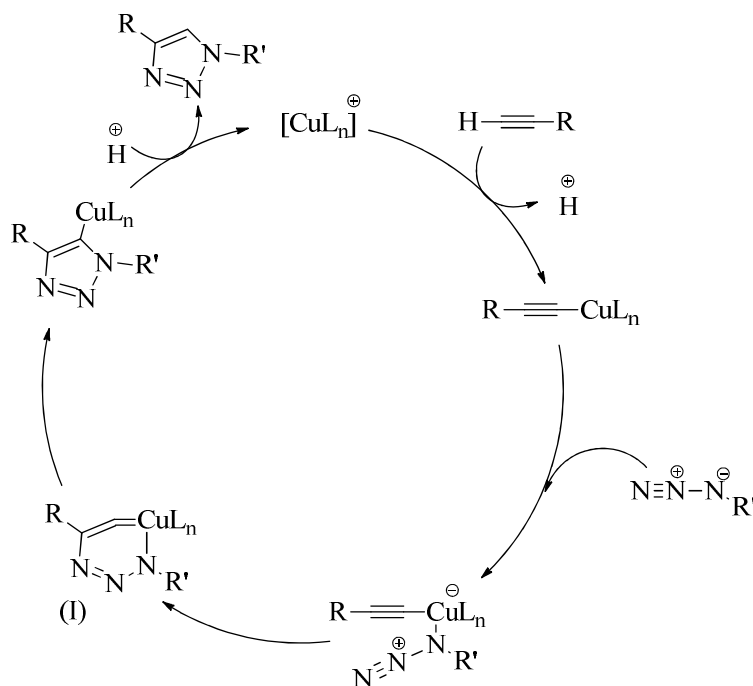
Scheme 2.18 CuAAC catalytic cycle.

In the optimized procedure followed by N. Varga[17] and developed in the group of Dr. J. Rojo (Seville, SP), Copper(II) Sulphate and the reducing agent Sodium Ascorbate were used as a combined source of Cu(I). The possible re-oxidation of Copper(I) was prevented by stabilizing it with Tris[(1-benzyl-1H-1,2,3-triazol-4-yl)methyl]amine (TBTA) and by using an excess of NaAscorbate (4 times with respect to Cu). Moreover, reactions were conducted in the dark, under nitrogen atmosphere and using degased and/or freshly distilled solvents.

A 1:1 mixture THF/H$_2$O was found suitable to dissolve all the reagents. The reagents were added to the reaction vessel in the following order: alkyne, TBTA, CuSO$_4$·5H$_2$O, Sodium Ascorbate and finally the azide monovalent ligand (1.1 eq. per each triple bond).

The final concentration of alkynes was 3-15 mM, depending on the solubility of the components and of the products in the solvent. When a concentration $\geq$ 10 mM in 1:1 THF:H$_2$O could be obtained, the reaction was stirred at room temperature for 12 -24 hours. For less soluble mixtures, the reaction was performed at lower concentrations (typically 3 mM) under microwave assisted conditions for 1-2 h at 60 °C. Yield varied from acceptable (50 %) to high (90 %).

The reaction was monitored by TLC and/or MALDI mass spectrometry (DHB or sinapinic acid matrix) until completion. In general, the formation of divalent and trivalent compounds could be monitored by TLC, while most complex hexavalent compounds were best analysed by MALDI mass. When intermediates were observed but the azide monovalent ligand was totally consumed, the latter was added together with additional 0.4 eq. of Sodium Ascorbate.

The crude was purified by size exclusion chromatography on a Sephadex LH20 column and by reverse phase chromatography, when required. The metal scavenger Quadrasil™-MP was used to remove copper salts either from the reaction mixtures before purification, or from a solution of the isolated final compound. This was required because copper, in a certain amount, is toxic for cells.[24] Avoiding cytotoxicity is crucial both for biological cellular tests and, of course, for *in vivo* applications.

2.4.4 Synthesis of the polyalkyne scaffolds

The hexavalent scaffold **2.24** was available in the laboratory. It was prepared according to Ref.[12] starting from bis(pentaerythritol) **2.23**, which underwent a Williamson etherification reaction with propargyl bromide using NaH as a base (Scheme **2.19**).
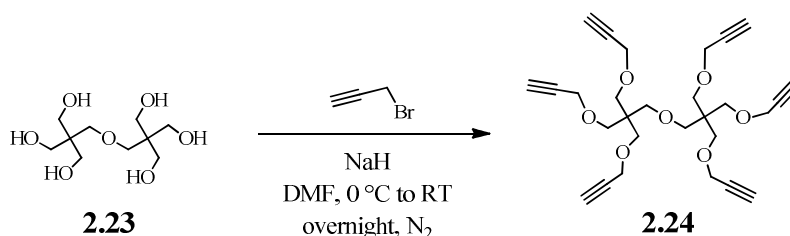
Scheme 2.19 Synthesis of the hexavalent scaffold **2.32**.

The trivalent scaffold **2.27** was synthesised as shown in Scheme **2.20**, starting from pentaerythritol **2.25**, which underwent a Williamson reaction with propargyl bromide to give compound **2.26**. **2.26.1** was formed as a co-product (20%) and was separated by flash chromatography. A second reaction with bis-(2-Chloroethyl) ether gave **2.27** (Scheme **2.20**).
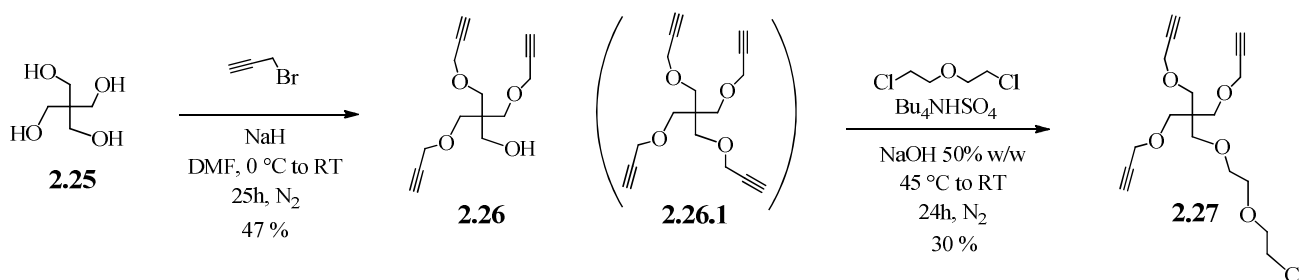
Scheme 2.20 Synthesis of the trivalent scaffold **2.31**.

2.4.5 Synthesis of the trivalent dendrons

The trivalent dendrons **2.1** and **2.2** (Scheme **2.2**) were produced by performing click reactions (see Paragraph 2.4) between the monovalent ligands **1.7** or **1.9** and the trivalent alkyne **2.27**. The

chloride-substituted dendrons **2.28** and **2.29** were converted in the corresponding azide-derivatives **2.1** and **2.2** through a chloride-azide reaction exchange catalysed by I⁻ (Scheme **2.21**).
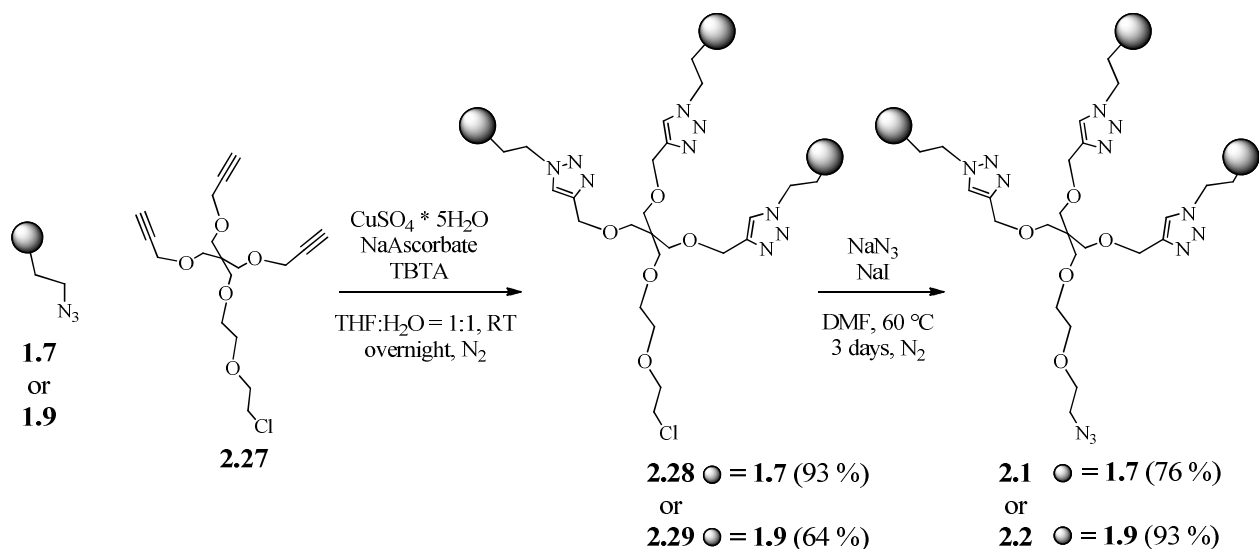
Scheme 2.21 General procedure to synthesize trivalent dendrimers **2.1** and **2.2**.

Remarkably, the purity of scaffold **2.27** was always assessed through TLC analysis prior each reaction, since it was demonstrated that it can degrade loosing propargyl functionalities to give alcohol **2.27.1** (Scheme **2.22**). The reaction between degraded scaffold and monovalent ligands would result in intermediate species that can't be separated from the desired final compound.
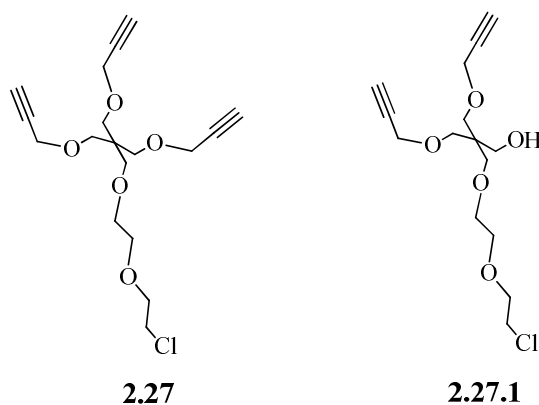
Scheme 2.22 2.27.1 results from the degradation of **2.27**.

2.4.6 Synthesis of elongated monovalent ligands

Linker **2.32** (Scheme **2.23**) was used to functionalize monovalent compounds **1.7** and **1.9**. It was obtained from the commercially available 3,7-Dioxa-1,9-nonanediol **2.30** that reacted with propargyl bromide in presence of NaH as the base, to give compound **2.31** (also the bis-

propargylated co-product **2.31.1** was obtained in 13 % yield and separated through flash chromatography on silica). The free hydroxyl group was then transformed into a tosylate to give compound **2.32**. This compound underwent a "click" reaction with **1.7** or **1.9**, obtaining respectively compounds **2.33** and **2.34**. A tosylate-azide exchange catalyzed by I⁻ gave **2.6** and **2.7** (Scheme **2.23**). Remarkably, final compounds were obtained not completely pure, still containing 1-3 % w/w of the tosilate salt; nevertheless, they were used without further purifications in the subsequent click reactions, where the salt didn't interfere.
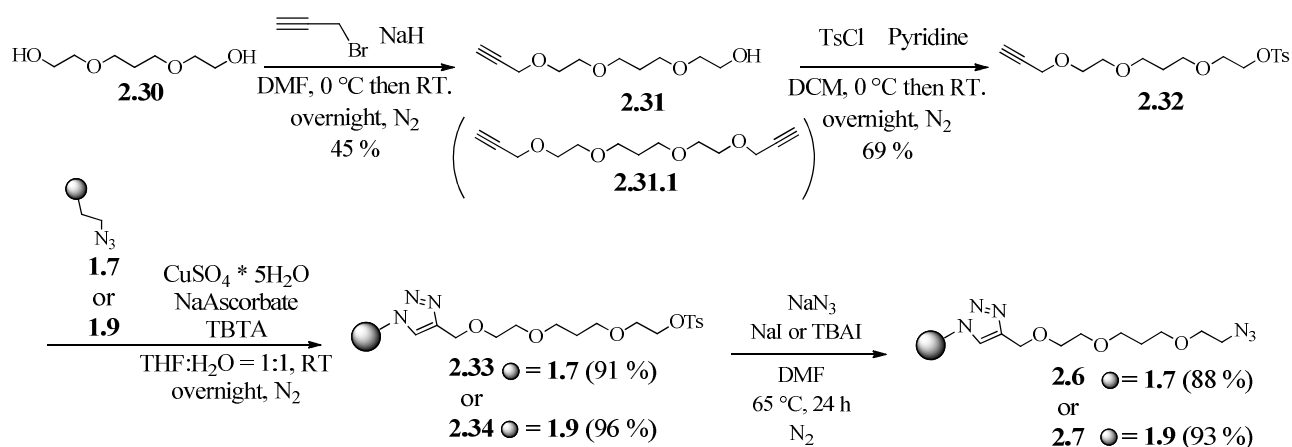
Scheme 2.23 Synthesis of elongated compounds **2.6** and **2.7**.

2.4.7 Synthesis of final molecules

The final molecules were synthesised coupling trivalent dendrons (**2.1**, **2.2**) or elongated monovalent ligands (**2.6**, **2.7**) or monovalent ligands (**1.7**, **1.9**), all bearing azide groups, on the terminal alkynes of the central scaffolds **2.3**, **2.4**, **2.5**, **2.28**. The general principle and reaction conditions of the CuAAC were explained in Paragraph 2.4.4. As previously reported, the cycloaddition was performed using copper(II) sulfate, *in situ* reduced by sodium ascorbate and stabilized by tris[(1-benzyl-1H-1,2,3-triazol-4-yl)methyl]amine (TBTA); azide-bearing compounds were used in slight excess (1.1 eq. per each triple bond).

Final obtained molecules are listed in Table **2.4**, together with their constituent moieties.

Structure R=	Fragment	🔵 Ligand 1.7	🔴 Ligand 1.9
	 2.1 or **2.2** **2.3**	**2.35** *PM30*	**2.43** *PM25*
	 2.1 or **2.2** **2.4**	**2.36** *PM32*	**2.44** *PM33*
	 2.1 or **2.2** **2.5**	**2.37** *PM31*	**2.45** *PM26*
	 2.6 or **2.7** **2.3**	**2.38** *PM34*	**2.46** *PM37*
	 2.6 or **2.7** **2.4**	**2.39** *PM35*	**2.47** *PM38*
	 2.6 or **2.7** **2.5**	**2.40** *PM36*	**2.48** *PM39*
	 1.7 or **1.9** **2.5**	**2.41** *PM41*	**2.49** *PM40*
	 1.7 or **1.9** **2.28**	**2.42** *PM09*	**2.50** *PM19*

Table 2.4 General structure of synthesised compounds, together with identification numbers and conventional names. Grey spheres represent monovalent ligands **1.7** or **1.9**. Derivatives of compound **1.7** are shown in **blue**, derivatives of compound **1.9** are shown in **red**.

All reactions were performed at room temperature, overnight and in the dark, except for derivatives of the trivalent dendrimers **2.2**. Its low solubility in water demanded for 4 final concentrations of the alkynes lower than 10 mM; therefore, reactions were accelerated under microwave irradiation at 60 °C; reaction times decreased to less than 2 h.

Compounds **2.35**, **2.38**, **2.43** and **2.46**, which are based on Rod1 **2.3**, were synthesised by directly performing a CuAAC between **2.3** and the required trivalent dendrimer or elongated monovalent ligand (Scheme **2.24**).
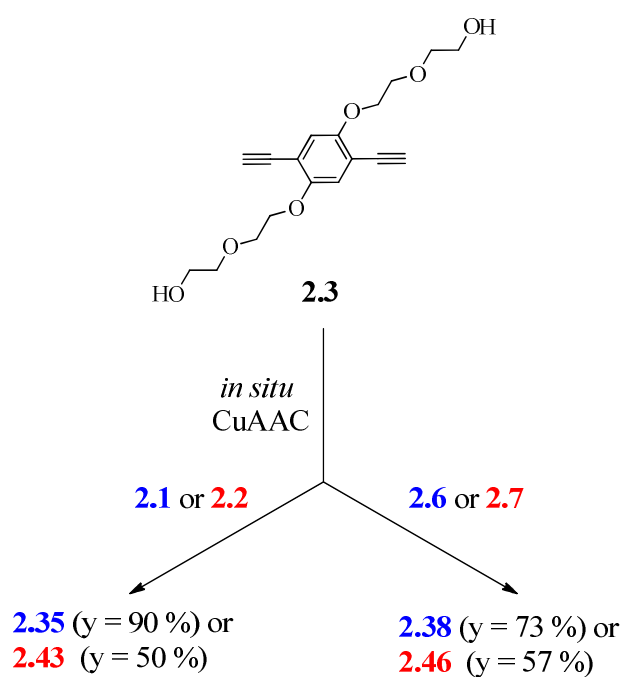
Scheme 2.24 Synthesis of compounds based on **Rod1**/**2.3**.

Rod2 (**2.4**) and Rod3 (**2.5**) were prepared immediately before performing the azide-alkyne cycloaddition by *in situ* desilylation of the corresponding tri-*iso*propyl-alkynylsilane TIPS-**2.4** (Scheme **2.25**) and TIPS-**2.5** (Scheme **2.26**). Coupling with the trivalent dendrons (**2.1**, **2.2**) or the elongated monovalent ligands (**2.6**, **2.7**) or with monovalent ligands **1.7** and **1.9** directly gave the final Rod2- and Rod3-based dendrimers.
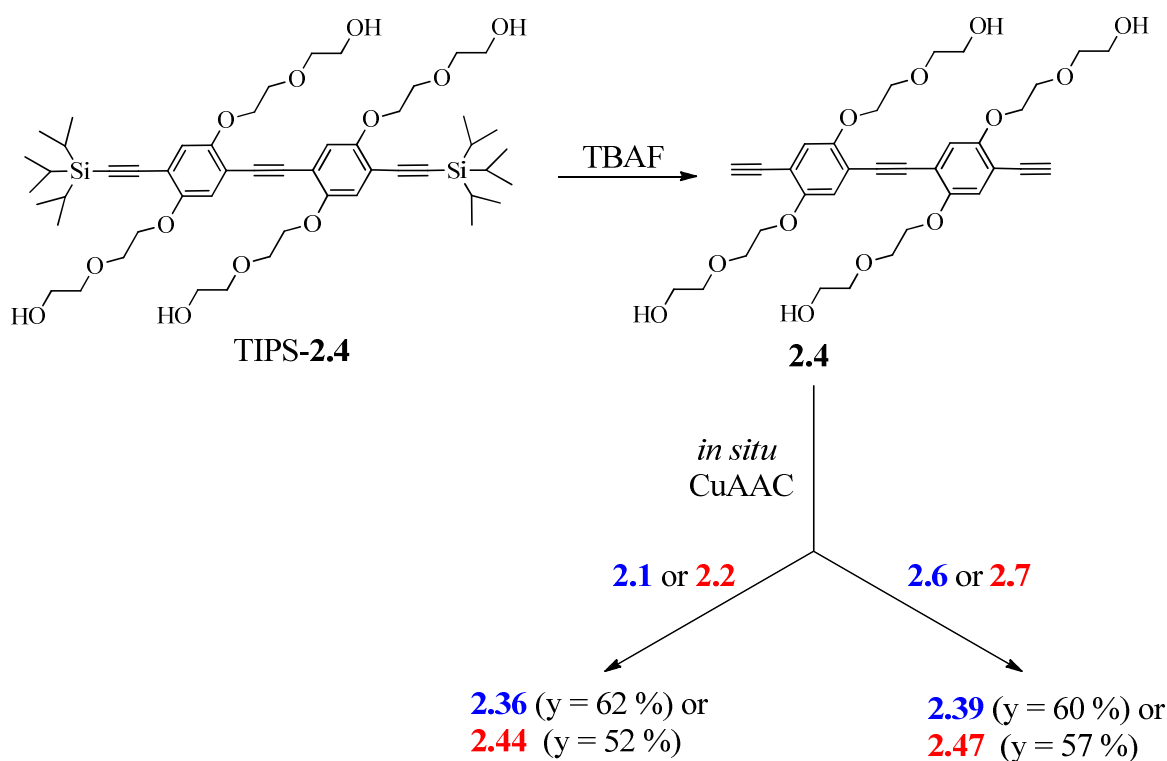
Scheme 2.25 Synthesis of compounds based on **Rod2/2.4**.
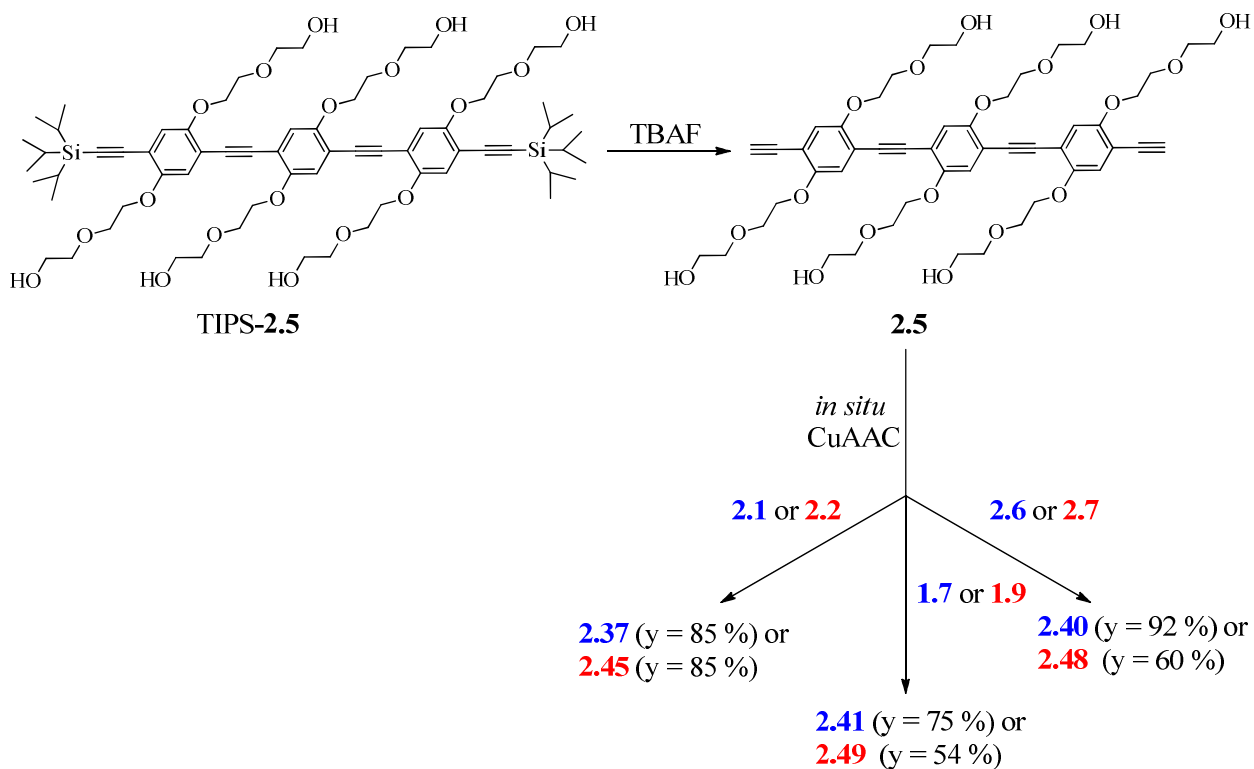
Scheme 2.26 Synthesis of compounds based on **Rod3/2.5**.

Hexavalent dendrimer-based compounds **2.42** and **2.50** were synthesised by coupling monovalent ligands on scaffold **2.24** (Scheme **2.27**). Also the purity of scaffold **2.28** was assessed through TLC

analysis before performing the reaction, thus avoiding the presence of degraded compounds missing propargly units.

Scheme 2.27 General procedure to synthesize hexavalent derivatives **2.42** and **2.50**.
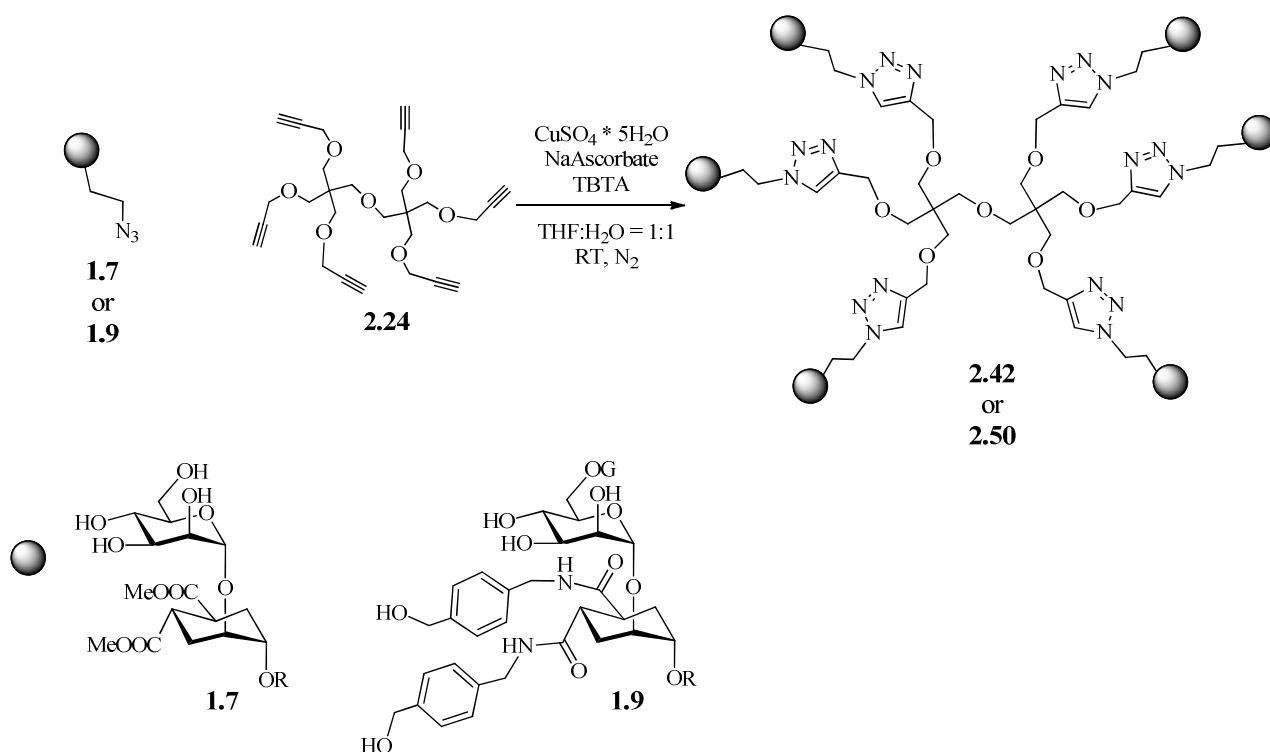
2.5 Computational Analysis

In order to predict the structural behavior of these compounds when interacting with DC-SIGN, the shape and size of the ligands were simulated by molecular dynamics (125-150 ns); analysis were performed by A. Bertaglia, Dr. G. Vettoretti and Dr. L. Belvisi. Compounds belonging to the **1.7**-series was used as model; for sake of simplicity, the PEG chains on the rods were replaced with methyl ethers.

To gauge the average dimension of the glycodendrimers and evaluate if they are potentially able to chelate DC-SIGN. The distance between Man-O3 atoms of two distal sugar residues in a multivalent structure was chosen as representative for its maximum extension in terms of binding capacities.

The simulations showed that, as previously described (see Ref.[12] and Paragraph 2.2), the hexavalent dendrimer **2.42** is structurally not long enough to bridge between two DC-SIGN binding sites. On the contrary, the presence of one rod, even the short one (scaffold **2.3** in compound **2.38**, Table **2.4**), gives rise to structures that in their most extended conformation could comfortably reach across. Indeed, all compounds **2.37**, **2.38**, **2.40** and **2.41** had maximum O3-O3 distance (Max d_{O3-O3}) values

longer than 40 Å. However, the flexibility associated to the long linker of **2.37**, **2.38**, and **2.40** induced sugars to fold over aromatic cores, so that the percentage of structures with an average O_3-O_3 distance ($<d_{O3-O3}>$) higher than 35 Å was < 5 %. Representative folded conformations of compounds **2.40** and **2.37** are shown in Figure **2.7**. A Type I conformation shows a compact structure where sugar residues fold over the aromatic core from the two opposite sides. On the contrary, Type II conformations are obtained when sugar moieties are found on the same side of the central scaffold. For divalent compound **2.40** both conformation types were observed. On the contrary, Type II conformations were preferentially assumed by hexavalent compound **2.37**, probably stabilized by Man-Man interactions (Figure **2.7**).
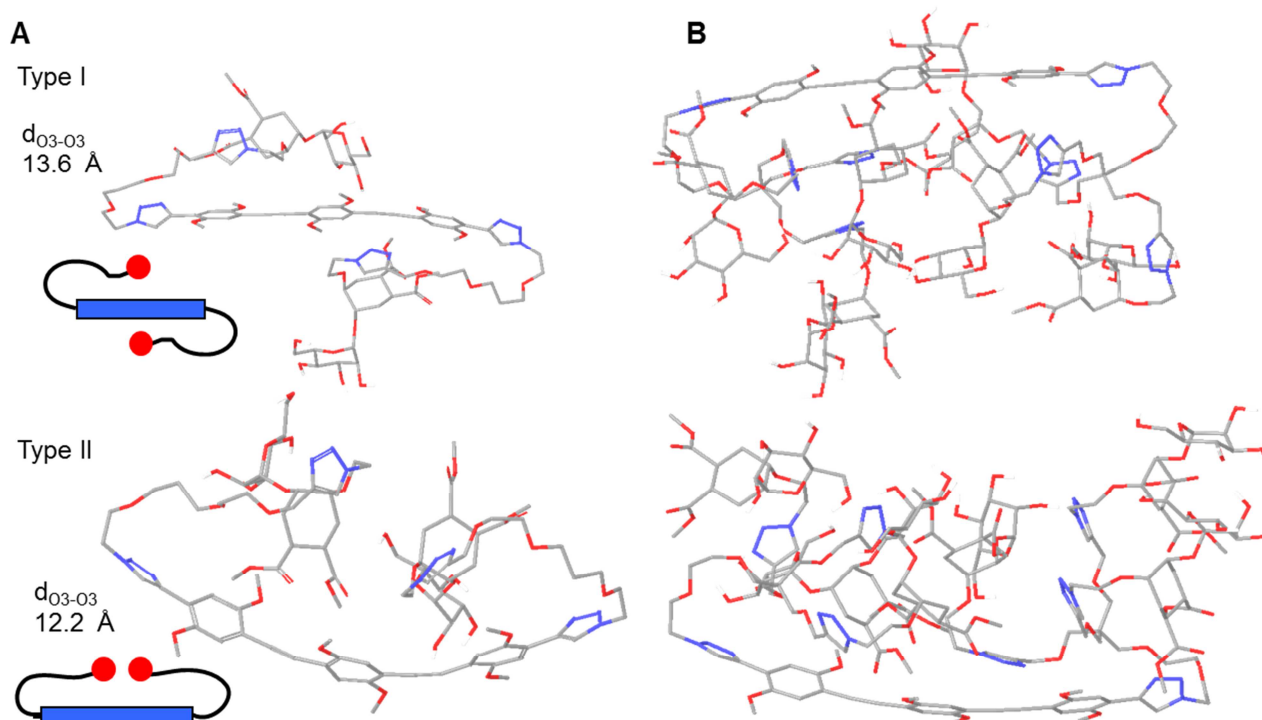
Figure 2.7 A) Structures of the most represented conformations sampled during the dynamic simulations of **2.40**. Two types of folds (Type I and Type II) were observed. B) Representative structures from the simulation of **2.37**: Type II folds are favored.

Remarkably, the most extended average structure was calculated for the dimeric compound **2.41**, having the short linker. This dimer features Max d_{O3-O3} and $< d_{O3-O3} >$ of 43.3 Å and 31.7 Å, respectively. Most importantly, 30 % of the structures sampled during the simulations displayed $d_{O3-O3} > 35$ Å. This result highlighted that, among the structures synthesised, compound **2.41** has an optimal preorganization to act as DC-SIGN chelating agent.

Dynamics simulations of the binding complexes formed by **2.41**, **2.40** and **2.38** and two DC-SIGN CRDs showed that they all are stable over the course of 25 ns. The structures of obtained complexes are reported in Figure **2.8**.
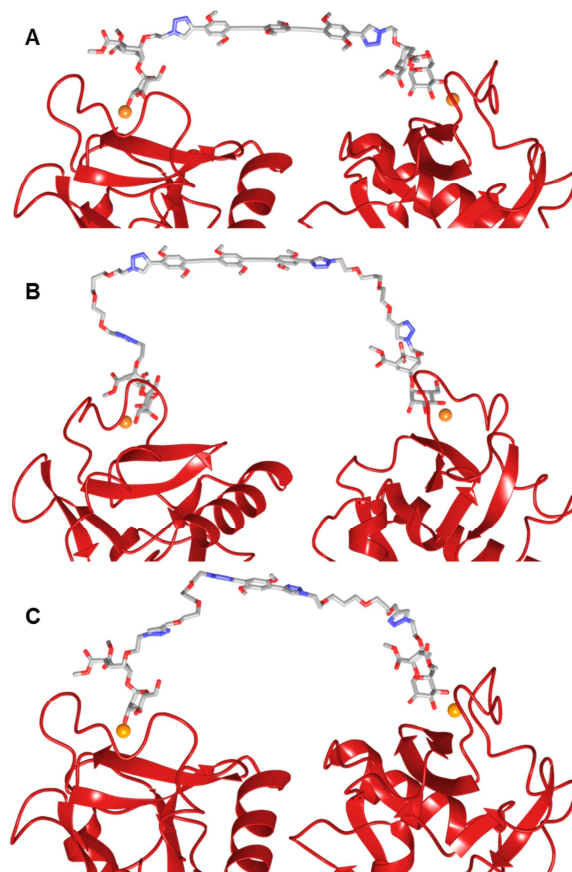
Figure 2.8 Docked complexes of divalent ligands A) **2.41**, B) **2.40** and C) **2.38** on two adjacent DC-SIGN CRDs.

2.6 Biological Characterization

With the aim to assess the biological relevance of synthesised compounds, we performed two types of assays. SPR inhibition assays were used to evaluate binding efficiency of the DC-SIGN ligands (see Paragraph 2.6.1). I performed these experiments in the laboratories of Prof. F. Fieschi, where I also expressed and purified DC-SIGN. The ability of compounds to inhibit the DC-SIGN-mediated HIV infection was investigated in a *trans*-infection model with DC-SIGN expressing cells and CD^{4+} T-lymphocytes. These latter experiments were performed by Dr. A. Berzi in the group of Prof. M. Clerici (see Paragraph 2.6.2). Finally, the cytotoxicity of compounds was also excluded (see Paragraph 2.6.3), a feature that makes them suitable for topical applications.

2.6.1 Surface Plasmon Resonance (SPR) Inhibition Assays

Surface Plamon Resonance (SPR) is a physical process that can occur when a beam of light hits a metallic surface and is reflected at the surface-solution interface. This resonance is possible only when the beam of light hits the surface at a certain angle Θ, the resonance angle, and it excites an electromagnetic field, named "evanescent" wave. By varying the mass of the surface, the suitable Θ that produces the evanescent wave changes as well. SPR technique is able to detect changes in terms of mass by monitoring in real time the changes in Θ. It gives back resonance signals (i.e. resonance units RU), proportional to mass change, versus time (Figure **2.9**).

An SPR assay allows to evaluate the interaction between one material immobilized over the surface, which is usually a gold layer, and another one flushing free in solution over the surface (Figure **1.7**).[25] When the binding occurs, the weight of the surface changes, in a way related to the mutual affinity of biding partners.
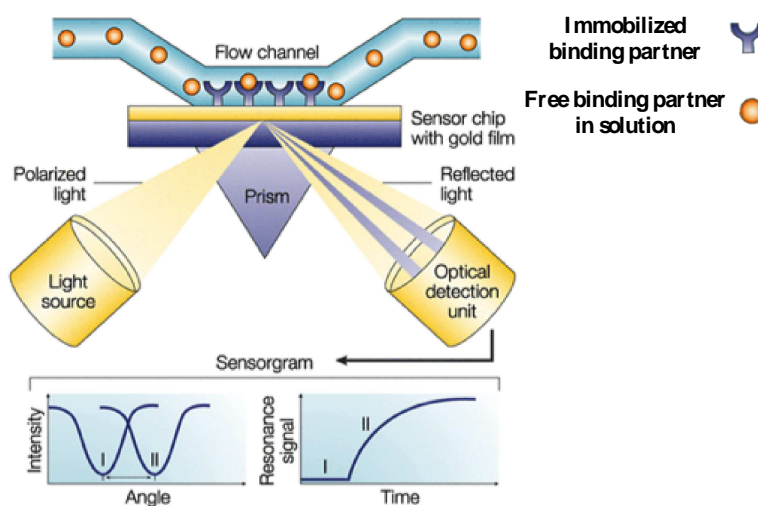
Figure 2.9 Surface plasmon resonance (SPR) detects the angle needed for the polarized light to excite the evanescent wave. The angle depends on the mass of the surface and can shift from I to II (bottom, left) when biomolecules bind to the surface, thus changing the mass of the surface layer. This angle change can be monitored in real time as a plot of resonance signal (proportional to mass change) versus time (bottom, right).

This technique was used to evaluate the ability of multivalent synthesised compounds to inhibit the binding of soluble tetrameric DC-SIGN extracellular domain (ECD) to mannosylated Bovine Serum Albumin (Man-BSA, carrying 15 tri-mannose residues per unit), immobilized over the gold surface. Man-BSA competes with the ligand in the binding to DC-SIGN, being itself a DC-SIGN ligand, and it was used as a mimic of gp120 glycoprotein. The efficiency of inhibition as a function of a compound's concentration is directly related to the ligand affinity toward DC-SIGN ECD. Since

what is measured is the residual protein able to bind to the surface where the competitor is immobilized, this experiment is referred to as *inhibition* or *competition* assay.

Preliminary SPR *direct* assays were also performed by the Fieschi group, evaluating the interaction between the ligands flushing over the gold surface where DC-SIGN ECD was immobilized. The interpretation of the obtained results is still on going.

2.6.1 Tested compounds

Tested compounds are listed in Table **2.2**. During the course of my thesis, these molecules were assigned a conventional name PolymanXY, and an abbreviation PMXY, for communication between the different groups involved. These abbreviations are shown in Table **2.2**, together with the structures and the numbering used so far. Their conventional abbreviated name PMXY will be used in the following paragraph.

The non-chelating dendrimers **2.42** (**PM09**) and **2.50** (**PM19**) were used as references.[12]

2.6.1.2 Experimental

2.6.1.2.1 DC-SIGN ECD production, expression and purification

2.6.1.2.1.1 Transformation of Ca^{2+}-competent E.coli strain

On ice, 5 µL of DC-SIGN ECD pET30 plasmid (produced by Dr. M. Thépaut, Institut de Biologie Structurale, Grenoble) were added to 200 µL of the Ca^{2+}-competent E.coli strain BL21(DE3). After being incubated for 30 minutes on ice, the resulted solution underwent a heat shock for 45 seconds in 42 °C water. Then it was put back on ice, before adding 1 ml of SOC broth (*sterile procedure*) and incubating at 37 °C for 1 hour. After solution centrifugation (5000 rpm, 5 minutes), the majority of the supernatant was discarded, leaving a small residual amount in the tube, in which the obtained pellet was resuspended (*sterile procedure*).

Resuspended cells were plated on a Petri dish with LB-Agar containing kanamycin antibiotic and incubated at 37 °C overnight (*sterile procedure*).

2.6.1.2.1.2 Preculture and culture of DC-SIGN ECD

Two clones selected from the Petri dish were inoculated to 100 mL of LB broth containing 50 µg/mL of kanamycin antibiotic (*sterile procedure*). The obtained solution was cultivated at 37°C overnight to produce the preculture.

The culture was started by inoculation of 50 mL of overnight preculture to 1 L of LB broth with 50 µg/mL kanamycin (*sterile procedure*). The cells were grown at 37 °C for 3 h.

Cell growth was controlled by measuring solution absorbance at 600 nm each (A = 1.86 at time of IPTG induction).

2.6.1.2.1.3 Overexpression of DC-SIGN ECD

DC-SIGN ECD over-expression was induced by addition of IPTG to final concentration of 1 mM and the culture was continued at 37 °C for 3 hours.

Cell growth was controlled by measuring solution absorbance at 600 nm each 20 minutes (**Figure 2.10**), and expression was confirmed by a 12 % polyacrylamide gel electrophoresis (PAGE) before and after induction (**Figure 2.11**).
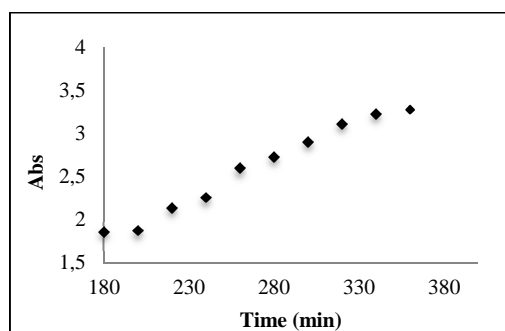
Figure 2.10 UV-Vis time-control of induction at λ = 600 nm.
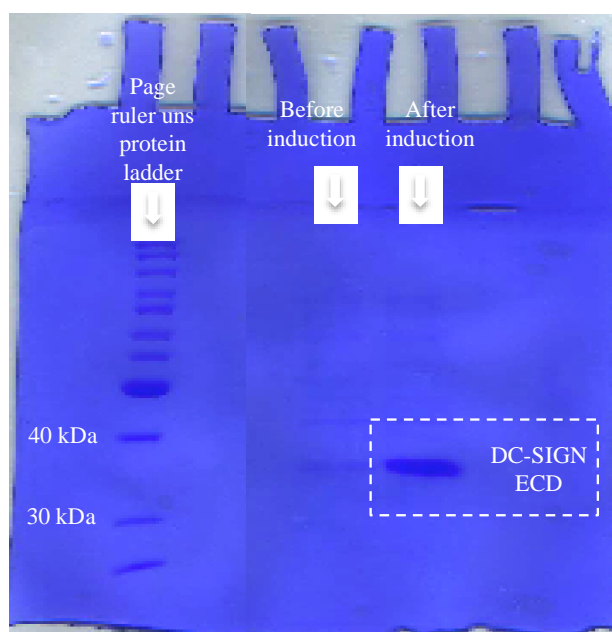
Figure 2.11 12 % polyacrylamide gel electrophoresis. Cell culture was controlled before and after the IPTG induction. *Page ruler uns protein ladder* is a pre-stained marker containing 11 proteins with known molecular weight. The DC-SIGN related spot corresponds to one monomeric extracellular domain.

The cells were harvested by centrifugation at 5000 rpm for 20 min at 4 °C and resuspended in the buffer consisting of 25 mM Tris-HCl (pH 8), 150 mM NaCl, 4 mM $CaCl_2$ (1 L pellet was resuspended in 30 mL of buffer) and stored at -20 °C.

2.6.1.2.1.4 Inclusion body extraction

To the pellet of 1 L culture already suspended in 30 mL of buffer (25 mM Tris-HCl pH 8, 150 mM NaCl, 4 mM $CaCl_2$), 1 tablet of "complete EDTA-free" protease inhibitor cocktail was added. The cells were disrupted by sonication in ice for a 2 minutes round at 90 % amplitude, using 2 s long sonications and 10 s long pauses in-between. The inclusion bodies together with cell debris were collected by centrifugation at 36800 rpm for 30 min at 4 °C.

The resulting pellets was resuspended using Potter- Elvehjem homogenizer in 20 mL of buffer containing 25 mM Tris-HCl (pH 8), 150 mM NaCl, 2 M urea and 1% Triton-X100, and centrifuged at 36800 rpm for 30 minutes at 4 °C. It was then rinsed by resuspending in 40 mL of 25 mM Tris-HCl (pH 8) and 150 mM NaCl buffer with Potter-Elvehjem homogenizer and centrifuging at 36800 for 30 min at 4 °C.

Inclusion bodies were solubilised with Potter-Elvehjem homogenizer in 60 mL of buffer containing 6 M Gdn-HCl, 150 mM NaCl, 25 mM Tris-HCl pH 8 and 0.01 % β-mercaptoethanol, and centrifuged at 36800 for 40 minutes at 4 °C to eliminate insoluble part. The presence of DC-SIGN ECD in the resulting supernatant was assessed by a 12 % polyacrylamide gel electrophoresis (PAGE). Protein was subsequently refolded (see following paragraph) without being freeze nor stored, otherwise losing its ability to renaturate.

2.6.1.2.1.5 Refolding

Solubilised DC-SIGN ECD was diluted with the same buffer (6 M Gdn-HCl, 150 mM NaCl, 25 mM Tris-HCl (pH 8) and 0.01 % β-mercaptoethanol) till the concentration (respect to the monomer) of 2 mg/mL was reached (211 mL). It was refolded by flash dilution (drop by drop) to 844 mL (final dilution 5X) of buffer consisting of 25 mM Tris-HCl (pH 8), 1.25 M NaCl, and 25 mM $CaCl_2$, at 4 °C. The resulting protein solution was dialyzed overnight against 6189 mL of 25 mM Tris-HCl (pH 8) buffer, at 4 °C. Two more dialyses (3 hours + 2 hours, at 4 °C), against 7000 mL of 25 mM Tris-HCl (pH 8), 150mM NaCl, and 4 mM $CaCl_2$ buffer, continued and finished the refolding. The precipitates were eliminated by centrifugation at 36800 rpm for 1 h at 4 °C.

For both the refolding and the dialysis, solubilised DC-SIGN ECD was divided in two batches. Each batch was refolded in 422 mL of buffer and dialyzed against 3095 mL and 3500 mL of buffer.

2.6.1.2.1.6 Purification

The purification of refolded DC-SIGN ECD was performed using automated purification protocol on an Akta Xpress FPLC system (MP3 platform, IBS Grenoble) at 4°C. Column used are a 20 mL Mannan-Agarose column (Sigma Aldrich Ref.: M9917) and a 125 mL Superose 12 column (GE Healthcare); gel filtration (GF) was cycled to fractionate the sample resulting from the Mannan-Agarose column in 2 mL injections.

• First step: Mannan-Agarose column 20 mL.

Equilibration buffer: 25 mM Tris (pH 8), 150 mM NaCl, 4 mM CaCl$_2$.

Elution buffer: 25 mM Tris (pH 8), 150 mM NaCl, 1 mM EDTA.

- Column equilibration with 50 mL of equilibration buffer at 2.5 mL/min.

- Loading of the whole sample at 2.5 mL/min.

- Column washing with 150 mL of equilibration buffer at 2.5 mL/min.

- Column elution with 100 mL of elution buffer at 2.5 mL/min and recovering of elution peak in a superloop (~20 mL of sample).

• Second step: Superose 12 125 mL (11 cycles).

GF buffer: 25 mM Tris (pH 8), 150 mM NaCl, 4 mM CaCl$_2$.

- Column equilibration with 150 mL of equilibration buffer at 1 mL/min.

- Loading of the sample from SuperLoop by fractions of 2 mL.

- Column elution with 150 mL of GF buffer at 1 mL/min, 1 mL fractions where collected when automatic peak detection occurred during elution in a 96-well deep well plate.

The best yield obtained was 30 mg of DC-SIGN ECD for 2 L culture.

2.6.1.2.2 SPR Assays set up

SPR inhibition assays were conducted using the Biacore 3000 instrument from Biacore-GE Healthcare. Sensor Chip CM4, amine coupling kit (including EDC, NHS and ethanolamine), HBS-P buffer (0.01 M HEPES (pH 7.4), 0.15 M NaCl, 0.005 % Surfactant P20) and 10 % P20 were from Biacore-GE Healthcare. Mannosylated bovine serum albumin Man α1-3[Man α1-6]Man BSA (Man-BSA, carrying 15 tri-mannose residues per unit) was from Dextra Laboratories Ltd.

Flow cells (Fc) 1 and 2 on a CM4 sensor chip were functionalized through the amine coupling procedure, using HBS-P buffer at a flow rate of 5 µL/min as the running buffer. The carboxymethyl dextran matrixe of the sensor chip was activated by injection of a 1:1 mixture of 0.2 M EDC and 0.05 M NHS (50 µL). One cell (Fc1) was functionalized with Man α1-3[Man α1-6]Man BSA (Man-BSA) (10 µg/mL solution of Man-BSA in 10 mM sodium acetate buffer pH 4), whereas the second one -Fc2- was used as reference and functionalized with BSA (100 µg/mL solution of BSA in 10 mM sodium acetate buffer pH4). The remaining activated but unbound carboxylic groups were blocked by the injection of 1 M ethanolamine pH 8 (30 µL). Finally, all surfaces were rinsed with 10 mM HCl (10 µL) and conditioned with 50 mM EDTA pH 8 (20 µL). On Fc1, the final response of immobilized level of Man-BSA was 1500 RU.

Glycodendrimers were solubilized in the running buffer consisting of 25 mM Tris-HCl (pH 8), 150 mM NaCl, 4 mM CaCl$_2$ and 0.005 % v/v P20, supplemented with 4 % DMSO for **1.9** derivatives, because of solubility problems.

13 µL of a mixture consisting of compounds plus 20 µM DC-SIGN ECD (concentration of the monomeric subunit) were injected over the surfaces. The concentration of DC-SIGN ECD was chosen according to its affinity for immobilized Man-BSA, resulting in a maximum response of about 3000 RU. Compounds were tested at increasing concentrations, up to 2 mM for divalent compounds and 0.9 mM for hexavalent derivatives. Lectin alone at the concentration of 20 µM was injected in order to determine its full activity. Bound lectin was removed with 5 µL of 50 mM EDTA (pH 8) to regenerate the surface.

2.6.1.2.3 Data analysis

Obtained sensograms show the binding responses expressed in terms of response unit (*RU*), and represent the amount of lectin bound to the surface in the function of time. Equilibrium binding responses are the maxima *RU* values reached and were obtained 150 s after the start of the injection. DC-SIGN ECD binding responses (R_{eq}) were corrected for the references *RU* arising from the interaction between DC-SIGN ECD and BSA (reference Fc2), thus avoiding the possible contribution of unspecific interactions with the BSA surface. In Figure **2.12** the series of sensograms obtained for several concentrations of compound **2.35/PM30** is shown as an example.
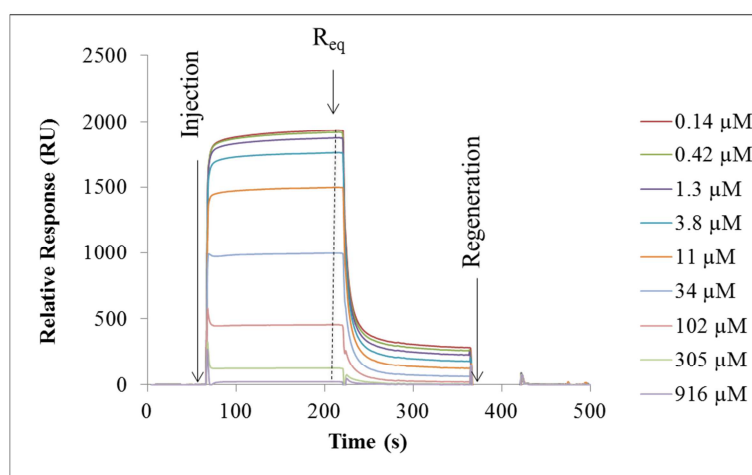
Figure 2.12 A mixture of **2.35/PM30** DC-SIGN ECD (20 µM) was injected over a CM4 sensor chip functionalized with Man-BSA (15 tri-mannoses on average). Obtained sensograms show the *Relative Response Units* (*RU*) in the function of time, indicating the amount of bound lectin corrected for the reference surface. DC-SIGN ECD binding responses (R_{eq}) were obtained 150 s after injection. The different sensograms correspond to different compound concentrations.

R_{eq} values were then converted to residual DC-SIGN ECD activity values by normalizing them with respect to the R_{eq} of the lectin alone (which was considered as a 100 % activity value), as shown in Figure **2.13** (again the behaviour of **2.35/PM30** is taken as an example).
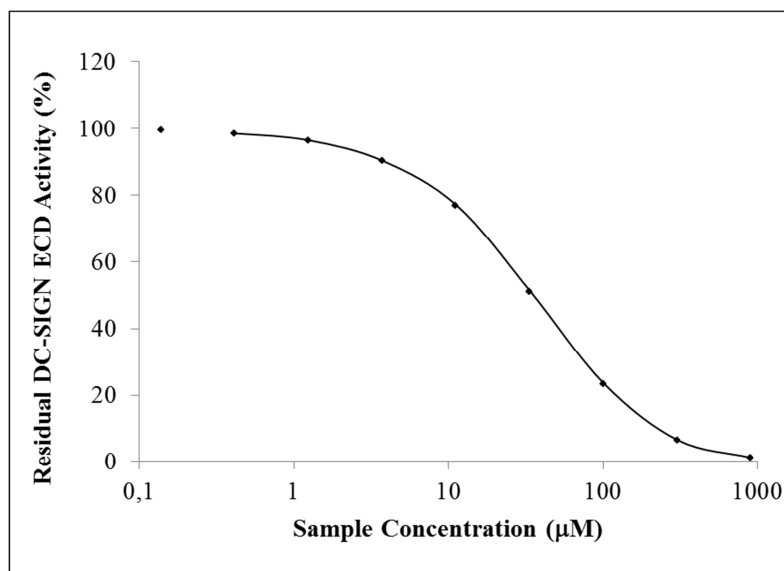
Figure 2.13 Residual DC-SIGN ECD activities in the presence of different concentration of compound **PM30** were obtained from the binding responses R_{eq} normalized with respect to the R_{eq} values of DC-SIGN ECD alone.

The plot of the residual DC-SIGN ECD activity (y, %) *versus* the corresponding compound concentration (Figure **2.13**) was fit using the 4-parametre logistic model (Equation **2.3**)

$$y = R_{hi} - \frac{R_{hi} - R_{low}}{1 + \left(\frac{Conc}{A_1}\right)^{A_2}}$$

Equation 2.3 4-parameter logistic model used to fit the plots of the residual DC-SIGN ECD activity (*y*, %) with respect to the corresponding compound concentration (*Conc*). R_{hi} and R_{lo} are maximum and minimum asymptotes, A_1 is the inflection point and A_2 is a slope of the curve.

Finally, IC_{50} values for each compound (i.e. the concentration needed to inhibit the binding of half of the injected protein to the BSA-Man surface) were calculated using Equation **2.4**.

$$IC_{50} = A_1 \cdot \left(\frac{R_{hi} - R_{lo}}{R_{hi} - 50} - 1\right)^{\frac{1}{A_2}}$$

Equation 2.4 Equation used to calculate IC_{50} values of each compound, i.e. the concentration needed to inhibit binding of 50 % of the DC-SIGN ECD on the BSA-Man surface.

2.6.1.3 Results and discussion

Sensograms relative to all tested compounds are reported in Figure **2.14A** (**1.9** derivatives) and Figure **2.14B** (**1.9** derivatives), whilst inhibition curves are shown in Figure **2.15A**, **2.15B** (**1.7** derivatives) and Figure **2.15C**, **2.15D** (**1.7** derivatives). Calculated IC_{50} values of tested compounds are reported in Figure **2.16A** (**1.9** derivatives) and Figure **2.16B** (**1.7** derivatives) and in Table **2.5** and **2.6**. Results obtained for compound **2.42/PM09** derive from another campaign previously conducted by Dr. Ieva Sutkeviciute.[26]
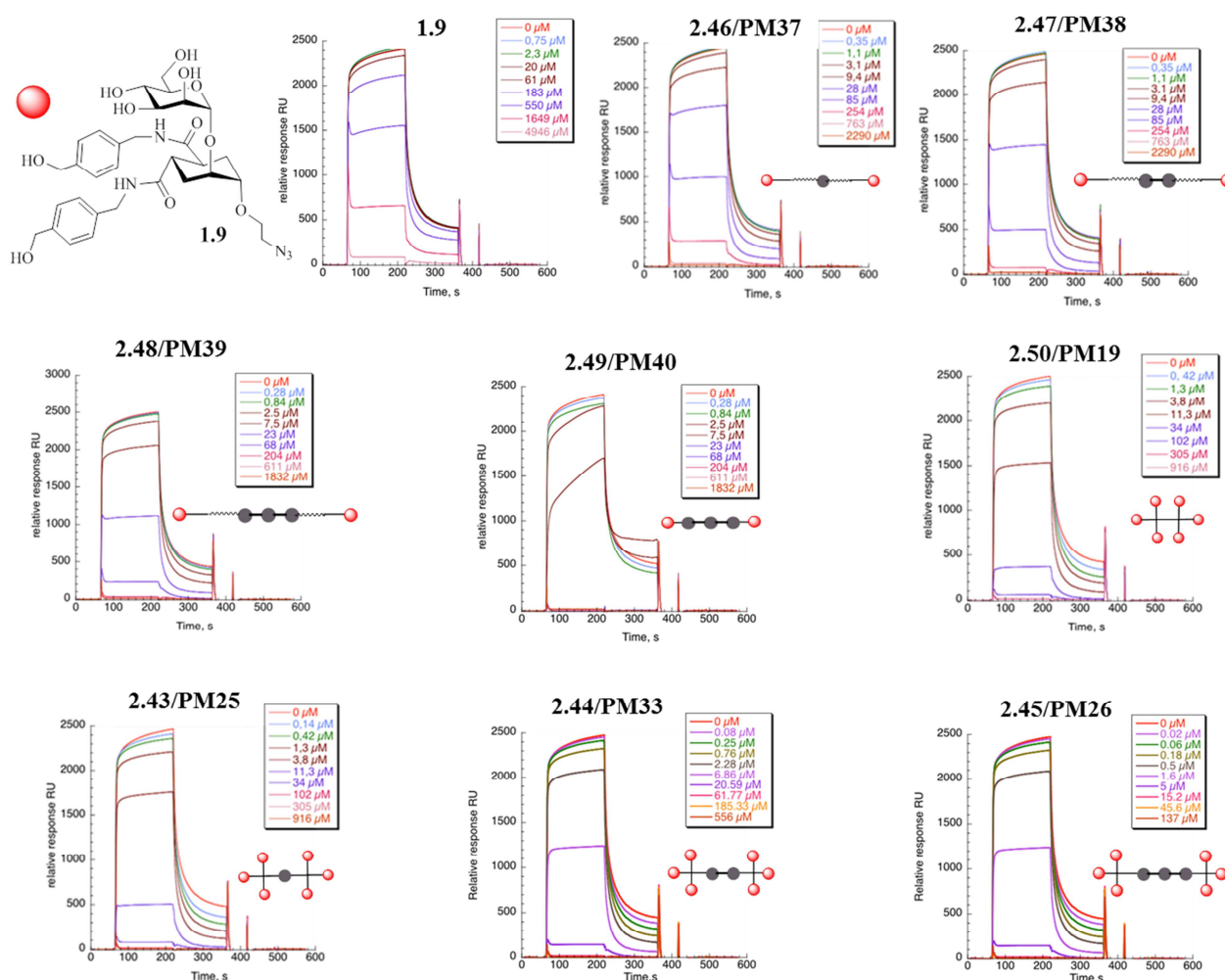
Figure 2.14A Inhibition of DC-SIGN interaction with BSA-Mannotriose surface. Compounds based on **1.9** at different concentrations were co-injected with DC-SIGN ECD (20 µM).

B) Multivalent compounds based on 1.7
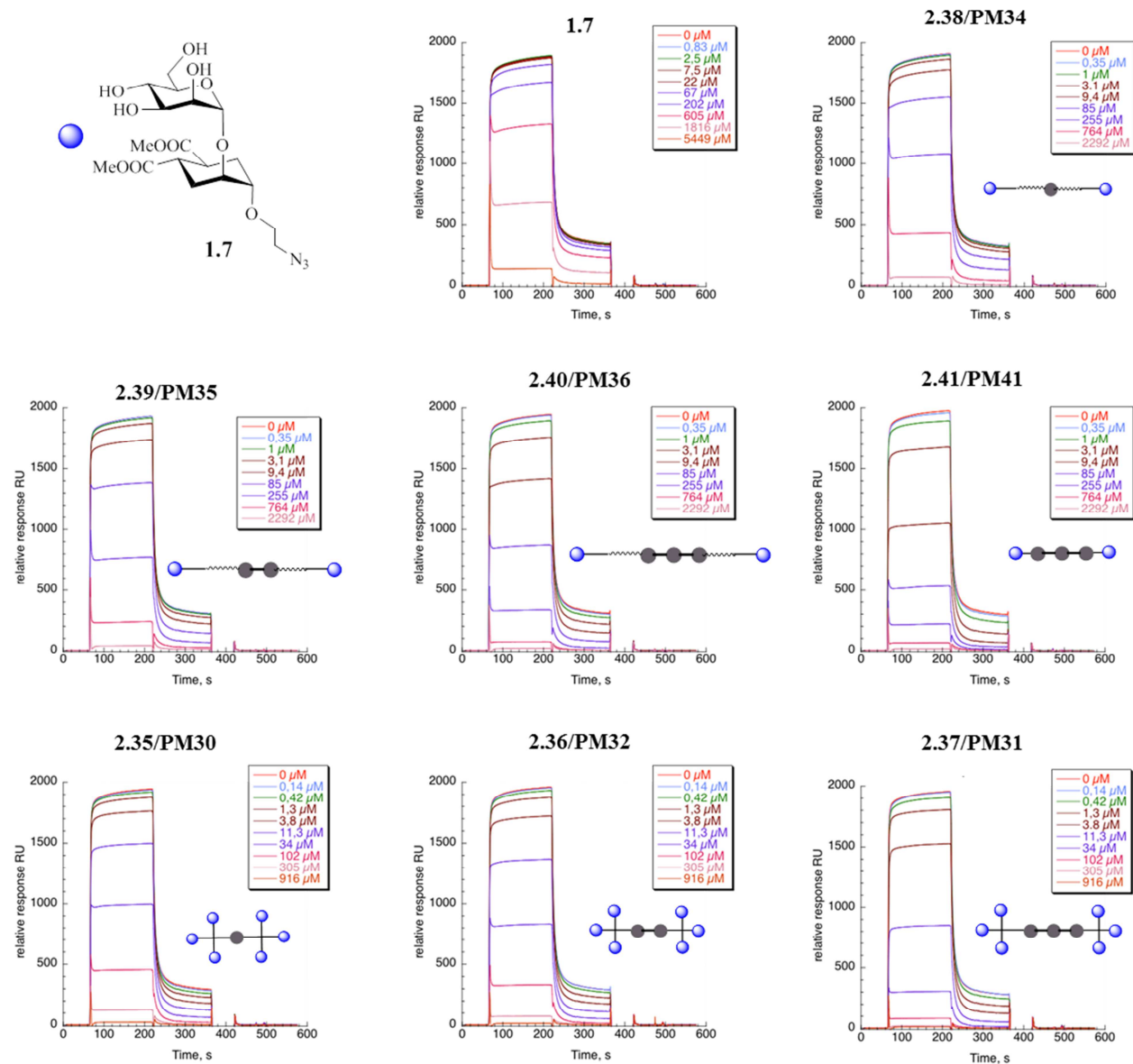
Figure 2.14B Inhibition of DC-SIGN interaction with BSA-Mannotriose surface. Compounds based on **1.7** at different concentrations were co-injected with DC-SIGN ECD (20 µM).

A

B

C

D
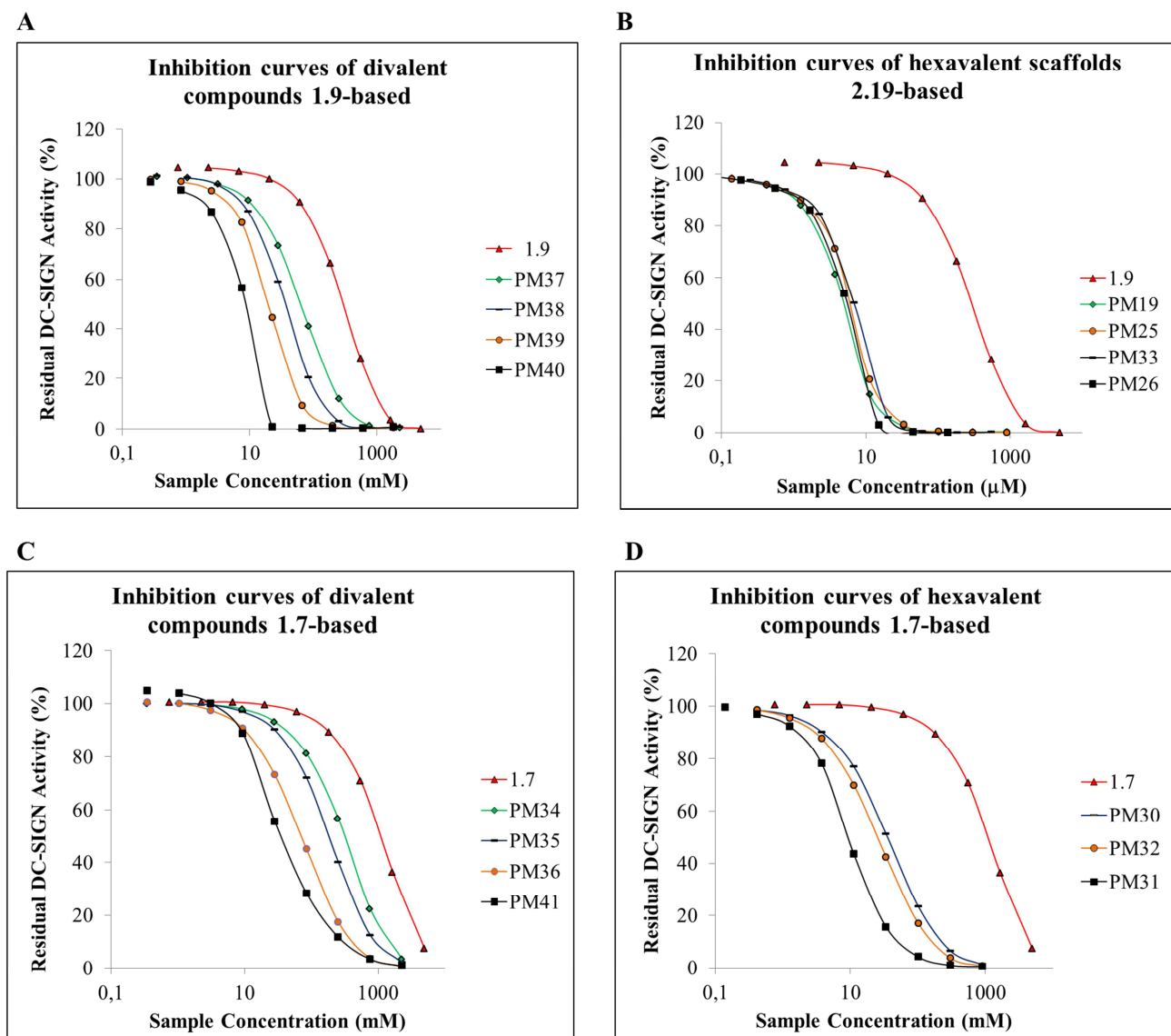
Figure 2.15 Inhibition curves of A) divalent and B) hexavalent **1.9**-based ligands and C) divalent and D) hexavalent **1.7**-based ligands. The ability of ligands to inhibit DC-SIGN-ECD binding to a CM4 Sensor Chip where Man-BSA (Man α1-3[Manα1-6]Man-BSA, 15 trimannose residues, on average) was immobilized was evaluated. The residual DC-SIGN-ECD activity (%) is plotted against ligand concentrations.
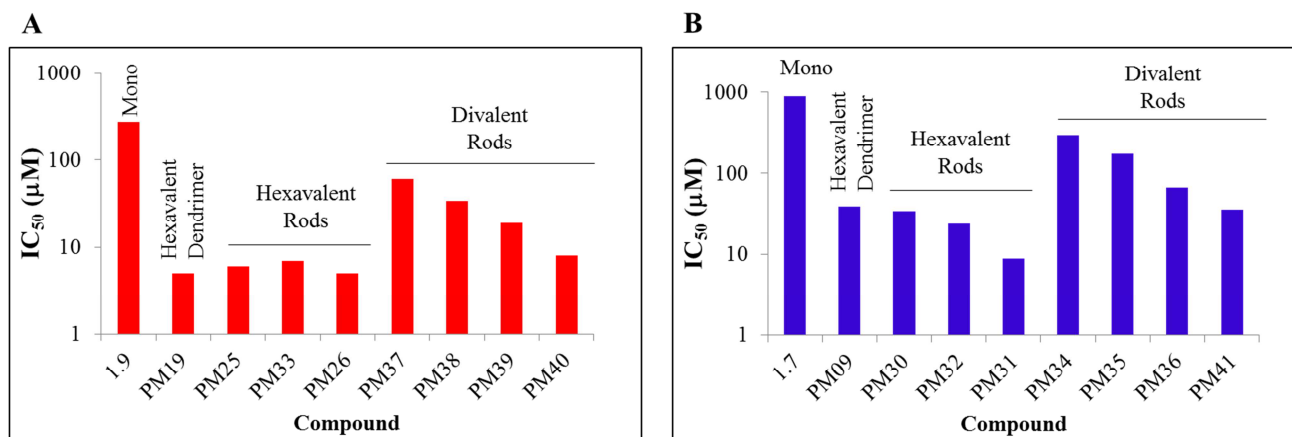
Figure 2.16 Activities of glycodendrimers bearing **1.9** (A, red bars) or **1.7** (B, blue bars) in inhibiting binding of DC-SIGN ECD (20 μM) to Man-BSA (Man α1-3[Manα1-6]Man-BSA, 15 trimannose residues, on average) immobilized on a CM4 Sensor Chip. *IC$_{50}$* are expressed as dendrimer concentration (μM).

The affinity improvements of multivalent ligands for DC-SIGN ECD with respect to the corresponding monovalent ones is expressed in terms of Relative Inhibitory Potency (*R.I.P.*), calculated according to Equation **2.5** and listed in Table **2.5** and **2.6**.

$$R.I.P. = \frac{IC_{50monovalent}}{IC_{50multivalent}.\,valency}$$

Equation 2.5 Relative Inhibitory Potency (*R.I.P.*) represents the improvement of a multivalent compound with respect to the corresponding monovalent ligands and it is corrected for its valency.
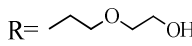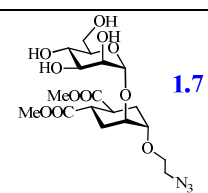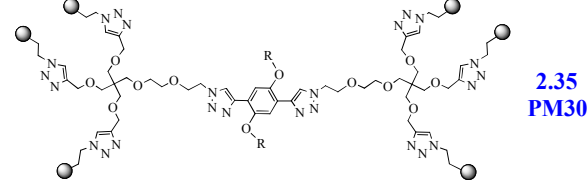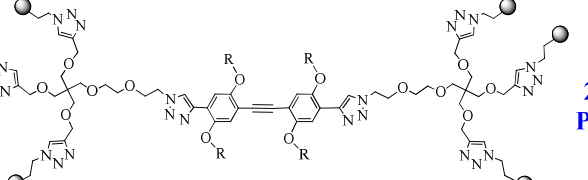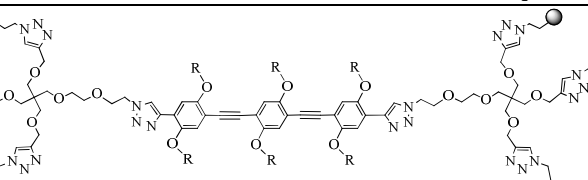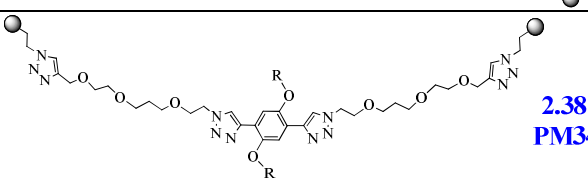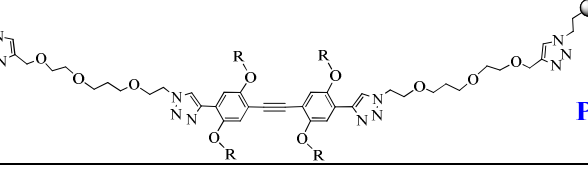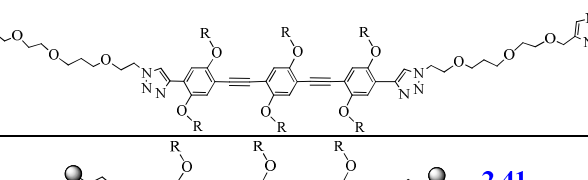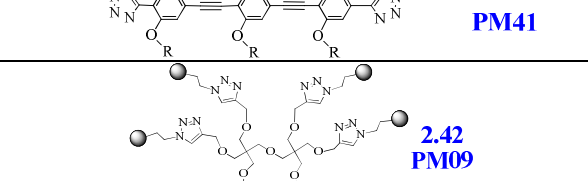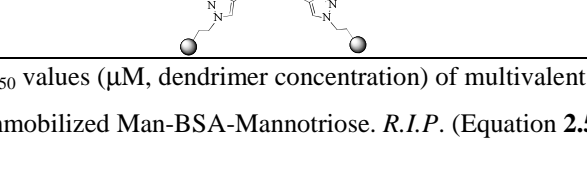
Structure	$R=$	Ligand 1.7	IC_{50} (μM)	R.I.P.
		1.7	901	1
		2.35 PM30	34	4
		2.36 PM32	24	6
		2.37 PM31	9	17
		2.38 PM34	295	2
		2.39 PM35	175	3
		2.40 PM36	67	7
		2.41 PM41	36	13
		2.42 PM09	39	4

Table **2.5** IC$_{50}$ values (μM, dendrimer concentration) of multivalent derivatives of **1.7** inhibiting binding of DC-SIGN ECD to immobilized Man-BSA-Mannotriose. *R.I.P.* (Equation **2.5**) of compounds are reported in round brackets.
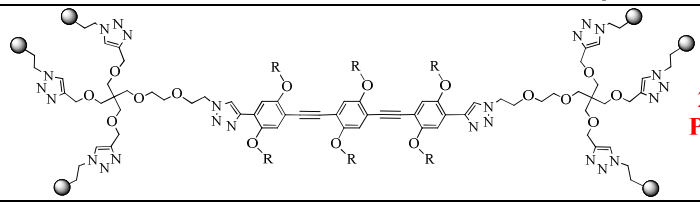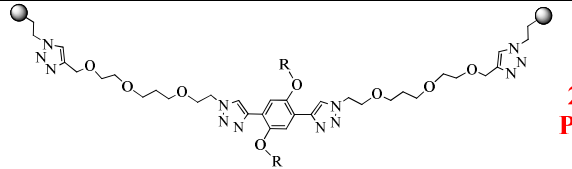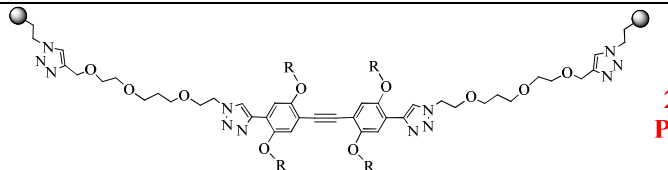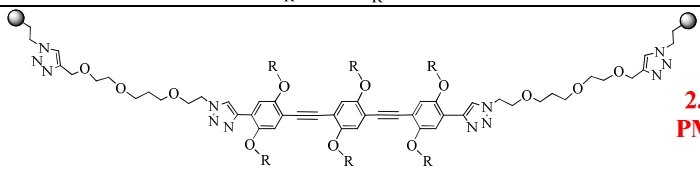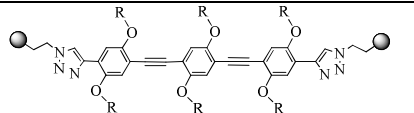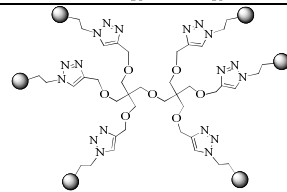
Structure	R= ～O～OH Ligand 1.9	IC_{50} (µM)	R.I.P.
1.9	271	1
2.43 PM25	5[a]	10
2.44 PM33	6[a]	8
2.45 PM26	7	7
2.46 PM37	5[a]	9
2.47 PM38	61	2
2.48 PM39	34	4
2.49 PM40	19	7
2.50 PM19	5	10

Table **2.6** IC$_{50}$ values (µM, dendrimer concentration) of multivalent derivatives of **1.9** inhibiting binding of DC-SIGN ECD to immobilized BSA-Mannotriose. *R.I.P.* (Equation **2.5**) of compounds are reported in round brackets. [a]Lower limit of the assay was reached.

Clear trends were shown by the compounds bearing **1.7** as ligand (Figure **2.16B**, Table **2.5**). Both in the divalent and in the hexavalent series, activity and relative inhibitory potency increased by increasing the length of the Rod. For divalent compounds, IC_{50} decreased from 295 μM (**2.38/PM34**, Rod1 derivative) to 67 μM (**2.40/PM36**, Rod3 derivative), corresponding to an increase of the Reletive Inhibitory Potency, respectively, from 2 to 7. A similar trend was observed for hexavalent compounds, showing IC_{50} values varying from 34 μM (**2.35/PM30**, Rod1 derivative, *R.I.P.* = 4) to 7 μM (**2.37/PM31**, Rod3 derivative, *R.I.P.* = 17). Remarkably, already the presence of the shortest Rod1 contributed to slightly increase compound activity, which was 39 μM (IC_{50}) for the hexavalent dendrimeric compound **2.42/PM09**. Also valency revealed to influence glycodendrimers potency; indeed, keeping the Rod equal, hexavalent molecules were more active than the corresponding divalent ones (*R.I.P.* values at least doubled, compare **2.35/PM30** with **2.38/PM34**, **2.36/PM32** with **3.39/PM35** or **2.37/PM31** with **2.40/PM36**). This is a clear demonstration of the involvement of the effective concentration C_{eff} in the multivalent effect (see Chapter 1.5). Indeed, simply by increasing the local concentration of one ligand at the binding site, activities were improved. Among divalent compounds, an improvement was obtained by reducing the length of the linker between the sugar moiety and Rod3, leading to an almost doubled activity of compound **2.41/PM41** (IC_{50} = 36 μM, *R.I.P.* = 13) with respect to **2.40/PM36** (IC_{50} = 67 μM, *R.I.P.* = 7). This can be explained by the tendency of the divalent compounds with the long linker to fold up, thus reducing the probability to expose the hydroxyl groups responsible for binding to DC-SIGN. Ac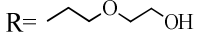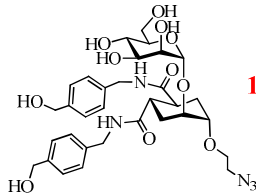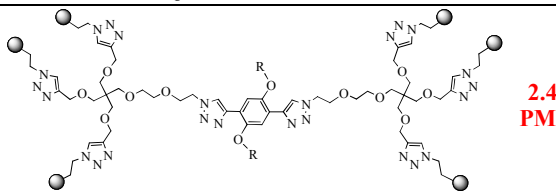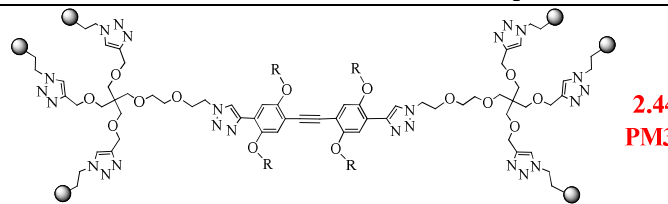cording to computational results, this tendency characterizes much less the short linker derivative (see Paragraph 2.5). From a thermodynamic point of view, **2.40/PM36** has to pay high energetic costs for reducing its degrees of freedom and assuming the optimal conformation to bind the lectin, thus decreasing its activity (see Chapter 1.5).

A similar trend was observed for divalent **1.9** derivatives, which showed IC_{50} values decreasing by increasing the length of the Rod (series **2.46/PM37**, **2.47/PM38**, **2.48/PM39**, Figure **2.16A**, Table **2.6**). Again, optimal activities characterized the divalent compound with the short linker, **2.49/PM40**, with IC_{50} = 8 μM and *R.I.P.* = 17. This confirmed that a good preorganization of a ligand, with flexibility and spatial distribution matching the target binding site, leads to powerful antagonists. On the contrary, activities of **1.9** hexavalent derivatives (**2.50/PM19**, **2.43/PM25**, **2.44/PM33** and **2.45/PM26**) didn't follow any apparent trend and showed similar IC_{50} values in the low μM range (5-7 μM, Figure **2.16A**). This occurred because the lower limit of the assay has been reached.

Indeed, considering that the IC_{50} is defined as the inhibitor concentration required for inhibiting -i.e. binding- the 50 % of the protein, in the case of 1:1 inhibitor-protein interactions, half of the protein

concentration would always be the lower limit value. In the case of our experimental setup with 20 µM DC-SIGN ECD (with respect to the monomer), assuming that every compound molecule binds one monomeric protein, IC_{50} values below 10 µM can no more be measured accurately. This can be observed also from inhibition curves of **2.44/PM33**, **2.45/PM26**, **2.49/PM40** (Figure **2.15A,B**), that do not have a sigmoidal shape.

2.6.2 *Trans*-infection Inhibition Assays

Selected Rod derivatives **PM25**, **PM26**, **PM39** and **PM40** and, for comparison, the hexavalent derivative **PM19**[12] (Table **2.2**) were tested as inhibitors of DC-SIGN-mediated HIV *trans*-infection of CD4^{+} T-Lymphocytes. They all bear compound **1.9** as monovalent ligand. B-THP-1 cells that overexpress DC-SIGN were used as a model of Dendritic Cells. This assay is referred to as a *trans*-infection assay because the virus is transmitted from B-THP to T-cells without having infected (i.e. being replicated in) B-THP-cells themselves (see Chapter 1.2).[27]

The tests were performed by Dr. A. Berzi in the group of Prof. M. Clerici (Università degli Studi di Milano).

B-THP-1/DC-SIGN cells were obtained by transfecting the B-THP-1 human B cell line with DC-SIGN expression vector. They were first incubated with artificial DC-SIGN ligands for 30 min at 37 °C and, subsequently, with HIV (the R5 tropic laboratory-adapted strain HIV-1) for 3 h at 37 °C, without removing the ligand. After an extensive washing step, B-THP-1/DC-SIGN cells were co-cultured with activated CD4^{+} lymphocytes for three days (37 °C). Viral infection of lymphocytes was assessed by measuring the p24 concentration in the culture supernatants through ELISA assays. p24 is a structural component of HIV-1 virus and it is therefore commonly used to evaluate the level of infection by HIV. In this assay B-THP-1 cells are model of Dendritic Cells, easier to be obtained and cultured. They only express DC-SIGN as lectin that can be recognized both by artificial ligands and HIV-1; therefore, they represent a cellular model of HIV anchoring on Dendritic Cells that take into consideration only the role of DC-SIGN.

In Figure **2.17**, obtained results are reported. Each point is the average of three different assays performed using CD4^{+} T-lymphocytes deriving from three different healthy donors. This explains the observed variability, since every donor may be naturally more or less prone to be infected. Every compound was tested in the range of concentration 1 – 50 µM. Cells not treated with DC-SIGN ligands and incubated with the medium (MED, Figure **2.17**) are the positive control. The level of *trans*-infection obtained in T-lymphocytes without inhibiting DC-SIGN can be considered as the maximum infection level (100 %). Also in this case it is possible to evaluate the IC_{50} value of one compound, defined as the concentration needed to decrease the infection level by half. It was

already assessed that B-THP-1 cells not transfected with DC-SIGN did not transmit the infection and can be used as negative control.[28]
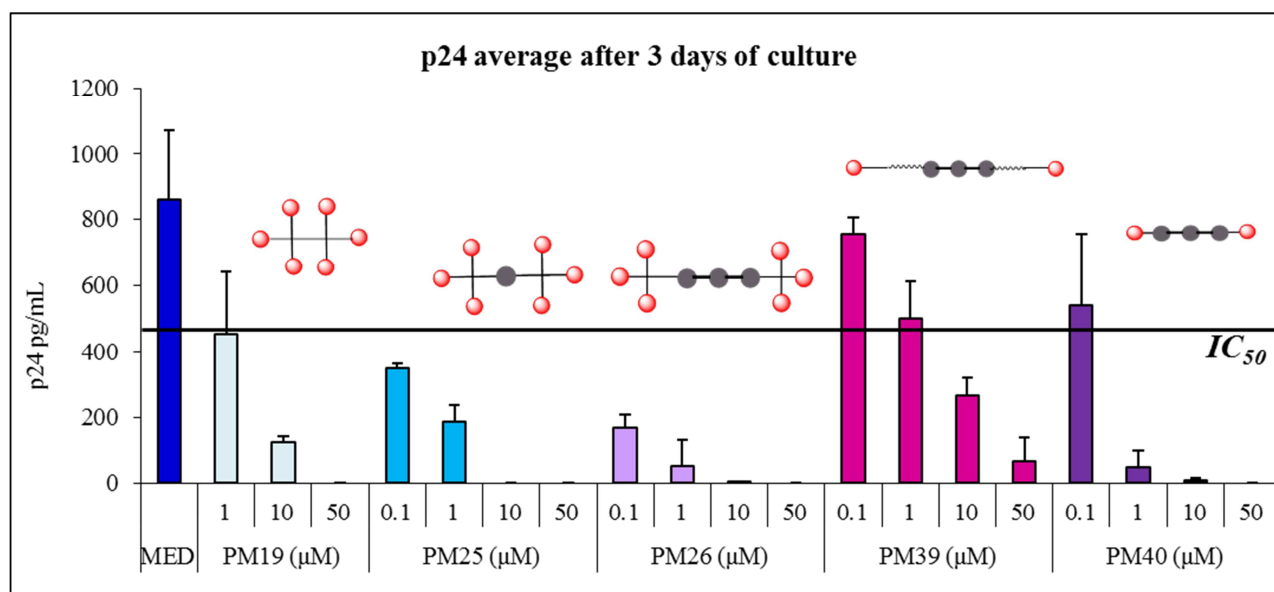
Figure 2.17 PM19, **PM25**, **PM26**, **PM39** and **PM40** were tested at the concentrations indicated as inhibitors of the T-lymphocytes HIV-infection. Virus was transmitted by B-THP-1/DC-SIGN cells, and p24 measured in the T-lymphocytes-culture supernatant reflected the level of infection. MED (blue bar) was the positive control, obtained without inhibiting DC-SIGN.

The activity trend observed for the hexavalent series (**PM19**, **PM25** and **PM26**) showed that already the presence of the small Rod1 in **PM25** allows for activity increase by at least one order of magnitude over **PM19**. Indeed, the IC_{50} value of **PM19** was confirmed to be about 1 µM (as previously reported),[12] whereas the one of **PM25** was lower than 0.1 µM. Compound **PM26**, bearing Rod3, was found to be even more active. The divalent series showed an IC_{50} of almost 1 µM for **PM39**, underlying that a divalent compound with Rod3 can have a similar activity than an hexavalent dendrimeric derivative (**PM19**). Compound **PM40**, with an IC_{50} around 0.1 µM, was one order of magnitude more active that **PM39**, demonstrating again that structural preorganization of one molecule leads to a strong antagonist when it matches the protein structure.

PM25, **PM26** and **PM40** were tested in a broader concentration range, from 0.01 to 50 µM (Figure **2.18**), and obtained points were fitted to 1:1 hyperbolic decay, in order to extrapolate IC_{50} values. Obtained values are 67 nM for **PM25**, 24 nM for **PM26** and 161 nM for **PM40**. These results confirmed again the importance of the Rod, showing that **PM25** and **PM26** are 15 and 40 times more active than **PM19** ($IC_{50} \approx 1$ µM) respectively. The presence of Rod3 that, according to computational prediction (see Paragraph 2.5), should allow the compound to chelate easily two

binding sites in the tetrameric DC-SIGN is reflected in an almost triple activity of **PM26** relative to **PM25**. Being the Rod equal, the increase in local ligand concentration generated by increasing the valency of the compounds (see **PM26** *vs* **PM40**) resulted again in higher antagonism activity.
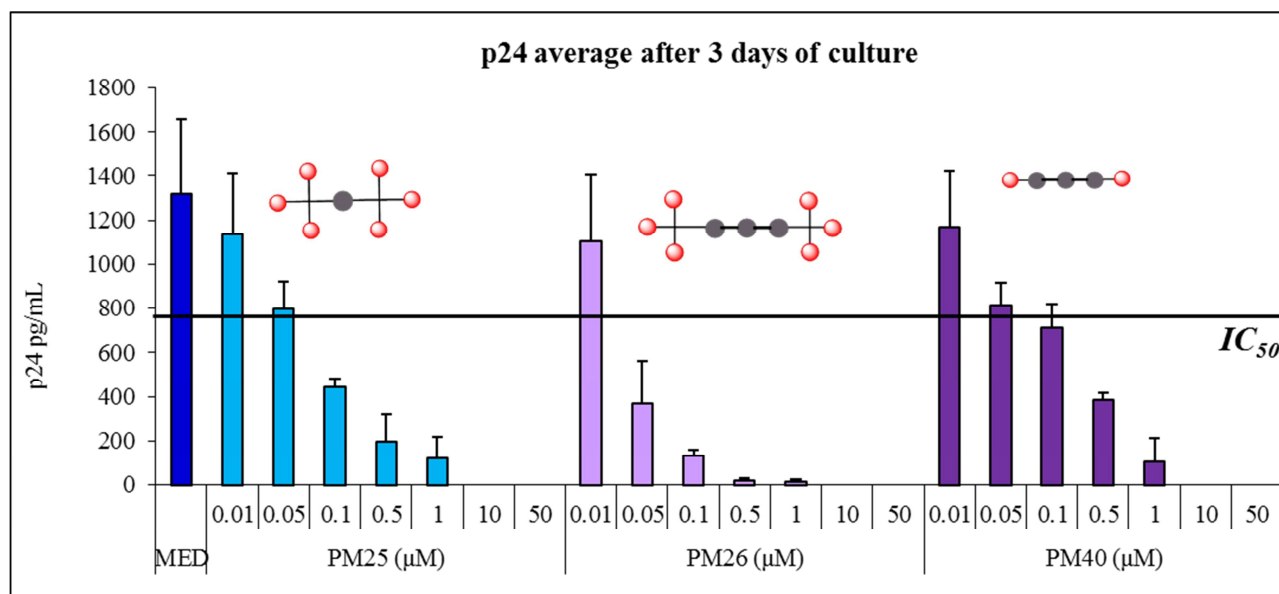
Figure 2.18 PM25, **PM26** and **PM40** were tested at the concentrations indicated as inhibitors of the T-lymphocytes HIV-infection. Virus was transmitted by B-THP-1/DC-SIGN cells, and p24 measured in the T-lymphocytes-culture supernatant reflected the level of infection. MED (blue bar) was the negative control, obtained without inhibiting DC-SIGN.

Remarkably, tested compounds **PM19**, **PM25**, **PM26** and **PM40** were the ones that didn't show any apparent trend in the SPR inhibition assay (see Paragraph 2.6.1). Results obtained here highlight that the presence and the length of the Rod do play an important role in compound's activity. This may confirm that the strange results coming from SPR assays were affected by an experimental limit.

2.6.3 Cytotoxicity

Cytotoxicity assays were performed by Dr. A. Berzi in the group of Prof. M. Clerici (Università degli Studi di Milano) on the selected compounds **PM25**, **PM26**, **PM39** and **PM40**.

Tests were performed using B-THP-1 cells overexpressing DC-SIGN, i.e. to the same cell line used for *trans*-infection inhibition assays (see Paragraph 2.6.2). Cells were incubated together with compounds at different concentrations and for different times; the amount of dead cells was measured using 7-Aminoactinomycin D (7-AAD) (Scheme **2.28**) after 3 hours and half and 24 hours of incubation. 7-AAD is a fluorescent chemical compound with a strong affinity for DNA. It is able to reach DNA only if cellular membranes are compromised, which happens in dead cells.

The percentage of cells positive to 7-AAD, evaluated through flow citometry (FACS), is a measure of the percentage of dead cells.
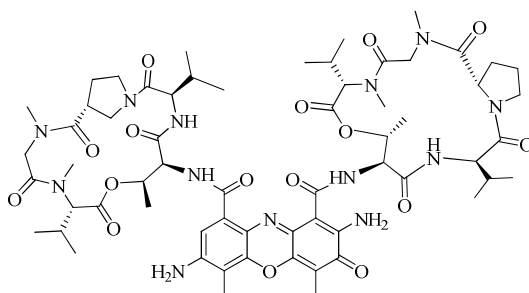
Scheme 2.28 The fluorescent dye 7-AAD used for evaluating the amount of dead cells.

Results indicated that Rod derivatives are not cytotoxic. Indeed, even after 24 hours of incubation, the amount of dead cells was below 2 %.

2.7 Conclusions

Monovalent ligands **1.7**[9] and **1.9**[8] and corresponding tetravalent, hexavalent and nonavalent compounds[12] (Figure **2.4**) had already been synthesised in our laboratories as DC-SIGN antagonists, using dendrimers based on a pentaerythritol core.

In principle, these dendrimers could be used to inhibit the binding of external pathogens that infect humans through the mucosal entry pathway recognizing DC-SIGN as their primary target.[4] Their affinity for DC-SIGN was assessed through SPR competition assays, reveling that the series derived from **1.9** was more active than the corresponding **1.7** one. Compounds affinity for the receptor increased also with the valency, as a result of multivalent effect. Interestingly, computational modelling revealed that the multivalent effect associated with these compounds can only be due to the so called statistical rebinding effect, or to mechanisms of protein clustering. Indeed, these dendrimers have a dimension that doesn't allow them to bridge two binding sites on the DC-SIGN tetramer. The distance between two contiguous DC-SIGN binding sites is about 4 Å, and the production of constructs able to bridge DC-SIGN could improve compounds activity exploiting also the chelation-binding mode.

For this reason, with the aim to improve the activity of artificial DC-SIGN ligands, rather that increasing the valency of the constructs, we've tried to rationally control the spacing of the ligands.

A library of multivalent compounds characterized by rigid rods of controlled length as the central scaffold units was designed and synthesised. Compounds are listed in Table **2.2**.

In order to dissect their relative contribution, the following elements were varied:

- **Ligand**: both ligand **1.7** and **1.9** were used.

- **Valency**: hexavalent and divalent compounds were synthesized.
- **Length of the Rod**: Rod1 (8 Å), Rod2 (12 Å) or Rod3 (24 Å) were used.
- **Length of the linker** separating monovalent ligands and the central scaffolds.

The possibility of these compounds to adopt conformations where two mannose residues are separated by more than 4 Å was assessed by computational modelling, thus confirming their ability to be potential chelating agents for DC-SIGN.

All compounds were tested as DC-SIGN ligands through an SPR inhibition assay, revealing first of all the importance of the monovalent ligands, since multivalent compounds based on **1.9** were always more active than those based on **1.7**. Investigating the **1.7** series, both the length of the rod and the valency of the materials were found to influence the biological activity. The increase of the rod length increased compounds β factor, and activities of hexavalent molecules were always higher than the ones of corresponding divalent constructs. Once the rod becomes long enough to allow simultaneous interaction of two ligands with two DC-SIGN binding sites, the loss of entropy associated with a long flexible linker becomes apparent, and a divalent compound with the short linker had a lower IC_{50} value than the corresponding divalent compound with the long linker. Hexavalent compounds of the **1.9** series were too active to be tested through the SPR competition assay, since they reached its intrinsic lower limit. Nonetheless, the ability of **1.9**-mutlivalent derivatives to inhibit the *trans*-infection of HIV virus from B-THP/DC-SIGN to CD^{4+} T lymphocytes was evaluated. Also in this case, inclusion of a rigid spacer in the dendrimer core improved the activity of the material with results that depend on the length of the spacer and on the overall valency of the system. Best results were obtained with compound **2.45/PM26**, displaying an IC_{50} value in the low nM range. This result compares well with DC-SIGN inhibition activities described in the literature for constructs (polymers, dendrimers or gold nanoparticles) of much higher valency.[29] Remarkably, the two tests (SPR and infection studies) differ radically in the way DC-SIGN is presented to the antagonists: as a soluble tetramer in the SPR assay, embedded in cellular membranes in the infection assay. Therefore, the SPR assay will also include protein aggregation effects that are much less likely to occur in the infection studies. Moreover, the results of cellular assays may depend also on other mechanisms, such as receptor internalization after ligand binding.

These results demonstrate how a rational design can lead to molecules with high antagonism potency even at relatively low valency. The possibility of controlling their size and their shape can lead to fully characterized compounds that can also be tuned to match sterical and molecular features of their targets, thus being selective.

In conclusion, the combination of three elements in the design of **2.45/PM26,** i.e. an effective (and selective) monovalent ligand, a rigid core of appropriate length and two trivalent dendrons, allowed to maximize the DC-SIGN antagonist activity of the construct taking advantage of both chelation and local ligand density effects.

2.8 Experimental

General procedures

Chemicals were purchased by commercial sources and used without further purification, unless otherwise indicated. When anhydrous conditions were required, the reactions were performed under nitrogen atmosphere. Anhydrous solvents were purchased from Sigma-Aldrich® with a content of water ≤0.005 %. THF was dried over Na/benzophenone and freshly distilled prior to use. Thin-layer chromatography (TLC) was performed on Silica Gel 60 F254 plates (Merck) with UV detection (254 nm and 365 nm) or using appropriate developing solutions. Flash column chromatography was performed on silica gel 230-400 mesh (Merck), according with the procedure described in literature.[30] Automated flash chromatography was performed on a Biotage® Isolera™ Prime system. Final compounds were purified by size-exclusion chromatography using Sephadex LH-20 from GE Helthcare Life Science® and through reverse phase automated flash chromatography (C18) when required. NMR experiments were recorded on a Bruker AVANCE 400 MHz instrument at 298 K. Chemical shifts (δ) are reported in ppm downfield from TMS as internal standard, coupling constants (J) in Hz. The ^{1}H and ^{13}C-NMR resonances of compounds were assigned with the assistance of COSY and HSQC experiments. HSQC experiments were also used to assign the chemical shift of protons overlapping with the solvent signals. The numbering for protons and carbons in the NMR characterization are shown on the molecules. Mass spectra were recorded on ThermoFischer LCQ apparatus (ESI ionization), Apex II ICR FTMS (ESI ionization-HRMS), Waters Micromass Q-Tof (ESI ionization-HRMS), or Bruker Daltonics Microflex MALDI-TOF apparatus. Specific optical rotation values were measured using a Perkin-Elmer 241, at 589 nm in a 1 mL cell.

General procedure for the CuAAC reaction. In the optimized Copper(I)-catalyzed Azide-Alkyne Cycloaddition (CuAAC) procedure, starting materials and reagents were added to the reaction mixture as solids or as solutions in water or THF. Water was degassed by bubbling with nitrogen and THF was freshly distilled. The reagents were added to the reaction vessel in the following order: alkyne (1 eq., solid or THF), TBTA (0.2 eq., THF), CuSO$_4$·5H$_2$O (0.1 eq., H$_2$O), Sodium Ascorbate (0.4 eq., H$_2$O) and finally the azide monovalent ligand (1.1 eq. per each triple bond, solid

or water solution). The final concentration of multivalent scaffold was 3-15 mM in a 1:1 THF:H$_2$O mixture, depending on the solubility of the components and the products in water. When a concentration $\geq$ 10 mM in 1:1 THF:H$_2$O could be obtained, the reaction was stirred at room temperature for 12 -24 hours, under nitrogen atmosphere and protected from light. For less soluble mixtures, the reaction was performed at lower concentrations (tipically 3 mM) under microwave assisted conditions for 1-2 h at 60 °C. In both cases, the reaction was monitored by TLC and/or MALDI mass spectrometry (DHB or sinapinic acid matrix) until completion. In general, the formation of divalent compounds could be monitored by TLC (eluent: CH$_2$Cl$_2$:MeOH:H$_2$O in a ratio that depended on molecules polarity) while hexavalent compounds were best analysed by MALDI mass (DHB or sinapinic acid matrix). When intermediates were observed but the azide monovalent ligand was totally consumed, the latter was added together with additional 0.4 eq. of sodium ascorbate. The crude was purified by size exclusion chromatography on a Sephadex LH20 column (Ø 3 cm, H 55 cm; eluent: MeOH) as MeOH solution and by reverse phase chromatography (C18; eluent: water with a gradient of MeOH from 0 % to 100 %), when required. The metal scavenger Quadrasil™-MP[31] was used to remove copper salts either from the reaction mixtures before purification, or from a solution of the isolated final compound. In either case, the suspension was stirred for 10 min and the resin filtered off.

Synthesis of 1,4-diiodo-2,5-dimethoxybenzene, 2.14
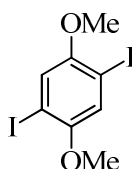
2.14

To a solution of H$_5$IO$_6$ (10 g, 42 mmol, 0.6 eq.) in 7 mL of MeOH, stirred for 10 min at room temperature, I$_2$ (11.5 g, 90.0 mmol, 1.25 eq.) was added; the resulting brownish solution was stirred for other 10 min. Finally, *p*-dimethoxybenzene (10 g, 72 mmol, 1 eq.) was slowly added. The reaction mixture was first stirred at room temperature for 40 min, then refluxed for 3 hours and finally stirred at room temperature overnight. The formation of a yellow precipitate was observed during time. TLS analysis (Hex:AcOEt 9:1) revealed that the reaction was complete. The crude was slowly dissolved in a Na$_2$S$_2$O$_5$ water solution (20g in 200 mL H$_2$O) and stirred at room temperature for 15 min. The precipitate was isolated using through Buckner funnel, washed with H$_2$O (50 mL) and MeOH (20 mL). The resulting 28 g of a not pure solid (**2.14**) were crystallized in *i*-propanol (200 mL), obtaining a not complete dissolution. The yellowish solid was recovered through

filtration (Buckner funnel) from the yellow solution, obtaining 20.9 g of pure product **2.14** (yield 74 %), with spectral data identical to those reported.[17,16].

^{1}H NMR (400 MHz, CDCl$_3$): δ 7.18 (s, 2H, Ar-<u>H</u>); 3.81 (s, 6H, OC<u>H</u>$_3$).

Synthesis of 2,5-diiodobenzene-1,4-diol, 2.15.
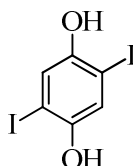
2.15

To a solution of **2.14** (10 g, 25.6 mmol, 1 eq.) in 250 mL of dry CH$_2$Cl$_2$ cooled at -78 °C, BBr$_3$ (1 M solution in MeOH, 77 mL, 3 eq.) was added dropwise under nitrogen atmosphere. The resulting brownish suspension was allowed to recover at room temperature; the reaction proceeded at RT and under nitrogen, overnight. TLS analysis (Hex:AcOEt 8:2) revealed that the reaction was complete. The reaction mixture was cooled to 0 °C and quenched with cold water (0 °C, 50 mL), leading to the formation of a white precipitated. The resulting mixture was diluted with AcOEt (500 mL) and washed with water (2 x 200 mL) and brine (2 x 200 mL); the organic phase was then dried over anhydrous sodium sulfate and concentrated, obtaining 10 g of not pure **2.15**. After a crystallization in CH$_2$Cl$_2$ (60 mL), the yellowish solid was isolated through bukner funnel from a brown solution, obtaining 7.8 g of pure product **2.15** (yield 84 %), with spectral data identical to those reported.[17,16].

^{1}H NMR (400 MHz, CDCl$_3$): δ 7.27 (s, 2H, Ar-<u>H</u>); 4.81 (bs, 2H, O<u>H</u>).

Synthesis of 2,2'-((((2,5-diiodo-1,4-phenylene)bis(oxy))bis(ethane-2,1-diyl))bis(oxy))diethanol, 2.16
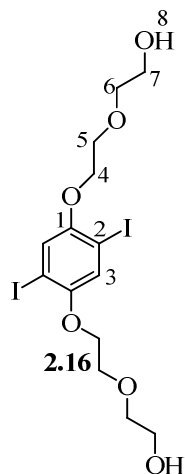
To a suspension of **2.15** (7.3 g, 20.2 mmol, 1 eq.) in 20 mL of dry DMF, 7.0 g of K_2CO_3 (7.0 g, 50.4 mmol, 2.5 eq.) were added, without obtaining complete dissolution; the resulting reddish suspension was stirred for 10 min at room temperature. Finally, 2-(2-Chloroethoxy)ethanol (8.5 mL, 70.7 mmol, 4 eq.) was added. The reaction mixture was stirred at RT for 20 min, than at 70 °C for 18 h, under nitrogen atmosphere. TLC analysis (Hex:AcOEt 3:7) revealed that the reaction was complete. The solvent was evaporated under reduced pressure, then the crude redissolved in AcOEt (500 mL) and washed with a water solution of $Na_2S_2O_5$ (10 g in 100 mL), water (3 x 100 mL) and brine (2 x 100 mL). A black solid remained insolubilized. The organic phase was dried over anhydrous sodium sulfate, then concentrated. The resulting brownish oil was purified through automated flash chromatography (silica, Hex with a gradient of AcOEt from 50 % to 90 %). 4.6 g of pure **2.16** were obtained (yield 44 %), with spectral data identical to those reported.[17,16].

^{1}H NMR (400 MHz, CDCl3): δ 7.22 (s, 2H, H$_3$), 4.11 – 4.07 (m, 4H, H$_4$), 3.88 – 3.84 (m, 4H, H$_5$), 3.76 – 3.72 (m, 4H, H$_7$), 3.71 – 3.76 (m, 4H, H$_6$), 1.67 (s, 2H, H$_8$).

Synthesis of 1,4-bis[2-(2-hydroxyethoxy)ethoxy]-2-[tris(1-methylethyl)silyl]ethynyl)-5-Iodobenzene, 2.18 and 1,4-bis[2-(2-hydroxyethoxy)ethoxy]-2,5-bis[tris(1-methylethyl)silyl]-ethynyl)benzene, TIPS-2.3.
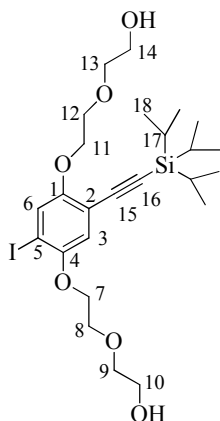
2.18
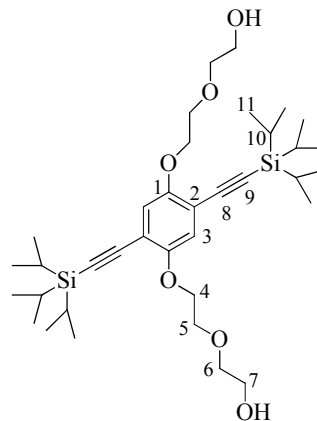
TIPS-2.3
TIPS-Rod1

2.16 (2.5 g, 4.63 mmol, 1 eq.), Pd(PPh$_3$)$_2$Cl$_2$ (130.0 mg, 0.185 mmol, 0.04 eq.), CuI (88.2 mg, 0.463 mmol, 0.1 equiv), and PPh$_3$ (121.3 mg, 0.463 mmol, 0.1 eq.) were placed into the reaction flask and dried under vacuum. Then reagents were dissolved in toluene (32 mL) and finally ethynyltriisopropylsilane (TIPS-acetylene, 1.56 mL, 6.94 mmol, 1.5 eq.) and Et$_3$N (6.5 mL) were added under nitrogen. The reaction was heated at 50 °C, under nitrogen atmosphere, overnight. TLC analysis (Hex:AcOEt 3:7) revealed that the reaction was complete (a trace of **2.16** was still observed). The reaction was then diluted with AcOEt and finally dried. The crude was purified through automated flash chromatography (Hex with a gradient of AcOEt from 5 % to 100 %), obtaining 905 mg of **2.18** (yield 33 %) and 1.26 g of **TIPS-2.3**, (yield 42 %). 470 mg of **2.16** were recovered, both with spectral data identical to those reported.[17,16]

Compound 2.18

^{1}H NMR (400 MHz, CDCl$_3$): δ 7.27 (s, 1H, H$_6$), 6.87 (s, 1H, H$_3$), 4.15 – 4.05 (m, 4H, H$_7$, H$_{11}$), 3.93 – 3.78 (m, 4H, H$_8$, H$_{12}$), 3.77 – 3.58 (m, 8H, H$_9$, H$_{10}$, H$_{13}$, H$_{14}$), 1.16 – 0.86 (m, 3H, H$_{17}$), 1.10 - 1.12 (m, 18H, H$_{18}$).

Compound TIPS-2.3

^{1}H NMR (400 MHz, CDCl$_3$): δ 6.89 (s, 2H, H$_3$), 4.15 – 4.09 (m, 4H, H$_4$), 3.85 – 3.80 (m, 4H, H$_5$), 3.74 – 3.67 (m, 4H, H$_7$), 3.66 – 3.59 (m, 4H, H$_6$), 1.29 – 0.91 (m, 6H, H$_{10}$), 1.10 – 1.12 (m, 38H, H$_{11}$).

Synthesis 1,4-bis[2-(2-hydroxyethoxy)ethoxy]-2,5-diethynylbenzene, 2.3
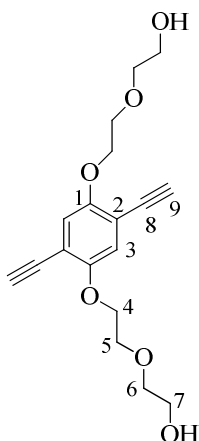
2.3

To a solution of **TIPS-2.3** (633 mg, 0.98 mmol, 1 eq.) in dry THF (3.3 mL), TBAF (1 M in THF, 2.0 mL, 1.96 mmol, 2 eq.) was added dropwise. The resulting solution was stirred for 45 min at room temperature, under nitrogen atmosphere. TLC analysis (CHCl$_3$:MeOH 95:5) revealed that the reaction was complete. The solvent was removed under reduced pressure and the crude was purified by automated flash chromatography (silica, CHCl$_3$ with gradient of MeOH from 0 to 5%) to afford 297 mg of pure product **2.3** (yield 91 %), with spectral data identical to those reported.[17,16]

Compound's characterization was identical to the one presented in Ref.[17,16]

¹H NMR (400 MHz, CDCl₃): δ 6.98 (2H, s, H$_3$), 4.16–4.10 (4H, m, H$_4$), 3.90–3.82 (4H, m, H$_5$), 3.76–3.70 (4H, m, H$_7$), 3.68–3.62 (4H, m, H$_6$), 3.34 (2H,s, H$_9$).

Synthesis of 2,2'-(((((2-(3-hydroxy-3-methylbut-1-yn-1-yl)-5-((triisopropylsilyl)ethynyl)-1,4-phenylene)bis(oxy))bis(ethane-2,1-diyl))bis(oxy))diethanol, 2.22

2.22
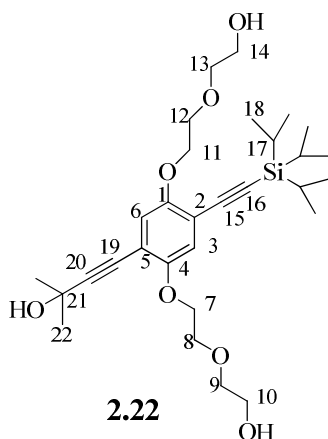
2.18 (50 mg, 84.4 μmol, 1 eq.), Pd(PPh$_3$)$_2$Cl$_2$ (3.0 mg, 4.22 μmol, 0.05 eq.) and CuI (1.0 mg, 4.22 μmol, 0.05 eq.) were dissolved in 260 μL of dry THF, under nitrogen atmosphere. DIPEA (34 μL) and finally 2-methylbut-3-yn-2-ol (10 μL, 0.1055 mmol, 1.25 eq.) were added. The reaction was stirred at room temperature and under nitrogen atmosphere overnight. TLC analysis (Hex:AcOEt 3:7) revealed that the reaction was complete. The reaction mixture was directly purified through flash chromatography (silica, Hex with a gradient of AcOEt from 50 % to 70 %), obtaining 39.3 mg of **2.22** as a yellowish oil (yield 85 %).

^{1}H NMR (400 MHz, CDCl$_3$): δ 6.90 (2s, 2H, H$_2$ and H$_5$), 4.15–3.95 (m, 4H, H$_7$, H$_{11}$), 3.95–3.88 (m, 2H, H$_8$) 3.86-3.82 (m, 2H, H$_{12}$), 3.78–3.75 (m, 2H, H$_9$), 3.70-3.74 (m, 4H, H$_{10}$, H$_{14}$), 3.62–3.67 (m, 2H, H$_{13}$) 2.55 (bs, 2H, OH), 1.59 (s, 6H, H$_{22}$), 1.18-1.10 (m, 21H, H$_{17}$, H$_{18}$).

^{13}C NMR (100 MHz, CDCl$_3$): 13C NMR (100 MHz, CD$_3$OD) δ 154.3, 154.2 (C$_4$, C$_1$); 117.8, 117.5 (C$_2$, C$_5$); 114.4, 113.9 (C$_3$, C$_6$); 102.8 (C$_{15}$); 100.71 (C$_{16}$); 97.08 (C$_{20}$); 77.80 (C$_{19}$); 72.8, 72.3 (C$_9$, C$_{13}$); 69.87, 69.86 (C$_8$, C$_{12}$); 69.3 (C$_7$, C$_{11}$); 65.1 (C$_{21}$); 62.1, 61.6 (C$_{10}$, C$_{14}$); 31.5 (C$_{22}$); 18.9 (C$_{18}$); 11.6 (C$_{17}$).

MS (ESI): calculated for [C$_{30}$H$_{48}$NaO$_7$Si]$^+$: 571.32; found: 571.5.

Synthesis of 2,2'-(((((2-ethynyl-5-((triisopropylsilyl)ethynyl)-1,4-phenylene)bis(oxy))bis(ethane-2,1-diyl))bis(oxy))diethanol, 2.21
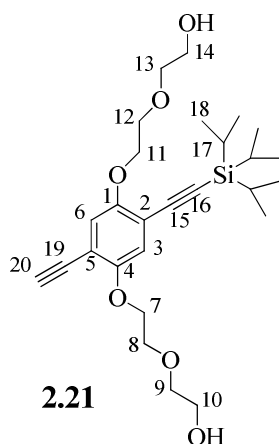
2.22 (27 mg, 0.05 mmol, 1 eq.) was dissolved in dry toluene (500 μL) and solid NaOH (7 mg, 0.18 mmol, 3.6 eq.) was added. The reaction was stirred for 6 h at 45 °C under nitrogen atmosphere and in the dark. TLC analysis (toluene:acetone 6:4) revealed that the reaction was not complete, but the side product **2.3** was starting forming. Therefore the mixture was diluted with CHCl$_3$:MeOH (97:3,

2 mL) and purified by flash chromatography (silica, Hex:AcOEt 4:6), obtaining 8.5 of pure product **2.21** (yield 35 %). 10 mg of **2.22** was also recovered.

¹H NMR (400 MHz, CDCl₃) δ 6.96, 6.95 (2s, 2H, H₂ and H₅), 4.25–4.10 (m, 4H, H₇, H₁₁), 3.90–3.80 (m, 4H, H₈, H₁₂), 3.75–3.60 (m, 8H, H₉, H₁₀, H₁₃, H₁₄), 3.35 (s, 1H, H₂₀), 2.05 (bs, 2H, OH) 1.45–1.00 (m, 21H, H₁₇, H₁₈).

¹³C NMR (100 MHz, CDCl₃): δ 154.3, 154.2 (C₄, C₁); 118.5, 118.3 (C₂, C₅); 115.4, 113.3 (C₃, C₆); 102.6 (C₁₅); 97.7 (C₁₆); 83.1, 80.0 (C₁₉, C₂₀); 72.9 (C₉, C₁₃); 69.9, 69.8, 69.7, 69.4 (C₇, C₈, C₁₁, C₁₂); 62.2 (C₁₀, C₁₄); 19.4 (C₁₈); 11.6 (C₁₇).

MS (ESI) calculated for $[C_{27}H_{42}NaO_6Si]^+$: 513.7; found: 513.4.

Synthesis of TIPS-2.4/TIPS-Rod2

TIPS-2.4
TIPS-Rod2
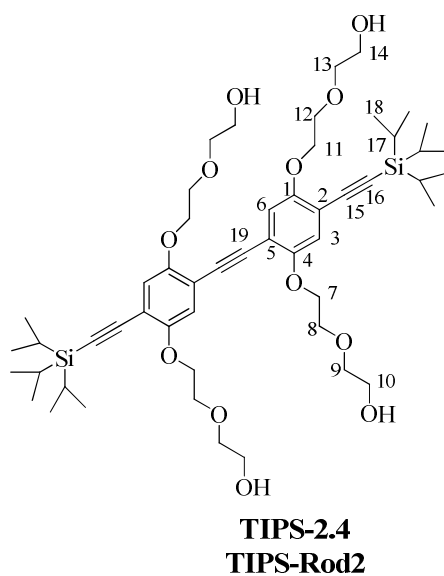
Compound **2.21** (24.2 mg, 0.05 mmol, 1 eq.), PdCl₂(PPh₃)₂ (2 mg, 0.003 mmol, 0.05 equiv) and CuI (1 mg, 0.005 mmol, 0.1 equiv) were dissolved in dry THF (245 μL) under nitrogen atmosphere. DIPEA (20 μL 0.11 mmol, 2 eq.) was added; finally **2.18** (36.7 mg, 0.061 mmol, 1.25 eq.) dissolved in THF (145 μL) and washed with remaining THF (100 μL) was added. The reaction mixture was stirred for 3 h at room temperature under nitrogen and in the dark. TLC analysis (CHCl₃:MeOH 10:0.5) revealed that the coupling was complete. The solvent was removed under reduced pressure and the resulting crude was purified by automated flash chromatography (silica, Hex with a gradient of AcOEt from 0 % to 10 %), to afford 38 mg of pure **TIPS-2.4** as a yellowish solid (yield 81 %). 12 mg of **2.21** were recovered.

¹H NMR (400 MHz, CD₃OD): δ 7.11 (2H, s, H$_2$), 7.05 (2H, s, H$_5$), 4.31–4.12 (8H, m, H$_7$, H$_{11}$), 3.95–3.80 (8H, m, H$_8$, H$_{12}$), 3.74–3.60 (16H, m, H$_9$, H$_{10}$, H$_{13}$, H$_{14}$), 1.45-1.00 (42H, m, H$_{17}$, H$_{18}$).

¹³C NMR (100 MHz, CD3OD, HSQC): δ 119.1, 118.0 (C$_5$, C$_2$); 73.79, 73.76 (C$_9$, C$_{13}$); 70.59, 70.54 (C$_7$, C$_8$, C$_{11}$, C$_{12}$); 62.01, 61.96 (C$_{10}$, C$_{14}$); 18.83 (C$_{18}$); 12.20 (C$_{17}$).

MS (ESI): calculated for [C$_{52}$H$_{82}$NaO$_{12}$Si$_2$]$^+$: 977.53; found: 978.0.

Synthesis of TIPS-2.5/TIPS-Rod3
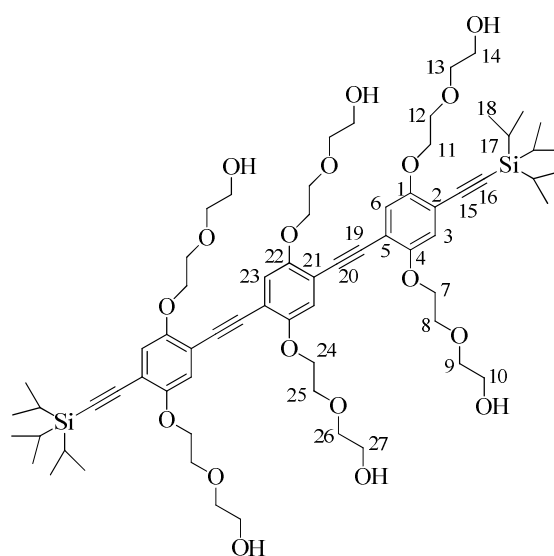
TIPS-2.5
TIPS-Rod3

2.3 (26 mg, 0.077 mmol, 1 eq.), Pd(PPh$_2$)$_2$C$_{l2}$, (2.7 mg, 0.004 mmol, 0.05 eq.) and CuI (2.8 mg, 0.008 mmol, 0.1 equiv) were dissolved in dry THF (350 μL) under nitrogen atmosphere. DIPEA (30.8 μL 0.177 mmol, 2.3 eq.) was added; finally **2.18** (100.4 mg, 0.169 mmol, 2.2 eq.) dissolved in THF (300 μL) and washed with remaining THF (120 μL) was added. The reaction was stirred at room temperature for 3 h, under nitrogen atmosphere and in the dark. TLC analysis (CH$_2$Cl$_2$:MeOH 9:1) revealed that the coupling was complete. The reaction mixture was concentrated under reduce pressure and purified through automated flash chromatography (silica, CHCl$_3$ with gradient of MeOH from 1 % to 20 %), affording 47.7 mg of pure product **TIPS-2.5** as yellow solid (yield 50 %), with spectral data identical to those reported.[17,16].

¹H NMR (400 MHz, CD₃OD): δ 7.16 (s, 2H, H$_2$), 7.12 (s, 2H, H$_5$), 7.05 (s, 2H, H$_{23}$), 4.31–4.12

(m, 12H, H$_7$, H$_{11}$, H$_{24}$), 3.97–3.80 (m, 12H, H$_8$, H$_{12}$, H$_{25}$), 3.76–3.56 (m, 24H, H$_9$, H$_{10}$, H$_{13}$, H$_{14}$, H$_{26}$, H$_{27}$), 1.35–0.98 (6H, m, H$_{17}$), 1.16–1.18 (m, 36H, H$_{18}$).

Synthesis of 3-(prop-2-yn-1-yloxy)-2,2-bis((prop-2-yn-1-yloxy)methyl)propan-1-ol, 2.26
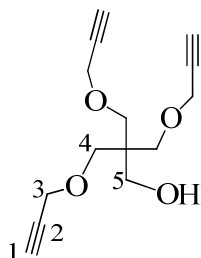
2.26

To a solution of pentaeritritol (0.5 g, 3.67 mmol, 1 eq.) in dry DMF (15 mL), sodium hydride (60 %, 0.48 g, 12.12 mmol, 3.3 eq.) was slowly added under nitrogen atmosphere at 0 ºC; not complete dissolution was obtained. The mixture was stirred at 0 ºC for 30 min, under flushing nitrogen. Then propargyl bromide (80% in toluene, 1.3 mL, 12.12 mmol effective, 3.3 eq.) was added. The reaction mixture was recovered at room temperature, then stirred under nitrogen overnight. TLC analysis (Hex:AcOEt 8:2) revealed that the reaction was complete. Reaction mixture was cooled at 0 °C and cold water (20 mL, 0 °C) was added. The product was extracted using Et$_2$O (3 x 50 mL). The resulting organic phase was dried over anhydrous sodium sulfate and concentrated. The crude was purified through flash chromatography (Hex with a gradient of AcOEt from 10 % to 30 %), obtaining 436 mg of pure product **2.26** (yield 47 %), with spectral data identical to those reported.[17,12]

^{1}H NMR (400 MHz, CDCl$_3$): δ = 4.14 (d, 6H, H$_2$, J_{3-1} = 2.3 Hz), 3.69 (s, 2H, H$_4$), 3.57 (s, 6H, H$_3$), 2.24 (t, 3H, H$_1$, J_{3-1} = 2.3 Hz).

Synthesis of 3-(3-(2-(2-chloroethoxy)ethoxy)-2,2-bis((prop-2-yn-1-yloxy)methyl)propoxy)prop-1-yne, 2.27

2.27
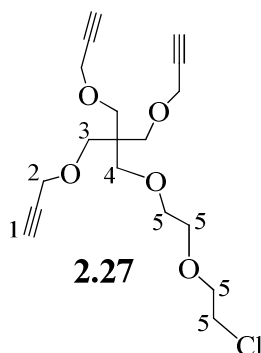
To a solution of **2.26** (434 mg, 1.73 mmol, 1 eq.) in bis(2-cloroethyl)eter (2.1 mL), (nBu)$_4$NHSO$_4$ (1.2 mg, 3.46 mmol, 2.1 eq.) and NaOH (aq. 50%, 2.6 mL) were slowly added at room temperature. Complete dissolution was not obtained. The reaction mixture was vigorously stirred at 45 ºC for 18 h, under nitrogen atmosphere. TLC analysis (Hex:AcOEt 6:4) revealed that the reaction was complete. CH$_2$Cl$_2$ (50 mL) and water (80 mL) were added; the resulting organic phase was separated and washed with distilled water (2 x 50 mL) and brine (50 mL), dried over anhydrous sodium sulphate and finally concentrated under reduced pressure. The crude was purified by flash chromatography (silica, Hex with a gradient of AcOEt from 5 % to 30 %), affording 170 mg of pure product **2.27** as a colorless oil (yield 30 %), , with spectral data identical to those reported. [17,12]

^{1}H NMR (300 MHz, CDCl$_3$): δ = 4.05 (d, 6H, H$_2$, J_{3-1} = 2.4 Hz), 3.70 (t, 2H, H$_8$, J_{7-8} = 5.9 Hz), 3.61 – 3.50 (m, 6H, H$_5$, H$_6$, H$_7$), 3.46 (s, 6H, H$_3$), 3.40 (s, 2H, H$_4$), 2.33 (t, 3H, H$_1$, J_{3-1} = 2.4 Hz).

Synthesis of trivalent glycodendron, 2.28
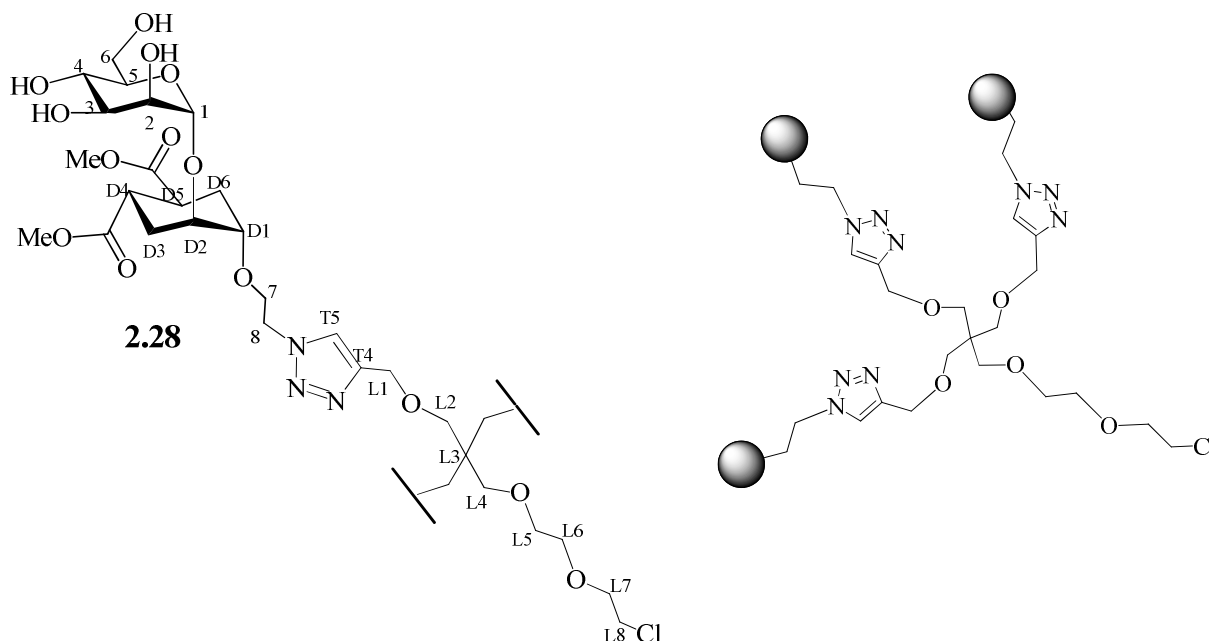
To scaffold (**2.27**) (40.4 mg, 113 µmol, 1 eq.) dissolved in THF (2.55 mL) under inert atmosphere at room temperature, reagents were added as solutions in the following order: TBTA in THF (12.0 mg, 22.6 µmol, 0.2 eq., in 0.95 mL), $CuSO_4 \cdot 5H_2O$ in water (2.8 mg, 11.3 µmol, 0.1 eq., in 0.56 mL) and Sodium Ascorbate in water (9.0 mg, 45.2 µmol, 0.4 eq., in 0.83 mL). The reaction mixture was stirred under inert atmosphere, at RT and in the dark for 10 min, then **1.7** in water was added (189.1 mg, 408 µmol, 3.6 eq., 2.5 mL). The THF and water volumes were adjusted to 4.4 mL each and the mixture was stirred for 18 h. TLC analysis ($CHCl_3$:MeOH:H_2O 8:2:0.5) revealed that the reaction was complete. Quadrasil™-MP (S/Cu 2:1, 15 mg) was added to the reaction mixture, which was stirred for 10 min, and then filtered off. The crude was dried, then redissolved in MeOH and purified by size exclusion chromatography on a Sephadex LH-20 (MeOH) column to give 186 mg of **2.28** as a white solid (yield 94 %), , with spectral data identical to those reported.[17,12].

^{1}H NMR (400 MHz, CD$_3$OD): δ 7.98 (s, 3H, H_{T5}), 4.90 (bs, 3H, H_1), 4.60 (t, 6H, H_8, J_{8-7} = 5 Hz), 4.55 (s, 6H, H_{L1}), 4.00 - 3.79 (m, 15H, H_2, H_{6a}, H_{D2}, H_7), 3.75 - 3.45 (m, 37H, H_{6b}, H_{D1}, H_3, H_{OMe}, H_4, H_5, H_{L5}, H_{L6}, H_{L7}, H_{L8}), 3.48 (s, 6H, H_{L2}), 3.43 (s, 2H, H_{L4}), 2.83 – 2.63 (m, 6H, H_{D4}, H_{D5}), 2.04-1.92 (m, 6H, H_{D3eq}, H_{D6eq}), 1.78 - 1.51 (m, 6H, H_{D3ax}, H_{D6ax}).

Synthesis of trivalent glycodendron, 2.21
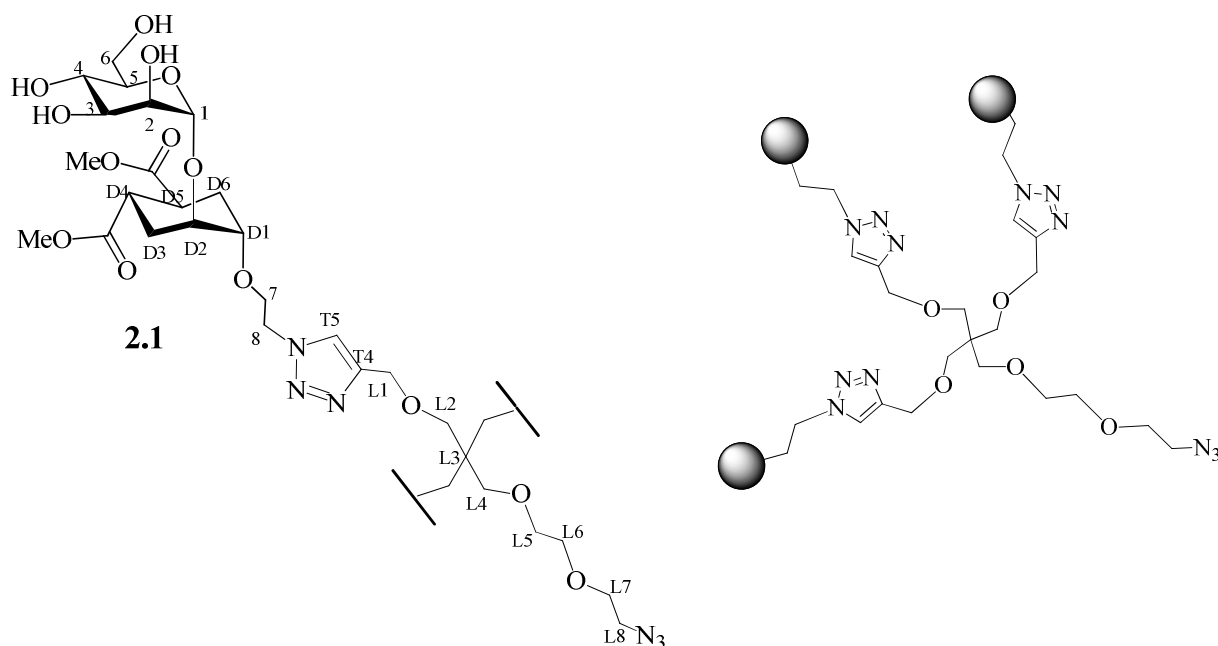
To a solution of **2.28** (123.6 mg, 0.07 mmol, 1 eq.) in DMF (1 mL), sodium azide (37 mg, 0.57 mmol, 8 eq.) was added. The reaction was stirred at 60 ºC for 3 days. A MALDI mass analysis (DHB matrix) revealed that the reaction was complete. The solvent was removed under reduced pressure and the resulting crude was purified by size exclusion chromatography (Sephadex LH20, MeOH) to afford 93.2 mg of pure product **2.1** as a white solid (yield 76 %), with spectral data identical to those reported.[17,12]

^{1}H NMR (400 MHz, CD3OD): δ 7.97 (s, 3H, H_{T5}), 4.90 (bs, 3H, H_1), 4.60 (t, 6H, H_8, J_{8-7} = 5 Hz), 4.55 (s, 6H, H_{L1}), 4.01 - 3.80 (m, 15H, H_2, H_{6a}, H_{D2}, H_7), 3.72 - 3.49 (m, 35H, H_{6b}, H_{D1}, H_3, H_{OMe}, H_4, H_5, H_{L5}, H_{L6}, H_{L7}), 3.48 (s, 6H, H_{L2}), 3.44 (s, 2H, H_{L4}), 3.40 – 3.32 (m, 2H, H_{L8}), 2.84-2.61 (m, 6H, $_{D4}$, H_{D5}), 2.05 – 1.95 (m, 6H, H_{D3eq}, H_{D6eq}), 1.77 - 1.46 (m, 6H, H_{D3ax}, H_{D6ax}).

Synthesis of trivalent glycodendron, 2.29
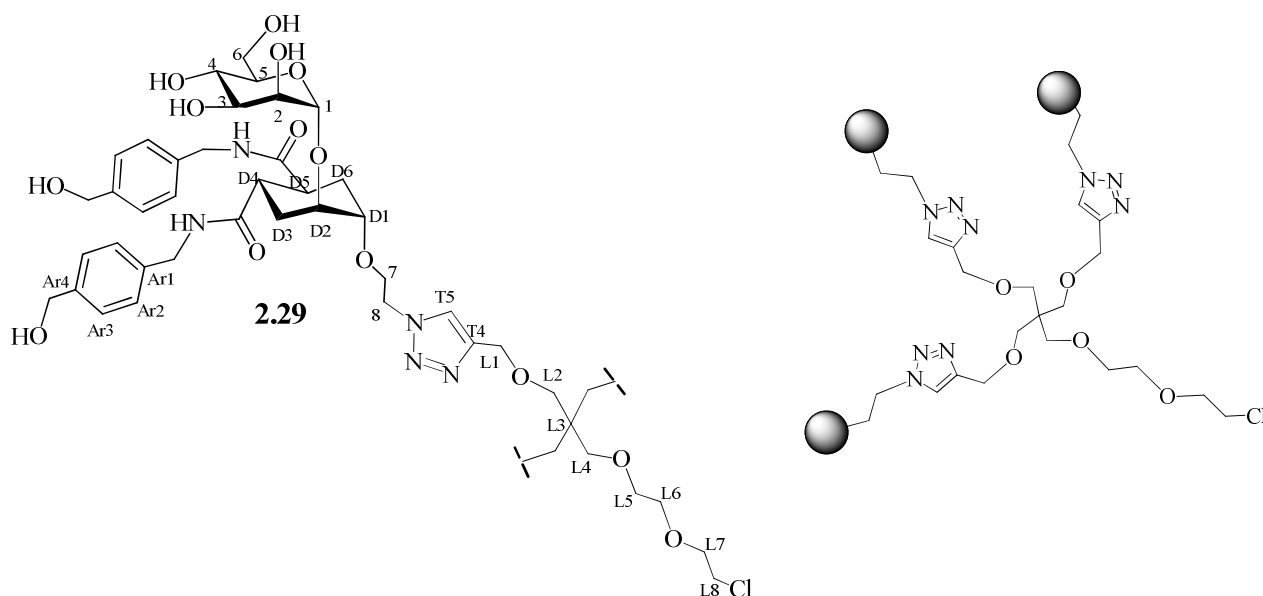
To scaffold (**2.27**) (32.1 mg, 89.9 µmol, 1 eq.) dissolved in THF (2.55 mL) under inert atmosphere at RT, reagents were added as solutions in the following order: TBTA in THF (9.5 mg, 18.0 µmol, 0.2 eq., in 0.96 mL), $CuSO_4 \cdot 5H_2O$ in water (2.2 mg, 9.0 µmol, 0.1 eq., in 0.24 mL) and Sodium Ascorbate in water (7.1 mg, 36.0 µmol, 0.4 eq., in 0.35 mL). The reaction mixture was stirred under inert atmosphere, at room temperature and in the dark for 10 min, then **1.9** in water was added (218 mg, 323.6 µmol, 3.6 eq., 1 mL). The THF and water volumes were adjusted to 2 mL each and the mixture was stirred for 18 h. MALDI mass (DHB matrix) revealed that the reaction was complete. Quadrasil™-MP (S/Cu 2:5, 15 mg) was added to the reaction mixture, which was stirred for 10 min, and then filtered off. The crude was dried, then redissolved in MeOH and purified by size exclusion chromatography on a Sephadex LH-20 (MeOH) column to give 110 mg of **2.29** as a white solid (yield 50 %), , with spectral data identical to those reported.[17,12].

^{1}H NMR (400 MHz, CD$_3$OD): δ = 7.98 (s, 3H, H_{T5}); 7.28 – 7.16 (m, 24H, H_{Ar2}, H_{Ar3}); 4.89 (br s, 3H, H_1); 4.58 – 4.50 (m, 6H, H_8); 4.55 (s, 12H, $\underline{CH_2}OH$); 4.48 (s, 6H, H_{L1}); 4.28 (s, 6H, $\underline{CH_2}NH$); 4.26 (s, 6H, $\underline{CH_2}NH$); 3.99 - 3.80 (m, 15H, H2, H_{6a}, H_{D2}, H_7); 3.73 - 3.61 (m, 11H, H_{6b}, H_{D1}, H_3, H_{L8}); 3.61-3.44 (m, 12H, H_4, H_5, H_{L5}, H_{L6}, H_{L7}), 3.42 (bs, 6H, H_{L2}), 3.39 (bs, 2H, H_{L4}), 2.90 – 2.76 (m, 6H, H_{D4}, H_{D5}), 1.96 – 1.68 (m, 12H, H_{D3}, H_{D6}).

Synthesis of trivalent glycodendron, 2.2

To a solution of **2.29** (140.4 mg, 0.06 mmol, 1 eq.) in DMF (0.8 mL), sodium azide (30.7 mg, 0.47 mmol, 8 eq.) was added. The reaction was stirred at 60 °C for 3 days. A MALDI mass analysis (DHB matrix) revealed that the reaction was complete. The solvent was removed under reduced pressure and the resulting crude was purified by size exclusion chromatography (Sephadex LH20, MeOH) to afford 130.4 mg of pure product **2.2** as a white solid (yield 93 %), with spectral data identical to those reported.[17,12]
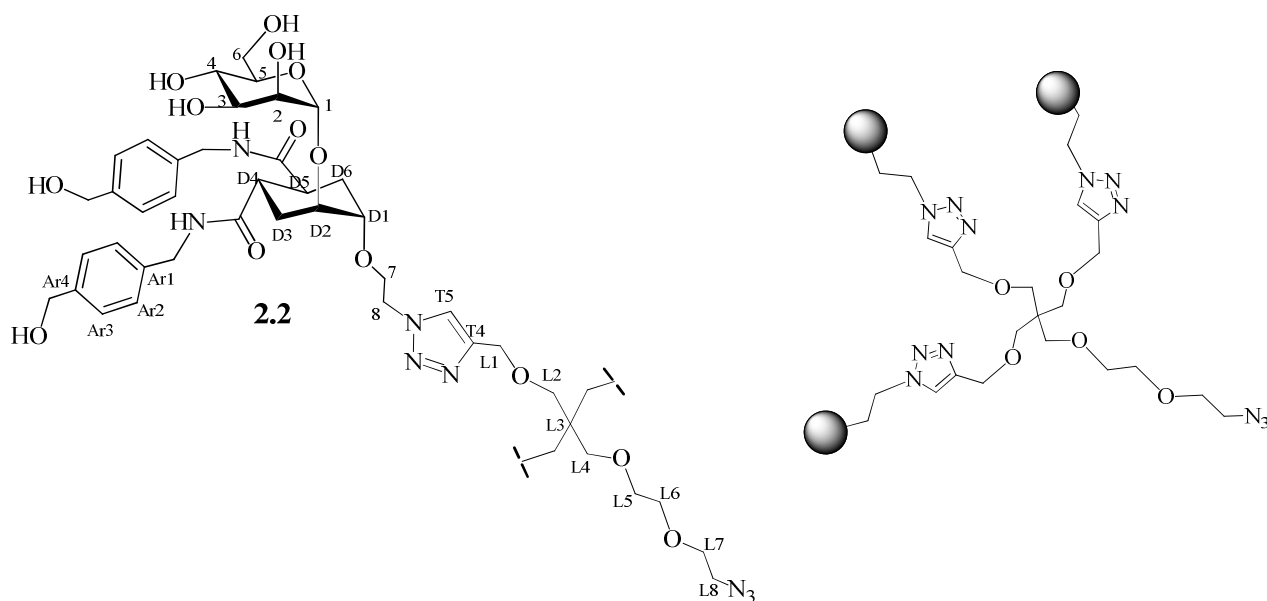
^{1}H NMR (300 MHz, CDCl3): δ = 7.98 (s, 3H, H_{T5}), 7.30 – 7.13 (m, 24H, H_{Ar2}, H_{Ar3}), 4.89 (bs, 3H, H_1), 4.60 – 4.50 (m, 6H, H_8), 4.55 (s, 12H, $\underline{C}H_2OH$), 4.48 (s, 6H, H_{L1}), 4.28 (s, 6H, $\underline{C}H_2NH$), 4.26 (s, 6H, $\underline{C}H_2NH$), 3.97 - 3.80 (m, 15H, H_2, H_{6a}, H_{D2}, H_7), 3.73 - 3.62 (m, 9H, H_{6b}, H_{D1}, H_3), 3.62 - 3.46 (m, 14H, H_4, H_5, H_{L5}, H_{L6}, H_{L7}, H_{L8}), 3.43 (bs, 6H, H_{L2}), 3.40 (bs, 2H, H_{L4}), 2.90 – 2.76 (m, 6H, H_{D4}, H_{D5}), 1.96 – 1.69 (m, 12H, H_{D3}, H_{D6}).
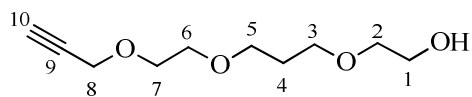
Synthesis of 2-(3-(2-(prop-2-yn-1-yloxy)ethoxy)propoxy)ethanol, 2.31

2.31

A stirred solution of 3,7-dioxa-1,9-nonanediol (130.9 mg, 0.8 mmol, 1 eq.) in dry DMF (3.5 mL) was slowly treated with NaH (60% in oil, 35.0 mg, 0.9 mmol, 1.1 eq.) at 0 °C under nitrogen atmosphere. After 30 min, propargyl bromide (80% in toluene, 94.5 μL, 0.9 mmol, 1.1 eq.) was added. The reaction mixture was left to warm to RT and stirred under nitrogen overnight. The reaction was quenched by slow addition of iced water and then concentrated under reduced pressure. The crude was purified by flash chromatography (Hex:AcOEt 3:7) affording 81 mg of pure **2.31** as a yellow oil (yield 50 %). Also 26 mg of the bis-propargyl ether byproduct was isolated as yellow oil (yield 13 %).

^{1}H NMR (400 MHz, CD$_3$OD): δ 4.19 (d, J = 2.4 Hz, 2H, H$_8$); 3.68 – 3.63 (m, 4H, H$_7$, H$_1$); 3.61 – 3.60 (m, 2H, H$_6$); 3.59 – 3.54 (m, 4H, H$_3$, H$_5$); 3.52 – 3.50 (m, 2H, H$_2$); 2.85 (t, J = 2.4 Hz, 1H, H$_{10}$); 1.84 (tt, J = 6.4 Hz, 1H, H$_4$).

^{13}C NMR (100 MHz, CD$_3$OD): δ 75.97 (C$_{10}$, C$_9$); 73.31 (C$_2$); 71.02 (C$_6$); 70.06 (C$_7$); 69.11 (C$_5$, C$_3$); 62.22 (C$_1$); 59.08 (C$_8$); 31.05 (C$_4$).

MS (ESI-HRMS): calculated for [C$_{10}$H$_{18}$O$_4$Na]$^+$: 225.10973; found = 225.10959.

Synthesis of 2-(3-(2-(prop-2-yn-1-yloxy)ethoxy)propoxy)ethyl 4-methylbenzenesulfonate, 2.32
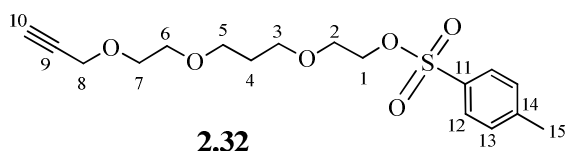
2.32

To a stirred solution of **2.31** (72.4 mg, 0.4 mmol, 1 eq.) in dry CH$_2$Cl$_2$ (500 μL), TsCl was added (102.4 mg, 0.5 mmol, 1.5 eq.), then pyridine (57.7 μL, 0.7 mmol, 2 eq.) was added at 0 °C under nitrogen atmosphere. The reaction mixture was left to warm to RT and stirred under nitrogen overnight. TLC analysis (Hex:AcOEt 3:7) revealed that the reaction was complete. CH$_2$Cl$_2$ (10 mL) was added and the mixture was washed with water (10 mL), HCl 1 M (10 mL), water (10 mL), NaHCO$_3$ sat. sol. (10 mL) and water again (10 mL). The organic phase was finally dried over anhydrous sodium sulfate and concentrated under reduced pressure. The crude was purified by flash

chromatography (Hex:AcOEt 65:35), affording 88 mg of pure compound **2.32** as a yellow oil (yield 69 %).

^{1}H NMR (400 MHz, CD$_3$OD): δ 7.80 (d, J = 8.3 Hz, 2H, H$_{12}$); 7.45 (d, J = 8.3 Hz, 2H, H$_{13}$); 4.18 (d, J = 2.4 Hz, 2H, H$_8$); 4.15 – 4.13 (m, 2H, H$_1$); 3.66 – 3.64 (m, 2H, H$_7$); 3.60 – 3.56 (m, 4H, H$_2$, H$_6$); 3.51 – 3.43 (m, 4H, H$_3$, H$_5$); 2.85 (t, J = 2.4 Hz, 1H, H$_{10}$); 2.46 (s, 3H, H$_{15}$); 1.74 (tt, J = 6.3 Hz, 1H, H$_4$).

^{13}C NMR (100 MHz, CD$_3$OD): δ 146.4 (C$_{11}$); 134.4 (C$_{14}$); 131.0 (C$_{13}$); 129.0 (C$_{12}$); 80.3 (C$_{10}$); 75.7 (C$_9$); 71.0 (C$_2$); 70.0 (C$_1$); 68.9 (C$_7$); 68.7 (C$_6$); 59.1 (C$_3$, C$_6$); 30.6 (C$_4$); 21.5 (C$_{15}$).

MS (ESI-HRMS): calculated for [C$_{17}$H$_{24}$O$_6$S$_1$Na]$^+$: 379.11858; found: 379.11815.

Synthesis of compound 2.33
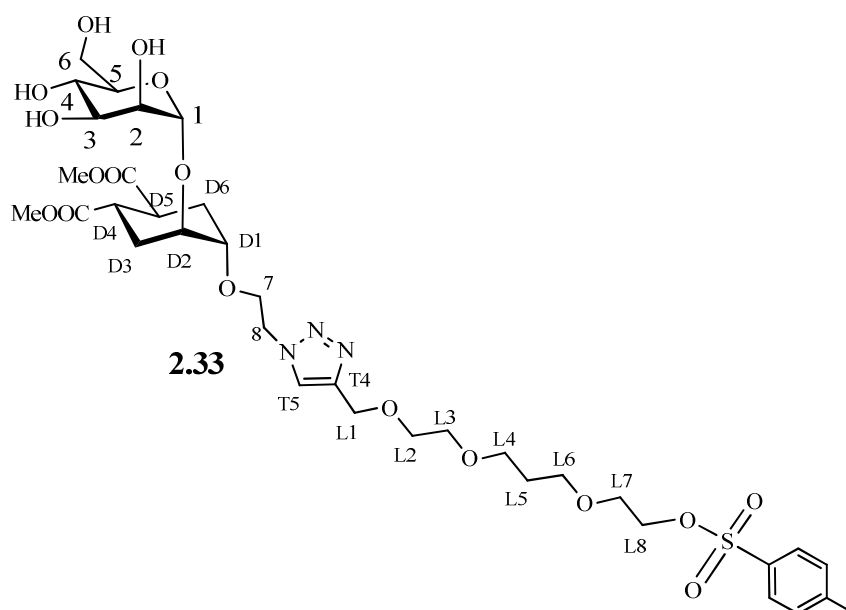
Reagents were added in the reaction vessel as solids or solutions in the following order: linker **2.32** as a solid (60.7 mg, 170 µmol, 1 eq.), TBTA in THF (18.0 mg, 34 µmol, 0.2 eq., 960 µL of THF), CuSO$_4$·5H$_2$O in H$_2$O (4.2 mg, 17 µmol, 0.1 eq., 226 µL of H$_2$O) and Sodium Ascorbate in H$_2$O (13.5 mg, 68 µmol, 0.4 eq., 530 µL of H$_2$O). The reaction mixture was stirred at room temperature, under nitrogen atmosphere and in the dark for 10 minutes. Then **1.7** (87.1 mg, 190 µmol, 1.1 eq.) was added as a solid. THF and H$_2$O volumes were adjusted to 4 mL each. The reaction was stirred at room temperature, under nitrogen atmosphere and in the dark. TLC analysis (Hex:AcOEt 7:3) showed total conversion of linker **2.32**; TLC (AcOEt:MeOH:H$_2$O 85:15:2.5) showed the formation of a single new product. Quadrasil™-MP (S/Cu 2:1, 20 mg) was added to the reaction mixture,

which was stirred for 10 minutes, and then filtered off. The solvent was removed under reduced pressure and the resulting mixture redissolved in MeOH and purified by size exclusion chromatography (Sephadex LH-20, MeOH), obtaining 126 mg of pure **2.33** as a colourless oil (yield 91 %).

¹H NMR (400 MHz, CD₃OD): δ 8.00 (s, 1H, H_{T5}); 7.79 (d, 2H, H_{OTs}, J = 8.3 Hz); 7.44 (d, 2H, H_{OTs}, J = 8.3 Hz); 4.89 (bs, 1H, H_1); 4.65 (s, 2H, H_{L1}); 4.60 (t, 2H, H_8, J = 5.0 Hz); 4.16 – 4.11 (m, 2H, H_{L8}); 3.98 – 3.85 (m, 4H, H_{6a}, H_{D2}, H_7); 3.82 – 3.80 (m, 1H, H_2); 3.70 – 3.61 (m, 11H, H_3, H_{6b}, H_{D1}, H_{L7}, H_{COOMe}); 3.61 – 3.44 (m, 10H, H_4, H_{L2}, H_{L3}, H_{L4}, H_{L6}, H_5); 2.82 – 2.62 (m, 1H, H_{D4}, H_{D5}); 2.45 (s, 3H, CH_3Ts), 2.02 – 1.94 (m, 2H, H_{D3eq}, H_{D6eq}); 1.79 – 1.66 (m, 3H, H_{L5}, H_{D3ax} or H_{D6ax}); 1.61 – 1.49 (m, 1H, H_{D3ax} or H_{D6ax}).

¹³C NMR (100 MHz, CD₃OD): δ 176.7 (COOMe); 146.5 ($C_{quatOTs}$); 145.9 (C_{T4}); 134.5 ($C_{quatOTs}$); 131.1 (C_{OTs}); 128.8 (C_{OTs}); 126. 1 (C_{T5}); 100.5 (C_1); 75.7 (C_5); 75.6 (C_3); 72.5 (C_{D1}); 72.4 (C_2); 72.1 (C_{D2}); 71.2 (C_{L2}, C_{L3}); 71. 0 (C_{L8}); 70.7 (C_{L7}); 69.4, 68.94, 68.91 (C_{L4}, C_{L6}); 68.6 (C_4); 68.4 (C_7); 65.0 (C_{L1}); 63.1 (C_6); 52.5 (COO**M**e); 51.7 (C_8); 40.1 (C_{D4}, C_{D5}); 31.0 (C_{L5}); 28.8 (C_{D3} or C_{D6}); 28.4 (C_{D3} or C_{D6}); 21.6 (**C**H₃Ts).

MS (ESI-HRMS): calculated for $[C_{35}H_{53}N_3O_{17}Na]^+$: 842.29879; found: 842.29713.

$[\alpha]_D{}^{25}$: 26.5 (c = 0.34, MeOH).

Synthesis of elongated monovalent ligand, 2.6

To a solution of **2.33** (117 mg, 140 µmol, 1 eq.) in DMF dry (1.5 mL), NaN₃ (37 mg, 570 µmol, 4 eq.) and Bu₄NI (6.0 mg, 16 µmol, 0.1 eq.) were added. The reaction mixture was stirred at 65 °C

under nitrogen for 20 h. ESI-MS analysis showed total conversion of the starting material. The solvent was removed under reduced pressure and the resulting crude was redissolved in MeOH and purified by size exclusion chromatography (Sephadex LH-20, MeOH), obtaining 89 mg of **2.6** as a white foam (yield 88 %), still cont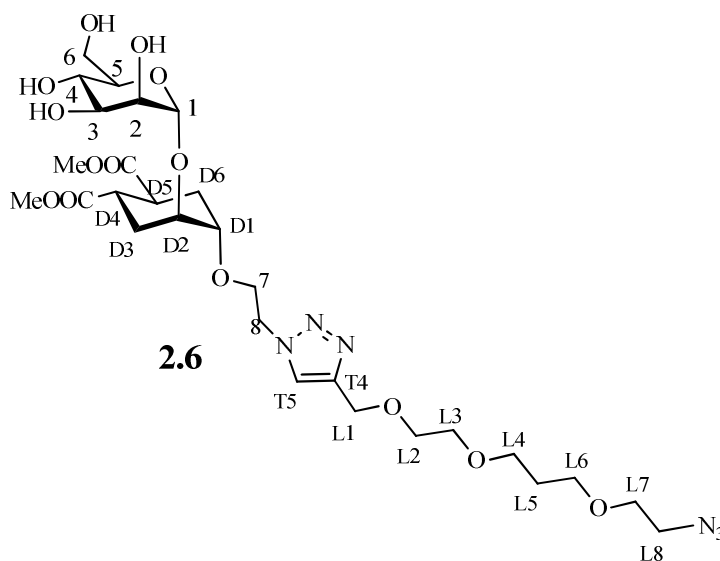aining 3 % (w/w, as measured by NMR integration) of a tosylate salt. Compound **2.6** was used for conjugation to the rods without further purifications.

^{1}H NMR (400 MHz, CD$_3$OD): δ 8.00 (s, 1H, H$_{T5}$); 4.89 (bs, 1H, H$_1$); 4.65 (s, 2H, H$_{L1}$); 4.60 (t, 2H, H$_8$, J = 5.1 Hz); 3.99 – 3.82 (m, 4H, H$_{6a}$, H$_{D2}$, H$_7$); 3.81 (dd, 1.7 Hz, 1H, H$_2$, J = 3.2); 3.70 – 3.60 (m, 15H, H$_3$, H$_{6b}$, COO$\underline{\text{Me}}$, H$_{D1}$, H$_{L2}$, H$_{L3}$, H$_{L7}$); 3.60 – 3.54 (m, 5H, H$_4$, H$_{L4}$, H$_{L6}$); 3.54 – 3.45 (m, 1H, H$_5$); 3.37 – 3.32 (m, 2H, H$_{L8}$); 2.82 – 2.64 (m, 2H, H$_{D4}$, H$_{D5}$); 2.02 – 1.95 (m, 2H, H$_{D3eq}$, H$_{D6eq}$); 1.84 (tt, 2H, H$_{L5}$, J = 6.3 Hz,); 1.77 – 1.49 (m, 2H, H$_{D3ax}$, H$_{D6ax}$).

^{13}C NMR (100 MHz, CD$_3$OD): δ 176.8; 176.7 ($\underline{\text{C}}$OOMe); 146.0 (C$_{T5}$); 100.5 (C$_1$); 75.7 (C$_5$); 75.6 (C$_3$); 72.5 (C$_{D1}$); 72.4 (C$_2$); 72.1 (C$_{D2}$); 71.2, 70.9, 70.7 (C$_{L2}$, C$_{L3}$, C$_{L7}$); 68.96, 68.90 (C$_{L4}$, C$_{L6}$); 68.6 (C$_4$); 68.4 (C$_7$); 65.0 (C$_{L1}$); 63.1 (C$_6$); 52.4 ($\underline{\text{C}}$OOMe); 51.8 (C$_8$); 51.6 (C$_{L8}$); 40.2, 40.1 (C$_{D4}$, C$_{D5}$); 31.1 (C$_{L5}$); 28.9 (C$_{D3}$, or C$_{D6}$); 28.2 (C$_{D3}$, or C$_{D6}$).

MS (ESI): calculated for [C$_{28}$H$_{46}$N$_6$O$_4$Na]$^+$: 713.7; found: 713.4.

Synthesis of compound 2.34
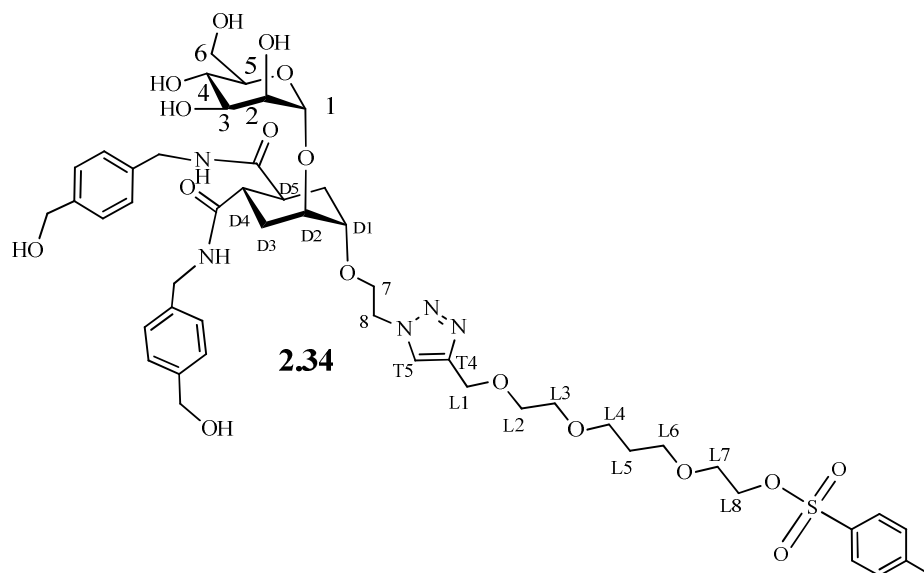
Reagents were added in the reaction vessel as solids or solutions in the following order: linker **2.32** as solid (55.8 mg, 160 µmol, 1 eq.), TBTA in THF (16.7 mg, 31 µmol, 0.2 eq., 960 µL of THF), CuSO$_4$·5H$_2$O in H$_2$O (3.9 mg, 16 µmol, 0.1 eq., 710 µL of H$_2$O) and Sodium Ascorbate in H$_2$O (12.4 mg, 63 µmol, 0.4 eq, 880 µL of H$_2$O). The reaction mixture was stirred at room temperature,

under nitrogen atmosphere and in dark for 10 minutes. Then **1.9** (115.9 mg, 170 µmol, 1.1 eq.) was added as solid. THF and H_2O volumes were adjusted to 4 mL each. The reaction continued overnight, stirred at room temperature, under nitrogen atmosphere and in dark. TLC analysis (Hex:AcOEt 7:3) showed total conversion of linker **2.32**; TLC (CHCl$_3$:MeOH:H$_2$O 85:25:2.5) showed the formation of a single new product. Quadrasil™-MP (S/Cu 2:1, 20 mg) was added to the reaction mixture, which was stirred for 10 minutes, and then filtered off. The solvent was removed under reduced pressure and the resulting mixture redissolved in MeOH and purified by size exclusion chromatography (Sephadex LH-20, MeOH), obtaining 155 mg of pure **2.34** as a colourless oil (yield 96 %).

^{1}H NMR (400 MHz, MeOD): δ 8.04 (s, 1H, H$_{T5}$); 7.78 (d, 2H, H$_{OTs}$, J = 8.3 Hz); 7.42 (d, 2H, H$_{OTs}$, J = 8.3 Hz); 7.28 – 7.19 (m, 8H, H$_{Ar2}$, H$_{Ar3}$); 4.90 (bs, 1H, H$_1$); 4.64 – 4.52 (m, 8H, H$_{L1}$, C$\underline{H}_2$OH, H$_8$); 4.30 – 4.28 (m, 4H, CH$_2$NH); 4.14 – 4.07 (m, 2H, H$_{L8}$); 4.02 – 3.81 (m, 5H, H$_2$, H$_{D2}$, H$_{6a}$, H$_7$); 3.72 – 3.65 (m, 3H, H$_{D1}$, H$_3$, H$_{6b}$); 3.62 – 3.59 (m, 2H, H$_{L7}$); 3.58 – 3.49 (m, 6H, H$_5$, H$_4$, H$_{L2}$, H$_{L3}$); 3.46 – 3.41 (m, 4H, H$_{L4}$, H$_{L6}$); 2.89 – 2.74 (m, 2H, H$_{D4}$, H$_{D5}$); 2.44 (s, 3H, C$\underline{H}_3$Ts); 1.97 – 1.74 (m, 4H, H$_{D3}$, H$_{D6}$); 1.70 (tt, J = 6.3 Hz, 2H, H$_{L5}$).

^{13}C NMR (100 MHz, MeOD): δ 176.9, 176.7 ($\underline{C}$ONH); 146.5 (C$_{quatOTs}$); 146.0 (C$_{T4}$); 141.5 (C$_{quatOTs}$); 139.1 (C$_{Ar1}$, C$_{Ar4}$); 134.4 (C$_{OTs}$); 131.1 (C$_{OTs}$); 128.4, 128.3, 128.2, 128.1 (C$_{Ar2}$, C$_{Ar3}$); 126.1 (C$_{T5}$); 100.3 (C$_1$); 76.2 (C$_3$); 75.54 (C$_5$); 72.53 (C$_{D1}$); 72.3 (C$_2$); 72.1 (C$_{D2}$); 71.1, 71.0, 70.7 (C$_{L2}$, C$_{L3}$, C$_{L8}$); 69.3, 68.9 (C$_{L4}$, C$_{L6}$, C$_{L7}$); 68.8 (C$_4$); 68.4 (C$_7$); 64.9 ($\underline{C}$H$_2$OH, C$_{L1}$); 63.1 (C$_6$); 51.6 (C$_8$); 43.6 ($\underline{C}$H$_2$NH); 41.8 (C$_4$, C$_5$); 30.8 (C$_{L5}$); 29.7 (C$_{D3}$ or C$_{D6}$); 28.9 (C$_{D3}$ or C$_{D6}$); 21.6 ($\underline{C}$H$_3$Ts).

MS (ESI): calculated for [C$_{49}$H$_{67}$N$_5$O$_{17}$SNa]$^+$: 1053.0; found: 1052.6.

[α]$_D$^{25}: 3.9 (c = 0.42, MeOH).

Synthesis of elongated monovalent ligand 2.7
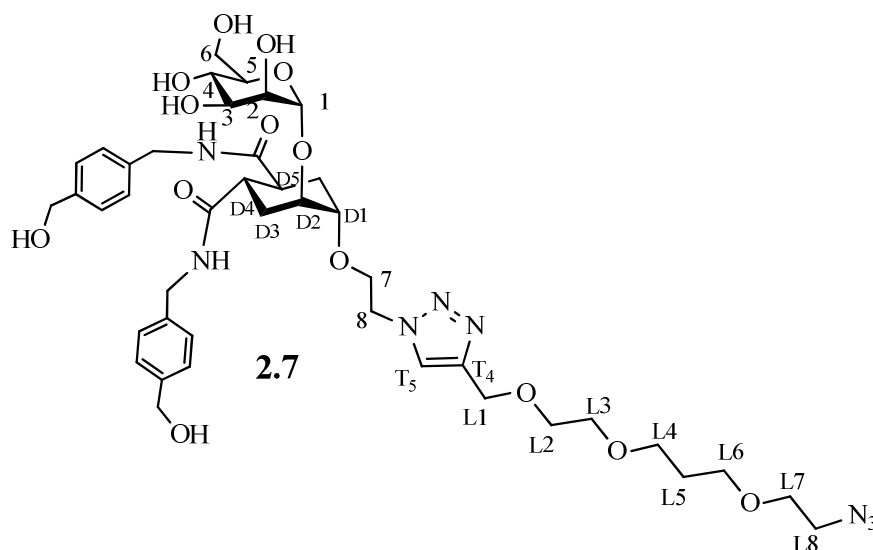

To a solution of **2.34** (147.8 mg, 140 µmol, 1 eq.) in DMF dry (1.5 mL), NaN_3 (37.3 mg, 570 µmol, 4 eq.) and NaI (3.5 mg, 23 µmol, 0.16 eq.) were added. The reaction mixture was stirred at 65 °C under nitrogen for 20 h. ESI-MS analysis showed total conversion of the starting material. The solvent was evaporated under reduced pressure and the resulting crude was redissolved in MeOH and purified by size exclusion chromatography (Sephadex LH-20, MeOH), obtaining 121 mg of **2.7** as a white foam (yield 93 %), still containing the 0.4 % (w/w, as measured by NMR integration) of a tosylate salt. Compound **2.7** was used for conjugation with the rods without further purifications.

^{1}H NMR (400 MHz): δ 8.05 (s, 1H, H_{T5}); 7.29 – 7.21 (m, 8H, H_{Ar2}, H_{Ar3}); 4.90 (bs, 1H, H_1); 4.63 – 4.53 (m, 8H, H_{L1}, CH2OH, H_8); 4.29 (d, 4H, H_{10}, $J = 5.5$ Hz); 4.01 – 3.82 (m, 5H, H_7, H_{D2}, H_{6a}, H_2); 3.71 – 3.64 (m, 3H, H_{D1}, H_3, H_{6b}); 3.63 – 3.55 (m, 6H, H_{L2}, H_{L3}, H_{L7}); 3.55 – 3.52 (m, 6H, H_4, H_5, H_{L4}, H_{L6}); 3.35 – 3.32 (m, 2H, H_{L8}); 2.92 – 2.71 (m, 2H, H_{D4}, H_{D5}); 1.99 – 1.69 (m, 6H, H_{D3}, H_{D6}, H_{L5}).

^{13}C NMR (100 MHz): δ 176.9, 176.7 (<u>C</u>ONH); 146.0 (C_{T4}); 141.5, 139.1 (C_{Ar1}, C_{Ar4}); 128.36, 128.34, 128.15, 128.13 (C_{Ar2}, C_{Ar3}); 126.1 (C_{T5}); 100.2 (C_1); 76.1 (C_3); 75.6 (C_5); 72.5 (C_{D1}); 72.3, 72.2, (C_2, C_{D2}); 71.1, 70.9, 70.7 (C_{L2}, C_{L3}, C_{L7}); 68.94, 68.87 (C_{L4}, C_{L6}); 68.78 (C_4); 68.4 (C_7); 64.9 (<u>C</u>H$_2$OH, C_{L1}); 63.1 ($C_{6a,b}$); 50.35 (C_{25}); 50.25 (C_8); 42.27 (<u>C</u>H$_2$NH); 40.36, 40.32 (C_{D4}, C_{D5}); 29.63 (C_{22}); 28.34 (C_{D3} or C_{D6}); 27.54 (C_{D3} or C_{D6}).

MS (ESI): calculated for $[C_{42}H_{60}N_8O_{14}]^+$: 923.9; found: 923.4.

Synthesis of hexavalent glycodendrimer 2.35

2.35
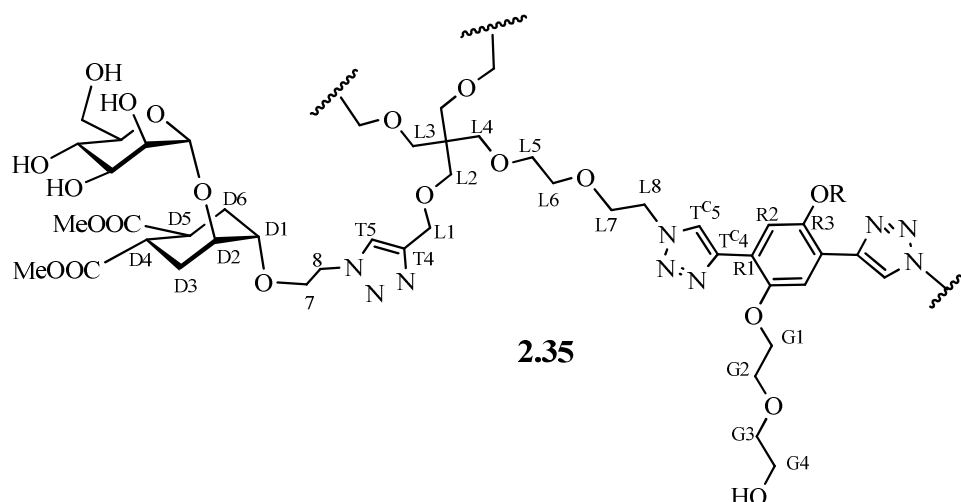
To a reaction vessel containing **2.3** (3.7 mg, 11.06 µmol, 1 eq.), reagents were added as solutions in the following order: TBTA in THF (1.17 mg, 2.21 µmol, 0.2 eq., 245 µL of THF), $CuSO_4 \cdot 5H_2O$ in H_2O (0.277 mg, 1.10 µmol, 0.1 eq., 44 µL of H_2O) and Sodium Ascorbate in H_2O (0.877 mg, 4.24 µmol, 0.4 eq., 82 µL of H_2O). The reaction mixture was stirred at room temperature, under nitrogen atmosphere and in the dark for 10 min. Then **2.1** (42.7 mg, 24.3 µmol, 2.2 eq.) in 1:1 THF:H_2O (200 µL) was added. THF and H_2O volumes were adjusted to 325 µL each. The reaction was stirred overnight, at RT, under nitrogen atmosphere and in the dark. TLC analysis (CH_2Cl_2:MeOH 9:1) revealed total consumption of **2.3**; mass analysis (MALDI, DHB or sinapinic acid matrix) confirmed that the reaction was complete. The crude mixture was directly loaded onto a Sephadex LH-20 column (MeOH) and purified by size exclusion chromatography, obtaining 38 mg of pure **2.35** as a white solid (yield 90 %). Copper salts were removed by adding Quadrasil™-MP (S/Cu 6.8:1, 5 mg) to a solution of the product in MeOH; the mixture was stirred for 10 min, then the resin was filtered off and the solvent evaporated.
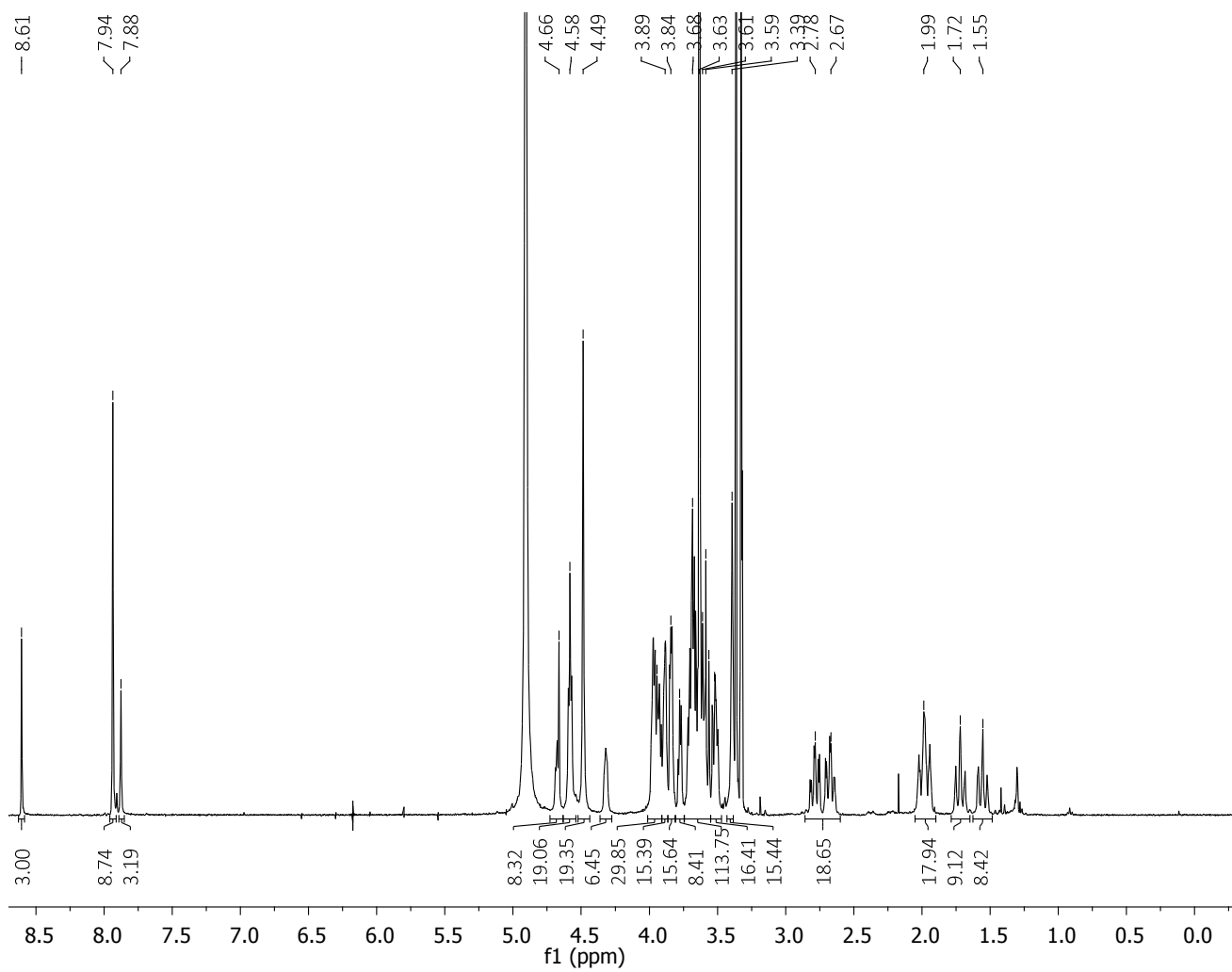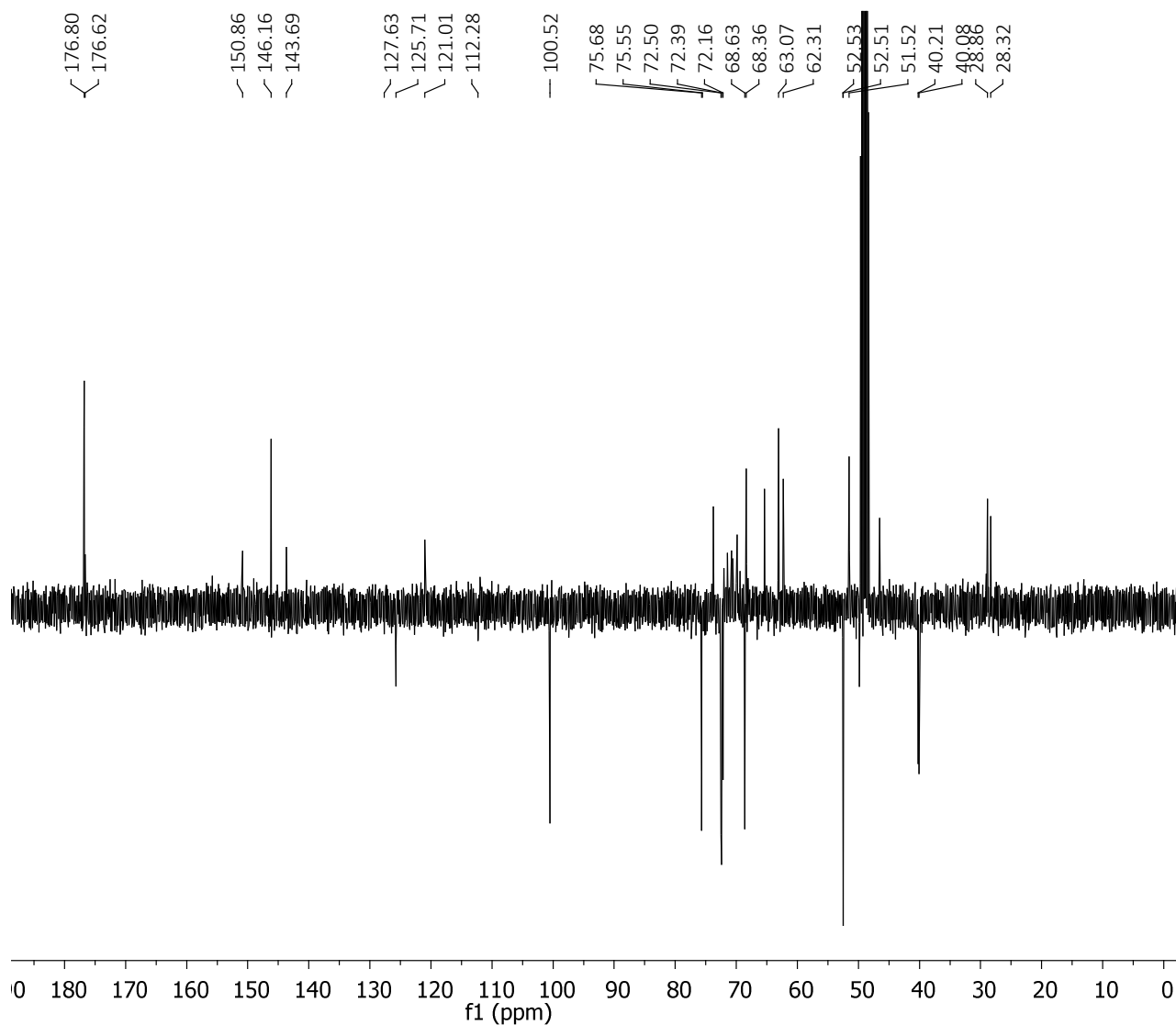
¹H NMR (400 MHz, CD₃OD): δ 8.59 (s, 2H, H$_{TC4}$); 7.92 (s, 6H, H$_{T4}$); 7.86 (s, 2H, H$_{R2}$); 4.89 (br s, 6H, H$_1$); 4.70 – 4.61 (m, 4H, H$_{L8}$); 4.57 (t, 12H, H$_8$, *J* = 4.8 Hz); 4.47 (s, 12H, H$_{L1}$); 4.31 (s, 4H, H$_{G1}$); 4.02 – 3.80 (m, 38H, H$_7$, H$_{6a}$, H$_2$, H$_{D2}$, H$_{L7}$, H$_{G2}$); 3.79 – 3.73 (m, 4H, H$_{G3}$); 3.72 – 3.63 (m, 22H, H$_{6b}$, H$_{D1}$, H$_3$, H$_{G4}$); 3.62 (s, 36H, COO<u>Me</u>); 3.60 – 3.54 (m, 10H, H$_4$, H$_{L5}$); 3.53 – 3.45 (m, 10H, H$_5$, H$_{L6}$); 3.38 (s, 12H, H$_{L2}$); 3.35 (s, 4H, H$_{L4}$); 2.77 (td, 6H, H$_{D4}$, *J* = 12.5, 3.5 Hz); 2.66 (td, 6H, H$_{D5}$, *J* = 12.2, 3.4 Hz); 2.05 – 1.88 (m, 12H, H$_{D3eq}$, H$_{D6eq}$); 1.70 (t, 6H, H$_{D6ax}$ or H$_{D3ax}$, *J* = 13.3 Hz); 1.54 (t, *J* = 12.7 Hz, 6H, H$_{D6ax}$ or H$_{D3ax}$).

¹³C NMR (100 MHz, CD₃OD): δ 176.8, 176.6 (<u>C</u>OOMe); 150.9 (C$_{R3}$); 146.2 (C$_{T4}$); 143.7 (C$_{TC4}$); 127.6 (C$_{TC5}$); 125.7 (C$_{T5}$); 121.0 (C$_{R1}$); 112.26 (C$_{R2}$); 100.5 (C$_1$); 75.7 (C$_5$); 75.6 (C$_3$); 73.7 (C$_{G3}$); 72.5 (C$_{D1}$); 72.4 (C$_2$); 72.2 (C$_{D2}$); 72.0 (C$_{L6}$); 71.5 (C$_{L5}$); 70.8 (C$_{L7}$); 70.6 (C$_{G2}$); 69.9 (C$_{L2}$, C$_{L4}$); 68.6 (C$_4$); 68.4 (C$_7$); 65.4 (C$_{L1}$); 63.1 (C$_6$); 62.3 (C$_{G4}$); 52.5, 52.5 (COO<u>Me</u>); 51.5 (C$_8$, C$_{L8}$); 46.55 (C$_{L3}$); 40.21 (C$_{D4}$); 40.08 (C$_{D5}$); 28.86 (C$_{D3}$ or C$_{D6}$); 28.32 (C$_{D3}$ or C$_{D6}$).

MS (ESI-HRMS): *m/z* calculated for $[C_{162}H_{247}N_{24}O_{82}]^+$: 3841.5929; found: 3841.5871 (after deconvolution).

$[\alpha]_D^{25}$: +29.5 (c = 0.65, MeOH).

Synthesis of hexavalent glycodendrimer 2.36

2.36
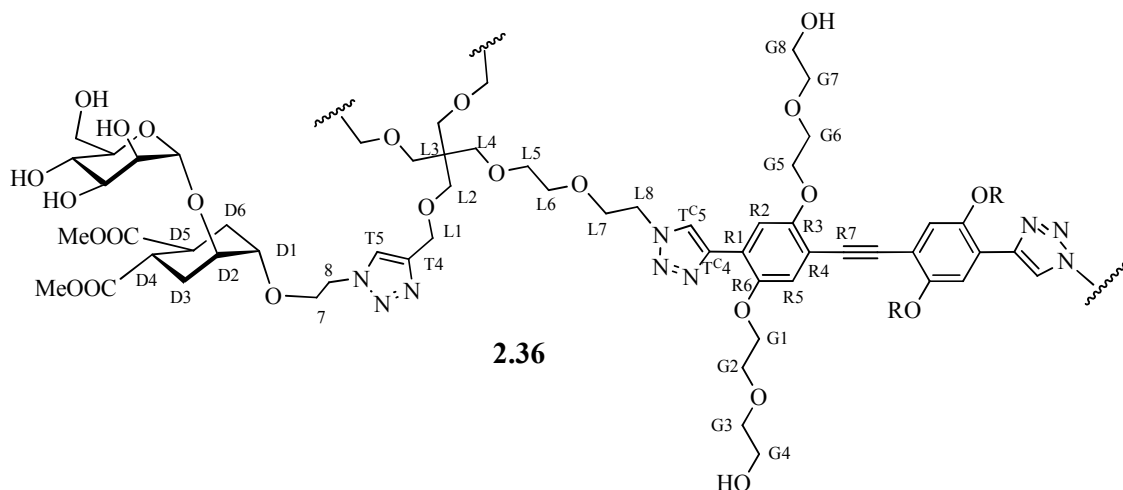
To a stirred solution of **TIPS-2.4** (5 mg, 5.2 µmol, 1 eq.) in THF (120 µL), TBAF (1 M in THF, 10.5 µL, 2 eq.) was added under nitrogen. After 1 h, TLC analysis (CH_2Cl_2:MeOH 9:1) showed that the desilylation reaction was complete. The CuAAC reagents were added as solutions in the following order: TBTA in THF (0.53 mg, 1.00 µmol, 0.2 eq., 21 µL of THF), $CuSO_4 \cdot 5H_2O$ in H_2O (0.13 mg, 0.52 µmol, 0.1 eq., 39 µL of H_2O) and Sodium Ascorbate in H_2O (0.40 mg, 2.08 µmol, 0.4 eq., 32 µL of H_2O). The reaction mixture was stirred at room temperature, under nitrogen atmosphere and in dark for 10 minutes. Then **2.1** (20 mg, 11.4 µmol, 2.2 eq.) was added as a solid. THF and H_2O volumes were adjusted to 150 µL each. The reaction was stirred overnight, at room temperature, under nitrogen atmosphere and in the dark. TLC analysis (CH_2Cl_2:MeOH 9:1) revealed total consumption of deprotected **2.4**; mass analysis (MALDI, DHB or sinapinic acid matrix) confirmed that the reaction was complete. Quadrasil™-MP (S/Cu 14.4:1, 5 mg) was added to the reaction mixture, which was stirred for 10 min, and then filtered off. The solvent was removed under reduced pressure and the resulting mixture was redissolved in MeOH and purified by size exclusion chromatography (Sephadex LH-20, MeOH), obtaining 13 mg of pure **2.36** as a yellow solid (yield 62 %).
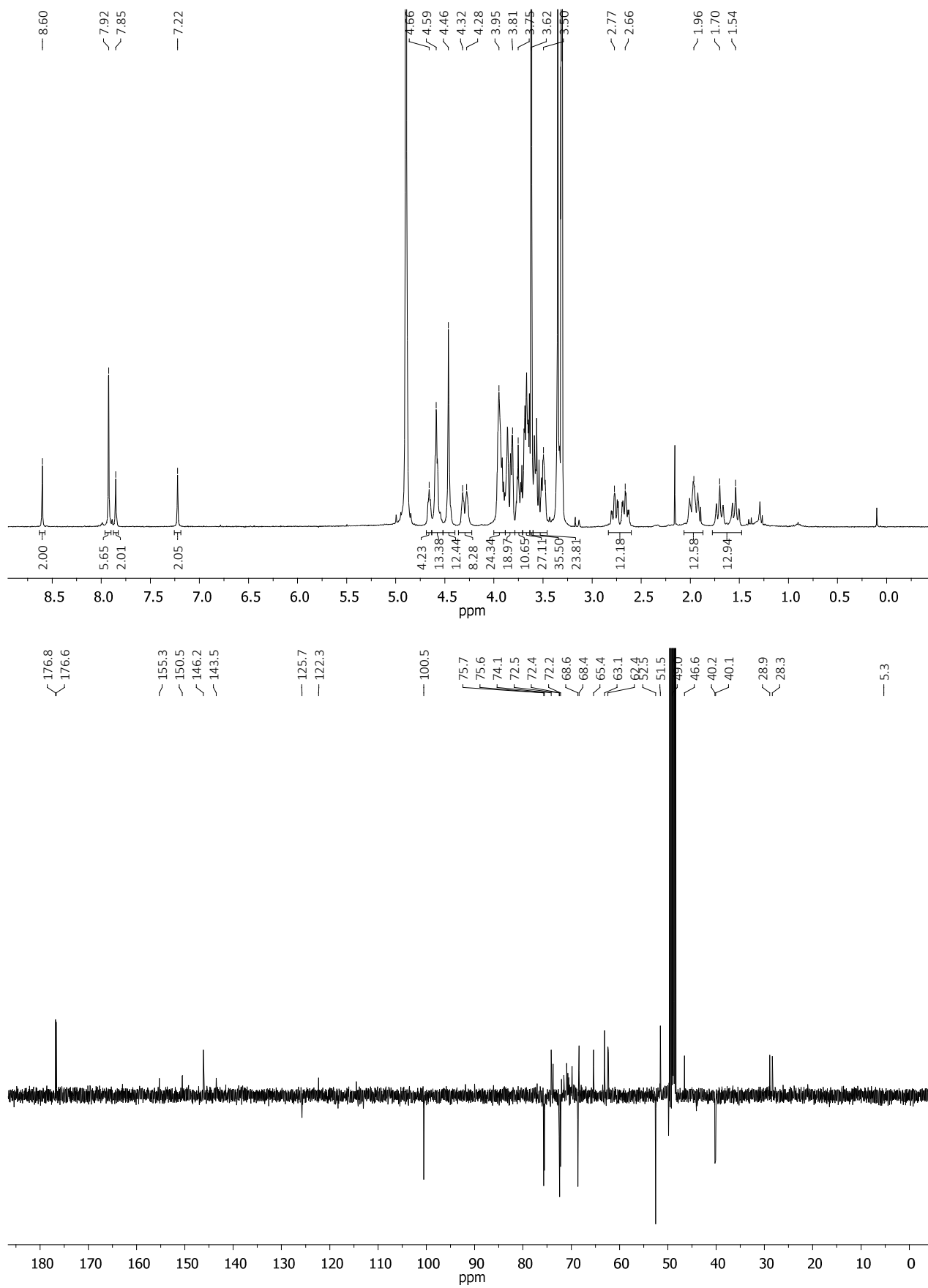
¹H NMR (400 MHz, CD₃OD): δ 8.60 (s, 2H, H$_{TC5}$); 7.92 (s, 6H, H$_{T5}$); 7.85 (s, 2H, H$_{R2}$); 7.22 (s, 2H, H$_{R5}$); 4.87 (br s, 6H, H$_1$); 4.69 – 4.63 (m, 4H, H$_{L8}$); 4.59 (t, 12H, H$_8$, J = 4.7 Hz); 4.46 (s, 12H, H$_{L1}$); 4.34 – 4.24 (m, 8H, H$_{G1}$, H$_{G5}$); 4.00 – 3.90 (m, 24H, H$_{G2}$, H$_{G6}$, H$_7$, H$_{L7}$); 3.90 – 3.79 (m, 18H, H$_{D2}$, H$_2$, H$_{6a}$); 3.79 – 3.71 (m, 8H, H$_{G4}$, H$_{G8}$); 3.71 – 3.63 (m, 26H, H$_{G3}$, H$_{G7}$, H$_3$, H$_{6b}$, H$_{D1}$); 3.62 (s, 36H, COO$\underline{Me}$); 3.60 – 3.53 (m, 10H, H$_4$, H$_{L5}$ or H$_{L6}$); 3.53 – 3.46 (m, 10H, H$_5$, H$_{L5}$ or H$_{L6}$); 3.35 (s, 16H, H$_{L2}$, H$_{L4}$); 2.77 (td, 6H, H$_{D4}$, J = 12.6, 3.4 Hz); 2.66 (td, 3.5 Hz, 6H, H$_{D5}$, J = 12.3); 2.03 – 1.91 (m, 12H, H$_{D3eq}$, H$_{D6eq}$); 1.75 – 1.49 (m, 12H, H$_{D3ax}$, H$_{D6ax}$).

¹³C NMR (100 MHz, CD₃OD): δ 176.8, 176.6 ($\underline{C}$OOMe); 155.3 (C$_{R6}$); 150.5 (C$_{R3}$); 146.2 (C$_{TC4}$); 143.5 (C$_{T4}$); 125.7 (C$_{TC5}$); 125.6 (C$_{T5}$); 122.3 (C$_{R1}$); 118.4 (C$_{R5}$); 114.5 (C$_{R2}$); 100.6 (C$_1$); 75.70 (C$_5$); 75.6 (C$_3$); 74.1, 73.8 (C$_{G3}$, C$_{G7}$); 72.5 (C$_{D1}$); 72.4 (C$_2$); 72.2 (C$_{D2}$); 72.0, 71.5 (C$_{L5}$, C$_{L6}$); 70.9, 70.7, 70.5 (C$_{G2}$, C$_{G6}$, C$_{G1}$); 69.9 (C$_{L2}$, C$_{L4}$); 69.5 (C$_{G5}$); 68.6 (C$_4$); 68.4 (C$_7$, C$_{L7}$); 65.4 (C$_{13}$); 63.1 (C$_6$); 62.4, 62.3 (C$_{G4}$, C$_{G8}$); 52.5, 52.5 (COO$\underline{Me}$); 51.6 (C$_8$, C$_{L8}$); 40.2, 40.1 (C$_{D4}$, C$_{D5}$); 28.9 (C$_{D3}$ or C$_{D6}$); 28.3 (C$_{D3}$ or C$_{D6}$).

MS (MALDI, matrix: sinapinic acid, solvent: MeOH): m/z calculated for $[C_{178}H_{267}N_{24}O_{88}]^+$: 4151.22; found: 4150.0.

MS (ESI-HRMS): calculated for $[C_{178}H_{266}N_{24}O_{88}]$: 4147.70772; found: 4147.71526 (after deconvolution).

[α]$_D^{25}$: +24.1 (c = 0.24, MeOH).

Synthesis of hexavalent glycodendrimer 2.37

2.37
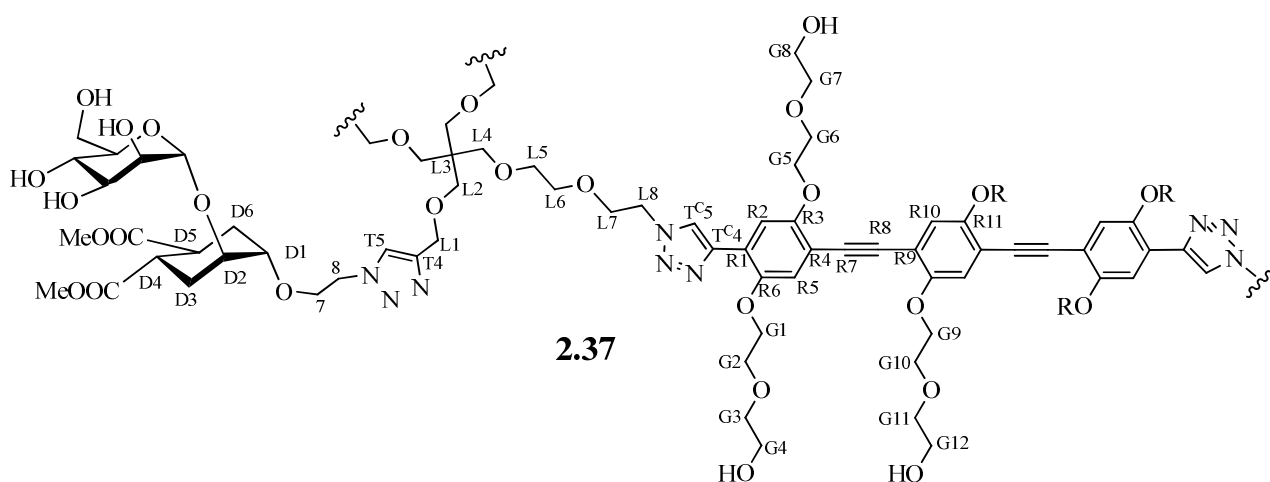
To a stirred solution of **TIPS-2.5** (12.4 mg, 9.82 µmol, 1 eq.) in THF (400 µL), TBAF (1 M in THF, 22 µL, 2 eq.) was added at room temperature under nitrogen. After 1 h, TLC analysis

(CH$_2$Cl$_2$:MeOH 9:1) showed that the desilylation reaction was complete. The CuAAC reagents were added as solutions in the following order: TBTA in THF (1.17 mg, 2.21 µmol, 0.2 eq., 160µL of THF), CuSO$_4$·5H$_2$O in H$_2$O (0.277 mg, 1.10 µmol, 0.1 eq., 56 µL of H$_2$O) and Sodium Ascorbate in H$_2$O (0.877 mg, 4.24 µmol, 0.4 eq., 74 µL of H$_2$O). The reaction mixture was stirred at room temperature, under nitrogen atmosphere and in the dark for 10 min. Then **2.1** (42.7 mg, 24.3 µmol, 2.2 eq.) was added as a solid. THF and H$_2$O volumes were adjusted to 500 µL each. The reaction was stirred overnight, at room temperature, under nitrogen atmosphere and in the dark. TLC analysis (CH$_2$Cl$_2$:MeOH 9:1) revealed total consumption of **2.5**; mass analysis (MALDI, DHB or sinapinic acid matrix) confirmed that the reaction was complete. The crude mixture was directly loaded onto a Sephadex LH-20 column (MeOH) and purified by size exclusion chromatography, obtaining 37 mg of pure **2.37** as yellow solid (yield 85%). Copper salts were removed by adding Quadrasil™-MP (S/Cu 6.8:1, 5 mg) to a **2.37** solution in MeOH; the mixture was stirred for 10 min, then the resin was filtered off and the solvent evaporated.
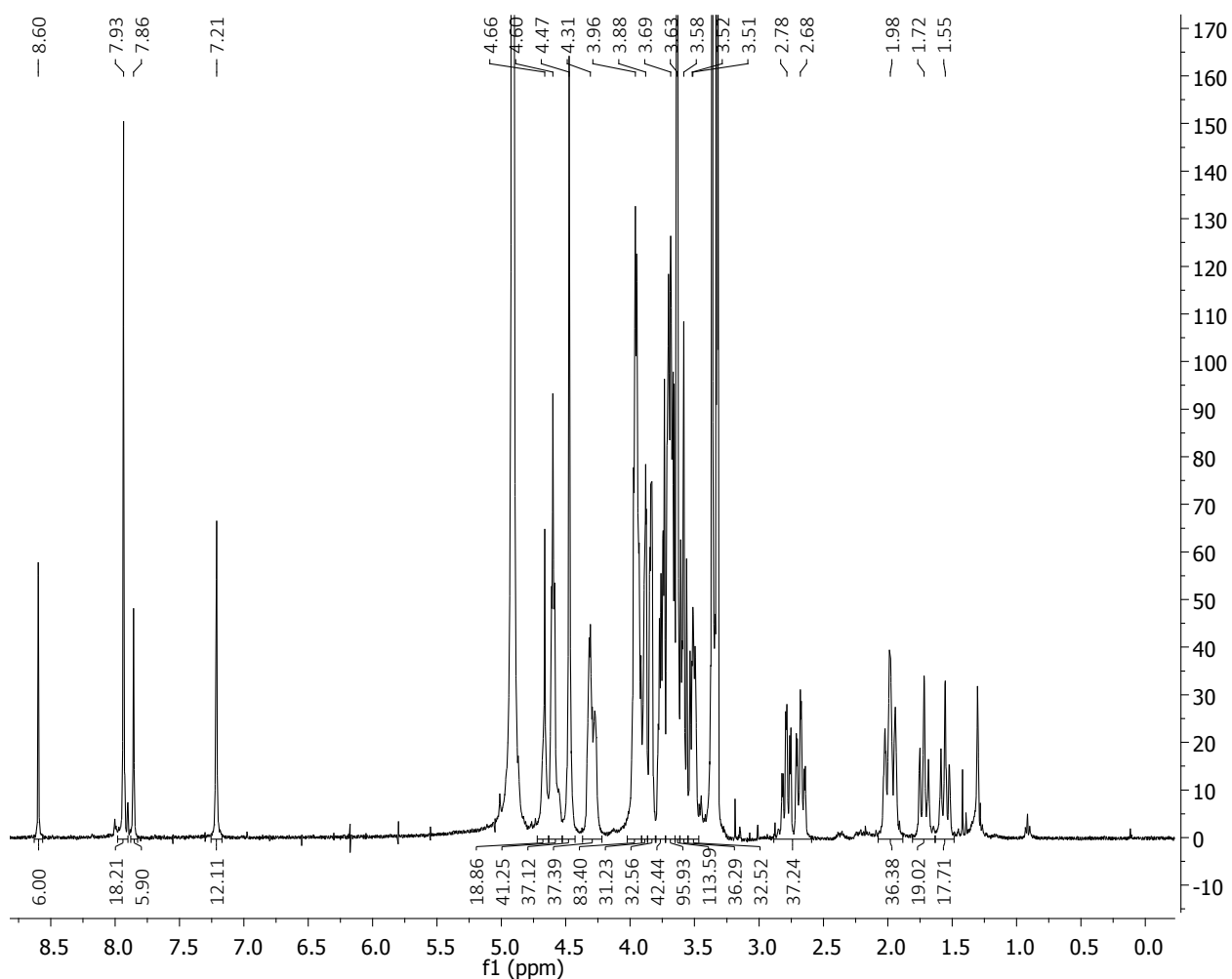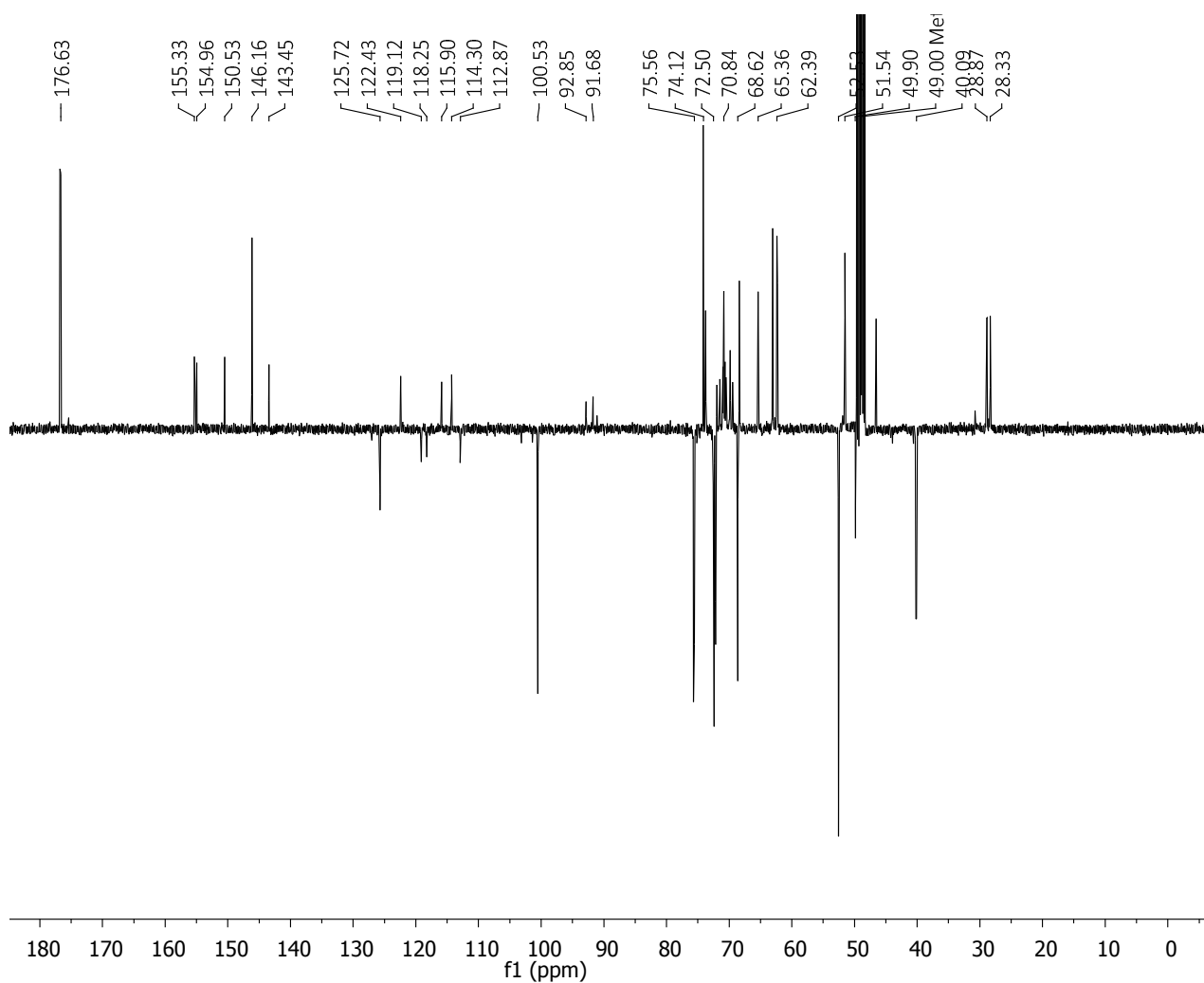
^{1}H NMR (400 MHz, CD$_3$OD): δ 8.58 (s, 2H, H$_{TC5}$); 7.92 (s, 6H, H$_{T5}$); 7.84 (s, 2H, H$_{R10}$); 7.20 (s, 4H, H$_{R2}$, H$_{R5}$); 4.89 (br s, 6H, H$_1$,); 4.65 (s, 4H, H$_{L8}$); 4.58 (t, 12H, H$_8$, J = 4.7 Hz); 4.46 (s, 12H, H$_{13}$); 4.35 – 4.21 (m, 12H, H$_{G1}$, H$_{G5}$, H$_{G9}$); 4.00 – 3.89 (m, 28H, H$_7$, H$_{L1}$, H$_{G2}$, H$_{G6}$, H$_{G10}$); 3.89 – 3.83 (m, 12H, H$_{D2}$, H$_{6a}$); 3.82 (dd, 1.6 Hz, 6H, H$_2$, J = 3.1); 3.78 – 3.71 (m, 12H, H$_{G3}$, H$_{G7}$, H$_{G11}$); 3.71 – 3.64 (m, 30H, H$_3$, H$_{6b}$, H$_{D1}$, H$_{G4}$, H$_{G8}$, H$_{G12}$); 3.62 (s, 36H, COO<u>Me</u>); 3.60 – 3.53 (m, 10H, H$_4$, H$_{L5}$); 3.53 – 3.45 (m, 10H, H$_5$, H$_{L6}$); 3.35 (s, 12H, H$_{L2}$); 3.33 (s, 4H, H$_{L4}$); 2.77 (td, 6H, H$_{D4}$, J = 12.4, 3.5 Hz); 2.66 (td, 6H, H$_{D5}$, J = 12.4, 3.5 Hz); 2.06 – 1.86 (m, 12H, H$_{D6eq}$, H$_{D3eq}$); 1.70 (t, J = 13.4 Hz, 6H, H$_{D6ax}$ or H$_{D3ax}$); 1.54 (t, J = 12.6 Hz, 6H, H$_{D6ax}$ or H$_{D3ax}$).

^{13}C NMR (100 MHz, CD$_3$OD): δ 176.8, 176.6 (<u>C</u>OOMe); 155.3, 155.0, 150.5, 146.2 (C$_{T4}$); 143.5 (C$_{TC4}$); 127.06 (C$_{TC5}$); 125.7 (C$_{T5}$); 122.4, 119.1 (C$_{R2}$); 118.3 (C$_{R5}$); 115.9, 114.3, 112.9 (C$_{R10}$); 103.2, 101.4, 100.5 (C$_1$); 92.8, 91.7, 91.1, 75.7 (C$_5$); 75.6 (C$_3$); 74.1, 73.7, 72.5 (C$_{D1}$); 72.4 (C$_2$); 72.2 (C$_{D2}$); 72.0 (C$_{L6}$); 71.5 (C$_{L5}$); 71.0, 70.9, 70.8, 70.7, 70.5, 69.8 (C$_{L2}$, C$_{L4}$); 69.5 (C$_{G9}$); 68.6 (C$_4$); 68.4 (C$_7$); 65.4 (C$_{L1}$); 63.1 (C$_6$); 62.4, 62.4, 62.3, 52.54, 52.53 (COO<u>Me</u>); 51.5 (C$_8$, C$_{L8}$); 46.6 (C$_{L3}$); 40.2 (C$_{D4}$); 40.1 (C$_{D5}$); 28.9 (C$_{D3}$ or C$_{D6}$); 28.3 (C$_{D3}$ or C$_{D6}$).

117

MS (ESI-HRMS): *m/z* calculated for $[C_{194}H_{287}N_{24}O_{94}]^+$: 4458.8404; found: 4457.8511 (after deconvolution).
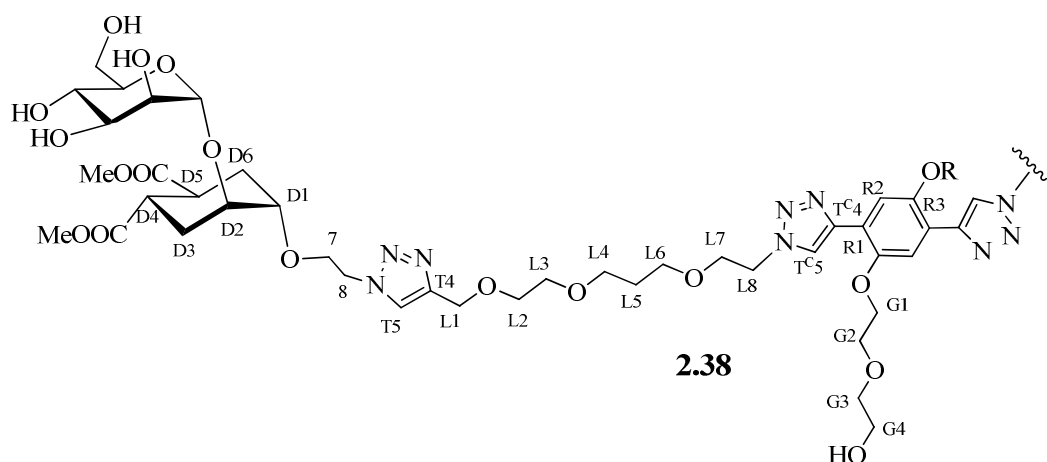
$[\alpha]_D^{25}$: +24.1 (c = 0.65, MeOH).

Synthesis of divalent glycodendrimer 2.38

2.38

In a reaction vessel containing **2.3** (4 mg, 12 µmol, 1 eq.), reagents were added as solutions in the following order: TBTA in THF (1.3 mg, 2.4 µmol, 0.2 eq., 80 µL of THF), $CuSO_4 \cdot 5H_2O$ in H_2O (0.3 mg, 1.2 µmol, 0.1 eq., 30 µL of H_2O) and Sodium Ascorbate in H_2O (1.0 mg, 4.8 µmol, 0.4 eq. 32 µL of H_2O). The reaction mixture was stirred at room temperature, under nitrogen atmosphere and in the dark for 10 min. Finally **2.6** (19.1 mg 97 % w/w, 26.8 µmol effective, 2.2 eq.) was added as solid. THF and H_2O volumes were adjusted to 270 µL each. The reaction was stirred at room temperature under nitrogen in the dark overnight. TLC analysis (CH_2Cl_2:MeOH 9:1) revealed total consumption of **2.3**; TLC ($CHCl_3$:MeOH:H_2O 75:25:2.5) revealed the presence of a single new species, together with a small amount of starting material **2.6**; mass analysis (MALDI, DHB or sinapinic acid matrix) confirmed that the reaction was complete. Quadrasil™-MP (S/Cu 6.3:1, 5 mg) was added to the reaction mixture, which was stirred for 10 min, and then filtered off. The solvent was removed under reduced pressure and the resulting mixture was redissolved in MeOH and purified by size exclusion chromatography (Sephadex LH-20, MeOH), obtaining 15 mg of pure **2.38** as a white solid (yield 73 %).
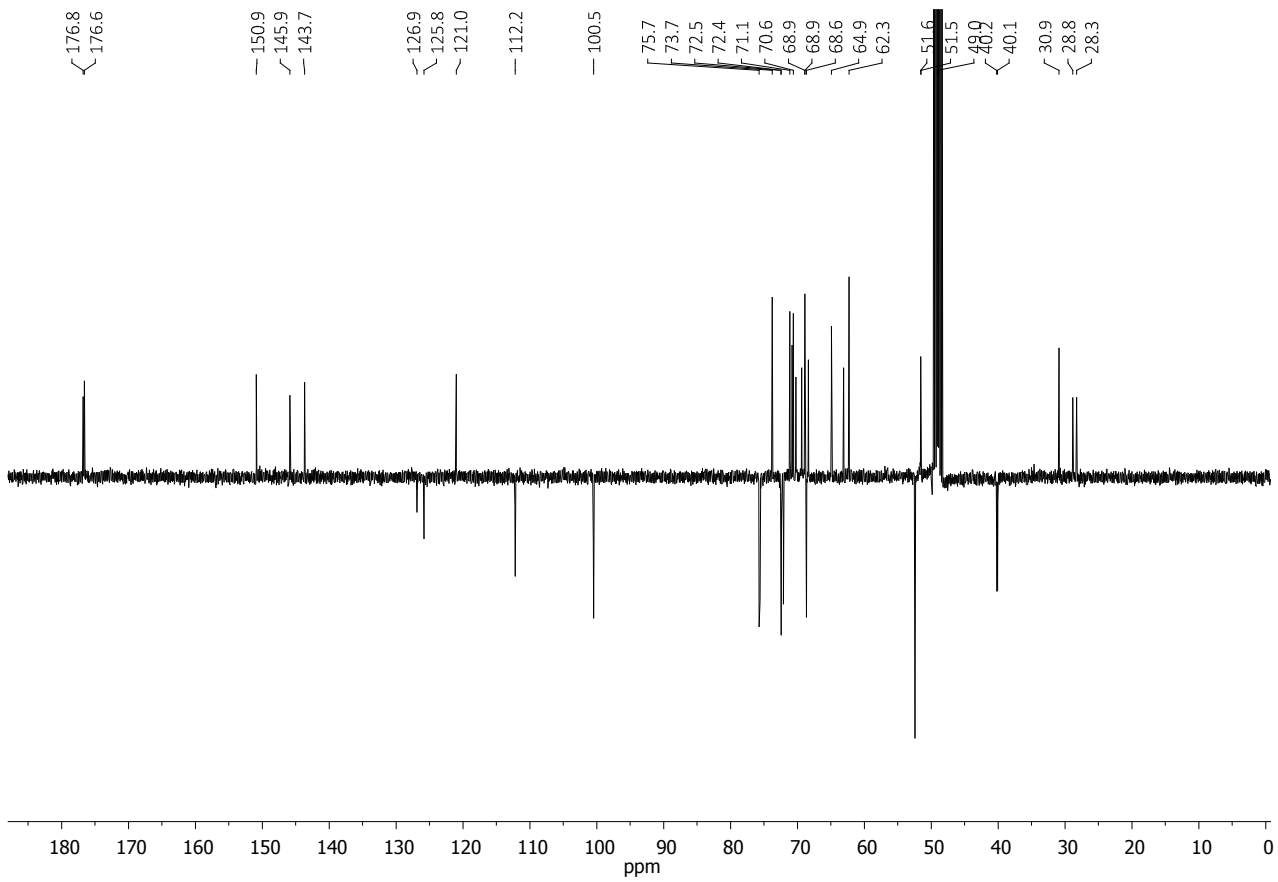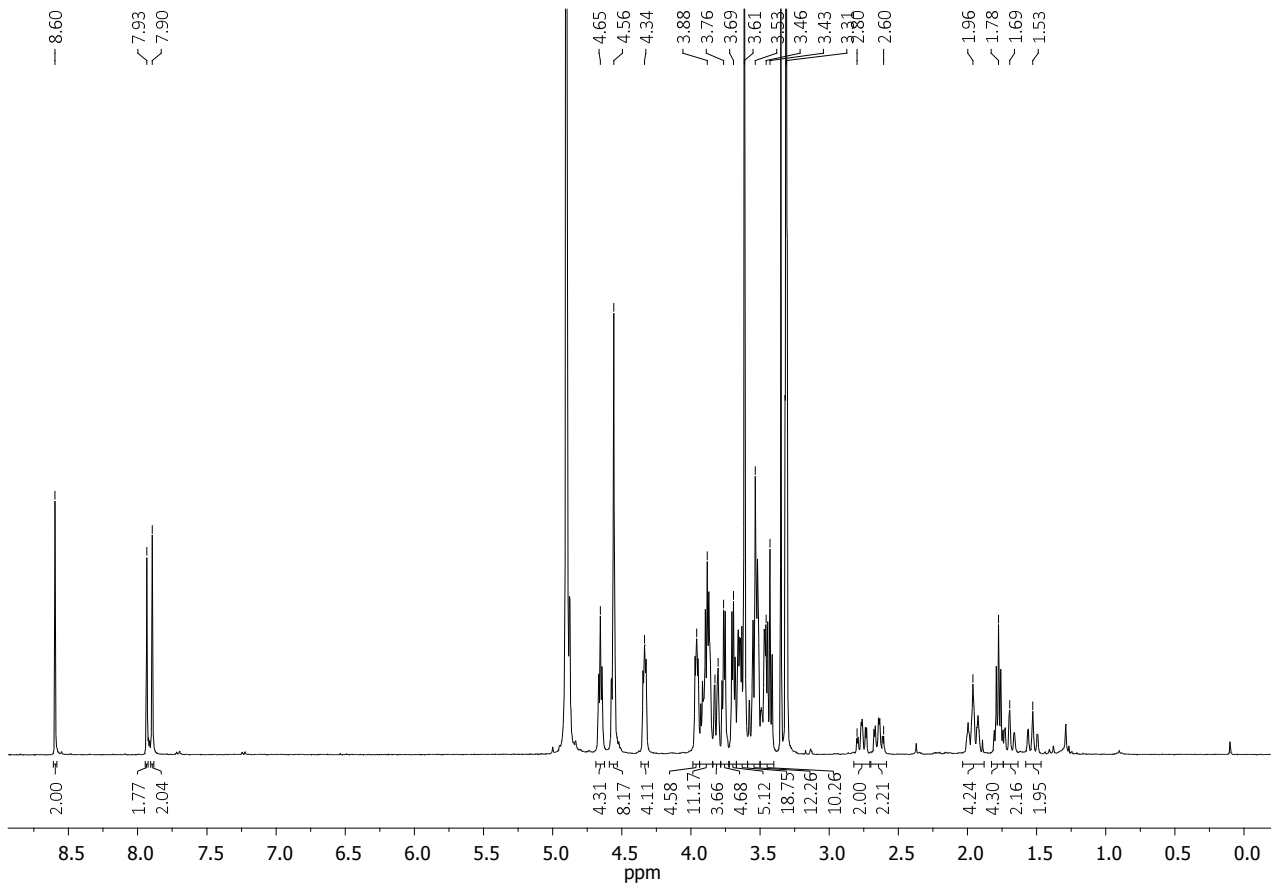
¹H NMR (400 MHz, CD₃OD): δ 8.60 (s, 2H, H$_{TC5}$); 7.93 (s, 2H, H$_{T5}$); 7.90 (s, 2H, H$_{R2}$); 4.88 (bs, 2H, H$_1$); 4.65 (t, 4H, H$_{L8}$, J = 4.9 Hz); 4.57 – 4.53 (m, 8H, H$_8$, H$_{L1}$); 4.36 – 4.31 (m, 4H, H$_{G1}$); 3.98 – 3.94 (m, 4H, H$_{G2}$); 3.94 – 3.84 (m, 10H, H$_{L7}$, H$_7$, H$_{D2}$); 3.83 – 3.80 (m, 4H, H$_{6a}$, H$_2$); 3.78 – 3.73 (m, 4H, H$_{G4}$); 3.71 – 3.68 (m, 4H, H$_{G3}$); 3.65 – 3.61 (m, 18H, H$_3$, H$_{6b}$, H$_{D1}$, COO<u>Me</u>); 3.59 – 3.50 (m, 10H, H$_5$, H$_{L2}$ or H$_{L3}$, H$_{L4}$ or H$_{L6}$); 3.50 – 3.39 (m, 10H, H$_4$, H$_{L2}$ or H$_{L3}$, H$_{L4}$ or H$_{L6}$); 2.76 (td, 2H, H$_{D4}$ or H$_{D5}$, J = 12.6, 3.5 Hz); 2.64 (td, 2H, H$_{D4}$ or H$_{D5}$, J = 12.6, 3.5 Hz); 2.04 – 1.88 (m, 4H, H$_{D3eq}$, H$_{D6eq}$); 1.78 (tt, 4H, H$_{L5}$, J = 6.2 Hz); 1.74 – 1.64 (m, 2H, H$_{D3ax}$ or H$_{D6ax}$); 1.59 – 1.47 (m, 2H, H$_{D3ax}$ or H$_{D6ax}$).

¹³C NMR (100 MHz, CD₃OD): δ 176.8, 176.6 (<u>C</u>OOMe); 150.9 (C$_{R3}$); 145.9 (C$_{TC4}$); 143.7 (C$_{T4}$); 126.9 (C$_{TC5}$); 125.8 (C$_{T5}$); 121.0 (C$_{R1}$); 112.2 (C$_{R2}$); 100.5 (C$_1$); 75.7 (C$_5$); 75.6 (C$_3$); 73.8 (C$_{G3}$); 72.5 (C$_{D1}$); 72.4 (C$_2$); 72.1 (C$_{D2}$); 71.2 (C$_{L2}$ or C$_{L3}$); 70.8 (C$_{G2}$); 70.6 (C$_{L2}$ or C$_{L3}$); 70.2 (C$_7$ or C$_{L7}$); 69.4 (C$_{G1}$); 68.89, 68.86 (C$_{L4}$, C$_{L6}$); 68.6 (C$_4$); 68.4 (C$_7$ or C$_{L7}$); 64.9 (C$_{L1}$); 63.1 (C$_6$); 62.3 (C$_{G4}$); 52.4 (COO<u>Me</u>); 51.6 (C$_8$); 51.5 (C$_{L8}$); 40.2, 40.1 (C$_{D4}$, C$_{D5}$); 30.9 (C$_{L5}$); 28.8 (C$_{D3}$ or C$_{D6}$); 28.3 (C$_{D3}$ or C$_{D6}$).

MS (MALDI, matrix: sinapinic acid, solvent: MeOH): m/z calculated for $[C_{74}H_{114}N_{12}O_{34}Na]^+$: 1738.4; found: 1738.0.

MS (ESI-HRMS): m/z calculated for $[C_{74}H_{114}N_{12}O_{34}Na_1]^+$: 1737.74526; found:1737.74278.

$[\alpha]_D^{25}$: +30.2 (c = 0.35, MeOH).

Synthesis of divalent glycodendrimer 2.39

2.39
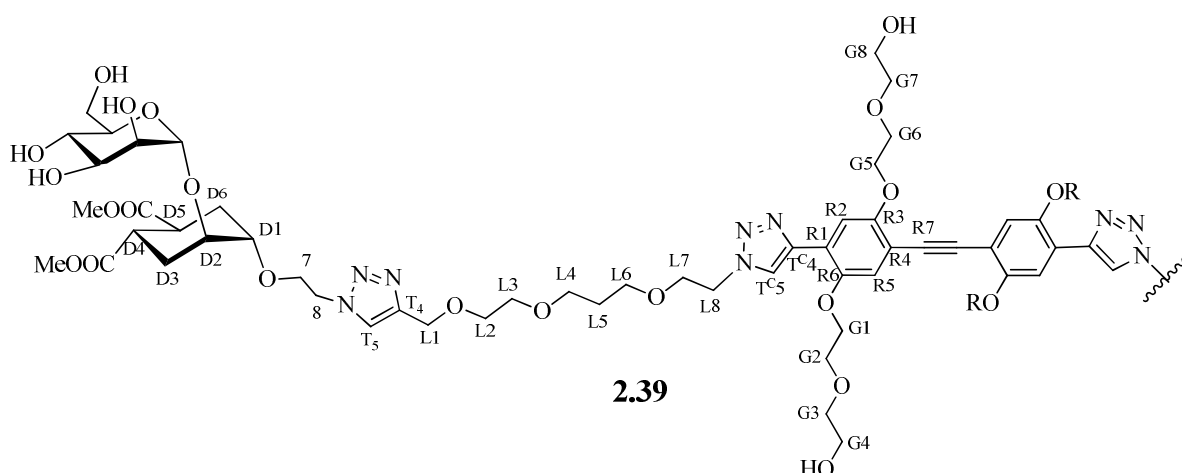
To a stirred solution of **TIPS2.4** (13.4 mg, 14 μmol, 1 eq.) in THF (300 μL), TBAF (1 M in THF, 28.0 μL, 2 eq.) was added under nitrogen. After 1 h, TLC analysis (CH₂Cl₂:MeOH 9:1) showed that

the desilylation reaction was complete. The CuAAC reagents were added as solutions in the following order: TBTA in THF (1.49 mg, 2.8 µmol, 0.2 eq., 120 µL of THF), CuSO$_4$·5H$_2$O in H$_2$O (0.35 mg, 1.4 µmol, 0.1 eq., 50 µL of H$_2$O) and Sodium Ascorbate in H$_2$O (1.06 mg, 5.6 µmol, 0.4 eq., 140 µL of H$_2$O). The reaction mixture was stirred at room temperature, under nitrogen atmosphere and in dark for 10 min. Finally **2.6** (22.3 mg 97 % w/w, 31.3 µmol effective, 2.2 eq.) was added as a solid. THF and H$_2$O volumes were adjusted to 450 µL each. The reaction was stirred at room temperature under nitrogen in the dark overnight. TLC analysis (CH$_2$Cl$_2$:MeOH 9:1) revealed total consumption of **2.4**; TLC (CHCl$_3$:MeOH:H$_2$O 75:25:2.5) revealed the presence of a single new species, together with a small amount of starting material **2.6**. Quadrasil™-MP (S/Cu 5.4:1, 5 mg) was added to the reaction mixture, which was stirred for 10 min, and then filtered. The solvent was removed under reduced pressure and the resulting mixture was redissolved in MeOH and purified by size exclusion chromatography (Sephadex LH-20, MeOH), obtaining 23 mg of **2.39** not pure**.** The remaining tetrabutylammonium salt was removed by automated reverse phase flash chromatography (C18, water with gradient of MeOH from 0 % to 100 %), obtaining 17 mg of pure **2.39** as a yellow solid (yield 60 %).
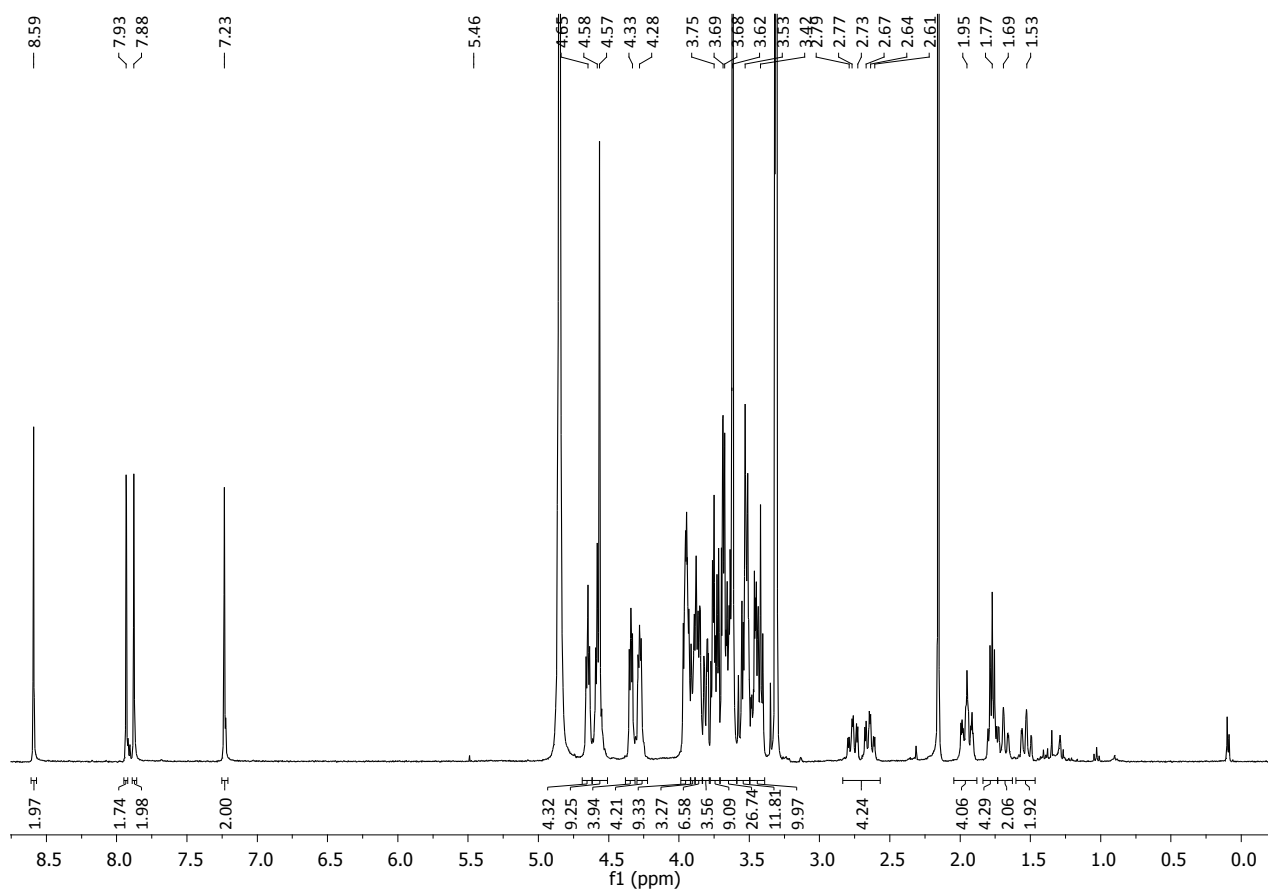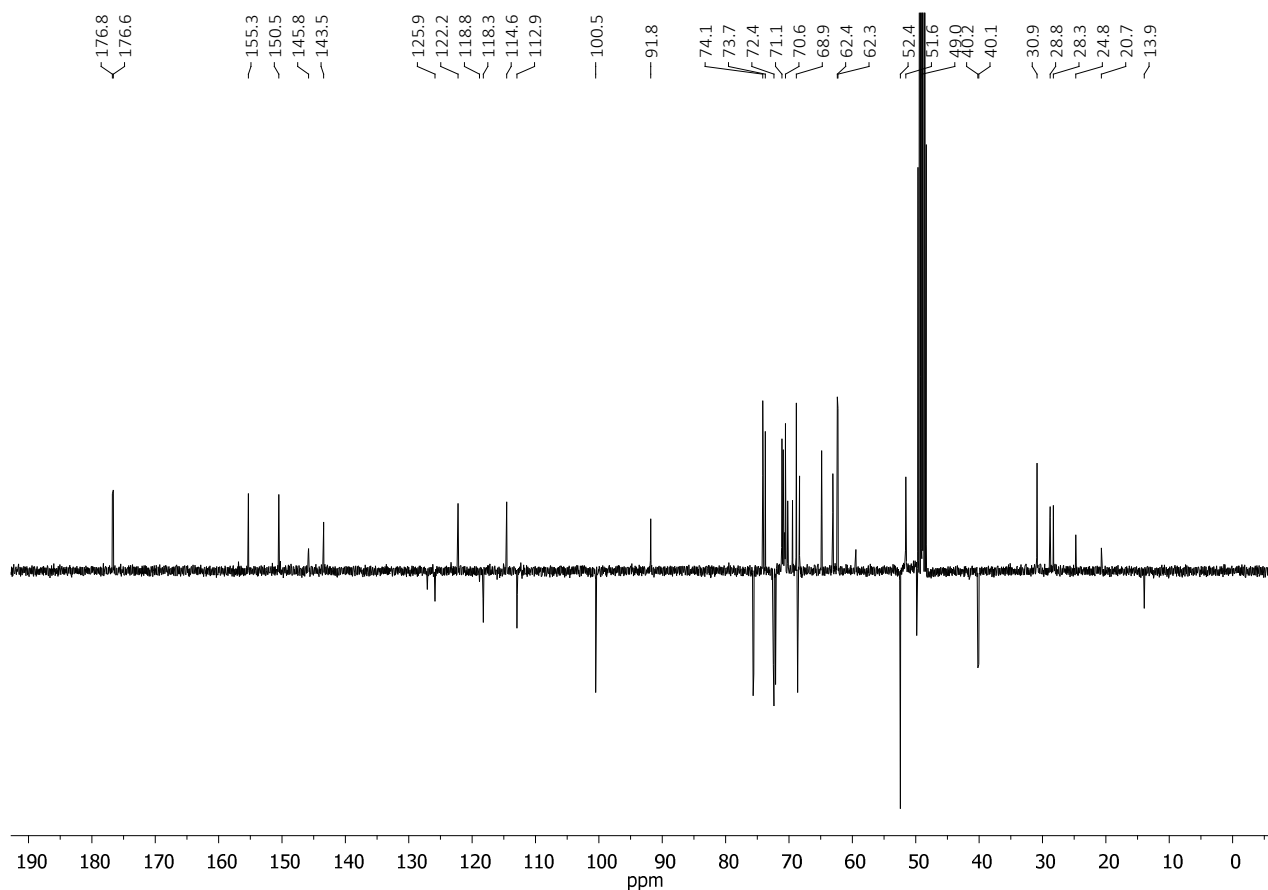
¹H NMR (400 MHz, CD₃OD): δ 8.58 (s, 2H, H$_{TC5}$); 7.94 (s, 2H, H$_{T5}$); 7.87 (s, 2H, H$_{R2}$); 7.22 (s, 2H, H$_{R5}$); 4.87 (br s, 2H, H$_1$); 4.64 (t, 4H, H$_{L8}$, J = 4.8 Hz); 4.62 – 4.52 (m, 8H, H$_8$, H$_{L1}$); 4.37 – 4.30 (m, 4H, H$_{G1}$); 4.30 – 4.22 (m, 4H, H$_{G5}$); 3.98 – 3.92 (m, 8H, H$_{G2}$, H$_{G6}$); 3.92 – 3.88 (m, 4H, H$_7$ or H$_{L7}$); 3.88 – 3.83 (m, 6H, H$_7$ or H$_{L7}$, H$_{D2}$); 3.83 – 3.78 (m, 4H, H$_{6a}$, H$_2$); 3.78 – 3.70 (m, 8H, H$_{G3}$, H$_{G4}$); 3.70 – 3.59 (m, 26H, H$_{G7}$, H$_{G8}$, H$_{6b}$, H$_{D1}$, H$_3$, COO<u>Me</u>); 3.59 – 3.47 (m, 12H, H$_{L4}$ or H$_{L6}$, H$_{L2}$ or H$_{L3}$, H$_4$, H$_5$); 3.47 – 3.37 (m, 8H, H$_{L4}$ or H$_{L6}$, H$_{L2}$ or H$_{L3}$); 2.76 (td, 2H, H$_{D4}$ or H$_{D5}$, J = 12.6, 3.6 Hz); 2.64 (td, 2H, H$_{D4}$ or H$_{D5}$, J = 12.6, 3.6 Hz); 1.95 (t, 4H, H$_{D3eq}$, H$_{D6eq}$, J = 14.2 Hz); 1.77 (tt, 4H, H$_{L5}$, J = 6.4 Hz); 1.72 – 1.64 (m, 2H, H$_{D3ax}$ or H$_{D6ax}$); 1.56 – 1.48 (m, 2H, H$_{D3ax}$ or H$_{D6ax}$).

¹³C NMR (100 MHz, CD₃OD): δ 176.8, 176.6 (<u>C</u>OOMe); 155.3 (C$_{R6}$); 150.5 (C$_{R3}$); 145.84 (C$_{TC4}$); 143.5 (C$_{T4}$); 127.1 (C$_{TC5}$); 125.9 (C$_{T5}$); 122.2 (C$_{R1}$); 118.8, 118.3 (C$_{R5}$); 114.6 (C$_{R4}$); 112.9 (C$_{R2}$); 100.5 (C$_1$); 91.8 (C$_{R7}$); 75.7 (C$_5$); 75.6 (C$_3$); 74.1, 73.7 (C$_{G3}$, C$_{G7}$); 72.5, 72.4 (C$_2$, C$_{D1}$); 72.1 (C$_{D2}$); 71.1 (C$_{L2}$ or C$_{L3}$); 71.0, 70.9 (C$_{G2}$, C$_{G6}$); 70.7 (C$_{G1}$); 70.6 (C$_{L2}$ or C$_{L3}$); 70.2 (C$_7$ or C$_{L7}$); 69.5 (C$_{G5}$); 68.9 (C$_{L4}$, C$_{L6}$); 68.6 (C$_4$); 68.4 (C$_7$ or C$_{L7}$); 64.9 (C$_{L1}$); 63.1 (C$_6$); 62.4, 62.3 (C$_{G4}$, C$_{G8}$); 52.4 (COO<u>Me</u>); 51.6 (C$_8$, C$_{L8}$); 40.2, 40.1 (C$_{D4}$, C$_{D5}$); 30.9 (C$_{L5}$); 28.8 (C$_{D3}$ or C$_{D6}$); 28.3 (C$_{D3}$ or C$_{D6}$).

MS (MALDI, matrix: sinapinic acid, solvent: MeOH): *m/z* calculated for [C₉₀H₁₃₄N₁₂O₄₀Na]⁺:

2047.0; found: 2046.4.

MS (ESI-HRMS): calculated for [C$_{90}$H$_{134}$N$_{12}$O$_{40}$]: 2022.88203; found: 2022.88641 (after deconvolution).

**[α]$_D$ ^{25}**: +16.1 (c = 0.50 MeOH).

Synthesis of divalent glycodendrimer 2.40

2.40
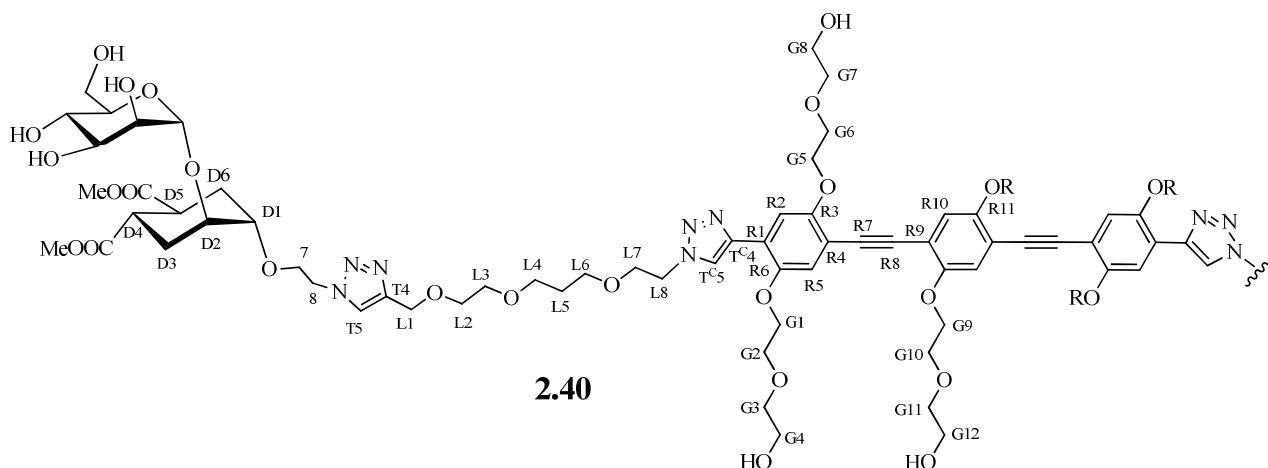
To a stirred solution of **TIPS-2.5** (13 mg, 10.5 µmol, 1 eq.) in THF (280 µL), TBAF (1 M in THF, 21.0 µL, 2 eq.) was added under nitrogen. After 1 h, TLC analysis (CH$_2$Cl$_2$:MeOH 9:1) showed that the desilylation reaction was complete. Then reagents were added as solutions in the following order: TBTA in THF (1.2 mg, 2.2 µmol, 0.2 eq., 50 µL of THF), CuSO$_4$·5H$_2$O in H$_2$O (0.3 mg, 1.1 µmol, 0.1 eq., 16 µL of H$_2$O) and sodium ascorbate in H$_2$O (0.9 mg, 4.4 µmol, 0.4 eq., 46 µL of H$_2$O). The reaction mixture was stirred at room temperature, under nitrogen atmosphere and in dark for 10 min. Finally **2.6** (16.8 mg 97 % w/w, 23.6 µmol effective, 2.2 eq.) was added as a solid. THF and H$_2$O volumes were adjusted to 350 µL each. The reaction was stirred at RT under nitrogen and in the dark overnight. TLC analysis (CH$_2$Cl$_2$:MeOH 9:1) revealed total consumption of **2.5**; TLC (CHCl$_3$:MeOH:H$_2$O 80:20:2.5) revealed the presence of a single new species, together with a small amount of starting material **2.6**; mass analysis (MALDI, DHB or sinapinic acid matrix) confirmed that the reaction was complete. Quadrasil™-MP (S/Cu 6.8:1, 5 mg) was added to the reaction mixture, which was stirred for 10 min, and then filtered off. The solvent was removed under reduced pressure and the resulting mixture was redissolved in MeOH and purified by size exclusion chromatography (Sephadex LH-20, MeOH), obtaining 23 mg of pure **2.40** as a yellow solid (yield 92 %).
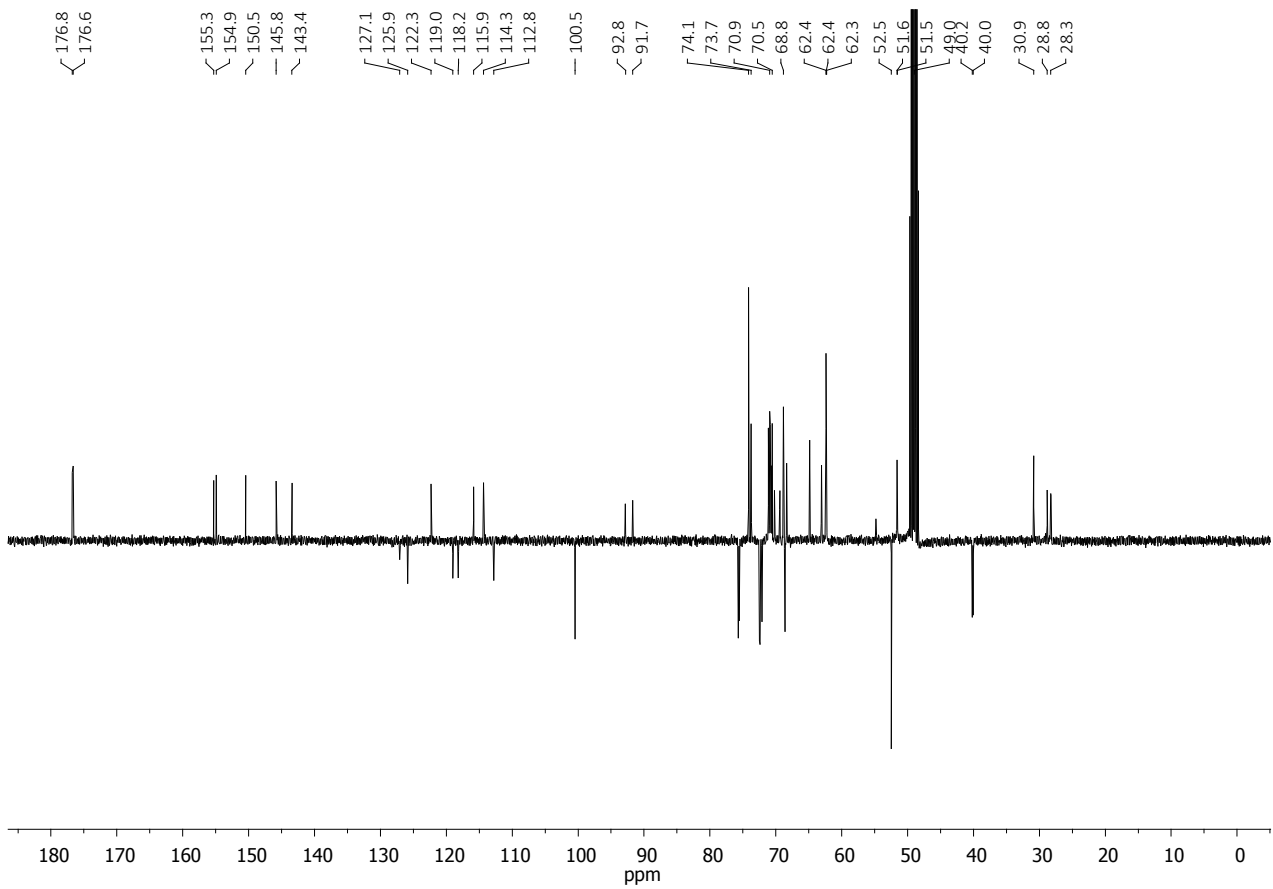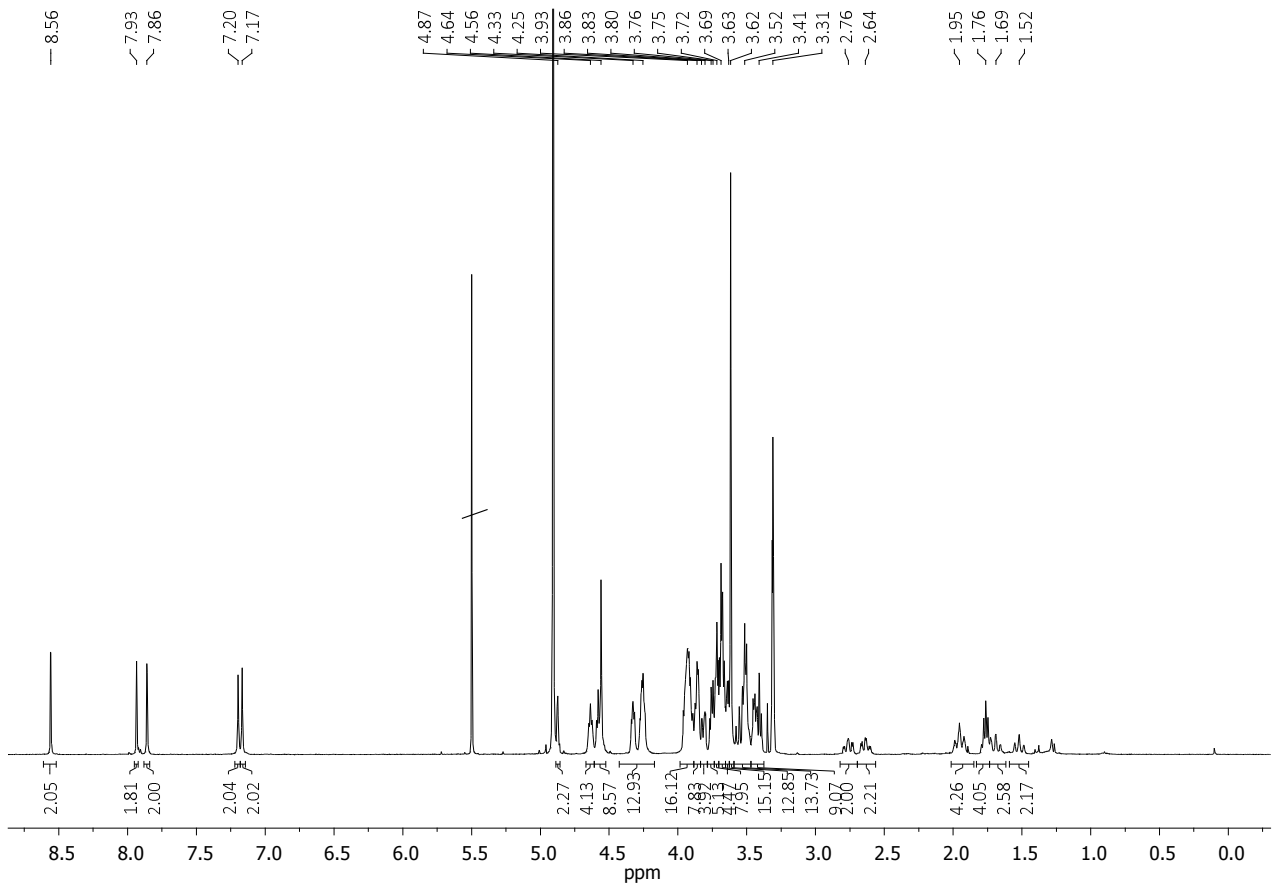
¹H NMR (400 MHz, CD₃OD): δ 8.56 (s, 2H, H$_{TC5}$); 7.93 (s, 2H, H$_{T5}$); 7.86 (s, 2H, H$_{R2}$); 7.20 (s, 2H, H$_{R5}$); 7.17 (s, 2H, H$_{R10}$); 4.87 (br s, 2H, H$_1$); 4.64 (t, 4H, H$_{L8}$, J = 4.7 Hz); 4.61 – 4.52 (m, 8H, H$_8$, H$_{L1}$); 4.34 – 4.24 (m, 12H, H$_{G1}$, H$_{G5}$, H$_{G9}$); 3.98 – 3.88 (m, 16H, H$_{G2}$, H$_{G6}$, H$_{G10}$, H$_7$ or H$_{L7}$); 3.88 – 3.84 (m, 8H, H$_7$ or H$_{L7}$, H$_{D2}$, H$_{6a}$); 3.84 – 3.78 (m, 4H, H$_2$, H$_{6b}$); 3.77 – 3.74 (m, 4H, H$_{G4}$); 3.74 – 3.70 (m, 8H, H$_{G3}$, H$_{G7}$); 3.70 – 3.66 (m, 12H, H$_{G8}$, H$_{G12}$, H$_{G11}$); 3.65 – 3.63 (m, 4H, H$_3$, H$_{D1}$); 3.62 (s, 12H, COO$\underline{\text{Me}}$); 3.59 – 3.47 (m, 12H, H$_{L4}$ or H$_{L6}$, H$_{L2}$ or H$_{L3}$, H$_4$, H$_5$); 3.46 – 3.39 (m, 8H, H$_{L2}$ or H$_{L3}$, H$_{L4}$ or H$_{L6}$); 2.76 (td, 2H, H$_{D4}$ or H$_{D5}$, J = 12.7, 3.6 Hz); 2.65 (td, 2H, H$_{D4}$ or H$_{D5}$, J = 12.7, 3.6 Hz); 2.01 – 1.90 (m, 4H, H$_{D3eq}$, H$_{D6eq}$); 1.83 – 1.73 (m, 4H, H$_{L5}$); 1.73 – 1.64 (m, 2H, H$_{D3ax}$ or H$_{D6ax}$); 1.57 – 1.47 (m, 2H, H$_{D3ax}$ or H$_{D6ax}$).

¹³C NMR (100 MHz, CD₃OD): δ 176.77, 176.62 ($\underline{\text{C}}$OOMe); 155.32, 154.92 (C$_{R6}$, C$_{R11}$); 150.46 (C$_{R3}$); 145.81 (C$_{TC4}$); 143.43 (C$_{T4}$); 127.09 (C$_{TC5}$); 125.87 (C$_{T5}$); 122.30 (C$_{R1}$); 119.00 (C$_{R10}$); 118.20 (C$_{R5}$); 115.86 (C$_{R4}$); 114.34 (C$_{R9}$); 112.79 (C$_{R2}$); 100.48 (C$_1$); 92.81, 91.70 (C$_{R7}$, C$_{R8}$); 75.68 (C$_5$); 75.57 (C$_3$); 74.12, 73.74 (C$_{G3}$, C$_{G7}$, C$_{G11}$); 72.47, 72.39 (C$_{D1}$, C$_2$); 72.09 (C$_{D2}$); 71.12 (C$_{L2}$ or C$_{L3}$); 70.93, 70.83 (C$_{G1}$, C$_{G5}$); 70.67 (C$_{G2}$, C$_{G6}$, C$_{G10}$); 70.55 (C$_{L2}$ or C$_{L3}$); 70.19 (C$_7$ or C$_{L7}$); 69.40 (C$_{G9}$); 68.84 (C$_{L4}$, C$_{L6}$); 68.61 (C$_4$); 68.34 (C$_7$ or C$_{L7}$); 64.86 (C$_{L1}$); 63.08 (C$_6$); 62.38, 62.36, 62.27 (C$_{G4}$, C$_{G8}$, C$_{G12}$); 54.83, 52.45 (COO$\underline{\text{Me}}$); 51.58, 51.53 (C$_{L8}$, C$_8$); 40.19, 40.05 (C$_{D4}$, C$_{D5}$); 30.85 (C$_{17}$); 28.81 (C$_{D3}$ or C$_{D6}$); 28.26 (C$_{D3}$ or C$_{D6}$).

MS (ESI-HRMS): calculated for [C$_{106}$H$_{154}$N$_{12}$O$_{46}$]: 2331.00802; found: 2331.00805 (after deconvolution).

$[\alpha]_D^{25}$: +8.5 (*c* 0.29, MeOH).

Synthesis of divalent glycodendrimer 2.41

2.41
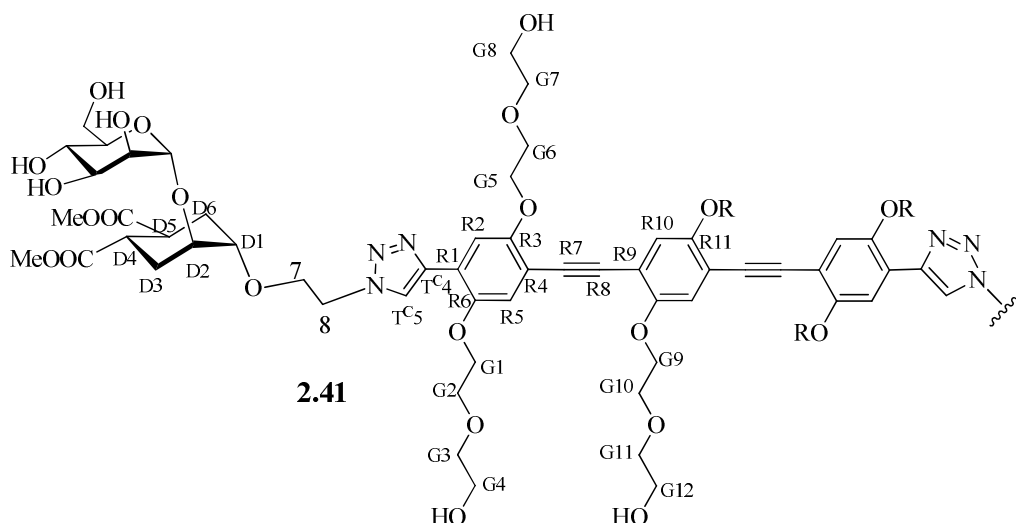
To a stirred solution of **TIPS-2.5** (16.2 mg, 12.8 µmol, 1 eq.) in THF (300 µL), TBAF (1 M in THF, 26.0 µL, 2 eq.) was added under nitrogen. After 1 h, TLC analysis (CH_2Cl_2:MeOH 9:1) showed that the desilylation reaction was complete. Then reagents were added as solutions in the following order: TBTA in THF (1.4 mg, 2.6 µmol, 0.2 eq., 100 µL of THF), $CuSO_4 \cdot 5H_2O$ in H_2O (0.32 mg, 1.28 µmol, 0.1 eq., 50 µL of H_2O) and sodium ascorbate in H_2O (1.01 mg, 5.1 µmol, 0.4 eq., 50 µL of H_2O). The reaction mixture was stirred at room temperature, under nitrogen atmosphere and in dark for 10 min. Finally **1.7** (13.1 mg, 28.2 µmol, 2.2 eq.) was added. THF and H_2O volumes were adjusted to 400 µL each. The reaction was stirred at RT, under nitrogen and in the dark overnight. TLC analysis (CH_2Cl_2:MeOH 9:1) revealed total consumption of **2.5**; TLC (CH_2Cl_2:MeOH:H_2O 80:20:2.5) showed the formation of a single new product and the remaining of a small amount of **1.7**. Quadrasil™-MP (S/Pd 5.9:1, 5 mg) was added to the reaction mixture, which was stirred for 10 min, and then filtered off. The solvent was removed under reduced pressure and the resulting mixture was redissolved in MeOH and purified by size exclusion chromatography (Sephadex LH-20, MeOH), obtaining 22 mg of **2.41** not pure. The remaining tetrabutylammonium salt was removed through automated reverse phase flash chromatography (C18, water with gradient of MeOH from 0 % to 100 %), obtaining 18 mg of pure **2.41** as a yellow solid (yield 71 %).
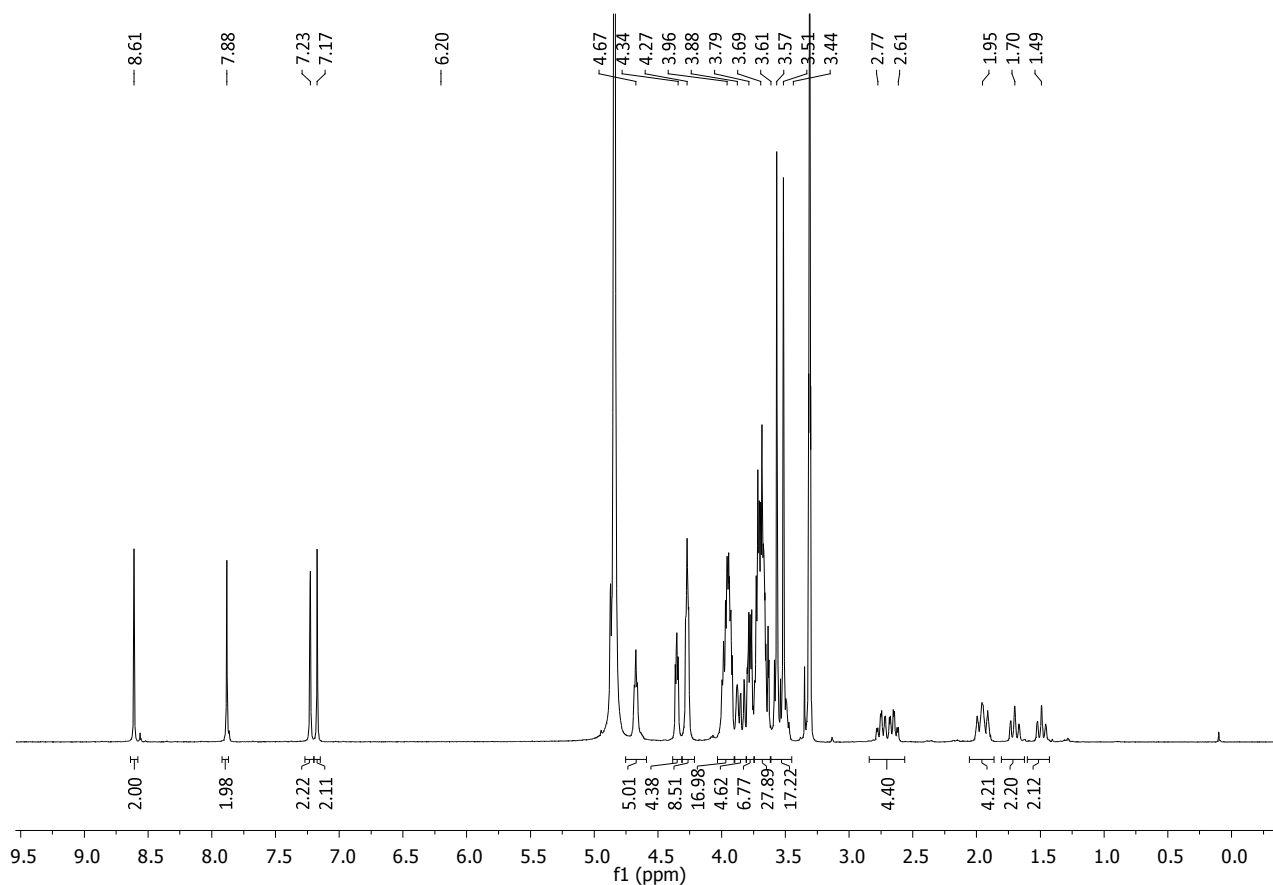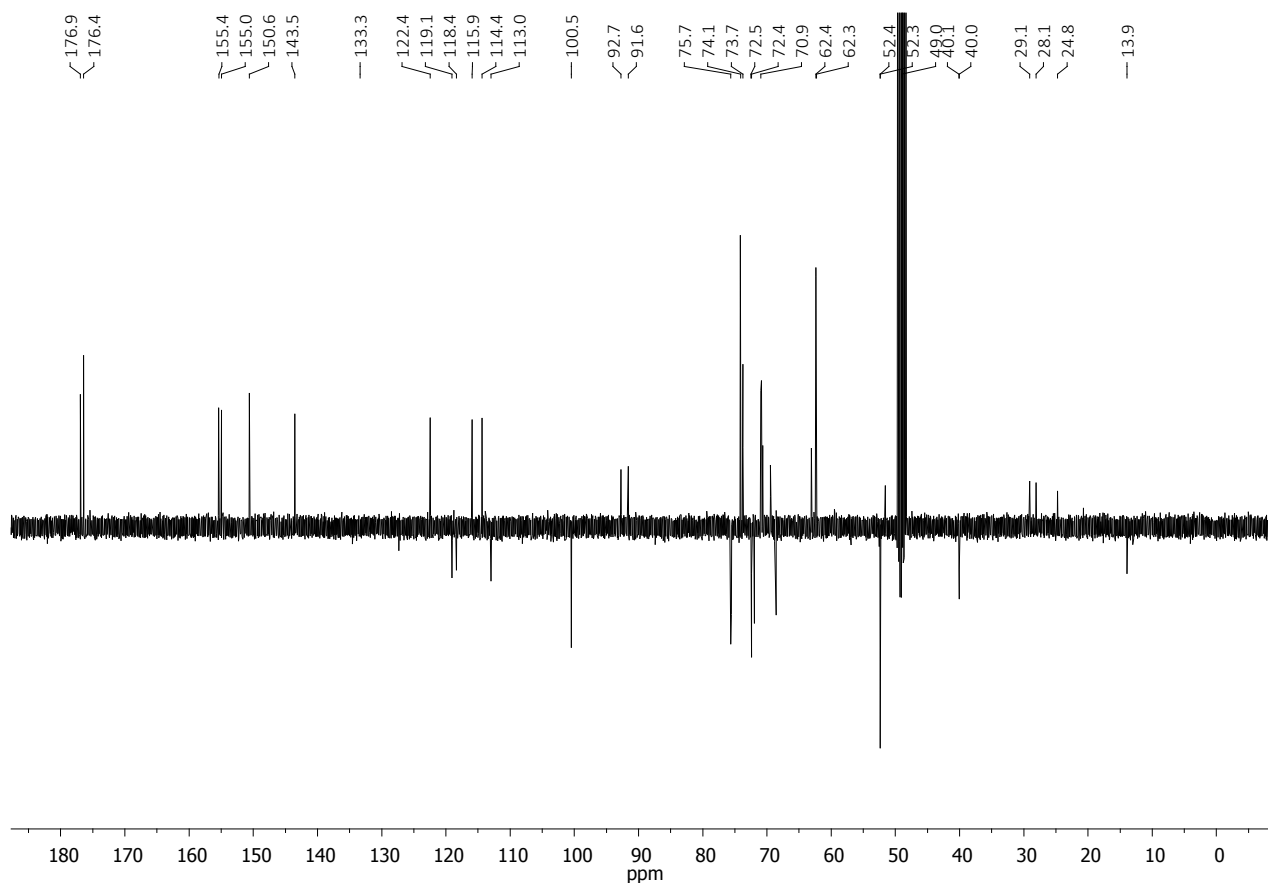
¹H NMR (400 MHz, CD₃OD): δ 8.61 (s, 2H, H_{TC5}); 7.88 (s, 2H, H_{R2}); 7.22 (s, 2H, H_{R5}); 7.17 (s, 2H, H_{R10}); 4.88 (br s, 2H, H_1); 4.67 (t, J = 4.6 Hz, 4H, H_8); 4.39 – 4.31 (m, 4H, H_{G9}); 4.30 – 4.21 (m, 8H, H_{G1}, H_{G5}); 4.00 – 3.91 (m, 16H, H_7, H_{G2}, H_{G6}, H_{G10}); 3.90 – 3.81 (m, 4H, H_{D2}, H_{6a}); 3.80 – 3.74 (m, 6H, H_2, H_{G12}); 3.74 – 3.63 (m, 26H, H_{D1}, H_3, H_{6b}, H_{G4}, H_{G8}, H_{G3}, H_{G11}, H_{G7}); 3.62 – 3.45 (m, 16H, COO$\underline{\text{Me}}$, H_4, H_5); 2.81 – 2.57 (m, 4H, H_{D4}, H_{D5}); 2.04 – 1.85 (m, 4H, H_{D3eq}, H_{D6eq}); 1.73 – 1.62 (m, 2H, H_{D3ax} or H_{D6ax}); 1.52 – 1.44 (m, 2H, H_{D3ax} or H_{D6ax}).

¹³C NMR (100 MHz, CD₃OD): δ 176.9, 176.4 ($\underline{\text{C}}$OOMe); 155.4, 154.9 (C_{R6}, C_{R11}); 150.6 (C_{R3}); 143.5 (C_{TC4}); 127.3 (C_{T4}); 122.5 (C_{R1}); 119.1 (C_{R10}); 118.4 (C_{R5}); 116.0, 114.3 (C_{R4}, C_{R9}); 113.0 (C_{R2}); 100.4 (C_1); 92.7, 91.7 (C_{R7}, C_{R8}); 75.6 (C_5); 75.5 (C_3); 74.1, 73.7 (C_{G3}, C_{G7}, C_{G11}); 72.5 (C_{D1}); 72.4 (C_2); 71.9 (C_{D2}); 70.9 (C_{G1} or C_{G5}); 70.9 (C_{G9}); 70.6 (C_{G2}, C_{G6}, C_{G10}); 69.4 (C_{G1} or C_{G5}); 68.6 (C_4); 68.5 (C_7), 63.1 (C_6); 62.4, 62.3 (C_{G4}, C_{G8}, C_{G12}); 52.4 (COO$\underline{\text{Me}}$); 51.6 (C_8); 40.1 (C_{D4}, C_{D5}); 29.1 (C_{D3} or C_{D6}); 28.1 (C_{D3} or C_{D6}).

MS (ESI): m/z calculated for $[C_{86}H_{120}N_6O_{40}Na_2]^{2+}$: 961.8; found: 961.9.

MS (ESI-HRMS): m/z calculated for $[C_{86}H_{120}N_6O_{40}]^+$: 1876.75403; found: 1876.76014.

[α]$_D$ ^{25}: +27.5 (*c* 0.59, MeOH).

Synthesis of hexavalent glycodendrimer 2.43

2.43
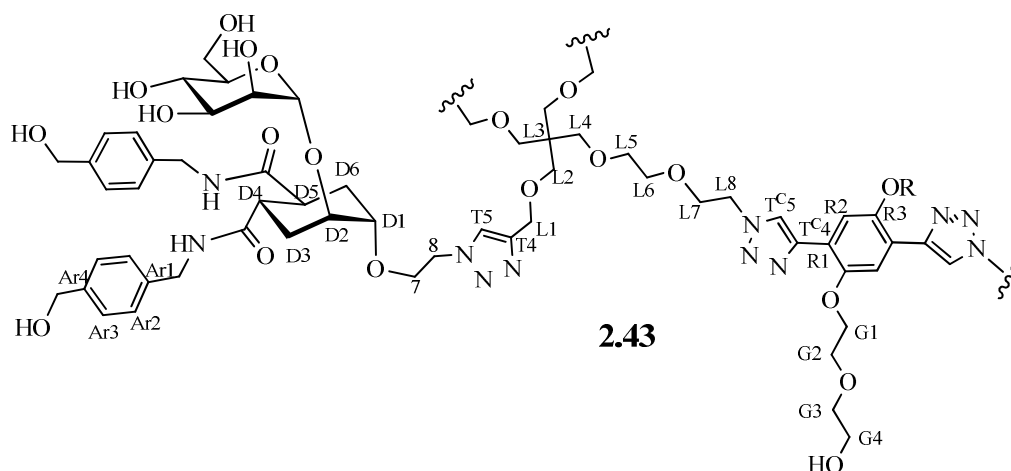
To a reaction vessel containing **2.3** (1.15 mg, .4 µmol, 1 eq.), reagents were added as solutions in the following order: TBTA in THF (0.36 mg, 0.69 µmol, 0.2 eq., 100 µL of THF), $CuSO_4 \cdot 5H_2O$ in H_2O (0.09 mg, 0.34 µmol, 0.1 eq., 50 µL of H_2O) and Sodium Ascorbate in H_2O (0.27 mg, 1.37 µmol, 0.4 eq, 50 µL of H_2O). The reaction mixture was stirred at room temperature, under nitrogen atmosphere and in dark for 10 min, then **2.2** (18 mg, 7.55 µmol, 2.2 eq.) was added as a solid. THF and H_2O volumes were adjusted to 500 µL each and The reaction mixture was heated at 60 °C under microwave irradiation for 90 min. TLC analysis (CH_2Cl_2:MeOH 9:1) revealed total consumption of **2.3**; mass analysis (MALDI, DHB or sinapinic acid matrix) confirmed that the reaction was complete. Quadrasil™-MP (S/Cu 22:1, 5 mg) was added to the reaction mixture, which was stirred for 10 min, and then filtered off. The solvent was removed under reduced pressure and the resulting mixture was redissolved in MeOH and purified by size exclusion chromatography (Sephadex LH-20, MeOH), obtaining 9 mg of pure **2.43** as a yellowish solid (yield 50 %).
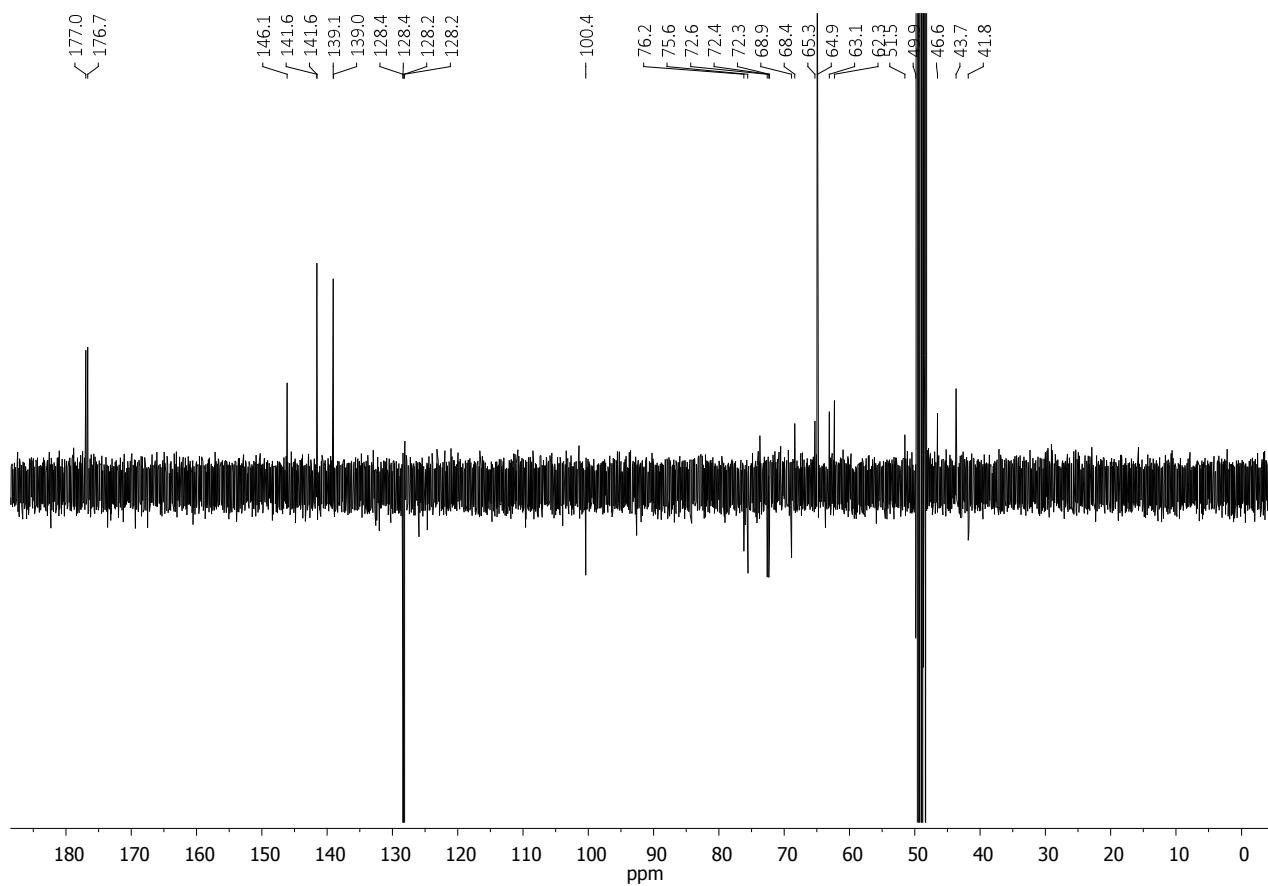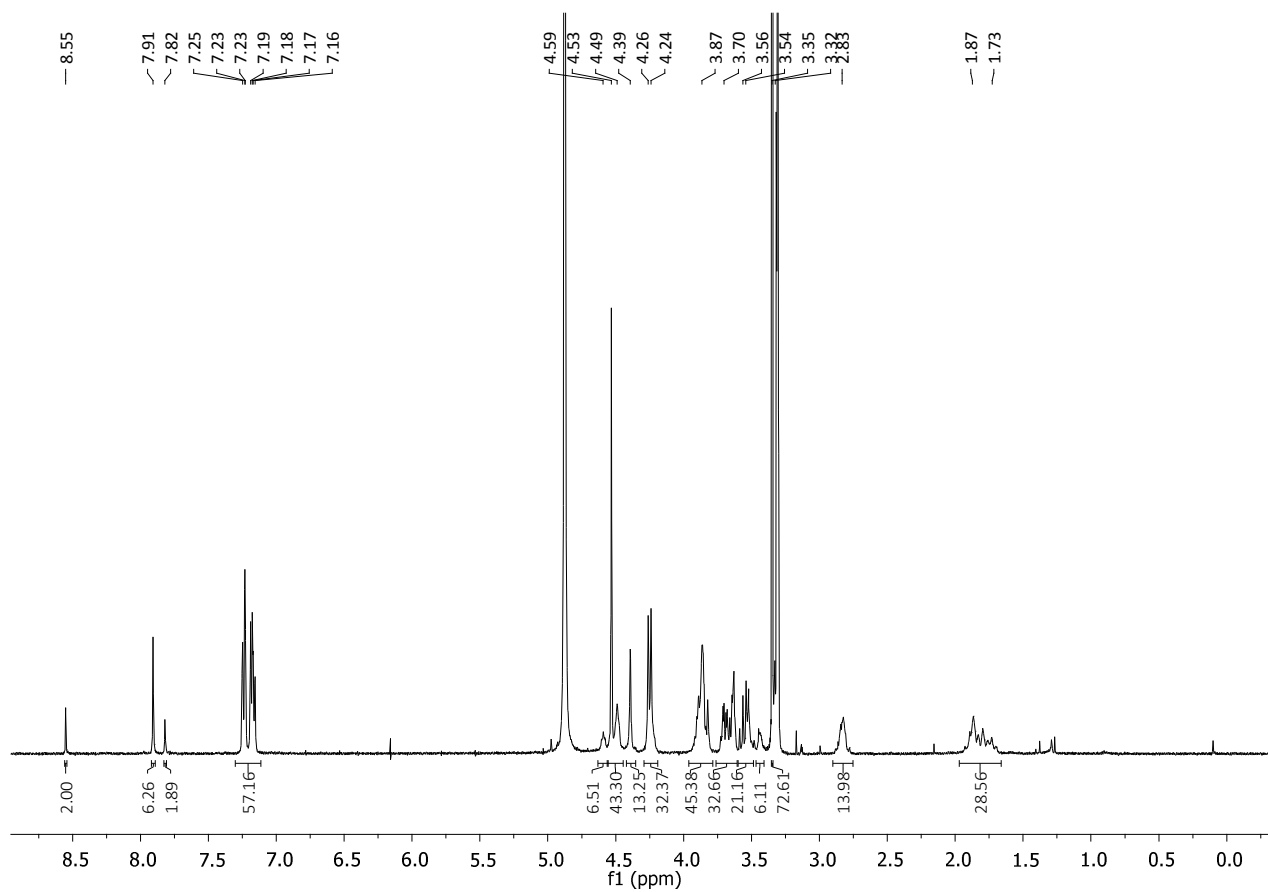
¹H NMR (400 MHz, CD₃OD): δ 8.55 (s, 2H, H_{TC5}); 7.90 (s, 6H, H_{T5}); 7.82 (s, 2H, H_{R2}); 7.27 – 7.12 (m, 48H, H_{Ar2}, H_{Ar3}); 4.88 (br s, 6H, H_1); 4.61 – 4.56 (m, 4H, H_{L8}); 4.53 (s, 24H, C$\underline{H}_2$OH); 4.50 – 4.44 (m, 12H, H_8); 4.40 (s, 12H, H_{L1}); 4.26 – 4.24 (m, 28H, C$\underline{H}_2$NH, H_{G1}); 3.93 - 3.85 (m, 32H, H_2, H_{D2}, H_7, H_{L7}, H_{G2}); 3.82 (bs, 6H, H_{6a}); 3.72 - 3.67 (m, 14H, H_{6b}, H_{G3}, H_{G4}); 3.65 – 3.62 (m, 12H, H_3, H_{D1}); 3.60 - 3.52 (m, 16H, H_4, H_5, H_{L5}); 3.45 – 3.44 (m, 4H, H_{L6}); 3.33 – 3.27 (m, 16H, H_{L2}, H_{L4}); 2.91 – 2.74 (m, 12H, H_{D4}, H_{D5}); 1.96 – 1.66 (m, 24H, H_{D3}, H_{D6}).

¹³C NMR (100 MHz, CD₃OD): δ 177.1, 176.8 ($\underline{C}$ONH); 146.3 (C_{T4}); 141.7, 141.7; 139.2, 139.2 (C_{Ar1}, C_{Ar4}); 128.6, 128.5, 128.3, 128.3 (C_{Ar2}, C_{Ar3}); 126.4 (C_{TC5}); 126.1 (C_{T5}); 112.6 (C_{R2}); 100.6 (C_1); 76.3 (C_3); 75.7 (C_5); 73.9 (C_{G3}); 72.6, 72.4, 72.3 (C_{D1}, C_{D2}, C_2); 71.9, 71.2 (C_{L5}, C_{L6}); 70.50 (C_{G2}); 69.83 (C_{L2}, C_{L4}); 68.7 (C_4); 69.0 (C_{G1}); 68.5 (C_7, C_{L7}); 65.5 (C_{L1}); 65.1 ($\underline{C}H_2OH$); 63.3 (C_6); 62.5 (C_{G4}); 51.7 (C_{L8}, C_8); 43.9 ($\underline{C}H_2NH$); 41.9 (C_{D4}, C_{D5}); 29.7 (C_{D3} or C_{D6}); 29.1 (C_{D3} or C_{D6}).

MS (MALDI, matrix: sinapinic acid, solvent: MeOH): m/z calculated for $[C_{246}H_{330}N_{36}O_{82}]^+$: 5103.4; found: 5102.6.

MS (ESI-HRMS): m/z calculated for $[C_{246}H_{330}N_{36}O_{82}]^+$: 5100.27592; found: 5100.29384 (after deconvolution).

[α]$_D$^{25}: -18.9 (c = 0.1, MeOH).

Synthesis of hexavalent glycodendrimer 2.44

2.44
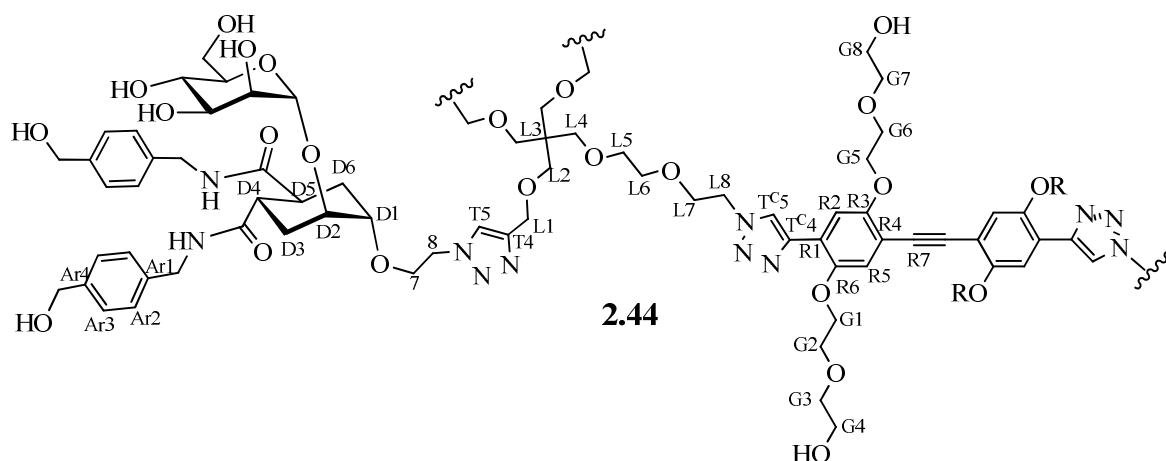
To a stirring solution of **TIPS-2.4** (4.1 mg, 4.38 µmol, 1 eq.) in THF (200 µL), TBAF (1 M in THF, 8.8 µL) was added under nitrogen. After 1 h, TLC analysis (CH₂Cl₂:MeOH 9:1) showed that the desilylation reaction was complete. The CuAAC reagents were added as solutions in the following order: TBTA in THF (0.47 mg, 0.9 µmol, 0.2 eq., 200 µL of THF), CuSO₄·5H₂O in H₂O (0.11 mg,

0.44 µmol, 0.1 eq., 150 µL of H_2O) and Sodium Ascorbate in H_2O (0.33 mg, 1.8 µmol, 0.4 eq., 150 µL of H_2O). The reaction mixture was stirred at room temperature, under nitrogen atmosphere and in the dark for 10 min. Then **2.2** (23 mg, 9.6 µmol, 2.2 eq.) was added as a solid. THF and H_2O volumes were adjusted to 600 µL each. The reaction mixture was heated at 60 °C under microwave irradiation for 60 min and then left stirring at room temperature overnight in the dark. TLC analysis (CH_2Cl_2:MeOH 9:1) revealed total consumption of **2.4**; mass analysis (MALDI, DHB or sinapinic acid matrix) confirmed that the reaction was complete. Quadrasil™-MP (S/Pd 17:1, 5 mg) was added to the reaction mixture, which was stirred for 10 minutes, and then filtered off. The solvent was removed under reduced pressure and the resulting mixture was redissolved in MeOH and purified by size exclusion chromatography (Sephadex LH-20, MeOH), obtaining 12 mg of pure **2.44** as a yellow solid (yield 52%).
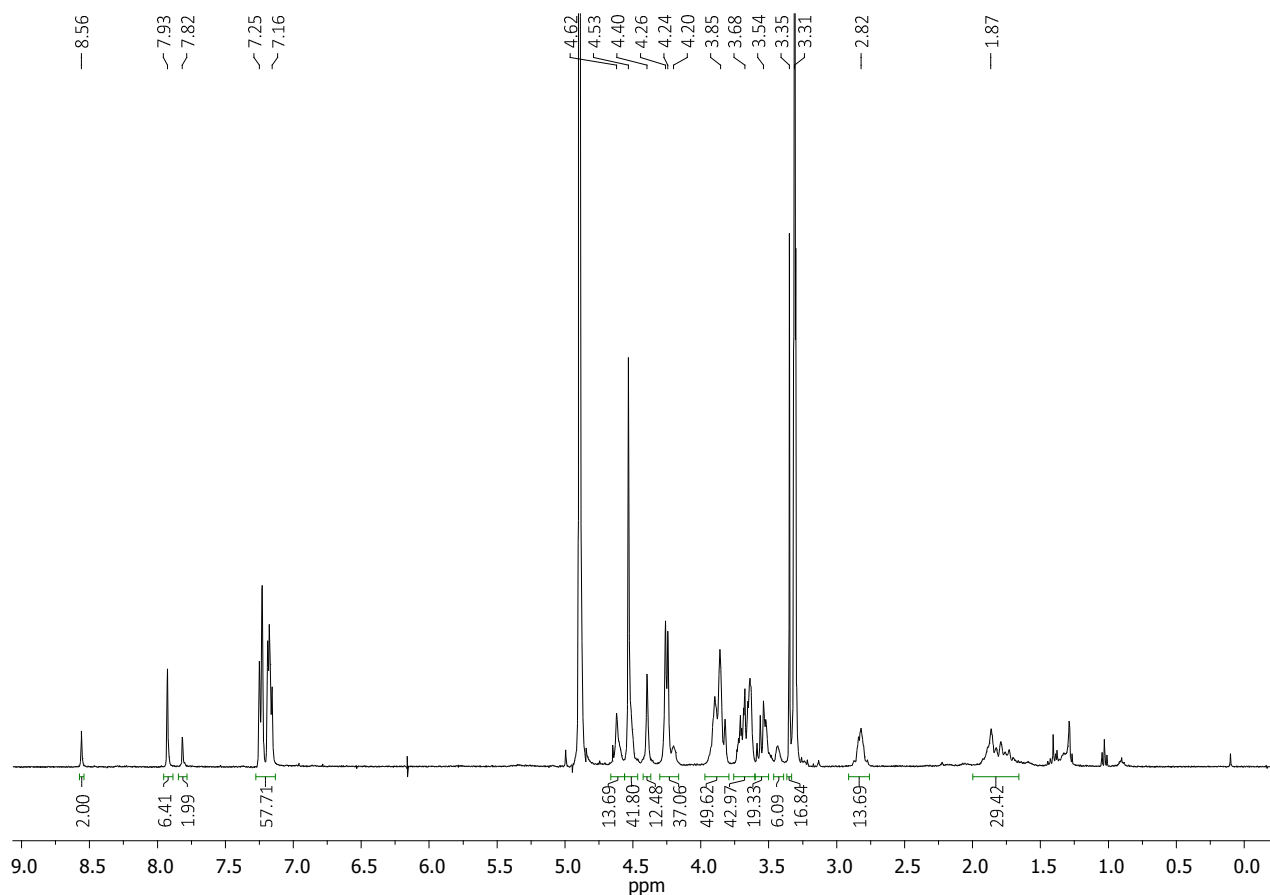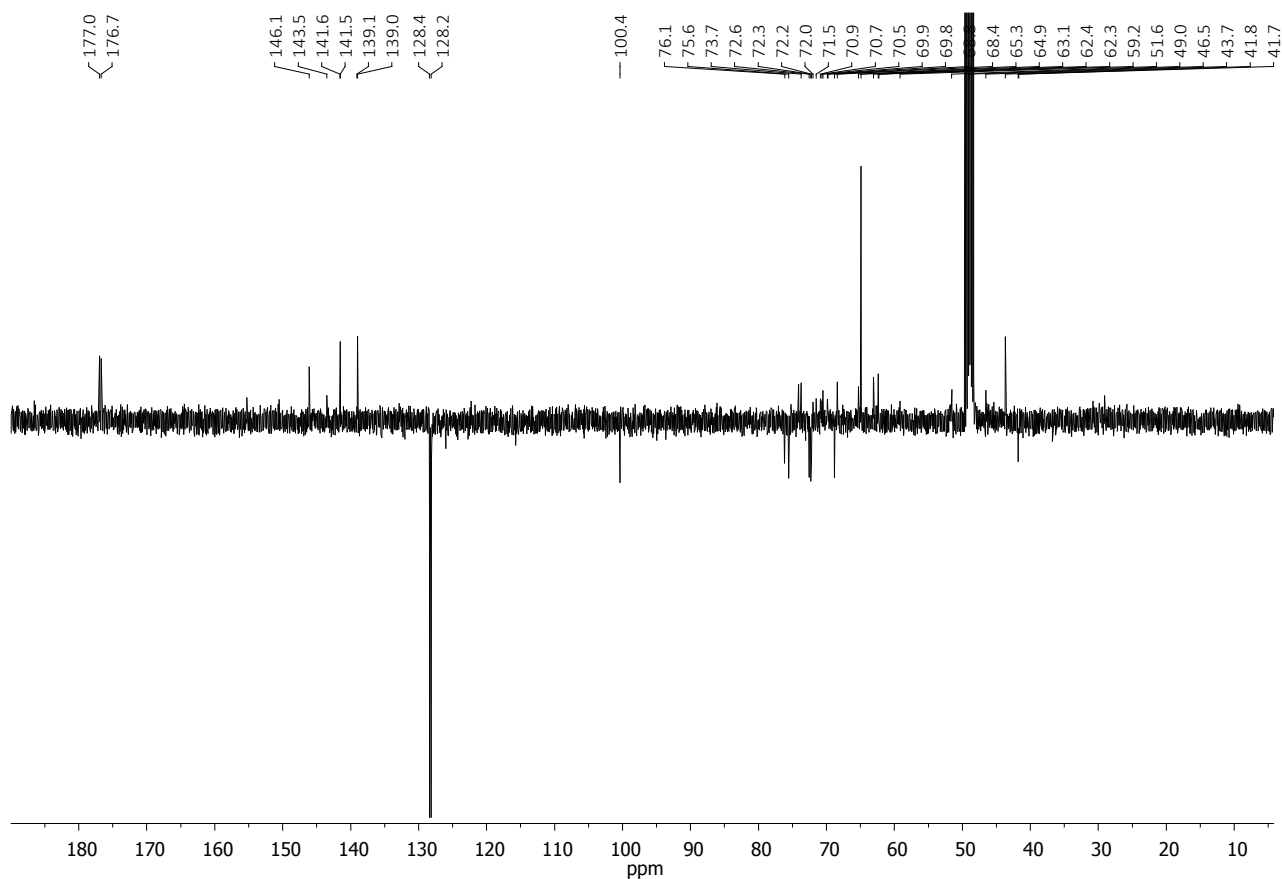
^{1}H NMR (400 MHz, CD$_3$OD): δ 8.56 (s, 2H, H$_{TC5}$); 7.93 (s, 6H, H$_{T5}$); 7.80 (s, 2H, H$_{R2}$); 7.25 – 7.16 (m, 50H, H$_{Ar2}$, H$_{Ar3}$, H$_{R5}$); 4.88 (br s, 6H, H$_1$); 4.65 – 4.60 (m, 4H, H$_{L8}$); 4.55 – 4.48 (m, 36H, C$\underline{H}_2$OH, H$_8$); 4.40 (s, 12H, H$_{L1}$); 4.29 – 4.16 (m, 32H, C$\underline{H}_2$NH, H$_{G1}$, H$_{G5}$); 3.95 - 3.80 (m, 42H, H$_2$, H$_{6a}$, H$_{D2}$, H$_7$, H$_{L7}$, H$_{G2}$, H$_{G6}$); 3.71 - 3.62 (m, 34H, H$_{6b}$, H$_{D1}$, H$_3$, H$_{G3}$, H$_{G7}$, H$_{G4}$, H$_{G8}$); 3.59 - 3.50 (m, 16H, H$_4$, H$_5$, H$_{L5}$); 3.45 - 3.42 (m, 4H, H$_{L6}$); 3.33 – 3.27 (m, 16H, H$_{L4}$, H$_{L2}$); 2.85 – 2.80 (m, 12H, H$_{D4}$, H$_{D5}$); 1.92 – 1.65 (m, 24H, H$_{D3}$, H$_{D6}$).

^{13}C NMR (100 MHz, CD$_3$OD): δ 179.0, 176.7 (CONH); 146.1 (C$_{T4}$); 143.5 (C$_{TC4}$); 141.6, 141.53; 139.1, 139.0 (C$_{Ar1}$, C$_{Ar4}$); 128.4, 128.2 (C$_{Ar2}$, C$_{Ar3}$); 126.3 (C$_{TC5}$); 125.7 (C$_{T5}$); 118.3 (C$_{R5}$); 112.7 (C$_{R2}$); 100.5 (C$_1$); 76.1 (C$_3$); 75.6 (C$_5$); 74.0 (C$_{G3}$, C$_{G7}$); 72.6 (C$_{D1}$); 72.3 (C$_2$, C$_{D2}$); 71.99, 71.49 (C$_{L5}$, C$_{L6}$); 70.8 - 69.5 (C$_{G1}$, C$_{G5}$, C$_{G2}$, C$_{G6}$, C$_{L2}$, C$_{L4}$); 68.8 (C$_4$); 68.3 (C$_7$, C$_{L7}$); 65.3 (C$_{L1}$); 64.9 (C$\underline{H}_2$OH); 63.0 (C$_6$); 62.3 (C$_{G4}$, C$_{G8}$); 51.5 (C$_{L8}$, C$_8$); 43.6 (C$\underline{H}_2$NH); 41.7 (C$_{D4}$, C$_{D5}$); 29.7 (C$_{D3}$ or C$_{D6}$), 29.0 (C$_{D3}$ or C$_{D6}$).

MS (MALDI, matrix: sinapinic acid, solvent: MeOH): *m/z* calculated for [C$_{262}$H$_{351}$N$_{36}$O$_{88}$]$^+$: 5412.3; found: 5413.2.

MS (ESI-HRMS): calculated for [C$_{262}$H$_{350}$N$_{36}$O$_{88}$]:5411.41100; found: 5411.42469 (after

deconvolution).

$[\alpha]_D^{25}$: -1.7 (c = 0.51, MeOH).

Synthesis of hexavalent glycodendrimer 2.45
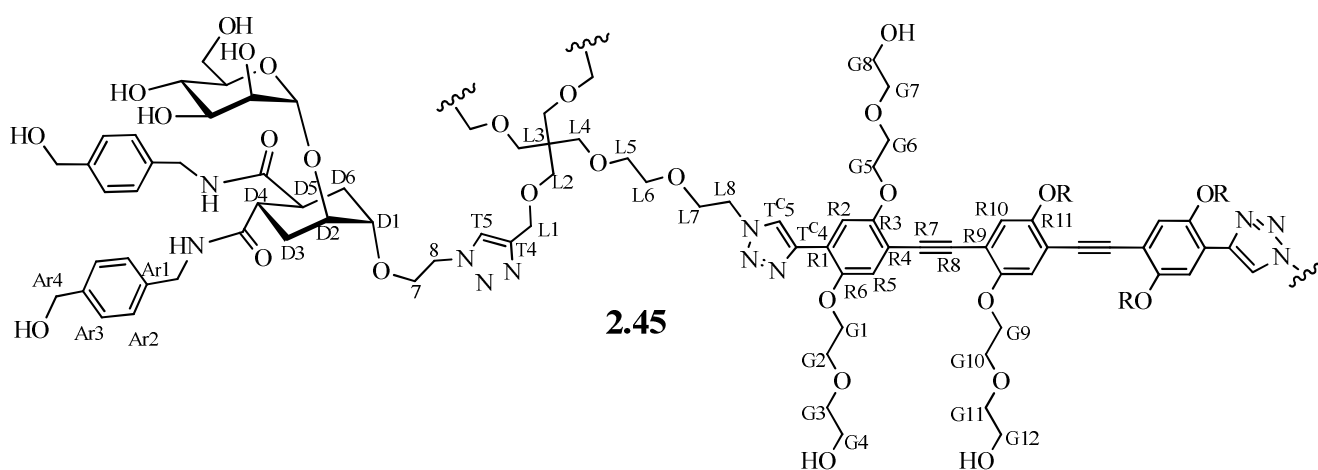
To a stirred solution of **TIPS-2.5** (3.2 mg, 2.5 µmol, 1 eq.) in THF (200 µL), TBAF (1 M in THF, 5.1 µL) was added under nitrogen atmosphere. After 1 h, TLC analysis (CH₂Cl₂:MeOH 9:1) showed that the desilylation reaction was complete. Then reagents were added as solutions in the following order: TBTA in THF (0.27 mg, 0.5 µmol, 0.2 eq., 100 µL of THF), CuSO₄·5H₂O in H₂O (0.06 mg, 0.25 µmol, 0.1 eq., 100 µL of H₂O), and sodium ascorbate in H₂O (0.20 mg, 1.0 µmol, 0.4 eq., 100 µL of H₂O). The reaction mixture was stirred at RT, under nitrogen atmosphere and in dark for 10 min. Then **2.2** (13.3 mg, 5.6 µmol, 2.2 eq.) was added as solid. THF and H₂O volumes were adjusted to 400 µL each. The reaction mixture was heated at 60 °C under microwave irradiation for 90 min. TLC analysis (CH₂Cl₂:MeOH 9:1) revealed total consumption of **2.5**; mass analysis (MALDI, DHB or sinapinic acid matrix) confirmed that the reaction was complete. Quadrasil™-MP (S/Cu 30:1, 5 mg) was added to the reaction mixture, which was stirred for 10 min, and then filtered off. The solvent was removed under reduced pressure and the resulting mixture was redissolved in MeOH and purified by size exclusion chromatography (Sephadex LH-20, MeOH), obtaining 12 mg of pure **2.45** as a yellowish solid (yield 85 %).
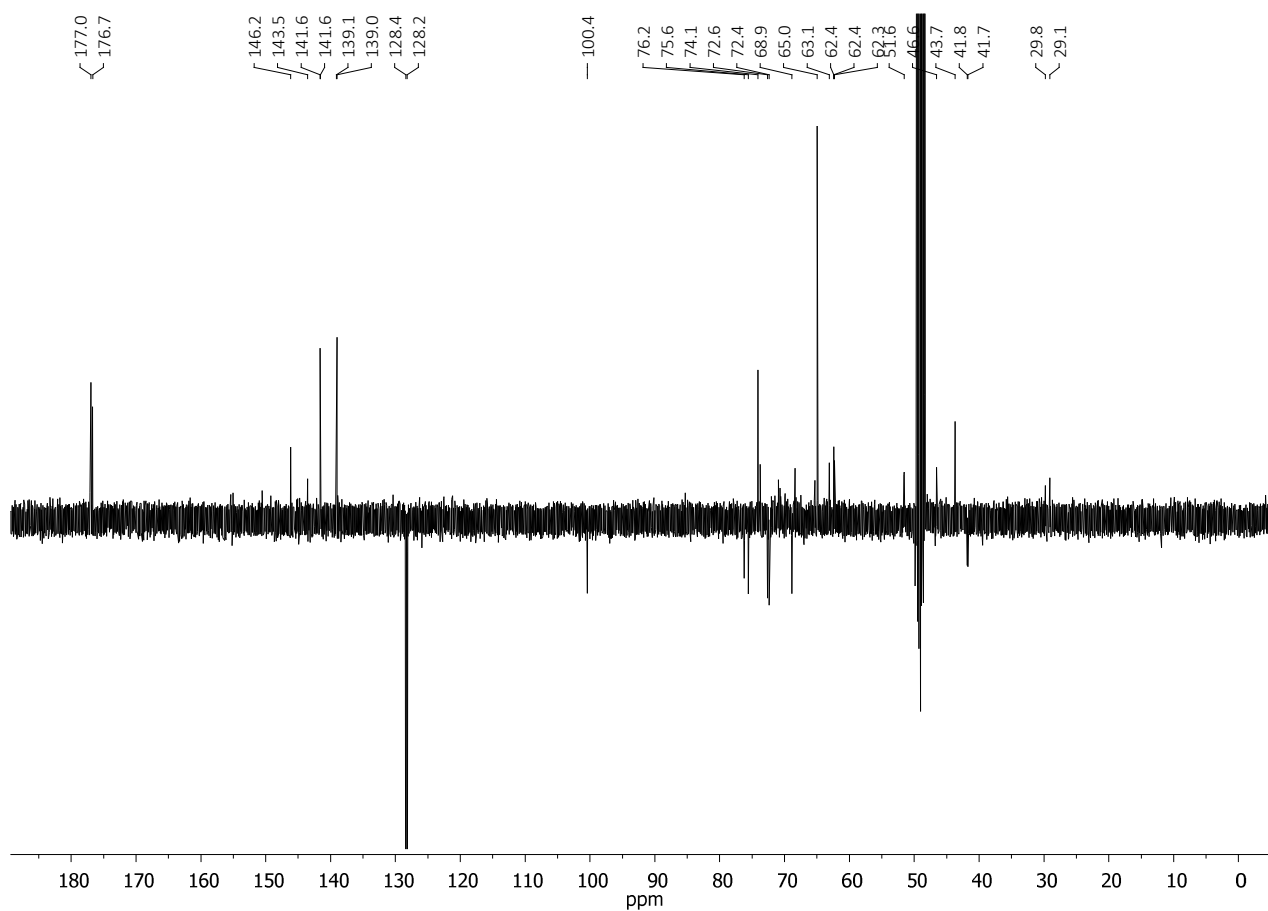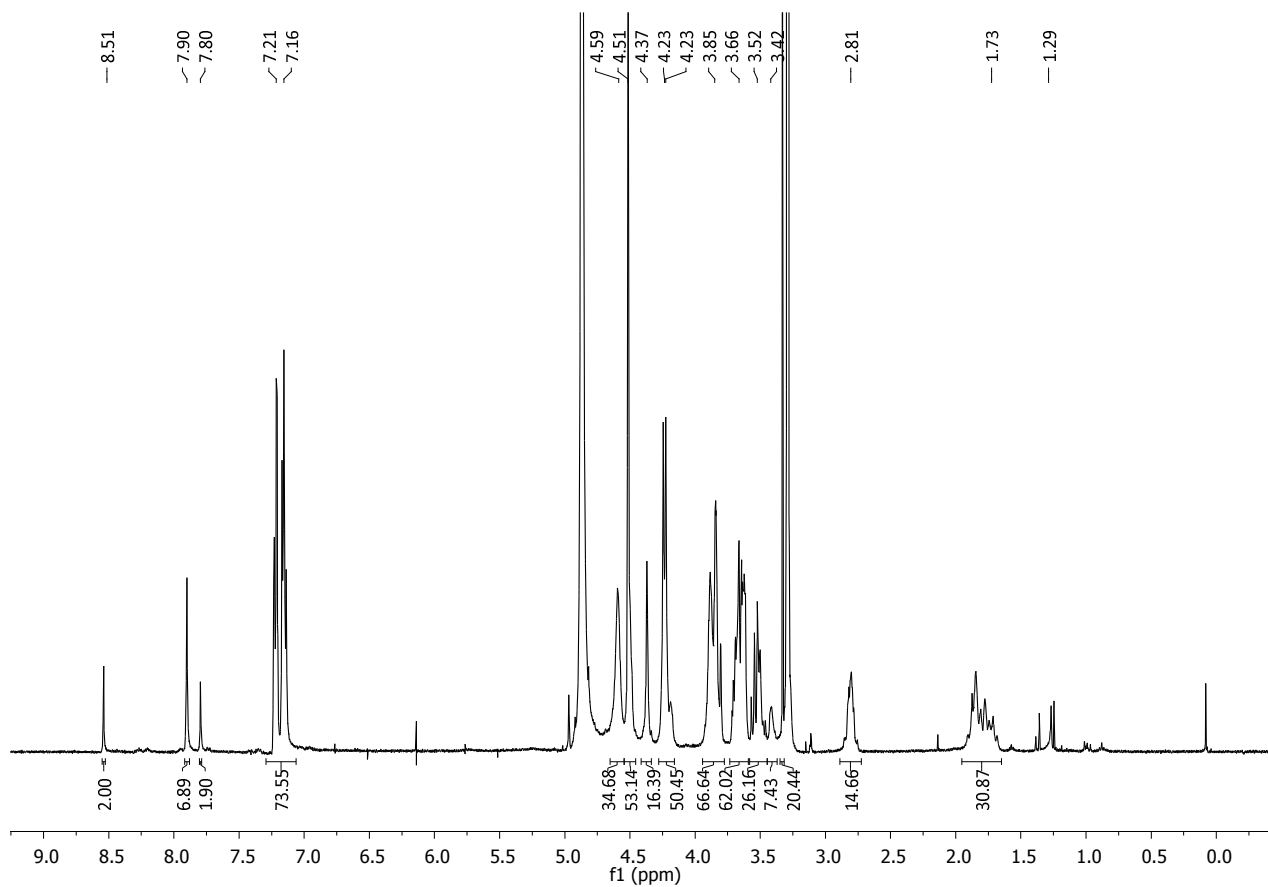
¹H NMR (400 MHz, CD₃OD): δ 8.56 (s, 2H, H_{TC5}); 7.92 (s, 6H, H_{T5}); 7.82 (s, 2H, H_{R2}); 7.28 – 7.13 (m, 52H, H_{Ar2}, H_{Ar3}, H_{R5}, H_{R10}); 4.88 (br s, 6H, H_1); 4.62 – 4.57 (m, 4H, H_{L8}); 4.56 – 4.48 (m, 36H, C$\underline{H}_2$OH, H_8); 4.39 (s, 12H, H_{L1}); 4.32 – 4.17 (m, 36H, C$\underline{H}_2$NH, H_{G1}, H_{G5}, H_{G9}); 3.95 - 3.79 (m, 46H, H_2, H_{6a}, H_{D2}, H_7, H_{L7}, H_{G2}, H_{G6}, H_{G10}); 3.75 - 3.61 (m, 42H, H_{6b}, H_{D1}, H_3, H_{G3}, H_{G7}, H_{G11}, H_{G4}, H_{G8}, H_{G12}); 3.60 - 3.39 (m, 16H, H_4, H_5, H_{L5}); 3.45 – 3.44 (m, 4H, H_{L6}); 3.33 – 3.27 (m, 16H, H_{L2}, H_{L4}); 2.89 – 2.75 (m, 12H, H_{D4}, H_{D5}); 1.96 – 1.66 (m, 24H, H_{D3}, H_{D6}).

¹³C NMR (100 MHz, CD₃OD): δ 177.1, 176.8 ($\underline{C}$ONH); 146.3 (C_{T4}); 143.7 (C_{TC4}); 141.7, 139.2, 139.2 (C_{Ar1}, C_{Ar4}); 128.6, 128.5, 128.3, 128.3 (C_{Ar2}, C_{Ar3}); 126.3 (C_{TC5}); 126.0 (C_{T5}); 119.3 (C_{R10}, C_{R5}); 113.5 (C_{R2}); 100.6 (C_1); 76.3 (C_3); 75.7 (C_5); 74.3, 74.3, 73.9 (C_{G3}, C_{G7}, C_{G11}); 72.6, 72.4, 72.3 (C_{D1}, C_2, C_{D2}); 72.3 – 69.0 (C_{L5}, C_{L6}, C_{L2}, C_{L4}, C_{G2}, C_{G6}, C_{G10}, C_{G1}, C_{G5}, C_{G9},); 69.0 (C_4); 68.5 (C_7, C_{L7}); 65.5 (C_{L1}); 65.1 ($\underline{C}$H₂OH); 63.3 (C_6); 62.6, 62.5, 62.5 (C_{G4}, C_{G8}, C_{G12}); 51.7 (C_{L8}, C_8); 43.9 ($\underline{C}$H₂NH); 42.0, 41.9 (C_{D4}, C_{D5}); 29.9 (C_{D3} or C_{D6}); 29.2 (C_{D3} or C_{D6}).

MS (MALDI, matrix: sinapinic acid, solvent: MeOH): m/z calculated for $[C_{278}H_{370}N_{36}O_{94}Na]^+$: 5743.1; found = 5744.6; calculated for $[C_{278}H_{370}N_{36}O_{94}]^+$: 5720.1; found = 5719.9.

MS (ESI-HRMS): m/z calculated for $[C_{278}H_{370}N_{36}O_{94}]^+$: 5716.52790; found = 5719.52543 (after deconvolution).

$[\alpha]_D^{25}$: -8.1 (c = 0.22, MeOH).

Synthesis of divalent glycodendrimer 2.46
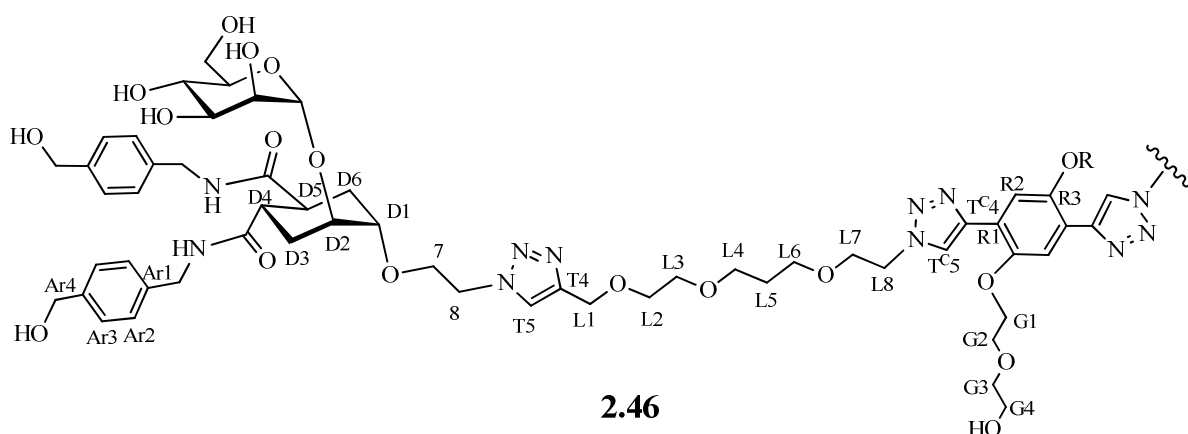
2.46

In a reaction vessel containing **2.3** (4 mg, 12 µmol, 1 eq.), reagents were added as solutions in the following order: TBTA in THF (1.3 mg, 2.4 µmol, 0.2 eq., in 68 µL of THF), CuSO₄·5H₂O in H₂O (0.3 mg, 1.2 µmol, 0.1 eq., 22 µL of H₂O) and Sodium Ascorbate in H₂O (0.95 mg, 4.8 µmol, 0.4 eq., 26 µL of H₂O). The reaction mixture was stirred at room temperature, under nitrogen

atmosphere and in dark for 10 min. Finally **2.7** (19.1 mg 99.6 % w/w, 26.6 µmol effective, 2.2 eq.) was added as solid. THF and H_2O volumes were adjusted to 250 µL each. The reaction was stirred at RT, under nitrogen and in the dark overnight. TLC analysis (CH_2Cl_2:MeOH 9:1) revealed total consumption of **2.3**; TLC (CH_2Cl_2:MeOH:H_2O 70:30:2.5) monitored the formation of a new polar species and the disappearance of another one having a slightly higher polarity relative to **2.7** (probably corresponding to the monosubstituted intermediate). Quadrasil™-MP (S/Cu 6.3:1, 5 mg) was added to the reaction mixture, which was stirred for 10 min, and then filtered off. The solvent was removed under reduced pressure and the resulting mixture was redissolved in MeOH and purified by size exclusion chromatography (Sephadex LH-20, MeOH), obtaining 20 mg of **2.46** not pure. The remaining tetrabutylammonium salt was removed through automated reverse phase flash chromatography (C18, H_2O with gradient of MeOH from 0 % to 100 %), obtaining 17 mg of pure **2.46** as a white solid (yield 65 %).
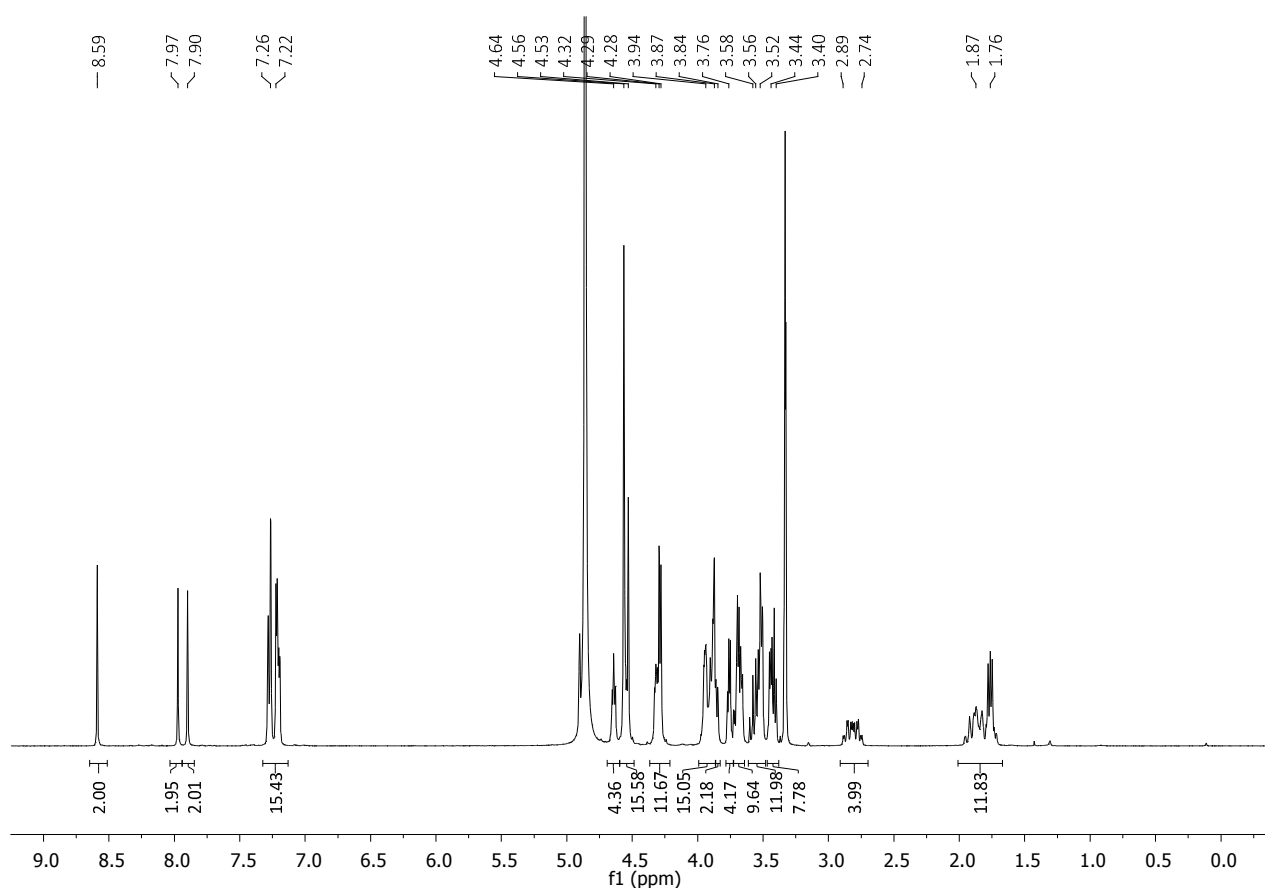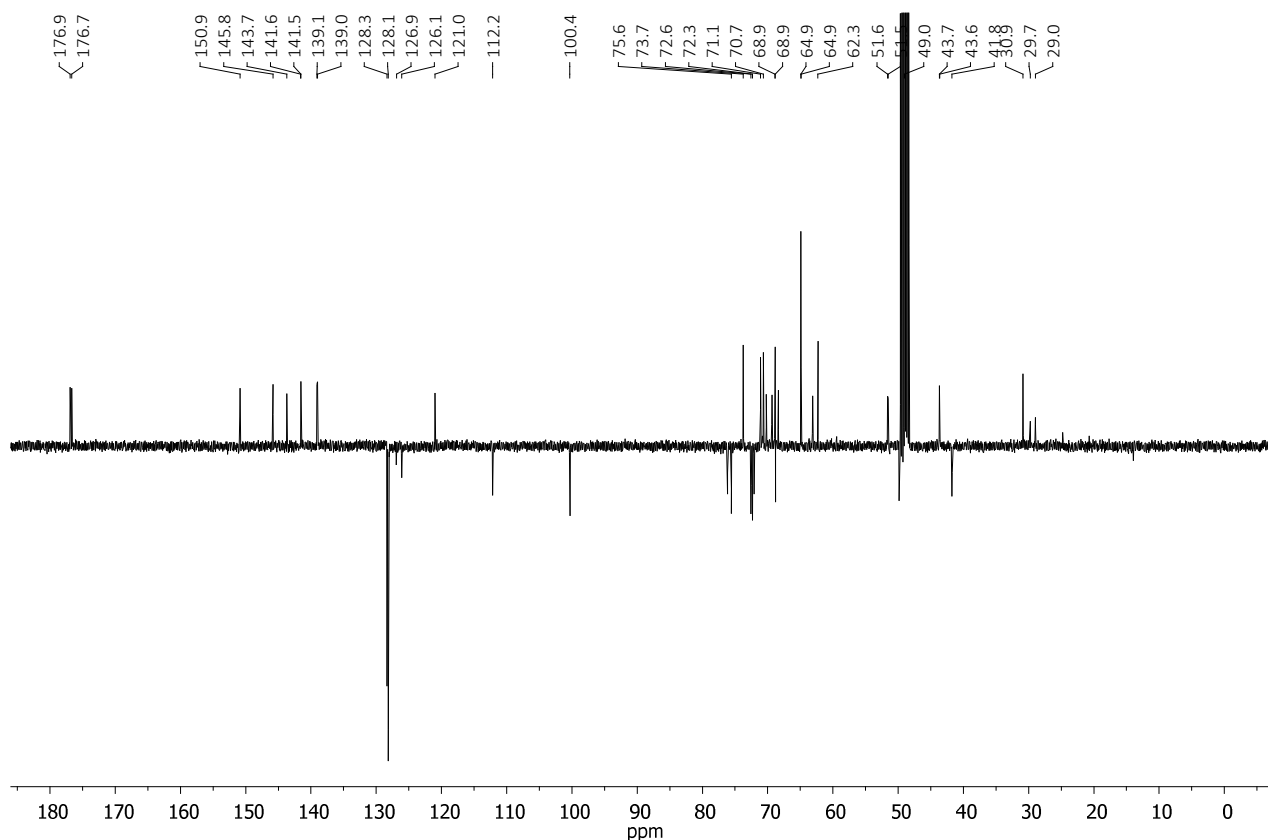
¹H NMR (400 MHz, CD₃OD): δ 8.58 (s, 2H, H$_{TC5}$); 7.96 (s, 2H, H$_{T5}$); 7.88 (s, 2H, H$_{R2}$); 7.30 – 7.15 (m, 16H, H$_{Ar2}$, H$_{Ar3}$); 4.89 (br s, 2H, H$_1$); 4.62 (t, 4H, H$_{L8}$, J = 4.9 Hz); 4.58 – 4.47 (m, 16H, H$_8$, C$\underline{H}_2$OH, H$_{L1}$); 4.29 (dd, 4.8 Hz, 12H, C$\underline{H}_2$NH, H$_{G1}$, J = 13.2); 3.96 – 3.85 (m, 16H, H$_{G2}$, H$_7$, H$_{L7}$, H$_2$, H$_{D2}$); 3.83 (d, 2H, H$_{6a}$, J = 5.0 Hz); 3.74 (t, J = 3.6 Hz, 4H, H$_{G4}$); 3.72 – 3.60 (m, 10H, H$_{G3}$, H$_3$, H$_{6b}$, H$_{D1}$); 3.58 – 3.48 (m, 12H, H$_5$, H$_{L1}$, H$_{L2}$, H$_4$); 3.45 – 3.36 (m, 8H, H$_{L6}$, H$_{L3}$); 2.89 – 2.71 (m, 4H, H$_{D4}$, H$_{D5}$); 1.97 – 1.78 (m, 8H, H$_{D3}$, H$_{D6}$); 1.78 – 1.71 (m, 4H, H$_{L5}$).

¹³C NMR (100 MHz, CD₃OD): δ 176.9, 176.7 ($\underline{C}$ONH); 150.9 (C$_{R3}$); 145.8 (C$_{TC4}$); 143.7 (C$_{T4}$); 141.6, 141.5, 139.1, 139.0 (C$_{Ar1}$, C$_{Ar4}$); 128.3, 128.2 (C$_{Ar2}$, C$_{A3}$); 126.9 (C$_{TC5}$); 126.1 (C$_{T5}$); 121.0 (C$_{R1}$); 112.2 (C$_{R2}$); 100.4 (C$_1$); 76.2 (C$_3$); 75.6 (C$_5$); 73.7 (C$_{G3}$); 72.6, 72.3, 72.1 (C$_{D1}$, C$_2$, C$_{D2}$); 71.1 – 70.2 (C$_{L2}$, C$_{L3}$, C$_{G1}$, C$_{G2}$); 69.3 (C$_{G1}$); 68.88, 68.86 (C$_{L4}$, C$_{L6}$); 68.81(C$_4$); 68.4 (C$_7$, C$_{L7}$); 64.9, 64.9 ($\underline{C}$H$_2$OH, C$_{L1}$); 63.1 (C$_6$); 62.3 (C$_{G4}$); 51.6, 51.5 (C$_8$, C$_{L8}$); 43.7, 43.6 ($\underline{C}$H$_2$NH); 41.8, 41.7 (C$_{D4}$, C$_{D5}$); 30.9 (C$_{L5}$); 29.7 (C$_{D3}$ or C$_{D6}$); 29.0 (C$_{D3}$ or C$_{D6}$).

MS (ESI-HRMS): m/z calculated for $[C_{102}H_{142}N_{16}O_{34}Na]^+$: 2157.97666; found: 2157.98424.

$[\alpha]_D^{25}$: -3.2 (*c* 0.39, MeOH).

Synthesis of divalent glycodendrimer 2.47

2.47
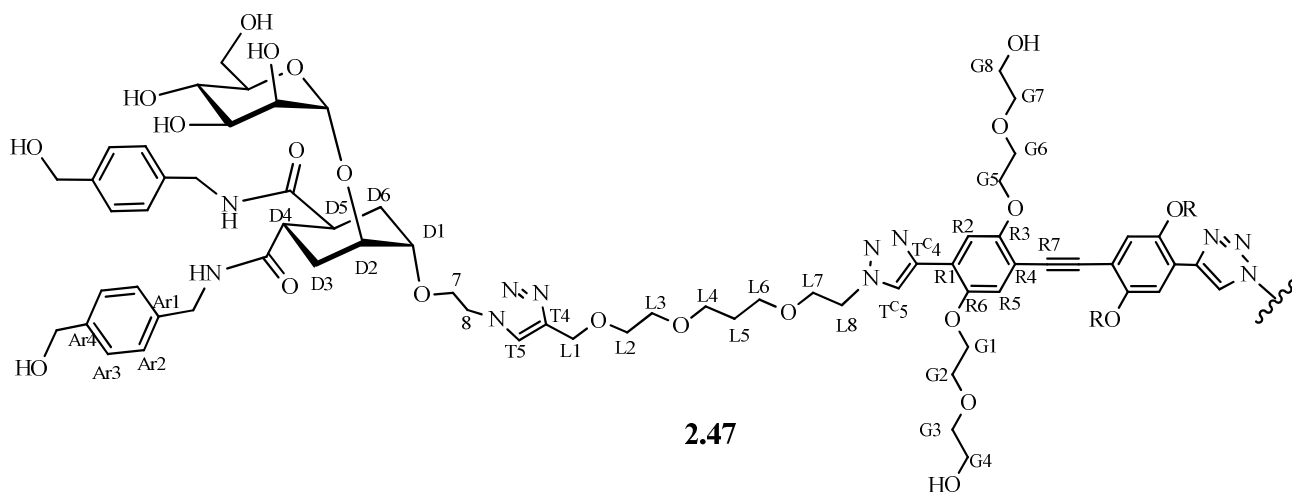
To a stirred solution of **TIPS-2.4** (12 mg, 12.6 µmol, 1 eq.) in THF (300 µL), TBAF (1 M in THF, 25.1 µL, 2 eq.) was added under nitrogen. After 1 h, TLC analysis (CH_2Cl_2:MeOH 9:1) showed that the desilylation reaction was complete. The CuAAC reagents were added as solutions in the following order: TBTA in THF (1.34 mg, 2.5 µmol, 0.2 eq., 75 µL of THF), $CuSO_4 \cdot 5H_2O$ in H_2O (0.31 mg, 1.3 µmol, 0.1 eq., 25 µL of H_2O) and Sodium Ascorbate in H_2O (0.96 mg, 5.0 µmol, 0.4 eq., 36 µL of H_2O). The reaction mixture was stirred at room temperature, under nitrogen atmosphere and in dark for 10 min. Finally **2.7** (25.3 mg 99.6 % w/w, 28 µmol effective, 2.2 eq.) was added as a solid. THF and H_2O volumes were adjusted to 400 µL each. The reaction was stirred at RT under nitrogen and in the dark overnight. TLC analysis (CH_2Cl_2:MeOH 9:1) revealed total consumption of **2.4**; TLC ($CHCl_3$:MeOH:H_2O 70:30:2.5) revealed the presence of a single new species, together with a small amount of starting material **2.7**. Quadrasil™-MP (S/Cu 5.8:1, 5 mg) was added to the reaction mixture, which was stirred for 10 min, and then filtered off. The solvent was removed under reduced pressure and the resulting mixture was redissolved in MeOH and purified by size exclusion chromatography (Sephadex LH-20, MeOH), obtaining 19 mg of **2.47** not pure**.** The remaining tetrabutylammonium salt was removed through automated reverse phase flash chromatography (C18, water with gradient of MeOH from 0 % to 100 %), obtaining 17 mg of pure **2.47** as a yellow solid (yield 57 %).
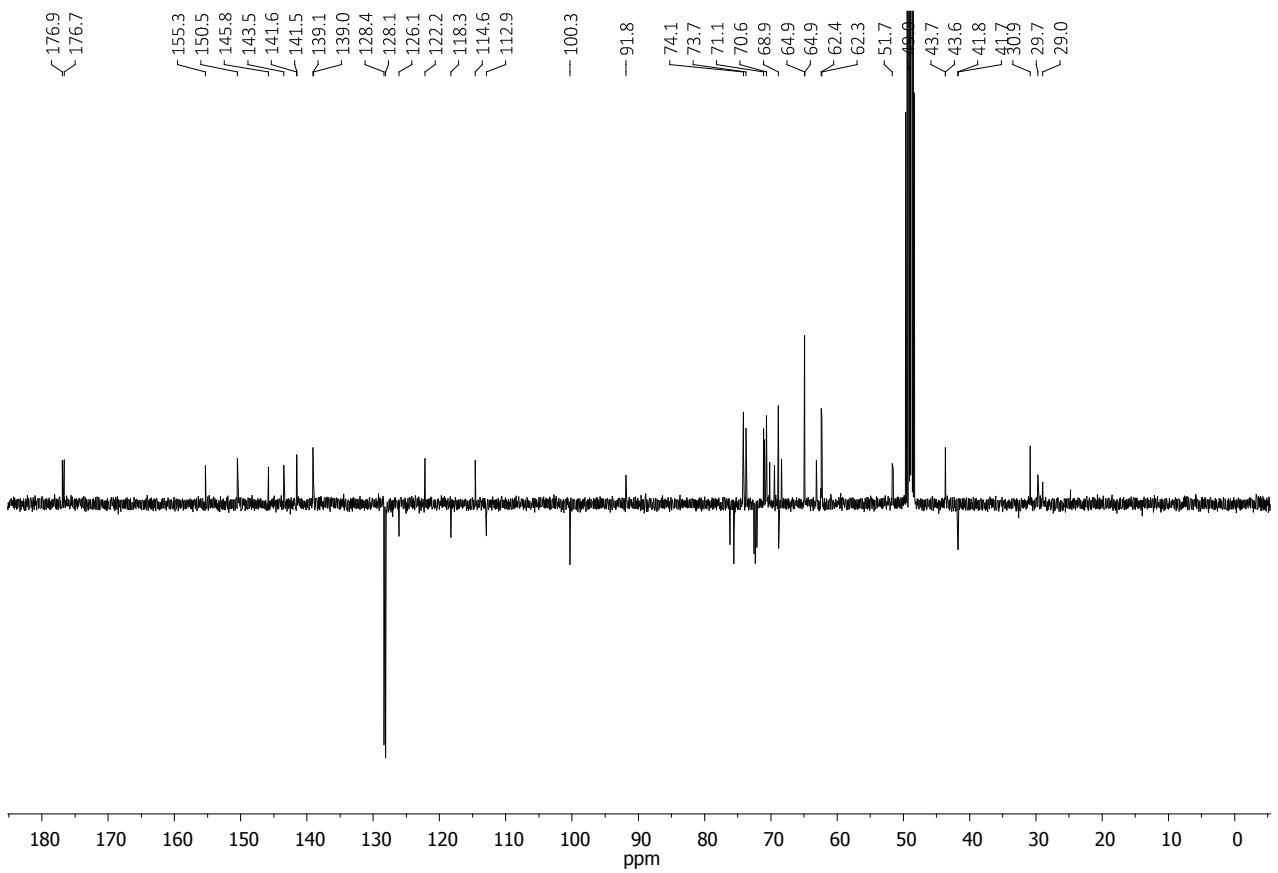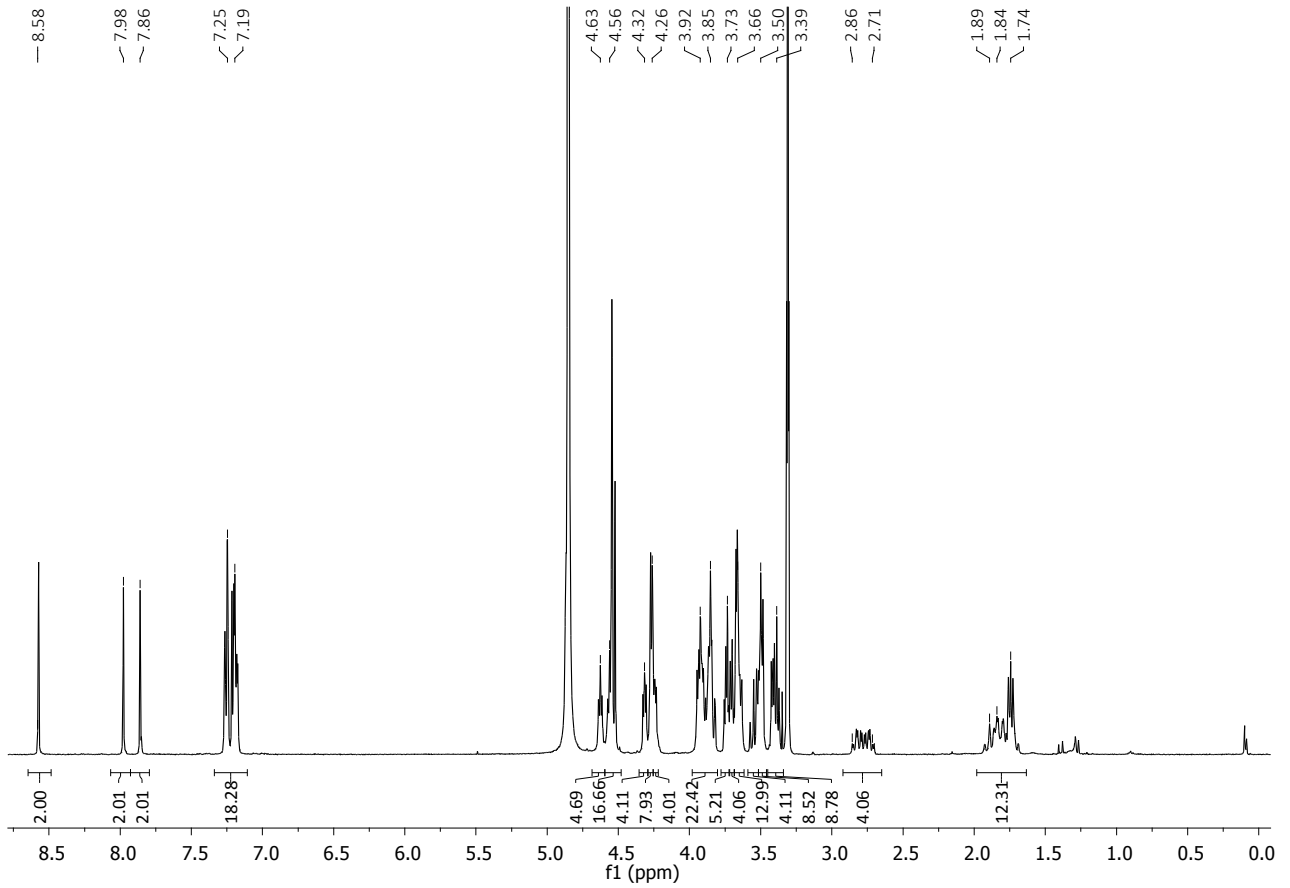
¹H NMR (400 MHz, CD₃OD): δ 8.57 (s, 2H, H_{TC5}); 7.98 (s, 2H, H_{TC}); 7.86 (s, 2H, H_{R2}); 7.26 – 7.17 (m, 18H, H_{Ar2}, H_{Ar3}, H_{R5}); 4.87 (br s, 2H, H_1); 4.66 – 4.59 (m, 4H, H_{L8}); 4.59 – 4.52 (m, 16H, H_8, C$\underline{H}_2$OH, H_{L1}); 4.35 – 4.29 (m, 4H, H_{G1}); 4.29-4.25 (m, 8H, C$\underline{H}_2$NH); 4.26 – 4.21 (m, 4H, H_{G5}); 3.95 – 3.82 (m, 24H, H_{G2}, H_{G6}, H_7, H_{L7}, H_{D2}, H_2, H_6); 3.78 – 3.73 (m, 4H, H_{G4}); 3.73 – 3.69 (m, 4H, H_{G3} or H_{G7}); 3.67 – 3.63 (m, 12H, H_{G8}, H_{G3} or H_{G7}, H_{D1}, H_3); 3.57 – 3.51 (m, 4H, H_4, H_5); 3.50 – 3.48 (m, 4H, H_{L2} or H_{L3}, H_{L4} or H_{L6}); 3.44 – 3.34 (m, 4H, H_{L2} or H_{L3}, H_{L4} or H_{L6}); 2.86 – 2.71 (m, 4H, H_{D4}, H_{D5}); 1.95 – 1.78 (m, 8H, H_{D3}, H_{D6}); 1.77 – 1.73 (m, 4H, H_{L5}).

¹³C NMR (100 MHz, CD₃OD): δ 176.9, 176.7 ($\underline{C}$ONH); 155.4 (C_{R6}); 150.5 (C_{R3}); 145.8 (C_{TC4}); 143.5 (C_{T4}); 141.6, 141.5, 139.1, 139.0 (C_{Ar1}, C_{Ar4}); 128.4, 128.2 (C_{Ar2}, C_{Ar3}); 127.1 (C_{TC5}); 126.1 (C_{T5}); 122.2 (C_{R1}); 118.3 (C_{R5}); 114.6 (C_{R4}); 112.9 (C_{R2}); 100.3 (C_1); 91.8 (C_{R7}); 76.2 (C_3); 75.6 (C_5); 74.1, 73.7 (C_{G3}, C_{G7}); 72.6, 72.3, 72.11 (C_{D1}, C_2, C_{D2}); 71.1 – 70.2 (C_{L2}, C_{L3}, C_{G1}, C_{G2}, C_{G6}); 69.5 (C_{G5}); 68.9 (C_{L4}, C_{L3}), 68.8 (C_4); 68.4 (C_7, C_{L7}); 64.92, 64.87 ($\underline{C}$H₂OH, C_{L1}); 63.1 (C_6); 62.4, 62.3 (C_{G8}, C_{G4}); 51.7, 51.5 (C_{L8}, C_8); 43.7, 43.6 ($\underline{C}$H₂NH); 41.8 (C_{D4}, C_{D5}); 30.9 (C_{L5}); 29.7 (C_{D3} or C_{D6}); 29.0 (C_{D3} or C_{D6}).

MS (ESI-HRMS): calculated for $[C_{118}H_{162}N_{16}O_{40}]$: 2443.11342; found: 2443.11450 (after deconvolution).

$[\alpha]_D^{25}$: +3.9 (*c* 0.95, MeOH).

Synthesis of divalent glycodendrimer 2.48

2.48
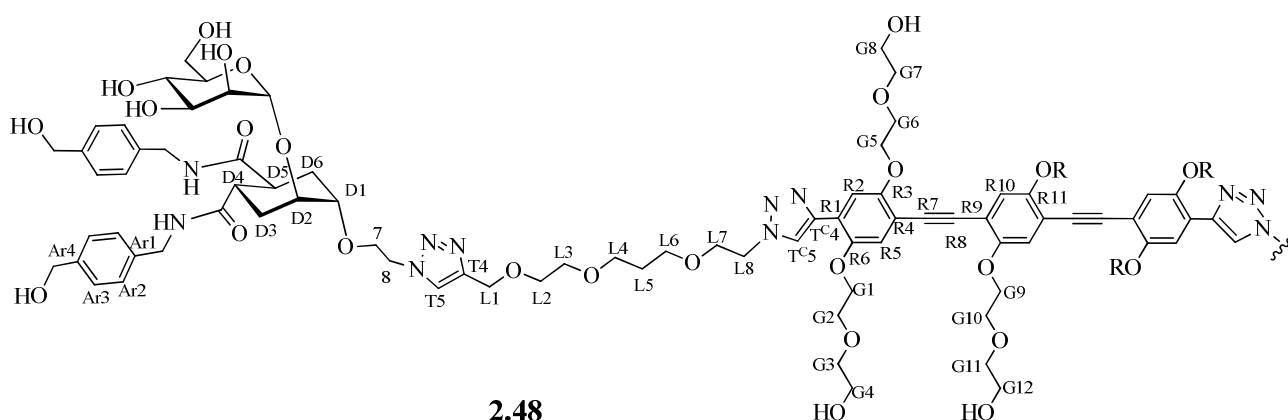
To a stirred solution of **TIPS-2.5** (12.4 mg, 10 µmol, 1 eq.) in THF (250 µL), TBAF (1 M in THF, 20.0 µL, 2 eq.) was added under nitrogen atmosphere. After 1 h, TLC analysis (CH₂Cl₂:MeOH 9:1) showed that the reaction was complete. Then reagents were added as solutions in the following

order: TBTA in THF (1.06 mg, 2.0 µmol, 0.2 eq., 34 µL of THF), CuSO₄·5H₂O in H₂O (0.25 mg, 1.0 µmol, 0.1 eq., 17 µL of H₂O) and Sodium Ascorbate in H₂O (0.79 mg, 4.0 µmol, 0.4 eq., 30 µL of H₂O). The reaction mixture was stirred at room temperature, under nitrogen atmosphere and in the dark for 10 min. Finally **2.7** (20.2 mg 99.6 % w/w, 22.3 µmol effective, 2.2 eq.) was added. THF and H₂O volumes were adjusted to 300 µL each. The reaction was stirred at room temperature under nitrogen and in the dark overnight. TLC analysis (CH₂Cl₂:MeOH 9:1) revealed total consumption of **2.5**; TLC (CH₂Cl₂:MeOH:H₂O 70:30:2.5) monitored the formation of a new polar species and the disappearance of another one having a slightly higher polarity relative to **2.7** (probably corresponding to the monosubstituted intermediate); mass analysis (MALDI, DHB matrix) confirmed that the reaction was complete. Quadrasil™-MP (S/Cu 7.5:1, 5 mg) was added to the reaction mixture, which was stirred for 10 min, and then filtered off. The solvent was removed under reduced pressure and the resulting mixture was redissolved in MeOH and purified by size exclusion chromatography (Sephadex LH-20, MeOH), obtaining 20 mg of **2.48** not pure. The remaining tetrabutylammonium salt was removed through automated reverse phase flash chromatography (C18, H₂O with gradient of MeOH from 0 % to 100 %), obtaining 17 mg of pure **2.48** as a yellow solid (yield 60 %).
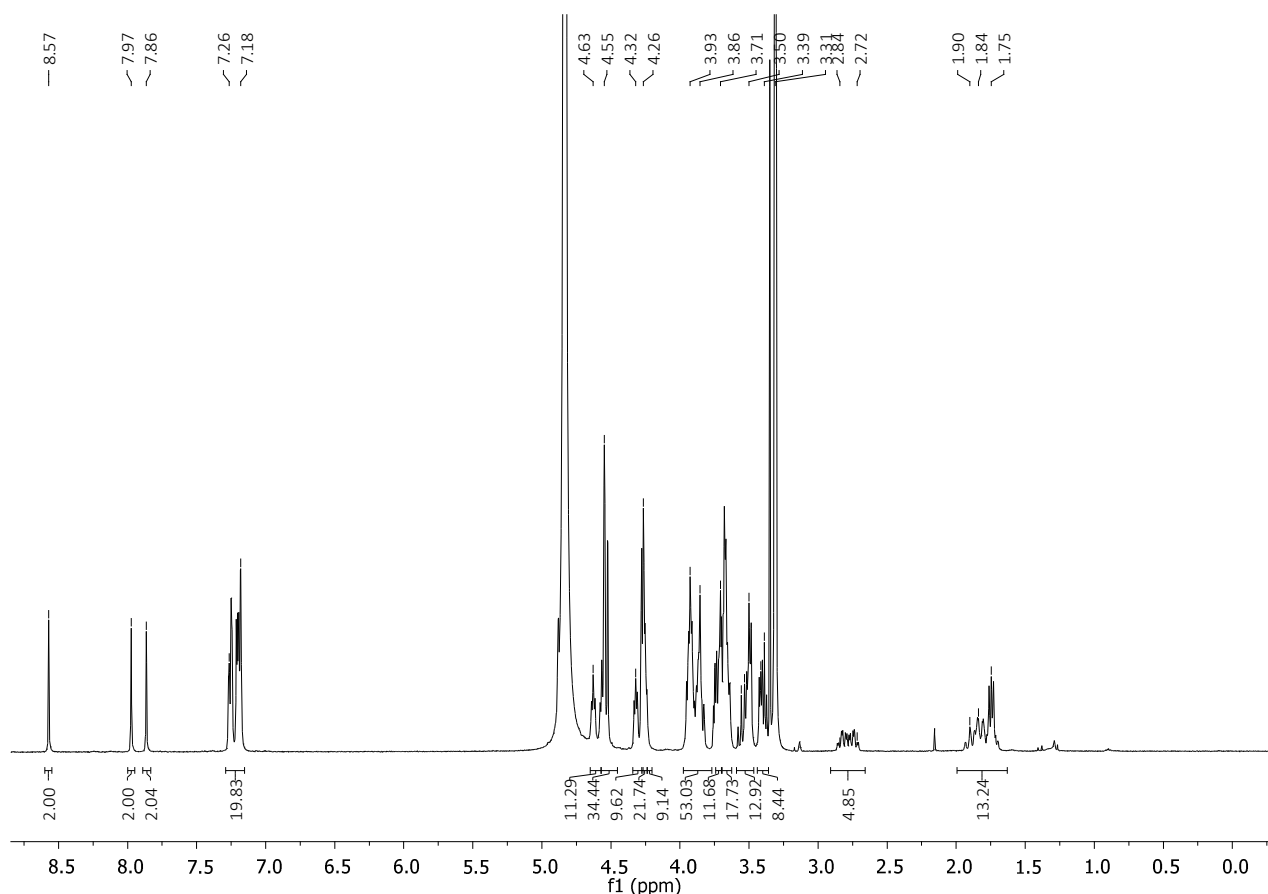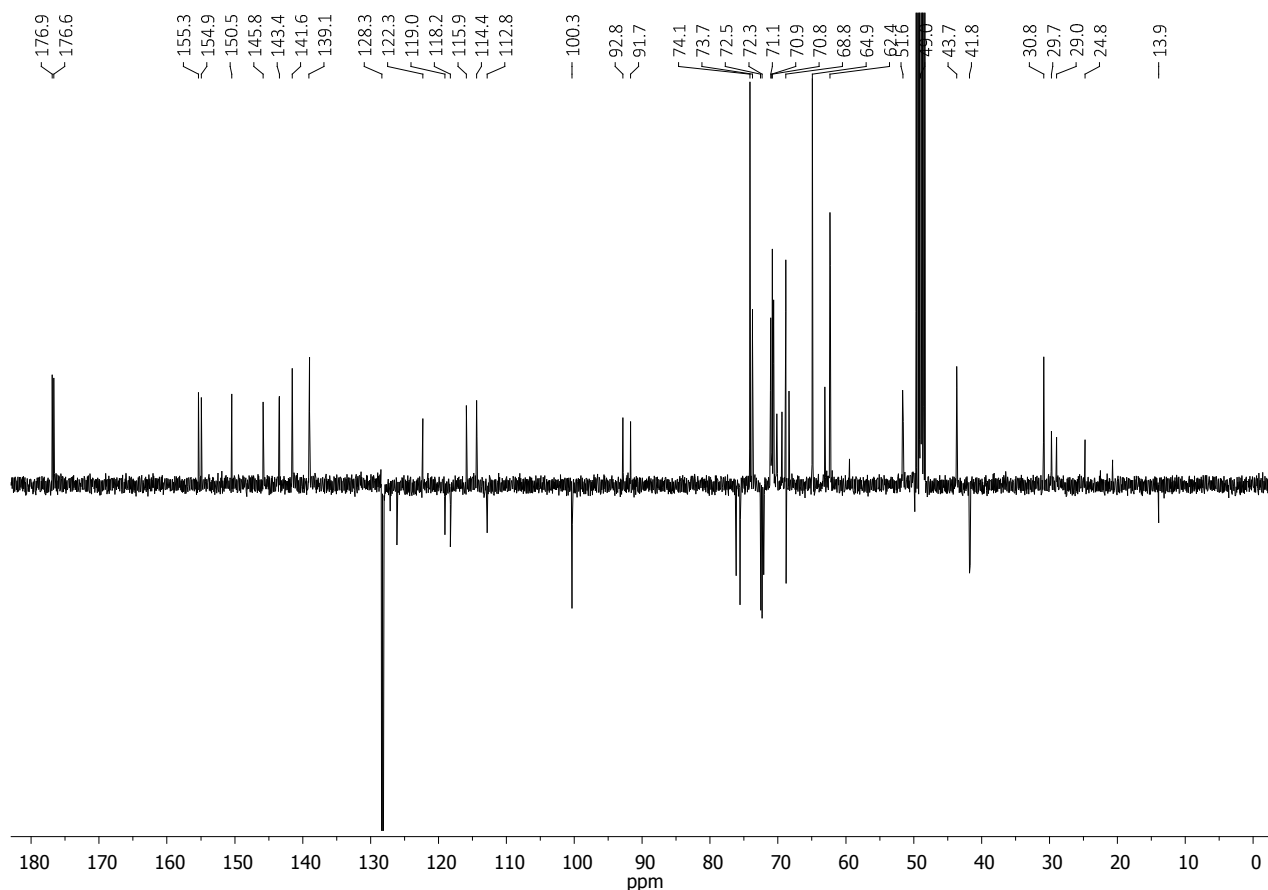
¹H NMR (400 MHz, CD₃OD): δ 8.56 (s, 2H, H$_{TC5}$); 7.98 (s, 2H, H$_{T5}$); 7.85 (s, 2H, H$_{R2}$); 7.28 – 7.15 (m, 20H, H$_{Ar2}$, H$_{Ar3}$, H$_{R5}$, H$_{R10}$); 4.87 (br s, 2H, H$_1$); 4.62 (t, 4H, H$_{L8}$, *J* = 4.8 Hz); 4.57 – 4.51 (m, 16H, H$_8$, C$\underline{H}_2$OH, H$_{L1}$); 4.34 – 4.29 (m, 4H, H$_{G1}$); 4.29 – 4.20 (m, 16H, H$_{G5}$, H$_{G9}$, C$\underline{H}_2$NH); 3.98 – 3.88 (m, 16H, H$_7$ or H$_{L7}$, H$_{G2}$, H$_{G6}$, H$_{G10}$); 3.88 – 3.80 (m, 10H, H$_7$ or H$_{L7}$, H$_{D2}$, H$_2$, H$_{6a}$); 3.77 – 3.61 (m, 30H, H$_{G4}$, H$_{G3}$, H$_{G7}$, H$_{G11}$, H$_{G8}$, H$_{G12}$, H$_{D1}$, H$_3$, H$_{6b}$); 3.59 – 3.51 (m, 4H, H$_4$, H$_5$); 3.50 – 3.47 (m, 8H, H$_{L2}$ or H$_{L3}$, H$_{L4}$ or H$_{L6}$); 3.43 – 3.33 (m, 8H, H$_{L2}$ or H$_{L3}$, H$_{L4}$ or H$_{L6}$); 2.89 – 2.70 (m, 4H, H$_{D4}$, H$_{D5}$); 1.93 – 1.80 (m, 8H, H$_{D3}$, H$_{D6}$); 1.78 – 1.69 (m, 4H, H$_{L5}$).

¹³C NMR (100 MHz, CD₃OD): δ 176.9, 176.7 ($\underline{C}$ONH); 155.4, 154.9 (C$_{R6}$, C$_{R11}$); 150.5 (C$_{R3}$); 145.8 (C$_{TC4}$); 143.5 (C$_{T4}$); 141.6, 141.5, 139.1, 139.0 (C$_{Ar1}$, C$_{Ar4}$); 128.4, 128.4, 128.15 (C$_{Ar2}$, C$_{Ar3}$); 127.1 (C$_{TC5}$); 126.1 (C$_{T5}$); 122.3 (C$_{R1}$); 119.0 (C$_{R5}$ or C$_{R10}$); 118.2 (C$_{R5}$ or C$_{R10}$); 115.9 (C$_{R4}$); 114.4 (C$_{R9}$); 112.8 (C$_{R2}$); 100.3 (C$_1$); 92.8, 91.7 (C$_{R7}$, C$_{R8}$); 76.2 (C$_3$); 75.6 (C$_5$); 74.1, 73.7 (C$_{G3}$, C$_{G7}$, C$_{G11}$); 72.5, 72.3, 72.1 (C$_{D1}$, C$_2$, C$_{D2}$); 71.1 (C$_{19}$ or C$_{20}$); 71.1 – 70.6 (C$_{G2}$, C$_{G6}$, C$_{G10}$, C$_{G5}$, C$_{G1}$, C$_{L2}$ or C$_{L3}$); 70.2 (C$_{D2}$); 69.4 (C$_{G9}$); 68.9 (C$_{L4}$, C$_{L6}$); 68.8 (C$_4$); 68.4 (C$_7$, C$_{L7}$); 64.9, 64.9 ($\underline{C}$H$_2$OH, C$_{L1}$); 63.1 (C$_6$); 62.4, 62.4, 62.3 (C$_{G4}$, C$_{G8}$, C$_{G12}$); 51.7, 51.5 (C$_{L8}$, C$_8$); 43.7, 43.6 ($\underline{C}$H$_2$NH); 41.8 (C$_{D4}$ or C$_{D5}$); 41.7 (C$_{D4}$ or C$_{D5}$); 30.9 (C$_{L5}$); 29.7 (C$_{D3}$ or C$_{D6}$); 29.0 (C$_{D3}$ or C$_{D6}$).

MS (MALDI, matrix: sinapinic acid, solvent: MeOH): *m/z* calculated for $[C_{134}H_{183}N_{16}O_{46}]^+$: 2754.0; found: 2752.3.

MS (ESI-HRMS): calculated for $[C_{134}H_{182}N_{16}O_{46}]$: 2751.23941; found: 2751.23567 (after deconvolution).

[α]$_D$ ^{25}: -4.6 (c = 0.33, MeOH).

Synthesis of divalent glycodendrimer 2.49

2.49
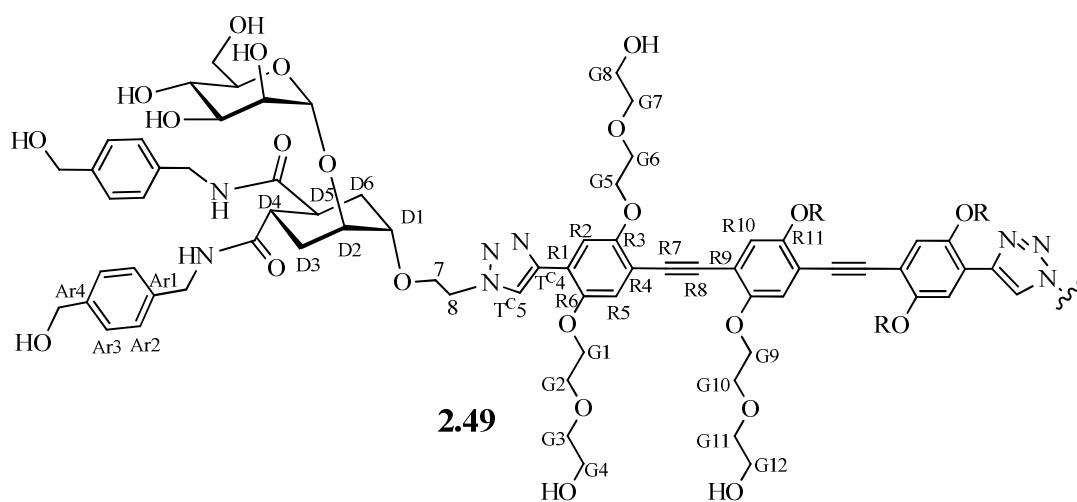
To a stirred solution of **TIPS-2.5** (11.5 mg, 9.1 µmol, 1 eq.) in THF (200 µL), TBAF (1 M in THF, 18.0 µL, 2 eq.) was added under nitrogen. After 1 h, TLC analysis (CH$_2$Cl$_2$:MeOH 9:1) showed that the desilylation reaction was complete. The CuAAC reagents were added as solutions in the following order: TBTA in THF (0.97 mg, 1.7 µmol, 0.2 eq., 50 µL of THF), CuSO$_4$·5H$_2$O in H$_2$O (0.22 mg, 0.9 µmol, 0.1 eq., 50 µL of H$_2$O) and Sodium Ascorbate in H$_2$O (0.72 mg, 3.6 µmol, 0.4 eq., 50 µL of H$_2$O). The reaction mixture was stirred at room temperature, under nitrogen atmosphere and in dark for 10 minutes. Finally **1.9** (13.5 mg, 20.0 µmol, 2.2 eq.) was added. THF and H$_2$O volumes were adjusted to 300 µL each. The reaction was stirred at RT, under nitrogen and in dark overnight. TLC analysis (CH$_2$Cl$_2$:MeOH 9:1) revealed total consumption of **2.5**; TLC (CH$_2$Cl$_2$:MeOH:H$_2$O 75:25:2.5) monitored the formation of a new polar species and the disappearance of another one having a slight higher polarity relative to **1.9** (probably corresponding to the monosubstituted intermediate). Quadrasil™-MP (S/Cu 8.3:1, 5 mg) was added to the reaction mixture, which was stirred for 10 minutes, and then filtered off. The solvent was removed under reduced pressure and the resulting mixture was redissolved in MeOH and purified by size exclusion chromatography (Sephadex LH-20, MeOH), obtaining 15 mg of **2.49** not pure. The remaining tetrabutylammonium salt was removed through automated reverse phase flash chromatography

(C18, H₂O with gradient of MeOH from 0 % to 100 %), obtaining 11 mg of pure **2.49** as a yellow solid (yield 54 %).
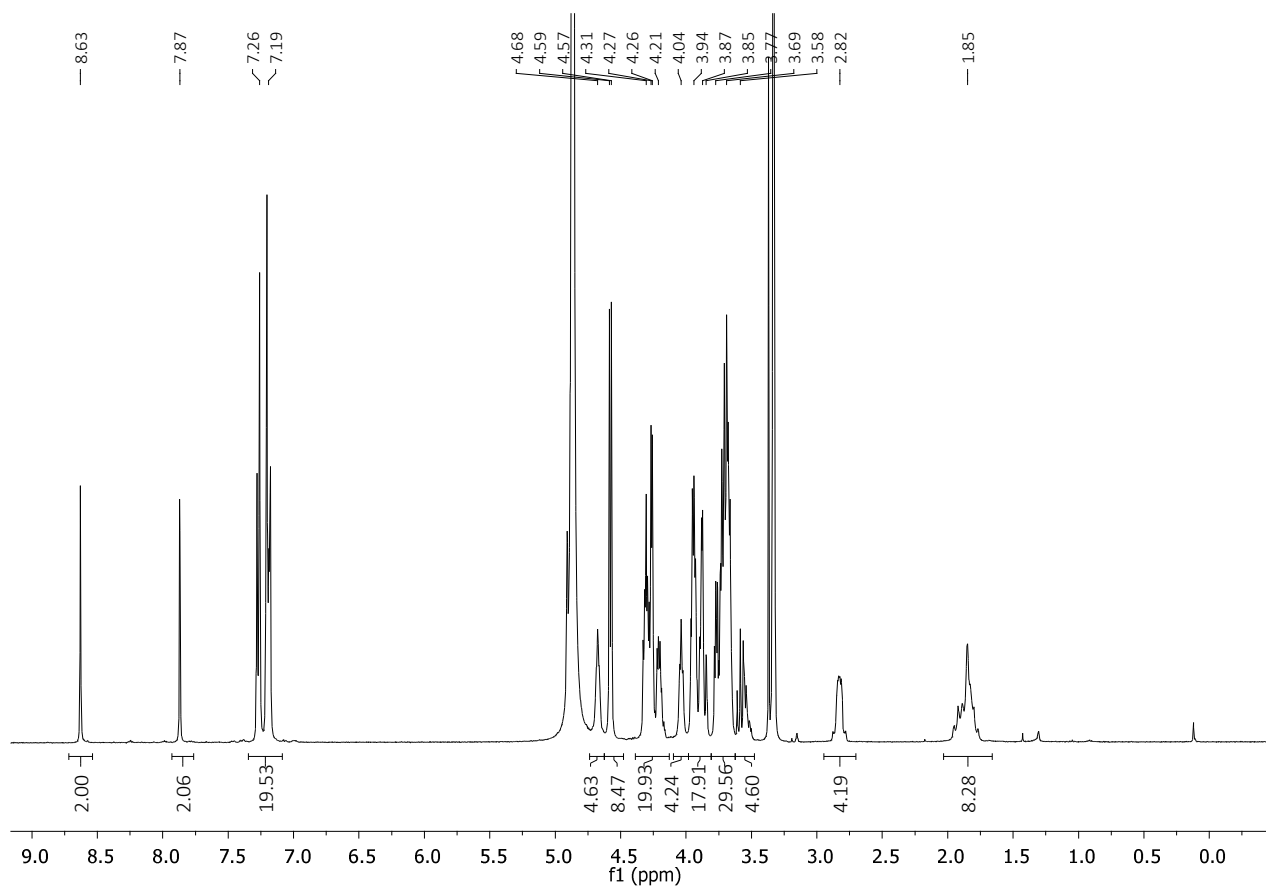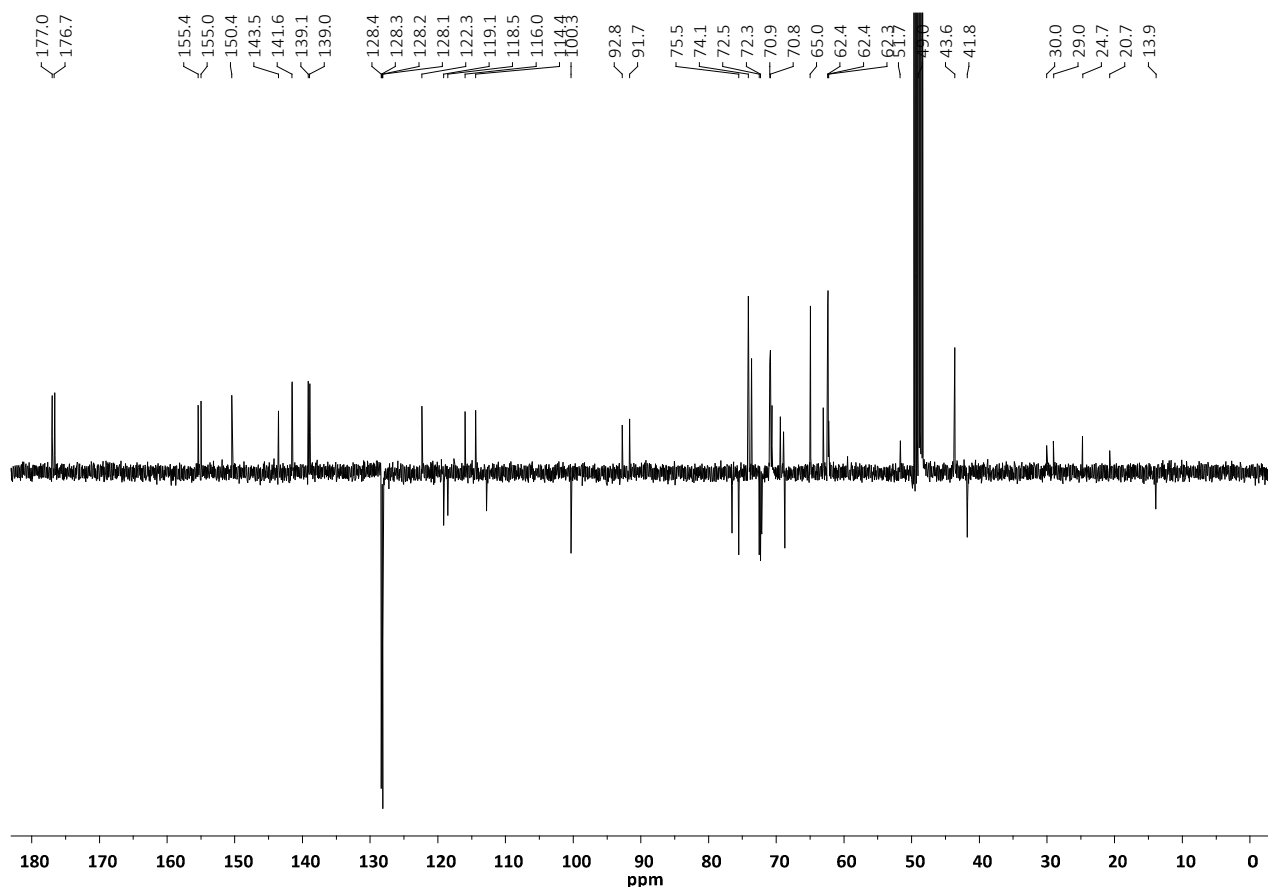
¹H NMR (400 MHz, CD₃OD): δ 8.61 (s, 2H, H$_{TC5}$); 7.84 (s, 2H, H$_{R2}$); 7.28 – 7.13 (m, 20H, H$_{Ar2}$, H$_{Ar3}$, H$_{R5}$, H$_{R10}$); 4.90 (br s, 2H, H$_1$); 4.68 – 4.61 (m, 4H, H$_8$); 4.56 (d, J = 6.2 Hz, 8H, C$\underline{H}_2$OH); 4.32 – 4.13 (m, 20H, C$\underline{H}_2$NH, H$_{G1}$, H$_{G5}$, H$_{G9}$); 4.01 (t, 4H, H$_7$, J = 4.8 Hz); 3.96 – 3.80 (m, 20H, H$_{G2}$, H$_{G6}$, H$_{G10}$, H$_2$, H$_{D2}$, H$_{G12}$); 3.78 – 3.61 (m, 28H, H$_6$, H$_{G3}$, H$_{G4}$, H$_{G8}$, H$_{G7}$, H$_{G11}$, H$_{D1}$, H$_3$); 3.60 – 3.48 (m, 4H, H$_4$, H$_5$); 2.88 – 2.75 (m, 4H, H$_{D4}$, H$_{D5}$); 1.94 – 1.60 (m, 8H, H$_{D3}$, H$_{D6}$).

¹³C NMR (100 MHz, CD₃OD): δ 177.0, 176.7 ($\underline{C}$ONH); 155.4, 155.0 (C$_{R6}$, C$_{R11}$); 150.4 (C$_{R3}$); 143.5 (C$_{TC4}$); 141.6, 139.1, 139.0 (C$_{Ar1}$, C$_{Ar4}$); 128.4, 128.3, 128.19, 128.15 (C$_{Ar2}$, C$_{Ar3}$); 127.0 (C$_{TC5}$); 122.4 (C$_{R1}$); 119.1, 118.5 (C$_{R5}$, C$_{R10}$); 116.0, 114.4 (C$_{R4}$, C$_{R9}$); 112.8 (C$_{R2}$); 100.3 (C$_1$); 92.8, 91.7 (C$_{R7}$, C$_{R8}$); 76.5 (C$_3$); 75.5 (C$_5$); 74.1 (C$_{G3}$, C$_{G7}$, C$_{G11}$); 72.5, 72.4, 72.2 (C$_2$, C$_{D1}$, C$_{D2}$); 71.0 - 70.7 (C$_{G2}$, C$_{G6}$, C$_{G10}$); 69.5, 68.9 (C$_{G1}$, C$_{G5}$, C$_{G9}$, C$_7$); 68.7 (C$_4$); 65.0 ($\underline{C}$H$_2$OH); 63.0 (C$_{G12}$); 62.4, 62.4 (C$_{G4}$, C$_{G8}$); 62.3 (C$_6$); 51.7 (C$_8$); 43.6 ($\underline{C}$H$_2$NH); 41.8 (C$_{D4}$, C$_{D5}$); 30.0 (C$_{D3}$ or C$_{D6}$); 29.0 (C$_{D3}$ or C$_{D6}$).

MS (ESI-HRMS): *m/z* calculated for [C$_{144}$H$_{148}$N$_{10}$O$_{40}$Na$_2$]$^{2+}$: 1171.48194; found: 1171.47672.

[α]$_D$^{25} : 1.7 (c = 0.75, MeOH).

Synthesis of hexavalent glycodendrimer 2.50
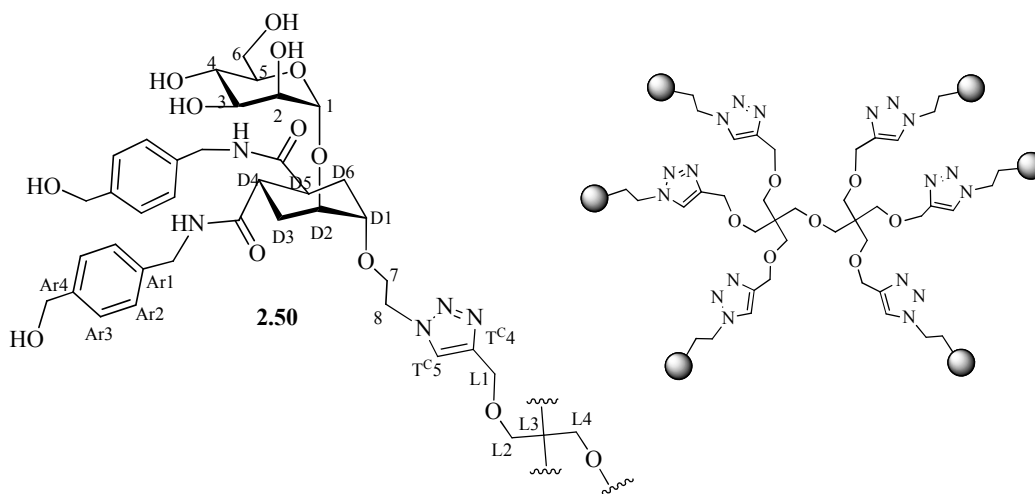
To a stirred solution of **2.24** (3.0 mg, 6.0 µmol, 1 eq.) in THF (50 µL), the CuAAC reagents were added as solutions in the following order: TBTA in THF (0.64 mg, 1.2 µmol, 0.2 eq., 50 µL of THF), CuSO$_4$·5H$_2$O in H$_2$O (0.15 mg, 0.6 µmol, 0.1 eq., 24 µL of H$_2$O) and sodium ascorbate in H$_2$O (0.48 mg, 2.4 µmol, 0.4 eq., 50 µL of H$_2$O). The reaction mixture was stirred at RT, under nitrogen atmosphere and in the dark for 10 minutes. Finally **1.9** (26.9 mg, 40.0 µmol, 6.6 eq.) was added. THF and H$_2$O volumes were adjusted to 550 µL each. The reaction was stirred at RT, under nitrogen and in dark overnight. TLC analysis (CHCl$_3$:MeOH:H$_2$O 55:45:7.5) revealed the presence of a single new species. Quadrasil™-MP (S/Pd 11.4:1, 5 mg) was added to the reaction mixture, which was stirred for 10 minutes, and then filtered off. The solvent was removed under reduced pressure and the resulting mixture was redissolved in MeOH purified by size exclusion chromatography (Sephadex LH-20, MeOH), obtaining 21 mg of pure **2.50** as a white solid (yield 77 %), with characterization data identical to those reported in Ref.[12,17].

^{1}H NMR (400 MHz, CDCl3): δ = 7.95 (s, 6H, H$_{TC5}$), 7.28 – 7.07 (m, 48H, H$_{Ar2}$, H$_{Ar3}$), 4.89 (br s, 6H, H$_1$), 4.54 (s, 24H, C_H$_2$OH), 4.51 - 4.45 (m, 12H, H$_8$), 4.44 (s, 12H, H$_{L1}$), 4.28 - 4.20 (m, 24H, C_H$_2$NH), 3.95 - 3.80 (m, 30H, H$_2$, H$_{6a}$, H$_{D2}$, H$_7$), 3.73 - 3.61 (m, 18H, H$_{6b}$, H$_{D1}$, H$_3$), 3.60 - 3.47 (m, 12H, H$_4$, H$_5$), 3.38 (br s, 12H, H$_{L2}$), 3.26 (br s, 4H, H$_{L4}$), 2.89 – 2.78 (m, 12H, H$_{D4}$, H$_{D5}$), 1.93 –1.69 (m, 24H, H$_{D3}$, H$_{D6}$).

Synthesis of monovalent control of glycodendrimer 2.49
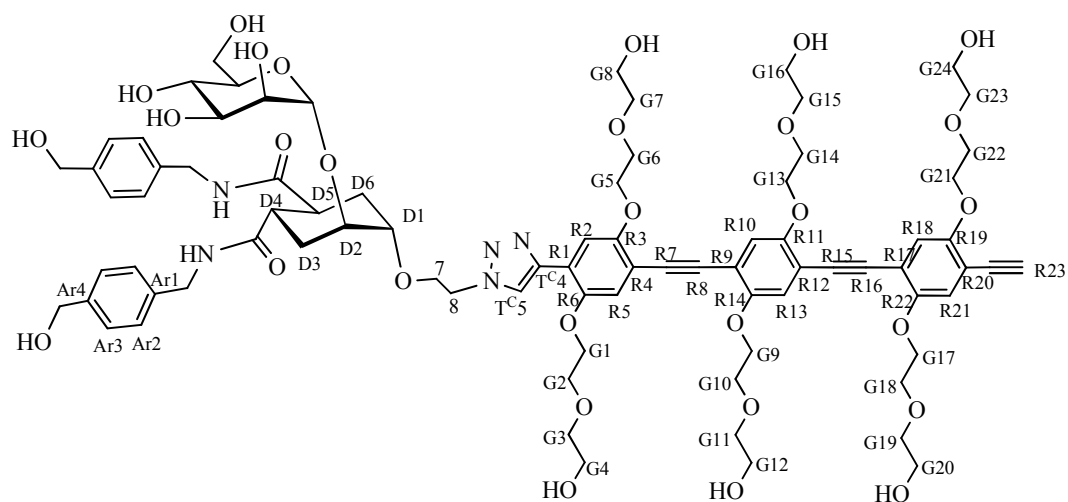
To a stirred solution of **TIPS-2.5** (6.4 mg, 5.0 µmol, 1 eq.) in THF (200 µL), TBAF (1 M in THF, 10.0 µL, 2 eq.) was added under nitrogen. After 1 h, TLC analysis (CH_2Cl_2:MeOH 9:1) showed that the desilylation reaction was complete. The CuAAC reagents were added as solutions in the following order: TBTA in THF (0.53 mg, 1.0 µmol, 0.2 eq., 100 µL of THF), $CuSO_4·5H_2O$ in H_2O (0.12 mg, 0.5 µmol, 0.1 eq., 80 µL of H_2O) and Sodium Ascorbate in H_2O (0.40 mg, 2.0 µmol, 0.4 eq., 80 µL of H_2O). The reaction mixture was stirred at room temperature, under nitrogen atmosphere and in dark for 10 minutes. Finally **1.9** (2.7 mg, 4.0 µmol, 0.8 eq.) was added as solid. THF and H_2O volumes were adjusted to 250 µL each. The reaction was stirred at RT, under nitrogen and in dark overnight. TLC analysis (CH_2Cl_2:MeOH 9:1) revealed total consumption of **2.5**; TLC (CH_2Cl_2:MeOH:H_2O 75:25:2.5) monitored the formation of a new polar species (that MALDI MS analysis –DHB matrix- confirmed to be the expected product), together also with small amounts of divalent **2.49** and residual starting material. Quadrasil™-MP (S/Cu 15:1, 5 mg) was added to the reaction mixture, which was stirred for 10 minutes, and then filtered off. The solvent was removed under reduced pressure and the resulting mixture was redissolved in MeOH and purified by size exclusion chromatography (Sephadex LH-20, MeOH, 1 drop in 4 seconds), obtaining 2.3 mg of final compound (yield 28 %).
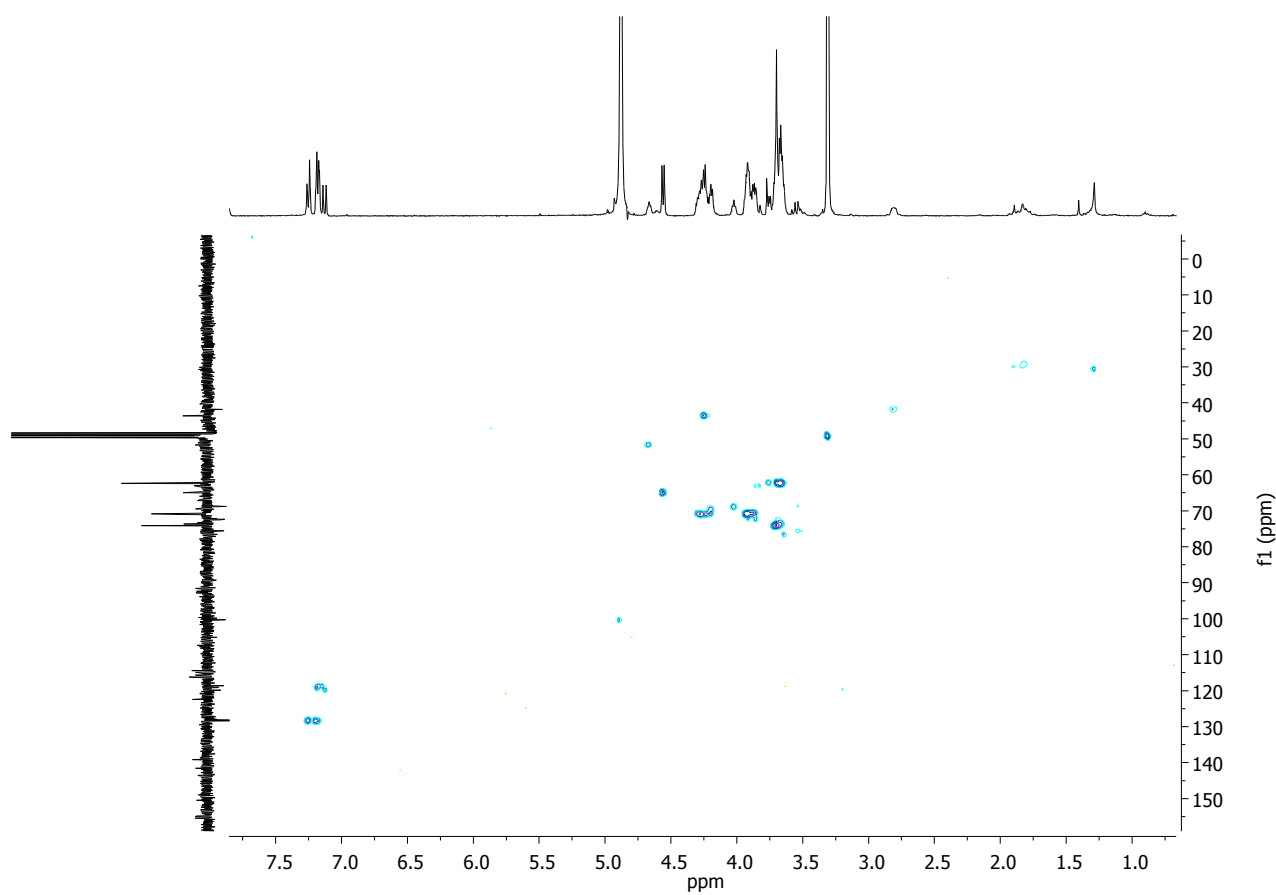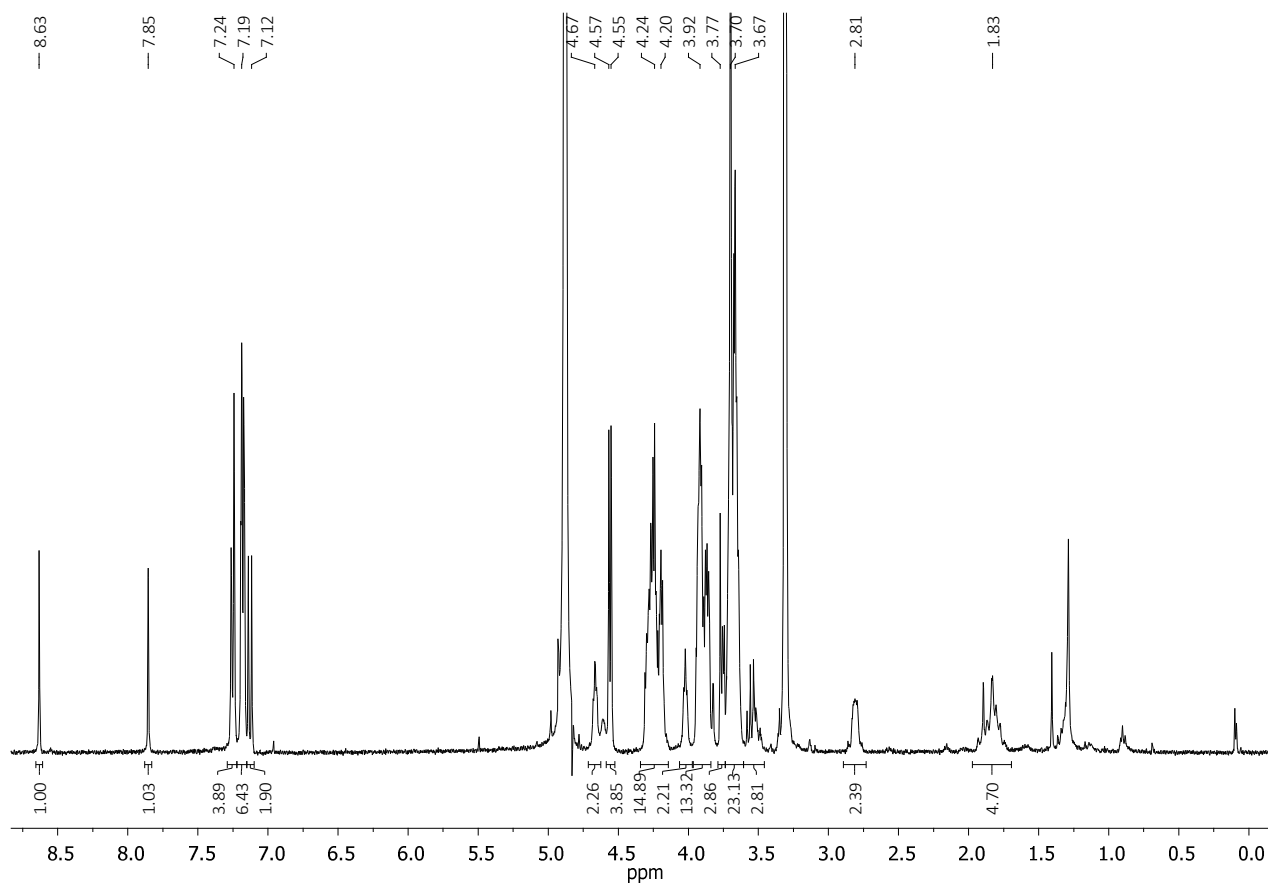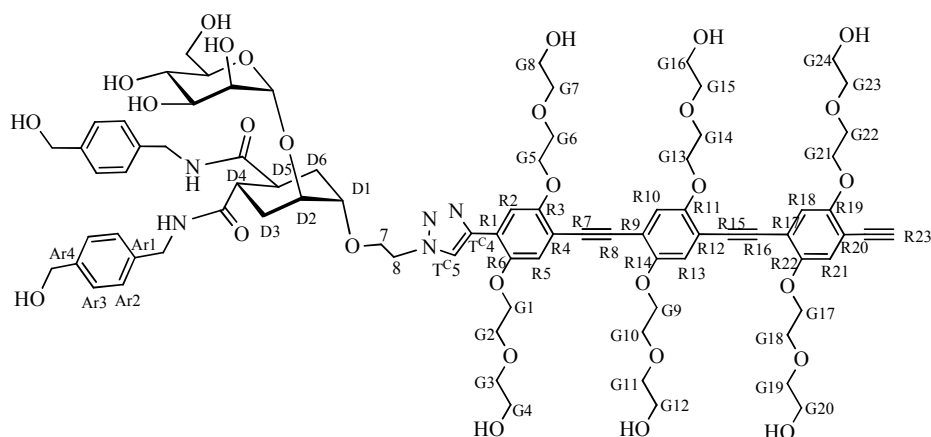
¹H NMR (400 MHz, CD₃OD): δ 8.63 (s, 1H, H$_{TC5}$), 7.85 (s, 1H, H$_{R2}$), 7.31 – 7.09 (m, 12H, H$_{Ar2}$, H$_{Ar3}$, H$_{R5}$, H$_{R10}$, H$_{R13}$, H$_{R18}$, H$_{R21}$), 4.71 – 4.64 (m, H$_8$), 4.59 – 4.53 (m, 4H, C$\underline{H}_2$OH), 4.35 – 4.13 (m, 16H, C$\underline{H}_2$NH, H$_{G1}$, H$_{G5}$, H$_{G9}$, H$_{G13}$, H$_{G17}$, H$_{G21}$), 4.07 – 3.98 (m, 2H, H$_7$), 3.97 – 3.80 (m, 16H, H$_{D2}$, H$_2$, H$_{G2}$, H$_{G6}$, H$_{G10}$, H$_{G12}$, H$_{G14}$, H$_{G18}$, H$_{G22}$), 3.79 – 3.60 (m, 26H, H$_{6a}$, H$_{6b}$, H$_3$, H$_{D1}$, H$_{G3}$, H$_{G7}$, H$_{G11}$, H$_{G15}$, H$_{G19}$, H$_{G23}$, H$_{G4}$, H$_{G8}$, H$_{G16}$, H$_{G20}$, H$_{G24}$), 3.60 – 3.46 (m, 2H, H$_5$, H$_4$), 3.59 – 3.45 (m, 3H), 2.90 – 2.73 (m, 2H, H$_{D4}$, H$_{D5}$), 1.96 – 1.72 (m, 6H, H$_{D3}$, H$_{D6}$).

¹³C NMR (100 MHz, CD₃OD): δ 177.01, 176.60 ($\underline{C}$ONH), 155.65, 155.45, 155.08, 154.97, 154.81 (C$_{R6}$, C$_{R11}$ C$_{R14}$, C$_{R19}$, C$_{R22}$), 150.72 (C$_{R3}$), 143.74 (C$_{TC4}$), 141.59, 141.53, 139.14, 138.92 (C$_{Ar1}$, C$_{Ar4}$), 128.38, 128.31, 128.19, 128.15 (C$_{Ar2}$, C$_{Ar3}$), 127.26 (C$_{TC5}$), 122.43 (C$_{R1}$), 119.86, 119.22, 119.04, 118.64 (C$_{R5}$, C$_{R10}$, C$_{R13}$, C$_{R18}$, C$_{R21}$), 116.23, 116.16, 115.67, 114.90, 114.44 (C$_{R4}$, C$_{R9}$, C$_{R12}$, C$_{R17}$, C$_{R20}$), 112.31 (C$_{R2}$), 100.31 (C$_1$), 76.01 (C$_5$), 75.55 (C$_3$), 74.10 (C$_{G3}$, C$_{G7}$, C$_{G11}$, C$_{G15}$, C$_{G19}$, C$_{G23}$), 72.54 (C$_2$), 72.36 (C$_{D2}$), 72.15 (C$_{D1}$), 71.26 – 70.55 (C$_{G2}$, C$_{G6}$, C$_{G10}$, C$_{G14}$, C$_{G18}$, C$_{G22}$, C$_{G1}$, C$_{G5}$, C$_{G9}$, C$_{G13}$, C$_{G17}$, C$_{G21}$), 69.22 (C$_7$), 69.03 (C$_4$), 64.88 ($\underline{C}$H$_2$OH), 63.01 (C$_{G12}$), 62.55 – 62.16 (C$_6$, C$_{G4}$, C$_{G8}$, C$_{G12}$, C$_{G16}$, C$_{G20}$, C$_{G24}$), 51.45 (C$_{G8}$), 43.67 ($\underline{C}$H$_2$NH), 41.95 (C$_{D4}$, C$_{D5}$), 25.56 (C$_{D3}$, C$_{D6}$).

MS (ESI-HRMS): *m/z* calculated for [C$_{82}$H$_{105}$N$_5$O$_{29}$Na$_2$]$^{2+}$: 834.83398; found: 834.83574.

[α]$_D$^{25} : -16.4 (c = 0.1, MeOH).

2.9 References

[1] T. B. Geijtenbeek; R. Torensma; S. J. van Vliet; G. C. van Duijnhoven; G. J. Adema; Y. van Kooyk; C. G. Figdor, Identification of DC-SIGN, a novel dendritic cell-specific ICAM-3 receptor that supports primary immune responses, *Cell* **2000**, 575.

[2] T. Mizuochi; T. J. Matthews; M. Kato; J. Hamako; K. Titani; J. Solomon; T. Feizi, Diversity of Oligossaccharide Structures on the Evelope Glycoprotein gp120 of Human Immunodeficiency Virus 1 from the Lymphoblastoid Cell Line H9, *The Journal of Biological Chemistry* **1990**, 8519.

[3] E. W. Adams; D. M. Ratner; H. R. Bokesch; J. B. McMahon; B. R. O'Keefe; P. H. Seeberger, Oligosaccharide and Glycoprotein Microarrays as Tools in HIV Glycobiology: Glycan-Dependent gp120/Protein Interactions, *Chemistry & Biology* **2004**, 875.

[4] Y. van Kooyk; T. B. Geijtenbeek, DC-SIGN: escape mechanism for pathogens, *Nat. Rev. Immunol.* **2003**, 697.

[5] R. J. Pieters, Maximising multivalency effects in protein–carbohydrate interactions, *Org. Biomol. Chem.*, **2009**, 2013.

[6] M. Mammen; S. Choi; G. M. Whitesides, Polyvalent Interactions in Biological Systems: Implications for Design and Use of Multivalent Ligands and Inhibitors, *Angew. Chem. Int. Ed.* **1998**, 2754.

[7] A. Bernardi; J. Jimenez-Barbero; A. Casnati; C. De Castro; T. Darbre; F. Fieschi; J. Finne; H. Funken; K. E. Jaeger; M. Lahmann; T. K. Lindhorst; M. Marradi; P. Messner; A. Molinaro; P. V. Murphy; C. Nativi; S. Oscarson; S. Penades; F. Peri; R. J. Pieters; O. Renaudet; J. L. Reymond; B. Richichi; J. Rojo; F. Sansone; C. Schaffer; W. B. Turnbull; T. Velasco-Torrijos; S. Vidal; S. Vincent; T. Wennekes; H. Zuilhof; A. Imberty, Multivalent glycoconjugates as anti-pathogenic agents, *Chem. Soc. Rev.* **2013**, 4709.

[8] N. Varga; I. Sutkeviciute; C. Guzzi; J. McGeagh; I. Petit-Haertlein; S. Gugliotta; J. Weiser; J. Angulo; F. Fieschi; A. Bernardi, Selective Targeting of Dendritic Cell-Specific Intercellular Adhesion Molecule-3-Grabbing Nonintegrin (DC-SIGN) with Mannose-Based Glycomimetics: Synthesis and Interaction Studies of Bis(benzylamide) Derivatives of a Pseudomannobioside, *Chem. Eur. J.* **2013**, 4786.

[9] J. J. Reina; S. Sattin; D. Invernizzi; S. Mari; L. Martínez-Prats; G. Tabarani; F. Fieschi; R. Delgado; P. M. Nieto; J. Rojo; A. Bernardi, 1,2-Mannobioside Mimic: Synthesis, DC-SIGN Interaction by NMR and Docking, and Antiviral Activity, *ChemMedChem* **2007**, 1030.

[10] M. Thépaut; C. Guzzi; I. Sutkeviciute; S. Sattin; R. Ribeiro-Viana; N. Varga; E. Chabrol; J. Rojo; A. Bernardi; J. Angulo; P. M. Nieto; F. Fieschi, Structure of a Glycomimetic Ligand in the Carbohydrate Recognition Domain of C-type Lectin DC-SIGN. Structural Requirements for Selectivity and Ligand Design, *J. Am. Chem. Soc*. **2013**, 2518.

[11] IC_{50} in SPR experiments depend on the exact functionalization of the chip.

[12] N. Varga; I. Sutkeviciute; R. Ribeiro-Viana; A. Berzi; R. Ramdasi; A. Daghetti; G. Vettoretti; A. Amara; M. Clerici; J. Rojo; F. Fieschi; A. Bernardi, A multivalent inhibitor of the DC-SIGN dependent uptake of HIV-1 and Dengue virus, *Biomaterials* **2014**, 4175.

[13] J. Luczkowiak; S. Sattin; I. Sutkeviciute; J. Reina; M. Sánchez-Navarro; M. Thépaut; L. Martínez-Prats; A. Daghetti; F. Fieschi; R. Delgado; A. Bernardi; J. Rojo, Pseudosaccharide functionalized dendrimers as potent inhibitors of DC-SIGN dependent Ebola pseudotyped viral infection, *Bioconj. Chem.* **2011**, 1354.

[14] G. Tabarani; M. Thépaut; D. Stroebel; C. Ebel; C. Vivès; P. Vachette; D. Durand; F. Fieschi, DC-SIGN Neck Domain Is a pH-sensor Controlling Oligomerization, *J. Biol. Chem.* **2009**, 21229.

[15] C. Manzo; J. A. Torreno-Pina; B. Joosten; I. Reinieren-Beeren; E. J. Gualda; P. Loza-Alvarez; C. G. Figdor; M. F. Garcia-Parajo; A. Cambi, The Neck Region of the C-type Lectin DC-SIGN Regulates Its Surface Spatiotemporal Organization and Virus-binding Capacity on Antigen-presenting Cells, *J. Biol. Chem.* **2012**, 38946.

[16] F. Pertici; N. Varga; A. van Duijn; M. Rey-Carrizo; A. Bernardi; R. J. Pieters, Efficient synthesis of phenylene-ethynylene rods and their use as rigid spacers in divalent inhibitors, *Beilstein J. Org. Chem*. **2013**, 215.

[17] N. Varga, *PhD Thesis*, **2012**.

[18] K. Sonogashira; Y. Tohda; N. Hagihara, A convenient synthesis of acetylenes: catalytic substitutions of acetylenic hydrogen with bromoalkenes, iodoarenes and bromopyridines, *Tetrahedron Letters* **1975**, 4467.

[19] J. J. Li, Name Reactions, Springer: 2014.

[20] P. Siemse; R. C. Livingston; F. Diederich, Acetylenic Coupling: A Powerful Tool in Molecular Construction, *Angew. Chem. Int. Ed*. **2000**, 2632.

[21] Q. Lu; K. Liu; H. Zhang; Z. Du, X. Wang; F. Wang, From Tunneling to Hopping: A Comprehensive Investigation of Charge Transport Mechanism in Molecular Junctions Based on Oligo(p-phenylene ethynylene)s, *ACS Nano* **2009**, 3861.

[22] a) V. V. Rostovtsev; L. G. Green; V. V. Fokin; K. B. Sharpless, A stepwise Huisgen cycloaddition process: copper(I)-catalyzed regioselective "ligation" of azides and terminal alkynes,

Angew. Chem. Int. Ed. **2002**, 2596. b) C. W. Tornoe; C. Caspar; M. Morten, Peptidotriazoles on Solid Phase: [1,2,3]-Triazoles by Regiospecific Copper(I)-Catalyzed 1,3-Dipolar Cycloadditions of Terminal Alkynes to Azides, *J. Org. Chem.* **2002**, 3057.

[23] C. Nolte; P. Mayer; B. F. Straub, Isolation of a Copper(I) Triazolide: A "Click" Intermediate, *Angew. Chem. Int. Ed.* **2007**, 2101.

[24] R. P. Singh; S. Kumar; R. Nada; R. Prasad, Evaluation of copper toxicity in isolated human peripheral blood mononuclear cells and it's attenuation by zinc: *ex vivo*, *Molecular and Cellular Biochemistry* **2006**, 13.

[25] M. Cooper, Optical biosensors in drug discovery, *Nat. Rev. Drug Discov.* **2002**, 515.

[26] I. Sutkeviciute, *PhD Thesis*, **2012**.

[27] L. Wu; V. N. KewalRamani, Dendritic-cell interactions with HIV: infection and viral dissemination, *Nat. Rev. Immunol.* **2006**, 859.

[28] S. Sattin; A. Daghetti; M. Thépaut; A. Berzi; M. Sánchez-Navarro; G. Tabarani; J. Rojo; F. Fieschi; M. Clerici; A. Bernardi, Inhibition of DC-SIGN-Mediated HIV Infection by a Linear Trimannoside Mimic in a Tetravalent Presentation, *Chem. Biol.* **2010**, 301.

[29] (a) O. Martinez-Avila, L. M. Bedoya, M. Marradi, C. Clavel, J. Alcami and S. Penades, Multivalent Manno-Glyconanoparticles Inhibit DC-SIGN-Mediated HIV-1 Trans-Infection of Human T Cells, *Chembiochem.* **2009**, 1806; (b) J. Luczkowiak, S. Sattin, I. Sutkeviciute, J. J. Reina, M. Sanchez-Navarro, M. Thepaut, L. Martinez-Prats, A. Daghetti, F. Fieschi, R. Delgado, A. Bernardi and J. Rojo, Pseudosaccharide Functionalized Dendrimers as Potent Inhibitors of DC-SIGN Dependent Ebola Pseudotyped Viral Infection, *Bioconjugate chemistry* **2011**, 1354; (c) C. R. Becer, M. I. Gibson, J. Geng, R. Ilyas, R. Wallis, D. A. Mitchell and D. M. Haddleton, High-Affinity Glycopolymer Binding to Human DC-SIGN and Disruption of DC-SIGN Interactions with HIV Envelope Glycoprotein, *J. Am. Chem. Soc.* **2010**, 15130.

[30] W. C. Still; M. Kahn; A. Mitra, Rapid Chromatographic Technique for Preparative Separations with Moderate Resolution, *J. Org. Chem.* **1978**, 2923.

[31] R. H. Lambeth; S. J. Pederson; M. Baranoski; A. M. Rawlett, Methods for removal of residual catalyst from polymers prepared by ring opening metathesis polymerization, *J. Polym. Sc. Pol. Chem.* **2010**, 5725.

Chapter 3

Fluorescence microscopy analysis of 2.45(PM26) interacting with DC-SIGN expressing cells

3.1 Receptor-mediated internalization of antigens

As stated in Chapter 1.1, antigen-presenting cells (APCs) recognize and capture antigens through their surface receptors. The recognition of antigens presented on APCs surface as Major Histocompatibility Complexes (MHC) by T lymphocytes activates the antigen-specific immune responses. When antigens are internalized by APCs and routed to acidic endosomes and lysosomes, they are presented to $CD4^+$ T helper cells as MHC type II complexes. On the contrary, when they are internalized into early endosomes, they are then presented as MHC type I complex to $CD8^+$ cytotoxic T cells.[1]

Dendritic Cells are antigen-presenting cells recognizing a plethora of pathogens through their Pathogen Recognition Receptors, amongst which surface receptor DC-SIGN.[2,3] Targeting DC-SIGN with artificial selective ligands is a strategy to prevent pathogens binding to human cells, thus running so-called anti-adhesive therapies. Remarkably, also artificial compounds can induce DC-SIGN internalization and can be routed to specific cellular organelles. Internalization of this kind of ligands can in principle stimulate an antigen-specific immune response. Knowing the fate of artificial compounds once internalized via DC-SIGN, it is possible to predict, evaluate and also modulate the type of activated immune response.

3.1.1 DC-SIGN-mediated internalization of antagonists: examples in the literature

In the literature, only a few examples of artificial ligands designed as DC-SIGN antagonists to prevent HIV infection were demonstrated to be internalized by cells expressing the DC-SIGN receptor. An explanation of the so small number of examples is that it is not possible to detect ligands inside cells if they are not fluorescent. Moreover, the label of ligands with fluorescent dyes can in principle affect their properties, at least in terms of toxicity and binding.

In 2012, the group of Rojo reported mannose- and fucose- based nonavalent dendrimers labelled with the fluorescent dye BODIPY (Scheme **3.1**) that are internalized by Dendritic Cells and routed to lysosomes.[4] The fate of internalized glycodendrimers was investigated using flow citometry, labelling early endosomes and late endosomes/lysosomes with appropriate markers.
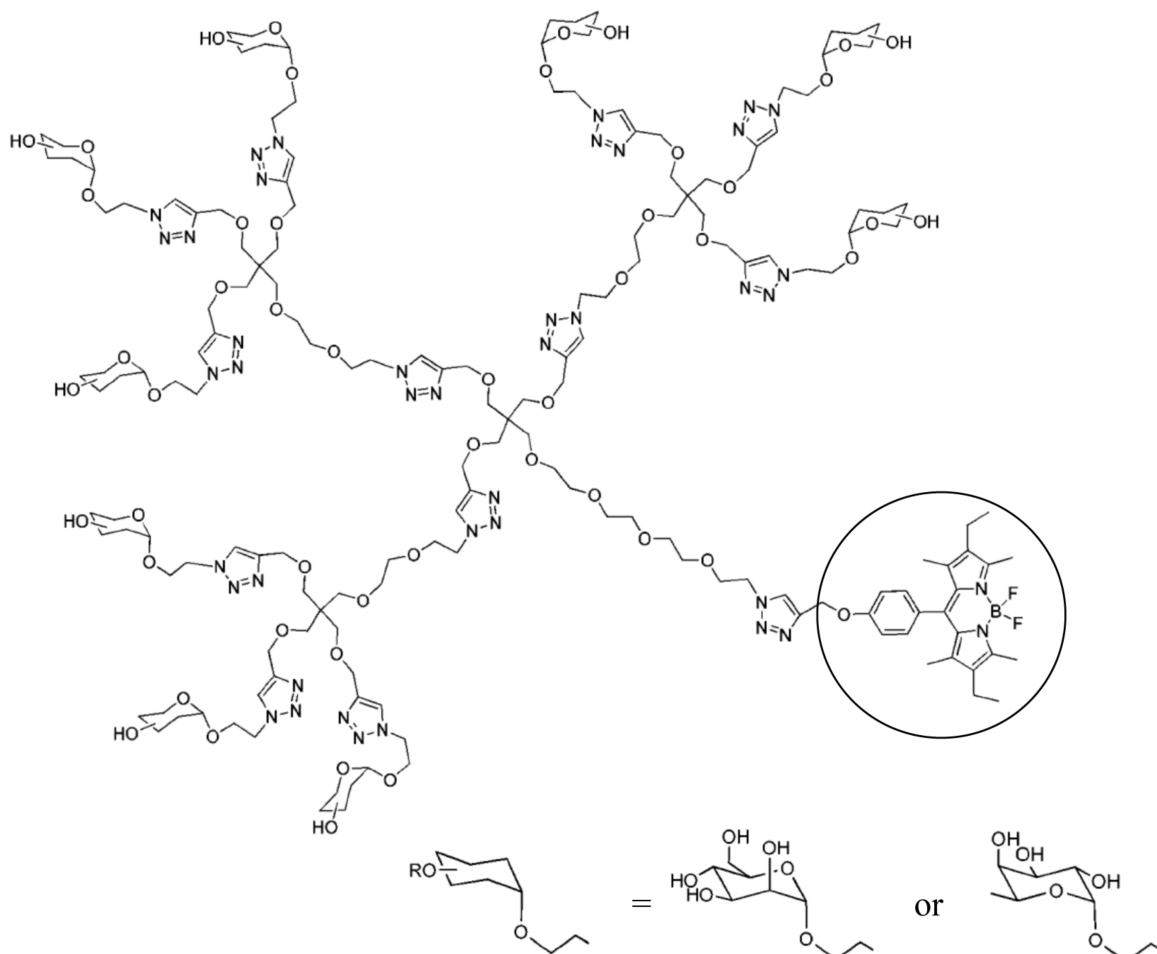
Scheme 3.1 Nonavalent glycodendrimers bearing mannose of fucose as sugar moieties and labelled with the fluorescent dye BODIPY (circled in black).[4]

In the same year, the group of Penades evaluated the internalization of mannosylated gold nanoparticles labelled with FITC -fluorescein isothyocyanate- (Scheme **3.2**) in immature Dendritic Cells.[5] FITC-nanoparticles were found to be internalized into early endosomes. Internalization experiments were carried out using confocal microscopy, analysing the colocalization between the fluorescence signals of the gold nanoparticles and those of markers of cellular organelles.
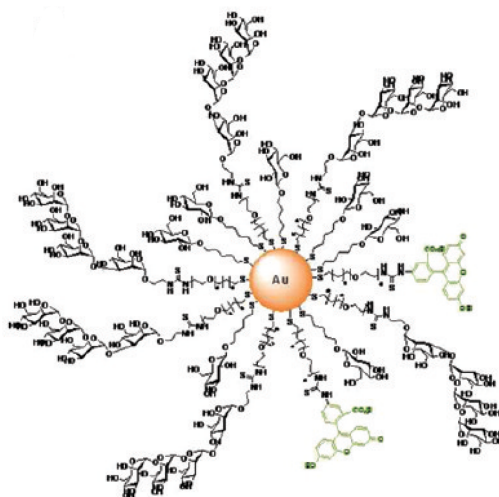
Scheme 3.2 Mannosylated-gold nanoparticles labelled with the FITC (coloured as green).[5]

Finally, the group of Kiessling showed that a non-carbohydrate glycomimetic compound based on Shikimic acid conjugated with BSA -bovine serum albumin- (Scheme **3.3**) and then coupled with a fluorescent dye was internalized by Raji Cells expressing DC-SIGN.[6] Authors also assessed the production of phosphor-JNK, a specific kinase involved in the dendritic cell maturation and the response to "danger" signals,[7] when Raji/DC-SIGN cells were treated with the glycoprotein surrogate. This observation demonstrated the possibility of initiating immune signalling events by using DC-SIGN artificial binders.
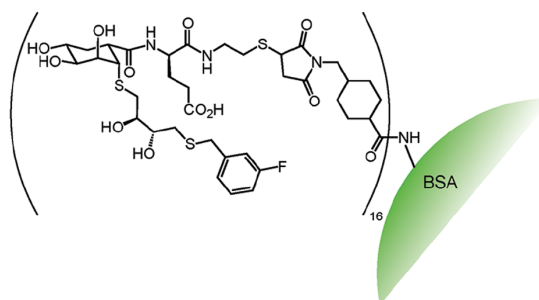
Scheme 3.3 Glycoprotein surrogate constituted by a Shikimic acid derivative connected to BSA and labelled with a fluorescent dye (not shown).[6]

3.2 Goal of the assays

Rod2, Rod3 and their derivatives are fluorescent molecules. We therefore decided to exploit their natural fluorescence to analyse their interaction with DC-SIGN and immature Dendritic Cells through fluorescence microscopy. **PM26** (Scheme **3.4)** was selected as target compound because of its higher biological activity in SPR and *trans*-infection competition assays (see Chapter 2.6). I

conducted all these experiments with the collaboration of B. Joosten visiting the group of Prof. A. Cambi at the Radboud University Medical Centre (Nijmegen, NL).
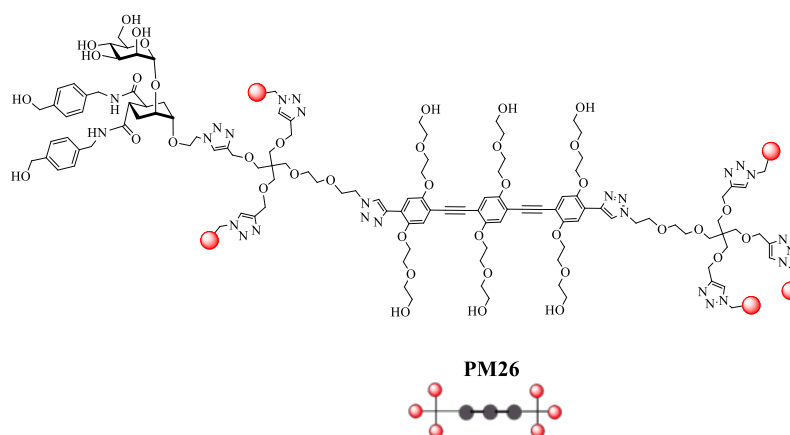
Scheme 3.4 Structure of compound **PM26**. Red sheres represent **1.9** ligand.

3.3 Intrinsic fluorescence properties of PM26 compound

Using a Perkin Elmer Fluorescence Spectrometer, the fluorescence properties of **PM26** in Hank's Balanced Salt Solution (HBSS) were investigated. As shown in Figure **3.1**, compound **PM26** was found to have an excitation maximum of 372 nm and emission maximum of 425 nm in HBSS. Also a shoulder, probably corresponding to a second fluorophore, was observed.
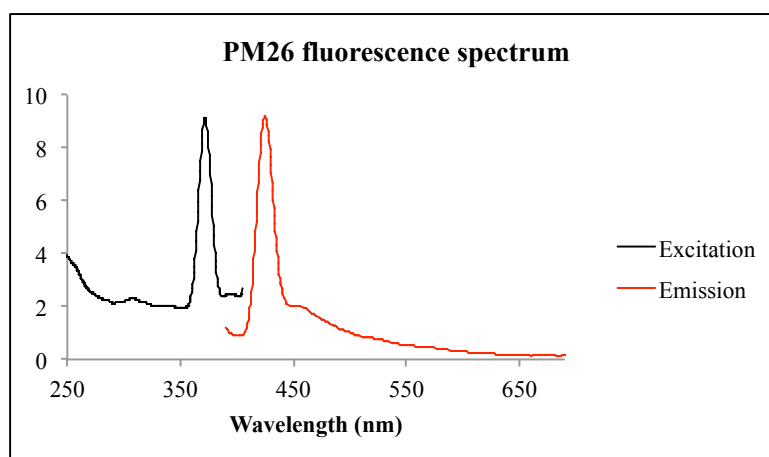
Figure 3.1 Excitation and emission spectra of 2.4 nM **PM26** in HBSS. Also a shoulder of the main peak can be observed.

PM26 emission in HBSS was found to decrease by decreasing the solution pH (Figure **3.2**). This is probably due to protonation of the triazole moieties (pKa = 9.3) directly linked to the central rod. Remarkably, the decrease of fluorescence involved more the shoulder (450-460 nm) than the main peack (425 nm). Indeed, the ratio between the fluorescent intensity observed in the range 420-430

nm and the fluorescent intensity observed in the range 450-460 nm increased by decreasing the pH (i.e. 1.81 when pH = 7.8; 1.88 when pH = 5.4; 2.12 when pH = 3.1; 2.49 when pH = 1.2). This suggests that the second emission (450-460 nm) is more pH dependant than the first one (425 nm).
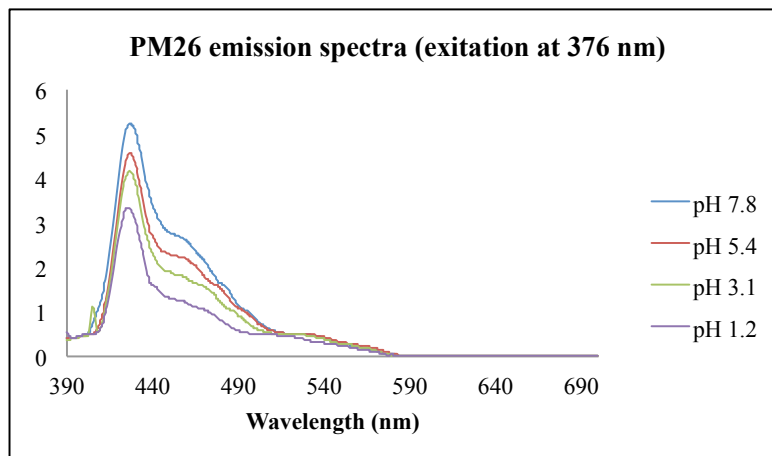
Figure 3.2 Emission spectra of 13 nM **PM26** in HBSS at different pH values. **PM26** was excited at 372 nm.

The observation of two emission bands is consistent with the detection of two fluorophores for compound **PM31** in HBSS (Figure **3.3A**). In that case, a first species absorbing at 376 nm and emitting at 426 nm (Figure **3.3B**) and a second species absorbing at 392 nm and emitting at 450 nm were observed (Figure **3.3C**).
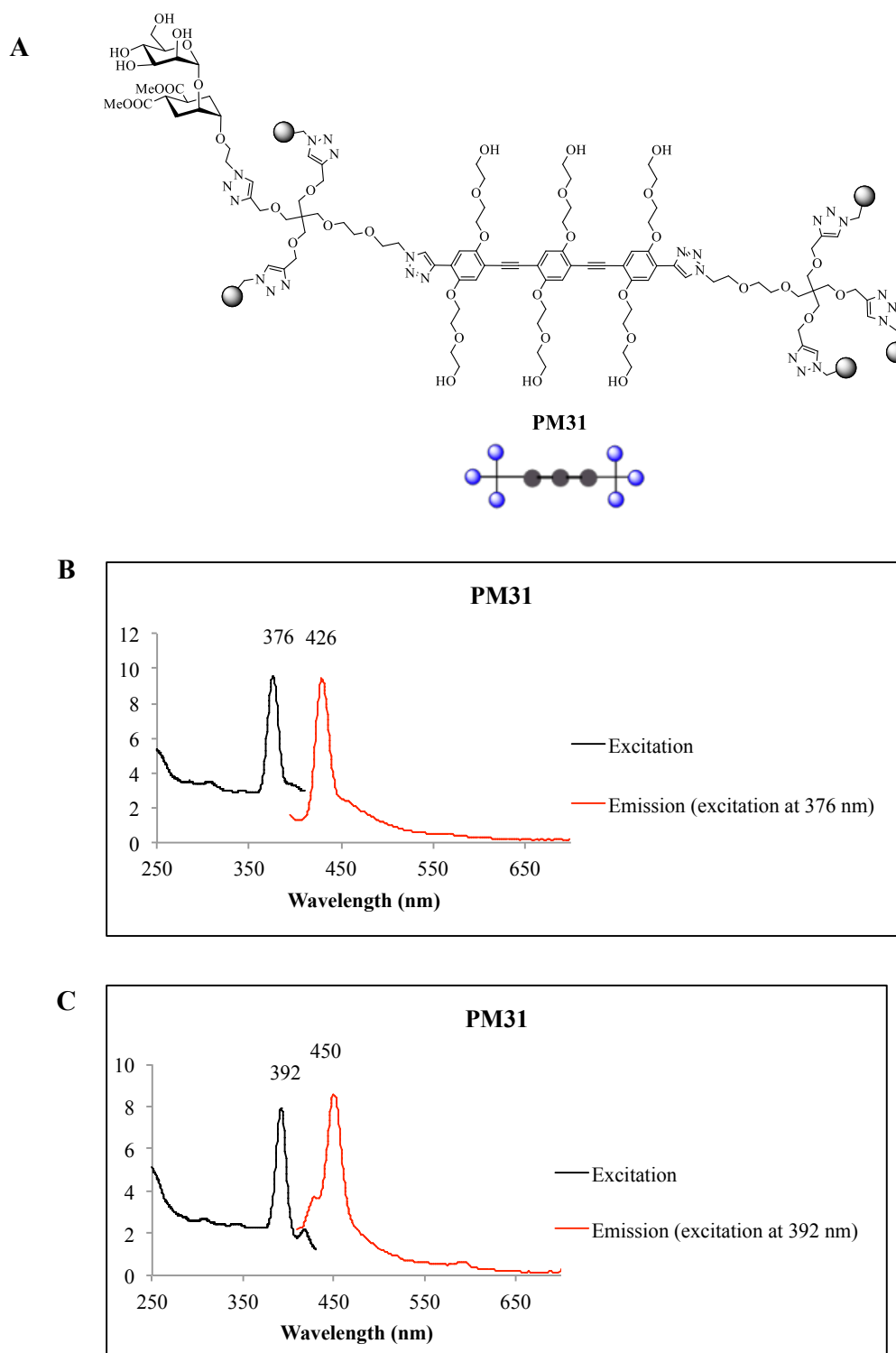
Figure 3.3 A) Structure of **PM31**; blue spheres represent ligand **1.7**. B) and C) Excitation and emission spectra of 4 nM **PM31** in HBSS.

The fluorescence of **PM26** was investigated also in the presence of 4 % paraformaldehyde (PFA), which is the reagent of choice used for fixing cells for microscopy analysis. In these conditions, a completely altered emission spectrum was observed (Figure **3.4**).
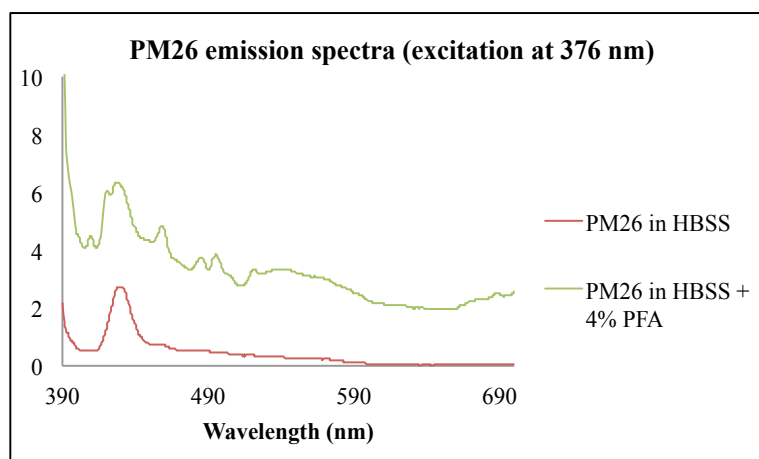
Figure 3.4 Emission spectra of 10 nM **PM26** in HBSS alone and in the presence of 4 % PFA. **PM26** was excited at 376 nm.

Finally, since microscopy analyses were conducted in the presence of specific fluorescent dyes, we recorded fluorescence spectra of **PM26** in the presence of selected Ovalbumin absorbing at 647 nm (i.e. OVA 647). At least in this wavelength region, we excluded that **PM26** emission is reduced by the presence of the dye (Figure **3.5**).
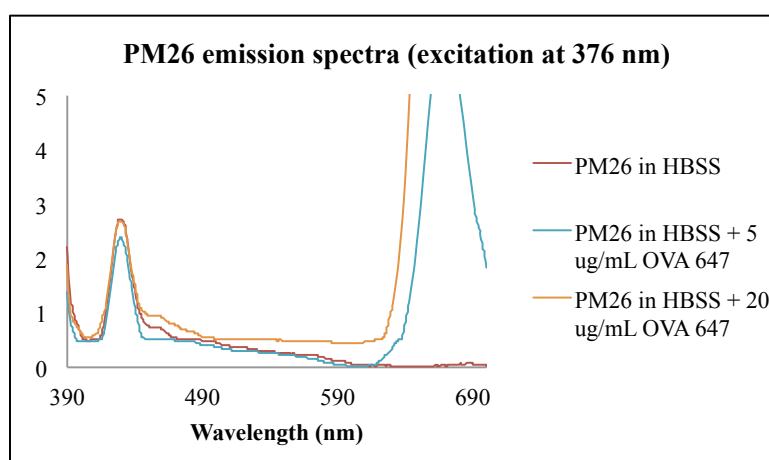
Figure 3.5 Emission spectra of 10 nM **PM26** in HBSS alone and in the presence of 5 μg/mL or 20 μg/mL of OVA647. **PM26** was excited at 376 nm.

3.4 Evaluation of DC-SIGN subdomain targeted by PM26

With the aim to investigate which is the preferential DC-SIGN region bound by *PM* compounds, the interaction between **PM26** and two different DC-SIGN mutants was evaluated. Together with DC-SIGN wild type (DC-SIGN-wt), also DC-SIGN lacking the CRD domain (DC-SIGN-ΔCRD) and DC-SIGN lacking the tandem repeats in the extracellular neck region (DC-SIGN-ΔRep) were investigated. The amount of **PM26** binding to the cell lines harbouring the wild type or the mutated DC-SIGN was then assessed by fluorescence microscopy.

3.4.1 Experimental

CHO cells stably expressing DC-SIGN-wt, ΔCRD and ΔRep were established by Lipofectamine^TM 2000 transfection. Cells plated on a 96-well plate were incubated with 100 μM **PM26** in HBSS for 30 min at room temperature. After thorough washing with HBSS, images were obtained using a commercial Leica DMI6000 epi fluorescence microscope with AFC equipped with a 63× oil immersion objective (HC PL APO 63x/1.40-0.60 OIL, Leica Microsystems) and filter system DAPI ET, GFP ET, DsRed ET and Y5 ET. **PM26** was excited at 340-380 nm; emission was recorded at 450-490 nm.

Images were analyzed using Fiji software.

3.4.2 Results and discussion

Cell pictures are shown in Figure **3.6** and the calculated mean fluorescence values are listed in Table **3.1**. Untransfected CHO cells were used as a negative control, both incubated with HBSS (obtaining no fluorescence signal) and with **PM26** (Figure **3.6A**). It was possible to observe that DC-SIGN-wt (Figure **3.6B**) and ΔRep (Figure **3.6D**) bound to fluorescent **PM26**, while the ΔCRD mutant did not show binding (Figure **3.6C**).

A   CHO + PM26

B   DC-SIGN-wt + PM26

C   ΔCRD + PM26

D   ΔRep + PM26
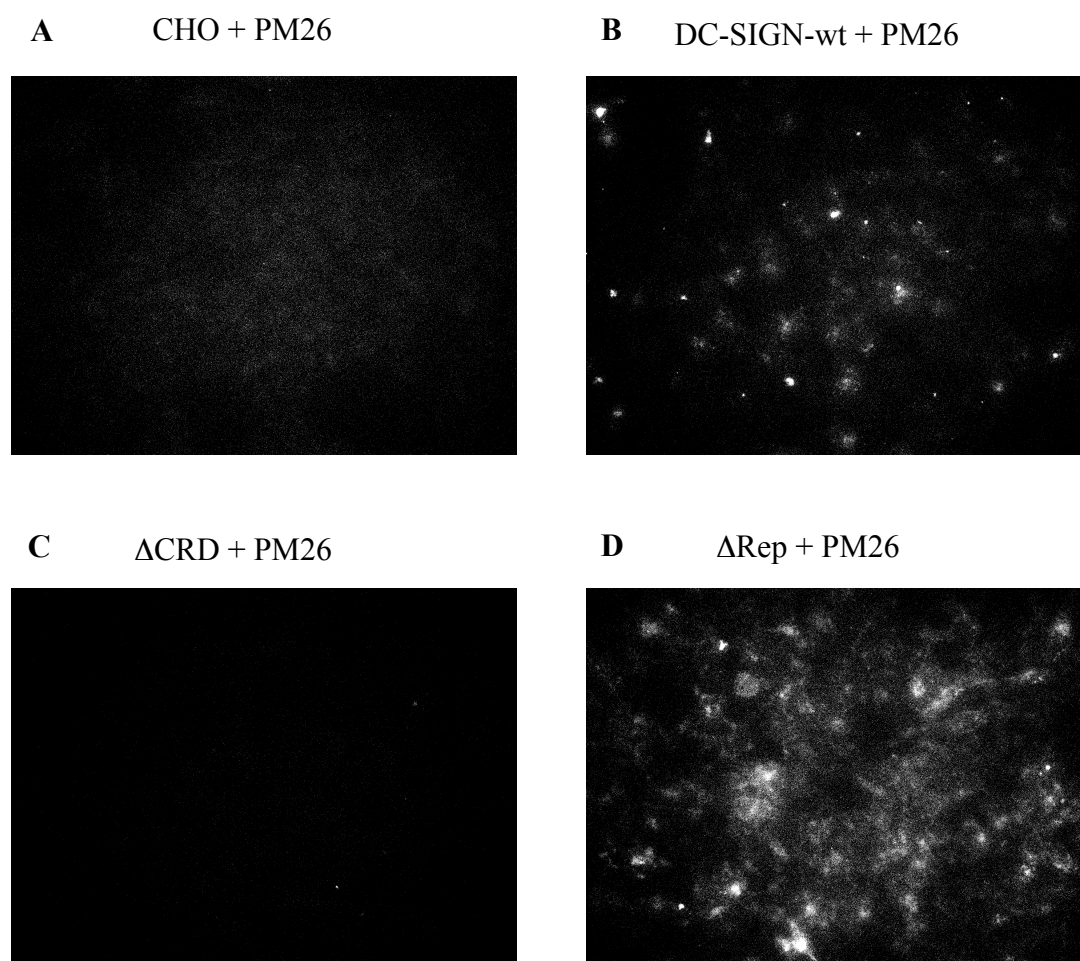
Figure 3.6 Specificity control of DC-SIGN binding to **PM26**. Cells incubated with **PM26** for 30 min at RT A) Negative control: untransfected CHO; B) CHO cells expressing DC-SIGN-wt; C) CHO cells expressing DC-SIGN-ΔCRD; D) CHO cells expressing DC-SIGN-ΔRep.

Entry	Imaged cells	Mean Fluorescence
1	CHO + HBSS (negative control)	112.6 ± 16.7
2	CHO + PM26 (negative control)	127.6 ± 14.2
3	CHO-DC-SIGN-wt + PM26	134.5 ± 10.2
4	CHO-DC-SIGN-ΔCRD + PM26	117.2 ± 5.2
5	CHO-DC-SIGN-ΔRep + PM26	162.9 ± 12.9

Table 3.1 Mean fluorescence of imaged cells calculated with ImageJ software.

The weak fluorescence intensity variation among all tested cell lines depends on the weak intrinsic fluorescence of **PM26**, which is not optimal for this fluorescence assay. Moreover, **PM26** excitation, with an incident beam set to wavelengths proper of the UV light (340-380 nm) couldn't be too strong, otherwise inducing both cellular autofluorescence and death.

Fluorescence values increased from CHO cells treated with HBSS and the same cell line treated with **PM26** (Table **3.1** Entries **1** and **2**); nevertheless, they decreased again for cells carrying DC-SIGN-ΔCRD incubated with **PM26** (Table **3.1**, Entry 4). The interaction between the compound and DC-SIGN-ΔRep was the strongest observed (Table **3.1**, Entry 5), even higher than that detected between **PM26** and DC-SIGN-wt (Table **3.1**, Entry 3). All these results could also be indicative of a different level of DC-SIGN expression on CHO cells. Nonetheless, the large difference in binding between **PM26** and DC-SIGN-ΔCRD (Figure **3.5C**, Table **3.1**, Entry 4) or DC-SIGN-ΔRep (Figure **3.5D**, Table **3.1**, Entry 5) assessed the selective binding of **PM26** with the CRD domain and not the neck domain on DC-SIGN.

3.5 PM26 internalization

3.5.1 PM26 internalization as a function of temperature

PM26 internalization in immature dendritic cells (iDCs) was assessed through confocal microscopy using *DiD* oil (1,1'-Dioctadecyl-3,3,3',3'-Tetramethylindodicarbocyanine Perchlorate) as a marker for the cellular membrane. The benefit of using confocal microscopy is the possibility to optically slice cellular samples (referred to *z-sections*), therefore observing both dorsal (top) and ventral (bottom) membranes and cross sections in the middle of the cells body.

3.5.1.1 Experimental

Human immature DCs were generated from peripheral blood monocytes of healthy donors[8] and they were allowed attaching to a Labtek 8-chamber slides in serum free RPMI medium. Cells were incubated with 50 μM **PM26** in HBSS both at 37 °C for 60 min and 4 °C for 20 min and washed with HBSS. Also cells incubated at 37 °C were stored at 4 °C for 20 min; indeed, at 4 °C cells were found to assume a round shape more suitable to perform *z-sections*. Cells were incubated with Did for 2 min at RT. After a washing step (HBSS), cells were fixed with 1 % paraformaldehyde for 20 min at RT, washed and blocked with 100 mM glycine in TBS (Tris-buffered saline) for 10 min at RT. Confocal images were obtained in a sequential manner using a commercial Leica SP8 SMD-WLL (Leica Microsystems) confocal microscope equipped with PMT and Hybrid detectors (HyD) and a 63× water immersion objective (HC PL APO 63×/1.2 W motCORR CS2, Leica Microsystems). **PM26** was excited at 405 nm. Images were analyzed using Fiji software.

3.5.1.2 Results and discussion

In Figure **3.7**, iDCs with labelled membrane (rendered as green) and treated with **PM26** (rendered as red) are presented. For each sample, optical slices were recorded, imaging both external membrane and cross sections. Negative controls were included.
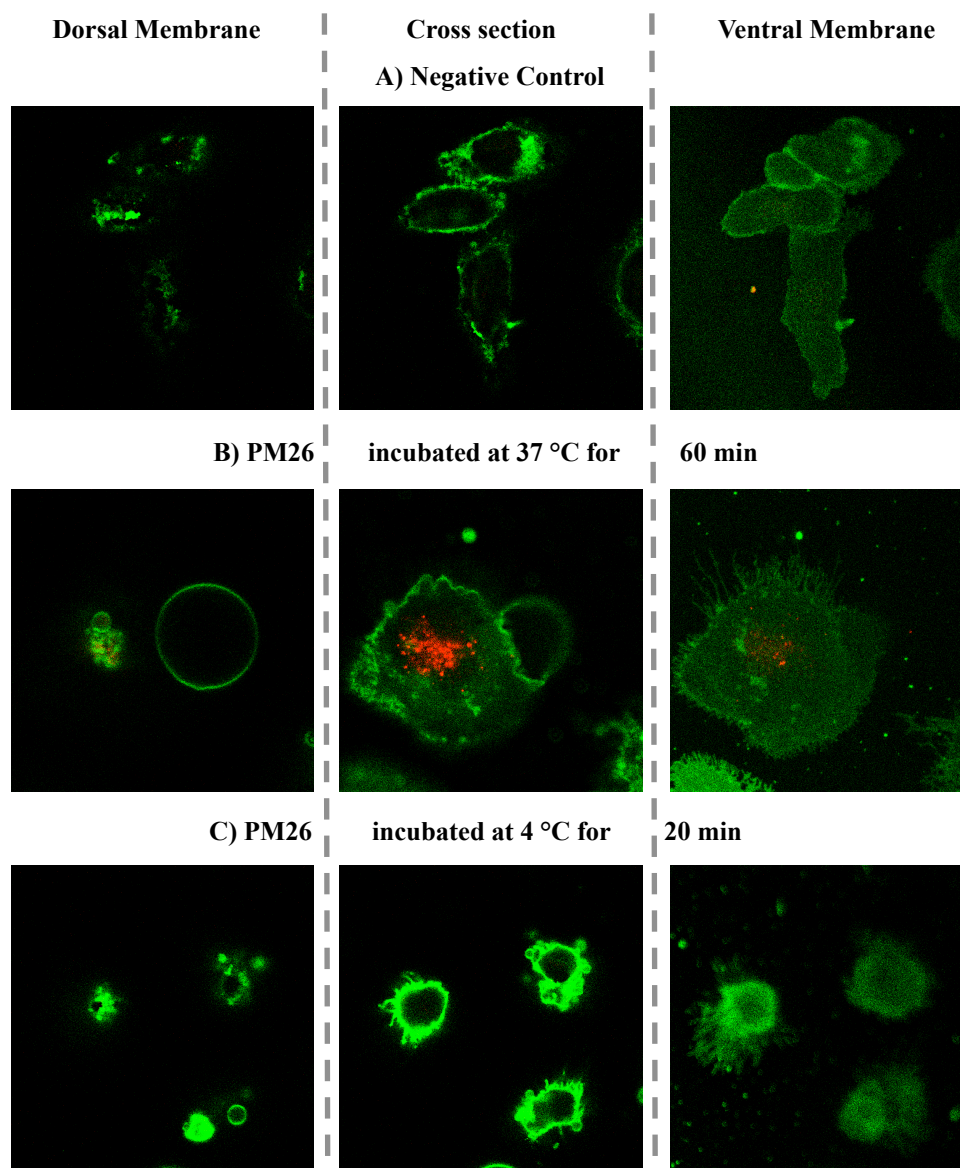
Figure 3.7 Optical slices of immature Dendritic Cells incubated with 50 μM **PM26** in HBSS and stained with Did as membrane marker Left: dorsal membrane; centre: middle of the cell body; right: ventral membrane. A) Negative control; B) iDCs were incubated with 50 μM of **PM26** at 37 °C for 60 min; C) iDCs were incubated with 50 μM of **PM26** at 4 °C for 20 min. Membrane is rendered as green; **PM26** is rendered as red.

PM26 incubated with DCs at 37 °C was internalized, reaching fluorescence levels 18 times above background levels, as shown in the cross section (Figure **3.7B**, centre); dorsal and ventral labelled membrane clearly show the absence of compound **PM26** on cells surface (Figure **3.7B** left and **3.7B**

right). Remarkably, no internalization occurred when compounds were incubated with iDCs at 4 °C. Since incubation of cells at 4 °C has been described as a method to inhibit energy-dependent internalization,[9,10] this result shows that **PM26** internalization is mediated by active mechanisms, as receptor-mediated internalization is.

Remarkably, also images recorded on live cells after 10 (Figure **3.8A**) and 20 min (Figure **3.8B**) of incubation at 37 °C showed internalization of **PM26** in the middle of cell body.
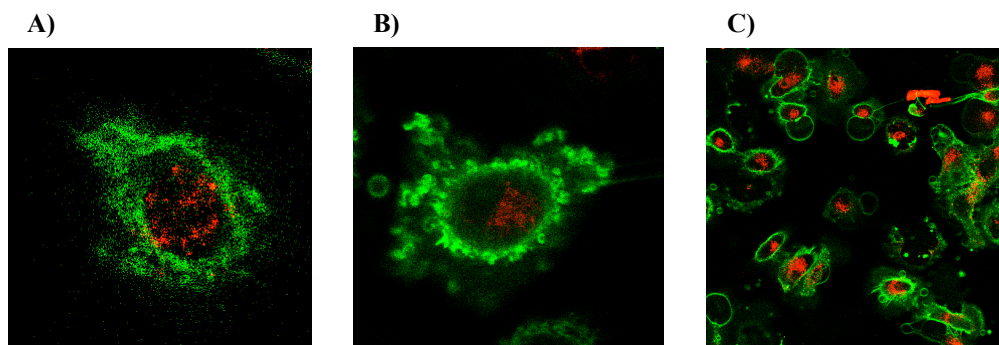
Figure 3.8 Optical slices of immature Dendritic Cells incubated with 50 μM **PM26** in HBSS (rendered as red) and stained with Did as membrane marker (rendered as green). A) Incubation for 10 min at RT, live cells; B) Incubation for 10 min at RT, live cells; C) Incubation for 60 min at 37 °C, fixed cells with 1 % PFA.

3.5.2 *PM*s compounds localization within immature Dendritic Cells

To study the internalization route of **PM26** in iDCs and its localization in intracellular compartments, fluorescent ovalbumin (OVA 488), Cholera Toxin Subunit B (CTB 647), Transferrin (633) and Lysotracker Red (577) were used. OVA,[11] Cholera Toxin[12] and Transferrin[13] are internalized by cells and routed to early endosomes compartments; therefore, once labelled with fluorescent dyes, they can be used to visualize these specific organelles. LysoTracker Red is a red-fluorescent dye for labelling and tracking acidic organelles in live cells, therefore it is selective for late endosomes and lysosomes. Also immature Dendritic Cells transfected with Rab5-GFP were used; Rab5 is a protein marker for early endosomes.

To understand also whether **PM26** follows DC-SIGN in the internalization route, a fluorescent antibody specific for DC-SIGN neck (DCN46 labelled first with biotin and then, as second step, with fluorescent streptavidin) was used.

Remarkably, the common procedure in which cells, after first being incubated with the fluorescent compound, are fixed and permeabilized to let antibodies specifically label cellular organelles could not be used. Indeed, after fixation with paraformaldehyde (4 %) followed by membrane permeabilization and many washing steps, **PM26** could not be detect any longer. The alteration of fluorescence in the presence of PFA (Figure **3.4**) was probably combined also with physical

removal of the compound that, once internalized, can in principle dissociate from DC-SIGN and exit the cell from the permeabilized membrane.

3.5.2.1 Experimental

Human immature DCs were generated from peripheral blood monocytes of healthy donors[8] and they were allowed to attach to a labtek 8 well chamber slides in serum free medium. Incubation with dyes was always followed by extensive washing steps with HBSS, unless otherwise stated. Cells were incubated with HBSS solution of 50 μM **PM26** plus fluorescent OVA, CTB or transferrin for 10 min at room temperature. In the case of transfected cells with labelled Rab5, incubation lasted for 2 min at room temperature. Lysotracker was added and not removed, after incubating cells with **PM26** for 20 min at room temperature or 2 hours at 37 °C. The colocalization experiments with labelled DC-SIGN were performed by incubating cells with DCN46 for 5 min at room temperature and, after washing steps, incubating cells with HBSS solution of 50 μM **PM26** plus Streptavidine-TxRed. Images were recorded through confocal microscopy (the apparatus was described in Paragraph 3.5.1) on live cells with at time chase dependent on experimental needs for setting the instrument up. The intracellular localization of **PM26** and dyes was assessed over time by confocal microscopy. **PM26** was excited at 405 nm, while dyes at the specific and required wavelength. In the case of experiment performed with OVA, CTB, transferrin, labelled Rab5 and labelled DC-SIGN, sequential images in time were recorded on the same cells. Unfortunately, the low staining intensity of CTB prevented us to draw conclusions.

Images were analyzed using Fiji software.

The degree of colocalization, expressed as **PM26** fraction overlapping with the dye, was calculated with Manders' coefficients with the JACoP plugin, using the automatic threshold.[14]

3.5.2.2 Results and discussion

Figure **3.9** shows selected immature dendritic cells presenting **PM26** stain (rendered as red) superimposed to the dye (rendered as green), for each dye at different time points. Colocalized stains result in yellow spots. In each figure, colocalization coefficients are plotted as histograms (Figure **3.10**).

A) PM26 + OVA 488

t = 8' chase   t = 10' chase   t = 15' chase   t = 20' chase   t = 30' chase   t = 40' chase

B) PM26 + Transferrin 633

t = 8' chase   t = 10' chase   t = 15' chase   t = 20' chase   t = 30' chase   t = 40' chase

C) PM26 + LysoTracker 577

Incubation 30' @ RT + 20' chase   Incubation 120' @ 37 °C + 20' chase

D) PM26 + Rab5

t = 5' chase   t = 6' chase   t = 8' chase   t = 10' chase   t = 15' chase   t = 20' chase

E) PM26 + DC-SIGN (DCN46 *vs* neck)

t = 6' chase   t = 8' chase   t = 10' chase   t = 15' chase   t = 20' chase   t = 30' chase

Figure 3.9 Pictures were obtained through confocal microscope; **PM26** is rendered as red and the dye is rendered as green. A) iDCs were incubated with **PM26** (50 µM) plus OVA 488 in HBSS, for 10 min at RT and analysed at indicated time chase. B) iDCs were incubated with **PM26** (50 µM) plus Transferrin in HBSS, for 10 min at RT and analysed at indicated time chase. C) iDCs were incubated with 100 µM **PM26** for 20 min at RT or 120 min at 37 °C; after a washing step, LysoTracker was added and cells were analysed at indicated time chase. D) Cells transfected with anti Rab5 were incubated with 50 µM **PM26** for 2 min at RT and analysed at indicated time chase. E) iDCs were incubated with DCN46 anti DC-SIGN-neck for 5 min at RT; after a washing step, **PM26** (50 mM) plus Streptavdine in HBSS were added for 10 min at RT. Cells were analysed at indicated time chase.
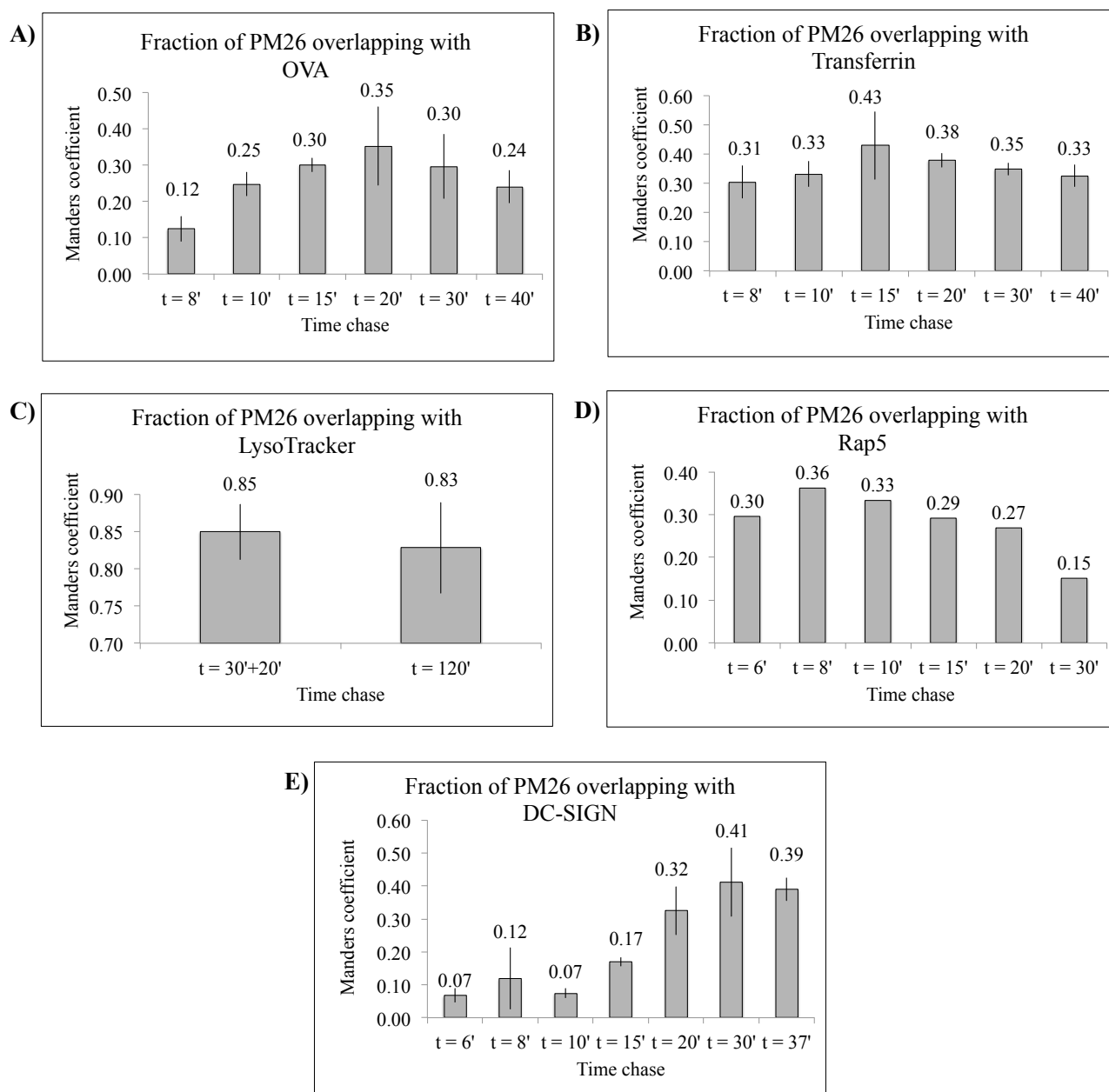
Figure 3.10 Manders' colocalization coefficients plot representing the fraction of **PM26** overlapping with A) OVA 488, B) Transferrin 633, C) LysoTracker 577, D) Rap5, E) stained DC-SIGN.

The colocalization of **PM26** and OVA (Figure **3.9A**, **3.10A**) gradually increased in time, reaching higher values after 20 min of chase; subsequent decrease of colocalization could indicate that **PM26** and the dye follow different endocytic routs. On the contrary, **PM26** colocalization with Transferrin (Figure **3.9B**, **3.10B**) remained almost constant over the time. The highest degree of colocalization was obtained between **PM26** and LysoTracker, reaching coefficient values higher that 0.8 (Figure **3.9C**, **3.10C**). Remarkably, Manders' coefficients indicating the overlapping of **PM26** with Lysosomes remained constant by increasing incubation times. Colocalization coefficients between **PM26** and Rab5 (Figure **3.9D**, **3.10D**) gradually increased from 5 min to 6 min of chase, reaching

the highest value < 0.4, but then started decreasing; this low colocalization level could derive also from a not perfect stain of Rab5 obtained in transfected cells.

The colocalization between **PM26** and DCN46 was surprisingly low, reaching medium values only after 15 min chase (Figure **3.9E**, **3.10E**). Assuming that **PM26** and DCN46 bind to different DC-SIGN tetramers, even if the were both added to cells in saturation concentrations, it is possible that they have different internalization kinetics and/or they follow different endocytosis routes. Indeed, **PM26** was demonstrated to bind DC-SIGN CRD (see Paragraph 4.4), and Tacken *et al.* demonstrated that DC-SIGN follows alternative endocytic pathways with prolonged residence in early endosomes when targeted via its neck region.[15] It is therefore possible that **PM26** and stained DCN46 are routed to the same organelles only after times chase > 15 min. It is also possible that a portion of DC-SIGN tetramers targeted by the antibody started to be internalized before the incubation with the compounds. Or, it is also possible that **PM26** has others binding receptors expressed on Dendritic Cells, not being totally selective for DC-SIGN. Further experiments would be needed to clarify this point.

3.6 Conclusions

Analysing **PM26** behaviour through fluorescence microscopy was rather challenging, since the compound doesn't have the optimal fluorescence properties required for this kind of analysis. First of all, it has to be excited at a high energy wavelength (i.e. around 400 nm, Figure **3.1**), which is detrimental for cells. Fixing cells with PFA was also not viable, since this alters Rod fluorescence (Figure **3.4**); therefore, more difficult experiments on live cells were mainly conducted. Moreover, **PM26** fluorescence decreases by increasing the acidity of the medium (Figure **3.3**). Therefore, once internalised in acidic compartments (early endosomes pH = 6.5-6.0; late endosomes and lysosomes pH = 5.5-4.5), it is less probable to detect the compound. Nevertheless, it was possible to draw relevant conclusions.

It was demonstrated that **PM26** binds DC-SIGN selectively *via* the CRD, since it was not able to interact with CHO ΔCRD cells, whereas it did bind CHO cells lacking the neck domain (Figure **3.6**). **PM26** appeared to be internalized inside immature Dendritic Cells. Internalization seemed to be receptor dependant, since it didn't occur at 4 °C (Figure **3.7**). Internalization happened already after 10 min of incubation at room temperature (Figure **3.8**). The specific internalization route of **PM26** was also investigated, finding that this dendrimer ends up in lysosomes (Figure **3.10C**). When an antigen is routed to lysosomes, it must do so through endosomes. Colocalization with Rab5 positive organelles, even if low (Figure **3.10D**), demonstrated that **PM26** transit *via* the early endosomes en route to the lysosomal compartments (Figure **3.8** and **3.9**). These results suggest that **PM26** could in

principle stimulate an immune response, and could therefore be used as adjuvant for vaccines. The immune response of iDCs associated to **PM26** internalization will be further investigated by Dr. A. Berzi (Università degli Studi di Milano).

The observed not very high colocalization level between **PM26** and DC-SIGN (Figure **3.10E**) demands for further investigation to evaluate both the kinetics associated to the internalization of DC-SIGN targeted with an anti-neck antiboby or with **PM26** and the selectivity of **PM26** for DC-SIGN itself. SPR and *trans*-inhibition assays (Chapter 2.6) clearly demonstrated the affinity of **PM26** to DC-SIGN, but it is also probable that other mannose-recognizing receptors expressed at the surface of DCs are able to bind it and to drive it inside cells.

3.7 References

[1] J. Banchereau; F. Briere; C. Caux; J. Davoust; S. Lebeque; Y. Liu, B.Pulendran; K. Palucka, Immunobiology of Dendritic Cells, *Annu. Rev. Immunol.* **2000**, 767.

[2] T. B. Geijtenbeek; R. Torensma; S. J. van Vliet; G. C. van Duijnhoven; G. J. Adema; Y. van Kooyk; C. G. Figdor, Identification of DC-SIGN, a novel dendritic cell-specific ICAM-3 receptor that supports primary immune responses, *Cell* **2000**, 575.

[3] Y. van Kooyk; B. Appelmelk; T. B.H. Geijtenbeek, A fatal attraction: Mycobacterium tuberculosis and HIV-1 target DC-SIGN to escape immune surveillance, *Trends in Mol. Med.* **2003**, 153.

[4] R. Ribeiro-Viana; J. J. García-Vallejo; D. Collado; E. Pérez-Inestrosa; K. Bloem; Y. van Kooyk; J. Rojo, BODIPY-Labeled DC-SIGN-Targeting Glycodendrons Efficiently Internalize and Route to Lysosomes in Human Dendritic Cells, *Biomacromol.* **2012**, 3209.

[5] B. Arnáiz; O. Martínez-Ávila; J. M. Falcon-Perez; S. Penadés, Cellular Uptake of Gold Nanoparticles Bearing HIV gp120 Oligomannosides, *Bioconjugate Chem.* **2012**, 814.

[6] L. R. Prost; J. C. Grim; M. Tonelli; L. L. Kiessling, Noncarbohydrate Glycomimetics and Glycoprotein Surrogates as DC-SIGN Antagonists and Agonists, *ACS Chem. Biol.* **2012**, 1603.

[7] S. K. Pathak; A. E. Skold; V. Mohanram; C. Persson; U. Johansson; A. L. Spetz, Activated apoptotic cells induce dendritic cell maturation via engagement of Toll-like receptor 4(TLR4), dendritic cell-specific intercellular adhesion molecule 3 (ICAM-3), grabbing nonintegrin (DC-SIGN), and beta 2 Integrins, *J. Biol. Chem.* **2012**, 13731.

[8] N. Romani; S. Gruner; D. Brang; E. Kämpgen; A. Lenz; B. Trockenbacher; G. Konwalinka; P. O. Fritsch; R. M. Steinman; G. Schuler, Proliferating dendritic cell progenitors in human blood, *J. Exp. Med.* **1994**, 83.

[9] B. J. Iacopetta; E. H. Morgan, The kinetics of transferrin endocytosis and iron uptake from transferrin in rabbit reticulocytes, *J. of Biol. Chem.* **1983**, 9108.

[10] J. Saraste; G. E. Palade; M. G. Farquhar, Temperature-sensitive steps in the transport of secretory proteins through golgi-complex in exocrine pancreatic-cells, *Proceedings of the National Academy of Sciences of the United States of America* **1986**, 6425.

[11] S. Burgdorf; A. Kautz; V. Böhnert; P. A. Knolle; C. Kurts, Distinct Pathways of Antigen Uptake and Intracellular Routing in CD4 and CD8 T Cell Activation, *Science* **2007**, 612.

[12] Y. Sugimoto; H. Ninomiya; Y. Ohsaki; K. Higaki; J. P. Davies; Y. A. Ioannou; K. Ohno, Accumulation of cholera toxin and GM1 ganglioside in the early endosome of Niemann–Pick C1-deficient cells, *Proc. Natl. Acad. Sci. USA* **2001**, 12391.

[13] E. M. van Dam; W. Stoorvogel, Dynamin-dependent Transferrin Receptor Recycling by Endosome-derived Clathrin-coated Vesicles, *Molecular Biology of the Cell* **2002**, 169.

[14] S. Bolte; F. P. Cordelières, A guided tour into subcellular colocalization analysis in light microscopy. *J. Microsc.* **2006**, 213.

[15] P. J. Tacken; W. Ginter; L. Berod; L. J. Cruz; B. Joosten; T. Sparwasser; C. G. Figdor; A. Cambi, Targeting DC-SIGN via its neck region leads to prolonged antigen residence in early endosomes, delayed lysosomal degradation, and cross-presentation, *Blood* **2011**, 4111.

Chapter 4

Morphological behaviour of ROD-based glycodendrimers in aqueous solution

4.1 Introduction

With the aim of interpreting the biological performances of synthesised compounds and to assess whether their biological activity depends on single molecules or aggregates, we studied their morphological behaviour in water and aqueous solutions. The hypothesis that they could form aggregates in water was related to their amphiphilic structure (Scheme **4.1A**) and to their rather low solubility in water (Table **4.1**). Derivatives based on the disaccharide **1.9** (Scheme **4.1B**), bearing aromatic amide moieties, have a lower solubility with respect to those based on **1.7** (Scheme **4.1C**).
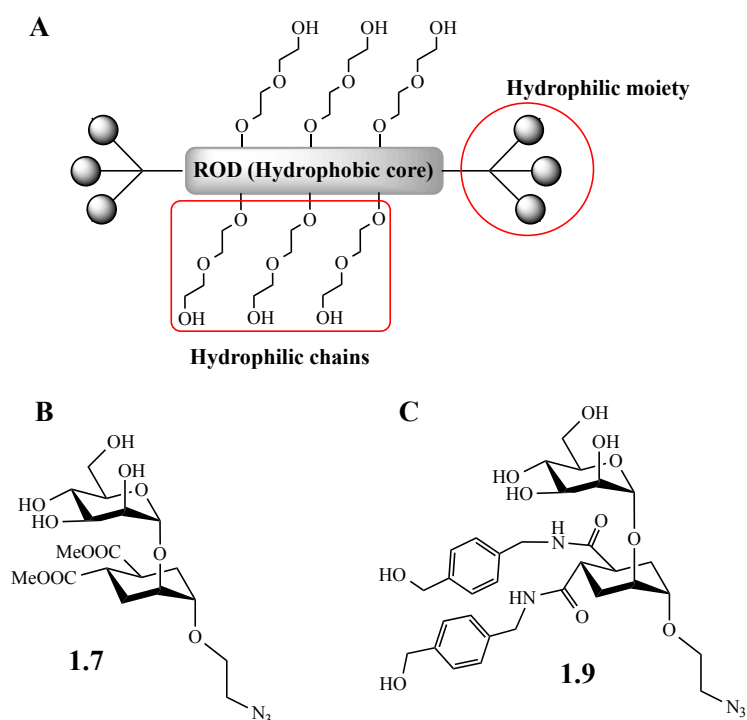
Scheme 4.1 A) Schematic representation of Rod derivatives, highlighting their amphiphilic structure; B) Structure of the disaccharide **1.7**; C) Structure of the disaccharide **1.9**.

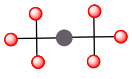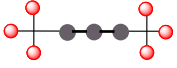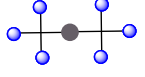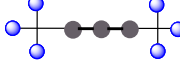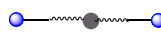| Compound				Max Solubility	Solvent
Name	**Ligand**	**Valency**	**Schematic structure**		
PM25	**1.9**	6		0.5 mM	H$_2$O
				1 mM	SPR buffer^a + 4% DMSO
PM26	**1.9**	6		0.15 mM	SPR buffer^a + 4% DMSO
PM30	**1.7**	6		≥ 5 mM	SPR buffer^a
PM31	**1.7**	6		≥ 5 mM	SPR buffer^a
PM34	**1.7**	2		≥ 5mM	SPR buffer^a
PM36	**1.7**	2		≥ 5 mM	SPR buffer^a

Table 4.1 Solubility ranges of compounds **PM25**, **PM26**, **PM30**, **PM31**, **PM34** and **PM36**.
^{a}SPR buffer consists of 25 mM Tris-HCl (pH 8), 150 mM NaCl, 4 mM CaCl$_2$, 0.005 % P20. The full structure of the compounds is shown in Chapter 2.

Water and/or buffer solutions of selected compounds were analysed through:
- Surface Tension determination, to evaluate if micelles are formed
- Diffusion-Ordered NMR Spectroscopy (DOSY), to determine particle size
- Transmission Electron Microscopy (TEM), to determine particle size
- Sedimentation Velocity Analytical Ultracentrifugation (SV-AUC), to determine particle size and homogeneity
- Dynamic Light Scattering (DLS), to determine particle size and polydispersity

Experimental sets up and results will be described in the following paragraphs.

4.2 Background

In the literature, a number of amphiphilic compounds that self-assemble in water has been described.

The group of Percec reported the preparation of several libraries of amphiphilic Janus dendrimers that self-assemble into stable bilayer vesicles, referred to as dendrimersomes, as well as in other complex architectures.[1] Janus dendrimers are non-symmetric dendrimers constituted by linking two chemically distinct dendritic building blocks, thus they terminate with two different functionalities. Amphiphilic Janus dendrimers bear a hydrophobic end and a hydrophilic one. Self-assembly was induced by injecting Janus dendrimers solutions (10-20 mg/mL in ethanol, tetrahydrofurane,

acetone or dimethylsulfoxide) in water or buffer. The nature of the spontaneous aggregates was evaluated through Cryogenic TEM (cryo-TEM), revealing that some Janus dendrimers form spherical dendrimersomes (Figure **4.1A**) and that others, on the contrary, form polygonal (**4.1B**) or tubolar (**4.1C**) dendrimersomes and spherical (**4.1D**) or rod-like, tubular and helical micelles (**4.1E**).
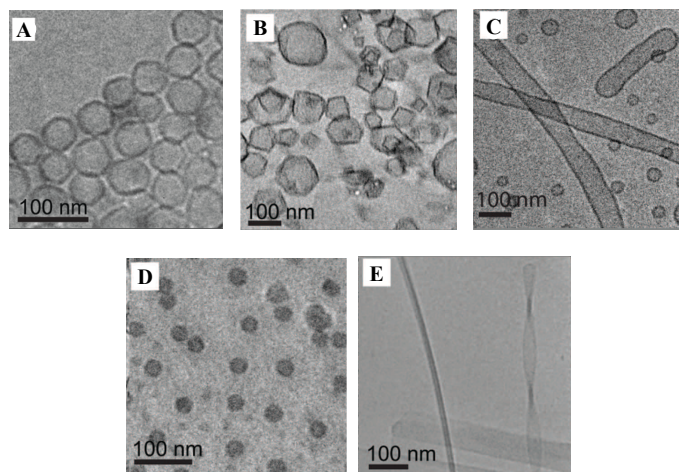
Figure 4.1 A) Spherical dendrimersomes B) Polygonal dendrimersomes C) Tubular dendrimersomes D) Spherical Micelles E) Rod-like, tubular and helical micelles.[1]

Compound **4.1** (Figure **4.2A**) was one of the dendrimers that aggregate as spherical dendrimersomes shown in Figure **4.1A**. The size and the polydispersity of the aggregates were evaluated through Dynamic Light Scattering of their aqueous dispersion. With a final concentration of 0.1 mg/mL in water, **4.1** produces dendrimersomes with an average size of 233 nm and a Polydispersity Index (PDI) of 0.08 (0 corresponds to a perfectly uniform size distribution, Figure **4.2B**). The ability of its simpler derivative **4.2** (Figure **4.3A**) to form dendrimersomes was confirmed also by modeling, showing that a vesicle is completely formed after 80 ns of simulation. Figure **4.3B** and **4.3C** represent the modelled dendrimersome and its cut-away view, respectively.

A   **4.1**

$R_1 = R_3 = OC_{12}H_{25};\ R_2 = H$

B   PDI: 0.080 +/- 0.02   Z-Average (nm): 233.2 +/- 1.70
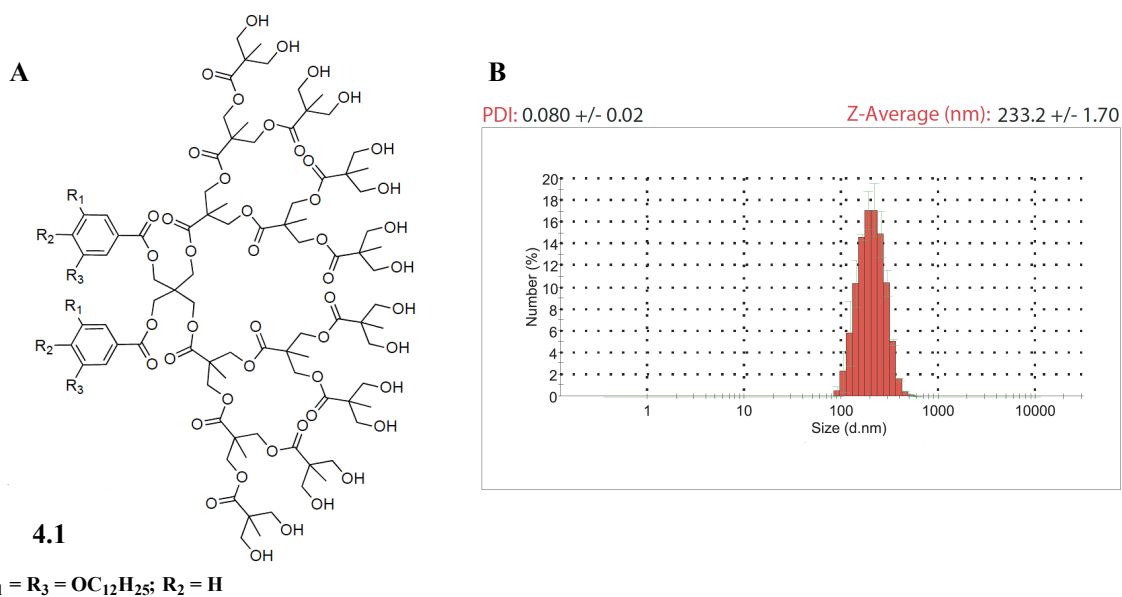
Figure 4.2 A) Janus dendrimer **4.1**; B) DLS evaluation of the size and the polydispersity of dendrimersomes formed by dispersing an ethanol solution of **4.1** in water (0.1 mg/mL final concentration in water).[1]

A   **4.2**

$R_1 = R_3 = OC_{12}H_{25};\ R_2 = H$

B   **C**
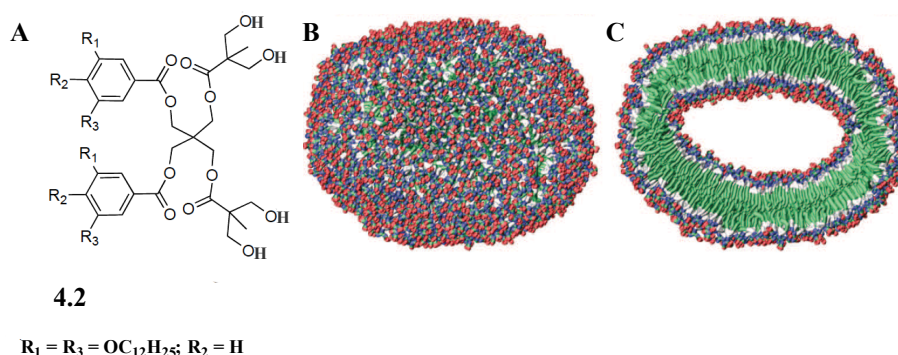
Figure 4.3 A) Janus dendrimer **4.2**; B) Computational simulation of a vesicle formed by compound **4.2**; C) Cut-away view of the vesicle. Hydroxyls groups are represented in red, alkane chains in green.[1]

The group of Prasad reported the formation of μm-sized aggregates by a pyrene-modified polyamidoamine dendrimer (PAMAM) **4.3** (Scheme **4.2**) in dichloromethane solution.[2] Aggregates were analysed by Scanning Electron Microscopy (SEM), revealing their doughnut-type shape (Figure **4.4**). This morphological behaviour is probably driven by hydrophobic interactions between pyrene units and hydrogen bonds between dendrimeric regions.
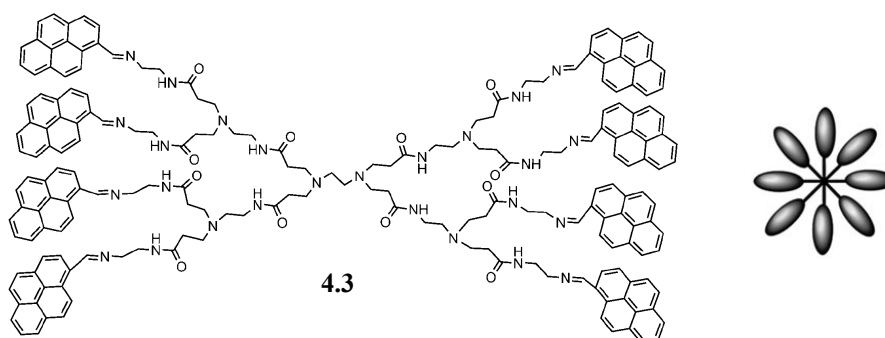
Scheme 4.2 Pyrene-modified polyamidoamine dendrimer **4.3** (left) and its schematic representation where grey ovals represent pyrene units (right).[2]
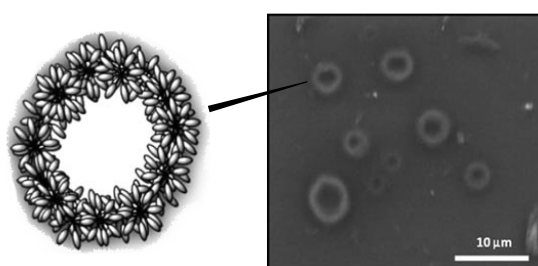
Figure 4.4 Schematic representation of a doughnut-shape aggregate in dichloromethane (left) and SEM images of aggregates (right).[2]

Also carbohydrates can be the polar head of the amphiphilic compounds. Byung-Sun *et al.* reported that rod-coil amphiphiles bearing mannose at one end of the coil self-assemble in water in a way that depends on the conformational behaviour of the monomer.[3] Compounds **4.4**, **4.5** and **4.6** (Scheme **4.3**) were synthesised and their morphological behaviour in water was assessed through TEM and DLS.
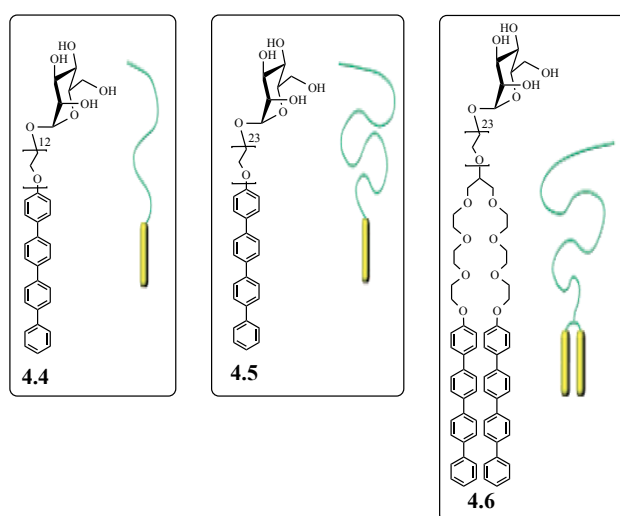
Scheme 4.3 Amphiphilic rod-coil molecules **4.4**, **4.5** and **4.6**, together with their schematic representations were the rod is yellow and the coil is green.[3]

Compound **4.4** self-assembled into bilayer vesicular structures with a diameter of 40 nm, where mannose moieties cover external surfaces (Figure **4.5A**, **4.5D**, **4.6A**). On the contrary, compound **4.5** spontaneously aggregated as micelles with a diameter of 20 nm, which corresponds approximately twice the extended molecular length of 10 nm -calculated through modeling- (Figure **4.5B**, **4.5E**, **4.6B**). Probably this behaviour depends on a more cone-shaped -conformation of its coil moiety that would not be able to fill all of the internal volume of a bilayer. Finally, compound **4.6** self-assembled into cylindrical micelles with, again, a diameter 20 nm long (Figure **4.5C**, **4.5F**). Probably, the strong π-π interaction among the aromatic moieties drives their preferential stacking.
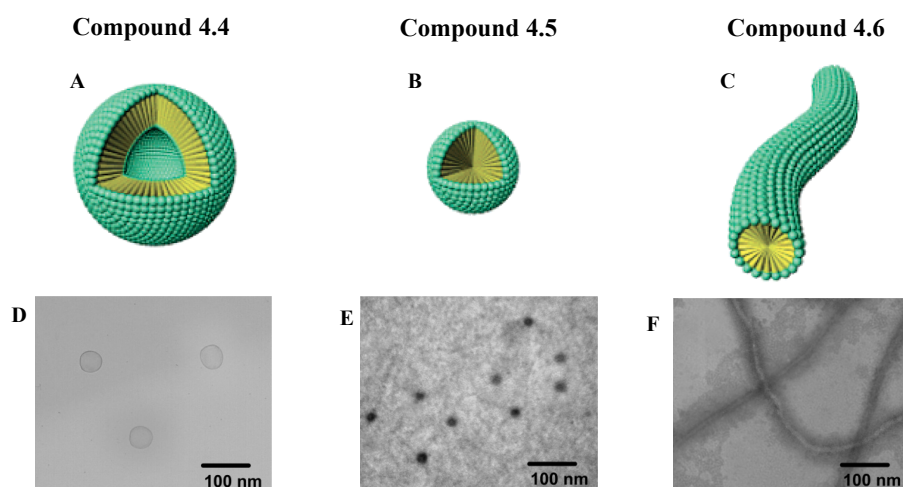
Figure 4.5 Up: schematic representation of the aggregates; down: TEM images of the aggregates. A,D) compound **4.4**; B,E) compound **4.5**; C,F) compound **4.6**.[3]
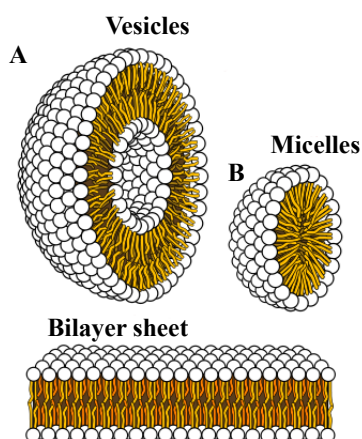
Figure 4.6 A vesicle (A) is formed when a bilayer sheet (down) turns and closes. B) In a typical micelle formed in aqueous solution, the hydrophilic external structure protects hydrophobic moieties from water.

Amphiphilic Janus dendrimers can bear carbohydrates in their hydrophilic part; in this case, they can be referred to as Janus glycodendrimers. The group of Percec reported also the self-assembling

of 51 Janus glycodendrimers when their THF or ethanol solutions are injected into water or buffer.[4] Besides the formation of aggregates with rigid membranes (Figure **4.7A**, **4.7B**), denoted as *solid* or *hard*, *fluid* or *soft* glycodendrimersomes were formed (Figure **4.7C**, **4.7D**).
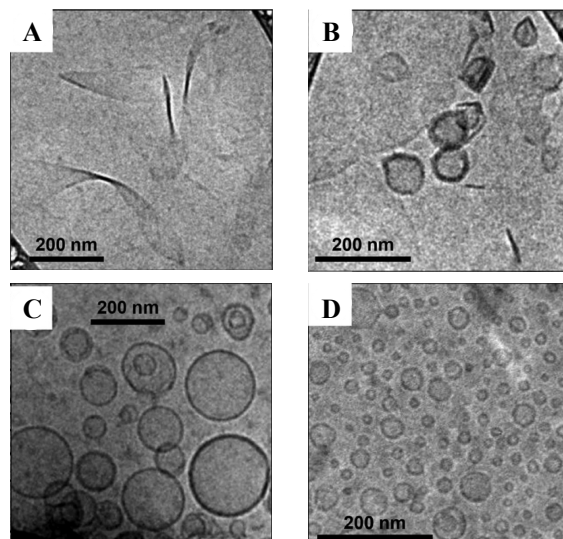
Figure 4.7 Cryo-TEM images of A) solid lamellae; B) solid glycodendrimersomes; C) and D) soft glycodendrimersomes.[4]

Authors remarked that Janus glycodendrimers with carbohydrate moieties attached via a tri(ethylene glycol) or tetra(ethylene glycol) spacer and with a 3,5-disubstituted linear or branched hydrophobic pattern (like compounds **4.7** and **4.8**, Scheme **4.4**) are more prone to form soft glycodendrimersomes with narrow molar mass and mass distribution (Scheme **4.4A**, **4.4B**).
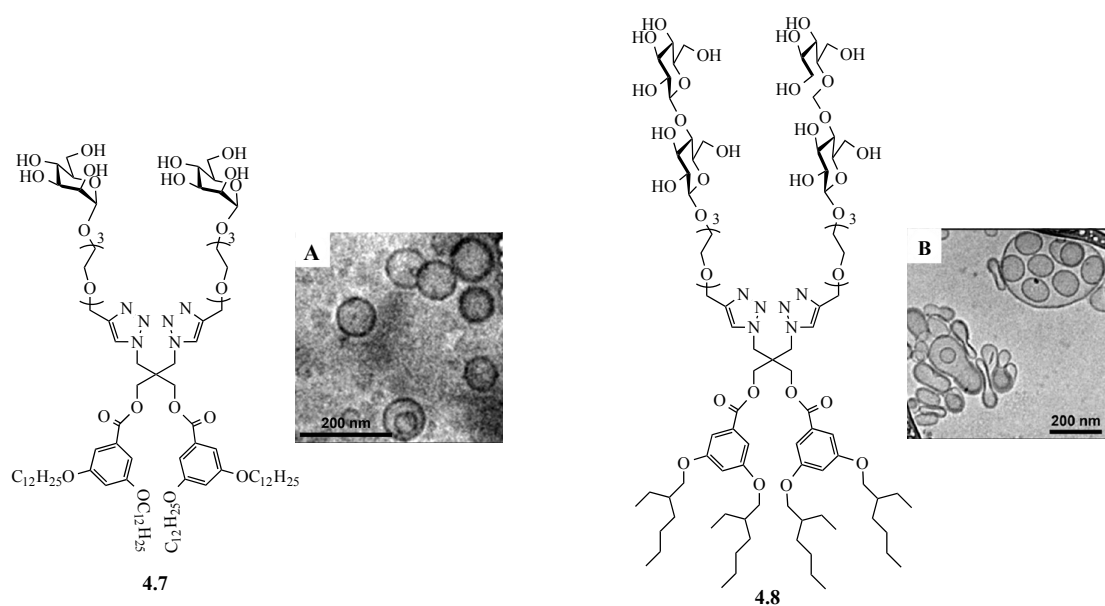
Scheme 4.4 Janus glycodendrimers **4.7** and **4.8** and cryo-TEM images of the soft glycodendrimersomes that they form when their THF or ethanol solutions are injected in water.[4]

Discotic amphiphilic molecules, such as **4.9** depicted in Scheme **4.5**, can form self-assembled columnar polymers in water.[5] **4.10** bears hydrophobic cores and oligo(ethylene oxide) side chains to increase its water solubility. Disks' stacking is driven by π-π hydrophobic interactions among aromatic cores; inter- and intramolecular hydrogen bonds fix the disks in a peculiar conformation. Aggregation was demonstrated by broad signals in the ^{1}H-NMR spectra, a red shift of the UV-Vis spectra and a strong fluorescence intensity. Compound **4.10** (Scheme **4.5**) was obtained decorating **4.9** with mannose moieties; from a mixture of compounds **4.9** and **4.10** in water, a multivalent self-assembled columnar glycol-polymers was obtained (Figure **4.8**).[6] Aggregation was confirmed by the high fluorescence of molecules.
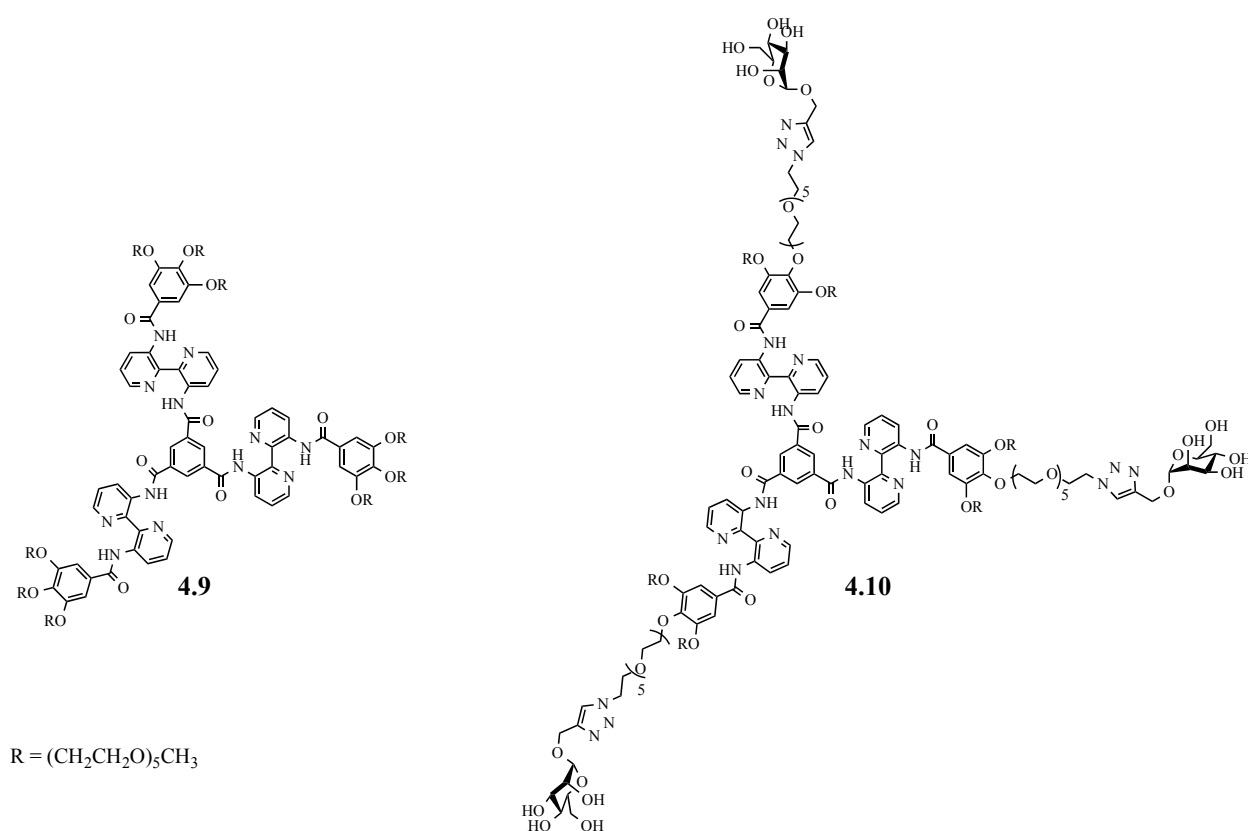
Scheme 4.5 Discotic compound **4.9** and its mannose derivative **4.10**.[5]
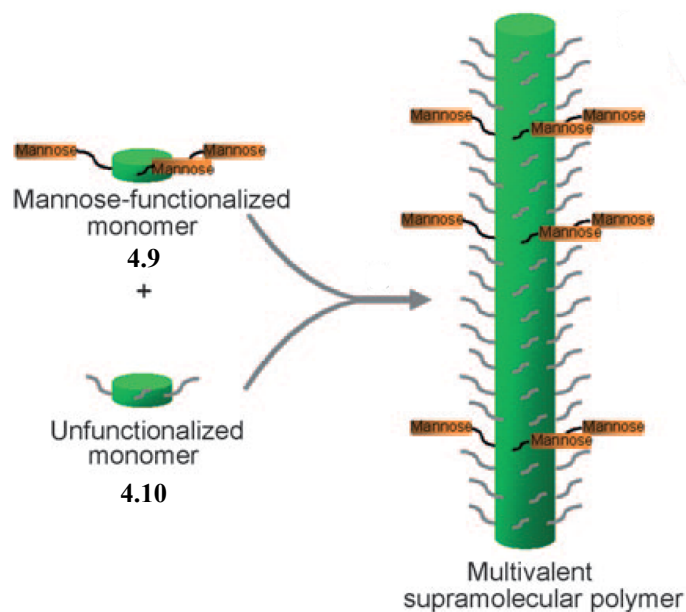
Figure 4.8 Self-assembled columnar glycopolymer from compounds **4.9** and **4.10** in water.[6]

4.3 Analysed molecules

In Scheme **4.6** the structure of all tested compounds are reported. For every N-valent compound, only one sugar is depicted: the others are replaced with a sphere for a matter of simplicity. Red sphere represent ligand **1.9**, blue sphere represent ligand **1.7**. Along the following paragraphs, the reader should refer to this scheme for molecular structures.
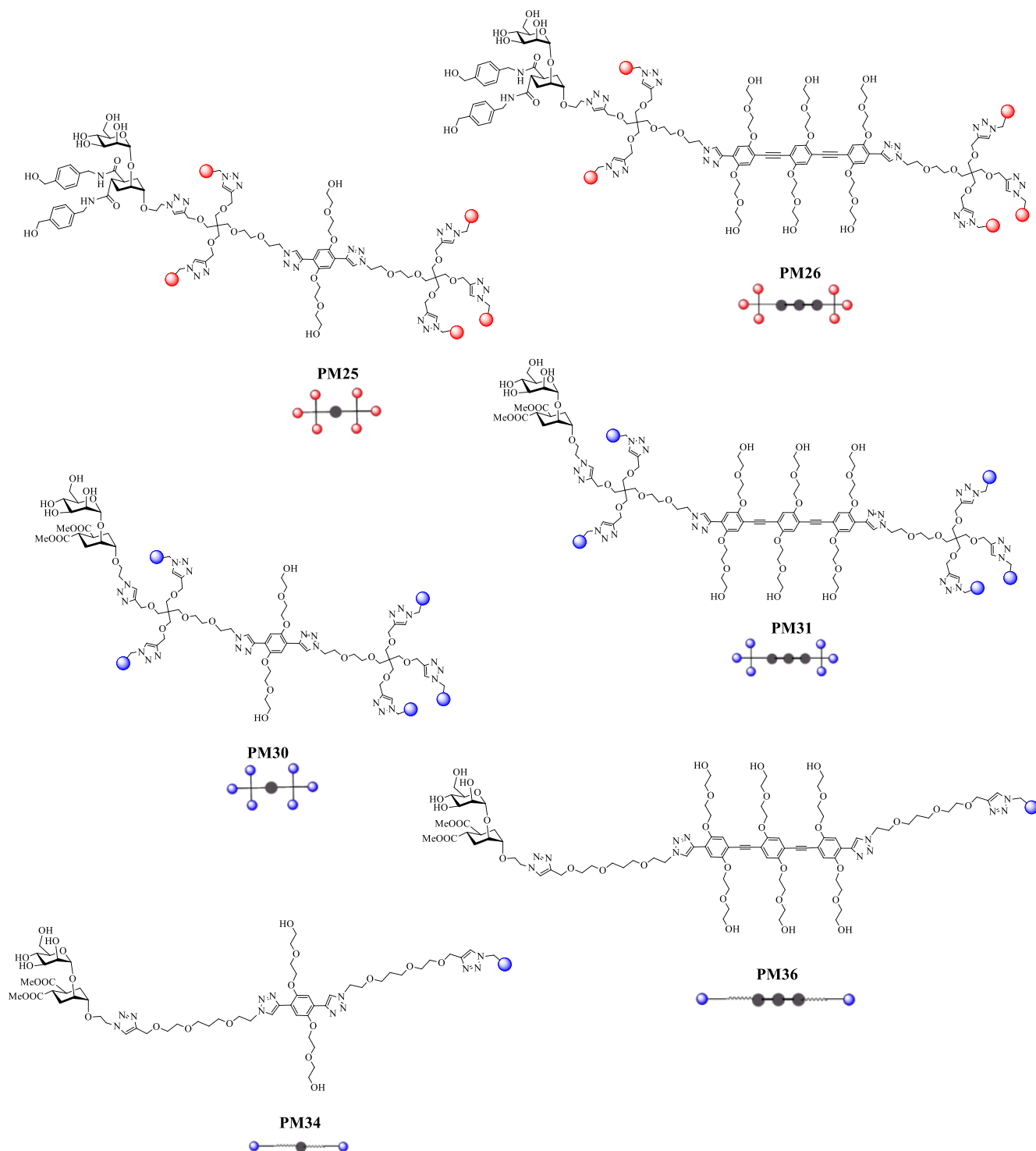
Scheme 4.6 Structures of tested compounds. Blue spheres represent ligand **1.7**, red spheres represent ligand **1.9**

4.4 UV-Visible absorption spectra

UV-Vis spectra of selected compounds in water were recorded as a matter of characterization. Rod1 derivatives (as **PM25**, **PM30** and **PM34**) showed absorption peaks at 331 and 283 nm, whereas Rod3 derivatives (as **PM26**, **PM31** and **PM36**) at 392 and 311 nm. The UV-Vis absorption spectrum of compound **PM34** is shown as an example (Figure **4.9**). Absorption bands are not sharp, but they are in agreement with those obtained from rods alone.[7]
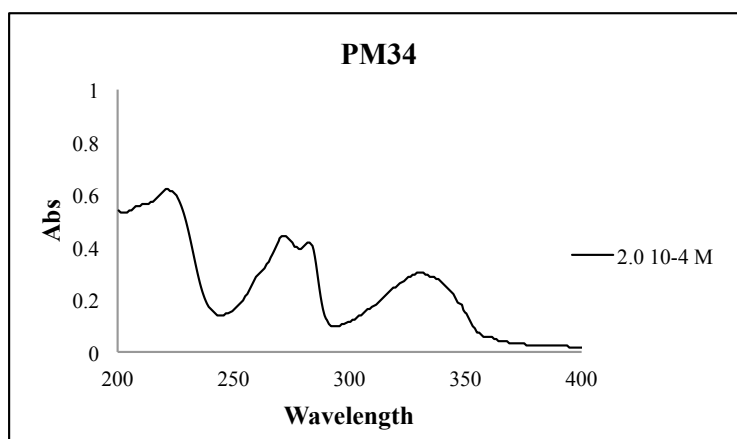
PM34

Figure 9 UV-Vis spectra of **PM34** $2.0 \cdot 10^{-4}$ M in water.

Remarkably, no absorption peak shift was observed by varying sample concentration in the range 10^{-3}-10^{-5} M. In principle, this could have been characteristic of different aggregative process existing at different concentrations.

4.5 Surface Tension determination

Within a liquid, bulk molecules experience a zero-value net force, being attracted at the same level by other molecules in every direction (Figure **4.10B**). On the contrary, molecules located at the surface of a liquid experiment a net inward force (Figure **4.10S**), thus they tend to move inwardly. When molecules leave the surface, this shrinks. Surface tension is the work done by the system in such a reduction of the area.
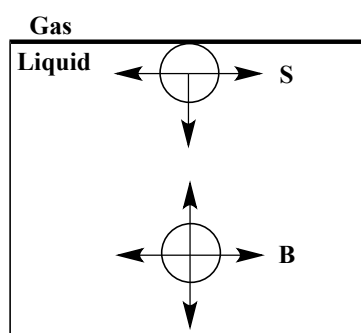
Figure 4.10 Non-equilibrate forces acting of a surface molecule (S) result in its inward movement; a bulk molecule (B) experiments a zero-value net force.

From a thermodynamic point of view, surface tension γ can be defined as in Equation **4.1** and represents the surface excess free energy.[8]

$$\gamma = \left(\frac{\delta G}{\delta A}\right)_{P,T}$$

Equation 4.1 Surface tension γ can be expressed as the increment in Gibbs free energy per unit increment in area.

Surfactants, i.e. materials that bear a hydrophilic head and a hydrophobic tail, are able to reduce the surface tension of water by adsorbing at the interphase liquid-gas. Indeed tails, which are not soluble in water, prevent the surfactants movement towards the bulk, which would result from attractive forces exerted on the hydrophilic heads (Figure **4.11**).
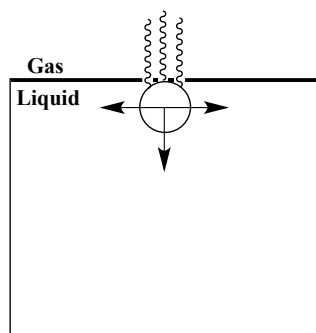
Figure 4.11 A surfactant reduces the surface tension of a liquid by adsorbing at the interphase liquid-gas.

By increasing surfactant concentration, amphiphilic molecules tend to accumulate at the surface of the liquid, thus gradually decrease surface tension. The Critical Micelle Concentration (CMC) is defined as the concentration at which surfactant molecules self-assemble in micelles. Micelles are spherical aggregates where the hydrophilic heads are in contact with the surrounding and the hydrophobic tails are protected in the micelle centre (Figure **4.6**, see Paragraph 4.2). After the CMC, surface tension doesn't decrease anymore because additional surfactant molecules go to micelles.

It is possible to evaluate the critical micelle concentration of a species by measuring surface tension as a function of concentration. The De Noüy method and the pendant drop one are the ones used in this PhD thesis.

With the De Noüy method, the surface tension of a liquid is determined in relation to the force needed for detaching a ring of wire from the surface (Figure **4.12A**). Besides surface tension value γ, this force depends also on the ring weight *W* and its perimeter, which corresponds to the periphery of the surface detached (Equation **4.2**, Figure **4.12B**).

A   Force

B

Ring

Liquid

$$F_{tot} = W_{ring} + 4\pi R\gamma$$

Equation 4.2
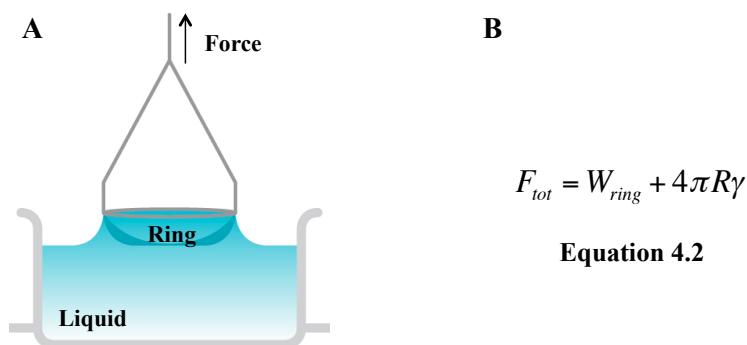
Figure 4.12 A) Ring method; B) The upward force F_{tot} needed to detach the ring from the liquid surface depends on the weight W_{ring} and the perimeter of the ring and on the surface tension γ of the liquid. R is ring's radius.

The pendant drop method relates the surface tension of a liquid to the shape of its drop hanging from a tip. As stated in Equation **4.3** (Figure **4.13**), surface tension γ depends on the drop equatorial diameter d_e, on a factor H also depending on drop's shape and on the difference in density $\Delta\rho$ between the liquid and the gas at the interphase; g is the gravitational constant.

A

Needle tip

ds

de   de

B

$$\gamma = \frac{\Delta\rho g d_e^2}{H}$$

Equation 4.3
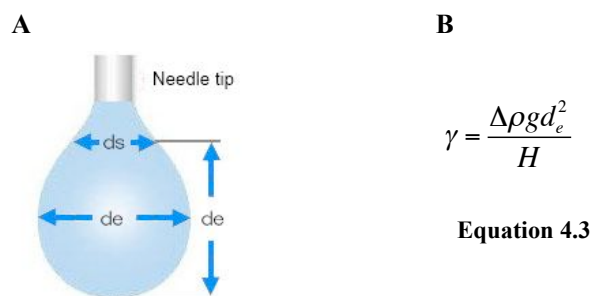
Figure 4.13 A) Pendant drop method; B) The surface tension γ is related on drop's equatorial diameter d_e; H value also depend on drop's shape; $\Delta\rho$ is the difference in density between the liquid and the gas at the interphase; g is the gravitational constant.

4.5.1 Experimental

Surface Tension analyses of selected compounds **PM34**, **PM36**, **PM30**, **PM31** (Scheme **4.6**, see Paragraph 4.2) solubilized in water at different concentrations were performed with the aim to evaluate the nature of the monomers and of possible the aggregates. These experiments were performed in collaboration with Dr. D. Meroni and Prof. S. Ardizzone, with the pendant drop method, which has the benefit of using only small quantities of the sample ($\approx$ 100-200 μL). Using a Krüss EasyDrop instrument equipped with DSA1 software, the shape of the pendent drop was fitted using Equation **4.3** (Figure **4.13**), which relates surface tension to the shape of the drop. A calibrated syringe was used.

One selected sample was analyzed with both the pendant drop and the more common De Noüy methods, obtaining comparable results, thus demonstrating the good accuracy of the pendant drop one ($\gamma_{PendantDrop}$ = 61.7 mN/m; $\gamma_{De\text{-}Nouy}$ = 58.0 mN/m). An analogous result was obtained also with milliQ water ($\gamma_{PendantDrop}$ = 71.8 mN/m; $\gamma_{De\text{-}Nouy}$ = 72.8 mN/m).

4.5.2 Results and discussion

Analogous trends were found for all analysed compounds; as shown in Figure **4.14**, surface tension decreases by increasing sample concentration. Remarkably, the classical behaviour of a surfactant that, after reaching the CMC, shows an almost invariant plateau was not observed. Nevertheless, the decrease of surface tension reflects the behaviour of molecules positively adsorbed at the interphase air-water, which is typical of molecules having two different functionalities. This corroborates the hypothesis that monomers have two explicit hydrophobic and hydrophilic functionalities. Surface tension tendency doesn't unequivocally indicate the presence of aggregates. On the contrary it suggests that, increasing sample concentration, the amount of free monomer that adsorbs at the interphase increases as well. In principle, it could also happen that aggregates are formed and they are able to adsorb at the interphase and participate to the γ decrease; this behavior is not possible for a micelle-like material, but it can't be excluded for more complex aggregates that can display hydrophobic moieties on their surface.
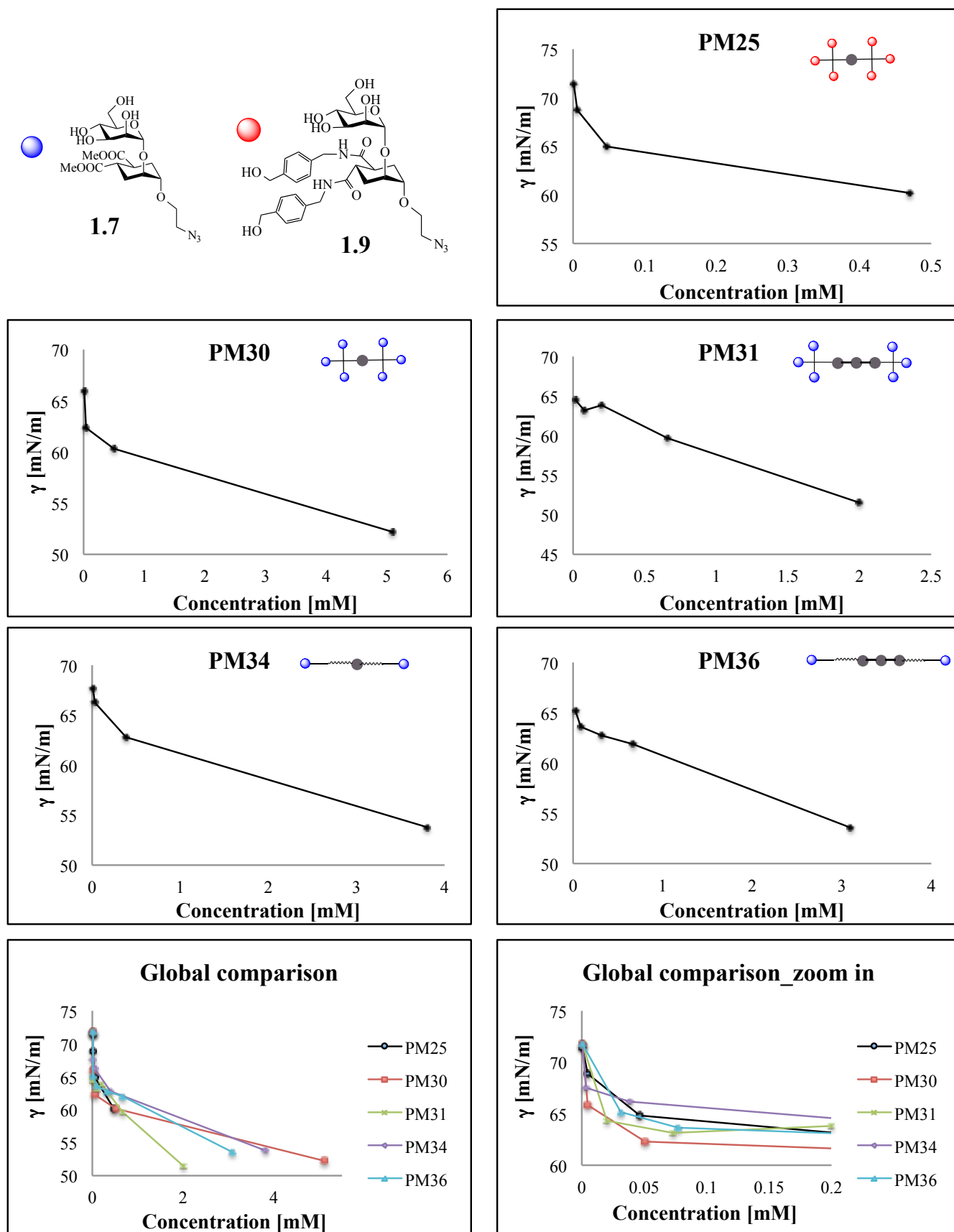
Figure 4.14 Surface tension trends of tested compounds **PM30**, **PM31**, **PM34**, **PM36** and **PM25** in water at concentrations indicated in the legends. Cartoons accompany compounds' name; blue spheres correspond to **1.7**, red spheres to **1.9**.

Comparing the curves displayed by all compounds, it is possible to observe a general more rapid decay at low concentrations; then, surface tension still decreases, but slighter. The comparison between **PM30** and **PM31** or **PM34** and **PM36** shows the relevance of the rod in the surface tension trend: being the valency equal, at mM concentrations, Rod3 derivatives (**PM31** and **PM36**) display lower γ values relative to corresponding Rod1 derivatives (**PM30** and **PM34**). But remarkably, compounds bearing Rod1 are the ones that show a faster γ decrease at low concentrations. If this behaviour is slight for **PM34** and **PM36**, **PM31** starts having lower γ values than **PM30** only at a concentration of ≈ 0.7 mM. Also the influence of the valency was assessed: being rod-length equal, hexavalent compounds (**PM30** and **PM31**) have lower surface tension values than the corresponding divalent ones (**PM34** and **PM36**). Thus, the presence of sugar moieties increases the ability of compounds to adsorb at the interphase. Interestingly, for compounds **PM30** and **PM34**, bearing Rod1, the valency effect is more marked at lower concentrations. All together, these results corroborate also the hypothesis that the less soluble compounds are, the lower is their surface tension (**PM31** less soluble than **PM30**; **PM36** less soluble than **PM34**, **PM31** less soluble than **PM36**, **PM30** less soluble than **PM34**, Table **4.1**, see Paragraph 4.1). The small concentration range in which **PM25** was tested is due to its low solubility in water (Table **4.1**, see Paragraph 4.1). This can explain also a trend that is difficult to compare with other ones.

4.6 Diffusion-Ordered NMR Spectroscopy (DOSY)

In the absence of a net force acting on them, molecular particles self-diffuse in solution (i.e. they randomly translate) as a consequence of their thermal energy; people refer to this motion as the Brownian one. The Stokes-Einstein equation (Equation **4.4**) relates the self-diffusion coefficient (D) to the temperature T, the viscosity of the medium η and the species' hydrodynamic radius R_H (which is the radius of an hypothetical hard sphere that diffuses at the same rate as the species itself).

$$D = \frac{k_b T}{6\pi\eta R_H}$$

Equation 4.4 Stokes-Einstein equation to calculate self-diffusion coefficients D; k_b is the Boltzmann constant.

Diffusion-Ordered NMR Spectroscopy (DOSY) is a technique able to evaluate the diffusion coefficients D of species in solution, and therefore their effective size.[9] By the use of an NMR gradient, molecules can be spatially labelled, i.e. marked depending on their position in the sample

tube. If they move after this encoding during the subsequent diffusion time Δ, their new position can be decoded by a second gradient. The measured signal is the integral over the whole sample volume, and the NMR signal intensity is attenuated depending on the diffusion time Δ and the gradient parameters. A DOSY experiment provides a two-dimensional matrix where chemical shifts are plotted along one axis and diffusion coefficients are plotted along the perpendicular one. The diffusion information is obtained by an inverse Laplace transformation of the signal decay data.

4.6.1 Experimental

In collaboration with Dr. I. Guzzetti and Dr. D. Potenza of the University of Milano, DOSY experiments were performed on compounds **PM34**, **PM36** and **PM31** in water (Scheme **4.6**, see Paragraph 4.3). **1.7** derivatives were chosen because of their higher solubility in water, that allows achieving millimolar concentrations suitable for NMR experiments. A range of concentrations from 4 mM to about 1 mM was tested. NMR spectra were recorded on a Bruker AVANCE 400 MHz instrument, in D_2O at 298 K. Diffusion coefficients were calculated with the module T1/T2 relaxation of the software Topspin, using the diffusion coefficient of D_2O (= 10^{-8} m^2/s) as internal standard. For each species and each concentration, reported *D* values are an average of diffusion coefficients obtained for four different protonic regions. The Stockes-Einstein equation (Equation **4.4**) allowed the calculation of hydrodynamic radii.

4.6.2 Results and discussion

Representative DOSY NMR 2D spectra are reported in Figure **4.15**, whereas diffusion coefficients *D* and corresponding hydrodynamic radii are listed in Table **4.2**.
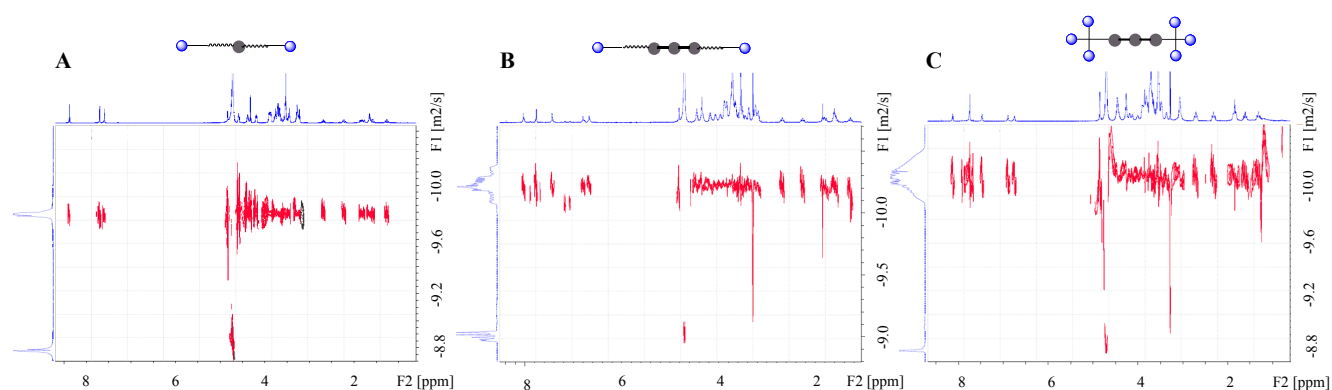
Figure 4.15 DOSY NMR spectra of compounds (D_2O, 298 K); diffusion coefficients are plotted along the vertical axis. A) **PM34** 3.9 mM; B) **PM36** 3.7 mM; C) **PM31** 4.0 mM. In the cartoons of tested molecules, blue spheres represent **1.7**.

A

PM34		
Concentration (mM)	**D (m²/s)**	**R_H (nm)**
3.89	1.66E-10	1.05
2.02	1.74E-10	1.00
1.33	//// too diluted	

B

PM36		
Concentration (mM)	**D (m²/s)**	**R_H (nm)**
4.00	1.09E-10	1.60
2.57	1.05E-10	1.66
1.89	1.1E-10	1.59
1.50	1.16E-10	1.51
1.24	1.15E-10	1.52
1.06	1.17E-10	1.49
0.5	1.25E-10	1.40

C

PM31		
Concentration (mM)	**D (m²/s)**	**R_H (nm)**
3.70	8.84E-11	1.98
2.45	8.92E-11	1.96
1.84	8.70E-11	2.01
1.47	9.58E-11	1.82
1.23	9.56E-11	1.83
1.02	/// too diluted	

Table 4.2 Concentrations of tested compounds, together with determined *D* and *R_H* values; A) **PM34**, B) **PM36**, C) **PM31**.

Obtained *D* and *R_H* values can be associated with the dimension of monomeric species, as predicted by Molecular Dynamics simulations described in Chapter 2.5. Maxima and averaged gyration radii calculated for the three compounds are listed in Table **4.3**. The gyration radius *Gyradius*, defined as the mass weighted average distance from the core of a molecule to each mass element in the molecule, can be compared with the hydrodynamic one in a first approximation. MD simulations were run for 25 ns in implicit solvent.

Compound	**Rod length (nm)**	**Max Gyradius (nm)**	**<Gyradius> (nm)**
PM34	0.8	1.81	0.78
PM36	2.2	2.32	0.97
PM31	2.2	2.20	1.09

Table 4.3 Maxima and averaged gyration radii of **PM34**, **PM36** and **PM31**. MD simulations were run for 25 ns in implicit solvent.

Being concentrations equal (3.85 ± 0.15 mM, Table **4.2**), the smallest compound **PM34** displayed the lowest R_H value. By increasing the length of the rod from 1 to 3 units, as in **PM36**, R_H value increased. This derives of course from bigger dimensions of **PM36** relative to **PM34**. In **PM31**, the presence of trivalent dendrons at the two ends of the longest rod resulted in a further increase of the averaged hydrodynamic radius. It is apparent that the size of R_H varies mostly with the length of the rod (50 % increase from **PM34** to **PM36**) and less with the valency of the molecule (25 % increase from **PM36** to **PM31**). This is also consistent with the results from MS simulations (Table **4.3**), which suggests how these molecules fold over. In the range of concentrations studied, little or no variation of R_H was observed.

The trend of the R_H values was reflected also in the shape of diffusion coefficients D. Indeed, the peak representing the diffusion coefficient of **PM34** was sharp (Figure **4.15A**), whilst it become broader by shifting to **PM36** and **PM31**. Less compact peaks associated to **PM36** and **PM31** could also indicate the presence of several subpopulations in dynamic equilibrium.

4.7 Transmission Electron Microscopy Imaging

Transmission Electron Microscopy is able to image soft matter that is hit by a focused beam of accelerated electrons. Since the sample has a thickness < 200 nm, it doesn't absorb electrons, whereas it transmits or scatters them. The number of transmitted electrons depends on the solid materials that they encounter; they finally hit a fluorescent screen that gives a brighter or darker image back. When electrons are transmitted, the image is bright, whereas in the regions where electrons have been diffracted by the sample, the image is dark. There is also a range of greys in between depending on how electrons have interacted with and scattered by the sample. From this, it is possible to obtain information with regard to the sample morphology.

In a conventional TEM instrument, sample is dried over a grid, while, performing a Cryo-TEM analysis, sample molecules are frozen in thin ice.

High-resolution transmission electron microscopy (HR-TEM) uses not only the transmitted, but also the scattered beams to create images; in that way, resolution can be improved.

Generally, being the resolution of a microscope defined as the distance between two details just separable from one another and directly proportional to the wavelength of the incident beam, the use of accelerated electron allows for a higher resolution relative to using photons. TEM resolution can be lower that 1 nm.

4.7.1 Experimental

Conventional TEM images were collected using a Zeiss LEO 912ab Energy Filtering TEM operating at an acceleration voltage of 120 kV, equipped with a CCD-BM/1K system. The sample preparation was carried out according to the following procedure. Aliquots of 5 µL of the *PM* solution were deposited onto Formvar-coated 300 mesh copper grids. The excess of water was then gently blotted using filter paper. When solvent evaporated at room temperature under atmospheric pressure for 24 h, the grids were negatively stained by 1.5 wt % phosphertungstic acid. The aggregates diameters were measured by the EsiVision software (Olympus,Germany).

CryoTEM imaging was executed at -178 °C using a Zeiss LIBRA 200FE-HR TEM, operating at 200 kV. Images were processed by means of the iTEM TEM Imaging Platform software (Olympus). The mean diameter and size distribution of the observed aggregates were obtained from a statistical analysis of over 270 aggregates.

4.7.2 Results and discussion

TEM images of compounds **PM31** and **PM26** were acquired. Images obtained with HR-TEM are displayed in Figure **4.16**. Compound **PM31** at a millimolar concentration resulted in a solid layer that couldn't be analysed (Figure **4.16A**). On the contrary, lower concentrations of both **PM31** (Figure **4.16A-C**) and **PM26** (Figure **4.16D-F**) revealed the presence of big aggregates, characterized by radii of hundreds of nanometres, together with a plethora of other smaller materials. In Figure **4.16**, big aggregates are circled in red, whereas smaller observable objects are circled in green. Stained samples (i.e. Figure **4.16C** and **4.16F**) allowed for better evaluation of the shape of aggregates, which displayed less dense and softer cores. In principle, they could be vesicles or doughnut-like materials.

A   B   C

D   E   F
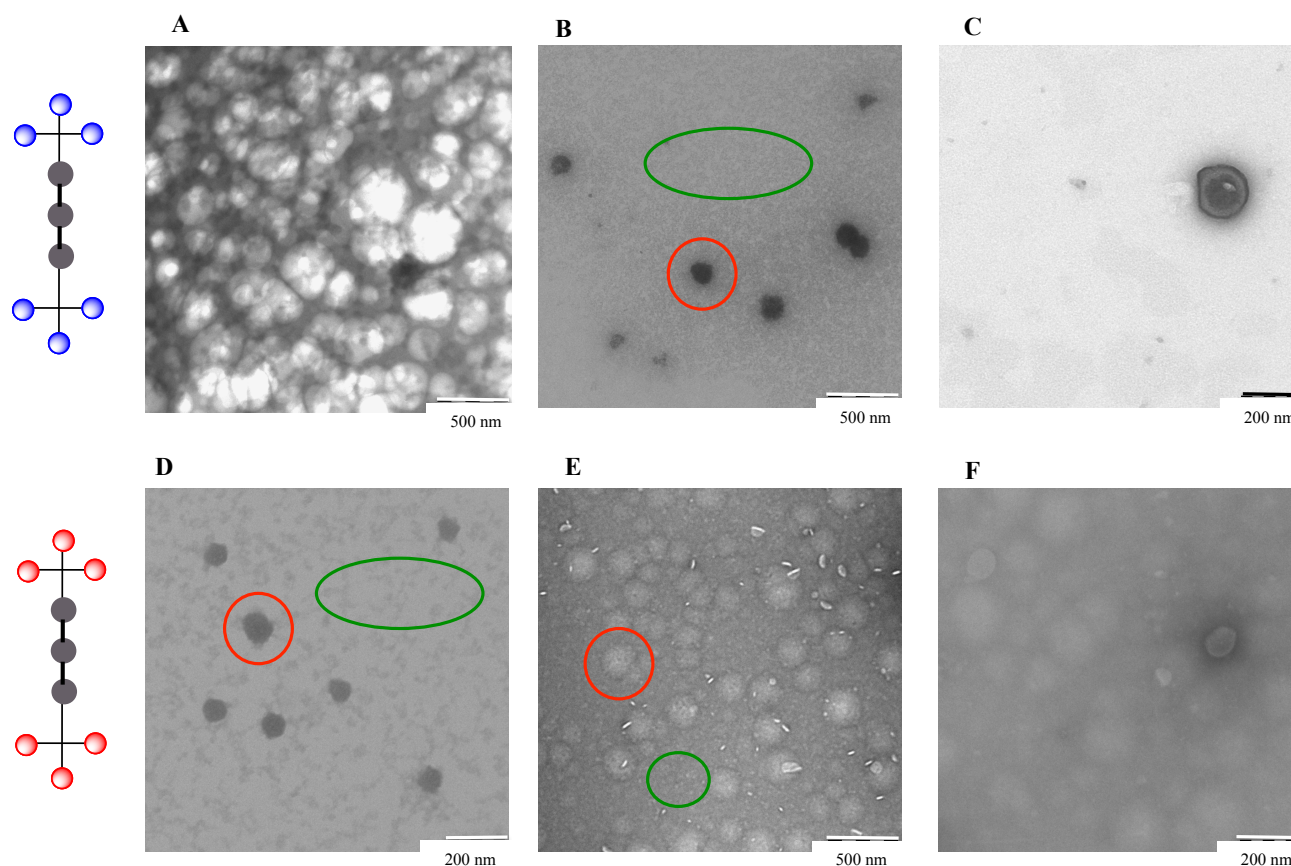
Figure 4.16 TEM images of A) **PM31** 2.2 mM; B) **PM31** 0.22 mM; C) **PM31** 0.22 mM stained;
D) **PM26** mM 0.11 mM; E) **PM26** 0.11 mM stained; F) **PM26** 0.011 mM stained.
Big aggregates are circled in red, small meterials are circled in greed. In the cartoons of tested molecules, blue spheres
represent monovalent ligand **1.7** and red spheres represent monovalent ligand **1.9**.

In order to assess if the drying step of sample preparation for the HR-TEM analyses induced the formation of aggregates, cryo-TEM images were also acquired on selected **PM26** (0.11 mM, Figure **4.17**). Again, hundreds-nanometre-sized aggregates were detected and still smaller objects can be observed in the background. Also this assays suggests that aggregates have a vesicle or doughnut-like shape (Figure **4.17**). In Table **4.4**, the diameter distribution calculated over 271 observed species is reported.
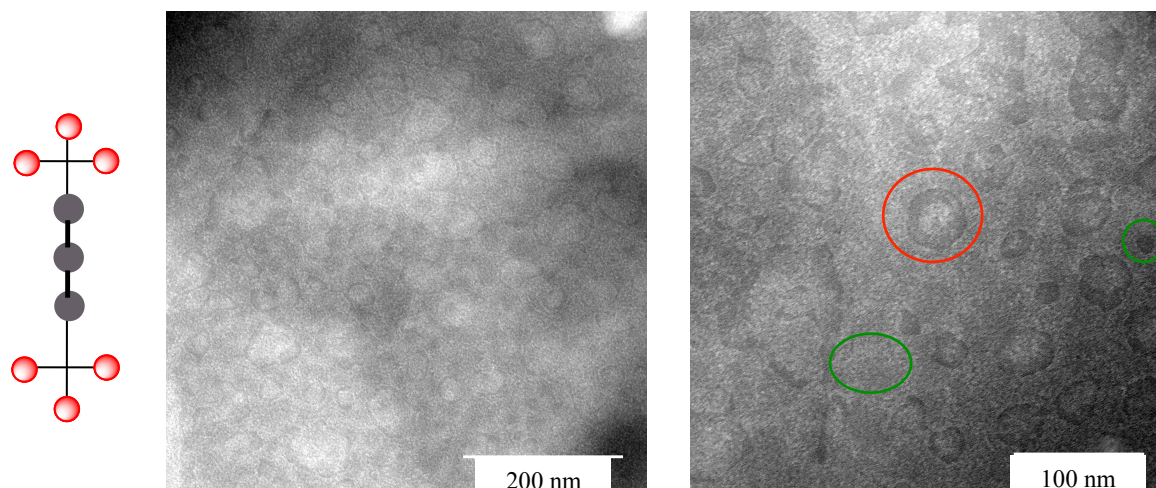
Figure 4.17 Cryo-TEM images of **PM26** 0.11 mM. Big aggregates are circled in red, small meterials are circled in green. In the cartoons of the tested molecule, red spheres represent **1.9**.

Mean	30 nm
Median	22 nm
Standard deviation	25 nm
Minimum	8 nm
Maximum	164 nm
Mode	15 nm

Table 4.4 Diameter distributions calculated over 271 aggregates, from Cryo-TEM images of **PM26** 0.11 mM.

Remarkably, the presence of aggregates was detected at a concentration in which the presence of micelles was excluded by surface tension determination analyses (see Paragraph 4.5).

4.8 Sedimentation Velocity Analytical Ultracentrifugation Analysis

Sedimentation velocity (SV-AUC) is an analytical ultracentrifugation method that measures at which rate molecules move in response to a high centrifugal force generated in a centrifuge. In a classical SV-AUC experiment, an initially uniform solution is placed in a cell; when the cell rotates, the solute sediments towards the bottom of the cell. By measuring the sample absorbance as a function of radial position and at different times, it is possible to evaluate how it changes within the cell. A sharp boundary between the depleted region (top) and the region that contains molecules is formed and, during time, it moves away from the meniscus (Figure **4.18**). For molecules obeying to the Lambert-Beer Law, concentrations at given times can be evaluated measuring absorbance. Normally, the absorbance of every sample is corrected by the absorbance of the solvent alone, which is placed as reference in a second sector of the cell. The rate of movement of the boundary,

which is referred to as sedimentation rate, can be measured and it provides values of the sedimentation coefficients of the species in solution. Sedimentation coefficient (*s*) can be expressed as in Equation **4.5**; it depends on the molar mass of the solute *M,* its partial specific volume $\bar{v}$ and its frictional coefficient *f,* which is linked to the shape and size of the particle.

$$s = \frac{M(1 - \bar{v}\rho)}{Nf}$$

Equation 4.5 Sedimentation coefficient *s*. The buoyant effective molar mass $M(1 - \bar{v}\rho)$ of a particle corrects the effects of buoyancy, i.e. the upward force exerted by the fluid that is displaced by the particle itself. $\bar{v}$ is the partial specific volume of the solute, i.e. the volume that each of its grams occupies in solution. ρ is the density of the solvent. *f* is proportional to the resistance exerted by the fluid to the solute motion, calculated according to Equation **4.6**. *N* is the Avogadro's number.

$$f = 6\pi\eta R_{\mathrm{H}}$$

Equation 4.6 Frictional coefficient *f*. It is related to solvent viscosity η and the particle hydrodynamic radius R_{H}. R_{H} can be expressed as a function of the radius of the anhydrous volume, R_{min}, which can be derived from *M* and $\bar{v}$. The frictional ratio $f/f_{\mathrm{min}} = R_{\mathrm{H}}/R_{\mathrm{min}}$, and it is related to the particle anisotropy and hydration.

Therefore, SV-AUC can provide information about both the molecular mass and the shape of particles.[10]
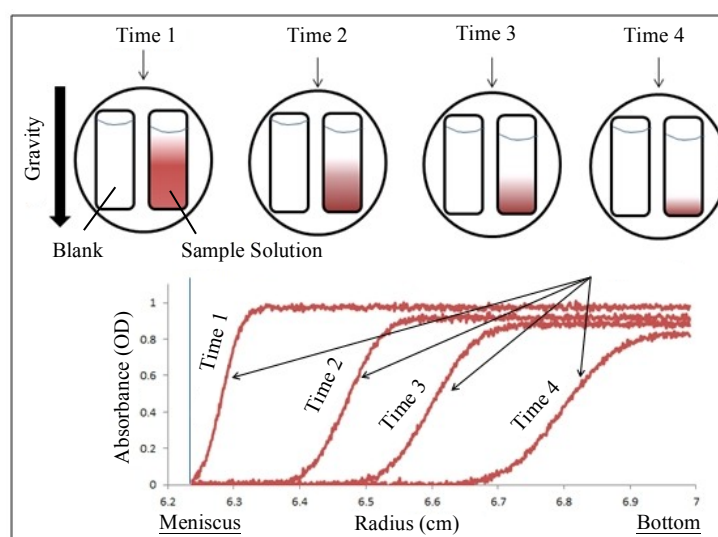

Figure 4.18 Principle of SV-AUC measurement.[11]

4.8.1 Experimental

In collaboration with V. Porkolab, A. Le Roy, Prof. F. Fieschi and Prof. C. Ebel, I performed SV-AUC analyses on selected glycodendrimer solutions at the Institut de Biologie Structurale of

Grenoble (FR). Compounds **PM25**, **PM26**, **PM30** and **PM31** (Scheme **4.6**, see Paragraph 4.2) were chosen to evaluate the effect of both the rod length and the sugar moiety on the eventual formation of aggregates. All compounds were solubilised in the same buffer used for the SPR inhibition studies (see Chapter 2.6.1), which consists of 25 mM Tris-HCl (pH 8), 150 mM NaCl, 4 mM CaCl$_2$, 0.005 % P20 ± 4 % DMSO. It should be noted that P20 is a surfactant, used in the SPR experiment to reduce non-specific interactions between the analytes and the surface; therefore, in principle, it could decrease also the non-specific aggregating interactions among glycodendrimers. In order to evaluate the role of the solvent, the behaviour of **PM25** and **PM30** was investigated also in water. Several concentrations were tested, trying to approach also compounds' solubility limits (see Paragraph 4.1). All tested samples are listed in Table **4.5**.

Sedimentation velocity experiments were performed in a Beckman XL-1 analytical ultracentrifuge using an AN-50 Ti rotor (Beckman instruments), at 20 °C. The experiments were carried out at 42000 rpm, using 50 µL, 100 µL or 430 µL samples in, respectively, two-channels 0.15 cm, 0.3 cm or 1.2 cm path length centerpieces equipped with sapphire windows (**Nanolytics GmbH**).

The absorption was monitored at several wavelengths, depending on the absorption behaviour and concentration of solutions, as indicated in Table **4.5**, with, typically, radial steps of 0.003 cm and time between profiles on a given sample of 20 min.

Compound	Solvent	Conc [mM]	λ monitored [nm]	Optical Path Length [mm]
PM25	Buffer	0.5	295	12
PM25	Buffer	0.1	295	12
PM25	H$_2$O	0.15	295	12
PM26	Buffer	0.15	391	1.5
PM26	Buffer	0.05	391	3
PM26	Buffer	0.015	391	12
PM30	Buffer	3.5	295	1.5
PM30	Buffer	1.0	295	1.5
PM30	H$_2$O	3.5	295	1.5
PM30	H$_2$O	1.0	295	1.5
PM31	Buffer	1.0	280	1.5
PM31	Buffer	0.5	280	1.5
PM31	Buffer	0.01	391	12

Table 4.5 Experimental conditions of tested compounds in SV-AUC assays.

Buffer = 25 mM Tris-HCl (pH 8), 150 mM NaCl, 4 mM CaCl$_2$, 0.005 % P20 ± 4 % DMSO.

The distribution of sedimentesion coefficients, *c(s),* were obtained from sedimentation velocity profiles, fitting with the SEDFIT software[12] the following parameters: meniscus, bottom and frictional ratio *f/f$_{min}$*. The partial specific volume ($\bar{v}$) of tested glycodendrimers was considered to be 0.7 cm^{3}g^{-1}, as a mean between values for hexose sugars and glycerol (about 0.6 and 0.77 cm^{3}g^{-1}).[13] Using SEDNTERP software, the viscosity and the density of the buffers were estimated to be, respectively, 0.01023 poise and 1.005 gcm^{-3}. Water viscosity (0.01002 poise) and density (0.998 gcm^{-3}) are tabulated. For a regularization procedure, a confidence level of 0.68 was used. In Figure **4.19A**, sedimentation velocity profiles of an illustrative sample are reported; in Figure **4.19B**, the table of fixed and fitted parameters to obtain the *c(s)* values are reported. The *c(s)* curve in Figure **4.19C** represents the distribution of sedimentation coefficients, *s*, expressed in Svedberg (S) units; the area under each peak is directly related to the absorption, and, therefore, quantifies the sedimenting species.
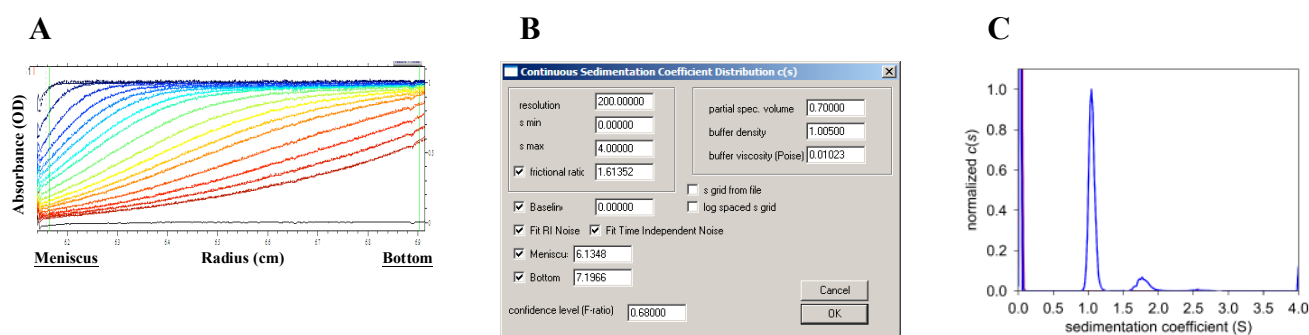
Figure 4.19 A) sedimentation velocity profiles; B) fixed and fitted parameters by Sedfit software; C) sedimentation coefficients distribution.

4.8.2 Results and discussion

Obtained sedimentation coefficients were compared with theoretical values expected if the molecules moved as globular compact particles in solution (therefore, having a frictional ratio *f/f$_{min}$* of 1.25), having *R$_H$* predicted values as reported in Table **4.6**.

Compound	Predicted R_H values (nm)			
	Monomer	Dimer	Trimer	Tetramer
PM30	1.28	1.61	1.84	2.03
PM31	1.34	1.69	1.94	2.13
PM25	1.40	1.77	2.02	2.23
PM26	1.46	1.84	2.10	2.31

Table 4.6 Predicted R_H values of compounds **PM30**, **PM31**, **PM25** and **PM26** both in water and in buffer. Values were calculated using f/f_{min} = 1.25 and $\bar{v}$ = 0.7 cm^{3}g^{-1}.

Buffer = 25 mM Tris-HCl (pH 8), 150 mM NaCl, 4 mM CaCl$_2$, 0.005 % P20 ± 4 % DMSO.

For all of the tested compounds in both buffer and water, prevalent species had sedimentation coefficients (*s*) very close to that of the corresponding monomers, revealing that they are mainly in the monomeric state (Figure **4.20.1**, **4.20.2**, **4.20.3**, **4.20.4**,). In a few cases, also sedimentation coefficients corresponding to dimeric, trimeric or tetrameric species were observed, but their amounts were always less than the 10 % on the total moles.

PM30
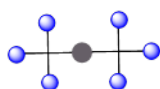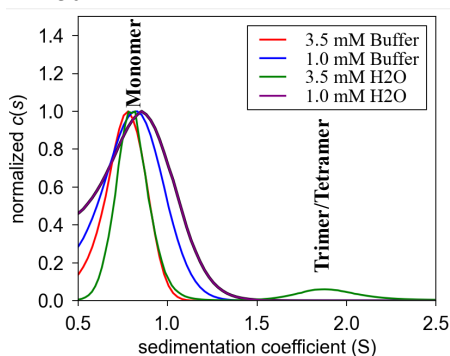
PM30	Slow Boundary		Fast Boundary		
Conc. [mM]	s_{exp}	s_{theo},mono[a]	s_{exp}	s_{theo},trimer[b]	s_{theo},tetramer[c]
3.5 in Buffer	0.75 (100 %)	0.77	///	1.60	1.94
1.0 in Buffer	0.78 (100 %)	0.77	///	1.60	1.94
3.5 in H$_2$O	0.81 (82 %)	0.80	1.91 (10 %)	1.66	2.01
1.0 in H$_2$O	0.81 (100 %)	0.80	///	1.66	2.01

Figure 4.20.1: *c(s)* distributions in sedimentation profiles of **PM30** solutions rotating at 42000 rpm at 298 K. In the table, experimental sedimentation coefficients, s_{exp}, are compared to expected theoretical ones, s_{theo}, for globular particles.

[a]Expected for a globular particle of R_H = 1.28 nm; [b]Expected for a globular particle of R_H = 1.84 nm; [c]Expected for a globular particle of R_H = 2.03 nm. Buffer = 25 mM Tris-HCl (pH 8), 150 mM NaCl, 4 mM CaCl$_2$, 0.005 % P20. In the cartoon of tested molecule, blue spheres represent **1.7**.
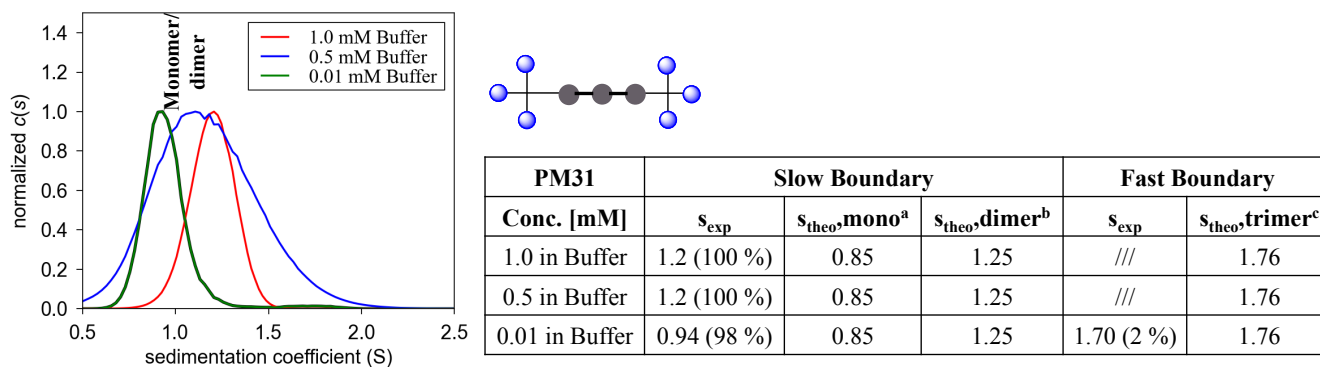
Figure 4.20.2: *c(s)* distributions in sedimentation profiles of **PM31** solutions rotating at 42000 rpm at 298 K. In the table, experimental sedimentation coefficients, s_{exp}, are compared to expected theoretical ones, s_{theo}, for globular particles. [a]Expected for a globular particle of R_H = 1.34 nm; [b]Expected for a globular particle of R_H = 1.94 nm. [c]Expected for a globula particle of R_H = 2.13 nm. Buffer = 25 mM Tris-HCl (pH 8), 150 mM NaCl, 4 mM CaCl$_2$, 0.005 % P20. In the cartoon of tested molecule, blue spheres represent **1.7**.

PM25

PM25	Slow Boundary		Fast Boundary		
Conc. [mM]	s_{exp}	s_{theo},**mono**[a]	s_{exp}	s_{theo},**dimer**[b]	s_{theo},**trimer**[c]
0.5 in Buffer	0.81 (96 %)	0.93	1.66 (4 %)	1.47	1.93
0.1 in Buffer	0.74 (100 %)	0.93	///	1.47	1.93
0.08 in H$_2$O	0.95 (100 %)	0.96	///	1.53	2.00

Figure 20.3: *c(s)* distributions in sedimentation profiles of **PM25** solutions rotating at 42000 rpm at 298 K. In the table, experimental sedimentation coefficients, s_{exp}, are compared to expected theoretical ones, s_{theo}, for globular particles. [a]Expected for a globular particle of R_H = 1.40 nm; [b]Expected for a globular particle of R_H = 1.77 nm; [c]Expected for a globular particle of R_H = 2.02 nm. Buffer = 25 mM Tris-HCl (pH 8), 150 mM NaCl, 4 mM CaCl$_2$, 0.005 % P20 + 4 % DMSO.

In the cartoon of tested molecule, red spheres represent **1.9**.

PM26

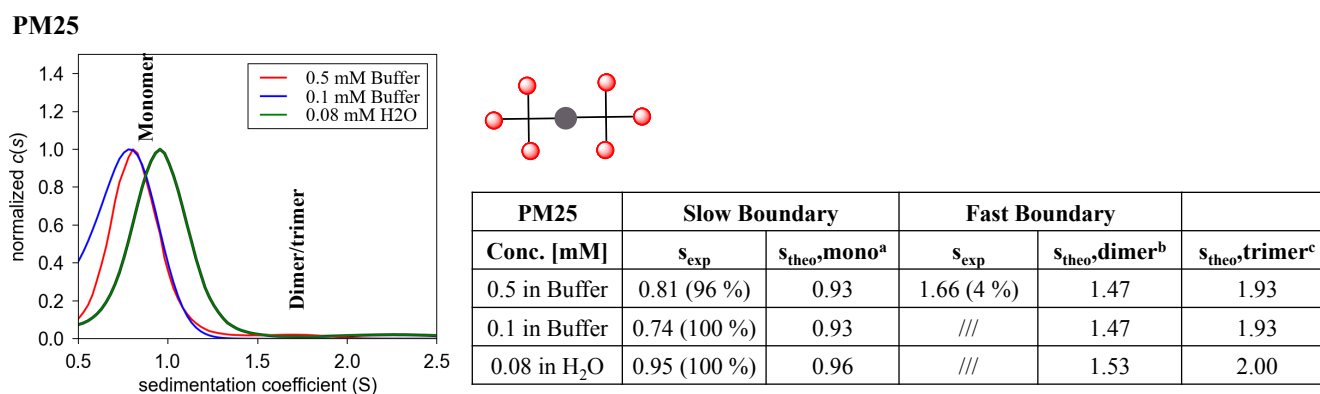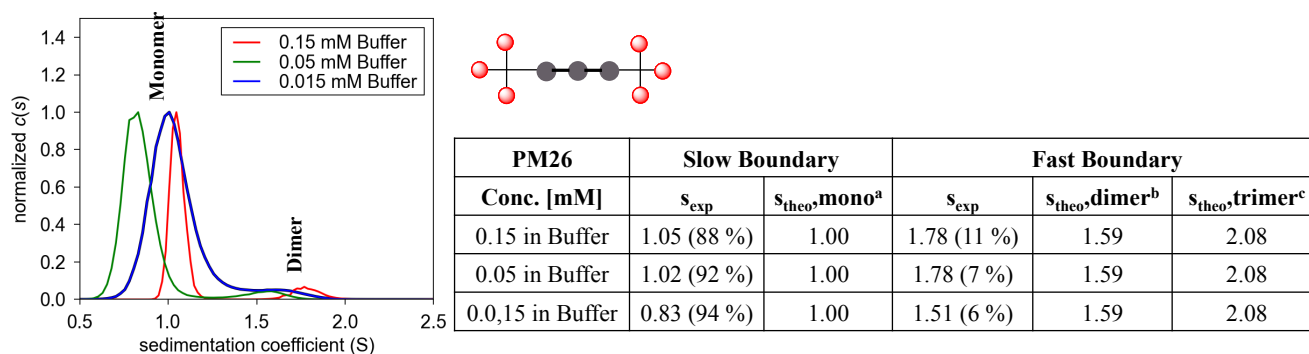| PM26	Slow Boundary		Fast Boundary		
Conc. [mM]	s_{exp}	s_{theo},mono[a]	s_{exp}	s_{theo},dimer[b]	s_{theo},trimer[c]
0.15 in Buffer	1.05 (88 %)	1.00	1.78 (11 %)	1.59	2.08
0.05 in Buffer	1.02 (92 %)	1.00	1.78 (7 %)	1.59	2.08
0.0,15 in Buffer	0.83 (94 %)	1.00	1.51 (6 %)	1.59	2.08

Figure 20.4: *c(s)* distributions in sedimentation profiles of **PM26** solutions rotating at 42000 rpm at 298 K. In the table, experimental sedimentation coefficients, s_{exp}, are compared to expected theoretical ones, s_{theo}, for globular particles. [a]Expected for a globular particle of R_H = 1.46 nm; [b]Expected for a globular particle of R_H = 1.84 nm; [c]Expected for a globular particle of R_H = 2.10 nm. Buffer = 25 mM Tris-HCl (pH 8), 150 mM NaCl, 4 mM $CaCl_2$, 0.005 % P20 + 4 % DMSO. In the cartoon of tested molecule, red spheres represent **1.9**.

These results highlight that **PM26** is the species more prone to form dimers, which exist in increasing amount (6 % - 11 %) at all tested concentrations (15 μM to 150 μM). This is in agreement with the fact that **PM26** is the compound less soluble in aqueous solutions.

In Table **4.7**, frictional ratios *f/f$_{min}$* obtained after the fitting process are listed; practically no differences were obtained by varying the solvent. It is possible to observe that **1.7** derivatives, with an averaged *f/fmin*=1.31 for **PM30** and 1.32 for **PM31**, behave similarly to globular compact particles in solution. On the contrary, **1.9** derivatives **PM25** (averaged *f/f$_{min}$* =1.54) and **PM26** (averaged *f/f$_{min}$*=1.60) have less compact shapes. However, the interpretation of these results is limited because they depend on the input on the partial specific volume of the compounds, for which we've considered only a default constant value.

Compound	Solvent	Conc [mM]	Fitted f/f_{min}
PM25	Buffer	0.5	1.55
PM25	Buffer	0.1	1.50
PM25	H_2O	0.15	1.57
PM26	Buffer	0.15	1.61
PM26	Buffer	0.05	1.60
PM26	Buffer	0.015	1.58
PM30	Buffer	3.5	1.36
PM30	Buffer	1.0	1.25
PM30	H_2O	3.5	1.33
PM30	H_2O	1.0	1.33
PM31	Buffer	1.0	1.42
PM31	Buffer	0.5	1.31
PM31	Buffer	0.01	1.23

Table 4.7 Frictional ratios obtained by fitting sedimentation velocity profiles; partial specific volume ($\bar{v}$) was fixed at 0.7 cm^{3}g^{-1}. Buffer = 25 mM Tris-HCl (pH 8), 150 mM NaCl, 4 mM CaCl$_2$, 0.005 % P20 ± 4 % DMSO.

Interestingly, except in one case, a loss of absorption was observed when the ultracentrifuge was speeded up from 3000 to 42000 rpm, as shown in Table **4.8**. This suggests that a portion of samples exists as large aggregates that are pelleted at high rotational speed. If this assumption is true, it is possible to say that, when large aggregates exist in solution, they can be removed by centrifugation. Remarkably, Rod1 derivatives (**PM25** and **PM30**, Table **4.8**) displayed a higher loss of absorption compared to Rod3 derivatives (**PM26** and **PM31**, Table **4.8**). Being the Rod equal, **1.9**-derivatives seemed to have a higher amount of aggregates that precipitate (compare **PM25** and **PM26** with **PM30** and **PM31**, Table **4.8**); this can be related to their lower solubility in aqueous solutions. Solvent (water or buffer) didn't seem to affect material precipitation.
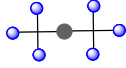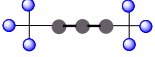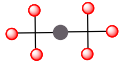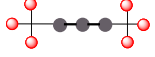
Absorption Variation (%)				
PM30	3.5 mM Buffer (λ = 295 nm)	1.0 mM Buffer (λ = 295 nm)	3.5 mM H$_2$O (λ = 295nm)	1.0 mM H$_2$O (λ = 295 nm)
	- 17%	- 23%	+ 8%	- 22%
PM31	1.0 mM Buffer (λ = 280 nm)	0.5 mM Buffer (λ = 280 nm)		
	- 14%	- 5%		
PM25	0.5 mM Buffer (λ = 295 nm)	0.1 mM Buffer (λ = 295 nm)	0.08 mM H$_2$O (λ = 295 nm)	
	- 32%	- 24%	- 24%	
PM26	0.15 mM Buffer (λ = 391 nm)	0.05 mM Buffer (λ = 391 nm)	0.015 mM Buffer (λ = 391 nm)	
	- 17%	- 19%	- 11%	

Table 4.8 Absorption variation (%) of tested samples speeding the rotor up from 3000 to 42000 rpm. If variation is positive (+), absorption increases; if variation is negative (-), absorption decreases. In the cartoons of tested molecules, blue spheres represent **1.7** and red spheres represent **1.9**. Buffer = 25 mM Tris-HCl (pH 8), 150 mM NaCl, 4 mM CaCl$_2$, 0.005 % P20 ± 4 % DMSO.

4.9 Dynamic Light Scattering Analysis

The electric field associated to a beam of light that hits matter induces a polarization of electrons in the molecules. Molecules become therefore a new source of light and they scatter light, i.e. they re-emit light in all directions. When molecules are experiencing a Brownian motion, the intensity *I* of the light scattered by an ensemble of particles varies in time, in a way related to their size.

A Dynamic Light Scattering (DLS) device irradiates the sample with a laser beam and, through a detector and digital correlator, measures the intensity fluctuations of the scattered light during the time. The correlation function *G(τ)* of the signal *I(t)*, which is expressed as in Equation **4.7**, allows for the determination of diffusion coefficients *D* of particles in solution (Figure **4.21**).[14]

$$G(\tau) = < I(t) \cdot I(t + \tau) >$$

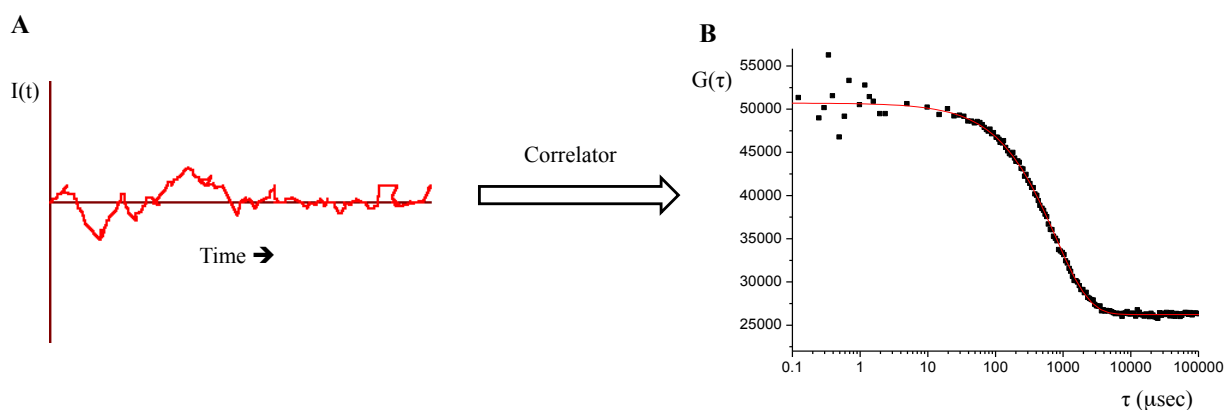**Equation 4.7** Correlation function of the signal *I(t)*.

A

B

Figure 4.21 A) In a Dynamic Light Scattering assay, a digital correlator measures the variation of the intensity *I* of the scattered light in time; B) intensity variations are evaluated through the correlation function *G(τ)*.

Indeed, for a system of identical particles, *G(τ)* takes the simple form of a single exponential relaxation: $G(\tau) \approx \exp(-\tau/\tau_c)$ with $\tau_c = 1/(2Dq^2)$, where q is the scattering vector, dependent on light wavelength and on the angle at which scattered light is collected; in practice, it corresponds to the inverse of the lengthscale at which particle rearrangement takes place producing dephasing of light and intensity fluctuations. It is possible to take polydispersity of the sample into account with slight modifications of the reported functional form (see below Equation **4.8**).

With the previously seen Stokes-Einstein equation (Equation **4.4**, see Paragraph 4.6) it is thus possible to calculate the hydrodynamic radius of the scattering species.

It should be noted that the intensity of the scattered light is proportional to the 6th power of R_H. This makes DLS highly sensitive to detect minor amounts of aggregates and less sensitve to monomeric species.

Preliminary DLS assays had been conducted at the Institut de Biologie Structurale (Grenoble, with Prof. C. Ebel) using a Dynapro Nanostar (Wyatt technology, Santa Barbara, CA, USA). Both monomers and aggregates had been detected (Figure **4.22**). Because of the much higher intensity scattered by aggregates, they dominate the intensity distribution. However, it was possible to extract the corresponding mass distribution, which is dominated by monomers. Results are not very accurate, since we considered approximate inputs (Rg model = sphere and dn/dc = 0.15, i.e. differential index of refraction associated to carbohydrates). Nevertheless, aggregates clearly appeared to represent only a small percentage of the molecules in solution. In the following sections we focus on their characterization.

PM26 0.15 mM in Buffer
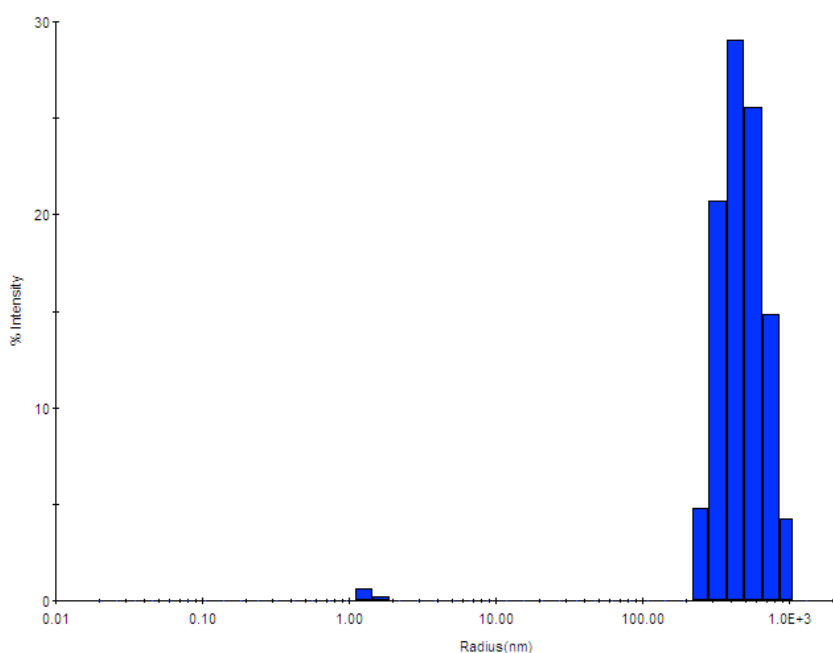
Density Distribution	Radius (nm)	% Intensity	% Mass
Peak 1	1.351	0.9	95.2
Peak 2	510.905	99.1	4.8

Figure 4.22 Size distributions extracted from DLS experiment for **PM26** on a Dynapro Nanostar. Tested concentration was 0.15 mM in buffer (25 mM Tris-HCl (pH 8), 150 mM NaCl, 4 mM CaCl$_2$, 0.005 % P20 + 4 % DMSO).

4.9.1 Experimental

Dynamic light scattering measurements were performed in collaboration with Dr. G. Zanchetta (University of Milano) on a ST100 Scitech Instruments apparatus. Data reported here were collected at a scattering angle of 90 °, corresponding to scattering vector q ~ 0.022 nm^{-1}.

Obtained correlation functions were fitted with Equation **4.8** using OriginPro8.5 software.

$$G = y_0 + A^{-(\frac{\tau}{\tau_c})^{\alpha}}$$

Equation 4.8 Equation used to fit the correlation functions. *G(τ)* is the correlation function.

The fitting allowed extrapolating the τ_c and α parameters. From τ_c values, it was possible to calculate the diffusion coefficient *D* of the scattering species. The stretching exponent α can give an estimate of the polidispersity of the system (when $\alpha = 1$, the single exponential decay is recovered, corresponding to a monodispersed system).

Finally, using the Stoke-Einstein Equation **4.4**, the R_H of species in solution can be determined.

Compounds were tested at different concentrations; before dissolution, compounds were filtered through a PTFE filter 0.45 μm, then lyophilized and re-solubilized in a filtered solvent (water or buffer, i.e. 25 mM Tris-HCl (pH 8), 150 mM NaCl, 4 mM $CaCl_2$, ± 4 % DMSO).

4.9.2 Results and discussion

All the samples at all concentrations displayed a single (stretched) exponential decay of the correlation function, indicating a monomodal particle size distribution. No evidence was found for a fast decay of the correlation function associated to the presence of free monomers, probably because of their weak scattered intensity. On the contrary, for all tested compounds, hundreds nanometer-sized aggregates were detected. The width of Gaussian distribution reported in Figure **4.23** corresponds to the largest value between the polydispersity estimated from the stretching exponent or from cumulant analysis of correlation functions and standard deviation are due to sample/measurement variability. Remarkably, no evidence was found for depolarized scattering signal, which would be expected from anisotropic assemblies. The polidispersity indication and the isotropic shape of the aggregates are in line with what we have observed in TEM images (see Paragraph 4.7).

Characteristic distributions for the tested compounds at different concentrations are reported in Figure **4.23**.
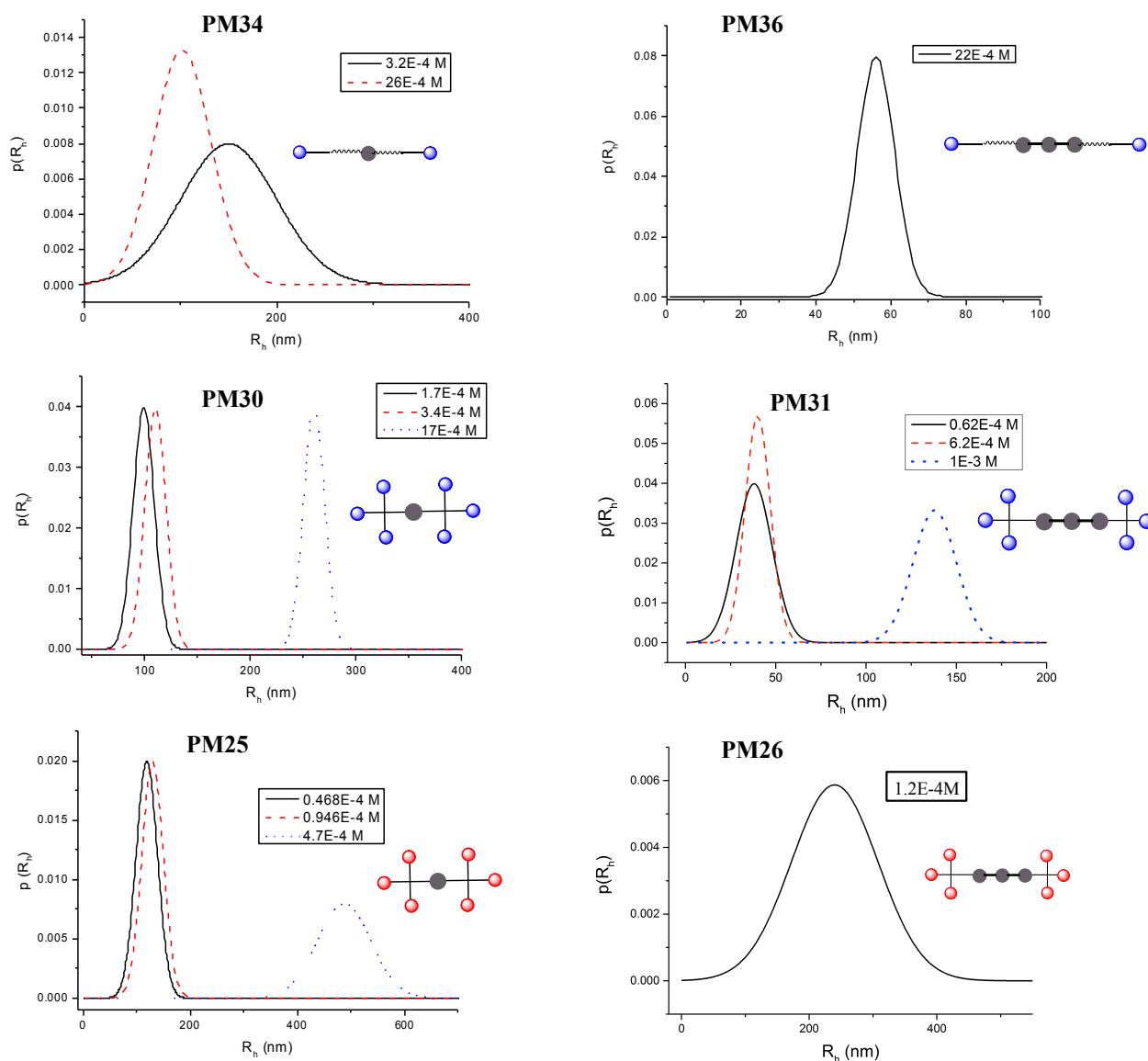
Figure 4.23 Size distributions extracted from DLS experiments for PM compounds at various concentrations (indicated in the panels). In the cartoons of tested molecules, blue spheres represent **1.7** and red spheres represent **1.9**.

In the case of **PM30**, **PM31**, **PM25** and **PM26** tested at a concentration with the same order of magnitude of their limit of solubility ($17 \cdot 10^{-4}$ M, $1 \cdot 10^{-3}$ M, $4.7 \cdot 10^{-4}$ M, $1.2 \cdot 10^{-4}$ M, see Table **4.1** for comparison), bigger species with R_H = 250, 150, 500 and 250 nm respectively were observed, probably corresponding to incipient precipitating materials. Otherwise, R_H didn't remarkably change varying the concentration. Interestingly, Rod1 derivatives (**PM30** and **PM34**) showed the presence of larger aggregates relative to molecules containing Rod3 (**PM34** *vs* **PM36** and **PM30** *vs* **PM31**). This is consistent with the observation, made by the AUC assays, that Rod1 subset lost higher percentages of absorption by speeding the rotor up from 3000 to 42000 rpm respect to the corresponding Rod3 one (**PM25** *vs* **PM26** and **PM30** *vs* **PM31**, see Paragraph 4.8).

The morphological behaviour of **PM31** at 0.62 mM was tested also at 40 °C, revealing that temperature doesn't affects significantly the size of the aggregates. Testing **PM31** at the same concentration both in water and in buffer also gave comparable results.

With the aim of confirming the nature of the aggregates and that they can be eliminated through centrifugation, DLS analysis of **PM31** 1 mM in water was performed before and after centrifugation. Different aliquots of the solutions were centrifuged for 1 h, 13 h or 40 h at 4000 rpm. Interestingly, already after 1 h, the intensity signal associated with aggregates decreased by about 50 %. Also the mean R_H shrank, probably because the bigger components of the Gaussian curve were removed first. *I(t)* and R_H kept decreasing by increasing the duration of the centrifugation reaching a plateau after a few hours. Remarkably, neither the intensity nor the hydrodynamic radius increased by stocking the 40 h-centrifuged sample for 4 weeks at 4 °C, indicating that, once removed, aggregates don't form anymore in these conditions. Results are reported in Figure **4.24A** and Figure **4.24B** and Table **4.9**.

An analogous experiment was conducted also on **PM26** 0.12 mM, but it was not possible to interpret results due to very low intensity values associated also to the pre-centrifuge sample, which didn't allow for a reliable fit of the correlation function.
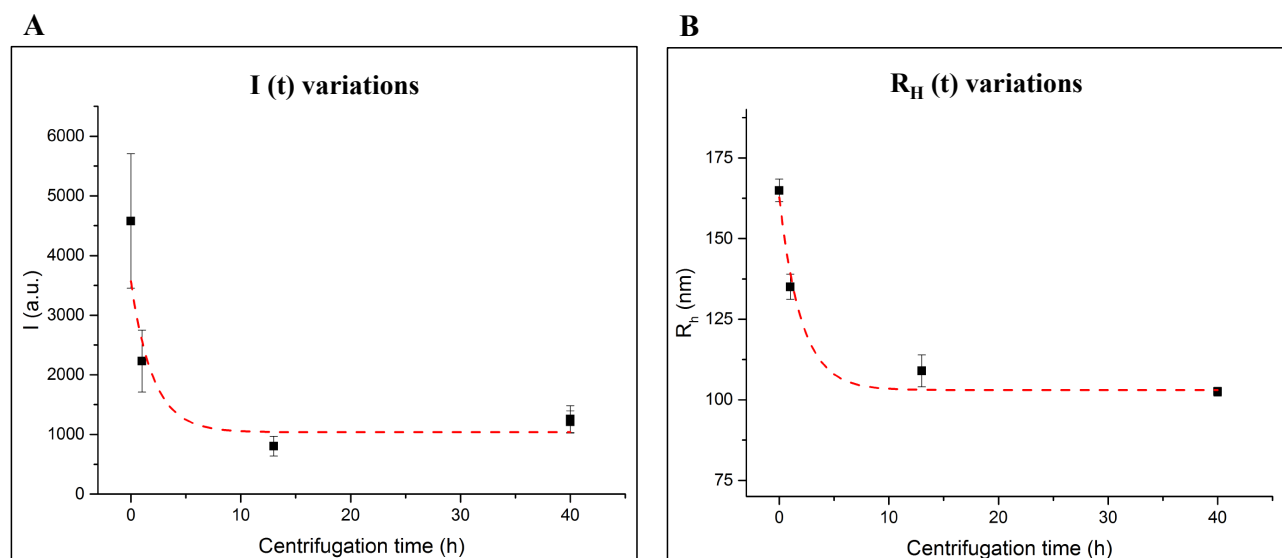
A

B

Figure 4.24 A) Intensity and B) R_H variations as a consequence of the centrifugation (4000 rpm) of **PM31** 1 mM in H$_2$O.

Centrifugation time (h)	Intensity (a.u.)	R_H (nm)
0	4579.2 ± 1591.2	164.9 ± 10.2
1	2230.1 ± 732.7	135.1 ± 11.1
13	803.9 ± 233.0	109.0 ± 13.9

| 40 | 1257.8 ± 317.8 | 102.6 ± 13.9 |
| 40* | 1210.5 ± 261.3 | 87.9 ± 2.6 |

Table 4.9 Intensity and R_H values vary as a consequence of the centrifugation (4000 rpm) of **PM31** 1 mM in H_2O. Values were obtained as a mean of two different measurements of the scattered light both at $\Theta = 90$ °C with respect to the incident laser beam. * Sample stored at 4 °C for 4 weeks after 40 h of centrifugation.

The loss of signal was investigated also through UV-Visible analyses. After centrifugation, the supernatant (65 µL) of the sample was separated through a syringe from the supposed pelleted-containing solution (30 µL). As reported in Tables **4.10** and **4.11**, after centrifugation lower absorption values were associated to supernatant solutions; in the case of **PM31**, this was consistent with an increase of the absorption in the pellet solution. Through these analyses, pelleted samples were found to be only a small percentage (< 10 %) of the overall solution. These absorbance variations are in line with those recorded through the spectrophotometer of the Analytical Ultracentrifugation machine (Table **4.8**).

Table 4.10 PM31 1 mM was tested through UV-Vis spectroscopy before and after centrifugation (40 h). Equal aliquots of the sample before the centrifugation and after the centrifugation (both supernatant and pellet) were diluted 1:10 before conducting the analysis.

Initial concentration	1 mM
Abs$_{391}$ pre	3.124
Abs$_{391}$ post_supernatant	3.034 (-3 %)
Abs$_{391}$ post_pellet	3.162 (+ 12 %)
Abs$_{315}$ pre	2.437
Abs$_{315}$ post_supernatant	2.222 (- 9%)
Abs$_{315}$ post_pellet	2.561 (+ 5 %)

Table 4.11 PM26 0.12 mM was tested through UV-Vis spectroscopy before and after centrifugation (13 h). After the centrifugation, only the supernatant was analysed, because the amount of the pellet ($\approx$ 30 mM) was to low.

Initial concentration	0.12 mM
Abs$_{391}$ pre	1.406
Abs$_{391}$ post_supernatant	1.291 (- 8%)
Abs$_{315}$ pre	0.716
Abs$_{315}$ post_supernatant	0.692 (- 3%)

4.10 Conclusions

DOSY NMR and SV-AUC analyses allowed to observed that the prevailing species in solution is monomeric for all tested compounds. Similarly, preliminary DLS examination of **PM26** confirmed that the mass distribution is dominated by monomers. Nevertheless, AUC revealed a loss in absorption by speeding the rotor up from 3000 to 42000 rpm, suggesting that there is a portion of the compounds that exists in an aggregate morphology and that pellets by centrifuging the sample. This aggregate material could be what was observed by TEM and Cryo-TEM and also by DLS analyses. In this last case, hundreds nanometer-size aggregates were clearly detected, their size not really being related to the concentration of sample, the temperature, the kind of ligand nor the length of the rod. DLS and UV-Vis analyses were used to validate the assumption that aggregates precipitate after centrifugation. DLS conducted on **PM31** 1 mM in water revealed a loss of intensity of the aggregate (- 50 %) already after 1 h of centrifugation. Recording samples absorptions of **PM31** 1 mM and **PM26** 0.12 mM in water before and after centrifugations revealed a 3-8 % reduction of absorption and therefore concentration, after centrifugation. These last results seem to confirm that a big portion (> 50 %) of aggregates can be removed through centrifugation and that aggregates represent only a small percentage (< 10 %) of the sample. Since the size of aggregates is not affected by temperature nor concentration, it is reasonable to assume that they are a portion of molecules that have failed to dissolve. Indeed, supernatant solutions removed after 40 h of centrifugation retain $\geq$ 90 % of the UV-Vis absorption intensity and do not show any new aggregate formation after 4 weeks at 4 °C. The tendency of the samples to pack together was shown also by the detection of dimers, trimers and tetramers through AUC, even if in very low amount. **PM26**, which is the less soluble compound among the synthesised ones (solubility limit $\approx$ 150 μM), formed the biggest aggregates (R_H = 200 nm, detected through DLS) and the highest amount of dimers ($\approx$ 10 %, detected through AUC).

Obtained results prompted us to conclude that all these compounds exert their biological activity as DC-SIGN binders and HIV-1 *trans*-infection inhibitors mainly as monomers. This hypothesis is supported by the fact that big aggregates should not be able to deeply affect the trend of obtained IC_{50} values. Indeed, even if the morphology of aggregates could in principle depend on the monomers, their resulting size and shape could not be related to the trend of IC_{50} variation, which was deeply size- and valency-dependant. Moreover, SPR experiments were always conducted centrifuging the sample before the analysis, thus removing at leas a considerable amount of aggregates. In parallel, *trans*-infection inhibition assays were conducted by dissolving the samples in DMSO, and then by diluting the resulting solution with the biological buffer; this way of solubilisation should be, in principle, more efficient.

Even if the formation of aggregates was found to be negligible for the biological activity of compounds, which still is their fundamental application, we wanted to evaluate their nature. TEM analyses suggest that they are similar to doughnut-shaped materials or to perforated vesicles. Surface tension analysis excluded the formation of micelles. Future computational analysis will be performed with the aim to evaluate which forces among monomers could drive the aggregation mechanism and predict possible structures.

4.11 References

[1] V. Percec; D. A. Wilson; P. Leowanawat; C. J. Wilson; A. D. Hughes; M. S. Kaucher; D. A. Hammer; D. H. Levine; A. J. Kim; F. S. Bates; K. P. Davis; T. P. Lodge; M. L. Klein; R. H. DeVane; E. Aqad; B. M. Rosen; A. O. Argintaru; M. J. Sienkowska; K. Rissanen; S. Nummelin; J. Ropponen, Self-Assembly of Janus Dendrimers into Uniform Dendrimersomes and Other Complex Architectures, *Science* **2010**, 1009.

[2] P. K. Lekha; Edamana Prasad, Tunable Emission of Static Excimer in a Pyrene-Modified Polyamidoamine Dendrimer Aggregate through Positive Solvatochromism, *Chem. Eur. J.* **2011**, 8609.

[3] K. Byung-Sun; H. Dong-Je; B. Jinyoung; L. Myongsoo, Controlled Self-Assembly of Carbohydrate Conjugate Rod-Coil Amphiphiles for Supramolecular Multivalent Ligands, *J. Am. Chem. Soc.* **2005**, 16333.

[4] V. Percec; P. Leowanawat; H. Sun; O. Kulikov; C. D. Nusbaum, T. M. Tran; A. Bertin; D. A. Wilson; M. Peterca; S. Zhang; N. P. Kamat; K. Vargo; D. Moock; E. D. Johnston; D. A. Hammer; D. J. Pochan; Y. Chen; Y. M. Chabre; T. C. Shiao; M. Bergeron-Brlek; S. André, R. Roy; H. Gabius; P. A. Heiney, Modular Synthesis of Amphiphilic Janus Glycodendrimers and Their Self-Assembly into Glycodendrimersomes and Other Complex Architectures with Bioactivity to Biomedically Relevant Lectins, *J. Am. Chem. Soc.*, **2013**, 9055.

[5] L. Brunsveld; B. G. G. Lohmeijer; J. A. J. M. Vekemans; E. W. Meijer, Chirality amplification in dynamic helical columns in water, *Chem. Commun.* **2000**, 2305.

[6] M. K. Müller; L. Brunsveld, A Supramolecular Polymer as a Self-Assembling Polyvalent Scaffold, *Angew. Chem. Int. Ed*. **2009**, 2921.

[7] Q. Lu; K. Liu; H. Zhang; Z. Du; X. Wang; F. Wang, From Tunneling to Hopping; A Comprehensive Investigation of Charge Transport Mechanism in Molecular Junctions Based on Oligo(*p*-phenylene ethynylene)s, *ACS Nano* **2009**, 3861.

[8] P. C. Hiemenz, *Principles of colloid and surface chemistry*, 1997.

[9] Y. Cohen; L. Avram; L. Frish, Diffusion NMR Spectroscopy in Supramolecular and Combinatorial Chemistry: An Old Parameter – New Insights, *Angew. Chem. Int. Ed*. **2005**, 520.

[10] Greg Ralston, *Introduction to Analytical Centrifugation*, Beckman 1993.

[11] www.coriolis-pharma.com

[12] a) P. Schuck, Size-distribution analysis of macromolecules by sedimentation velocity ultracentrifugation and lamm equation modeling. *Biophys. J.* **2000**, 1606; b) www.analyticalultracentrifugation.com

[13] H. Durchschlag, *Thermodynamic data for Biochemistry and Biotechnology*, Springer-Verlag, 1986.

[14] B. J. Berne; R. Pecora, *Dynamic Light Scattering*, 1976.

Chapter 5

DC-SIGN *vs* Langerin: synthesis of 6-amino-pseudo-dimannosides

5.1 Langerin

     As stated in Paragraph 1.3.1, Langerin is a C-type lectin expressed by a subset of Antigen Presenting Cells (APCs); it is specific for mannose or related sugars (e.g. glucose and fucose) that show two adjacent hydroxyl groups free to chelate Ca^{2+} ions in the carbohydrate recognition domain (CRD) of the protein.[1] Langerin is involved in the recognition and degradation of HIV-1 virus,[2] which probably happens in subdomains of the endosomal compartments named Birbeck granules.[3] Since Langerin has an efficient role against HIV virus, anti-adhesive therapeutic strategies, aimed to use artificial ligands to antagonize DC-SIGN or other receptors involved in HIV infection, must not target Langerin. In this Ph.D. project, DC-SIGN is the target of *ad hoc* synthesised ligands (see Chapter 2); the design and synthesis of ligands that bind DC-SIGN but not Langerin is mandatory. A rational approach for producing selective ligands takes into account the morphology of the receptors binding sites and aims to synthesise ligands that have higher affinity for the one targeted and lower or no affinity for the others. In previous studies, we have already shown that our current lead, ligand **1.9**, is rather selective for DC-SIGN *vs* Langerin.[4]**Errore. Il segnalibro non è definito.** However, since multivalency can increase the affinity even of weak ligands, refinement of the monovalent antagonist seems to be the most practical way to control the selectivity issue. In order to do so, in the course of my thesis we have explored some structural modifications of **1.7** and **1.9**, based on diffractional analysis of the lectin structures.

The extracellular domain of Langerin consists of a neck region and a CRD; coiled-coil structures in the neck regions lead to the formation of trimers where the three carbohydrate recognition domains are spaced by a distance of 41.5 Å (Figure **5.1A**; in Figure **5.1B** tetrameric DC-SIGN ECD is shown for comparison). Stabilizing interactions occur among neck regions, but also between the neck of one monomer and the CRD of another one and between two adjacent CRDs.[5]
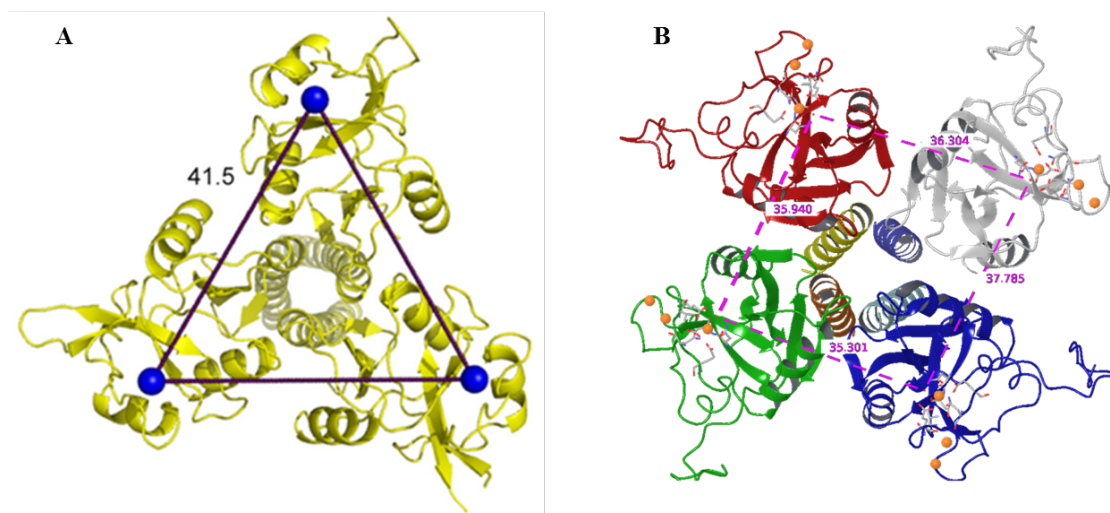

Figure 5.1 A) Trimer of Langerin (a truncated version); blue spheres represent Ca^{2+} ions.[5] B) Tetramer of DC-SIGN (a

truncated version); orange spheres represent Ca^{2+} ions.[6]

A unique feature of Langerin with respect to DC-SIGN is the presence of two positively charged lysine residues (Lys 299 and Lys313) in its binding site.[7]

Screening the glycan array of the Consortium for Functional Glycomics, the group of Weis demonstrated that 50 µg/mL of fluorescently-labelled Langerin significantly binds only high mannose oligosaccharides, few structures with terminal 6-sulfated galactose residues and the blood group B epitope (Galα1-3(Fucα1-2)Gal) (Figure **5.2**).
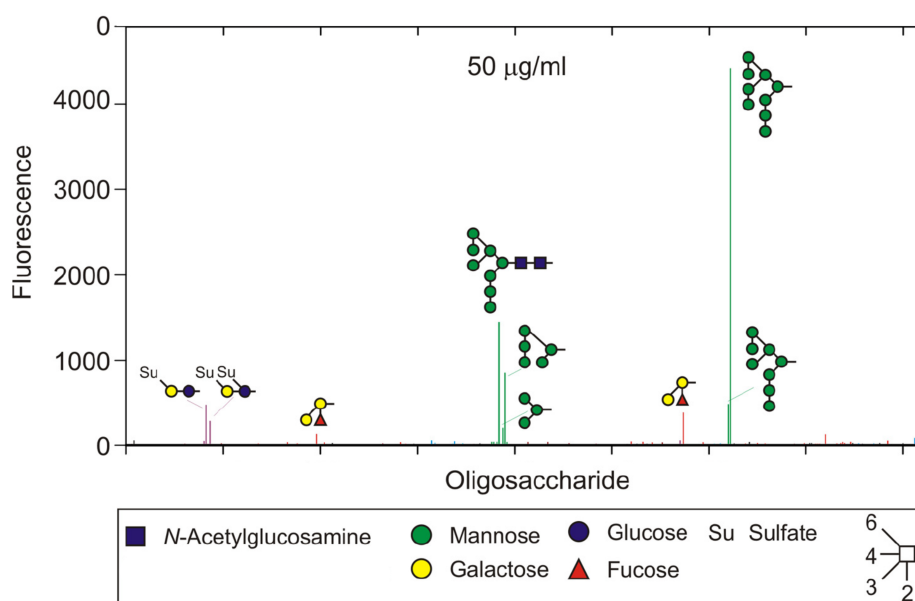

Figure 5.2 Ability of fluorescent Langerin to bind oligosaccharides. Ligands that gave highest signals are identified and reported as coloured bars.

The same group solved the crystal structure of monomeric Langerin CRD bound to various carbohydrate ligands. Manα1-2Man-containing compounds preferentially bind Langerin CRD with the 3-OH and 4-OH groups of the non-reducing end, leaving the 2-OH group free to form hydrogen bonds with Lys299. In that case, both chains extended either from the reducing end or from the 6-position of the nonreducing end can be accommodated. The reducing end can then form extra contacts with the protein (Figure **5.3A**). The interaction between Langerin and 6-SO$_4$-Gal is remarkable, since Langerin binds galactose more weakly than mannose and fucose.[1] This interaction is driven by the SO_4^{2-} group that forms salt bridges with Lys299 and Lys 313. These charge-charge interactions can therefore compensate the absence of hydroxyl groups properly oriented to chelate Ca^{2+} ions (Figure **5.3B**). The blood group B epitope binds Langerin with the equatorial 2-OH and 3-OH groups of the fucose moiety; the 4-OH group forms hydrogen bonds

with the Lys299 (Figure **5.3C**). The non-reducing galactose residue is involved in other interactions with the protein, while the central one is positioned away from the binding site (Figure **5.3D**).
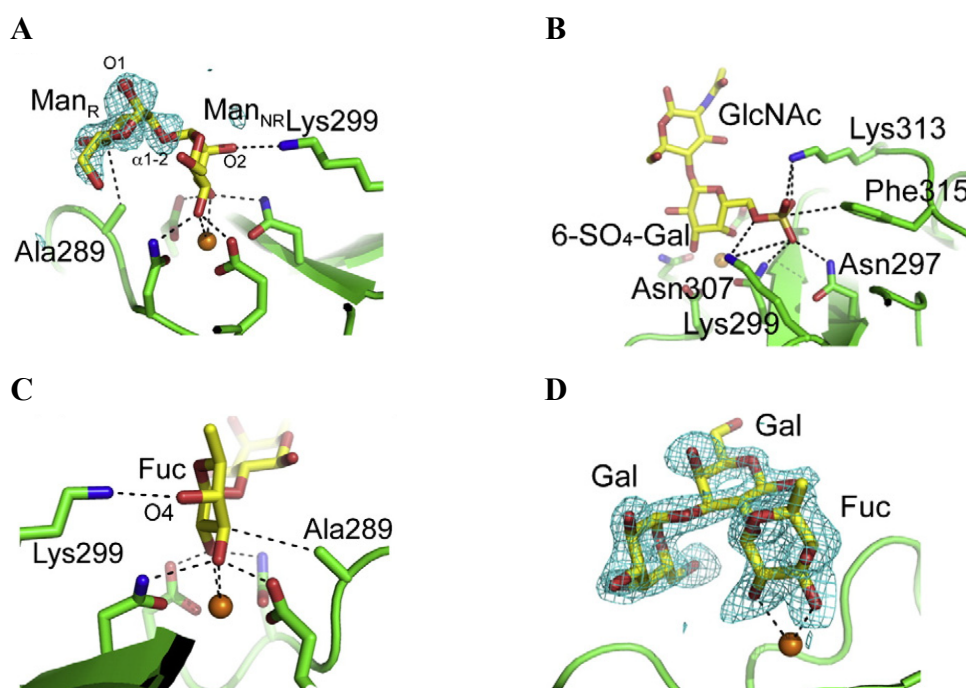

Figure 5.3 Interactions between oligosaccharides and the monomeric Langerin CRD. Carbohydrate ligands are: A) Manα1-2Man, B) 6-SO$_4$-Gal-GlcNAc, C) and D) blood group B epitope: Galα1-3(Fucα1-2)Gal. Orange spheres represent Ca^{2+} ions.

5.2 Artificial monovalent mannose-based ligands not targeting Langerin

Knowing the structure of the binding sites of DC-SIGN and Langerin, it is possible to design ligands with a high affinity towards the target DC-SIGN and with a lower ability to be recognized by Langerin.

In previous works conducted by our and Prof. F. Fieschi's group,[8,9] **1.9** (Scheme **5.1A**, Figure **5.5**) was found to be not only a good monovalent DC-SIGN inhibitor (see Chapter 2.2), but also to be more active towards DC-SIGN than Langerin, showing a gain in selectivity of 6 times over the monovalent ligand **1.7** (Scheme **5.1B**, Figure **5.5**). Further improvements were obtained by replacing the 6-OH group in the mannose residue of **1.7** with an -NH$_2$ group. The final compound **5.1** was tested as a receptor antagonist by SPR, displaying a doubled affinity towards DC-SIGN with respect to **1.7** and a 4 times higher selectivity against Langerin.

Scheme 5.1 Structures of monovalent ligands A) **1.9**, B) **1.7**, C) **5.1**.
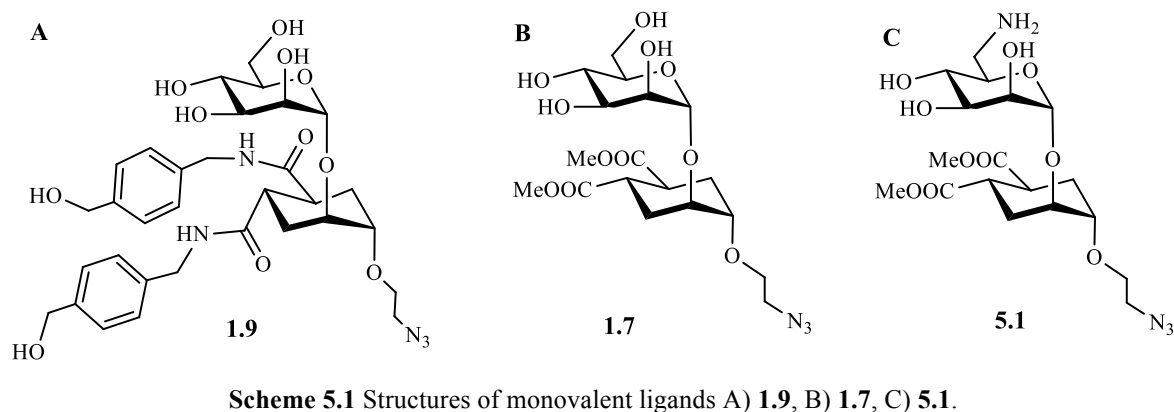
The better affinity for DC-SIGN may arise from positive interactions between the amino group and carboxylic side chains in the vicinity of the Ca^{2+} binding site, as predicted by docking studies (J. McGeagh, Anterio GmbH, unpublished results). NMR studies confirmed that **5.1** interacts with DC-SIGN in solution as its lead compounds **1.7** (Figure **5.4**, P. M. Nieto, unpublished results). Thus, it coordinates Ca^{2+} ions in the binding site with 3-OH and 4-OH of the mannose residue, and the cyclohexane ring participates in the interaction through van der Waals contacts (Figure **5.4**).[10]
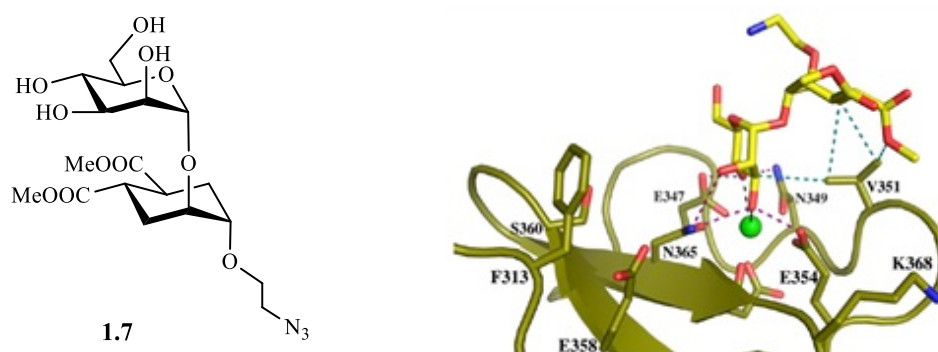

Figure 5.4 A) Structure of **1.7** and B) X-ray structure of the DC-SIGN complex.[10] The protein is shown in olive, **1.7** in yellow and the Ca^{2+} is a green sphere. Nitrogen and oxygen atoms are, respectively, blue and red. Hydrogen bonds are shown as dashed purple lines, Ca^{2+} coordination bonds are dashed black lines, and key van der Waals interactions are indicated by dashed blue lines.

The primary amine group in **5.1** should be largely protonated at physiological pH thus, in principle, increasing the compound solubility in water. Furthermore, the presence of positively charged groups can lead to electrostatic repulsions with the Lysine residues in Langerin binding site, explaining the lower affinity of this compound for Langerin. Crystal structures resolved in the group of Weis showed the proximity of the 6- position of the non-reducing mannose moiety of the disaccharide Manα1-2Man to Lys299 (Figure **5.3A**).[5]

In the course of previous PhD program (Varga 2012,[8] Sutkeviciute 2012[9]), interactions between

compounds and the two lectins were evaluated through SPR competition assays (described in Chapter 2.6.2), measuring *IC$_{50}$* values (Figure **5.5**).
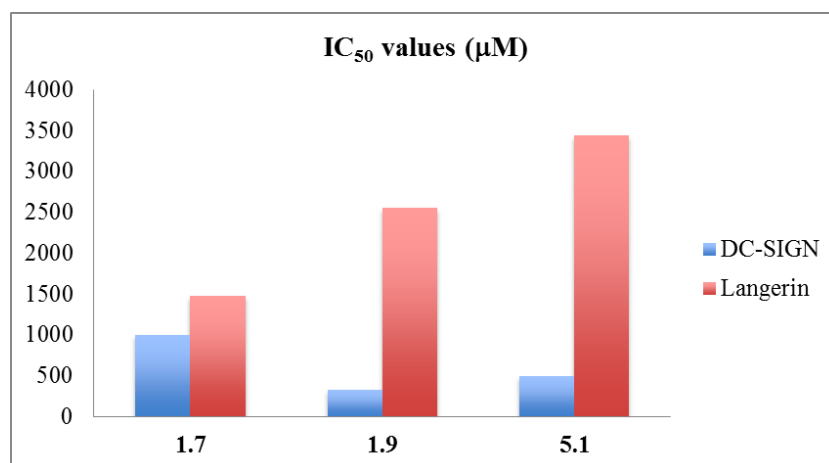

Figure 5.5 *IC$_{50}$* values (μM) of compounds **1.7**, **1.9** and **5.1** inhibiting the anchoring of DC-SIGN ECD (blue bars) or Langerin (red bars) on a highly mannosylated sensor chip.[8]

Combining the positive effects of amide groups on the cyclohexyl moiety (**1.9**) and -NH$_2$ groups on the mannose residue could result in a potent DC-SIGN ligand, selective with respect to Langerin. In the course of my thesis, ligand **5.2** (Scheme **5.2**) was synthesised on this purpose.
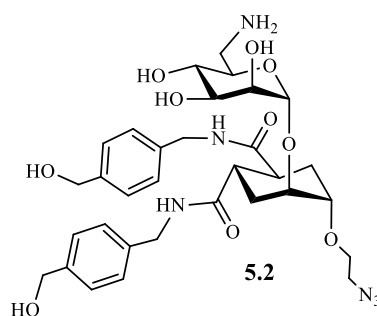
Scheme 5.2 Structure of **5.2**.

5.2.1 Synthesis

As for compounds **1.7** and **1.9** (see Chapter 2.4), the synthesis of compounds **5.1** and **5.2** was accomplished by combining one mannose donor activated as trichloroacetimidate at the anomeric position (**5.3**, Scheme **5.3**) with a cyclohexane derivative conveniently substituted (Scheme **5.3**). Cyclohexane derivatives **5.4** and **5.5** are analogous of compounds **2.9** and **2.10** presented in Chapter 2.4, but they bear a chloride atom rather than an azide on the ether tether. The glycosylation reaction led to **5.6** or **5.7** respectively (Scheme **5.3**), precursors of the final compounds. Final molecules **5.8** and **5.9** were isolated as Trifluoroacetate salts of the 6-amine (Scheme **5.3**).
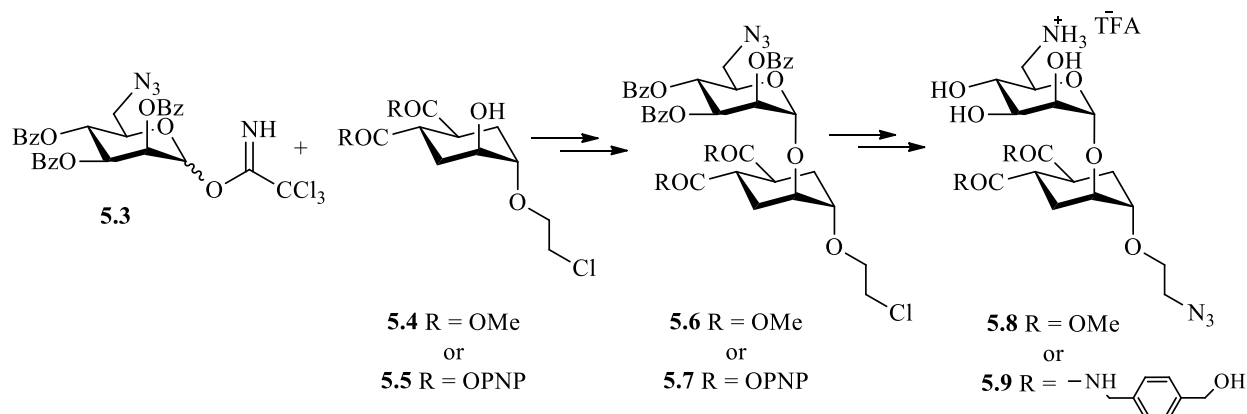
Scheme 5.3 A glycosylation reaction connects a trichloroacetimidate mannose derivative **5.3** and a cyclohexane conveniently substituted **5.4** or **5.5** yielding a precursors **5.6** or **5.7** of desired 6-NH$_2$ derivatives. Final compounds were isolated as TFA salts **5.8** and **5.9**.

Although **5.8** had already been synthesised within the group by Dr. Norbert Varga,[8] the synthesis of the mannose derivative **5.3** was optimized in this PhD thesis using a new procedure depicted in Scheme **5.4, route B**. The primary hydroxyl group of mannose was first activated as a tosylate, using tosyl chloride in the presence of pyridine, giving compound **5.10** (α anomer). When a tosylate-azide reaction exchange was performed at this stage, it yielded the desired compound **5.11**, in a mixture with an undesired byproduct (Scheme **5.4, route A**). ESI mass analysis revealed that the byproduct has the same molecular weight of compound **5.12**. This bicyclic molecule, coming from an intramolecular cyclisation where the 2-hydroxyl function has displaced the tosylate group, can be the actual byproduct according to ¹H-NMR data. No further investigation were performed to fully characterize its structure. The byproduct not only did reduce reaction yields (up to 0 % in one case), but it was also difficult to remove. Several reaction conditions listed in Table **5.1** were tried in vain to avoid the formation of **5.12**. Changing the solvent (DMF, DMA, H$_2$O, H$_2$O:DMA 1:1, H$_2$O:DMF 1:1), the reaction time (overnight or several days) and also using microwave irradiation, desired compound **5.11** was never obtained pure nor recovered pure after a chromatographic purification step.

| Catalyst	Solvent	[5.10]	Temperature (°C)	Time	Byproduct
Bu$_4$NI	DMF	0.5 M	60, batch	2 days	Yes
///	DMA	0.6 M	50, batch	3 days	Yes
///	DMA	0.6 M	50, batch	Overnight	Yes

///	H₂O	0.15 M	50, batch	Overnight	Yes
///	DMA:H₂O	0.64 M	60, MW	6 h	Yes
///	DMF:H₂O	0.6 M	65, MW	6 h	Yes
///	DMF	0.6 M	60 °C, MW	6 h	Yes

Table 5.1 Reaction conditions to synthesise compound **5.11**. The formation of byproduct was investigated. MW = microwave irradiation.

A more suitable reaction pathway involved first the protection of the residual free –OH groups in **5.10** as benzoate derivatives, performed in the presence of benzoyl chloride and 4-dimethylaminopyride (DMAP) as catalyst to give compound **5.13** (α–anomer). Reaction times and temperatures were optimized to minimize both the formation of a byproduct where the tosylate group is replaced by a chloride anion and the presence of an intermediate with a residual non-protected hydroxyl group (probably the one in 2- position for a matter of steric hindrance). Highest yields were obtained by performing the reaction at room temperature overnight in pyridine.

The subsequent tosylate-azide reaction exchange (60 °C, DMA) gave a mixture of α and β anomers of **5.14** in good yields. When Bu₄NI was used as catalyst and reaction times were around 24 hours, the side-reaction involving the deprotection of the anomeric hydroxyl group was less favored, giving ≈ 15 % of the not-expected compound **5.15**.

Selective deprotection of the anomeric position using methylamine afforded **5.15** (α–anomer). Activation of the anomeric hydroxyl group, yielding the α-anomer of compound **5.3**, was performed using freshly distilled trichloroacetonitrile in the presence of DBU as the catalytic base. After flash chromatography, protected compound **5.3** was obtained in 70 % yield, and almost 20 % of the starting material **5.15** was recovered.
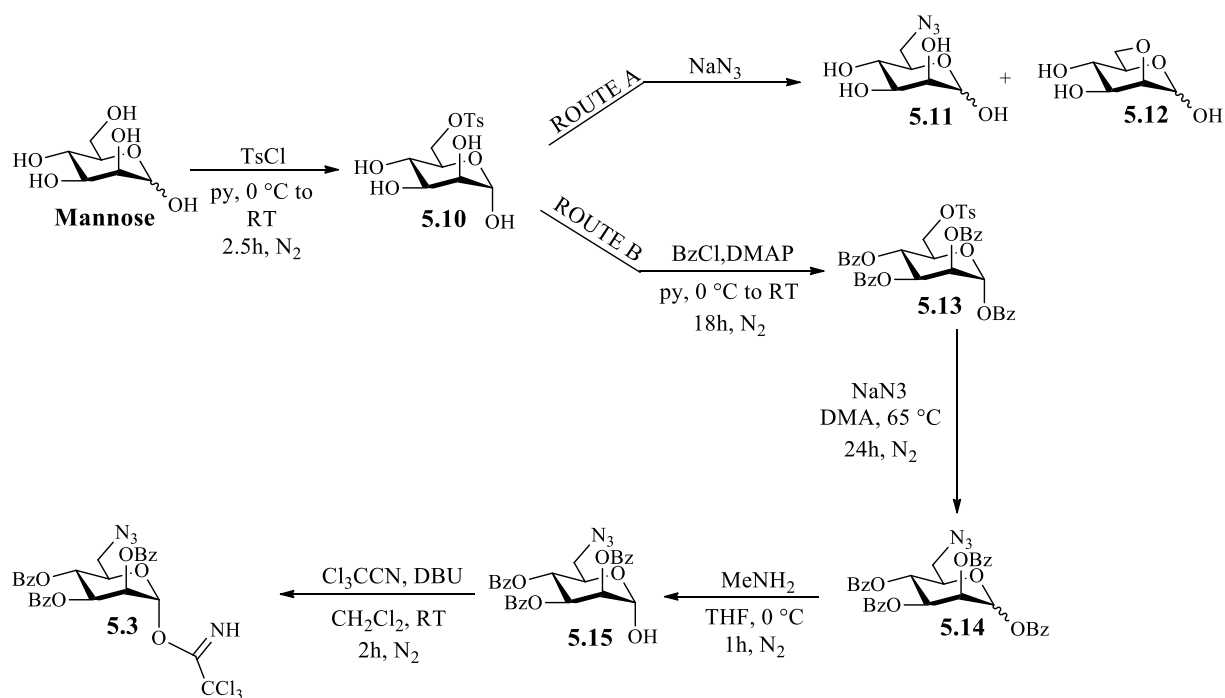
Scheme 5.4 Reaction pathway to obtain the activated glycosyl donor **5.3**. Route A was performed by Dr Norbert Varga;[8] Route B was optimized one during this PhD thesis.

The synthesis of **5.8** (Scheme **5.5**) involved a trimethylsilyltriflate-catalized glycosylation reaction between **5.3** and the cyclohexyl donor **5.4**. 1.5 g of compound **5.4** were available in the laboratory, synthesised by Dr. Norbert Varga in 92 % overall yield from diacid **5.19** (shown in Scheme **5.6**) following a procedure described in Ref.[11].

After the glycosylation step, the benzoyl protecting groups in **5.6** were removed using 0.18 M sodium methoxide in methanol (Zemplen's conditions, Scheme **5.5**), obtaining compound **5.16**. The azide group in the 6- position of the sugar moiety was reduced (H$_2$/Pd-C) in the presence of a slight excess of Boc$_2$O (1.5 eq.) and the amine was obtained directly protected as ^{t}butylcarbamate derivative **5.17**. A chloride-azide reaction exchange gave compound **5.18**; 100 mg were produced. The Boc removal was performed using trifluoroacetic acid in CH$_2$Cl$_2$ ($\approx$ 30 % v/v), at room temperature for 1 hour to afford **5.8** (Scheme **5.5**).

Reactions shown in Scheme **5.5** were performed by the undergraduate student M. Valletta under my supervision.
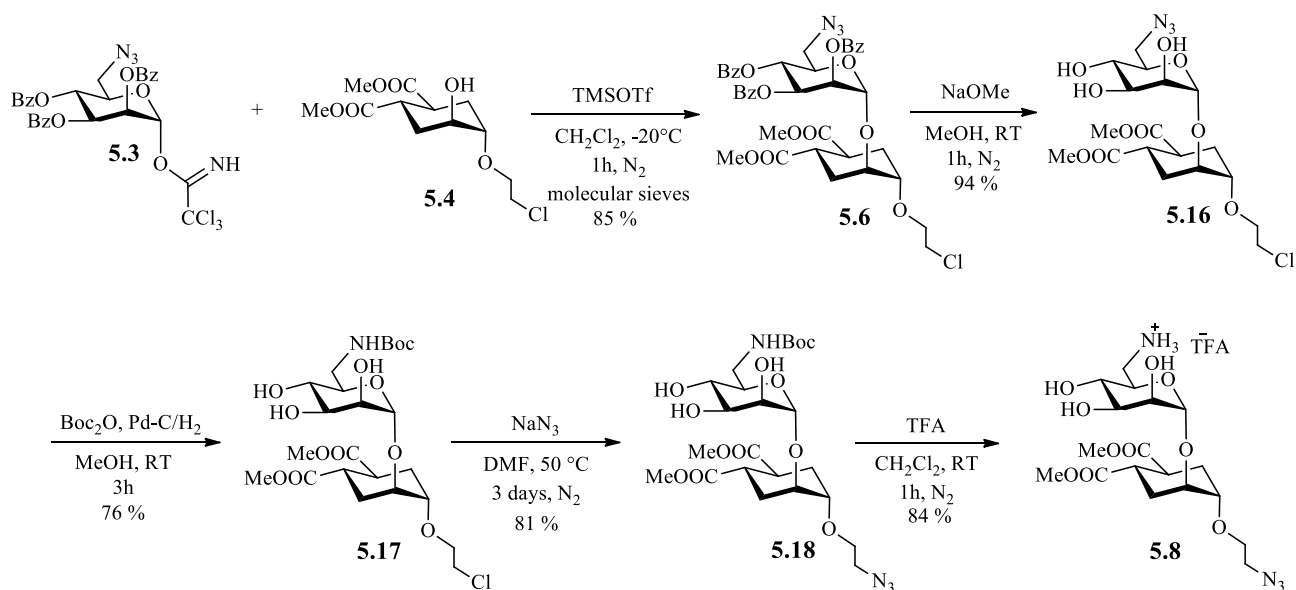
Scheme 5.5 Synthesis of **5.8** derivative as a trifluoroacetate salt.

An analogous reaction pathway was used to synthesise compound **5.9**. In this case, glycosylation step (Scheme **5.8**) involved **5.3** and the cyclohexyl donor **5.5** (Scheme **5.6**). **5.5** was synthesised according to the procedure shown in Scheme **5.6** and described by our group in Ref.[4]. Only the first step, where the acid groups of the diacid **5.19** are activated as *p*-NO$_2$-phenyl esters to give **5.20**, was improved by performing the basic workup to remove the remaining not-reacted phenol with NaHCO$_3$ $_{sat.sol.}$ at 0 °C. The following reaction steps involved the oxidation of the double bond to give the epoxyde **5.21** and the ring opening with chloroethanol assisted by Copper(II)triflate to give compound **5.5**. 1.3 g of **5.5** were obtained in 35 % overall yield.
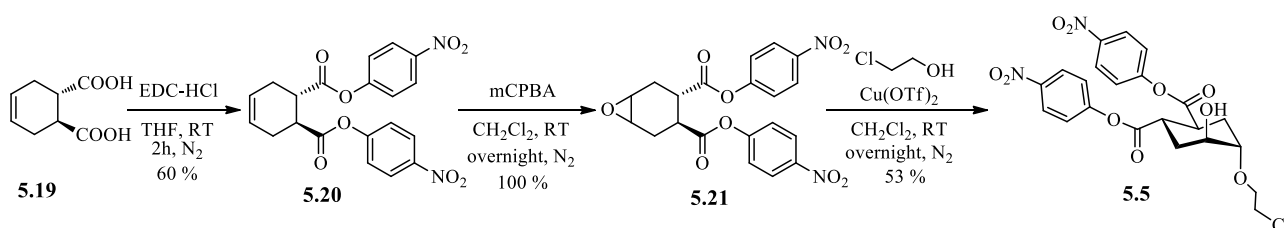

Scheme 5.6 Synthesis of the acceptor cyclohexyl derivative **5.5**.

After the glycosylation reaction to afford compound **5.7** (Scheme **5.8**), *p*-NO$_2$-phenyl ester groups were displaced by the benzylic amine **5.24** to obtain compound **5.25**. 800 mg of **5.24** were already available in the laboratory, obtained from the commercially available methyl(4-aminomethyl)benzoate·HCl **5.22** in 79 % overall yield. As shown in Scheme **5.8**, the free amine was first restored using a Na$_2$CO$_3$ solution, then the methylester was reduced to benzyl alcohol using LiAlH$_4$. Treatment of **5.25** under Zemplen's conditions (0.18 mM MeONa in MeOH) yielded compound **5.26** (Scheme **5.7**). The azide group in the 6- position of the mannose derivative was

223

reduced under hydrogen atmosphere in the presence of Boc$_2$O, obtaining **5.27**. This time Lindlar Palladium was used as catalyst because Pd/C could reduce the -CH$_2$-OH group on the amide moiety to -CH$_3$. Finally, a chloride-azide reaction exchange led to compound **5.28** in high yield, even if long reaction times (2-3 days) were required; 200 mg of **5.28** were produced. Final compound **5.9** was obtained again as trifluoroacetate salt, after Boc deprotection using trifluoroacetic acid in CH$_2$Cl$_2$ (100 or 50 % v/v (Scheme **5.7**). A Boc deprotection reaction in the presence of HCl in MeOH didn't afford the desired compound.

Compound **5.9** was synthesised in collaboration with V. Porkolab (Institut de Biologie Structurale, Grenoble), who visited our laboratories.
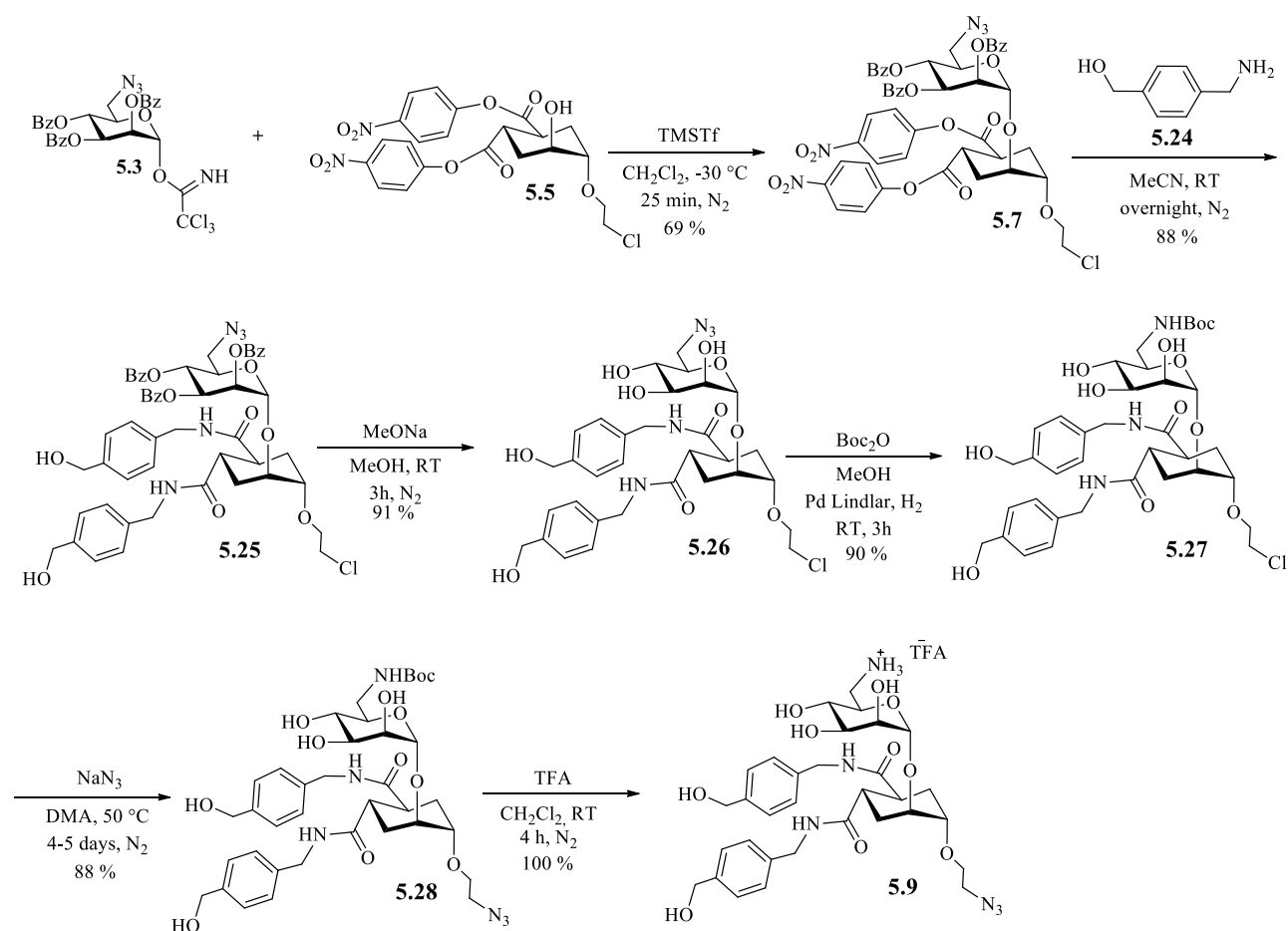
Scheme 5.7 Synthesis of 6-NH$_2$-Man030 derivative as a trifluoroacetate salt **5.9**.
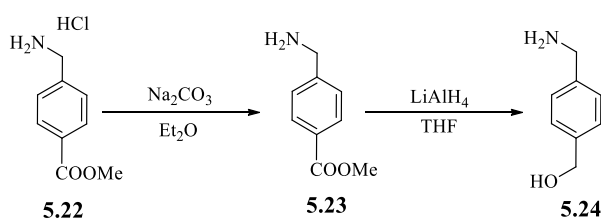
Scheme 5.8 Synthesis of amine **5.24**.

5.2.2 Biological assays

5.2.2.1 Surface Plasmon Resonance Inhibition Assays

6-NH$_2$- derivatives were analyzed as trifluoroacetate salts (**5.8** and **5.9**). The affinity of **5.8** for DC-SIGN and its selectivity with respect to Langerin was investigated through SPR inhibition assays, as reported (Figure **5.5**, Paragraph 5.2). Analogous assays were performed on **5.9**. In contrast with the behavior shown by **5.8** *vs* **1.7**, the replacement of the 6-OH group in **1.9** with a primary amine led to a only slight affinity improvement: **5.9** was found to be only 1.3 times more active towards DC-SIGN than the corresponding compound **1.9**. But, remarkably, **5.9** was totally selective for DC-SIGN over Langerin. Indeed, it was not possible to detect any binding of **5.9** with Langerin even at high compound concentration (4.5 mM). Results are reported in Table **5.2**.

IC_{50} values (mM) towards the two lectins		
Compound	**DC-SIGN**	**Langerin**
1.9	0.3	2.6
5.9	0.25	No binding

Table 5.2 IC_{50} (mM) values of compounds **1.9** and **5.9** inhibiting the anchoring of DC-SIGN ECD or Langerin to a highly mannosylated sensor chip. **5.9** did not inhibit Langerin anchoring at any concentration up to 4.5 mM, therefore it was not possible to determine an IC_{50} value.

5.2.2.2 Isothermal Titration Calorimetry

Isothermal Titration Calorimetry (ITC) was used to determine thermodynamic parameters associated with binding of **5.9** to DC-SIGN ECD. I performed this assays at the Institut de Biologie Structurale of Grenoble with the collaboration of V. Porkolab, Prof. F. Fieschi and M. Trovaslet.

A 5 mM solution of **5.9** in a buffer consisting of 25 mM Tris (pH 8), 150 mM NaCl, 4 mM CaCl$_2$ was titrated into a solution of DC-SIGN ECD (566 μM with respect to the binding sites, i.e. concentration of one single CRD) in the same buffer at 25 °C.

Fitting data allowed to obtained K_D = 171.8 μM, ΔH = -9.54 kJ/mol and stoichiometric value n = 1.07. The n value confirmed a mode of binding in which one single compound **5.9** binds only one CRD. In Table **5.3** thermodynamic fitted and calculated thermodynamic parameters are listed.

| K_A	K_D	n	ΔH	ΔG	ΔS
5820 M^{-1}	171.8 μM	1.07	-9.54 kJ/mol	21.48 kJ/mol	40.06 J/(mol K)

Table 5.3 Thermodynamic parameters associated with the interaction between **5.9** and DC-SIGN ECD. K_A, n and ΔH were obtained by fitting data. K_D was obtained as $1/K_A$. ΔG was obtained from the equation $\Delta G = -RTlnK_A$; $R = 8.314$ J mol^{-1} K^{-1}; T is temperature expressed in Kelvin. ΔS was obtained from the equation $\Delta G = \Delta H - T\Delta S$.

In a first approximation, K_D and IC_{50} values can be compared. ITC experiments revealed a higher affinity of **5.9** towards DC-SIGN ECD with respect to data obtained with the SPR competition experiments ($K_D = 172$ μM *vs* $IC_{50} = 254$ μM). Nevertheless, the two values have the same order of magnitude and differentiate less than a factor of 2, showing the reliability of the two methods.

ITC experiments have been previously conducted by Dr. I. Sutkeviciute to evaluate the interaction between DC-SIGN ECD and compound **1.7**.[9] On the contrary, the thermodynamic behaviour of compound **1.9** was never investigated. She titrated 12.7 mM of **1.7** into lectin solution (71 μM with respect to binding sites). Fitting one binding site model on the data with an assumed stoichiometry value n fixed to 1 yielded a K_D value of 990.10 ± 19.7 μM, in strong agreement with IC_{50} values (i.e. 900-1000 μM, depending on the campaign) found through SPR inhibition assays. Unfortunately, low affinity prevented the reliable interaction enthalpies and entropies to be obtained.

### 5.2.2.3 Saturation Transfer Difference (STD) NMR assay

To confirm that the binding mode of **5.2** to DC-SIGN is the same of **1.7** and **2.1**, Saturation Transfer Difference (STD) NMR experiments will be performed in the group of Prof. P. Nieto. The trifluoroacetate-derivative **5.9** will be used for the investigation and, in particular, it will be converted to molecule **5.9.1** (Scheme **5.9**). It was indeed already demonstrated that the presence of the triazole units allows the splitting of the axial and equatorial signals of the D3 and D6 cyclohexane protons (Scheme **5.9**), without affecting the binding mode.[10]
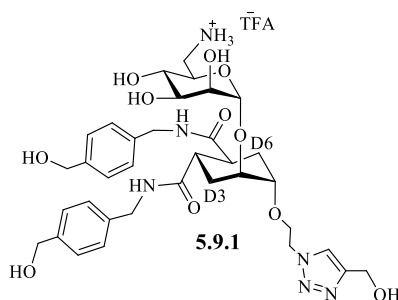
Scheme 5.9 5.9.1 maintain the same binding mode of **5.9**, but its ^{1}H NMR spectrum is more easy to interpreter because it is possible to discriminate between axial and equatorial D3 and D6 protons.

5.3 Artificial multivalent mannose-based ligands potentially not targeting Langerin

5.1 and **5.2** were used to decorate multivalent scaffolds, in order to obtain multivalent compounds with higher affinity towards DC-SIGN and potentially improved selectivity over Langerin. The hexavalent scaffold **2.24** depicted in Scheme **5.10A** was functionalised with both monovalent carbohydrates **5.1** and **5.2**, as well as the scaffold **2.5/Rod3** (Scheme **5.10B**). Nonavalent scaffold **5.24** (Scheme **5.10C**), on the contrary, was used to prepare only multivalent derivatives of **5.2**. All these scaffolds are characterized by a chemically solid backbone and are decorated with terminal triple bonds to be coupled with the azide functions of the monovalent ligands.
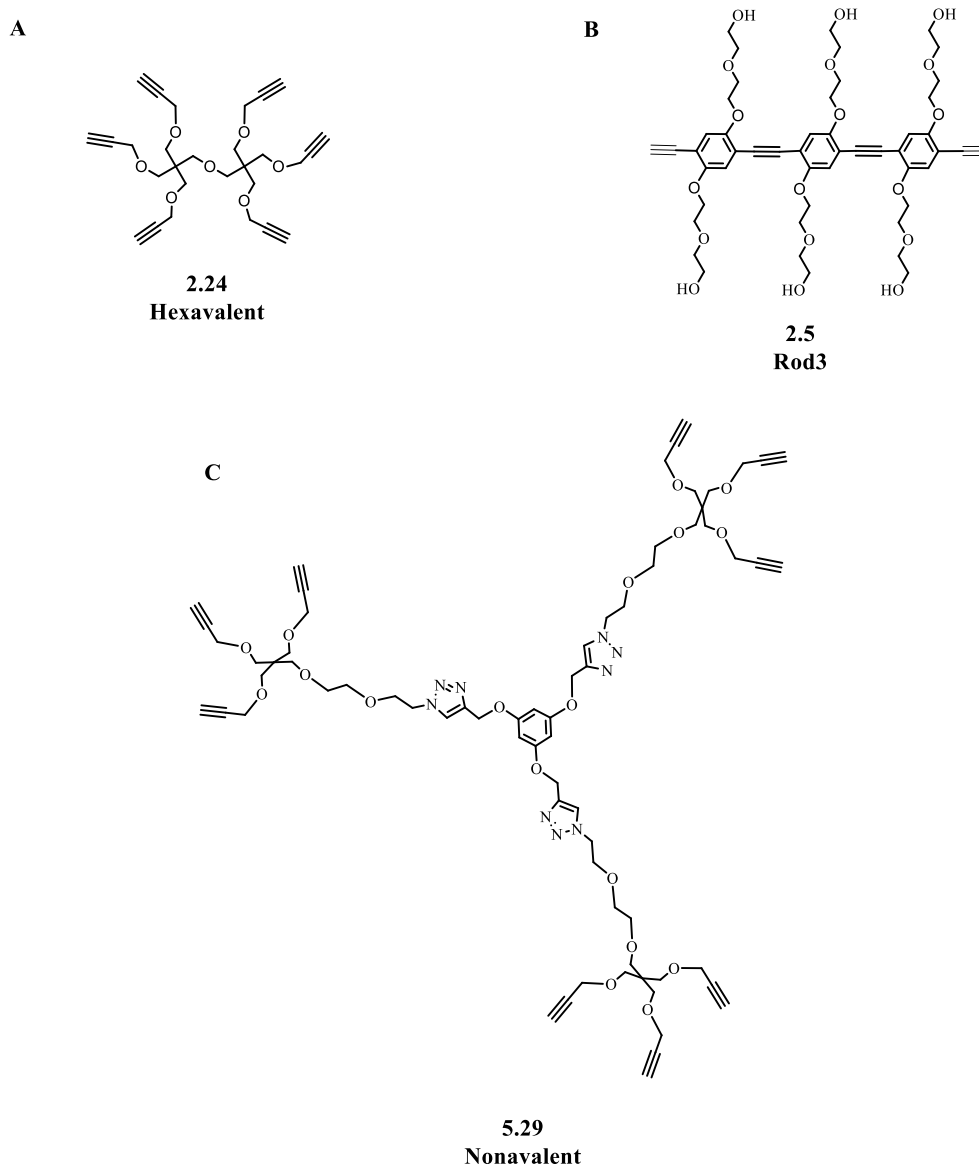
Scheme 5.10 Structure of multivalent ligands to be decorated with **5.1** and **5.2**. A) hexavalent scaffold **2.24**; B) divalent Rod3 **2.5**; C) nonavalent scaffold **5.29**.

According to computational studies performed in these laboratories and described in Chapter 2.5, hexavalent derivatives based on **2.24** should exploit only the statistical rebinding effect or protein aggregation to improve their affinity for the target receptor.[12] On the contrary, divalent **Rod3** derivatives should be able to assume extended conformations that allow for a simultaneous binding of two different subunits within one single DC-SIGN tetramer, thus exploiting the chelation effect.[13] A stated in Paragraph 5.2, the primary amine group of **5.1** and **5.2** could in principle be protonated at physiological pH; we wanted to exploit this feature to synthesis a nonavalent compound based on **5.2** more soluble in aqueous solution.

5.3.1 Synthesis

5.3.1.1 Synthesis of the scaffolds

Hexavalent and nonavalent scaffolds were available in the laboratory and prepared according to Ref.[12] The synthetic pathway to achieve the hexavalent scaffold **2.24** was already described in Chapter 2.4**.**

The synthesis of the nonavalent derivative was accomplished by coupling a trivalent sugar dendron **5.45** (Scheme **5.16**) on the aromatic-based trivalent core **5.31** (Scheme **5.11**). The synthesis of **5.45** involved the trivalent scaffold **2.27** (see Chapter 2.4) and it will be explained in the following Paragraph 5.3.1.2. The aromatic trivalent core **5.31** was synthesised with 1,3,5-trihydroxybenzene **5.30** performing a Williamson etherification reaction with propargyl bromide in the presence of K_2CO_3 as the base (Scheme **5.11**). 200 mg of **5.31** were obtained in 60 % yield.
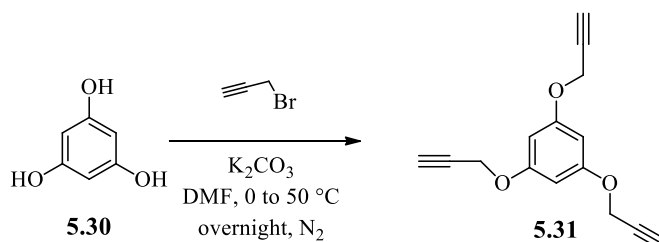
**Scheme 5.11** Synthesis of the trivalent aromatic core **5.31**.

Rod3 **2.5** was synthesised as described in Chapter 2.4.

5.3.1.2 Synthesis of final multivalent compounds

Multivalent compounds were synthesised by combining monovalent ligands bearing an azide group and the central cores functionalized with terminal triple bonds. The copper(I)-catalyzed 1,3-dipolar cycloaddition between an alkyl azide and a terminal alkyne functional groups (CuAAC or click

reaction) is a regioselective and catalyzed variation of an *Huisgens cycloaddition*. Principles of the click chemistry were explained in Chapter 2.4.

The goal of the investigation was to decorate hexavalent, Rod3 and novavalet scaffolds (bearing the terminal alkyne groups, Scheme **5.10**) with 6-NH$_2$-derivatives (Scheme **5.12**), bearing the azide group. We initially wondered which was the best monovalent ligand to undergo a click reaction, among the –Boc protected (Scheme **5.12A**), the trifluoroacetate salt (Sceme **5.12B**) or the free amine derivatives (Scheme **5.12C**).
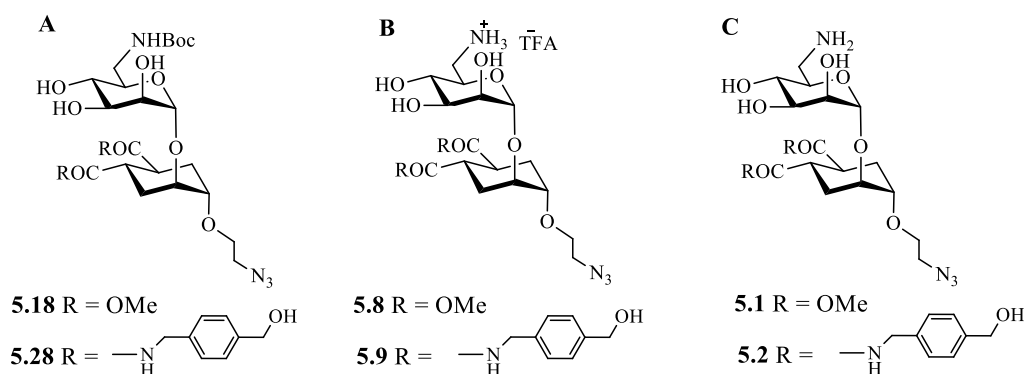
Scheme 5.12 Monovalent ligands bearing an azide group that, in principle, could react with terminal triple bonds in a Copper(I) catalyzed click reaction. A) –Boc derivative; B) trifluoroacetate salt; C) free amine.

A first attempt was performed on compound **5.8**, as a TFA salt, which reacted with the hexavalent core **2.24**. Even after 24 h, the reaction did not go to completion and MALDI mass detected the presence of tetravalent and pentavalent intermediates. Several trials were done to achieve total conversion of the starting materials, such as adding other portions of monovalent ligand **5.8** and heating under microwave irradiation (60 °C). Nonetheless, the reaction did not go to completion. Size exclusion chromatography afforded a mixture of tetra and pentavalent species together with the hexavalent one (**5.32**), which couldn't be isolated pure (Scheme **5.13**).
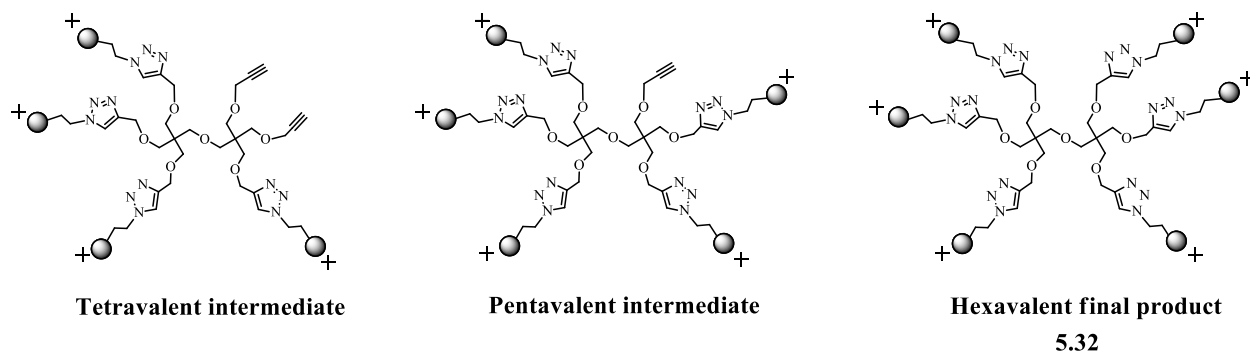
Scheme 5.14 The reaction between **5.8** and the hexavalent scaffold **2.24** afforded the desired hexacationic compound **5.32**, together with tetravalent and pentavalent intermediates.

A possible explanation of this behavior is the thermodynamic difficulty of forming an hexacationic species, probably due to electrostatic repulsion. Moreover, it is possible that the amino functions on the sugar coordinate and deactivate Cu(I), thus blocking the catalytic cycle. This last assumption would be true also using the derivative with the free amine, (Scheme **5.12C**). For these reasons, click chemistry was performed between multivalent scaffolds and monovalent ligands with the amine protected as Boc-derivative, i.e. compounds **5.18** and **5.28** (Scheme **5.12A**). Final compounds were purified by size exclusion chromatography and automated reverse phase chromatography when needed.

Compounds **5.18** and **5.28** reacted with the hexavalent scaffold **2.24** to afford hexavalent Boc-protected species (**5.33** and **5.38** respectively, Scheme **5.14**). The general procedure already explained in Chaper 2.4 was followed: 1.1 eq. of azide derivative per each triple bond; $CuSO_4*5H_2O$ (0.1 eq.), Sodium Ascorbate (0.4 eq.) and TBTA (0.2 eq.) were used in catalytic amount; reactions were performed in a 1:1 THF/H_2O mixture, under nitrogen atmosphere and in the dark at room temperature; final concentration of the scaffold was between 5 and 10 mM. Also in this case, the purity of scaffold **2.24** was always checked through TLC analysis immediately befor the reaction.
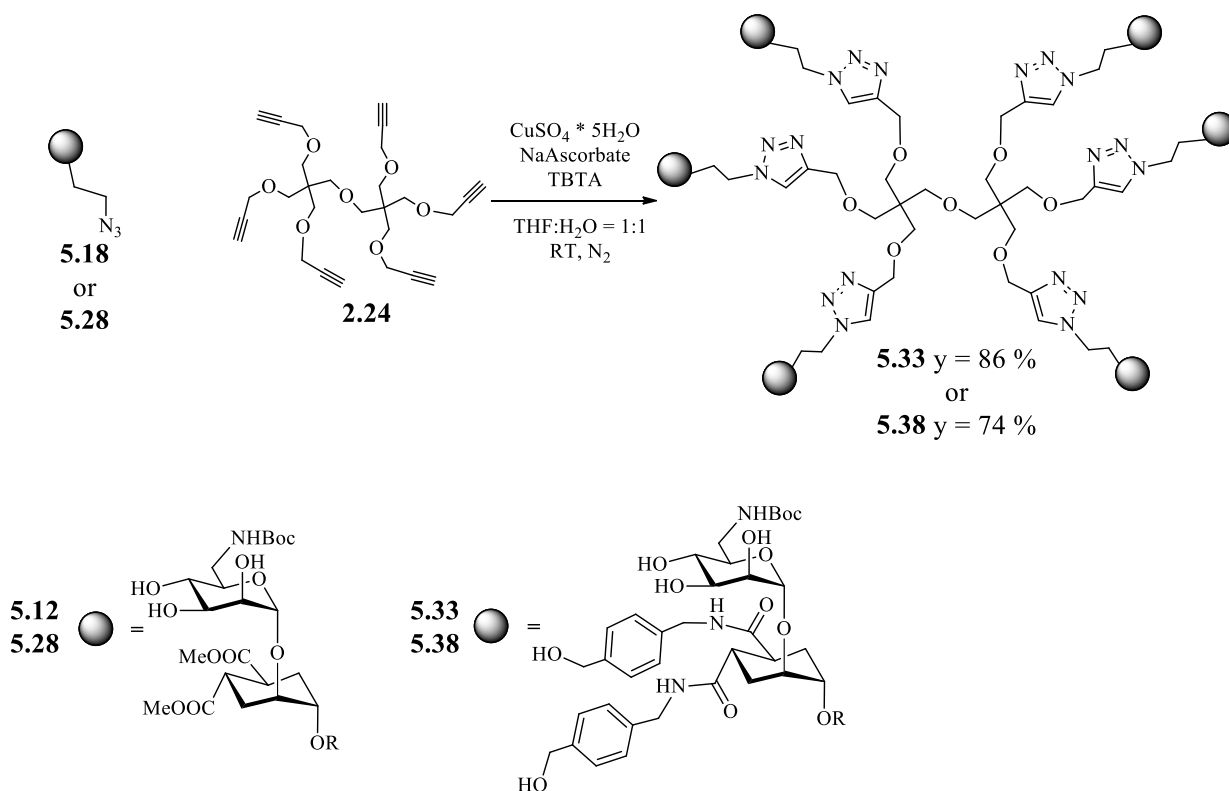
Scheme 5.14 General procedure to synthesise hexavalent derivatives **5.33** and **5.38**.

Analogous click reactions were conducted between **5.18** or **5.28** and **Rod3 (2.5**, Scheme **5.16)**. **Rod3 (2.5)** was formed *in situ*, after removal of triisopropylsilyl protecting group from compound **TIPS-Rod3 (TIPS-2.5)** and subsequently underwent the CuAAC reaction to give, respectively, compounds **5.35** or **5.41** (Scheme **5.16**).
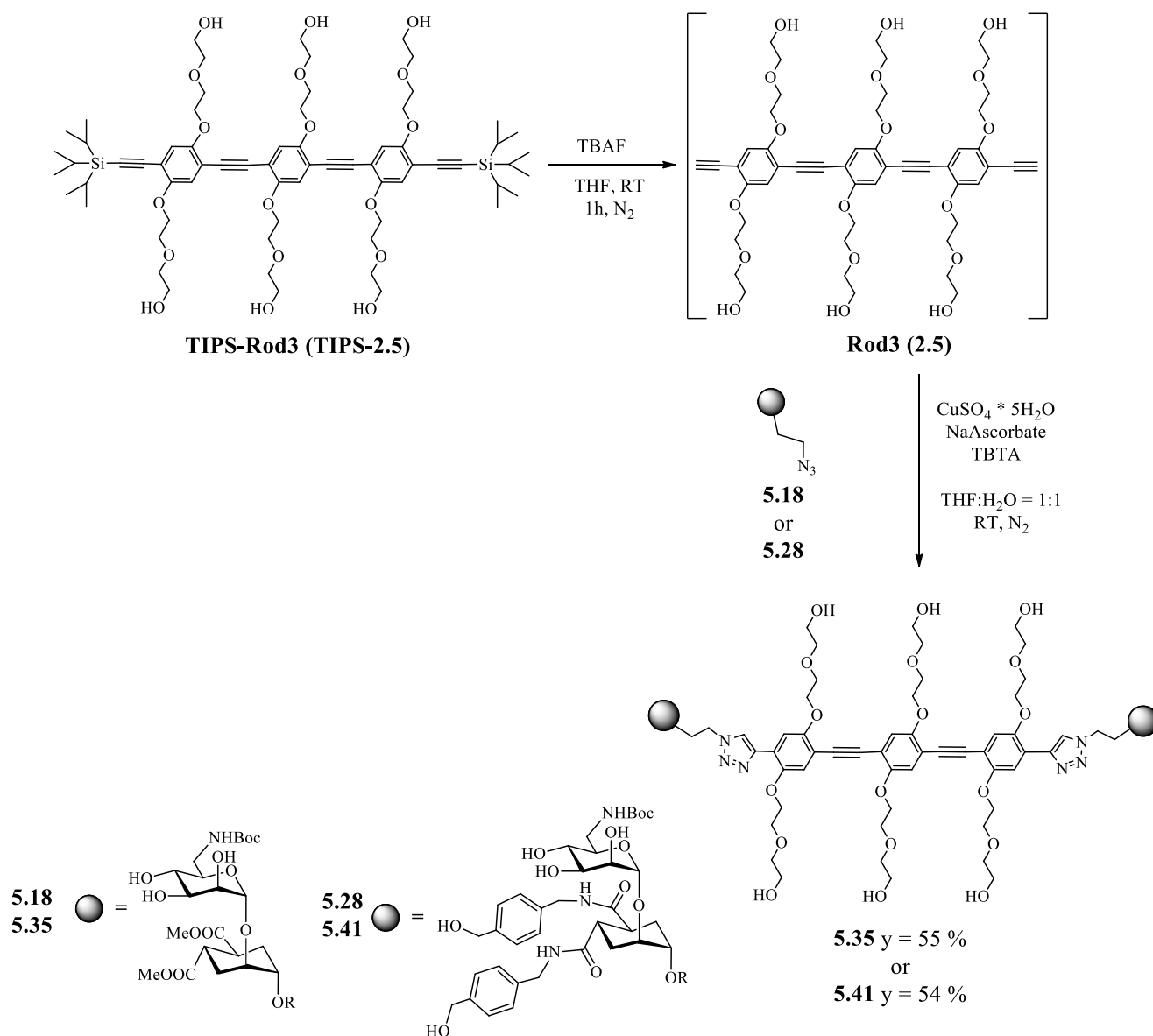
Scheme 5.15 General procedure to synthesise divalent Rod3 derivatives **5.35** and **5.41**.

As stated in Paragraph 5.3.1.1, the synthesis of the nonavalent derivative implies coupling between of three trivalent dendrons onto a central aromatic trivalent core. Only the nonavalent presentation of **5.2** was synthesised. The trivalent dendron **5.44** was produced by performing a click reaction between **5.28** and the trivalent core **2.27** (Scheme **5.16**). The terminal chloride was then replaced by an azido group through a chloride-azide reaction exchange. Obtained compound **5.44** underwent

then a further click reaction on scaffold **5.31** to give the desired nonavalent construct **5.46** (Scheme **5.16**).
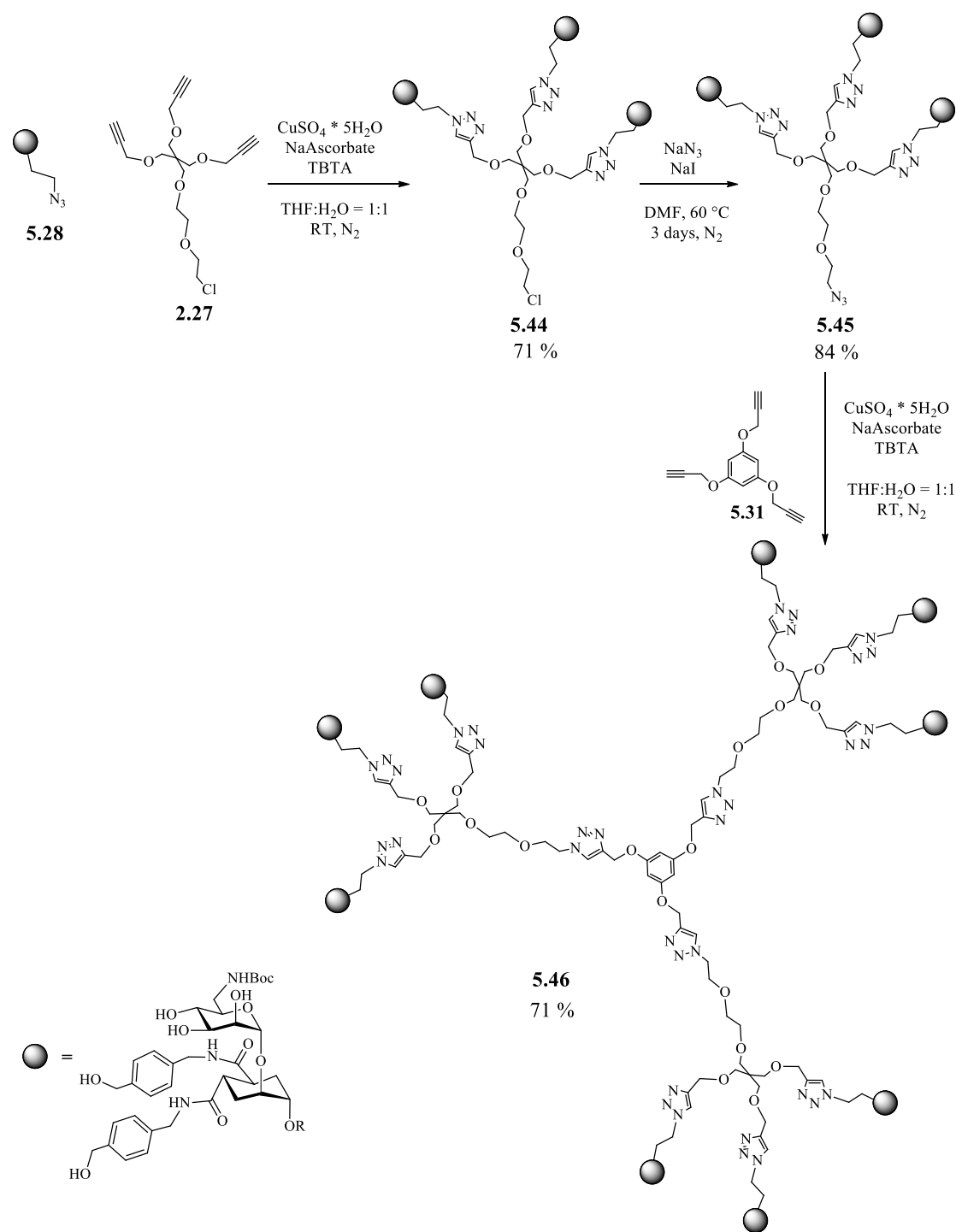
Scheme 5.16 General procedure to synthesise nonavalent **5.46**.

Boc- protecting groups were removed from the multivalent derivatives using trifluoroacetic acid in CH$_2$Cl$_2$ as solvent (TFA was used from 20 to 50 % v/v) Multivalent cationic compounds were obtained always with almost quantitative yields without any purification. The excess of TFA was

eliminated through co-evaporation with toluene and Et₂O (Scheme **5.17**). A deprotection reaction with HCl in dioxane did not afford the desired compound.
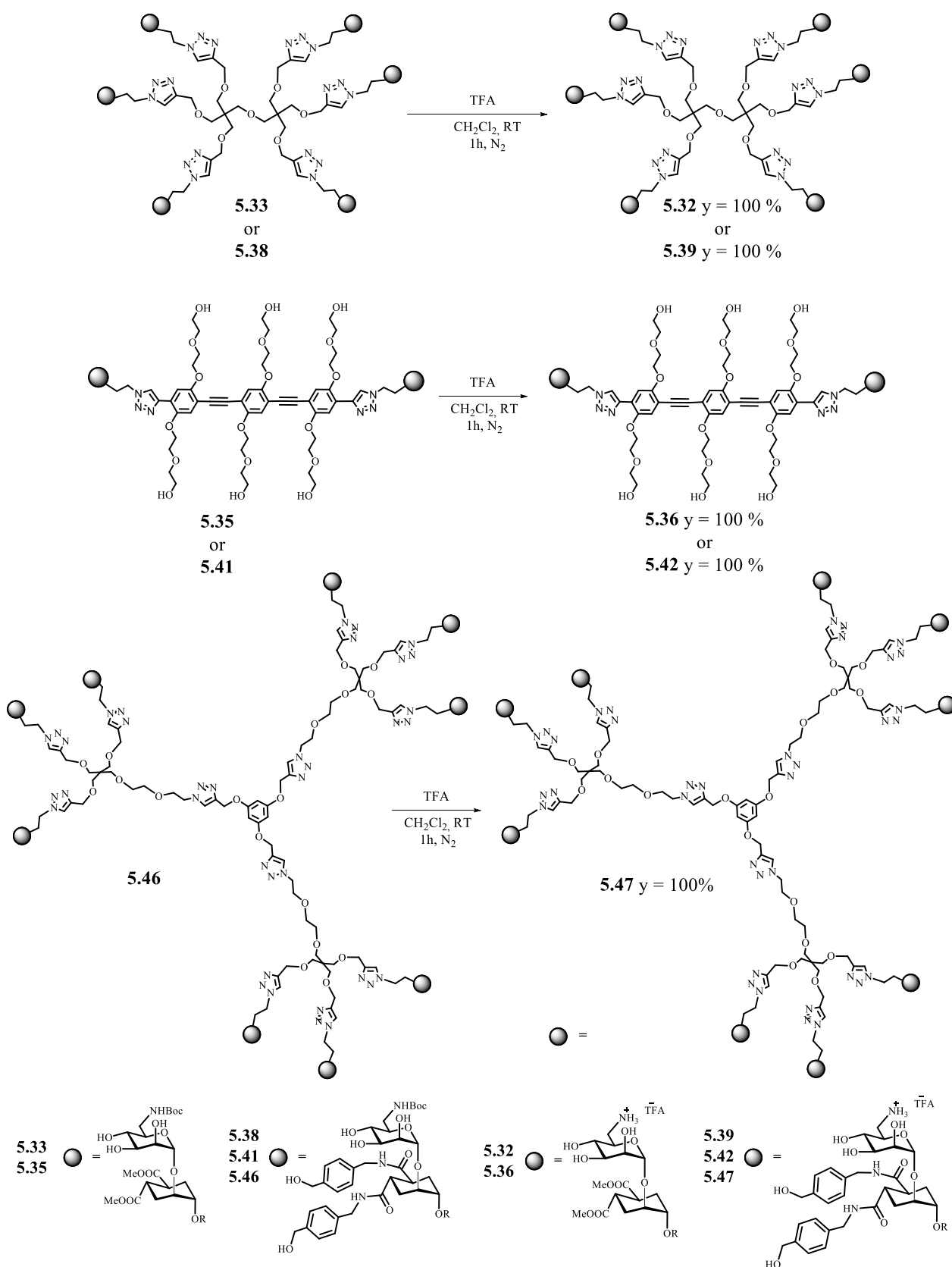
Scheme 5.17 General procedure for the Boc- removal in the presence of TFA in CH₂Cl₂.

The formation of the TFA-salt derivatives in **5.32** and **5.36** bearing ligand **5.8** was assessed by TLC analyses (developed with ninhydrin) and NMR analysis in MeOH. On the contrary, TLC analysis of **5.39**, **5.42** and **5.47** bearing ligand **5.9** was difficult to interpret and extensive NMR characterization was avoided, in order not to expose the compounds to nucleophiles (MeOD; D_2O). Therefore, only MALDI mass was used for characterization.

Remarkably, ^{1}H NMR spectra of cationic deprotected compounds sometimes showed signals splitting (Figure **5.6**), probably due to the presence of equilibriums in solution between species with either the free amine or the salt and/or between species with either neutral or protonated triazoles. MS spectra (MALDI) were consistent with a fully deprotected compound; the NMR spectra were not analyzed further.
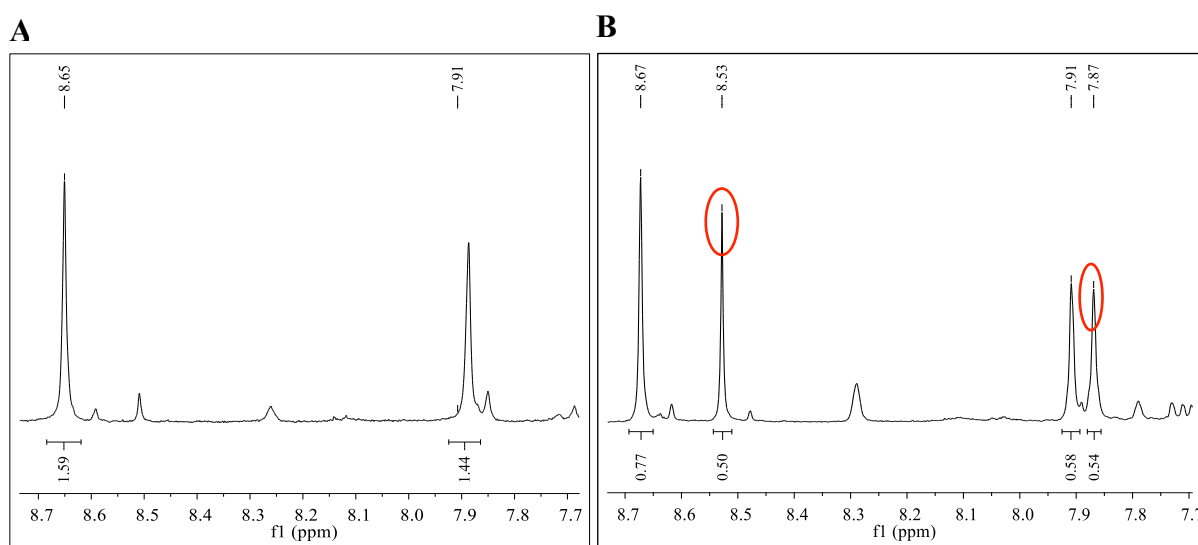

Figure 5.6 ^{1}H NMR spectra of **5.33** (Boc-derivative, A) and **5.32** (TFA-derivative, B) in MeOH zoomed in the aromatic region between 8.7 and 7.7 ppm. Red circles highlight new signals probably deriving from equilibriums between different species. Integrals were obtained by fixing to 4H a multiplet at 2.7 ppm.

The free amine functionalities were restored treating with an excess (> 10 eq. per each amine) of Amberlyst A21 (tertiary amine groups) [14] pre-washed with CH_2Cl_2, THF and finally MeOH. The reaction was shaken and not stirred, in order to avoid resin breaking; 3 h were arbitrarily chosen as reaction times (Scheme **5.18**). Remarkably, final nonavalent construct **5.48** had a rather low solubility in MeOH (< 300 nM).
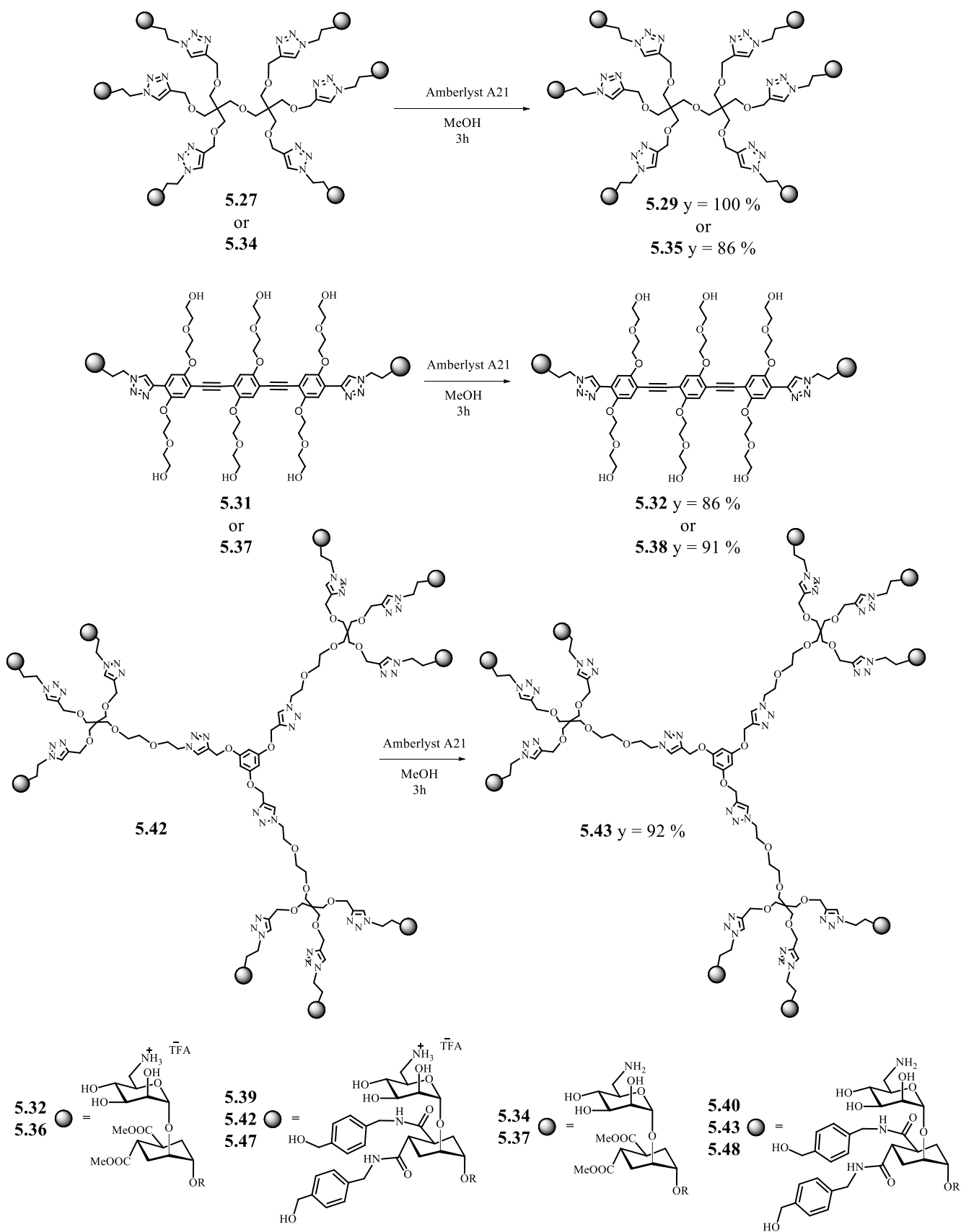
Scheme 5.18 General procedure for the TFA⁻ removal in the presence of Amberlyst A-21 in MeOH.

For **5.34** and **5.37**, bearing ligand **5.1**, it was possible to compare ^{1}H-NMR spectra (**5.32** or **5.36** before and **5.34** or **5.37** after the resin-based reaction exchange). The signals of the CH_2 group in the 6-position of the sugar moiety were slightly shifted in the two species, and their shape changed from sharper in the salt (**5.32** in Figure **5.6A**), to broader in the free amine (**5.34** in Figure **5.6B**). Moreover, trazole C-H signals that were found splitted in the salt derivatives (**5.32**) reverted to sharp singlets in **5.34** (Figure **5.6C**).
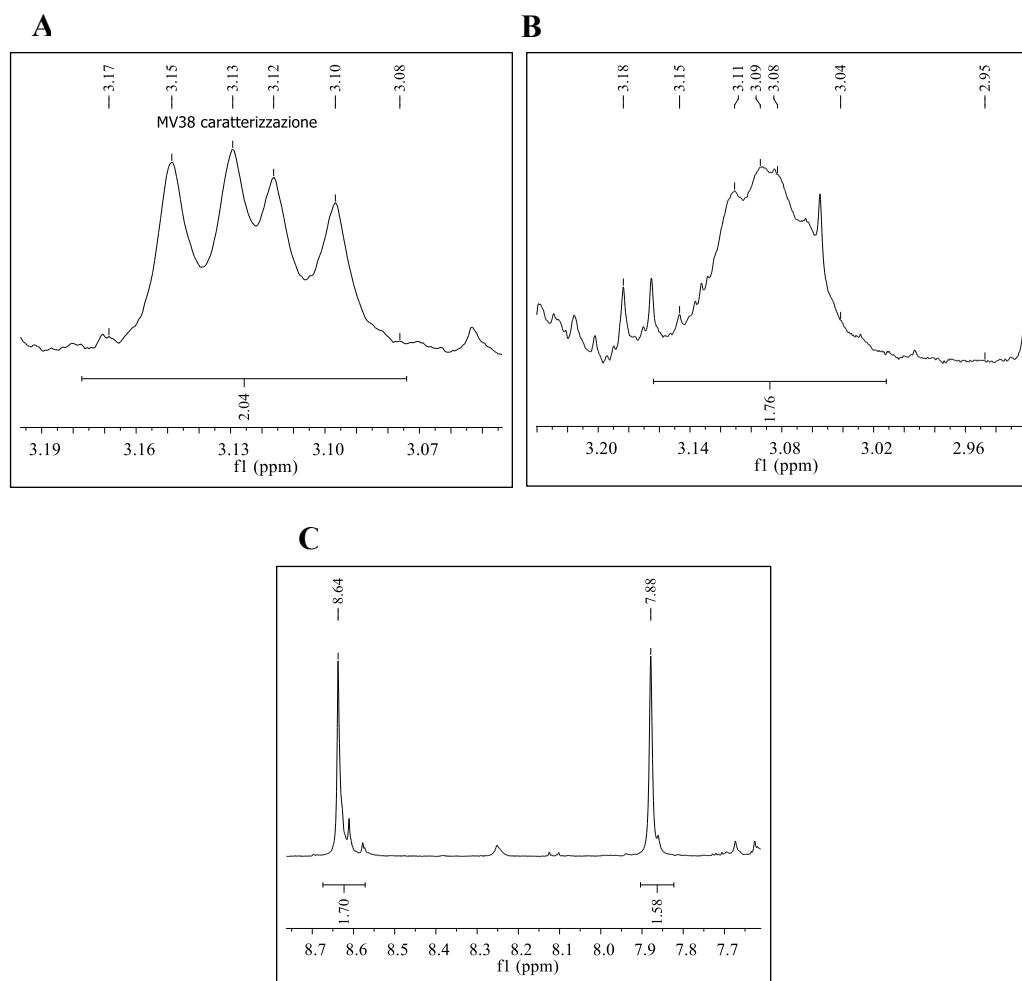

Figure 5.6 ^{1}H NMR spectra of **5.32** (TFA-derivative, A) and **5.34** (free amine, B) in MeOH zoomed on the CH_2 in the 6- position of the sugar moiety. (C) ^{1}H NMR spectrum of **5.34** in MeOH zoomed in the aromatic region between 8.7 and 7.7 ppm, showing single peaks not splitted anymore. Integrals were obtained by fixing to 4H a multiplet at 2.7 ppm.

5.3.2 Compounds nomenclature

Also this library of compounds was assigned a conventional name Polyman43-47-**PM43-47**. Structures of obtained compounds together with conventional names are reported in Table **5.4**
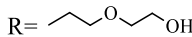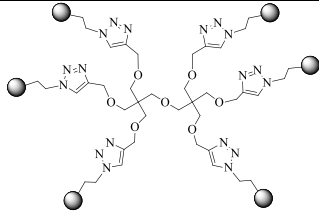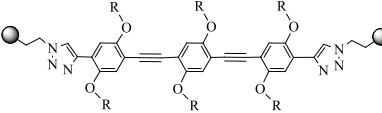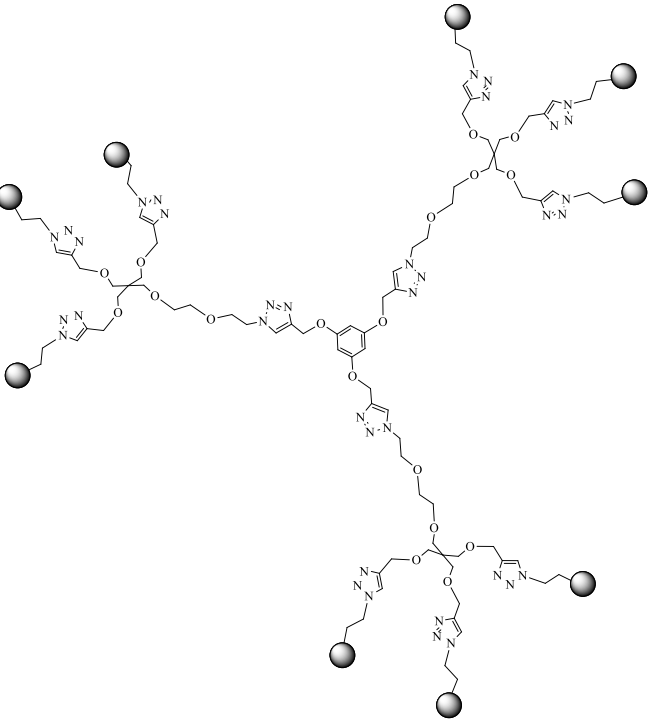
Structure	Ligand 5.1	Ligand 5.2
R= (structure)		
	5.34 *PM43*	5.40 *PM45*
	5.37 *PM44*	5.46 *PM46*
	///	5.48 *PM47*

Table 5.4 General structure of synthesised compounds, together with identification numbers and conventional names. Grey spheres represent monovalent ligands **5.1** or **5.2**.

5.3.3 Biological Assays

Biological analysis to be performed on 6-NH$_2$-derivatives are still on-going, with the aim to evaluate:

- Compounds affinity for DC-SIGN, through SPR assays
- Compounds affinity for Langherin (i.e. selectivity), through SPR assays
- Compounds ability to inhibit DC-SIGN-mediated HIV infection, through *trans*-infection inhibition assays performed of BTHP/DC-SIGN cells as Dendritic Cells model.

5.3.3.1 Citotoxicity

It is known that polycationic species can be cytotoxic.[15,16] They are able to neutralize the negatively-charged cell surface, thus inducing membrane damage which is followed by a decrease of the metabolic activity and cellular death. Cellular metabolic activity can be measured through i.e. the Method of Transcriptional and Translational (MTT) assay, which assesses the proper functionality of mithocondria, the principal cellular energy source. Once internalized, polycations can disrupt also the plasma, nuclear, mitrocondrial, endosomial and lysosomial membranes and they can interact with cytoskeleton elements. Multivalent *PM*s compounds bearing free amine groups are cationic once solubilized at physiological pH. For these reason, **5.34/PM43** was chosen to conduct preliminary cytotoxicity assays, performed by Dr. A. Berzi and Prof. M. Clerici (Università degli Studi di Milano) using the protocol described in Chapter 2.6.3.

The tests were performed by using B-THP-1 cells overexpressing DC-SIGN and belonging to the same cell line used for *trans*-infection inhibition assays (see Chapter 2.6.2). Cells were incubated together with **5.34** at different concentrations and after different times; the amount of dead cells was measured using the fluorescent dye 7-AAD. 3 hours and half and 72 hours were chosen because they are characteristic of the HIV-*trans* infection assays set up (see Chapter 2.6.2)

Results (Figure **5.8**) indicated that **5.34/PM43** is cytotoxic at concentrations ≥ 100 μM after 24 hours of incubation. Increasing incubation times, also lower concentrations (50 μM) were found to be toxic. Nevertheless, with respect to the behavior of the analogous compound bearing **1.9** as ligand,[12] we can assume that **5.34/PM43** would be active already at concentrations lower than 50 μM.
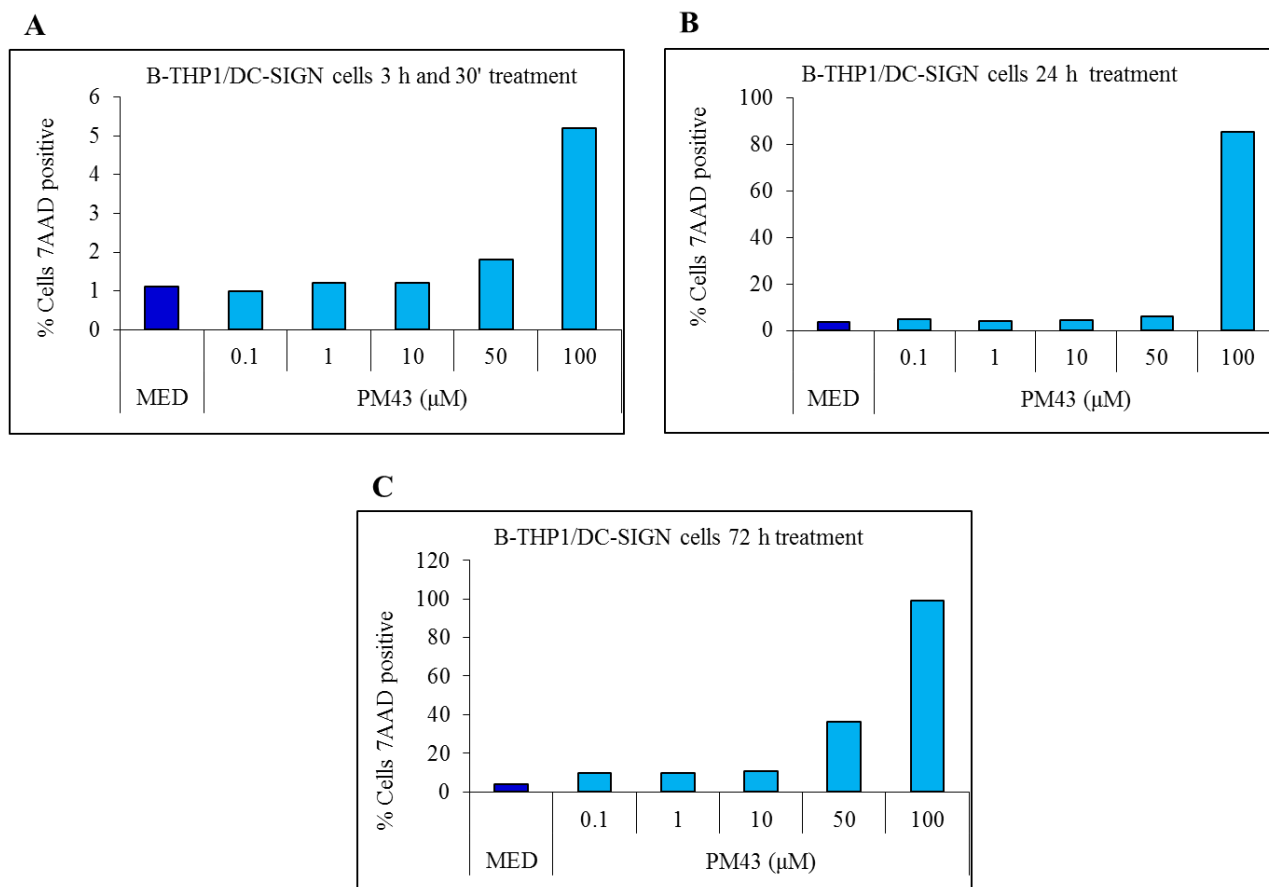
A

B

C

Figure 5.8 Percentage of dead cells (i.e. positive to the 7AAD dye) with respect to **5.34/PM43** concentration. Cytotoxicity was measure after 3 h and 30' (A), 24 h (B) and 72 h (C). MED represents the negative control, i.e. cells not treated with the compound.

5.4 Experimental

General procedures

Chemicals were purchased by commercial sources and used without further purification, unless otherwise indicated. When anhydrous conditions were required, the reactions were performed under nitrogen atmosphere. Anhydrous solvents were purchased from Sigma-Aldrich® with a content of water ≤0.005 %. THF was dried over Na/benzophenone and freshly distilled prior to use. Thin-layer chromatography (TLC) was performed on Silica Gel 60 F254 plates (Merck) with UV detection (254 nm and 365 nm) or using appropriate developing solutions. Flash column chromatography was performed on silica gel 230-400 mesh (Merck), according with the procedure described in literature.[17] Automated flash chromatography was performed on a Biotage® Isolera™ Prime system. Final compounds were purified by size-exclusion chromatography using Sephadex LH-20 from GE Helthcare Life Science® and through reverse phase automated flash chromatography (C18) when required. NMR experiments were recorded on a Bruker AVANCE 400 MHz instrument

at 298 K. Chemical shifts (δ) are reported in ppm downfield from TMS as internal standard, coupling constants (J) in Hz. The ^{1}H and ^{13}C-NMR resonances of compounds were assigned with the assistance of COSY and HSQC experiments. HSQC experiments were also used to assign the chemical shift of protons overlapping with the solvent signals. The numbering for protons and carbons in the NMR characterization are shown on the molecules. Mass spectra were recorded on ThermoFischer LCQ apparatus (ESI ionization), Apex II ICR FTMS (ESI ionization-HRMS), Waters Micromass Q-Tof (ESI ionization-HRMS), or Bruker Daltonics Microflex MALDI-TOF apparatus. Specific optical rotation values were measured using a Perkin-Elmer 241, at 589 nm in a 1 mL cell.

General procedure for the CuAAC reaction. In the optimized Copper(I)-catalyzed Azide-Alkyne Cycloaddition (CuAAC) procedure, starting materials and reagents were added to the reaction mixture as solids or as solutions in water or THF. Water was degassed by bubbling with nitrogen and THF was freshly distilled. The reagents were added to the reaction vessel in the following order: alkyne (1 eq., solid or THF), TBTA (0.2 eq., THF), $CuSO_4 \cdot 5H_2O$ (0.1 eq., H_2O), Sodium Ascorbate (0.4 eq., H_2O) and finally the azide monovalent ligand (1.1 eq. per each triple bond, solid or water solution). The final concentration of multivalent scaffold was 3-15 mM in a 1:1 THF:H_2O mixture, depending on the solubility of the components and the products in water. When a concentration $\geq$ 10 mM in 1:1 THF:H_2O could be obtained, the reaction was stirred at room temperature for 12 -24 hours, under nitrogen atmosphere and protected from light. For less soluble mixtures, the reaction was performed at lower concentrations (tipically 3 mM) under microwave assisted conditions for 1-2 h at 60 °C. In both cases, the reaction was monitored by TLC and/or MALDI mass spectrometry (DHB or sinapinic acid matrix) until completion. In general, the formation of divalent compounds could be monitored by TLC (eluent: CH_2Cl_2:MeOH:H_2O in a ration that depended on the polarity of the molecule) while hexavalent compounds were best analysed by MALDI mass (DHB or sinapinic acid matrix). When intermediates were observed but the azide monovalent ligand was totally consumed, the latter was added together with additional 0.4 eq. of sodium ascorbate. The crude was purified by size exclusion chromatography on a Sephadex LH20 column (Ø 3 cm, H 55 cm; eluent: MeOH) as MeOH solution and by reverse phase chromatography (C18; eluent: water with a gradient of MeOH from 0 % to 100 %), when required. The metal scavenger Quadrasil™-MP[18] was used to remove copper salts either from the reaction mixtures before purification, or from a solution of the isolated final compound. In either case, the suspension was stirred for 10 min and the resin filtered off.

Synthesis of 6-(*p*-toluensulfonyl)-D-mannopyranose, **5.10**

5.10
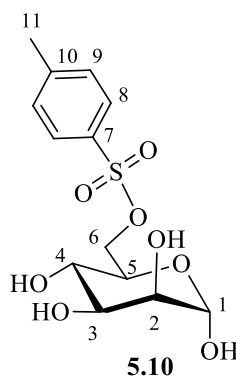
To a stirred suspension of D-mannose (4 g, 0.22 mol, 1 eq.) in 10 mL of dry pyridine, a solution of TsCl (6.35 g, 0.33 mol, 1.5 eq.) in 12 mL of dry pyridine was added drop by drop at 0°C under inert atmosphere, obtaining a light blue mixture. The reaction was stirred under nitrogen atmosphere for 2.5 h; TLC analysis (CH_2Cl_2:MeOH 8:2) revealed that the tosylation was complete. Pyridine was evaporated under reduced pressure and a dark green mixture was obtained; the crude was redissolved in CH_2Cl_2:MeOH 9:1 and purified over a sodium carbonate pad (Ø = 4 cm, h = 4 cm). The resulting solution was evaporated and purified again by flash chromatography (CH_2Cl_2:MeOH 9:1) to give 3.21 g of final product (**5.10**) as a white solid (yield 48 %). The α anomer was obtained, with spectral data identical to those reported.[8]

^{1}H-NMR (400 MHz, CD3OD): δ 7.80 (d, 2H, H_8, J_{8-9} =8.3 Hz), 7.43 (d, 2H, H_9, J_{8-9} = 8.3 Hz), 5.00 (d, 1H, H_1, J_{1-2} = 1.4 Hz), 4.39 - 4.23 (m, 1H, H_{6a}), 4.19 – 4.07 (m, 1H, H_{6b}), 3.93 - 3.82 (m, 1H, H_5), 3.75 (dd, 1H, H_2, J_{1-2} = 1.4 Hz, J_{3-2} = 3.3 Hz), 3.70 (dd, 1H, H_3, J_{3-4} = 9.3 Hz, J_{3-2} = 3.3 Hz), 3.51 (t, 1H, H_4, J_{3-4} = 9.3), 2.45 (s, 1H, H_{11}).

Synthesis of (1,2,3,4-*O*-tetrabenzoyl)-6-(*p*-toluensulfonyl)-D-mannopyranose, **5.13**

5.13
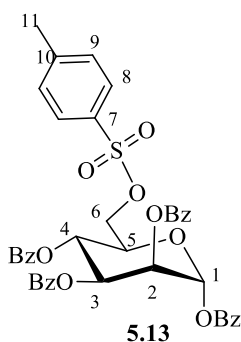
To a stirred solution of **5.10** (3.21 g, 9.59 mmol, 1 eq.) in 32 mL of dry pyridine, BzCl (10.78 g, 76.7 mmol, 8 eq.) and DMAP (0.117 g, 0.96 mmol, 0.1 eq.) were added under inert atmosphere at 0 °C, obtaining a yellow mixture. The room temperature was restored and the reaction was stirred for 18 h under nitrogen atmosphere; TLC analysis (Hex:AcOEt 8:2) revealed that the benzoylation was complete. The reaction was diluted with 90 mL of Et_2O and washed with HCl 1M (2 x 100 mL), $NaHCO_{3sol.\ sat.}$ (2 x 100 mL) and water (3 x 100 mL); the organic phase was dried over Na_2SO_4 anhydrous and the solvent was evaporated. The crude was purified by flash chromatography (silica, Hex:AcOEt 8:2) to give 5.31 g of final product (**5.13**) as a white solid (yield 74 %). The α anomer was obtained.

¹H-NMR (400 MHz, CDCl₃): δ 8.17-7.20 (m, 24H; H_{Bz}, H_9, H_{10}), 6.48 (d, 1H, H_1, J_{1-2} = 1.9 Hz), 5.98-5.96 (m, 2H, H_3, H_4), 5.80 (dd, 1H, J_{2-3} = 2.7, J_{1-2} = 1.9 Hz), 4.45-4.40 (m, 1H, H_5), 4.34 (dd, 1H, H_{6a}, J_{6a-6b} = 11.3, J_{6a-5} = 2.5 Hz), 4.25 (dd, H_{6b}, J_{6b-6a} = 11.3, J_{6b-5} = 4.8 Hz).

¹³C NMR (100 MHz, CDCl₃): δ 165.75, 165.33, 165.32, 163.83 (CO_{Bz}), 145.01 (C_7), 134.29, 133.96, 133.81, 133.63 (CH_{Bz}), 132.63 (C_{10}), 130.33, 130.24, 129.99, 129.94, 129.87 (CH_{Bz}, C_9), 129.03 (C_{quatBz}), 129.00, 128.92 (CH_{Bz}, C8), 128.86, 128.79, 128.76 (C_{quatBz}), 128.66, 128.58, 128.24 (CH_{Bz}), 91.14 (C_1), 71.20 (C_5), 69.89 (C_3), 69.44 (C_2), 67.79 (C_6), 66.24 (C_4), 21.78 (C_{11}).

MS (ESI): calculated for: $[C_{41}H_{34}O_{12}SNa]^+$ = 773.2, found: 773.5
Calculated for dimer: $[C_{82}H_{68}O_{24}S_2Na]^+$ = 1523.4, found: 1523.3

Synthesis of (1,2,3,4-*O*-tetrabenzoyl)-6-(azido)-D-6-deoxymannopyranose, 5.14

5.14
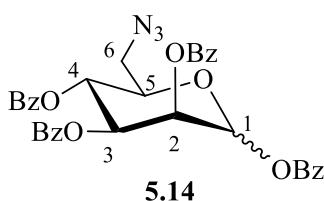
To a stirred solution of **5.13** (2.69 g, 3.46 mmol, 1 eq.) in 8 mL of dry DMA, NaN_3 (680 mg, 10.4 mmol, 3 eq.) and Bu_4NI (128 mg, 0.35 mmol, 0.1 eq.) were added under inert atmosphere, obtaining a not completed dissolved reddish reaction mixture. The reaction was heated at 60 °C and stirred overnight; TLC analysis (Hex:AcOEt 7:3) revealed that the reaction was complete. The solvent was concentrated under reduced pressure to 4 mL. The crude was dissolved in 20 mL of Et_2O and washed with water (3 x 20 mL); then the organic phase was dried over Na_2SO_4 anhydrous and the

solvent evaporated. The crude was purified by flash chromatography (silica, Hex:AcOEt 9:1) to give 1.57 g of final product (**5.14**) as a white solid (yield 72 %). Obtained ratio of two anomers: β/α = 0.58.

^{1}H-NMR (400 MHz, CDCl$_3$):

<u>α anomer</u>: δ 8.20 – 7.20 (m, 20H, H$_{Bz}$), 6.60 (d, 1H, H$_1$, J_{1-2} = 2.0 Hz), 6.05 – 6.00 (m, 1H, H$_4$), 5.88 – 5.85 (m, 1H, H$_2$), 5.74 – 5.63 (m, 1H, H$_3$), 4.41 – 4.34 (m, 1H, H$_5$), 3.55 – 3.41 (m, 2H, H$_{6a}$, H$_{6b}$).

<u>β anomer</u>: δ = 8.20 – 7.20 (m, 20H, H$_{Bz}$), 6.36 (d, 1H, H$_1$, J_{1-2} = 1.1 Hz), 6.07 (dd, 1H, H$_2$, J_{1-2} = 1.1 Hz, J_{3-2} = 3.2 Hz), 5.94 (pt, 1H, H$_4$, J_{4-3} = J_{4-5} = 9.8 Hz), 5.75 (dd, 1H, H$_3$, J_{3-4} = 9.8 Hz, J_{3-2} = 3.2), 4.20 – 4.13 (m, 1H, H$_5$), 3.61 (dd, 1H, H$_{6a}$, J_{5-6a} = 2.8 Hz, J_{6a-6b} = 13.5 Hz), 3.53 (dd, 1H, H$_{6b}$, J_{5-6a} = 5.5 Hz, J_{6a-6b} = 13.5 Hz).

^{13}C NMR (100 MHz, CDCl$_3$):

<u>α anomer</u>: δ = 165.9, 165.6, 165.6, 164.3 (CO$_{Bz}$); 134.3, 133.9, 133.8, (CH$_{Bz}$); 130.8, 130.4, 130.3, 130.0 (CH$_{Bz}$); 129.5 (Cquat$_{Bz}$); 129.1, 129.0 (CH$_{Bz}$); 128.8 (Cquat$_{Bz}$); 128.8, 128.6 (CH$_{Bz}$); 91.4 (C$_1$); 74.9 (C$_5$); 69.5 (C$_4$); 68.6 (C$_3$); 67.2 (C$_2$); 51.1 (C$_6$).

<u>β anomer</u>: δ = 165.9, 165.6, 165.6, 164.3 (CO$_{Bz}$); 134.0, 133.9, 133.8, 133.7 (CH$_{Bz}$); 130.4, 130.3, 130.0 (CH$_{Bz}$); 129.5 (Cquat$_{Bz}$); 128.9, 128.8 (CH$_{Bz}$); 128.8 (Cquat$_{Bz}$); 128.7, 128.6 (CH$_{Bz}$); 91.3 (C$_1$); 74.9 (C$_5$); 71.5 (C$_3$); 69.5 (C$_2$); 67.3 (C$_4$); 51.1 (C$_6$).

MS (ESI) calculated for: $[C_{34}H_{27}N_3O_9Na]^+$: 644.6, found: 644.3.

**Synthesis of (2,3,4-*O*-tribenzoyl)-6-(azido)-D-6-deoxymannopyranose, 5.15**
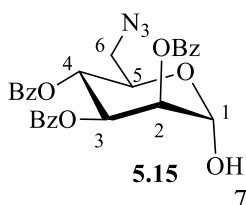
To a stirred solution of **5.15** (1.01 g, 1.62 mmol, 1 eq.) in 4.6 mL of dry THF, MeNH$_2$ (0.8 mL, 6.48 mmol, 4 eq.) was added under inert atmosphere at 0 °C. After 1 h of stirring, a TLC analysis (Hex:AcOEt 7:3) revealed that the debenzoylation of the anomeric hydroxyl group was complete. The solvent and methyl amine were evaporated and the crude was purified by flash chromatography

(silica, Hex:AcOEt 8:2) to give 783 mg of final product (**5.15**) as a light yellow solid (yield 93 %). Only the α anomer was obtained; with spectral data identical to those reported.[8]

¹H-NMR (400 MHz, CDCl₃): δ 8.13 – 8.04 (m, 2H, H$_{Bz}$), 8.00 – 7.90 (m, 2H, H$_{Bz}$), 7.87 – 7.75 (m, 2H, H$_{Bz}$), 7.67– 7.56 (m, 1H, H$_{Bz}$), 7.55 – 7.45 (m, 3H, H$_{Bz}$), 7.43 – 7.32 (m, 3H, H$_{Bz}$), 7.29 – 7.18 (m, 2H, H$_{Bz}$), 5.96 (dd, 1H, H₃, J_{3-4} = 10.0 Hz, J_{3-2}= 3.3), 5.87 (pt, 1H, H₄, J_{4-3} = J_{4-5}= 10.0 Hz), 5.71 (dd, 1H, H₂, J_{1-2} = 1.6 Hz, J_{3-2} = 3.3 Hz), 5.52 (d, 1H, H₁, J_{1-2} = 1.6 Hz), 4.54 – 4.43 (m, 1H, H₅), 3.51 – 3.45 (m, 2H, H$_{6a,b}$), 3.35 (bs, 1H, H₇).

Synthesis of (1*S*,2*S*,4*S*,5*S*) (2,3,4-*O*-tribenzoyl)-6-(azido)-D-6-deoxymannopyranosyl trichloroacetoimidate, 5.3
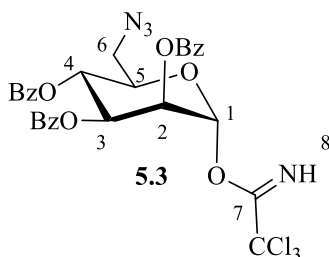
To a stirred solution of **5.15** (786 mg, 1.52 mmol, 1 eq.) in 5.1 mL of dry CH₂Cl₂, freshly distilled Cl₃CCN (0.762 mL, 7.60 mmol, 5 eq.) and DBU (45 μL, 0.30 mmol, 0.2 eq.) were added under inert atmosphere. After 2 h of stirring at room temperature, a TLC analysis (Hex:AcOEt 7:3) revealed that the formation of the trichloroacetoimidate was completed. The solvent was evaporated and the crude was purified by flash chromatography (silica, Hex:AcOEt 8:2) to give 567 mg of final product (**5.3**) as a light yellow solid (yield 71 %). Only α anomer was obtained, with spectral data identical to those reported.[8]

¹H-NMR (400 MHz, CDCl₃): δ 8.88 (s, 1H, H₈), 8.13 – 8.08 (m, 2H, H$_{Bz}$), 7.97 – 7.93 (m, 2H, H$_{Bz}$), 7.83 – 7.78 (m, 2H, H$_{Bz}$), 7.65 – 7.59 (m, 1H, H$_{Bz}$), 7.55 – 7.46 (m, 3H, H$_{Bz}$), 7.45 – 7.33 (m, 3H, H$_{Bz}$), 7.29-7.22 (m, 2H, H$_{Bz}$), 5.56 (d, 1H, H1, J_{1-2} = 1.8 Hz), 5.99 (pt, 1H, H₄, J_{4-3} = J_{4-5} = 9.8 Hz), 5.95-5.86 (m, 2H, H₂, H₃), 4.48 – 4.41 (m, 1H, H₅), 3.54 (dd, 1H, H$_{6a}$, J_{5-6a} = 2.8 Hz, J_{6a-6b} = 13.6 Hz), 3.49 (dd, 1H, H$_{6b}$, J_{5-6a} = 5.4 Hz, J_{6a-6b}= 13.6 Hz).

Synthesis of (1*S*,2*S*,4*S*,5*S*) 1,2-Cyclohexanedicarboxylic acid, 4-(2-chloroethoxy)-5-((2,3,4-*O*-tribenzoyl)-6-azido-α-D-6-deoxymannopyranosyloxy)-1,2-dimethyl ester, 5.6

5.6
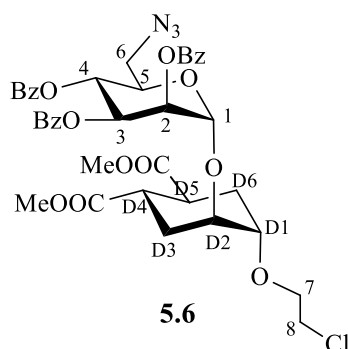
5.4 (127 mg, 0.43 mmol, 1 eq.) and **5.3** (314 mg, 0.47 mmol, 1.1 eq.) were coevaporated with toluene 3 times. Under inert atmosphere, molecular sieves (4Å) were added and the mixture was kept under vacuum overnight. Then the mixture was dissolved under inert atmosphere in 4.3 mL of dry CH_2Cl_2 and cool down at -30°C. Finally, TMSOTf (16 μL, 0.09 mmol, 0.2 eq.) was added drop by drop, and the reaction was stirred for 1 h. A TLC analysis (Hex:AcOEt 7:3) revealed that the glycosylation reaction was complete. The reaction was quenched by the addition of dry Et_3N (200 μL) and stirred for other 15 min. Restored the room temperature, the mixture was filtered over celite pad and the solvent evaporated; the crude was purified by flash chromatography (silica, Hex with gradient of AcOEt from 0 % to 50 %) to give 291 mg of final product α-anomer (**5.6**) as a white solid (yield 85 %). Spectral data were identical to those reported.[8]

^{1}H-NMR (400 MHz, CDCl₃): δ 8.1 – 8.05 (m, 2H, H_{Bz}), 7.99 – 7.89 (m, 2H, H_{Bz}), 7.83 – 7.74 (m, 2H, H_{Bz}), 7.65 – 7.56 (m, 1H, H_{Bz}), 7.55 – 7.46 (m, 3H, H_{Bz}), 7.45 – 7.33 (m, 3H, H_{Bz}), 7.29 –7.17 (m, 2H, H_{Bz}), 5.84 – 5.76 (m, 2H, H_3, H_4), 5.66 (dd, 1H, H2, $J_{2\text{-}1}$ = 1.9 Hz, $J_{2\text{-}3}$ = 2.7 Hz), 5.24 (d, 1H, H_1, $J_{1\text{-}2}$ = 1.6 Hz), 4.29 (pt, 1H, H_5, $J_{6a\text{-}5}$ = $J_{5\text{-}4}$ = 7.2 Hz), 4.06 (dd, 1H, H_{D2}, $J_{D1\text{-}D2}$ = 4.0 Hz, $J_{D2\text{-}3 \text{ or } 6}$ = 7.8 Hz), 3.93 – 3.83 (m, 1H, H_{7a}), 3.81 – 3.67 (m, 8H, H_{7b}, H_2, H_{10}), 3.63 (t, 2H, H_8, $J_{8\text{-}7}$ = 5.77 Hz), 3.57 (dd, 1H, H_{6a}, $J_{6b\text{-}5}$ = 7.2 Hz, $J_{6a\text{-}6b}$ = 13.3 Hz), 3.40 (dd, 1H, H_{6a}, $J_{6b\text{-}5}$ = 2.3 Hz, $J_{6a\text{-}6b}$ = 13.3 Hz), 3.13 - 3.00 (m, 2H, H_{D4}, H_{D5}), 2.17 – 1.97 (m, 4H, H_{D3}, H_{D6}).

Synthesis of (1*S*,2*S*,4*S*,5*S*) 1,2-Cyclohexanedicarboxylic acid, 4-(2-chloroethoxy)-5-(6-azido-α-D-deoxymannopyranosyloxy)-1,2-dimethyl ester, 5.16

5.16
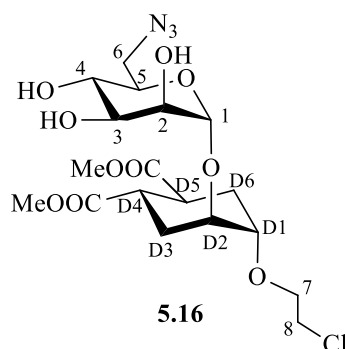
To a stirred suspension of **5.6** (269 mg, 0.34 mmol, 1 eq.) in 3.4 mL of dry MeOH, 1 M MeONa in MeOH (500 μL, 0.51 mmol, 1.5 eq.) was added under inert atmosphere. Only after the addition of the base, the starting material **5.6** fully dissolved. The reaction was stirred for 1.5 h under inert atmosphere. A TLC analysis (CHCl$_3$:MeOH 95:5) revealed that the debenzoylation reaction was complete. The reaction was quenched by the addition of Amberlite IR120 H$^+$ until pH 7 was reached and then filtered; ìthe filtrate was concentrated and the crude was purified by flash chromatography (silica, CHCl$_3$:MeOH 95:5) to give 157 mg of final product (**5.16**) as a colourless oil (yield 96%). Spectral data were identical to those reported.[8]

^{1}H-NMR (400 MHz, CD$_3$OD): δ 4.95 (d, 1H, H$_1$, $J_{1\text{-}2}$ = 1.6 Hz), 4.03 – 3.99 (m, 1H, H$_{D2}$), 3.94–3.89 (m, 1H, H$_{6a}$), 3.88 – 3.76 (m, 4H, H$_2$, H$_3$, H$_7$), 3.75 – 3.71 (m, 1H, H$_{D1}$), 3.71 - 3.64 (m, 9H, H$_8$, H$_5$, H$_{10}$), 3.61 – 3.54 (m, 1H, H$_4$), 3.51 (dd, 1H, H$_{6a}$, $J_{6a\text{-}6b}$ = 13.0 Hz, $J_{6a\text{-}5}$ = 2.1 Hz), 3.43 (dd, 1H, H$_{6a}$, $J_{6a\text{-}6b}$ = 13.0 Hz, $J_{6a\text{-}5}$ = 8.1 Hz), 3.00 – 2.81 (m, 2H, H$_{D4}$, H$_{D5}$), 2.21 - 1.94 (m, 2H, H$_{D3ax}$, H$_{D6ax}$), 1.94 – 1.72 (m, 2H, H$_{D3eq}$, H$_{D6eq}$).

Synthesis of (1*S*,2*S*,4*S*,5*S*) 1,2-Cyclohexanedicarboxylic acid, 4-(2-chloroethoxy)-5-(6-*N*-carbo-*t*-butoxy-α-D-6-deoxymannopyranosyloxy)-1,2-dimethyl ester, 5.17

5.17
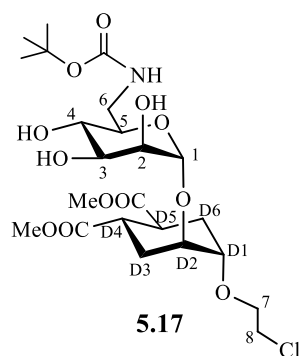
To a stirred solution of **5.16** (155 mg, 0.32 mmol, 1 eq.) in 32 mL of dry MeOH, Boc$_2$O (105 mg, 0.48 mmol, 1.5 eq.) and Pd-C (catalytic) were added under inert atmosphere. The mixture was stirred for 3 h under hydrogen atmosphere. A TLC analysis (CHCl$_3$:MeOH 95:5) revealed that the reaction was complete. The mixture was filtered over a celite pad and the solvent was evaporated; the crude was purified by flash chromatography (silica, CHCl$_3$ with a gradient of MeOH from 2 % to 5 %) to give 142 mg of final product (**5.17**) as a colourless oil (yield 80 %). Spectral data were identical to those reported.[8]

^{1}H-NMR (400 MHz, CD$_3$OD): δ 4.90 (d, 1H, H$_1$, $J_{1\text{-}2}$ = 1.6 Hz), 4.98 – 3.93 (m, 1H, H$_{D2}$), 3.85–3.74 (m, 3H, H$_2$, H$_7$), 3.72 – 3.62 (m, 10H, H$_{10}$, H$_{D1}$, H$_8$, H$_3$), 3.62 – 3.45 (m, 3H, H$_4$, H$_5$, H$_{6a}$), 3.19 (dd, 1H, H$_{6b}$, $J_{6a\text{-}6b}$ = 13.3 Hz, $J_{6a\text{-}5}$ = 5.1 Hz), 2.97 – 2.78 (m, 2H, H$_{D4}$, H$_{D5}$), 2.14 - 1.98 (m, 2H, H$_{D3ax}$, H$_{D6ax}$), 1.86 – 1.71 (m, 2H, H$_{D3eq}$, H$_{D6eq}$) , 1.44 (s, 9H, *t*Bu).

Synthesis of (1*S*,2*S*,4*S*,5*S*) 1,2-Cyclohexanedicarboxylic acid, 4-(2-azidoethoxy)-5-(6-*N*-carbo-*t*-butoxy-α-D-6-deoxymannopyranosyloxy)-1,2-dimethyl ester, 5.18


5.18
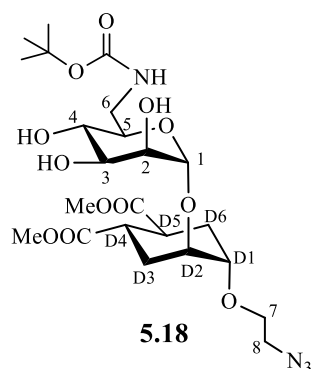
To a stirred solution of **5.17** (132 mg, 0.24 mmol, 1 eq.) in 3 mL of dry DMF, NaI (3.6 mg, 0.024 mmol, 0.1 eq.) and NaN$_3$ (77 mg, 1.18 mmol, 5 eq.) were added under inert atmosphere at room temperature. The reaction was heated to 50 °C and stirred for 3 days. ^{1}H-NMR analysis assessed the completion of the reaction. The solvent was evaporated and the crude was purified with flash chromatography (silica, CHCl$_3$:MeOH 95:5) to give 117 mg of final product (**5.18**) as a colourless oil (yield 88 %). Spectral data were identical to those reported.[8]

^{1}H-NMR (400 MHz, CD$_3$OD): δ 4.84 (d, 1H, H$_1$, $J_{1\text{-}2}$ = 1.6 Hz), 3.93 – 3.89 (m, 1H, H$_{D2}$), 3.78 – 3.77 (m, 1H, H$_2$), 3.74 – 3.64 (m, 2H, H$_7$), 3.65 – 3.55 (m, 8H, H$_{10}$, H$_{D1}$, H$_3$), 3.51 – 3.36 (m, 3H, H$_4$, H$_5$, H$_{6a}$), 3.31 (t, 2H, H$_8$, $J_{7\text{-}8}$ = 4.7 Hz), 3.12 (dd, 1H, H$_{6b}$, $J_{6a\text{-}6b}$ = 13.5 Hz, $J_{6a\text{-}5}$ = 5.4 Hz), 2.90

– 2.72 (m, 2H, H$_{D4}$, H$_{D5}$), 2.08 - 1.92 (m, 2H, H$_{D3ax}$, H$_{D6ax}$), 1.80 – 1.63 (m, 2H, H$_{D3eq}$, H$_{D6eq}$), 1.46 (s, 9H, *t*Bu).

Synthesis of (1*S*,2*S*,4*S*,5*S*) 1,2-Cyclohexanedicarboxylic acid, 4-(2-azidoethoxy)-5-(6-*N*-amino-α-D-6-deoxymannopyranosyloxy)-1,2-dimethyl ester, 5.8

5.8
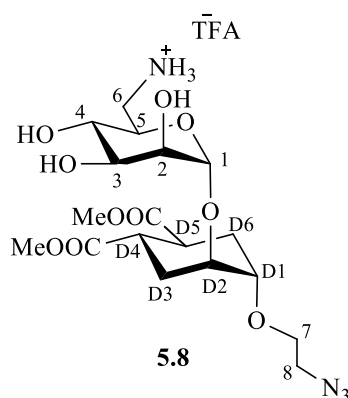
Compound **5.18** (52.3 mg, 0.094 mmol, 1 eq.) was dissolved in CH$_2$Cl$_2$ (3.7 mL); TFA (1.2 mL, 166 eq.) was added. The resulting solution was stirred at room temperature for 1h. TLC analysis (CHCl$_3$:MeOH 85:15) revealed that the reaction was complete. The solvent was removed under reduce pressure; the crude was washed and dried twice with diethyl ether. 54.4 mg of **5.8** were obtained as a white solid (yield 100 %). Spectral data were identical to those reported.[8]

^{1}H-NMR (400 MHz, CD$_3$OD): δ 4.98 (d, 1H, H$_1$, J_{1-2} = 1.6 Hz), 4.04 – 3.89 (m, 1H, H$_{D2}$), 3.87 (dd, 1H, H$_2$, J_{1-2} = 1.6 Hz, J_{3-2} = 3.0 Hz), 3.82 – 3.76 (m, 1H, H$_{7a}$), 3.74 – 3.63 (m, 9H, H$_{10}$, H$_{D1}$, H$_3$, H$_{7b}$), 3.63 – 3.50 (m, 2H, H$_4$, H$_5$), 3.42 – 3.34 (m, 2H, H$_8$), 3.19 (dd, 1H, H$_{6a}$, J_{6a-6b} = 13.2 Hz, J_{6a-5} = 2.6 Hz), 3.04 – 2.79 (m, 3H, H$_{6b}$, H$_{D4}$, H$_{D5}$), 2.20 – 2.00 (m, 2H, H$_{D3ax}$, H$_{D6ax}$), 1.88 – 1.70 (m, 2H, H$_{D3eq}$, H$_{D6eq}$).

**Synthesis of (1*S*,2*S*) 4-cyclohexene-1,2-dicarboxylic acid bis(*p*-nitro-phenylester), 5.20**

5.20
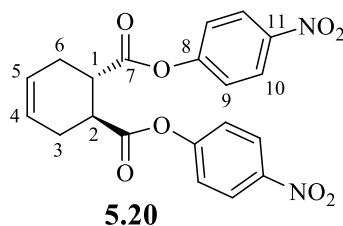
To a solution of (1S,2S)-4-Cyclohexane-1,2-dicarboxylic acid,(+) **5.19** (1.27 g, 7.5 mmol, 1 eq.) in dry THF (75 mL) under nitrogen atmosphere, EDC-HCl (5.0 g, 26.1 mmol, 3.5 eq.) was added. After 10 minutes, *p*-nitrophenol (3.13 g, 22.5 mmol, 3 eq.) was added. The solution was stirred at room temperature for 2 h. TLC analysis (Hex:AcOEt 6:4) revealed that the reaction was complete. The solvent was removed under reduce pressure and the crude was taken up in AcOEt (240 mL). The organic phase was washed with 1M HCl (2 x 120 mL), NaHCO$_3$ $_{sat.sol.}$ (0 °C, 2 x 100 mL) and H$_2$O (2 x 120 mL) and the dried over Na$_2$SO$_4$ anhydrous. The crude was concentrated under reduced pressure to obtain 1.95 g **5.20** as a pale yellow solid (yield 62 %).

^{1}H NMR (400 MHz, CDCl$_3$): δ = 8.26-8.24 (m, 4H, H$_{10}$); 7.26-7.23 (m, 4H, H$_9$); 5.83 (d, *J* = 3.0 Hz, 2H, H$_4$, H$_5$); 3.24-3.21 (m, 2H, H$_1$, H$_2$); 2.78-2.68 (m, 2H, H$_{3ps-eq}$, H$_{6ps-eq}$); 2.47-2.36 (m, 2H, H$_{3ps-ax}$, H$_{6ps-ax}$).

^{13}C NMR (CDCl$_3$): δ = 172,6, 171,5 (C$_7$); 155.4 (C$_{11}$); 145.7 (C$_8$); 125.5 (C$_{10}$); 124.9 (C5, C$_4$); 122.5 (C$_9$); 41.5 (C$_1$, C$_2$); 28.0 (C$_3$, C$_6$).

[α]$_D$^{25}: +129.6 (c = 1 in CHCl$_3$)

Synthesis of (3*S*,4*S*) 7-Oxabicyclo [4.1.0]heptane-3,4-dicarboxylic acid bis(*p*-nitro-phenyl-ester), 5.21
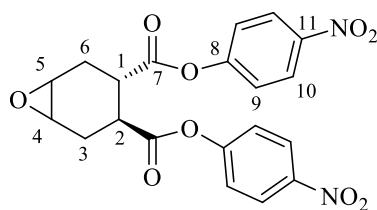
5.21

Compound **5.20** (1.9 g, 4.65 mmol, 1 eq.) was dissolved in dry CH$_2$Cl$_2$ (16 mL). 77 % *m*CPBA (1.3 g, 5.8 mmol effective, 1.2 eq.) was added. The solution was stirred at room temperature under nitrogen atmosphere overnight. TLC analysis (Hex:AcOEt 6:4) revealed that the reaction was complete. The organic phase was washed with NaHCO$_3$ $_{sat.\ sol.}$ (2 x 60 mL), H$_2$O (60 mL) and brine (60 mL) and then dried over Na$_2$SO$_4$ anhydrous. The crude was concentrated under pressure, to obtain 2.05 g of **5.21** as a pale yellow solid (yield 100 %).

^{1}H NMR (400 MHz, CDCl$_3$): δ = 8.28-8.23 (m, 4H, H$_{10}$); 7.30-7.25 (m, 4H, H$_9$); 3.46-3.44 (m, 1H, H$_4$ or H$_5$); 3.40-3.38 (m, 1H, H$_4$ or H$_5$); 3.37-3.27 (m, 1H, H$_1$ or H$_2$); 3.16-3.04 (m, 1H, H$_1$ or H$_2$);

2.85-2.75 (m, 1H, H$_{3eq}$ or H$_{6eq}$); 2.64 (m, 1H, H$_{3eq}$ or H$_{6eq}$); 2.46-2.37 (m, 1H, H$_{3ax}$ or H$_{6ax}$); 2.26-2.16 (m, 1H, H$_{3ax}$ or H$_{6ax}$).

^{13}C NMR (100 MHz, CDCl$_3$): δ = 172.6, 171.5 (C$_7$); 155.4, 155.3 (C$_8$); 149.9 (C$_{11}$); 125.5 (C$_{10}$); 122.5, 122,6 (C$_9$); 51.8, 50.3 (C$_4$, C$_5$); 40.1, 38.1 (C$_1$, C$_2$); 26.8, 26.3 (C$_3$, C$_6$).

MS (ESI) calculated for [C$_{20}$H$_{16}$N$_2$O$_9$Na]$^+$: 451.3, found: 452.0

[α]$_D^{25}$: +82.2 (c = 1.1 in CHCl$_3$).

Synthesis of (1*S*,2*S*,4*S*,5*S*) 1,2-Cyclohexanedicarboxylic acid, 4-hydroxy-5-(2-chloroethoxy)-1,2-bis(4-nitro)phenyl ester, 5.5

5.5
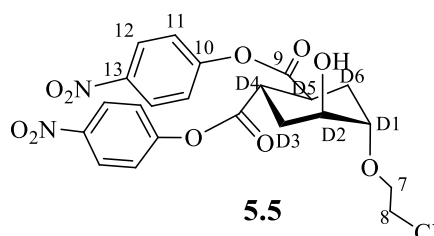
To a solution of **5.21** (2.0 g, 4.67 mmol, 1 eq.) in a minimum amount of dry CH$_2$Cl$_2$ (3.6 mL), 2-chloroethanol (4.7 mL, 70.0 mmol, 15 eq.) and Cu(OTf) $_2$ (272.76 mg, 0.75 mmol, 0.2 eq) were added. The solution was stirred at room temperature overnight. After completion of the reaction (TLC Hex:AcOEt 1:1), the crude was concentrated under reduce pressure and purified by flash chromatography (silica, Hex:AcOEt 6:4). 1.3 g of final compound **5.5** were obtained as yellowish oil (yield 54 %). **5.5** contained the 3 % w/w of free *p*-NO$_2$-phenol, but it was used without further purifications.

^{1}H NMR (400 MHz, CDCl$_3$): δ = 8.29–8.25 (m, 4H, H$_{12}$); 7.28-7.24 (m, 4H, H$_{11}$); 4.19-4.16 (m, 1H, H$_2$); 3.95–3.90 (m, 1H, H$_{7a}$); 3.81–3.76 (m, 1H, H$_{7b}$); 3.69–3.66 (m, 3H, H$_8$, H$_1$); 2.50–2.36 (m, 2H, H$_4$, H$_5$); 2.37–2.14 (m, 4H, H$_3$, H$_6$).

^{13}C NMR (100 MHz, CDCl$_3$): δ = 172.9, 172.9 (C$_9$); 155.6 (C$_{10}$); 145.8, 145.7 (C$_{13}$); 125.6 (C$_{12}$); 122.7, 122,7 (C$_{11}$); 76.5 (C$_1$); 69.5 (C$_7$); 66.5 (C$_2$); 43.6 (C$_8$); 39.6, 39.1 (C$_4$, C$_5$); 30.7, 27.3 (C$_3$, C$_6$).

Synthesis of (1*S*,2*S*,4*S*,5*S*) 1,2-Cyclohexanedicarboxylic acid, 4-(2-chloroethoxy)-5-[(2,3,4,-tri-O-benzoyl)-6-azido-α-D-6-deoxymannopyranosyloxy]-1,2-bis(*p*-nitrophenyl ester), 5.7


5.7
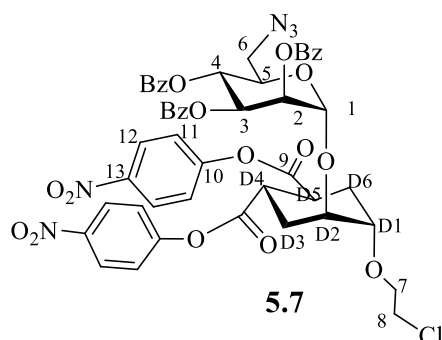
The acceptor **5.5** (381 mg, 0.755 mmol, 1 eq.) and the donor **5.3** (450 mg, 0.68 mmol, 0.9 eq.) were coevaporated with toluene three times. Powdered and activated acid washed 4 Å molecular sieves were added; the mixture was kept under vacuum overnight and then dissolved in 7.6 mL of dry CH$_2$Cl$_2$. After cooling at -30°C, TMSOTf (27 µL, 0.15 mmol, 0.2 eq.) was added and the reaction was stirred under nitrogen flushing for 1 h. TLC analysis (Hex:AcOEt 7:3) revealed that the reaction was complete. The mixture was quenched with dry Et$_3$N (300 µL) and the mixture warmed to room temperature and filtered over a celite pad. The filtrate was was evaporated at reduce pressure and the crude purified by flash chromatography (silica, Hex with gradient of AcOEt from 0 % to 40 %), obtaining 484.7 mg of **5.7** as yellowish solid (yield 69 %). **5.7** contained the 2 % w/w of free *p*-NO$_2$phenol, but it was used without further purifications.

^{1}H NMR (400 MHz, CDCl$_3$): δ = 8.36-8.24 (m, 4H, H$_{12}$); 8.13-8.07 (m, 2H, H$_{Bz}$); 8.01-7.93 (m, 2H, H$_{Bz}$); 7.84-7.76 (m, 2H, H$_{Bz}$); 7.73-7.61 (m, 1H, H$_{Bz}$); 7.59-7.48 (m, 4H, H$_{Bz}$); 7.48-7.38 (m, 4H, H$_{Bz}$); 7.34-7.28 (m, 4H, H$_{11}$); 5.90 (dd, 1H, H$_3$, J_{3-2} = 3.1 Hz, J_{3-4} = 10.0 Hz); 5.84 (t, 1H, H$_4$, J_{4-3} = 3.1 Hz, J_{4-5} = 10.0 Hz); 5.76-5.75 (m, 1H, H$_2$); 5.35 (bs, 1H, H$_1$); 4.35-4.19 (m, 2H, H$_5$, H$_{D2}$); 4.06-3.93 (m, 2H, H$_{7a}$, H$_{D1}$); 3.93-3.80 (m, 1H, H$_{7b}$); 3.71 (t, 1H, H$_8$, J_{8-7} = 5.5 Hz); 3.63 (dd, 1H, H$_{6a}$, J_{6a-5} = 7.8 Hz, J_{6a-6b} = 13.3 Hz); 3.52-3.36 (m, 3H, H$_{6b}$, H$_{D5}$, H$_{D4}$); 2.63-2.44 (m, 2H, H$_{D3eq}$, H$_{D6eq}$); 2.32-2.17 (m, 2H, H$_{D3ax}$, H$_{D6ax}$).

^{13}C NMR (100 MHz, CDCl$_3$): δ = 171.9, 171.8 (C$_9$); 165.6, 165.4, 165.3 (CO$_{Bz}$); 155.1, 155.1 (C$_{10}$); 145.4, 145.3 (C$_{13}$); 133.6, 133.7, 133.3 (CH$_{Bz}$); 129.7, 129.6, 129.5 (CH$_{Bz}$); 128.8, 128.5, 128.3 (Cquat$_{Bz}$); 128.5, 128.4, 128.3 (CH$_{Bz}$); 125.1, 125,0 (C$_{12}$); 122.3, 122.2 (C$_{11}$); 96.4 (C$_1$); 74.1 (C$_{D1}$); 72.1 (C$_{D2}$); 71.9 (C$_5$) 71.1 (C2); 70.2 (C$_7$); 69.7 (C3); 67.3 (C4); 51.2 (C6); 42.7 (C8); 38.7, 38.6 (C$_{D4}$, C$_{D5}$); 27.3, 26.5 (C$_{D3}$, C$_{D6}$).

Synthesis of (1*S*,2*S*,4*S*,5*S*) *N*¹,*N*²-bis(4-(hydroxymethylene)benzyl),1,2-Cyclohexanedi-carboxamide,4-(2-chloroethoxy)-5-[2,3,4-tri-*O*-benzoyl-6-azido-α-D-6-deoxy-mannopyranosyloxy], 5.25
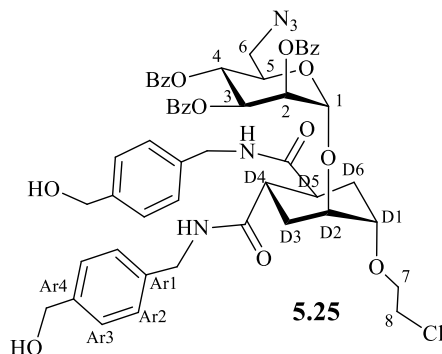

To a solution of compound **5.7** (464 mg, 0.47 mmol, 1 eq.) in dry MeCN (2 mL), a solution of (4-(aminomethyl)phenyl)methanol **5.24** (193.4 mg, 1.41 mmol, 3 eq.) in MeCN (3.7 mL) was added drop by drop. The reaction was stirred under nitrogen atmosphere, at room temperature overnight. TLC analysis (CHCl₃:(CH₃)₂O 65:35) revealed that the reaction was complete. The solvent was evaporated under reduce pressure and the crude purified by flash chromatography (silica, CHCl₃:(CH₃)₂O 65:35) obtaining 413.4 mg of **5.25** as a white solid (yield 88 %).

¹H NMR (400 MHz, CDCl₃): δ = 8.06-7.95 (m, 4H, H$_{Bz}$); 7,71-7, 69 (m, 2H, H$_{Bz}$); 7.64, 7.60 (m, 1H, H$_{Bz}$); 7.56-7.365 (m, 6H, H$_{Bz}$, H$_{Ar3}$); 7.27-7.14 (m, 8H, H$_{Bz}$, H$_{Ar2}$); 5.88-5.86 (m, 2H, H₃, H₄); 5.69-6.67 (m, 1H, H₂); 5.27 (bs, 1H, H₁); 4.68–4.53 (m, 4H, C$\underline{H}$₂OH); 4.45–4.27 (m, 5H, C$\underline{H}$₂NH, H₅); 4.13-4.08 (m, 1H, H$_{D2}$), 3.88–3.77 (m, 3H, H₇, H$_{D1}$); 3.71 (t, 2H, H₈, *J*$_{8-7}$ = 5.6 Hz); 3.53 (dd, 1H, H$_{6a}$, *J*$_{6a-6b}$ = 13.3 Hz, *J*$_{6a-5}$ = 6.9 Hz); 3.45 (dd, 1H, H$_{6b}$, *J*$_{6b-6a}$ = 13.3 Hz, *J*$_{6b-5}$ = 2.0 Hz); 3.14–2.97 (m, 2H, H$_{D4}$, H$_{D5}$); 2.34–2.18 (m, 2H, H$_{D3eq}$, H$_{D6eq}$); 2.09–1.98 (m, 2H, H$_{D3ax}$, H$_{D6ax}$).

¹³C NMR (100 MHz, CDCl3): δ = 174.7, 174.6 ($\underline{C}$ONH); 166.3, 166.2,166.1 (CO$_{Bz}$); 140.3, 140.2 (C$_{Ar1}$); 137.9, 137.8 (C$_{Ar4}$); 133.8, 133.7, 133.4, 133.3 (CH$_{Bz}$); 130.4, 130.4, 130.2 (CH$_{Bz}$); 129.1, 128.9, 128.8 (C$_{Ar2}$, C$_{Ar3}$); 128.1, 128.0, 127.7 (CH$_{Bz}$); 95.9 (C₁); 73.9, 73.6 (C$_{D1}$, C$_{D2}$); 71.3 (C₂, C₅); 68.7 (C₇); 69.5, 67.4 (C₄, C₃); 64.8 ($\underline{C}$H₂OH); 50.1 (C₆); 43.2, 41,1 ($\underline{C}$H₂NH, C₈); 40.8, 40.6 (C$_{D4}$, C$_{D5}$); 27.8, 27.7 (C$_{D3}$, C$_{D6}$).

Synthesis of (1*S*,2*S*,4*S*,5*S*) *N*¹,*N*²-bis(4-(hydroxymethylene)benzyl),1,2-Cyclohexane-dicarboxamides-4-(2-chloroethoxy)-5-[6-azido-α-D-6-deoxy-mannopyranosyloxy], 5.26

5.26
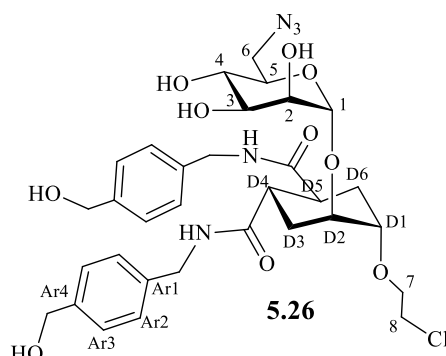
The compound **5.25** (413.3 mg, 0.41 mmol, 1 eq.) was dissolved in dry MeOH (4.1 mL), under nitrogen atmosphere at room temperature, and a solution of sodium methoxide in MeOH (1 M, 620 µL, 0.620 mmol, 1.5 eq.) was added. The reaction was stirred under nitrogen atmosphere at room temperature for 2.5 h; TLC analysis (CH_2Cl_2:MeOH 85:15) revealed that the reaction was complete. The mixture was purified by flash chromatography (silica, CH_2Cl_2:MeOH 85:15) to afford 260 mg of **5.26** as a white solid (yield 91 %).

¹H NMR (400 MHz, CD₃OD): δ = 7.27 (d, 4H, H_{Ar3}, *J* = 8.1 Hz); 7.22 (d, 4H, H_{Ar2}, *J* = 8.1 Hz); 4.95 (bs, 1H, H_1); 4.56 (s, 4H, C$\underline{H}_2$OH); 4.29 (s, 4H, C$\underline{H}_2$NH); 4.03-4.02 (m, 1H, H_{D2}); 3.93-3.81 (m, 1H, H_2); 3.86 (dd, 1H, H_{7a}, $J_{7a\text{-}7b}$ = 10.9 Hz, $J_{7a\text{-}8}$ = 5.4 Hz); 3.78 (dd, 1H, H_{7b}, $J_{7b\text{-}7a}$ = 10.9 Hz, $J_{7b\text{-}8}$ = 5.7 Hz); 3.79-3.63 (m, 5H, H_{D1}, H_8, H_5, H_3); 3.58-3.53 (m, 1H, H_4); 3.49-3.41 (m, 2H, H_6); 3.01-2.82 (m, 2H, H_{D4}, H_{D5}); 2.05-1.85 (m, 4H, H_{D3}, H_{D6}).

¹³C NMR (100 MHz, CD₃OD): δ = 176.9, 176.6 ($\underline{C}$ONH); 141.5, 141.3 (C_{Ar4}); 139.1, 139.0 (C_{Ar1}); 128.3, 128.3 (C_{Ar2}); 128.2, 128.2 (C_{Ar3}); 97.2 (C_1); 75.1 (C_{D1}); 75.0 (C_{D2}); 71.3 (C_5, C_2); 70.7 (C_7); 69.5 (C_3); 67.4 (C_4); 65.1 ($\underline{C}H_2$OH); 51.3 (C_6); 44.3 (C_8); 43.7 ($\underline{C}H_2$NH); 41.1 (C_{D4}, C_{D5}); 29.08, 28.7 (C_{D3}, C_{D6}).

MS (ESI HRMS) calculated for $[C_{32}H_{42}ClN_5O_{10}Na]^+$: 714.25124; found: 714.25095.

[α]$_D$²⁵: -12.04 (c = 0.25 in MeOH)

Synthesis of (1*S*,2*S*,4*S*,5*S*) *N*¹,*N*²-bis(4-(hydroxymethylene)benzyl),1,2-Cyclohexane-dicarboxamides-4-(2-chloroethoxy)-5-[6-*N*-carbo-*t*-butoxy-α-D-6-deoxymannopyranosyloxy], 5.27
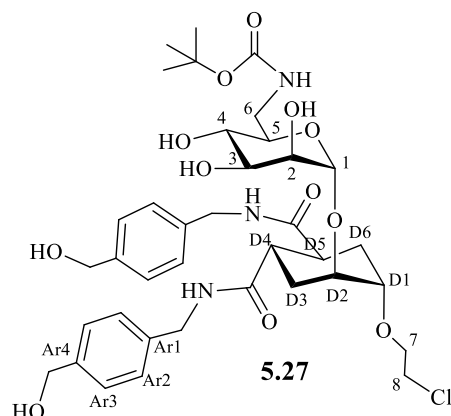
To a solution of **5.26** (88.8 mg, 0.128 mmol, 1 eq.) and Boc$_2$O (42 mg, 0.192 mmol, 1.5 eq.) in dry MeOH (12.8 mL), Pd Lindlar was added in catalytic amount. The reaction was stirred under H$_2$ (1 atm) at room temperature for 5 h. TLC analysis (RP H$_2$O:MeOH 4:6) revealed that the reaction was complete. The reaction was filtered through a celite pad and washed with MeOH. The filtrate was purified by flash chromatography (silica, CH$_2$Cl$_2$ with a gradient of MeOH from 10 % to 15 %). The crude was concentrated under reduce pressure to yield 88.2 mg of **5.27** as a white foam (yield 90 %).

¹H NMR (400 MHz, CD$_3$OD): δ = 7.27 (m, 4H, H$_{Ar3}$); 7.21 (m, 4H, H$_{Ar2}$); 4.90 (bs, 1H, H$_1$); 4.56 (s, 4H, C$\underline{H}_2$OH); 4.28 (s, 4H, C$\underline{H}_2$NH); 3.99-3.98 (m, 1H, H$_{D2}$); 3.89-3.88 (m, 1H, H$_2$); 3.84 (dd, 1H, H$_{7a}$, $J_{7a\text{-}7b}$ = 11.1 Hz, $J_{7a\text{-}8}$ = 5.6 Hz); 3.78 (dd, 1H, H$_{7b}$, $J_{7b\text{-}7a}$ = 11.1 Hz, $J_{7b\text{-}8}$ = 5.4 Hz); 3.74-3.61 (m, 4H, H$_3$, H$_8$, H$_{D1}$); 3.59-3.43 (m, 3H, H$_4$, H$_5$, H$_{6b}$); 3.27-3.10 (m, 1H, H$_{6a}$); 3.01-3.81 (m, 2H, H$_{D4}$, H$_{D5}$); 1.97-1.87 (m, 4H, H$_{D3}$, H$_{D6}$); 1.44 (s, 9H, *t*Bu).

¹³C NMR (100 MHz, CD$_3$OD): δ = 177.3, 177.0 ($\underline{C}$ONH); 141.2, 141.0, (C$_{Ar4}$); 139.8, 139.6 (C$_{Ar1}$); 128.6, 128.4 (C$_{Ar2}$); 127.5, 127.2 (C$_{Ar3}$); 100.6 (C$_1$); 80.3 (C$_{quat t Bu}$); 75.8 (C$_3$); 74.7 (C$_{D1}$); 72.2 (C$_{D2}$); 72.7 (C$_{D2}$); 72.2 (C$_2$); 70.4 (C$_7$); 69.5 (C$_4$); 64.9, 64.8 ($\underline{C}$H$_2$OH); 53.1 (C$_6$); 44.4 (C$_8$); 43.7, 43.6 ($\underline{C}$H$_2$NH); 42.4, 42.2 (C$_6$); 41.8 (C$_{D4}$, C$_{D5}$); 29.8, 29.4 (C$_{D3}$, C$_{D6}$); 28.2 (C$_{t Bu}$).

MS (ESI) calculated for [C$_{37}$H$_{52}$N$_3$O$_{12}$Na]$^+$: 788.32; found: 788.31

[α]$_D$²⁵: +9.28 (c = 0.21 in MeOH)

Synthesis of (1*S*,2*S*,4*S*,5*S*) *N*₁,*N*₂-bis(4-(hydroxymethylene)benzyl),1,2-Cyclohexane-dicarboxamides-4-(2-azidoethoxy)-5-[6-*N*-carbo-*t*-butoxy-α-D-6-deoxymannopyranosyloxy], 5.28

5.28
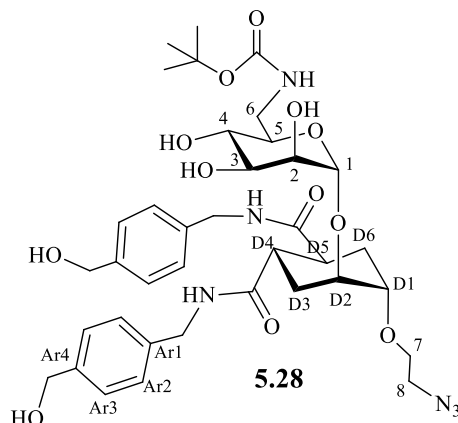
To a solution of **5.27** (250 mg, 0.326 mmol, 1 eq.) in dry DMF (4 mL), sodium azide (106 mg, 1.63 mmol, 5 eq.) was added. The reaction was stirred at 50 °C under nitrogen atmosphere for 3 days. ¹H NMR analysis assessed the completion of the reaction. The solvent was removed under reduce pressure and the crude was purified by flash chromatography (silica, CH₃Cl:MeOH 85:15) to afford 222.8 mg of **5.28** as a white foam (yield 88 %).
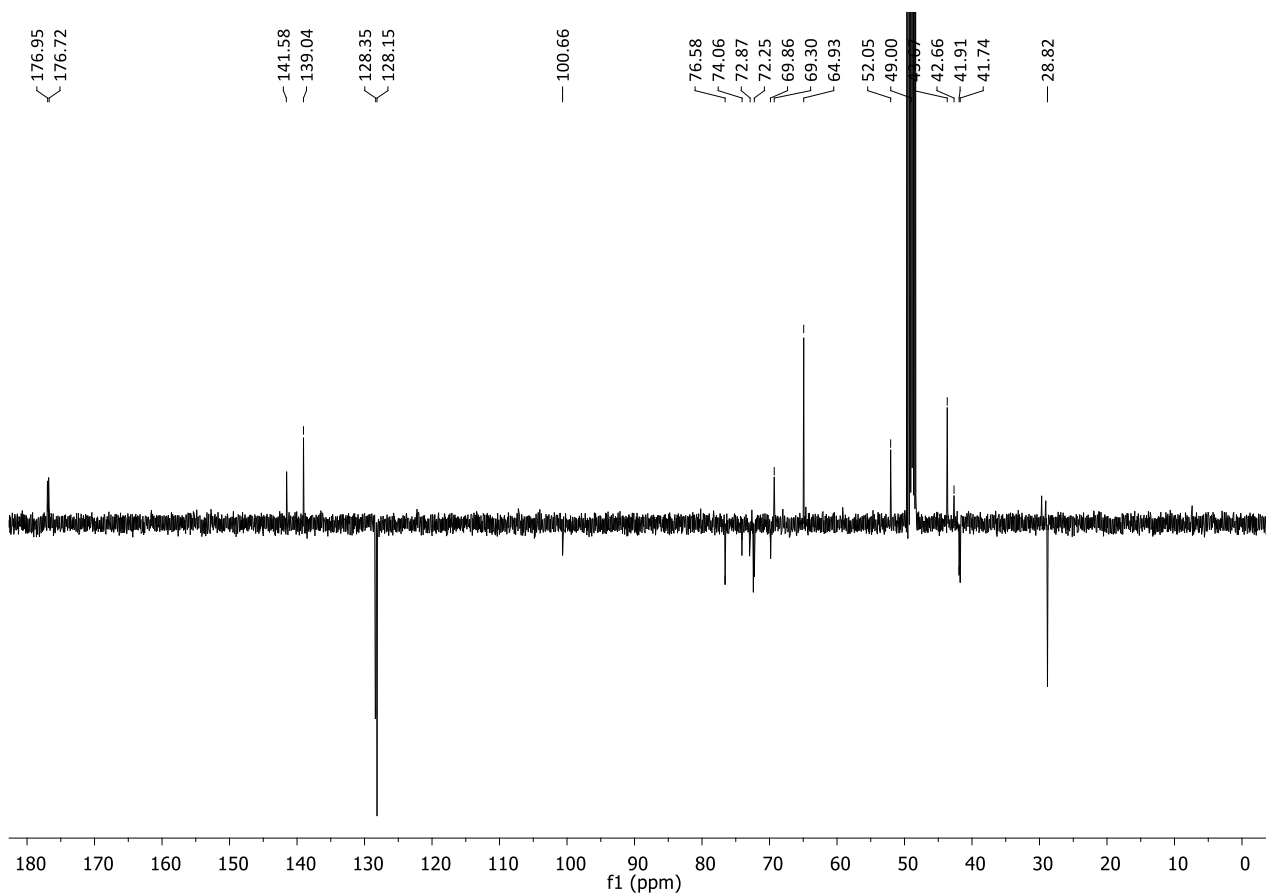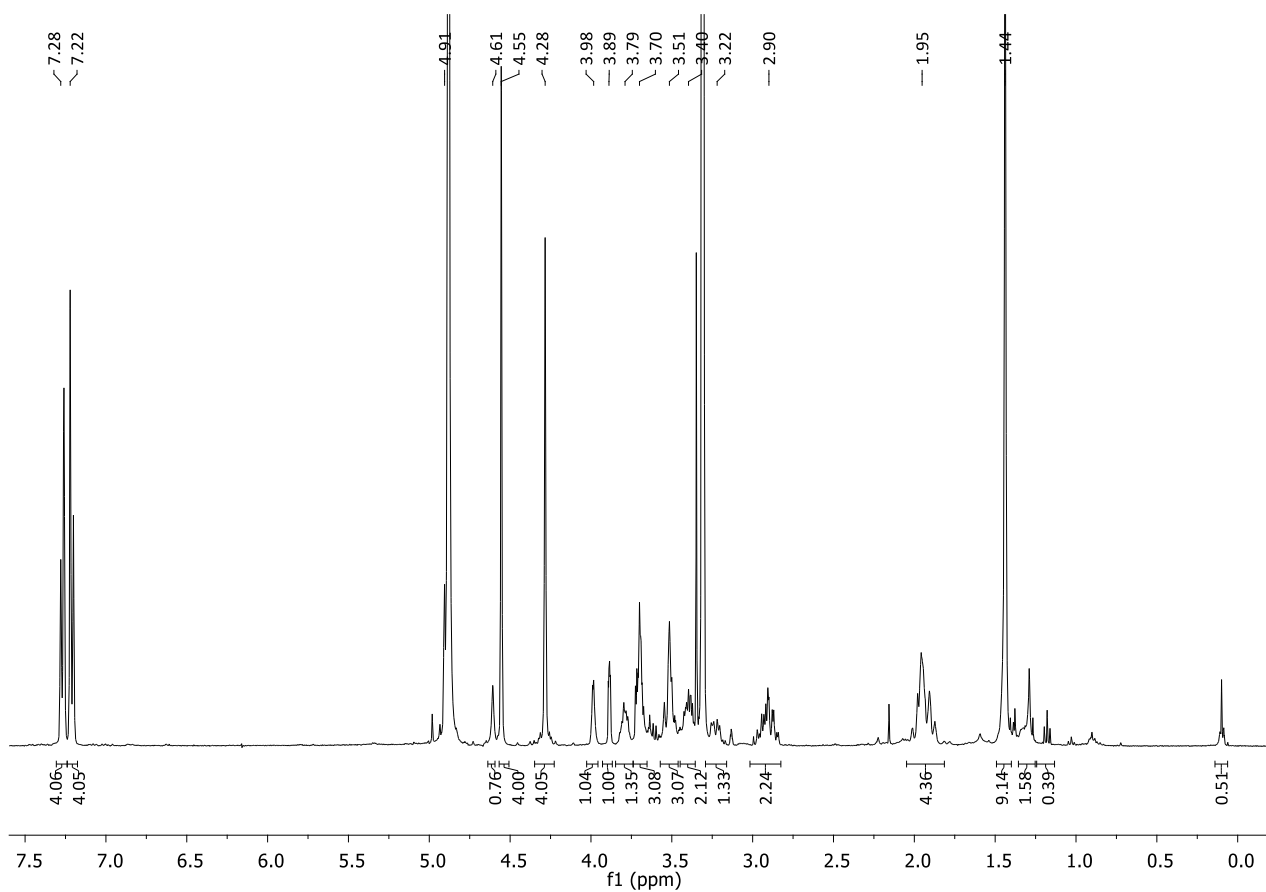
^{1}H NMR (400 MHz, MeOD): δ = 7.28 (d, 4H, H$_{Ar3}$, *J* = 8.0 Hz); 7.22 (d, 4H, H$_{Ar2}$, *J* = 8.0 Hz); 4.91 (bs, 1H, H$_1$); 4.55 (s, 4H, C$\underline{H}_2$OH); 4.28 (s, 4H, C$\underline{H}_2$NH); 3.99-3.98 (m, 1H, H$_{D2}$); 3.89-3.88 (m, 1H, H$_2$); 3.83-3.75 (m, 1H, H$_{7a}$); 3.73-3.66 (m, 3H, H$_{7b}$, H$_3$, H$_{D1}$); 3.56-3.46 (m, 3H, H$_{6a}$, H$_4$, H$_5$); 3.43-3.35 (m, 2H, H$_8$); 3.26-3.17 (m, 1H, H$_{6b}$); 3.03-2.78 (m, 2H, H$_{D4}$, H$_{D5}$); 2.04-1.85 (m, 4H, H$_{D3}$, H$_{D6}$); 1.44 (s, 9H, *t*Bu).

^{13}C NMR (100 MHz, MeOD): δ= 176.9, 176.8 ($\underline{C}$ONH); 141.5, 141.5, (C$_{Ar4}$); 138.9, 138.9 (C$_{Ar1}$); 128.3, 128.3 (C$_{Ar2}$); 128.2, 128.2 (C$_{Ar3}$); 101.2 (C$_1$); 80.4 (C$_{quat t Bu}$); 76.3 (C$_{D1}$); 75.1 (C$_5$); 72.9 (C$_{D2}$); 72.3 (C$_2$); 72.2 (C$_3$); 70.4 (C$_4$); 69.5 (C$_7$); 64.7 ($\underline{C}$H$_2$OH); 51.9 (C$_8$); 43.9 ($\underline{C}$H$_2$NH); 42.8, 42.8 (C$_6$); 42.4 (C$_{D4}$, C$_{D5}$); 29.6, 29.4 (C$_{D3}$, C$_{D6}$); 28.2 (C$_{t Bu}$).

MS (ESI HRMS) calculated for $[C_{37}H_{52}N_6O_{12}Na]^+$: 795.35354 ; found: 795.35211.

[α]$_D$^{25}: + 9.94 (c = 0.90 in MeOH).

Synthesis of (1S,2S,4S,5S) N_1,N_2-bis(4-(hydroxymethylene)benzyl)-1,2-Cyclohexane-dicarboxamides-4-(2-azidoethoxy)-5-[6-amino-α-D-6deoxymannopyranosyloxy], 5.9
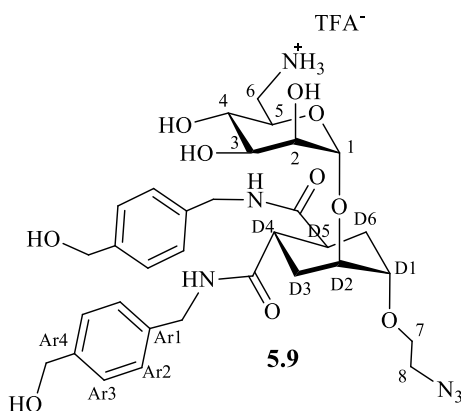
Compound **5.28** (25.5 mg, 0.033 mmol, 1eq) was dissolved in TFA (400 μL, 5.220 mmol, 158 eq.). The resulting solution was stirred at 35 °C for 4h. After completion of the reaction (TLC analysis (CHCl$_3$:MeOH 85:15) revealed that the reaction was complete. The solvent was removed under reduce pressure and the crude residue was washed and dried twice with Et$_2$O. 25 mg of **5.9** were obtained as a white solid (yield 100 %).
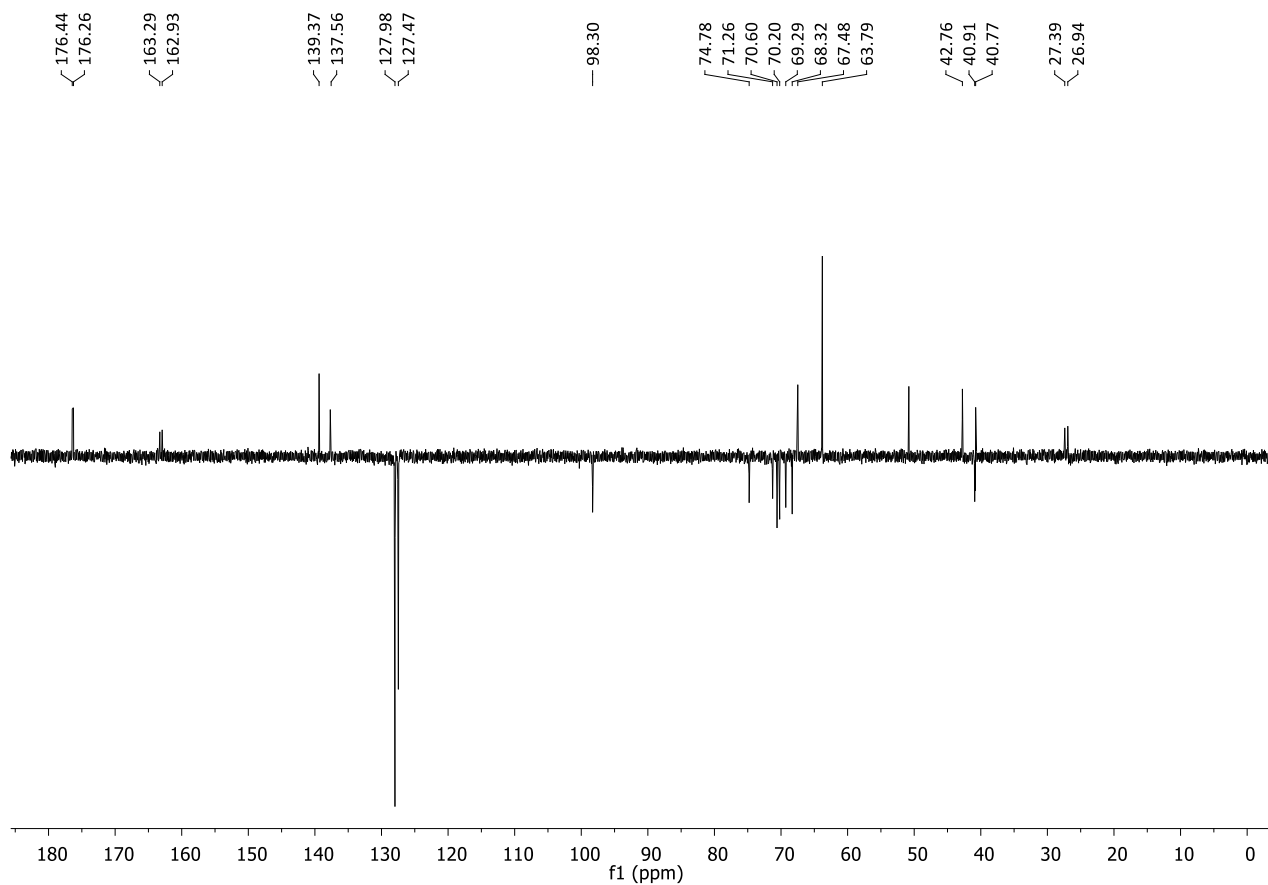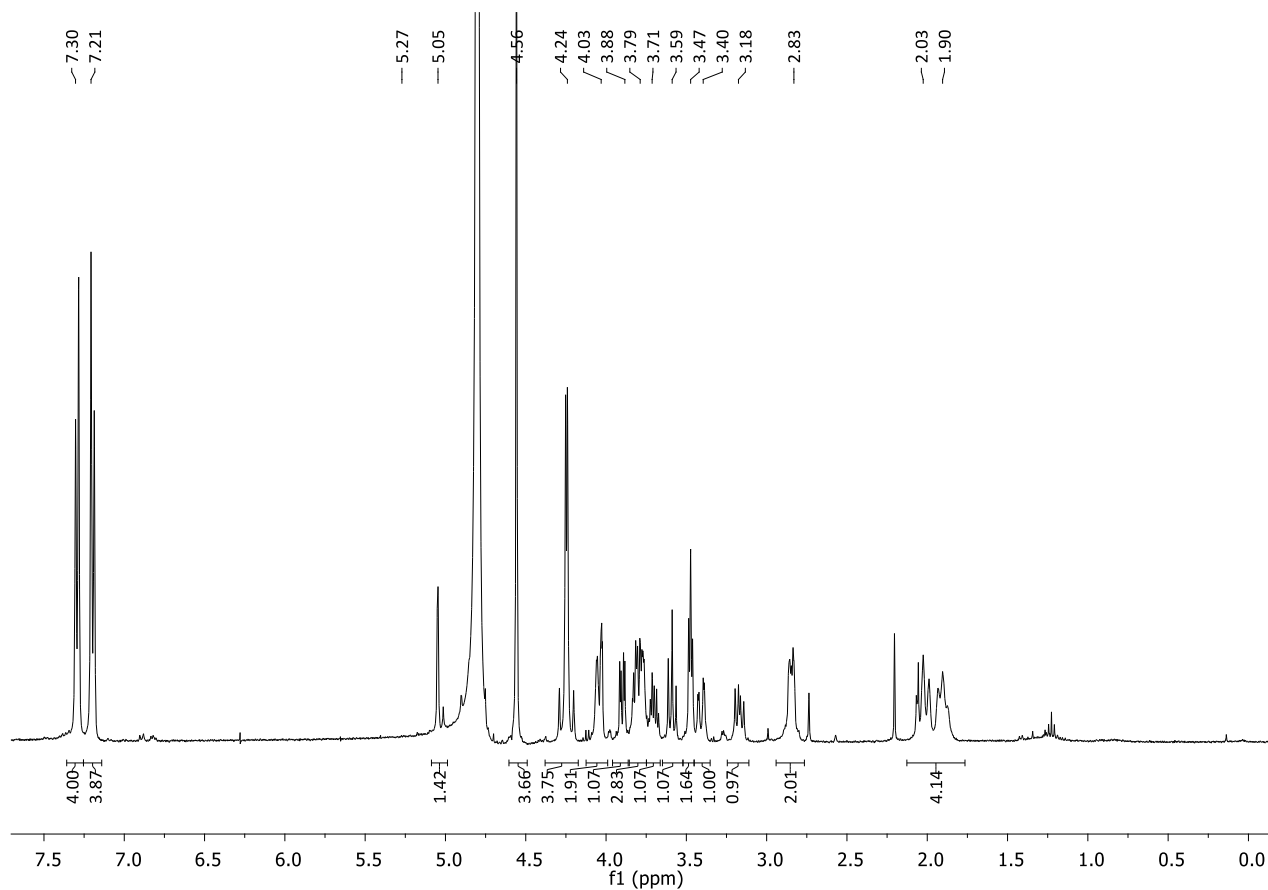
¹H NMR (400 MHz, D₂O) δ = 7.29 (d, 4H, H$_{Ar3}$, *J* = 8.1 Hz); 7.20 (d, 4H, H$_{Ar2}$, *J* = 8.1 Hz); 5.01 (bs, 1H, H$_1$); 4.56 (s, 4H, C$\underline{H}_2$OH); 4.29-4.20 (m, 4H, C$\underline{H}_2$NH); 4.06-4.02 (m, 2H, H$_{D2}$, H$_2$); 3.90 (dd, 1H, H$_{D1}$, *J* = 8.1 Hz); 3.84-3.76 (m, 3H, H$_3$, H$_5$, H$_{7a}$); 3.72-3.67 (m, 1H, H$_{7b}$); 3.59 (t, 1H, H$_4$, *J$_{4-3}$* = *J$_{4-5}$* = 9.7 Hz); 3.47 (t, 1H, H$_8$, *J$_{8-7}$* = 4.8 Hz); 3.41 (dd, 1H, H$_{6a}$, *J$_{6a-6b}$* = 13.3 Hz, *J$_{6a-5}$* = 2.8 Hz); 3.17 (dd, 1H, H$_{6b}$, *J$_{6b-6a}$* = 13.3 Hz, *J$_{6b-5}$* = 8.3 Hz); 2.86-2.83 (m, 2H, H$_{D4}$, H$_{D5}$); 2.07-1.88 (m, 4H, H$_{D3}$, H$_{D6}$).

¹³C NMR (100 MHz, D₂O): δ= 176.4, 176.3 ($\underline{C}$ONH); 163.0, 163.0 (CO$_{TFA}$); 139.4 (C$_{Ar4}$), 137.7, 137.7, (C$_{Ar1}$); 128.0, (C$_{Ar2}$); 127.5, (C$_{Ar3}$); 98.3 (C$_1$); 74.5 (C$_3$); 71.1 (C$_2$); 70.5 (C$_{D2}$); 70.1 (C$_{D1}$); 69.1 (C$_5$); 68.1 (C$_4$); 67.3, 67.3 (C$_7$); 63.7 ($\underline{C}$H$_2$OH); 50.6 (C$_8$); 42.8, 42.8 ($\underline{C}$H$_2$NH); 40.9, 40.8 (C$_{D4}$, C$_{D5}$), 40.8 (C$_6$); 27.4, 27.0 (C$_{D3}$, C$_{D6}$).

MS (ESI HRMS) calculated for [C$_{32}$H$_{44}$N$_6$O$_{10}$Na]$^+$: 695.30111, found: 695.29999.

[α]$_D$^{25}: +2.55 (c = 0.32 in H₂O)

Synthesis of pseudo-disaccharide, 5.9.1
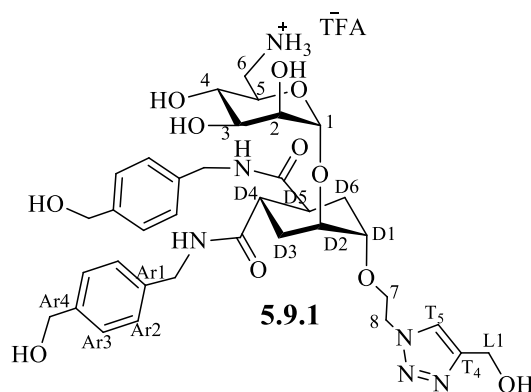
To a stirred solution of propargyl bromide (3.9 mg, 70.0 μmol, 5 eq.) in THF (40 μL), under inert atmosphere atroom temperature, reagents were added as solutions in the following order: TBTA in THF (1.5 mg, 1.64 μmol, 0.2 eq. in 360 μL), CuSO₄·5H₂O in water (0.34 mg, 1.4 μmol, 0.1 eq., in 34 μL), Sodium Ascorbate in water (1.1 mg, 5.6 μmol, 0.4 eq., in 75 μL). The reaction mixture was stirred under inert atmosphere, at room temperature and in the dark for 5 min, then **5.9** in H₂O (11 mg, 14.0 μmol, 1 eq.) was added as solid. The THF and water volumes were adjusted to 400 μL each and the mixture was stirred for 18 h, at room temperature, under nitrogen atmosphere and in dark. A ESI mass analysis assessed the formation of the product. Quadrasil™-MP (S/Cu 5.4:1, 5 mg) was added to the reaction mixture, which was stirred for 10 min, and then filtered off. The crude was dried, then redissolved in H₂O and purified by automated reverse phase chromatography

(H$_2$O with a gradient of MeOH from 0 to 50 %), to give 7.9 mg of **5.9.1** as a colourless solid (yield 77 %).

^{1}H NMR (400 MHz, D$_2$O): δ 8.04 (s, 1H, H$_{T5}$), 7.36-7.13 (m, 8H, H$_{Ar2}$, H$_{Ar3}$), 4.91 (bs, 1H, H$_1$), 4.65 − 4.59 (m, 8H, H$_8$, C$\underline{H}_2$OH (Ar), H$_{L1}$), 4.29 − 4.17 (m, 4H, C$\underline{H}_2$NH), 4.06 − 3.97 (m, 2H, H$_2$, H$_{7a}$), 3.97 − 3.90 (m, 2H, H$_{7b}$), 3.90 − 3.81 (m, 2H, H$_{D2}$, H$_3$), 3.80 − 3.72 (m, 1H, H$_5$), 3.62-3.53 (m, 2H, H$_{D1}$, H$_4$), 3.41 (dd, 1H, H$_{6a}$, $J_{6a\text{-}6b}$ = 13.3, $J_{6a\text{-}5}$ = 2.9 Hz), 3.21 − 3.12 (m, 1H, H$_{6b}$), 2.79-2.68 (m, 1H, H$_{D4}$), 2.55-2.41 (m, 1H, H$_{D5}$), 1.91-1.78 (m, 3H, H$_{D4}$, H$_{D5}$), 1.59-1.49 (m, 1H, H$_{D6ax}$).

^{13}C NMR (100 MHz, D$_2$O): δ 176.40, 176.20 ($\underline{C}$ONH), 139.47, 139.44, 137.78, 137.68 (C$_{Ar1}$, C$_{Ar4}$), 128.06, 127.55, 127.52 (C$_{Ar2}$, C$_{Ar3}$), 125.53 (C$_{T5}$), 98.33 (C$_1$), 74.47 (C$_{D1}$), 71.15 (C$_3$), 70.62 (C$_{D2}$), 70.22 (C$_2$), 69.33 (C$_5$), 68.39 (C$_4$), 67.04 (C$_7$), 63.88 ($\underline{C}$H$_2$OH (Ar)), 54.85 (C$_{L1}$), 50.78 (C$_8$), 49.17, 42.84 ($\underline{C}$H$_2$NH), 42.77 (C$_6$), 40.85, 40.79 (C$_{D4}$, C$_{D6}$), 27.44, 26.94 (C$_{D3}$, C$_{D6}$).

MS (ESI HRMS) calculated for [C$_{35}$H$_{49}$N$_6$O$_{11}$Na]$^+$: 729.34538, found: 729.34792.


[α]$_D^{25}$: +1.65 (c = 0.40 in H$_2$O)

Synthesis of hexavalent glycodendrimer, 5.33
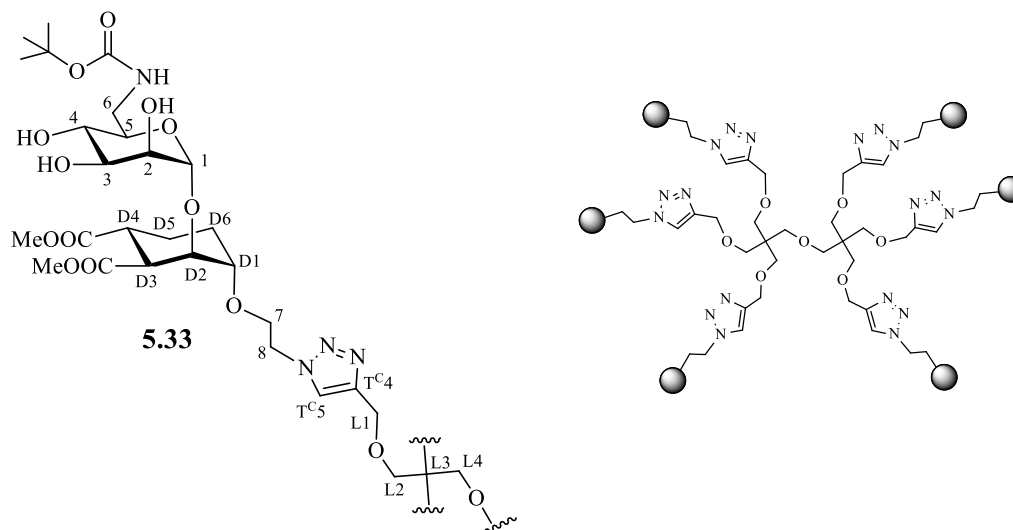
To hexavalent central scaffold **2.24** (3.96 mg, 8.21 µmol, 1 eq.) under inert atmosphere at room temperature, reagents were added as solutions in the following order: TBTA in THF (0.87 mg, 1.64 µmol, 0.2 eq. in 100 µL), CuSO$_4$·5H$_2$O in water (0.24 mg, 0.82 µmol, 0.1 eq., in 100 µL), Sodium Ascorbate in water (0.65 mg, 3.28 µmol, 0.4 eq., in 100 µL). The reaction mixture was stirred under inert atmosphere, at room temperature and in the dark for 5 min, then **5.18** in THF (10.1 mg, 18

μmol, 6.6 eq., in 200 μL). The THF and water volumes were adjusted to 650 μL each and the mixture was stirred for 18 h, at room temperature, under nitrogen atmosphere and in dark. A MALDI mass analysis (DHB or sinapinic acid matrix) assessed the formation of the product. Quadrasil™-MP (S/Cu 9.2:1, 5 mg) was added to the reaction mixture, which was stirred for 10 min, and then filtered off. The crude was dried, then redissolved in MeOH and purified firstly by size exclusion chromatography on a Sephadex LH-20 (MeOH) column and then by automated reverse phase chromatography (H$_2$O with a gradient of MeOH from 0 to 100 %), to give 27.5 mg of **5.33** as a colourless solid (yield 86%).
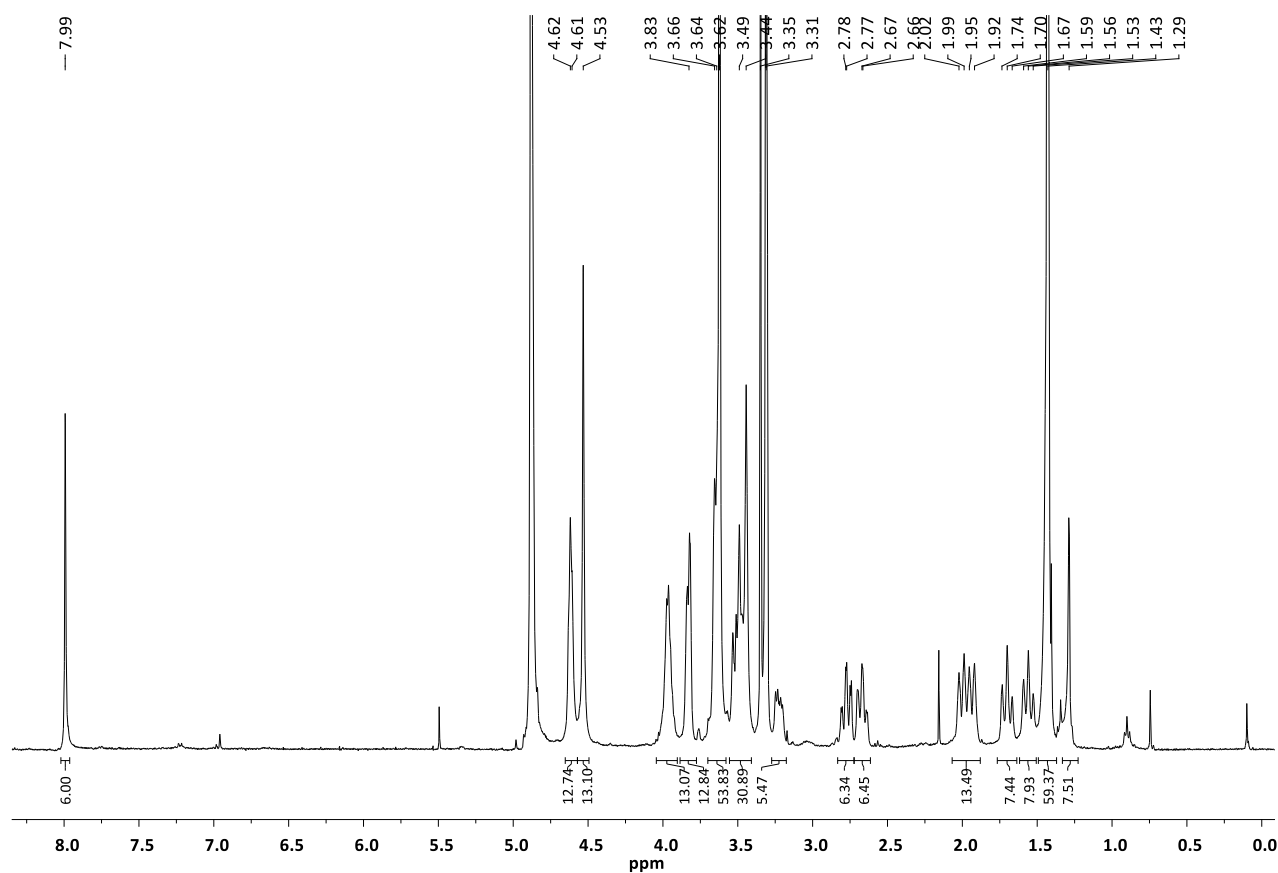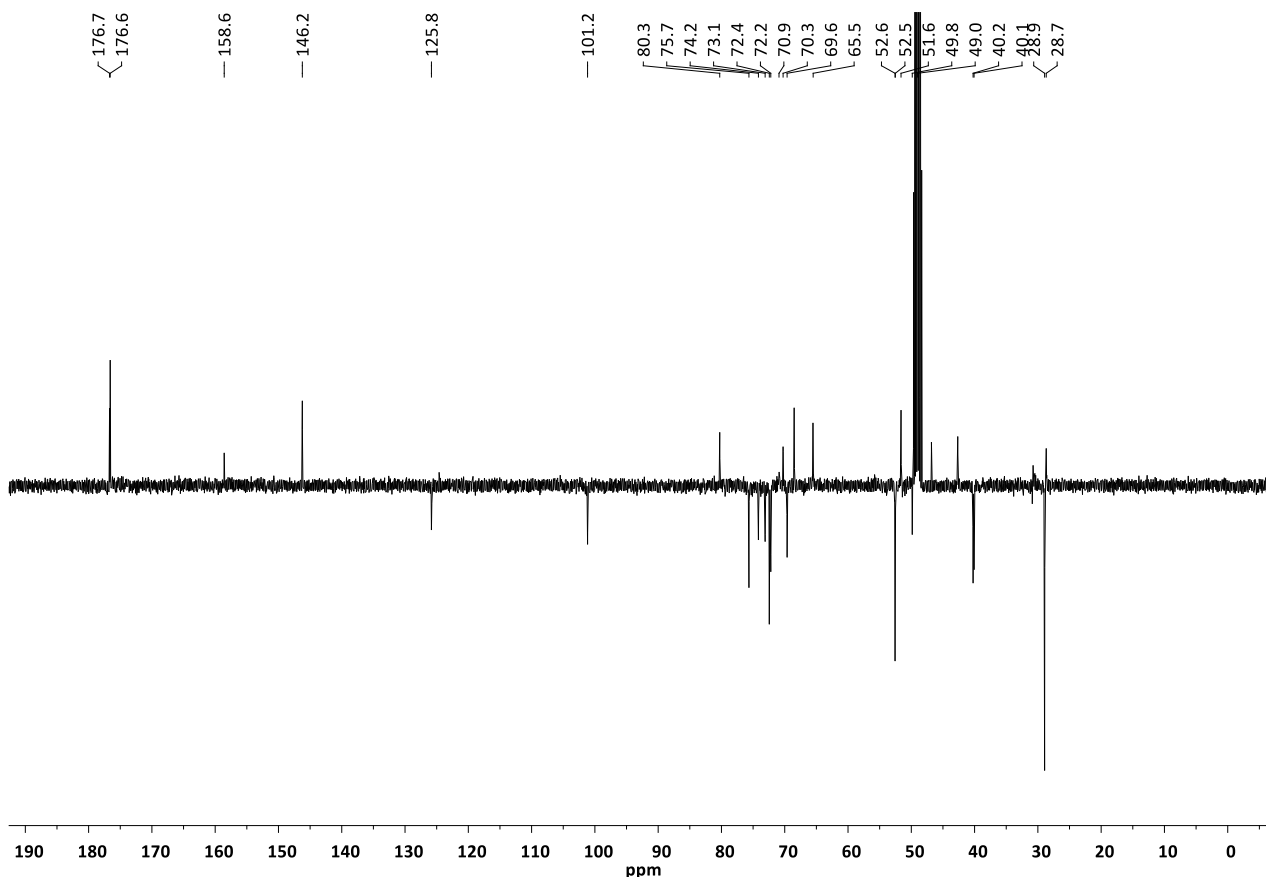
¹H-NMR (400 MHz, CD₃OD): δ 7.99 (s, 6H, H$_{TC5}$), 4.90 (bs, 6H, H$_1$), 4.65-4.58 (m, 12H. H$_8$), 4.53 (bs, 12H, H$_{L1}$), 4.03-3.91 (m, 12H, H$_7$), 3.87-3.78 (m, 12H, H$_2$, H$_{D2}$), 3.68-3.59 (m, 48H, H$_3$, H$_{D1}$, H$_{OMe}$), 3.55-3.41 (m, 30H, H$_{L2}$, H$_4$, H$_5$, H$_{6a}$), 3.33 (s, 4H, H$_{L4}$), 3.27 – 3.17 (m, 6H, H$_{6b}$), 2.82-2.62 (m, 12H, H$_{D4}$, H$_{D5}$), 2.05-1.89 (m, 12H, H$_{D3eq}$, H$_{D3eq}$), 1.77-1.49 (m, 12H, H$_{D3ax}$, H$_{D6ax}$), 1.43 (s, 54H, H$_{tBu}$).

¹³C-NMR (100 MHz, CD₃OD): δ 176.69, 176.59 (<u>C</u>OOMe), 158.57 (<u>C</u>OOtBu), 146.23 (C$_{TC4}$), 125.83 (C$_{TC5}$), 101.16 (C$_1$), 80.27 (C$_{quat t Bu}$), 75.66 (C$_{D1}$), 74.16 (C$_5$), 73.10, 72.44, 72.20 (C$_3$, C$_{D2}$, C$_2$), 70.91 (C$_{L4}$), 70.26 (C$_4$), 69.63 (C$_{L2}$), 68.44 (C$_7$), 65.51 (C$_{L1}$), 52.57, 52.53 (C$_{OMe}$), 51.62 (C$_8$), 46.82 (C$_{L3}$), 42.66 (C$_6$), 40.24, 40.08 (C$_{D4}$, C$_{D5}$), 28.94 (C$_{tBu}$), 28.68 (C$_{D3}$, C$_{D6}$).

MS (MALDI, DHB matrix): calculated for [C$_{166}$H$_{262}$N$_{24}$O$_{79}$Na]$^+$: 3859.0, found: 3860.0

[α]$_D^{25}$: +27 (c = 0.4 of MeOH)

Synthesis of hexavalent glycodendrimer, 5.32
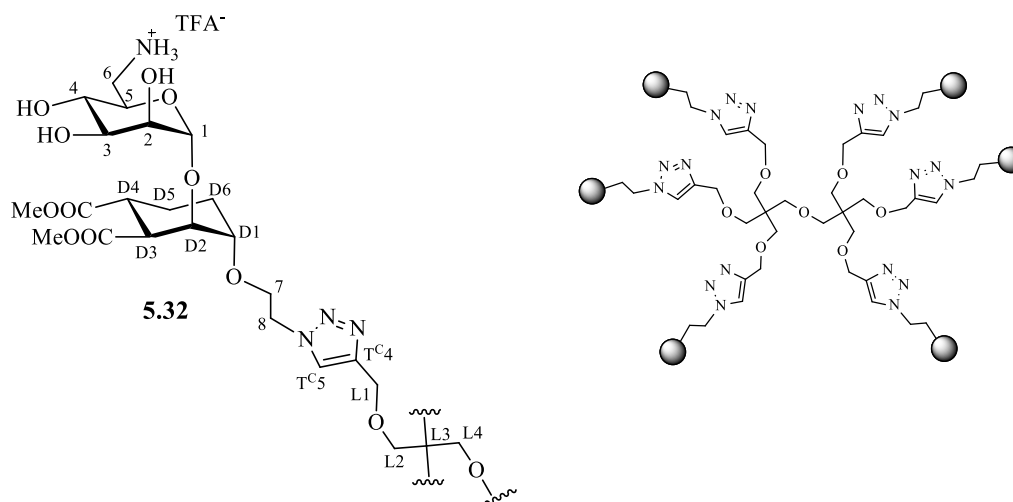
To a stirred suspension of **5.33** (20.4 mg, 5.30 μmol, 1 eq.) in 1.5 mL of dry CH_2Cl_2, TFA (500 μL, 6.5 mmol, 100 eq.) was added under inert atmosphere, obtaining a complete dissolution of the starting material. The reaction was stirred for 1.5 h, at room temperature and under nitrogen atmosphere. A TLC analysis ($CHCl_3$:MeOH:H_2O 8.5:1.5:0.2) revealed that the reaction was complete. The reaction mixture was dried and washed with Et_2O (3 x 2 mL), affording 21 mg of final product (**5.32**) as a colourless oil (yield 100 %).
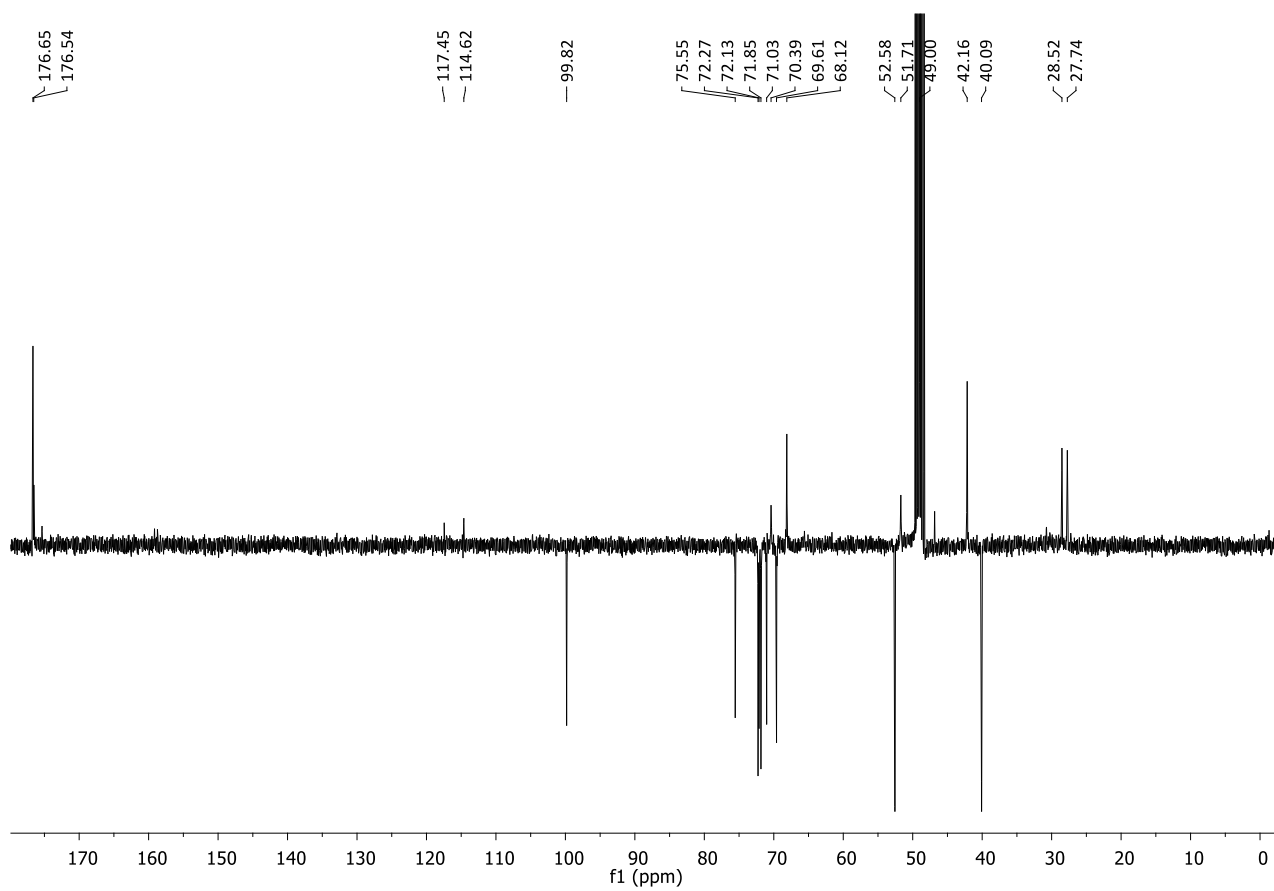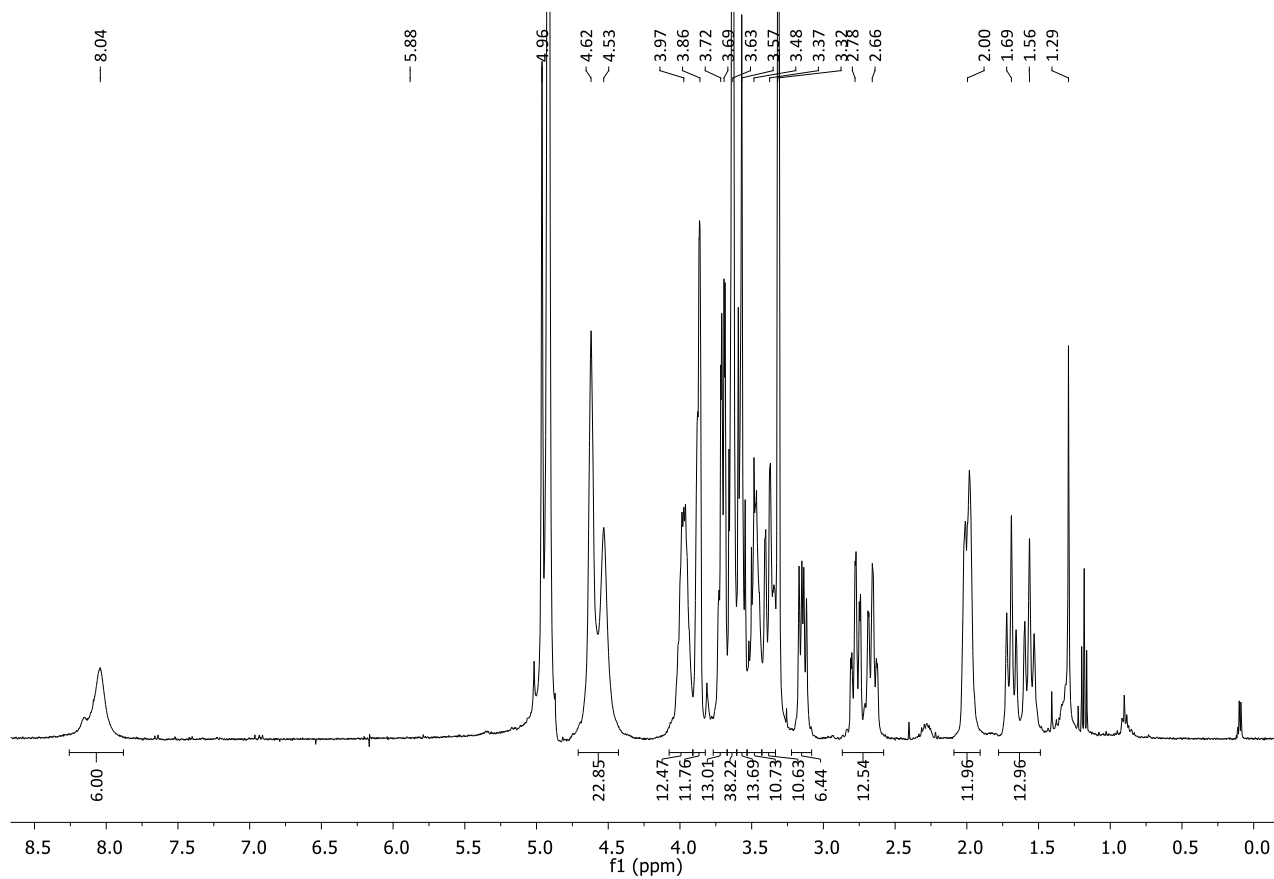
^{1}H NMR (400 MHz, CD$_3$OD): δ 8.04 (s, 6H, H$_{TC5}$), 4.96 (bs, H6, H$_1$), 4.68-4.57 (m, 12H, H$_8$), 4.53 (bs, 12H, H$_{L1}$), 4.05 – 3.90 (m, 12H, H$_7$), 3.90 – 3.83 (m, 12H, H$_{D2}$, H$_2$), 3.76 – 3.67 (m, H$_3$, H$_5$), 3.63 (s, 36H, OMe), 3.60-3.54 (m, 12H, H$_4$, H$_{D1}$), 3.51-3.43 (m, H$_{12}$, C$_{L2}$), 3.42 – 3.34 (m, 6H, H$_{6a}$), 3.34 (s, H$_{L4}$), 3.14 (dd, 6H, H$_{6b}$ J_{6b-6a} = 13.0, J_{6a-5} = 7.7 Hz), 3.82-3.60 (m, 12H, C$_{D4}$, C$_{D5}$), 2.05-1.92 (m, 12H, H$_{D3eq}$, H$_{D3eq}$), 1.77-1.49 (m, 12H, H$_{D3ax}$, H$_{D6ax}$).

^{13}C NMR (100 MHz, CD$_3$OD): δ 176.65, 176.54 (COOMe), 125.90 (C$_{TC5}$), 99.82 (C$_1$), 75.55 (C$_{D1}$), 72.27, 72.13, 71.85, 71.03 (C$_2$, C$_{D2}$, C$_3$, C$_5$), 70.84 (C$_{L4}$), 70.39 (C$_{L2}$), 69.61 (C$_4$), 68.12 (C$_7$), 52.58 (C$_{OMe}$), 51.71 (C$_8$), 42.16 (C$_6$), 40.09 (C$_{D4}$, C$_{D5}$), 28.52, 27.74 (C$_{D3}$, C$_{D6}$).

MS (MALDI, DHB matrix): calculated for [C$_{136}$H$_{215}$N$_{24}$O$_{67}$]$^+$: 3258.3, found: 3258.8

[α]$_D^{25}$ was not performed because NMR analysis revealed the presence of a mixture of products in equilibrium in solution.

Synthesis of hexavalent glycodendrimer, 5.34
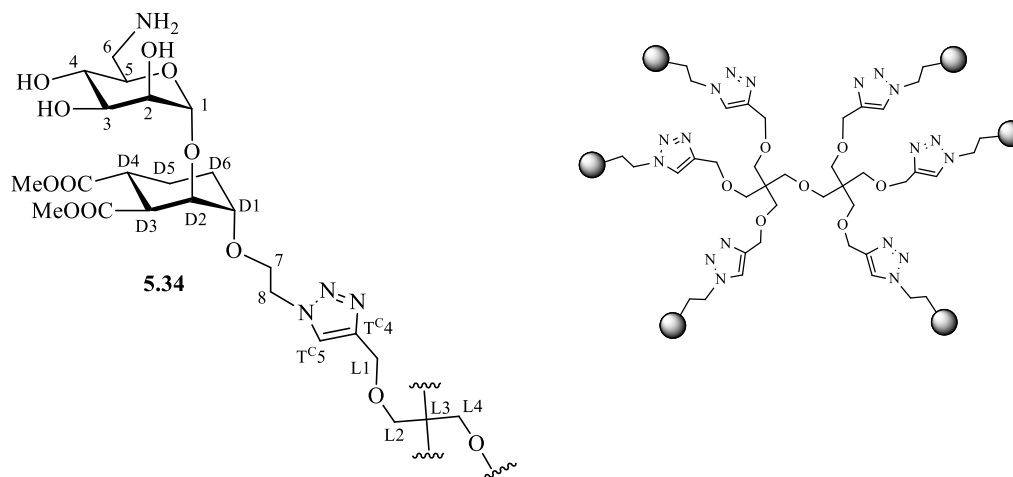
To a shaken solution of **5.32** (21 mg, 5.3 µmol, 1 eq.) in 2.5 mL of dry MeOH, Amberlyst A21® (60 mg, 10 eq.) was added under inert atmosphere at room temperature; the reaction was shaken at 1500 rpm for 3 h. Then the crude was filtered on a cotton pad to remove the resin, washed with MeOH and then dried. 17.3 mg of final product **5.34** were obtained as a colourless oil (yield 100 %).
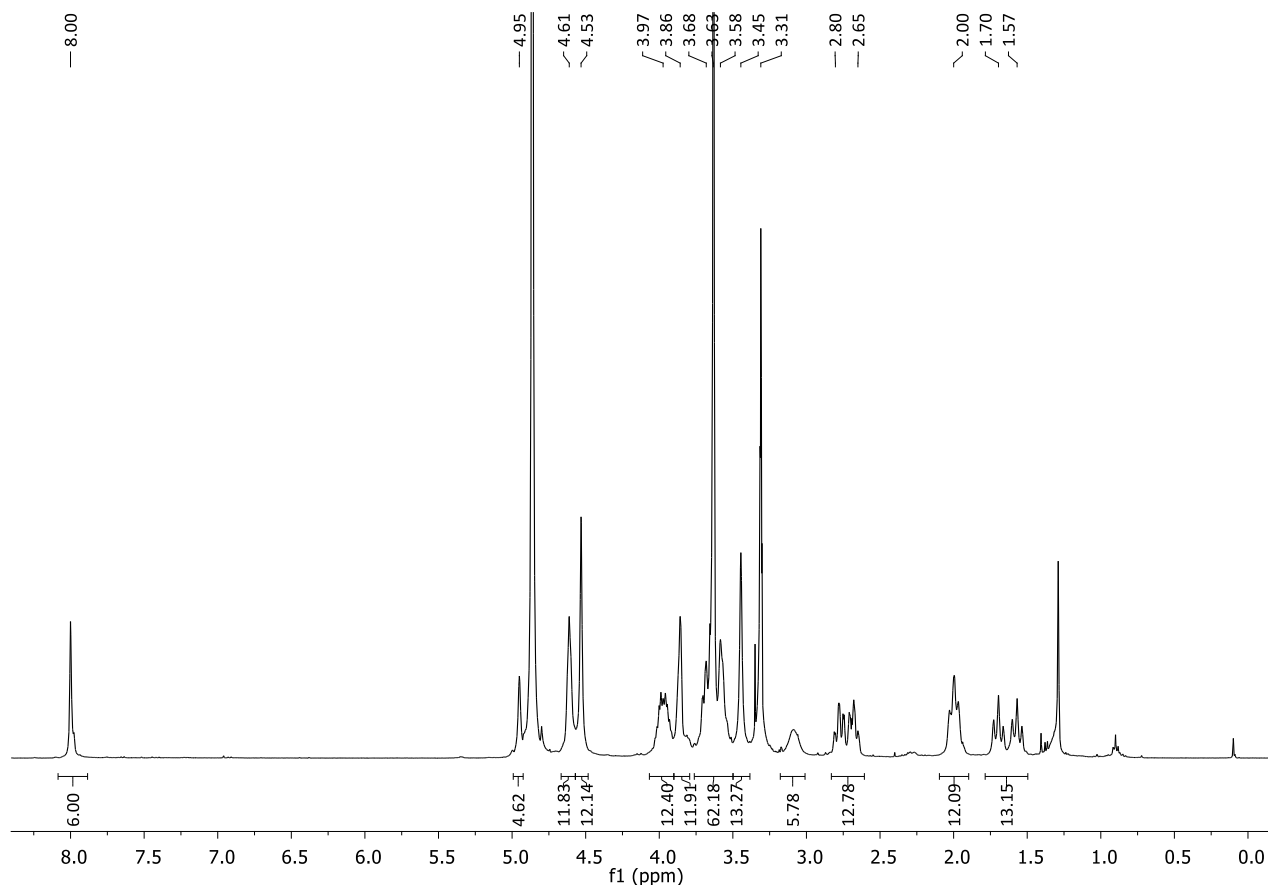
^{1}H-NMR (400 MHz, CD$_3$OD): δ 8.00 (s, 6H, H$_{TC5}$), 4.96 (bs, 6H, H$_1$), 4.66-4.58 (m, 12H, H$_8$), 4.58-4.48 (bs, 12H, H$_{L1}$), 4.05-3.91 (m, 12H, H$_7$), 3.91-3.86 (m, 12H, H$_2$, H$_{D2}$), 3.74-3.51 (m, 60H, H$_3$, H$_4$, H$_5$, H$_{D1}$, H$_{OMe}$), 3.45 (bs, H$_{L2}$), 3.17-3.02 (m, 6H, H$_{6a}$), 2.88-2.60 (m, 12H, H$_{D5}$, H$_{D4}$), 2.08-1.91 (m, 12H, H$_{D3eq}$, H$_{D6eq}$), 1.78-1.48 (m, 12H, H$_{D6ax}$, H$_{D3ax}$).

MS (ESI-HRMS): Calculated for [C$_{136}$H$_{214}$N$_{24}$O$_{67}$Na$_2$]$^{2+}$: 1651.19454, found:1651.22786.

[α]$_D^{25}$: +33.5 (c = 0.42 in MeOH).

Synthesis divalent glycodendrimer, 5.35
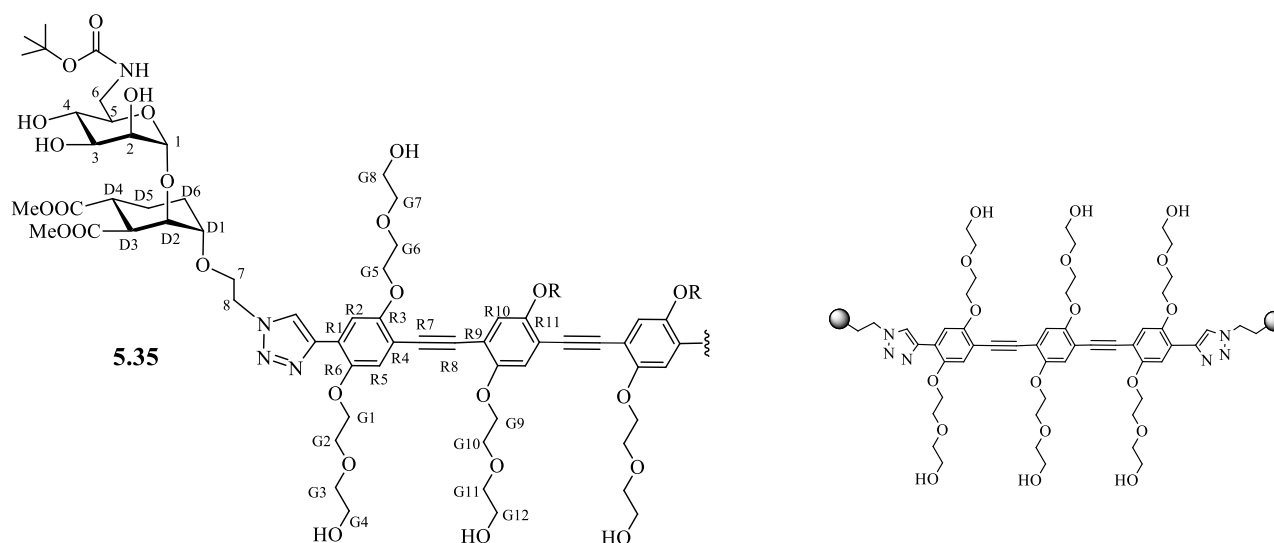
To a stirred solution of **TIPS-2.5** (15.1 mg, 12 µmol, 1 eq.) in 300 µL of dry THF, TBAF (1M in THF, 24 µL, 2 eq.) was added under inert atmosphere and the mixture was stirred for 1 h; a TLC analysis (CHCl$_3$:MeOH 9:1) revealed that the desilylation reaction was complete. Then reagents were added as solutions in the following order: TBTA in THF (1.26 mg, 2.40 µmol, 0.2 eq, in 100 µL), CuSO$_4$·5H$_2$O in water (0.35 mg, 1.20 µmol, 0.1 eq., in 100 µL) and Sodium Ascorbate in water (0.94 mg, 4.80 µmol, 0.4 eq., in 100 µL), and the reaction mixture was stirred under inert atmosphere at room temperature and in the dark for 5 min. Then **5.18** in THF (14.8 mg, 26.2 µmol, 2.2 eq., in 200 µL) was added to the mixture. THF and water volumes were adjusted to 900 µL each. The mixture was stirred for 18 h under inert atmosphere, at room temperature and in the dark. A MALDI mass analysis (DHB or synapinic matrix) assessed the formation of the product. The reaction was quenched by the addition of Quadrasil™-MP (S/Cu 6.2:1, 5 mg), which was added to the reaction mixture, stirred for 20 min and then filtered off. The crude was dried, redissolved in MeOH and purified firstly by size exclusion chromatography on a Sephadex LH-20 (MeOH) and then by automated reverse phase chromatography (H$_2$O with a gradient of MeOH from 0 % to 100 %), to give 13.7 mg of **5.35** as a yellow solid (yield 55 %).
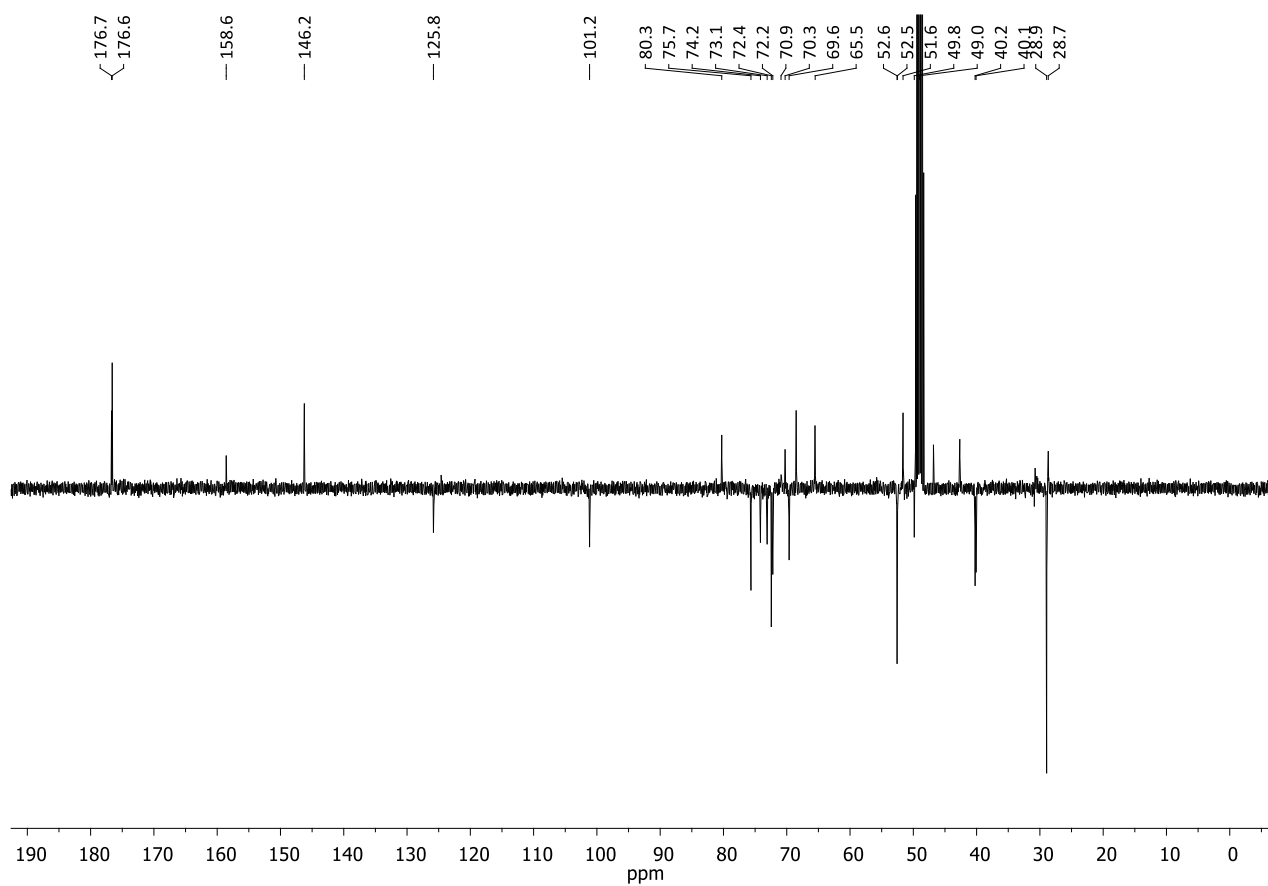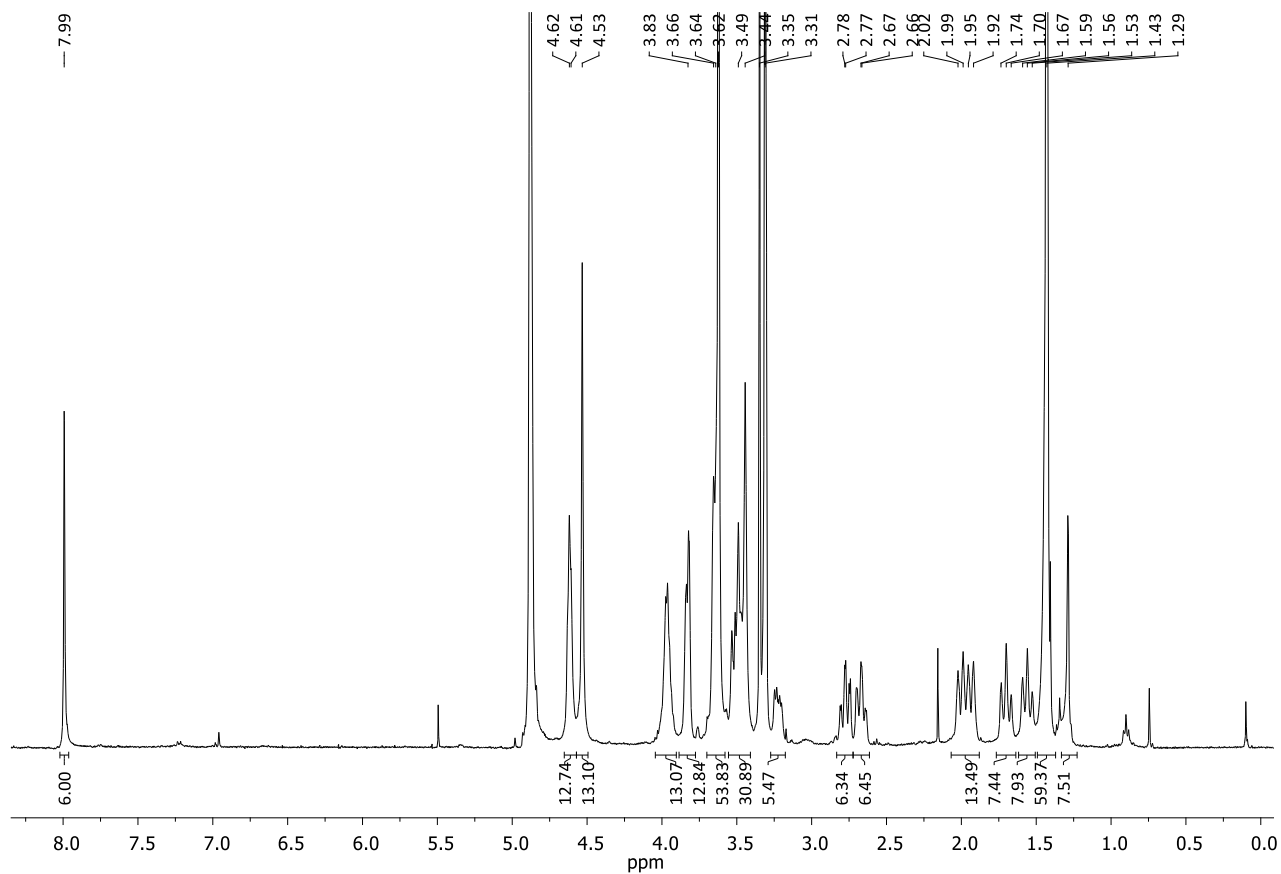
¹H-NMR (400 MHz, CD₃OD): δ 8.64 (s, 2H, H11), 7.90 (s, 2H, HR3), 7.25 (s, 2H, H$_{R5}$), 7.19 (s, 2H, H$_{R10}$), 4.83 (bs, 2H, H$_1$), 4.72-4.63 (m, 4H, H$_8$), 4.40-7.24 (m, 12H, H$_{G1}$, H$_{G5}$, H$_{G9}$), 4.04-3.88 (m, 16H, H$_{G2}$, H$_{G6}$, H$_{G10}$, H$_7$), 3.84-3.67 (m, 28H, H$_2$, H$_{D2}$, HG4, HG8, HG12, HG3, HG11, HG7), 3.66-3.61 (m, 4H, H3, HD1), 3.60-3.42 (m, 14H, H$_{6a}$, H$_{O\underline{Me}}$), 3.25-3.13 (m, 2H, H$_{6a}$), 2.79-2.58 (m, 4H, H$_{D4}$, H$_{D5}$), 2.02-1.84 (m, 4H, H$_{D3eq}$, H$_{D6eq}$), 1.73-1.59 (m, 4H, H$_{D3ax}$, H$_{D6ax}$), 1.45 (m, 18H, *t*Bu).

¹³C-NMR (100 MHz, CD₃OD): δ 176.84, 176.36 (<u>C</u>OOMe), 158.96 (<u>C</u>OO*t*Bu), 155.19, 154.95 (C$_{R10}$, C$_{R5}$), 149.79 (C$_{R3}$), 143.90 (C$_{TC4}$), 127.53 (C$_{TC5}$), 121.92 (C$_{R1}$), 119.14, 118.68 (C$_{R5}$, C$_{R10}$), 116.30, 114.11 (C$_{R4}$, C$_{R9}$), 111.99 (C$_{R2}$), 101,02 (C$_1$), 92.92, 91.10 (C$_{R7}$, C$_{R8}$), 80.33 (C$_{quat t Bu}$), 76.84 (C$_{D1}$), 74.15 (C$_5$), 74.15, 73.90 (C$_{G3}$, C$_{G7}$, C$_{G11}$), 72.95, 72.41, 71.99 (C$_{D2}$, C$_2$, C$_3$), 71.02, 70.94, 70.89, 70.85, 70.68 (C$_{G2}$, C$_{G5}$, C$_{G6}$, C$_{G9}$, C$_{G10}$), 69.57 (C$_4$), 69.41 (C$_{G1}$), 69.05 (C$_7$), 62.38, 62.37, 62.30 (C$_{G4}$, C$_{G8}$, C$_{G12}$), 52.34 (C$_{O\underline{Me}}$), 51.61 (C$_8$), 42.47 (C$_6$), 40.02 (C$_{D4}$, C$_{D5}$), 28.59, 28,02 (C$_{tBu}$, C$_{D6}$, C$_{D3}$)

MS (MALDI, DHB matrix): calculated for [C$_{96}$H$_{139}$N$_8$O$_{42}$]$^+$: 2077,2, found: 2076.9

[α]$_D$^{25}: +24 (c = 0.82 in MeOH)

Synthesis of divalent glycodendrimer 5.36
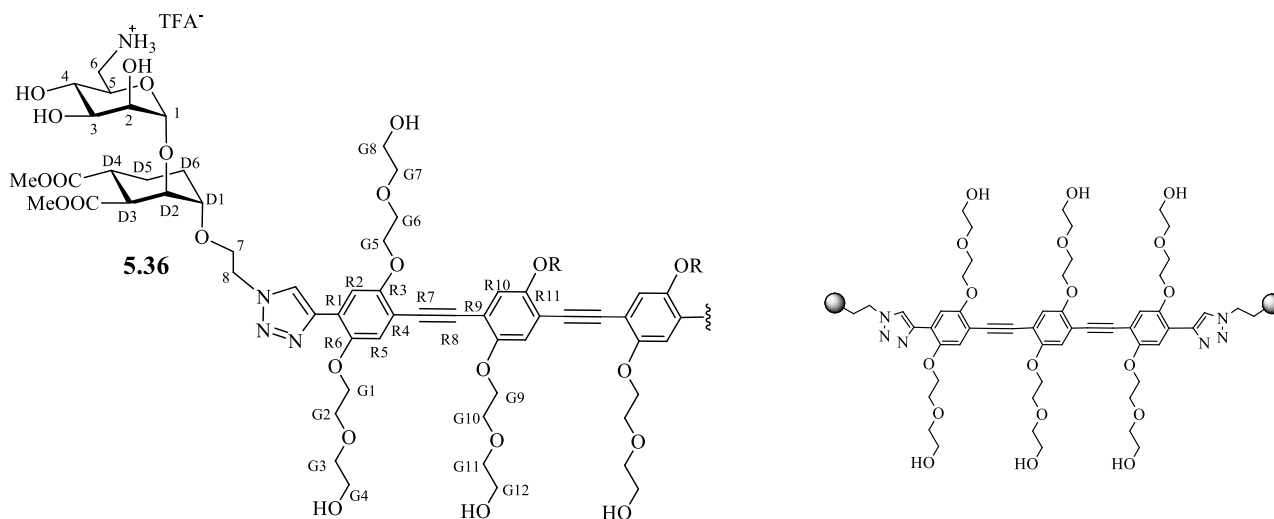
To a stirred solution of **5.35** (13.7 mg, 6.6 μmol, 1 eq.) in 1.8 mL of dry CH₂Cl₂, TFA (600 μL, 7.8 mmol, 120 eq.) was added. The reaction mixture was stirred for 1.5 h, under inert atmosphere and at room temperature. A TLC analysis (CHCl₃:MeOH:H₂O 8.5:1.5:0.2) revealed that the cleavage of Boc was complete. The crude was dried coevaporating with Et₂O (2 x 3 mL), to afford 13.9 mg of final product **5.36** as a yellow oil (yield 100 %).

8.64
7.88
7.24
7.18
4.91
4.69
4.50
4.35
4.27
3.98
3.96
3.82
3.78
3.72
3.68
3.58
3.53
3.31
3.13
3.12
2.71
1.97
1.67
1.49
1.28

2.00
1.81
2.32
2.00
4.24
1.32
5.67
8.22
22.78
9.99
26.64
19.15
2.50
5.03
5.63
3.86
3.15

f1 (ppm)

176.79
176.23
155.41
154.98
150.67
122.33
119.08
118.39
115.95
114.61
113.20
99.68
92.63
91.61
74.13
74.10
73.72
72.22
71.81
70.99
70.84
62.36
62.28
51.59
49.00
42.17
40.02
30.75
28.74
27.47

f1 (ppm)
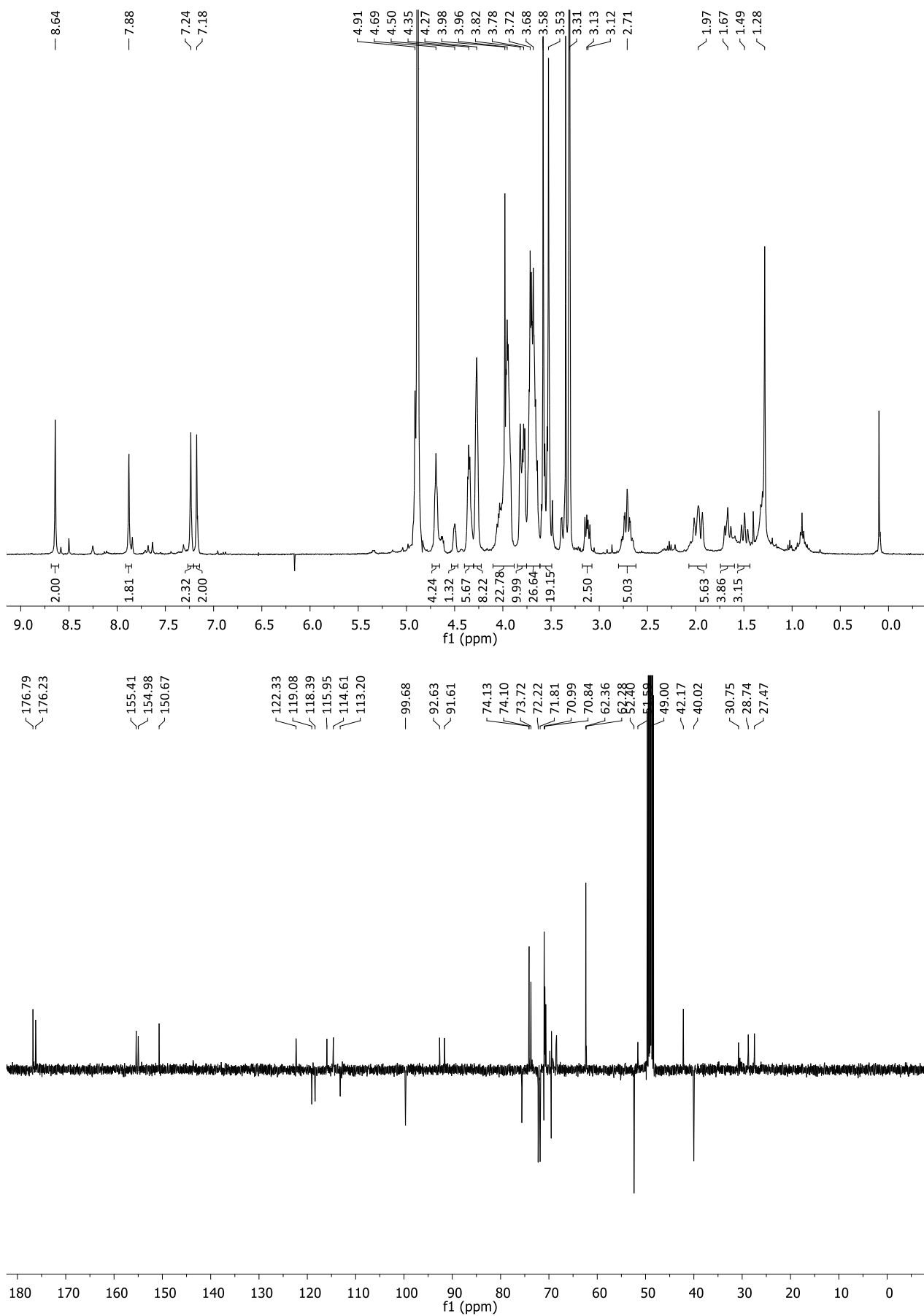
¹H-NMR (400 MHz, CD₃OD): δ 8.64 (s, 2H, H₁₁), 7.88 (s, 2H, H_{R3}), 7.24 (s, 2H, H_{R6}), 7.18 (s, 2H, H_{R11}), 4.92 (bs, 2H, H₁), 4.76-4.66 (m, 4H, H₈), 4.42-4.22 (m, 12H, H_{G9}, H_{G1}, H_{G5}), 4.10-3.89 (m, 16H, H_{G2}, H_{G6}, H_{G10}, H₇), 3.89-3.61 (m, 32H, H_{D2}, H₂, H₃, H₅, H_{G3}, H_{G4}, H_{G7}, H_{G8}, H_{G11}, H_{G12}), 3.61-3.49 (m, 16H, H_{OMe}, H_{D1}, H₄), 3.42-3.36 (m, 2H, H_{6a}), 3.19-3.07 (m, 2H, H_{6b}), 2.81-2.64 (m, 4H, H_{D5}, H_{D4}) 2.09-1.90 (m, 4H, H_{D3eq}, H_{D6eq}), 1.74-1.43 (m, 4H, H_{D3ax}, H_{D6ax}).

¹³C-NMR (100 MHz, CD₃OD): δ 176.94, 176.17 (COOMe), 155.41, 154.85 (C_{R6}, C_{R11}), 150.80 (C_{R3}), 143.54 (C_{TC5}), 122.46 (C_{R1}), 119.22, 118.49 (C_{R5}, C_{R10}), 116.01, 114.61 (C_{R4}, C_{R9}), 113.13 (C_{R2}), 99.72 (C₁), 92.71, 91.65 (C_{R7}, C_{R8}), 75.60 (C_{D1}), 74.10, 73.72 (C_{G3}, C_{G7}, C_{G11}), 72.22, 71.89, 71.81, 71.04 (C_{D2}, C₂, C₃, C₅), 70.99, 70.84, 70.65, 69.80 (C_{G2}, C_{G5}, C_{G6}, C_{G9}, C_{G10}), 69.52 (C₄), 69.47 (C₇), 68.55 (C_{G1}), 62.36, 62.28 (C_{G4}, C_{G8}, C_{G12}), 52.40 (C_{OMe}), 51.59 (C₈), 42.17 (C₆), 40.02 (C_{D4}, C_{D5}), 28.74, 27.47 (C_{D3}, C_{D6}).

**MS (MALDI, DHB matrix)**: calculated for $[C_{86}H_{122}N_8O_{38}]^+$: 1876,9, found: 1876.5

$[\alpha]_D^{25}$ was not performed because NMR analysis revealed the presence of a mixture of products in equilibrium in solution.

Synthesis of divalent glycodendrimer 5.37
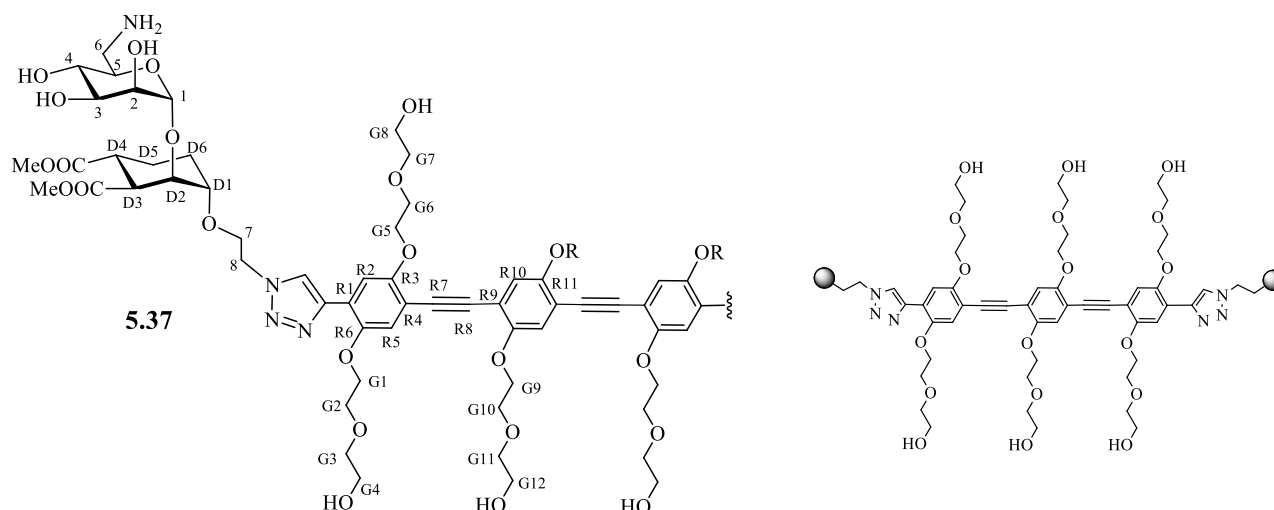
To a shaken solution of **5.36** (13.9 mg, 6.6 μmol, 1 eq.) in 1.6 mL of MeOH, Amberlyst A21® (60 mg, 50 eq.) was added, under inert atmosphere at room temperature and the reaction was shaken at 1500 rpm for 3 h. Then the crude was filtered on a cotton pad to remove the resin, washed with MeOH and then dried. 10.6 mg of final product **5.37** were obtained as a yellowish oil (yield 86 %).
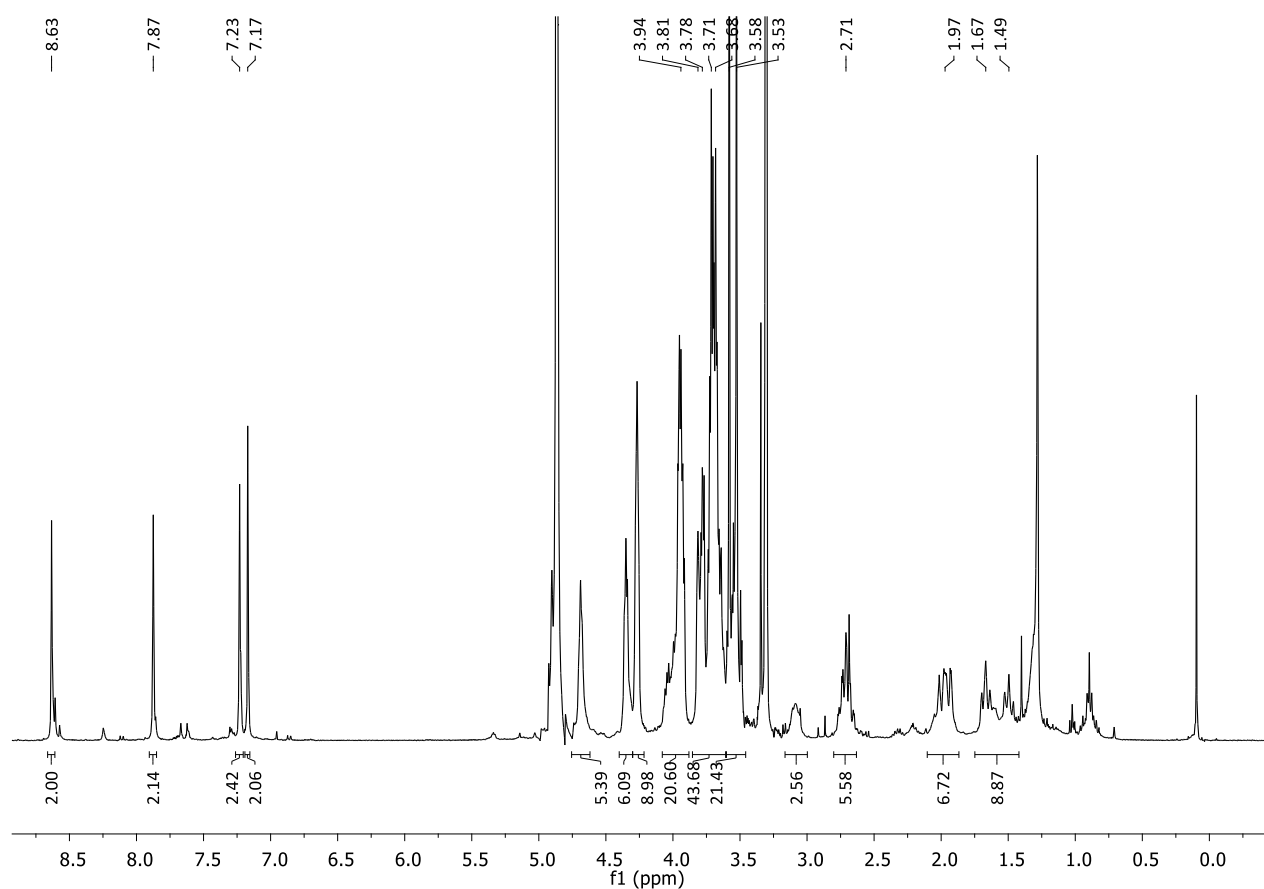
¹H-NMR (400 MHz, CD₃OD): δ 8.63 (s, 2H, H$_{TC5}$), 7.87 (s, 2H, H$_{R3}$), 7.24 (s, 2H, H$_{R5}$), 7.17 (s, 2H, H$_{R10}$), 4.90 (m, 2H, H$_1$), 4.72-4.64 (m, 4H, H$_8$), 4.43-4.17 (m, 12H, H$_{G9}$, H$_{G1}$, H$_{G5}$), 4.10-3.89 (m, 16H, H$_{G2}$, H$_{G6}$, H$_{G10}$, H$_7$), 3.86-3.60 (m, 32H, H$_{D2}$, H$_2$, H$_3$, H$_5$, H$_{G3}$, H$_{G4}$, H$_{G7}$, H$_{G8}$, H$_{G11}$, H$_{G12}$), 3.62-3.46 (m, 16H, H$_{O\underline{Me}}$, H$_5$, H$_{D1}$), 3.14-3.01 (m, 2H, H$_{6b}$), 2.79-2.65 (m, 4H, H$_{D4}$, H$_{D5}$), 2.11-1.87 (m, 4H, H$_{D3eq}$, H$_{D6eq}$), 1.72-1.4 (m, 4H, H$_{D3ax}$, H$_{D6ax}$).

MS (ESI-HRMS): Calculated for: $[C_{86}H_{123}N_8O_{38}Na]^{2+}$: 949.39180, found: 949.93389

[α]$_D^{25}$: +18.1 (c = 0.53 in MeOH).

Synthesis of hexavalent glycodendrimer, 5.38
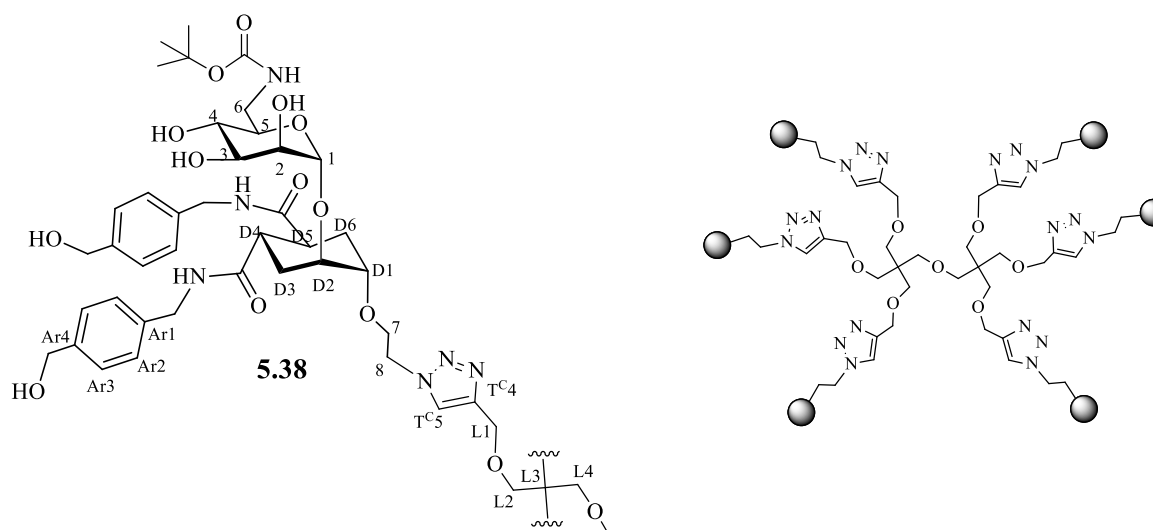
To Hexa(2-propynyloxymethyl)bispentaeritritol **2.24** (2.4 mg, 4.96 μmol, 1 eq.) dissolved in THF (100 μL) under inert atmosphere at room temperature, reagents were added as solutions in the following order: TBTA in THF (0.5 mg, 1.0 μmol, 0.2 eq., in 50 μL), $CuSO_4 \cdot 5H_2O$ in water (0.12 mg, 0.5 μmol, 0.1 eq., in 50 μL) and Sodium Ascorbate in water (0.4 mg, 2.0 μmol, 0.4 eq., in 50 μL). The reaction mixture was stirred under inert atmosphere, at room temperature and in the dark for 5 min, then **5.28** in H_2O was added (25.3 mg, 32.7 μmol, 6.6 eq., in 350 μL). The THF and water volumes were adjusted to 450 μL each and the mixture was stirred for 24 h. A MALDI mass analysis (DHB matrix) assessed the formation of the product. Quadrasil™-MP (S/Cu 15.1:1, 5 mg) was added to the reaction mixture, which was stirred for 10 min, and then filtered off. The crude was dried, then redissolved in MeOH and purified by size exclusion chromatography on a Sephadex LH-20 (MeOH) column. 18.9 of **5.38** were obtained as a white solid (yield 74 %).
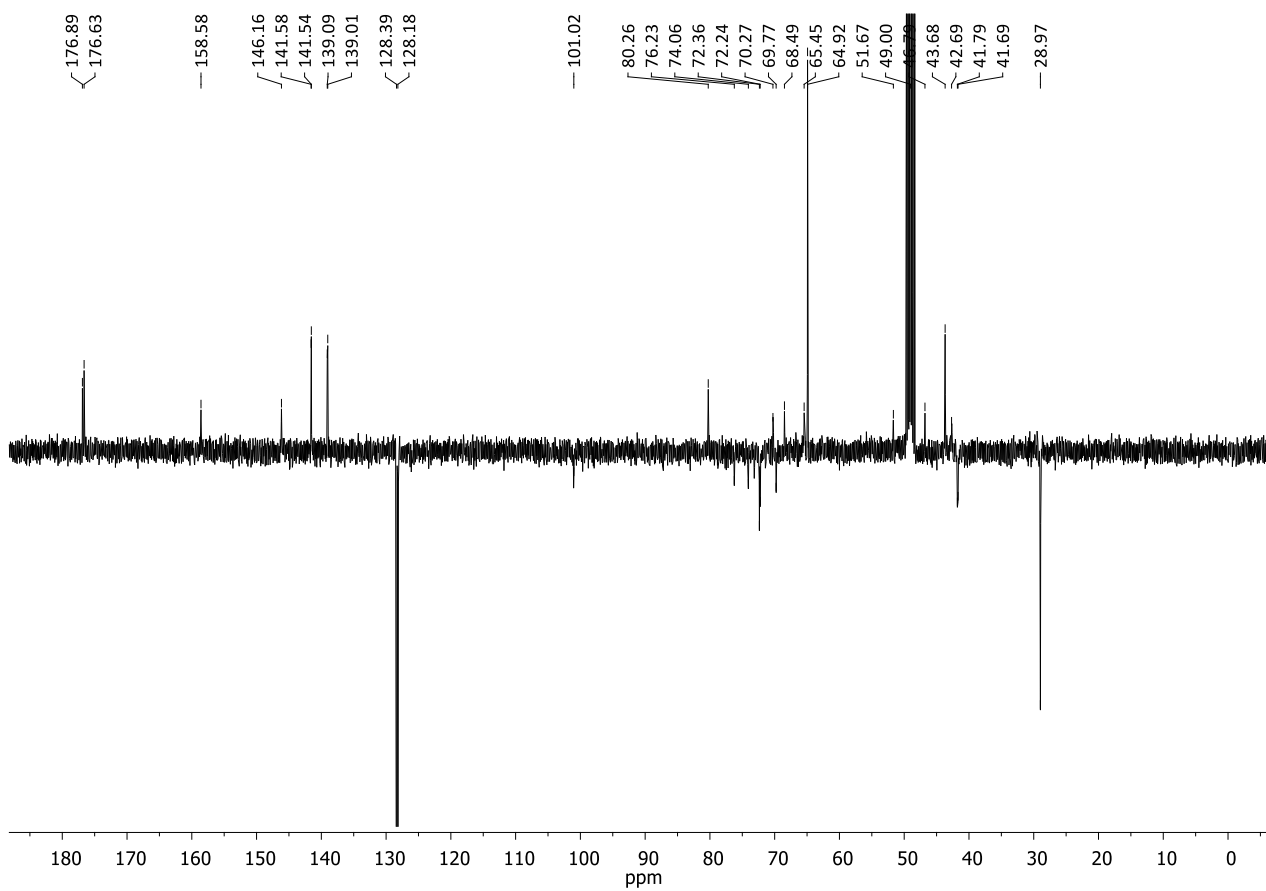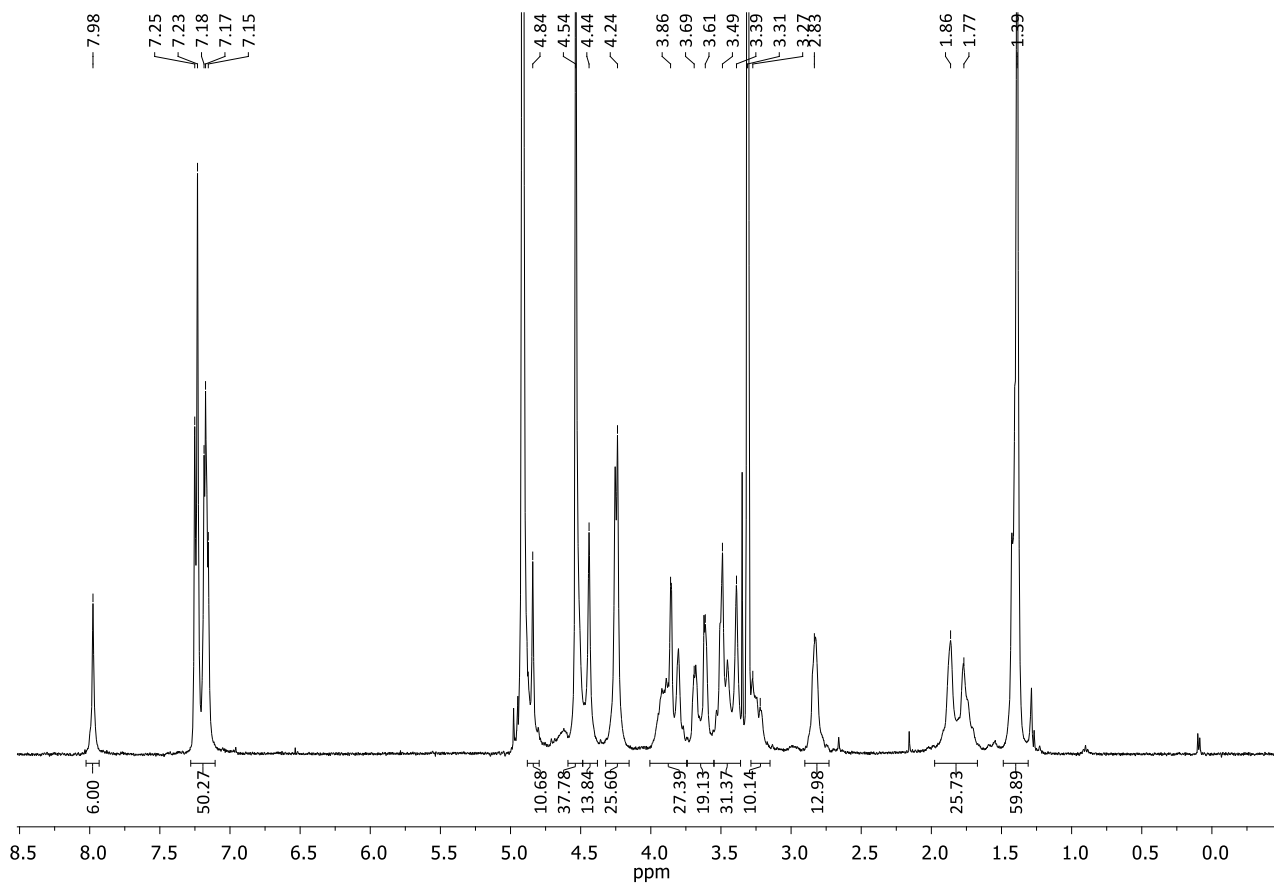
¹H NMR (400 MHz, CD₃OD): δ 7.98 (s, 6H, H$_{TC5}$), 7.32 – 7.06 (m, 48H, H$_{Ar2}$, H$_{Ar3}$), 4.84 (s, 6H, H$_1$), 4.60-4.40 (m, 48H, H8, H$_{L1}$, C$\underline{H}_2$OH), 4.30-4.20 (s, 24H, C$\underline{H}_2$NH), 4.00-3.74 (m, 24H; H$_7$, H$_2$, H$_{D2}$), 3.73-3.58 (m, 12H, H$_3$, H$_{D1}$), 3.56-3.35 (m, 34H, H$_4$, H$_5$, H$_{6a}$, H$_{L2}$, H$_{L4}$), 3.20-3.27 (m, 6H, H$_{6b}$), 2.75-2.84 (m, 12H, H$_{D4}$, H$_{D5}$), 1.90-1.70 (m, 24H, H$_{D3}$, H$_{D6}$), 1.39 (s, 36H, *t*Bu).

¹³C NMR (100 MHz, CD₃OD): δ 176.89, 176.63 ($\underline{C}$ONH), 158.58 ($\underline{C}$OO*t*Bu), 146.16 (C$_{TC4}$), 141.58, 141.54, 139.09, 139.00 (C$_{Ar1}$, C$_{Ar4}$), 128.39 (C$_{Ar2}$, C$_{Ar3}$), 128.18 (C$_{TC5}$), 101.02 (C$_1$), 80.26 (C$_{quat t Bu}$), 76.23 (C$_{D1}$), 74.06 (C$_5$), 72.36, 72.24 (C$_{D2}$, C$_2$, C$_3$), 70.27 (C$_{L2}$, C$_{L4}$), 69.77 (C$_4$), 68.49 (C$_7$), 65.45, 64.92 ($\underline{C}$H₂OH, C$_{L1}$), 51.67 (C$_8$), 46.79 ($\underline{C}$H₂NH), 43.68 (C$_6$), 42.69 (C$_{D4}$, C$_{D5}$), 41.79, 41.69, 28.97 (C$_{D3}$, C$_{D6}$, C$_{tBu}$).

MS (MALDI, DHB matrix): calculated for [C$_{250}$H$_{346}$N$_{36}$O$_{79}$Na]$^+$: 5142.6, found: 5145.3

[α]$_D$^{25}: -2.3 (c = 0.24 in MeOH)

**Synthesis of hexavalent glycodendrimer, 5.39**
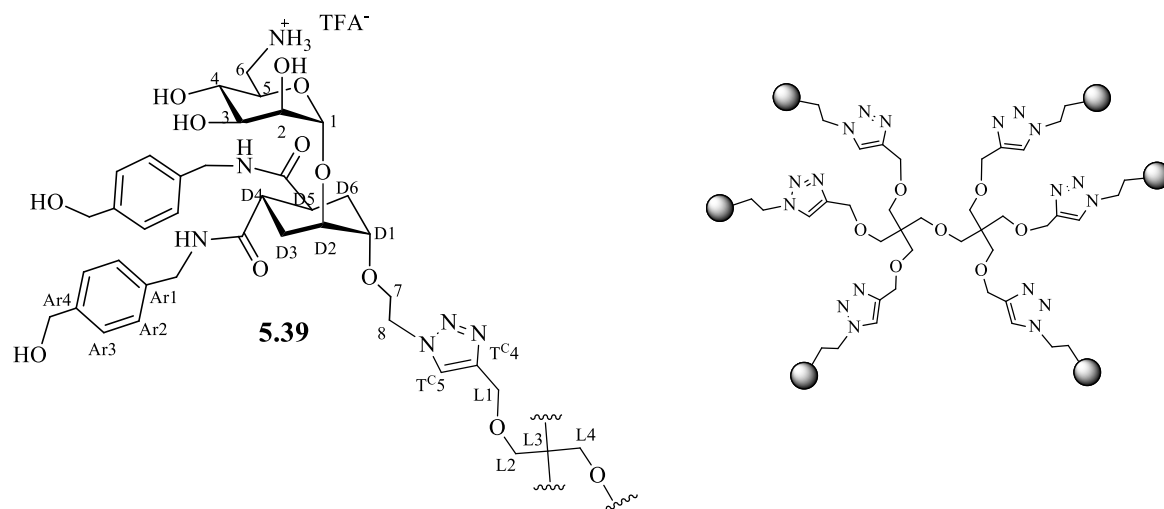
To a stirred solution of **5.38** (4.9 mg, 0.96 μmol, 1 eq.) in 125 μL of dry CH₂Cl₂, 125 μL of TFA (170 eq.) were added under inert atmosphere. The reaction was stirred for 1 h, at room temperature and under nitrogen atmosphere. A TLC analysis (CHCl₃:MeOH:H₂O 7:3:0.5) revealed that the reaction was complete. The reaction mixture was dried and washed with Et₂O (3 x 2 mL), affording 5.0 mg of final product (**5.39**) as a whit-brownish solid (yield 100 %).

Synthesis of hexavalent glycodendrimer, 5.40
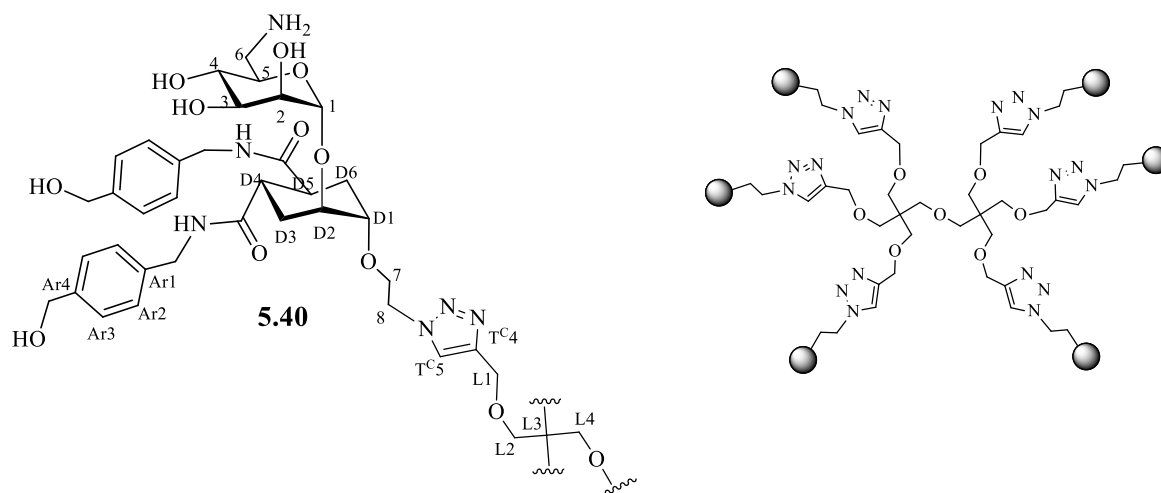
To a shaken solution of **5.39** (4.9 mg, 1.0 μmol, 1 eq.) in 700 μL of ry MeOH, Amberlyst A21® (16 mg, 100 eq.) was added, under inert atmosphere at room temperature, and the reaction was shaken at 1500 rpm for 3 h. Then the crude was filtered on a cotton pad to remove the resin, washed with MeOH and then dried. 4.5 mg of final product **5.40** were obtained as a white solid (yield 86%).
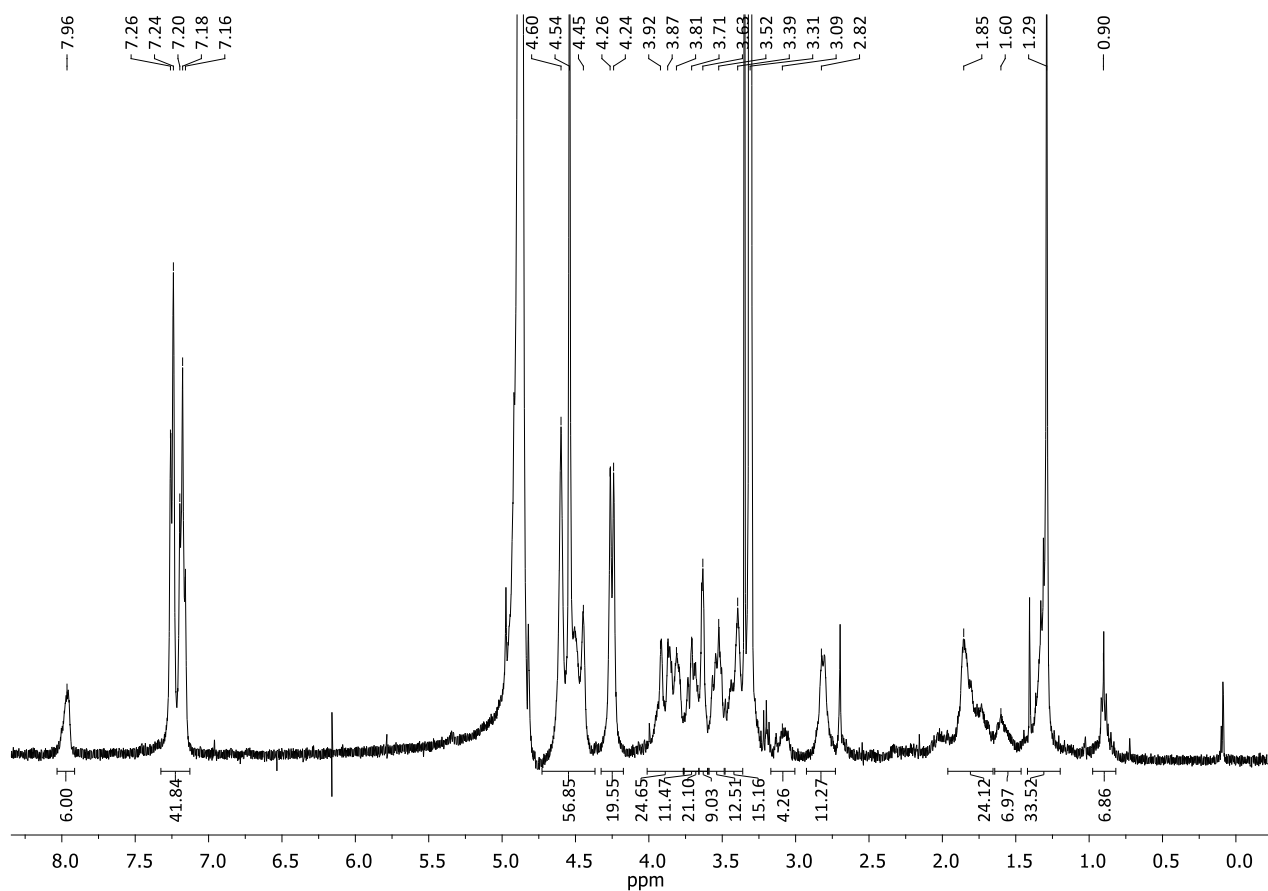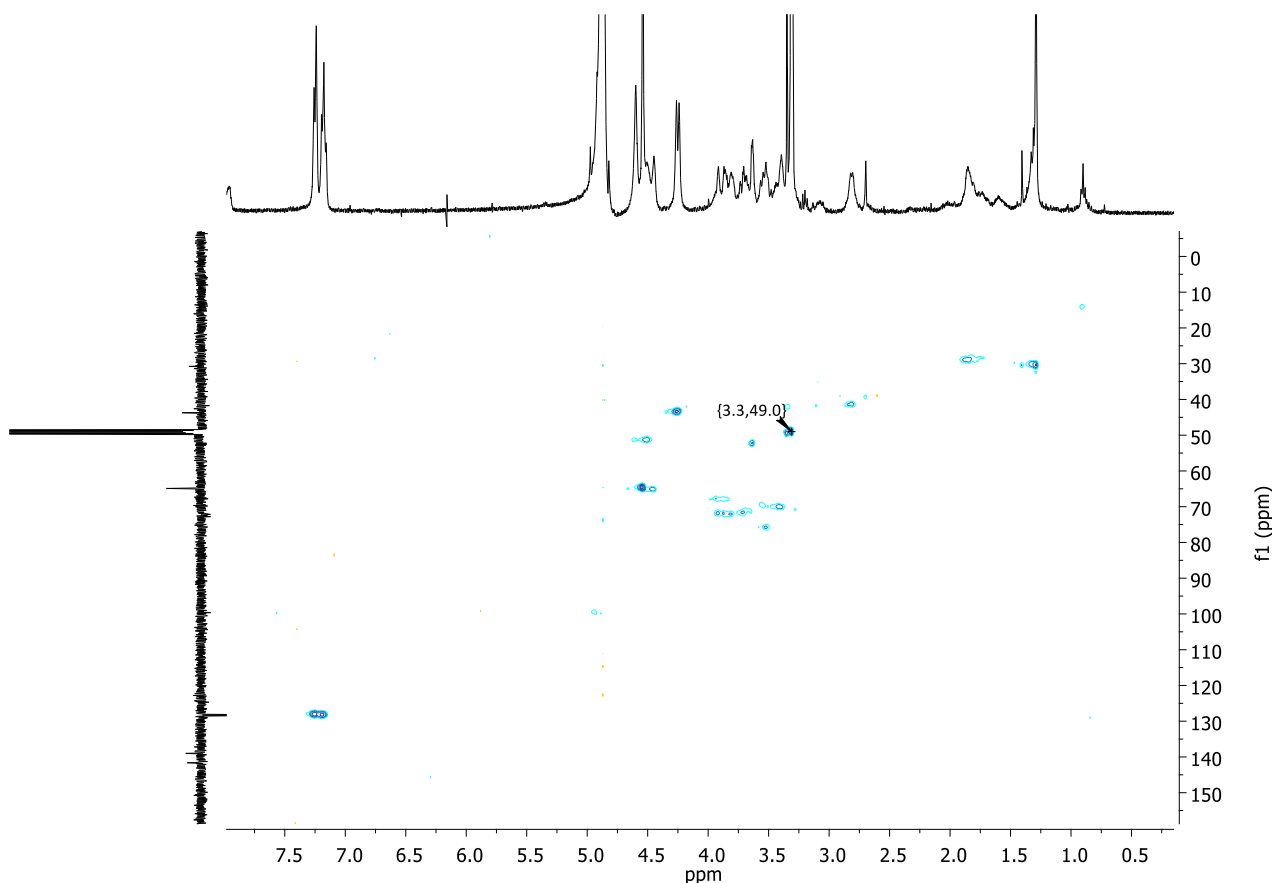
^{1}H NMR (400 MHz, CD$_3$OD): δ 7.98 (s, 6H; H$_{TC5}$), 7.32 − 7.12 (m, 48H, H$_{Ar2}$, H$_{Ar2}$), 4.72 − 4.37 (m, 48H, CH$_2$OH, H$_8$, H$_{L1}$), 4.20-4.28 (m, 24H, C$\underline{H}_2$NH), 4.00 − 3.75 (m, 24H, H$_7$, H$_2$, H$_{D2}$), 3.73-3.70 (m, 12H, H$_3$, H$_5$), 3.60-3.39 (m, 22H, H$_4$, H$_{L1}$, H$_{L2}$), 3.32 (6H, H$_{6a}$), 3.05-3.20 (m, 6H, H$_{6b}$), 2.75-2.85 (m, 12H, H$_{D4}$, H$_{D5}$), 1.90-1.60 (m, 24H, H$_{D3}$, H$_{D6}$).

^{13}C NMR (100 MHz, CD$_3$OD): δ 176.56 ($\underline{C}$ONH), 141.62 (C$_{TC4}$), 139.46, 139.39, 138.99 (C$_{Ar1}$, C$_{Ar2}$), 128.41 (C$_{Ar2}$, C$_{Ar3}$), 128.21 (C$_{TC5}$), 99.73 (C$_1$), 75.75 (C$_{D1}$), 72.16, 72.08, 71.90, 71.55 (C$_2$, C$_{D2}$, C$_3$, C$_5$), 70.11 (C$_{L2}$, C$_{L4}$), 69.64 (C$_4$), 67.93 (C$_7$), 65.17, 64.73 ($\underline{C}$H$_2$OH, C$_{L1}$), 51.27 (C$_8$), 43.73 ($\underline{C}$H$_2$NH), 42.64 (C$_6$), 41.71 (C$_{D4}$, C$_{D5}$), 30.85 (C$_{D3}$, C$_{D6}$).

$[\alpha]_D^{25}$: -3.9 (c = 0.15 in MeOH)

Synthesis of divalent glycodendrimer, 5.41
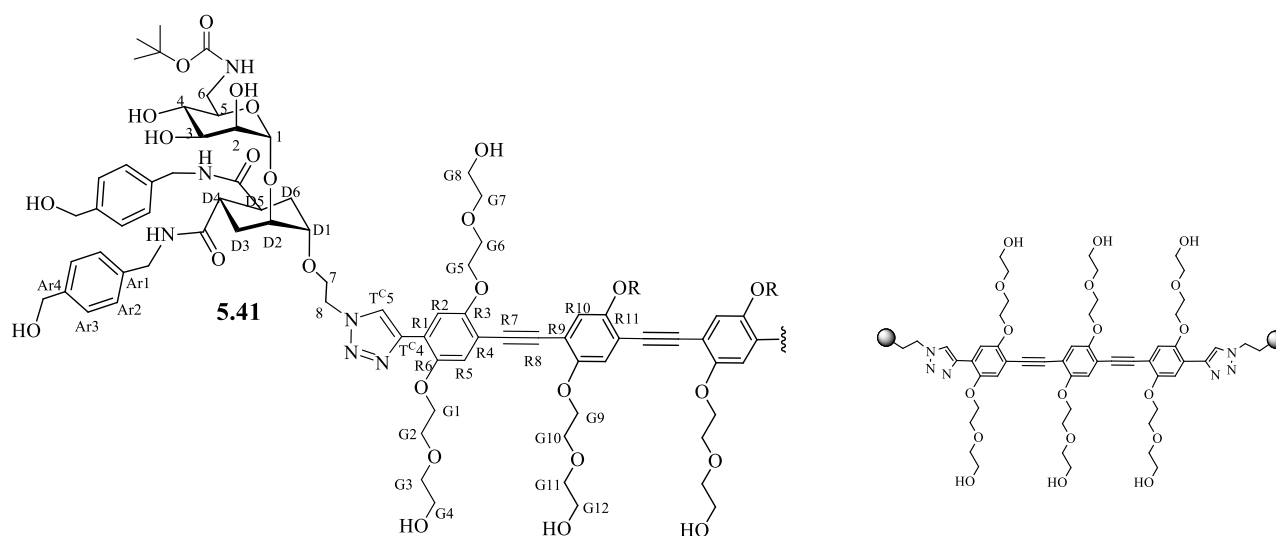
To a stirred solution of **TIPS-2.5** (8.1 mg, 6.4 µmol, 1 eq.) in 200 µL of THF, TBAF (1M in THF, 12.8 µL, 12.8 µmol, 2 eq.) was added under inert atmosphere and the mixture was stirred for 1 h; a TLC analysis (CHCl$_3$:MeOH 9:1) revealed that the desilylation reaction was complete. Then reagents were added as solutions in the following order: TBTA in THF (0.68 mg, 1.28 µmol, 0.2 eq, in 120 µL), CuSO$_4$·5H$_2$O in water (0.16 mg, 0.64 µmol, 0.1 eq., in 60 µL) and Sodium Ascorbate in water (0.51 mg, 2.56 µmol, 0.4 eq., in 60 µL). The reaction mixture was stirred, under inert atmosphere at room temperature in the dark, for 5 min. Then **5.28** in water (10.5 mg, 14.1 µmol, 2.2 eq., in 200 µL) was added to the mixture; THF and water volumes were adjusted to 320 µL each. The mixture was stirred for 18 h under inert atmosphere, at room temperature and in the dark. A MALDI mass analysis (DHB matrix) assessed the formation of the product. The reaction was quenched by the addition of Quadrasil™-MP (S/Cu 11.8:1, 5 mg), which was added to the reaction mixture, stirred for 20 min and then filtered off. The crude was dried, redissolved in MeOH and purified first by size exclusion chromatography on a Sephadex LH-20 (MeOH) and then by automated reverse phase chromatography (H$_2$O with a gradient of methanol from 0 % to 100 %), to give 8.7 mg of **5.41** as a yellowish solid (yield 54 %).
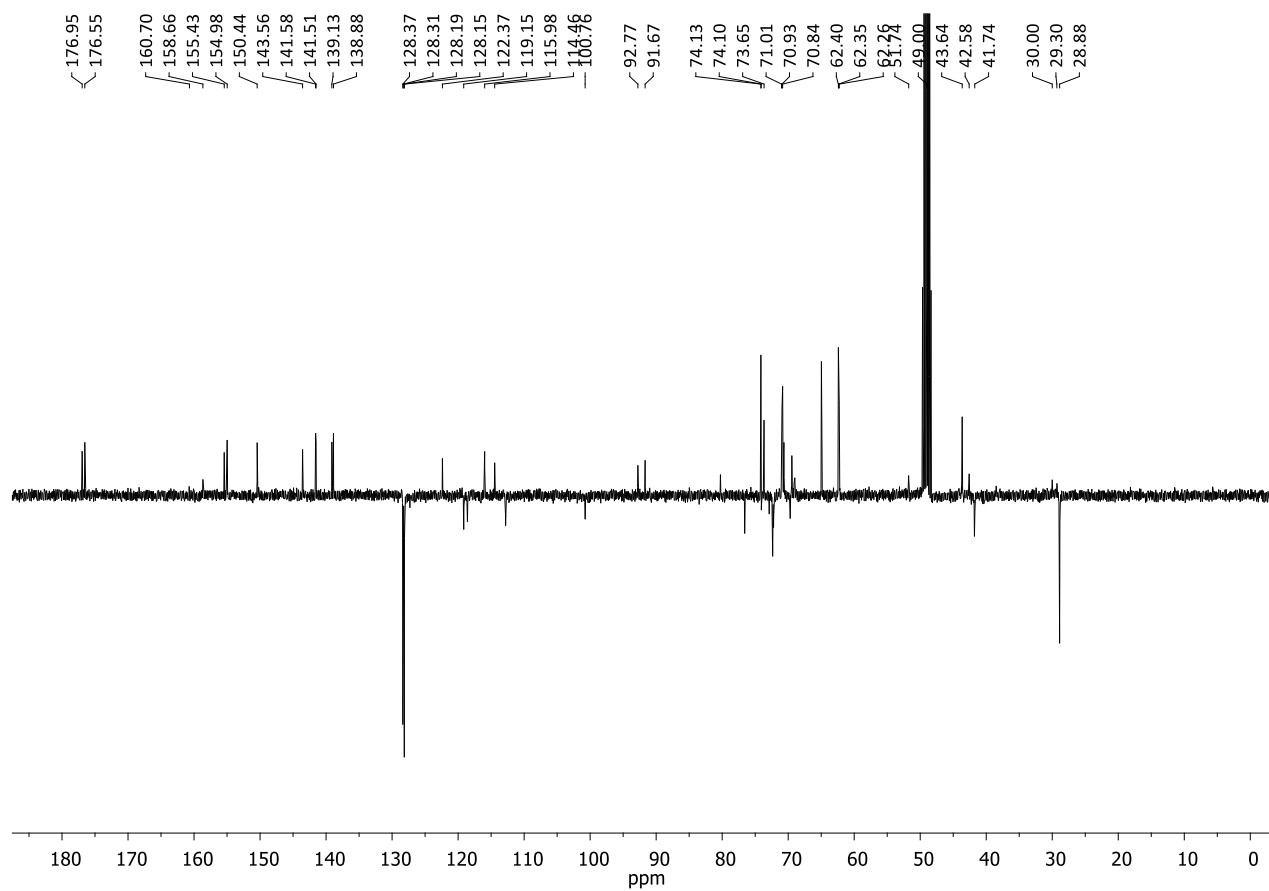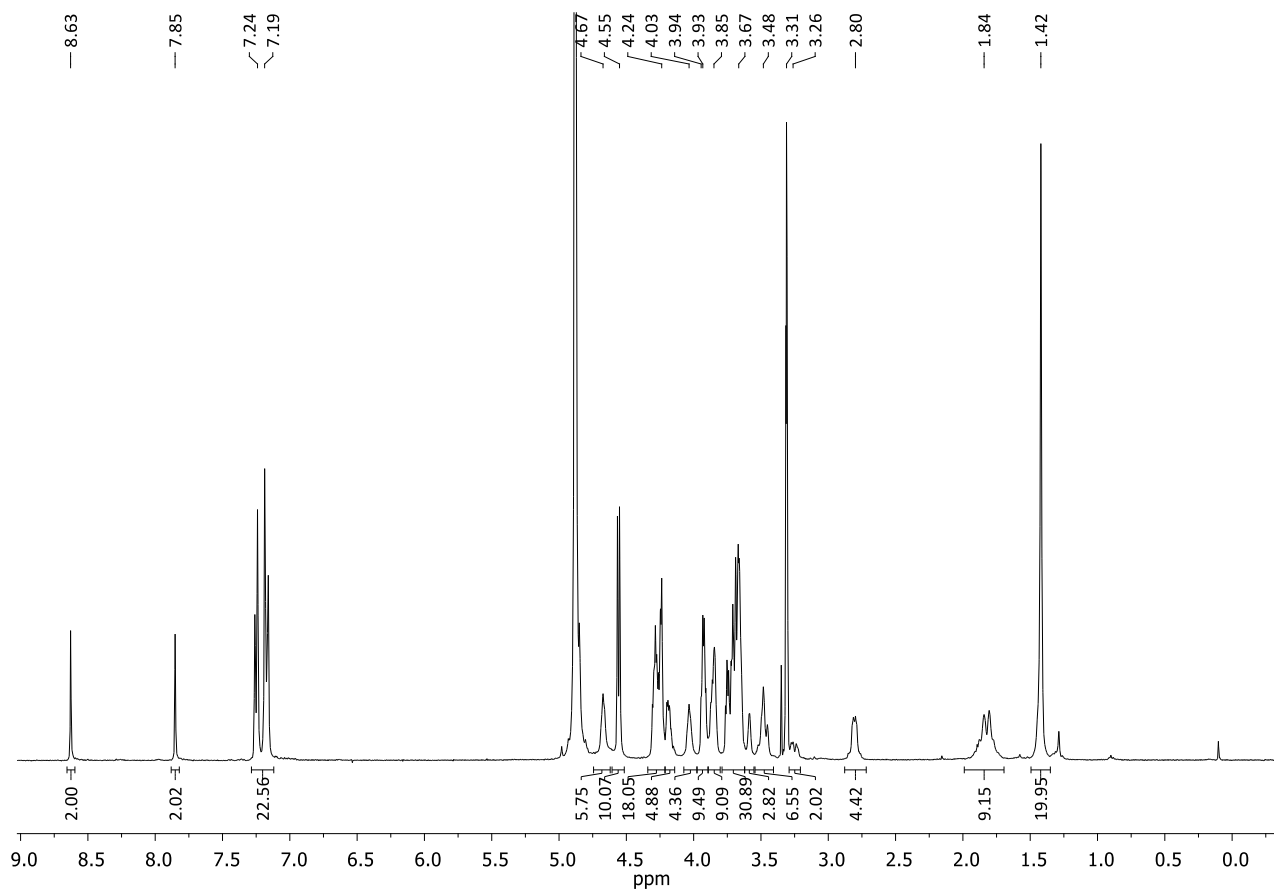
¹H NMR (400 MHz, CD₃OD): δ 8.63 (s, 2H, H_{TC5}), 7.85 (s, 2H, H_{R2}), 7.33-7.10 (m, 20H, H_{R10}, H_{R5}, H_{Ar2}, H_{Ar3}), 4.91 (bs, 2H, H_1), 4.72-4.60 (m, 4H, H_8), 4.59-4.50 (m, 8H, CH_2OH), 4.35-4.13 (m, 20H, CH_2NH, H_{G1}, H_{G5}, H_{G9}), 4.08-3.96 (m, 4H, H_7), 3.95-3.80 (m, 16H, H_2, H_{D2}, H_{G2}, H_{G6}, H_{G10}), 3.78 – 3.62 (m, 26H, H_3, H_{G3}, H_{G7}, H_{G11}, H_{G4}, H_{G8}, H_{G12}), 3.62-3.57 (m, 1H, H_{D1}), 3.52-3.40 (H_4, H_5), 3.31 (2H, H_{6a}), 3.30-3.22 (m, 2H, H_{6b}), 2.85-2.70 (m, 4H, H_{D4}, H_{D5}), 1.90-1.70 (m, 8H, H_{D3}, H_{D6}), 1.42 (s, 18H, *t*Bu).

¹³C NMR (100 MHz, CD₃OD): δ 176.95, 176.55 ($\underline{C}OONH$), 158.66 ($\underline{C}OOtBu$), 155.43, 154.98 (C_{R6}, C_{R11}), 150.44 (C_{R3}), 143.56 (C_{TC4}), 141.58, 141.51, 139.13, 138.88 (C_{Ar1}, C_{Ar4}), 128.37, 128.31, 128.19, 128.15 (C_{Ar2}, C_{Ar3}), 127.41 (C_{TC5}), 122.37 (C_{R1}), 119.15, 118.58 (C_{R5}, C_{R10}), 115.98, 114.46 (C_{R4}, C_{R9}), 112.81 (C_{R2}), 100.76 (C_1), 92.77, 91.67 (C_{R7}, C_{R8}), 80.26 ($C_{quat\,tBu}$), 76.59 (C_{D1}), 74.13, 74.10 (C_{G3}, C_{G7}), 74.03 (C_5), 73.65 (C_{G11}), 72.87, 72.35, 72.21 (C_2, C_{D2}, C_3), 71.01, 70.93, 70.84, 70.65 (C_{G5}, C_{G9}, C_{G2}, C_{G6}, C_{G10}), 69.69 (C_4), 69.44 (C_{G1}), 68.99 (C_7), 64.947, 64.94 ($\underline{C}H_2OH$), 62.40, 62.35, 62.26 (C_{G4}, C_{G8}, C_{G12}), 51.74 (C_8), 43.64 ($\underline{C}H_2NH$), 42.58 (C_6), 41.74 (C_{D4}, C_{D5}), 30.00, 29.30 (C_{D3}, C_{D6}), 28.88 (C_{tBu}).

MS (MALDI, DHB matrix): calculated for $[C_{124}H_{166}N_{12}O_{42}Na]^+$: 2519.7, found: 2517.9

$[\alpha]_D^{25}$: -0.9 (c = 0.38 in MeOH)

Synthesis of divalent glycodendrimer, 5.42
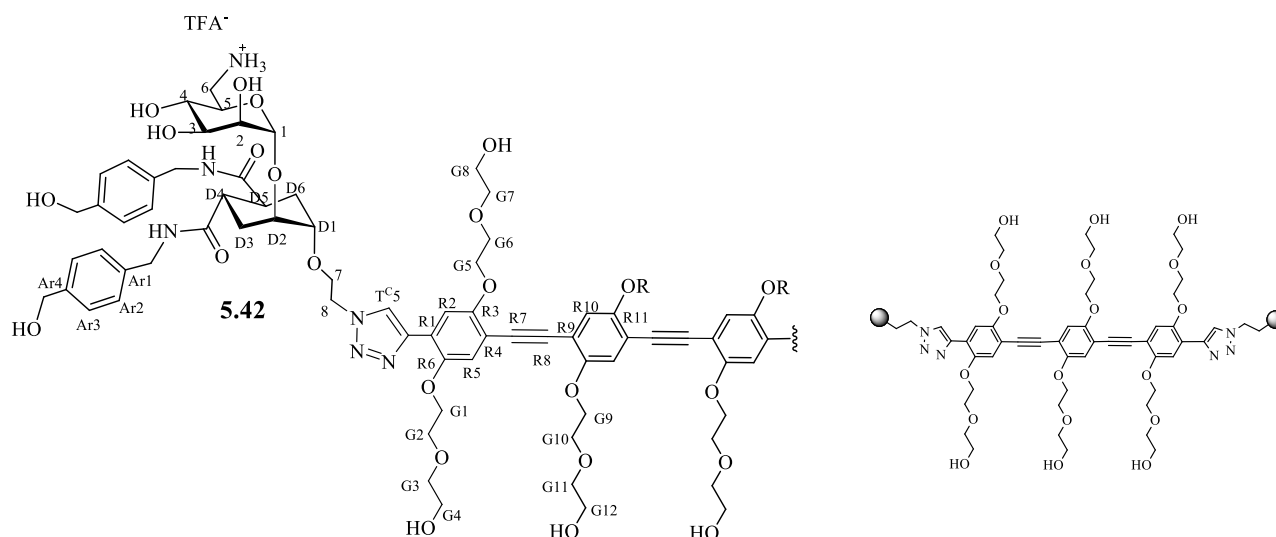
To a stirred solution of **5.41** (8.7 mg, 3.5 µmol, 1 eq.) in 500 µL of CH_2Cl_2, TFA (500 µL) was added, under inert atmosphere at room temperature and the mixture was stirred for 1 h. TLC (CHCl₃:MeOH:H₂O 7.5:5.5:0.25) and MALDI mass (HCCA matrix) analysis revealed that the
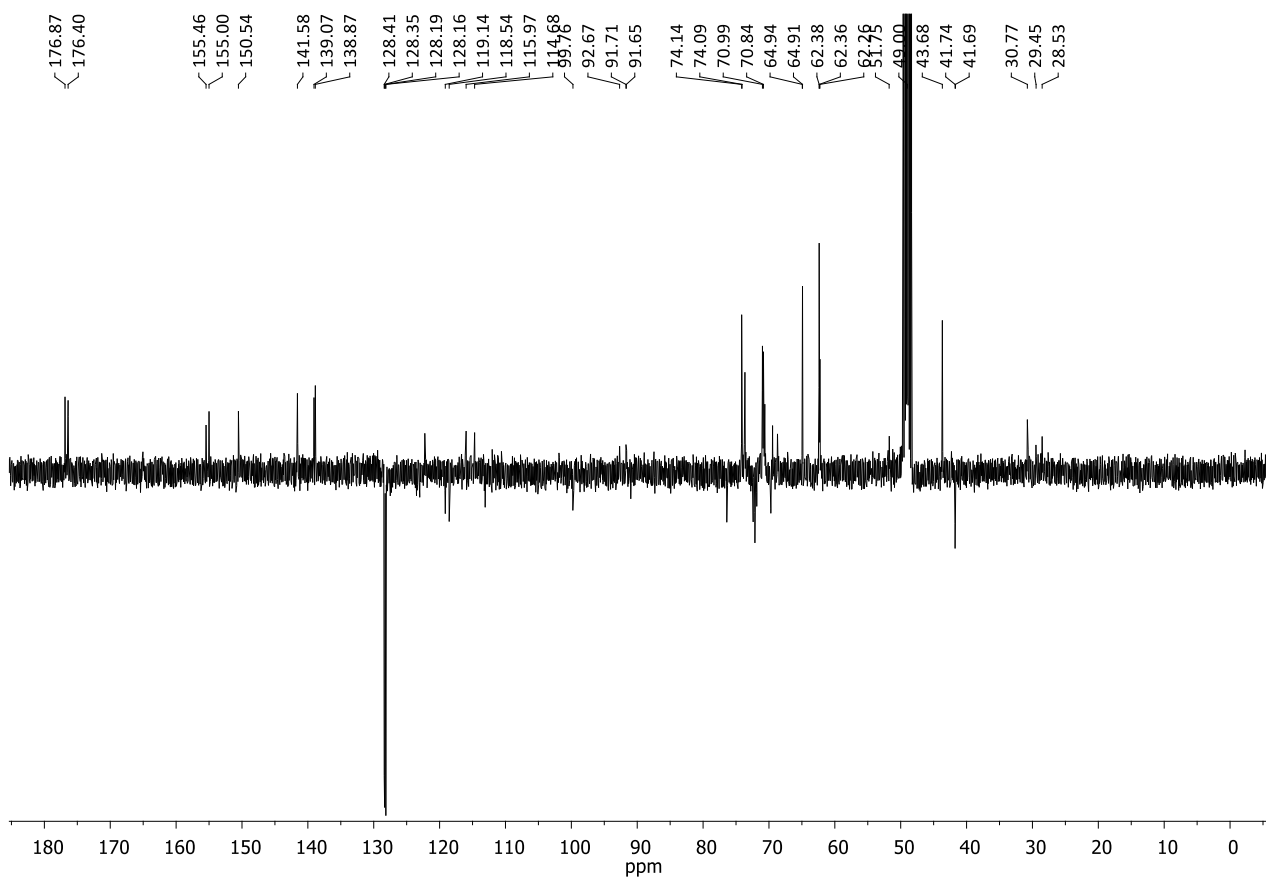
reaction was complete. The crude was dried coevaporating with Et$_2$O (3 x 1 mL), to afford 8.7 mg of final product **5.42** as a yellow oil (yield 100 %).

MS (MALDI, HCCA matrix): calculated for [C$_{114}$H$_{150}$N$_{12}$O$_{38}$Na]$^+$: 2319.5, found: 2319.0

Synthesis of divalent glycodendrimer, 5.43
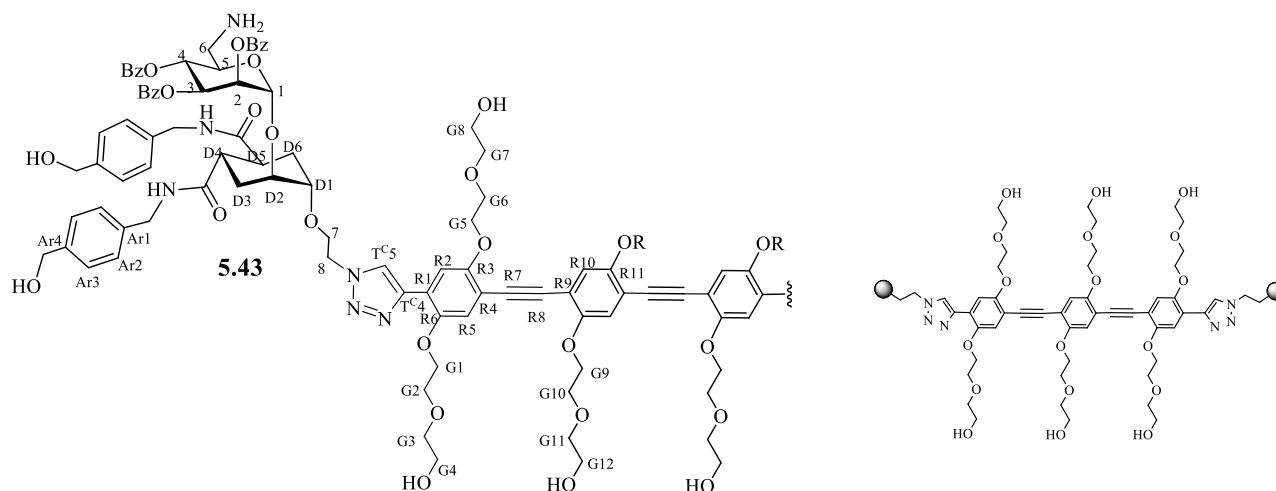
To a shaken solution of **5.42** (8.7 mg, 3.5 μmol, 1 eq.) in 1.7 mL of dry MeOH, Amberlyst A21$^®$ (60 mg, 100 eq.) was added, under inert atmosphere at room temperature and the reaction was shaken at 1500 rpm for 3 h. Then the crude was filtered on a cotton pad to remove the resin, washed with MeOH and then dried. 7.3 mg of final product **5.43** were obtained as a yellowish oil (yield 91 %).

8.64
7.85
7.25
7.19
4.55
4.25
3.92
3.69
3.54
3.31
3.11
2.80
1.82
1.29

2.00
0.61
1.71
1.11
20.69
3.90
3.01
8.70
20.10
5.37
13.83
31.66
5.84
2.02
2.30
4.73
9.30
0.70
8.60
2.66

9.0 8.5 8.0 7.5 7.0 6.5 6.0 5.5 5.0 4.5 4.0 3.5 3.0 2.5 2.0 1.5 1.0 0.5 0.0
ppm

176.87
176.40
155.46
155.00
150.54
141.58
139.07
138.87
128.41
128.35
128.19
128.16
119.14
118.54
115.97
114.68
99.76
92.67
91.71
91.65
74.14
74.09
70.99
70.84
64.94
64.91
62.38
62.36
51.26
51.75
49.00
43.68
41.74
41.69
30.77
29.45
28.53

180 170 160 150 140 130 120 110 100 90 80 70 60 50 40 30 20 10 0
ppm

¹H NMR (400 MHz, CD₃OD): δ 8.64 (s, 2H, H$_{TC5}$), 7.85 (s, 2H, H$_{R2}$), 7.28-7.10 (m, 20H, H$_{R10}$, H$_{R5}$, H$_{Ar2}$, H$_{Ar3}$), 4.91 (bs, 2H, H$_1$), 4.72-4.50 (m, 12H, H$_8$, C$\underline{H}_2$OH), 4.37-4.12 (m, 20H, C$\underline{H}_2$NH, H$_{G1}$, H$_{G5}$, H$_{G9}$), 4.10-3.99 (m, 4H, H$_7$), 3.95-3.80 (m, 14H, H$_2$, H$_{G2}$, H$_{G6}$, H$_{G10}$), 3.79 − 3.63 (m, 30H, H$_{D2}$, H$_3$, H$_5$, H$_{G3}$, H$_{G7}$, H$_{G11}$, H$_{G4}$, H$_{G8}$, H$_{G12}$), 3.58-3.45 (m, 4H, H$_4$, H$_{D1}$), 3.3-40-3.33 (m, 2H, H$_{6a}$), 3.20-3.07 (m, 2H, H$_{6b}$), 2.85-2.70 (m, 4H, H$_{D4}$, H$_{D5}$), 1.90-1.70 (m, 6H, H$_{D3}$, H$_{D6}$).

¹³C NMR (100 MHz, CD₃OD): δ 176.87, 176.40 ($\underline{C}$ONH), 155.46, 155.00 (C$_{R6}$, C$_{R11}$), 150.54 (C$_{R3}$), 141.63, 141.58, 139.07, 138.87 (C$_{Ar1}$, C$_{Ar4}$), 128.41, 128.35, 128.19, 128.16 (C$_{Ar2}$, C$_{Ar3}$), 127.33 (C$_{TC5}$), 122.24 (C$_{R1}$), 119.14, 118.54 (C$_{R5}$, C$_{R10}$), 116.64, 115.97, 115.91, 114.68 (C$_{R4}$, C$_{R9}$), 113.08 (C$_{R2}$), 99.76 (C$_1$), 92.67, 91.71 (C$_{R7}$, C$_{R8}$), 76.40 (C$_{D1}$), 74.14, 74.09, 73.65 (C$_{G3}$, C$_{G7}$, C$_{G11}$), 72.40, 72.13, 71.85 (C$_3$, C$_5$, C$_2$, C$_{D2}$), 70.99, 70.84, 70.63 (C$_{G5}$, C$_{G9}$, C$_{G2}$, C$_{G6}$, C$_{G10}$), 69.71 (C$_4$), 69.45 (C$_{G1}$), 68.70 (C$_7$), 64.94, 64.91 ($\underline{C}$H$_2$OH), 62.38, 62.36, 62.26 (C$_{G4}$, C$_{G8}$, C$_{G12}$), 51.75 (C$_8$), 43.68 ($\underline{C}$H$_2$NH), 41.74 (C$_{D4}$, C$_{D5}$), 41.69 (C$_6$), 30.77, 29.45 (C$_{D3}$, C$_{D6}$).

MS (ESI, HRMS): calculated for: [C$_{144}$H$_{150}$N$_{12}$O$_{38}$Na$_2$]$^{2+}$: 1170.99948; found: 1171.03374

[α]$_D$^{25}: -0.5 (c = 0.32 in MeOH)

Synthesis trivalent glycodendrimer, 5.44
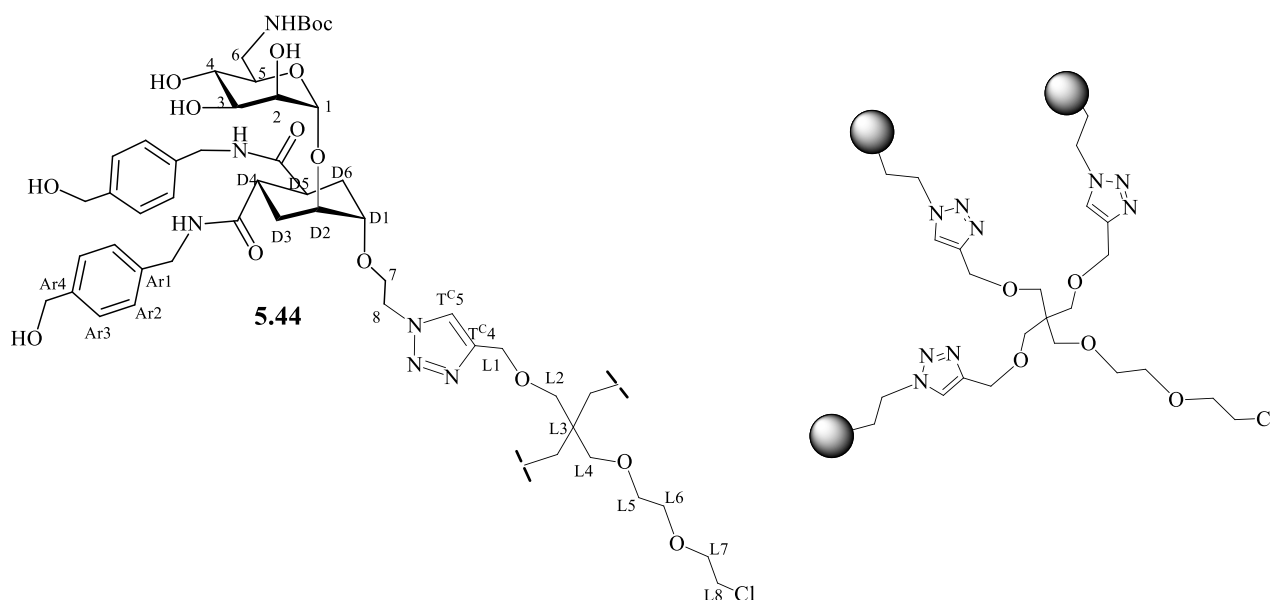
To scaffold **2.27** (7.0 mg, 19.6 μmol, 1 eq.) dissolved in THF (150 μM) under inert atmosphere at room temperature, reagents were added as solutions in the following order: TBTA in THF (2.1 mg, 3.9 μmol, 0.2 eq., in 200 μL), CuSO$_4$·5H$_2$O in water (0.48 mg, 1.96 μmol, 0.1 eq., in 200 μL) and Sodium Ascorbate in water (1.55 mg, 7.84 μmol, 0.4 eq., in 200 μL). The reaction mixture was

stirred under inert atmosphere, at room temperature and in the dark for 5 min, then **5.28** in water was added (50.0 mg, 64.7 μmol, 3.3 eq., 400 μL). The THF and water volumes were adjusted to 900 μL each and the mixture was stirred for 18 h. A MALDI mass analysis (DHB Matrix) assessed the formation of the product. Quadrasil™-MP (S/Cu 1.9:1, 5 mg) was added to the reaction mixture, which was stirred for 20 min and then filtered off. The crude was dried, then redissolved in MeOH and purified by size exclusion chromatography on a Sephadex LH-20 (MeOH) column to give 37.2 mg of **5.44** as a colourless solid (yield 71 %).

^{1}H NMR (400 MHz, CD$_3$OD): δ 8.01 (s, 3H, H$_1$), 7.33 – 7.17 (m, 24H, H$_{Ar2}$, H$_{Ar3}$), 4.65-4.44 (m, 24H, H$_8$, H$_{L1}$, C$\underline{H}_2$OH), 4.34-4.22 (m, 12H, C$\underline{H}_2$NH), 4.03-3.91 (m, 6H, H$_7$), 3.90-3.87 (m, 3H, H$_2$), 3.87-3.81 (m, 3H, H$_{D2}$), 3.75-3.39 (m, 28H, H$_{D1}$, H$_3$, H$_2$, H$_{6a}$, H$_{L2}$, H$_{L4}$, H$_{L5}$, H$_{L6}$, H$_{L7}$, H$_{L8}$), 3.30-3.20 (m, 3H, H$_{6b}$), 2.92-2.75 (m, 6H, H$_{D4}$, H$_{D5}$), 2.01-1.68 (m, 12H, H$_{D3}$, H$_{D6}$), 1.43 (s, 9H, *t*Bu).

^{13}C NMR (100 MHz, CD$_3$OD): δ 176.85, 176.63 ($\underline{C}$ONH), 158.58 ($\underline{C}$OO*t*Bu), 146.17 (C$_{T4}$), 141.58, 139.07, 138.98 (C$_{Ar1}$, C$_{Ar4}$), 128.38, 128.16 (C$_{Ar2}$, C$_{Ar3}$), 126.07 (C$_{T5}$), 100.95 (C$_1$), 80.24 (C$_{quat\it{t}Bu}$), 76.25 (C$_{D1}$), 74.05 (C$_5$), 73.00 (C$_{D2}$), 72.44, 72.34, 72.25, 72.09, 71.34, 70.75, 70.07 (C$_3$, C$_2$, C$_{L2}$, C$_{L4}$, C$_{L5}$, C$_{L6}$, C$_{L7}$), 69.79 (C$_4$), 68.49 (C$_7$), 65.34, 64.92 (C$_{L1}$, $\underline{C}$H$_2$OH), 51.69 (C$_8$), 46.57 (C$_{L3}$), 44.10 (C$_{L8}$), 43.67 ($\underline{C}$H$_2$NH), 42.66 (C$_6$), 41.78, 41.70 (C$_{D4}$, C$_{D5}$), 29.81, 29.35 (C$_{D3}$, C$_{D6}$), 28.91 (C$_{\it{t}Bu}$).

MS (MALDI, DHB matrix): calculated for [C$_{129}$H$_{182}$ClN$_{18}$O$_{41}$]$^+$: 2676.4, found: 2676.0
calculated for [C$_{129}$H$_{181}$ClN$_{18}$O$_{41}$Na]$^+$: 2698.4, found: 2698.9

[α]$_D^{25}$: 1.6 (c = 0.75 in MeOH)

Synthesis of trivalent glycodendrimer, 5.45
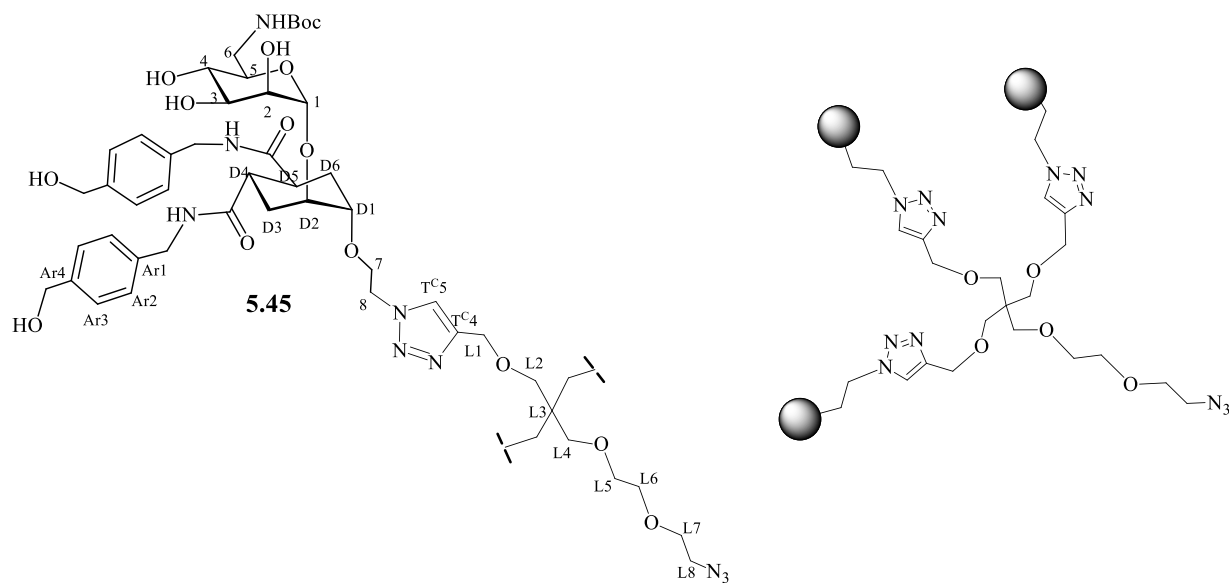
To a solution of **5.44** (37.2 mg, 13.9 μmol, 1 eq.) in dry DMF (200 μL), sodium azide (4.5 mg, 69 μmol, 5 eq.) and NaI (0.2 mg, 1.4 μmol, 0.1 eq.) were added. The reaction was stirred at 50 °C for 6 days, assessing the total conversion of the starting material by MALDI MS analysis (matrix DHB). The solvent was removed under reduce pressure and the crude residue was purified by size exclusion chromatography on a Sephadex LH-20® column to give 31.4 mg of **5.45** as a colourless solid (yield 84 %).
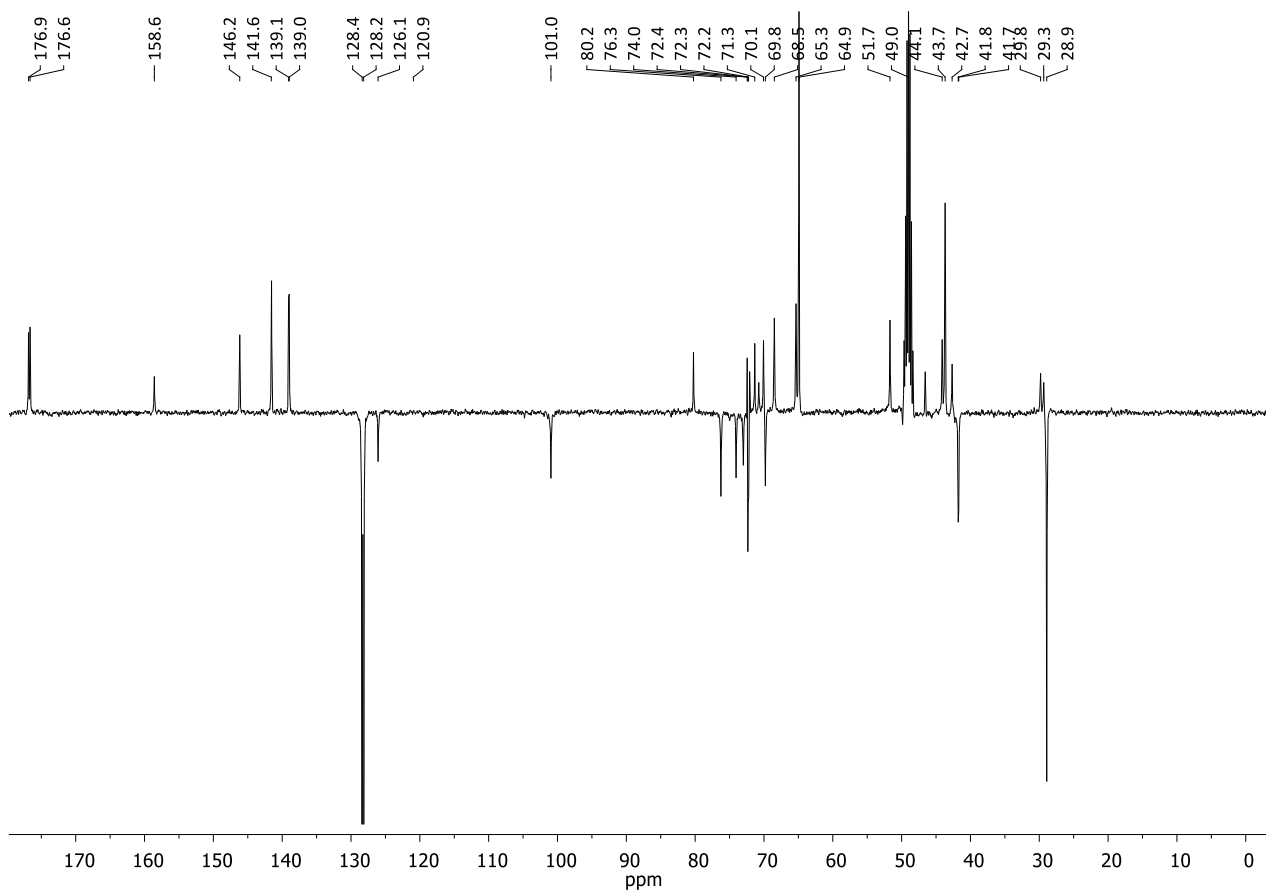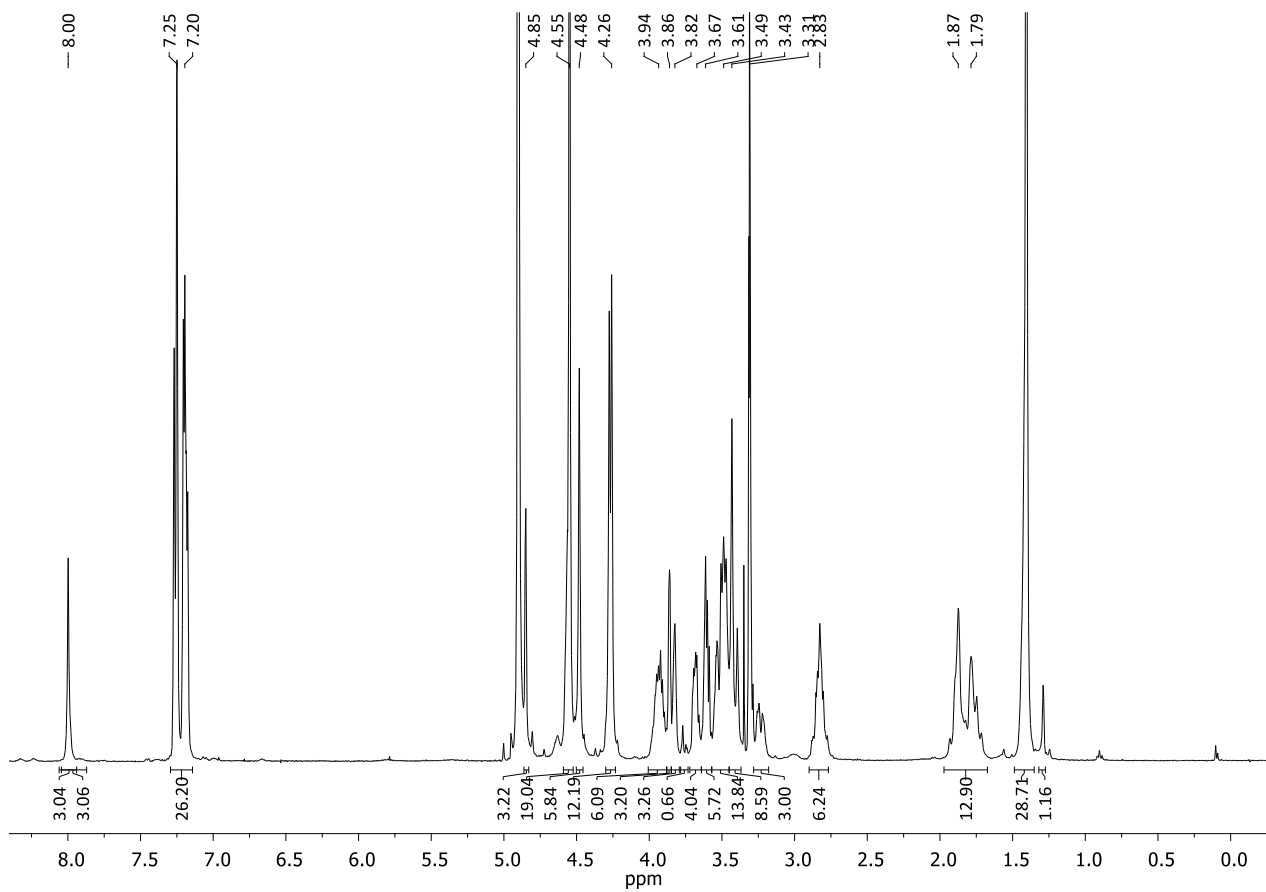
¹H NMR (400 MHz, CD₃OD): δ 8.00 (s, 1H, H_{T5}), 7.30 – 7.15 (m, 24H, H_{Ar2}, H_{Ar3}), 4.85 (bs, 3H, H_1), 4.65-4.45 (m, 24H; H_8, H_{L1}, $C\underline{H}_2OH$), 4.50-4.40 (m, 12H, $C\underline{H}_2NH$), 4.00-3.88 (m, 6H, H_7), 3.88-3.84 (m, 3H, H_2), 3.84-3.80 (m, 3H, H_{D2}), 3.72-3.65 (m, 3H, H_3), 3.57-3.33 (m, 26H, H_{D1}, H_{L2}, H_{L4}, H_{L5}, H_{L6}, H_{L7}, H_4, H_5, H_{6b}), 3.28-3.18 (m, 3H, H_{6b}), 2.91 – 2.76 (m, 6H, H_{D4}, H_{D5}), 1.96-1.68 (m, 12H, H_{D3}, H_{D6}), 1.41 (s, 18, *t*Bu).

¹³C NMR (100 MHz, CD₃OD): δ 176.86, 176.64 ($\underline{C}ONH$), 158.58 ($\underline{C}OOt$Bu), 146.13 (C_{T4}), 141.58, 141.53, 139.07, 138.98 (C_{Ar1}, C_{Ar4}), 128.37 (C_{Ar2}, C_{Ar3}), 128.16 (C_{T5}), 100.96 (C_1), 80.24 ($C_{quat t Bu}$), 76.24 (C_{D1}), 74.05 (C_5), 72.34 (C_{D2}), 72.23, 72.15, 71.40, 71.15, 70.76, 70.12, 69.78 (C_3, C_2, C_{L2}, C_{L4}, C_{L5}, C_{L6}, C_{L7}), 68.49 (C_4), 65.32 (C_7), 64.91 (C_{L1}, $\underline{C}H_2OH$), 51.78, 51.69 (C_8, C_{L8}), 46.57 (C_{L3}), 43.66 ($\underline{C}H_2NH$), 42.65, 41.77 (C_6), 41.69 (C_{D4}, C_{D5}), 29.82, 29.33 (C_{D3}, C_{D6}), 28.91 (C_{tBu}).

MS (MALDI, DHB matrix): calculated for $[C_{129}H_{181}N_{21}O_{41}Na]^+$: 2704.9, found: 2704.4

$[\alpha]_D^{25}$: -0.2 (c = 0.55 in MeOH)

Synthesis of nonavalent glycodendrimer, 5.46
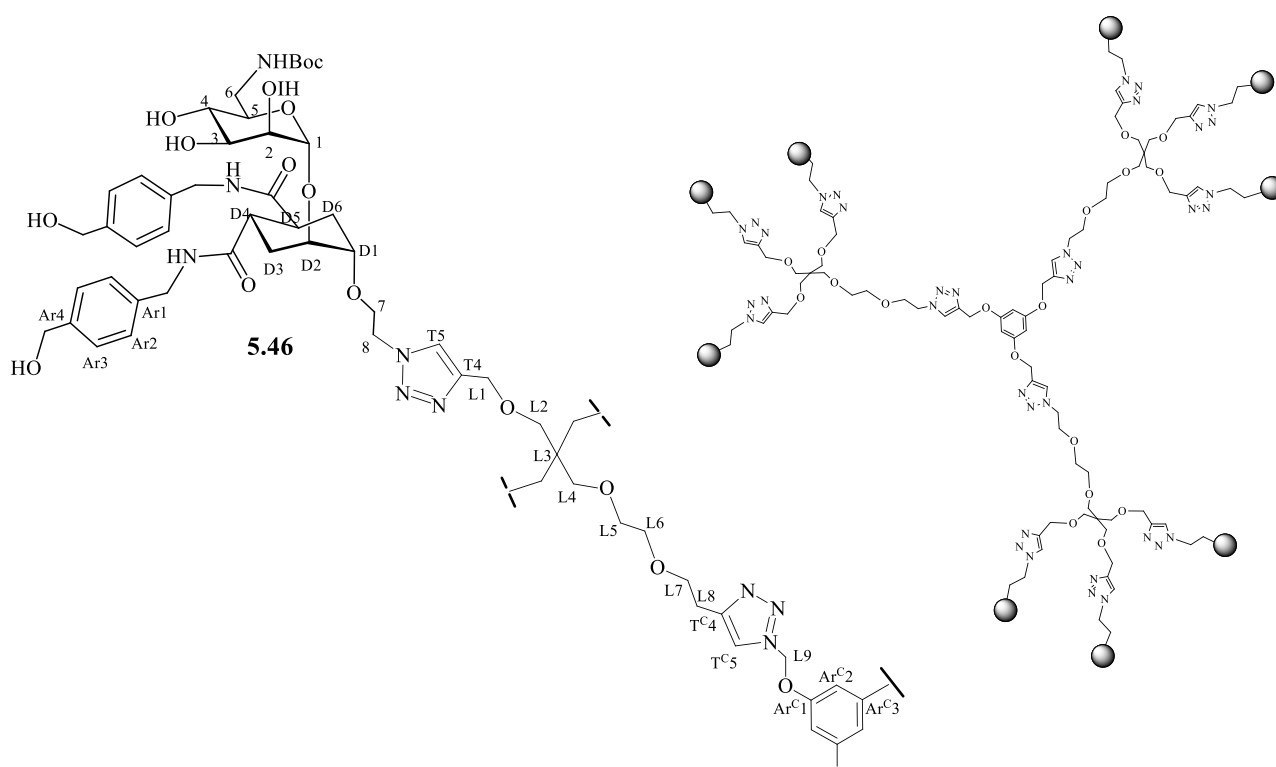
To freshly purified scaffold (**5.31**) (0.54 mg, 2.26 µmol, 1 eq.) dissolved in 40 µL of THF, under inert atmosphere at room temperature, reagents were added as solutions in the following order:

TBTA in THF (0.24 mg, 0.45 µmol, 0.2 eq., in 40 µL), CuSO$_4$·5H$_2$O in water (0.06 mg, 0.23 µmol, 0.1 eq., in 25 µL), Sodium Ascorbate in water (0.18 mg, 0.9 µmol, 0.4 eq., in 25 µL). The reaction mixture was stirred under inert atmosphere, at room temperature and in the dark for 5 min, then **5.45** in water (20 mg, 7.5 µmol, 3.3 eq., in 100 µL). The THF and water volumes were adjusted to 200 µL each and the mixture was stirred for 18 h. A MALDI mass analysis (DHB Matrix) assessed the formation of the product. Quadrasil™-MP (S/Pd 32.8:1, 5 mg) was added to the reaction mixture, which was stirred for 10 min, and then filtered off. The crude was dried, then redissolved in MeOH and purified firstly by size exclusion chromatography on a Sephadex LH-20 (MeOH) column to give 14.4 mg of **5.46** as a colorless solid (yield 77 %).
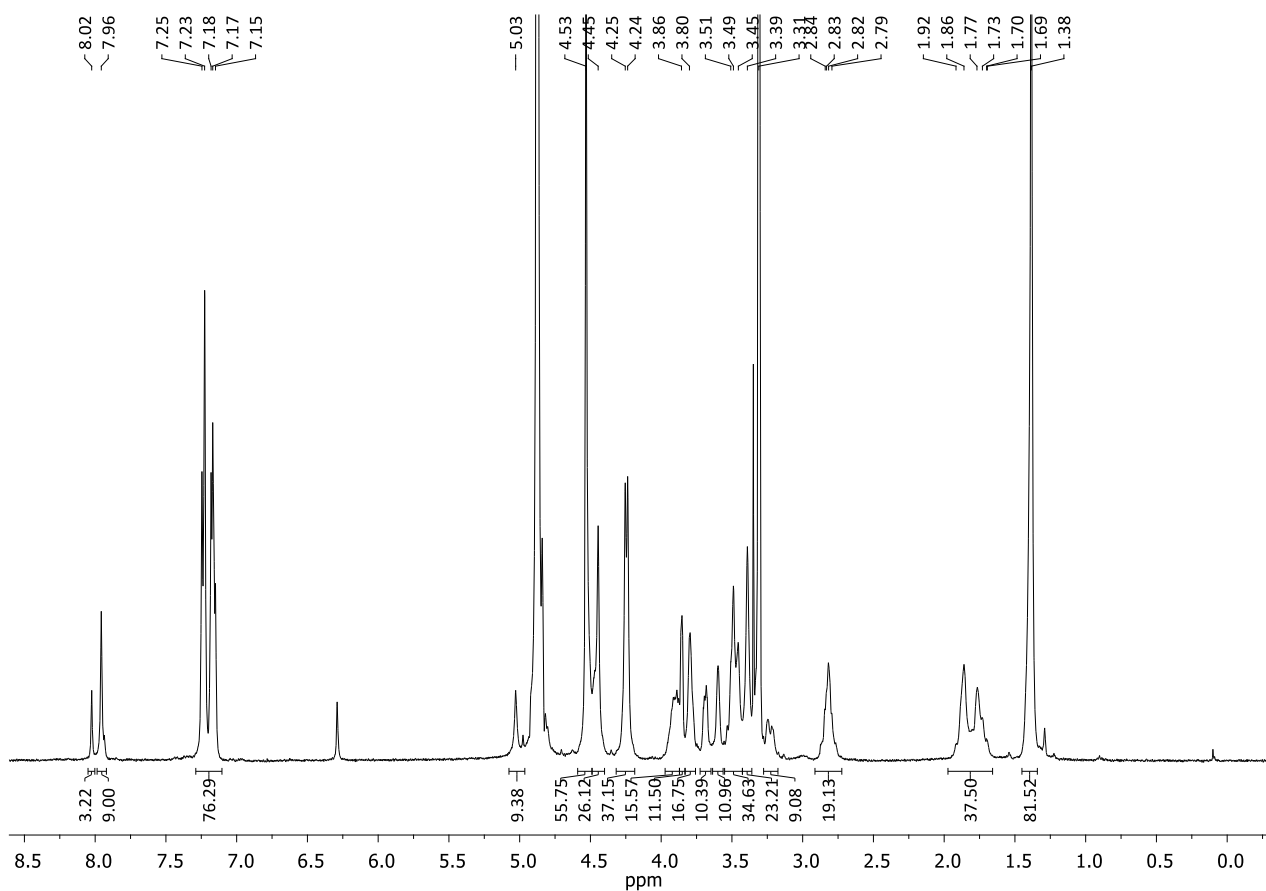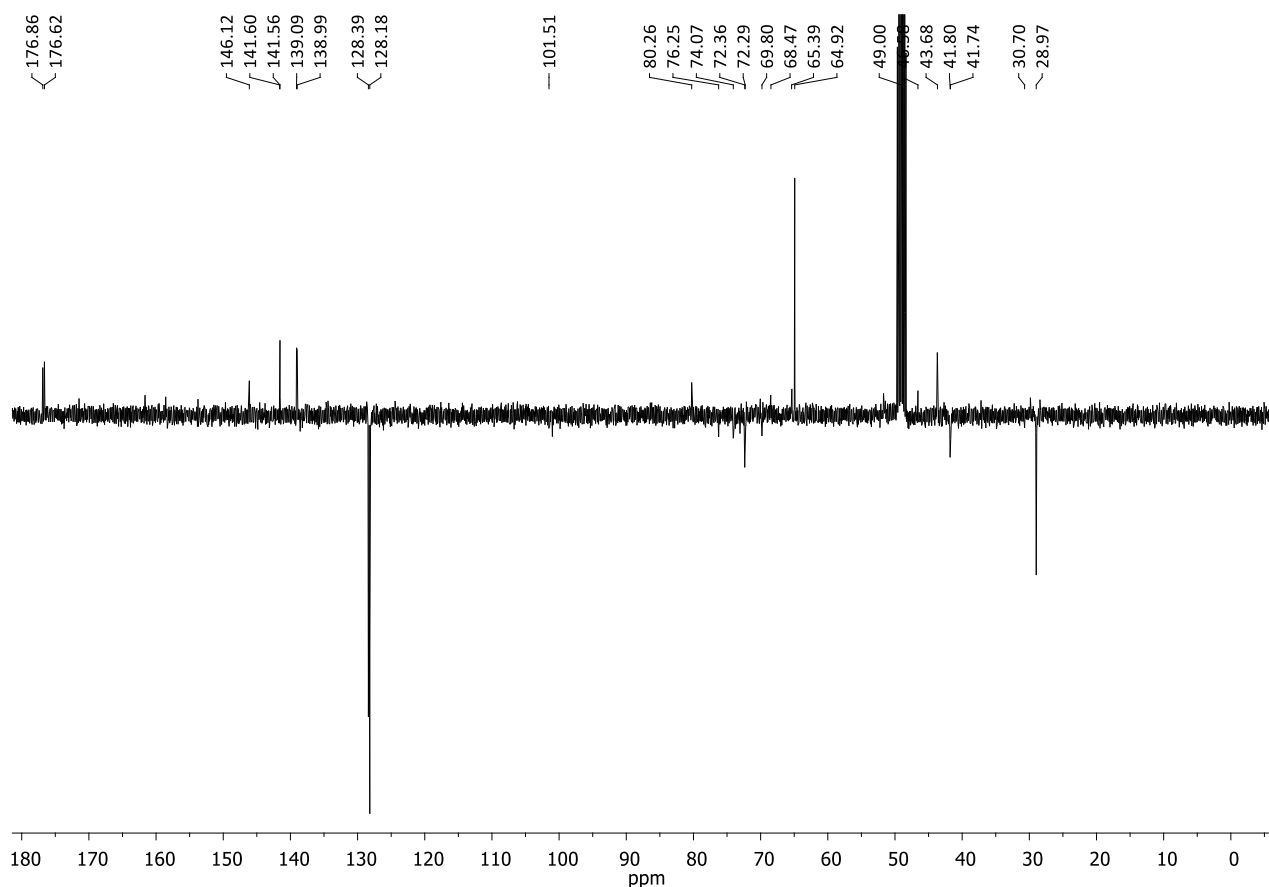
1H NMR (400 MHz, CD3OD): δ 8.02 (s, 3H, H_{TC5}), 7.96 (s, 9H, H_{T5}), 7.28-7.10 (m, 72H, H_{Ar2}, H_{Ar3}), 6.34 (s, 3H, H_{ArC2}), 4.80 (bs, 9H, H_1), 4.55-4.30 (m, 78H, H_8, H_{L1}, H_{L8}, C$\underline{H}_2$OH), 4.28-4.20 (m, 36H, C$\underline{H}_2$NH), 4.00-3.75 (m, 42H, H_7, H_2, H_{D2}, H_{L7}), 3.70-3.68 (m, 9H, H_3), 3.63 − 3.55 (m, 9H, H_{D1}), 3.53-3.33 (m, 9H, H_5, H_4, H_{L2}, H_{L4}, H_{L5}, H_{L6}, H_{6a}), 3.29-3.20 (m, 9H, H_{6b}), 2.80-3.70 (m, 18H, H_{D4}, H_{D5}), 1.86-1.56 (m, 36H, H_{D3}, H_{D6}), 1.38 (s, 81H, tBu).

13C NMR (100 MHz, CD3OD): δ 176.86, 176.62 ($\underline{C}$ONH), 146.12 (C_{T4}, C_{TC4}), 141.60, 141.56, 139.09, 138.99 (C_{Ar1}, C_{Ar4}), 128.39, 128.18 (C_{Ar2}, C_{Ar3}), 101.51 (C_1), 80.26 ($C_{quat t Bu}$), 76.25 (C_{D1}), 74.07 (C_5), 72.36-69.80 (C_2, C_{D2}, C_3, C_4, C_{L2}, C_{L4}, C_{L5}, C_{L6}), 68.47 (C_7), 65.39, 64.92 (C_{L1}, $\underline{C}$H$_2$OH), 51.67 (C_{L8}, C_8), 46.58 (C_{L3}), 43.68 ($\underline{C}$H$_2$NH), 41.80, 41.74 (C_6), 30.70 (C_{D3}, C_{D6}), 28.97 ($C_{t Bu}$).

MS (MALDI, DHB matrix): calculated for $[C_{402}H_{555}N_{63}O_{126}Na]^+$: 8309.1, found: 8319.7

[α]$_D^{25}$: -2.5 (c = 0.31 in MeOH)

Synthesis of nonavalent glycodendrimer, 5.47
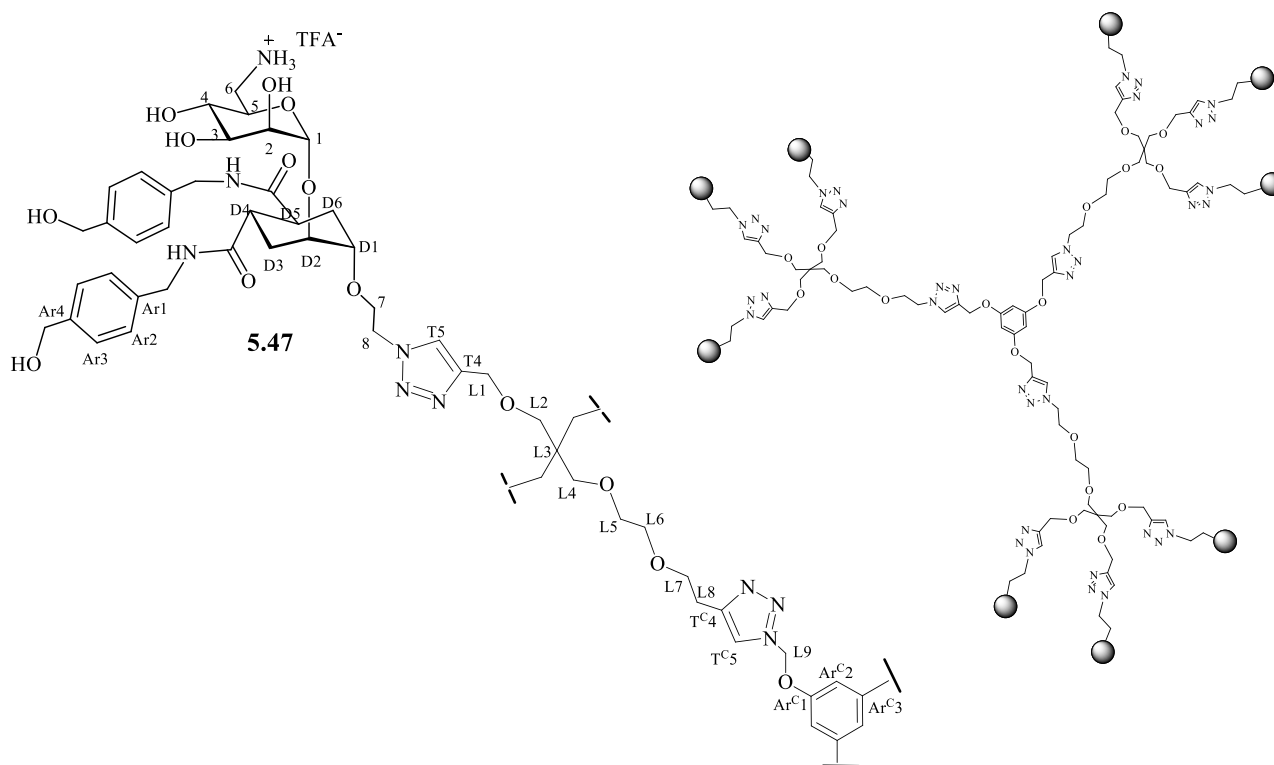
To a stirred solution of **5.46** (6.0 mg, 0.72 μmol, 1 eq.) in 100 μL of dry CH_2Cl_2, 100 μL of TFA were added under inert atmosphere. The reaction was stirred for 2 h, at room temperature and under nitrogen atmosphere. A MALDI mass analysis (HCCA matrix) revealed that the reaction. The reaction mixture was dried and washed with Et_2O (3 x 1 mL), affording 6.0 mg of final product (**5.47**) as a brownish solid (yield 100 %).

MS (MALDI, DHB matrix): calculated for $[C_{357}H_{484}N_{63}O_{108}]^+$: 7386.0, found: 7382.6

Synthesis of nonavalent glycodendrimer, 5.48
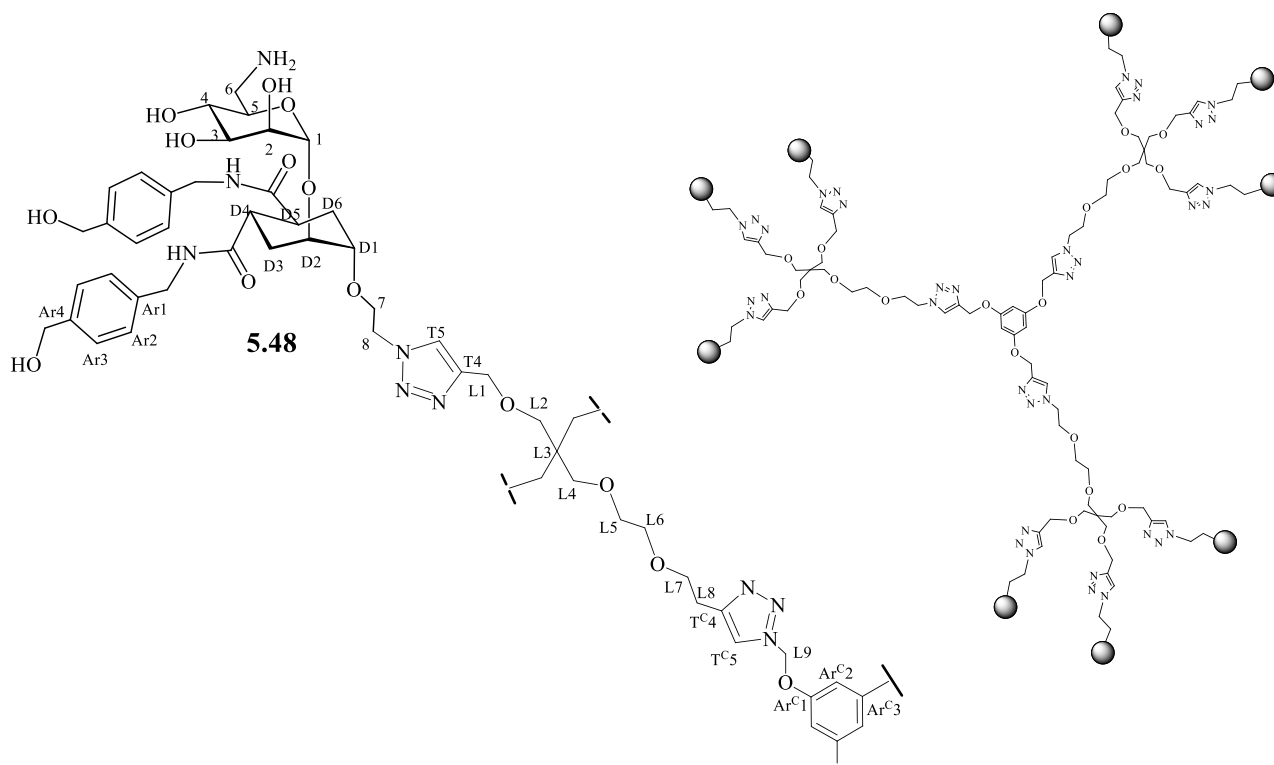
To a shaken solution of **5.47** (6 mg, 7.24 µmol, 1 eq.) in 550 µL of dry MeOH, Amberlyst A21$^{®}$ (12 mg, 100 eq.) was added, under inert atmosphere at room temperature, and the reaction was shaken at 1500 rpm for 3 h. Then the crude was filtered on a cotton pad to remove the resin, washed with MeOH and then dried. 4.91 mg of final product **5.48** were obtained as a brownish solid (yield 92 %).

NMR (CD$_3$OD): compound **5.48** has a too low solubility in CD$_3$OD to acquire interpretable ^{1}H and ^{13}C NMR spectra.

MS (MALDI, HCCA matrix): calculated for $[C_{357}H_{484}N_{63}O_{108}]^+$: 7386.0, found: 7384.1

[α]$_D$^{25}: /// (5 mg of **5.48** were not soluble in 2 mL of MeOH)

5.5 References

[1] N. S. Stambach; M. E. Taylor, Characterization of carbohydrate recognition by langerin, a C-type lectin of Langerhans cells, *Glycobiol.* **2003**, 401.

[2] L. de Witte, A. Nabatov; M. Pion; D. Fluitsma; M. A. de Jong; T. de Gruijl; V. Piguet; Y. van Kooyk; T. B. Geijtenbeek, Langerin is a natural barrier to HIV-1 transmission by Langerhans cells, *Nat. Med.* **2007**, 367.

[3] J. Valladeau; O. Ravel; C. Dezutter-Dambuyant; K. Moore; M. Kleijmeer; Y. Liu; V. Duvert-Frances; C. Vincent; D. Schmitt; J. Davoust; C. Caux; S. Lebecque; S. Saeland, Langerin, a Novel C-Type Lectin Specific to Langerhans Cells, Is an Endocytic Receptor that Induces the Formation of Birbeck Granules, *Immunity* **2000**, 71.

[4] N. Varga; I. Sutkeviciute; C. Guzzi; J. McGeagh; I. Petit-Haertlein; S. Gugliotta; J. Weiser; J. Angulo; F. Fieschi; A. Bernardi, Selective Targeting of Dendritic Cell-Specific Intercellular Adhesion Molecule-3-Grabbing Nonintegrin (DC-SIGN) with Mannose-Based Glycomimetics: Synthesis and Interaction Studies of Bis(benzylamide) Derivatives of a Pseudomannobioside, *Chem. Eur. J.* **2013**, 4796.

[5] H. Feinberg; A. S. Powlesland; M. E. Taylor; W. I. Weis, Trimeric Structure of Langerin, *J. Biol. Chem.* **2010**, 13285.

[6] G. Tabarani; M. Thépaut; D. Stroebel; C. Ebel; C. Vivès; P. Vachette; D. Durand; F. Fieschi, DC-SIGN Neck Domain Is a pH-sensor Controlling Oligomerization, *J. Biol. Chem.* **2009**, 21229.

[7] L. Chatwell; A. Holla; B. B. Kaufer; A. Skerra, The carbohydrate recognition domain of Langerin reveals high structural similarity with the one of DC-SIGN but an additional, calcium-independent sugar-binding site, *Mol. Immunol.* **2008**, 1981.

[8] N. Varga, *PhD Thesis*, **2012**.

[9] I. Sutkeviciute, *PhD Thesis*, **2012**.

[10] M. Thépaut; C. Guzzi; I. Sutkeviciute; S. Sattin; R. Ribeiro-Viana; N. Varga; E. Chabrol; J. Rojo; A. Bernardi; J. Angulo; P. M. Nieto; F. Fieschi, Structure of a Glycomimetic Ligand in the Carbohydrate Recognition Domain of C-type Lectin DC-SIGN. Structural Requirements for Selectivity and Ligand Design, *J. Am. Chem. Soc.* **2013**, 2518.

[11] J. J. Reina; S. Sattin; D. Invernizzi; S. Mari; L. Martínez-Prats; G. Tabarani; F. Fieschi; R. Delgado; P. M. Nieto; J. Rojo; A. Bernardi, 1,2-Mannobioside Mimic: Synthesis, DC-SIGN Interaction by NMR and Docking, and Antiviral Activity, *Chem. Med. Chem.* **2007**, 1030.

[12] N. Varga; I. Sutkeviciute; R. Ribeiro-Viana; A. Berzi; R. Ramdasi; A. Daghetti; G. Vettoretti; A. Amara; M. Clerici; J. Rojo; F. Fieschi; A. Bernardi, A multivalent inhibitor of the DC-SIGN dependent uptake of HIV-1 and Dengue virus, *Biomaterials* **2014**, 4175.

[13] S. Ordanini; N. Varga; V. Porkolab; M. Thépaut; L. Belvisi; A. Bertaglia; A. Palmioli; A. Berzi; D. Trabattoni; M. Clerici; F. Fieschi; A. Bernardi, Designing nanomolar antagonists of DC-SIGN-mediated HIV infection: ligand presentation using molecular rods, *Chem. Commun.* **2015**, 3816.

[14] Natarajan, S.; Yurek, A., Ganesan, A., Rapid deprotection of N-Boc amines by TFA combined with free base generation using basic ion-exchange resins. *Molecular Diversity,* **2005**, 9**,** 291.

[15] L. Parhamifar; A. K. Larsen; A. C. Hunter; T. L. Andresenc; S. M. Moghimi, Polycation cytotoxicity: a delicate matter for nucleic acid therapy—focus on polyethylenimine, *Soft Matter* **2010**, 6, 4001.

[16] D. Fischera; Y. Lib; B. Ahlemeyerc; J. Krieglsteinc; T. Kissela, In vitro cytotoxicity testing of polycations: influence of polymer structure on cell viability and hemolysis, *Biomaterials* **2003**, 1121.

[17] W. C. Still; M. Kahn; A. Mitra, Rapid Chromatographic Technique for Preparative Separations with Moderate Resolution, *J. Org. Chem.* **1978**, 2923.

[18] R. H. Lambeth; S. J. Pederson; M. Baranoski; A. M. Rawlett, Methods for removal of residual catalyst from polymers prepared by ring opening metathesis polymerization, *J. Polym. Sc. Pol. Chem.* **2010**, 5725.

Chapter 6

Conclusions

In this thesis, the synthesis of multivalent mannose-based compounds as effective DC-SIGN antagonists is described. DC-SIGN is a tetrameric C-type lectin expressed on the surface of Dendritic Cells and responsible for the early stage of several viral infections, like the HIV one. Constructs here synthesised were equipped with two active pseudo-disaccharide ligands already developed in our laboratories: **1.7** and **1.9** (Figure **6.1**), based on one mannose residue connected to a functionalized cyclohexane. Compound **1.9** was already demonstrated to be 3 times more active towards DC-SIGN than **1.7** (*IC₅₀* = 300 μM *vs* 1000 μM, respectively, calculated through SPR inhibition assays using BSA-Mannotrioside as competitor).
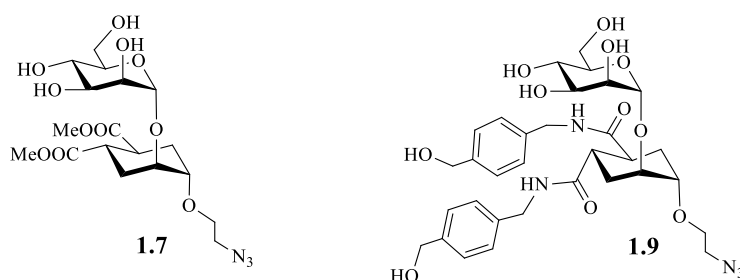

Figure 6.1 Structure of pseudo-mannobioside identified as lead DC-SIGN ligands in the Bernardi group.

It is well known from the literature and from previous studies conducted in the group that multivalent ligands are able to bind to their biological target tighter than to the corresponding monovalent ones. Indeed, the synthesis of tetravalent, hexavalent and nonavalent presentations of both **1.7** and **1.9** (Figure **6.2**) led to more powerful compounds, displaying an activity that increased by increasing the valency. Remarkably, multivalency amplified the difference in the activity between the simple monovalent ligands, since multivalent compounds based on **1.9** were now one order of magnitude more active than those based on **1.7** (SPR competition assays).
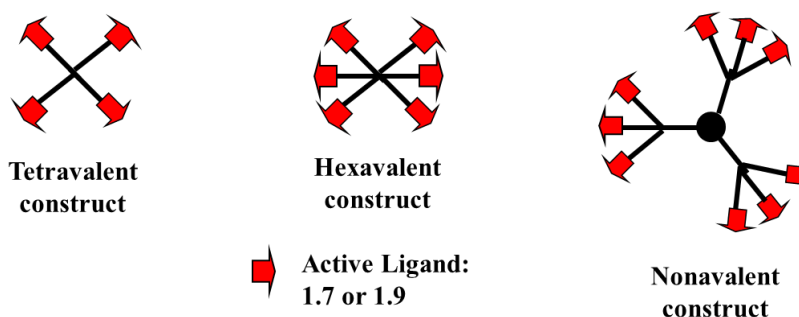

Figure 6.2 Schematic structure of tetravalent, hexavalemt and nonavalent compounds based on **1.7** and **1.9** previously synthesised in our group.

Nonetheless, computational studies demonstrated that the multivalent effect associated to these compounds can be due only to the statistical rebinding effect or to protein clustering. A chelating binding mechanism was excluded, since the distance between two binding sites in DC-SIGN is about 4 nm, whilst artificial tetravalent and hexavalent compounds were not able to cover a distance longer than 36 Å. Nonavalent derivatives based on **1.9** had a rather low solubility in water ($\leq$ 1 mM), suggesting that an approach based only on increased valency is limiting, at least for optimized and functionalized compounds like **1.9**.

For these reason, in this thesis we've strived to obtain compounds, based on **1.7** and **1.9**, able to exploit also the chelating effect, still with a relative low valency. We therefore designed compounds characterized by molecular rod cores, that should be able to control the relative disposition of active ligands, thus allowing the overall molecule to span the distance required to bridge two DC-SIGN binding sites. As molecular rods, we used three phenylene-ethynylene-based molecules (Rod1-3), having three different lengths (Figure **6.3A**). They were synthesisd starting from the commercially available *p*-dimethoxybenzene and making extensive use of Sonogashira coupling reactions with orthogonally protected alkynes.

With the aim to exploit both chelation and statistical rebinding mechanisms, hexavalent compounds (Figure **6.3B**) were synthesised by connecting two trivalent dendrons to the rods. In order to deeply investigate the role of valency, corresponding divalent compounds were produced (Figure **6.3C**). They were equipped with monovalent ligands elongated with a flexible linker having the same length of the dendron chain. Finally, the influence of the linker flexibility was explored by producing also divalent compounds directly combining monovalent ligands with Rod3 (Figure **6.3D**). This library of artificial compounds was synthesised exploiting Copper-catalyzed azide-alkyne cycloadditions to couple the biological active moieties (i.e. trivalent dendrons, elongated monovalent ligands and simple monovalent ligands), all equipped with an azido group, with the terminal alkynes of the rods. Final compounds were purified using size exclusion chromatography and reverse phase chromatography and characterized through NMR and MALDI spectroscopy.
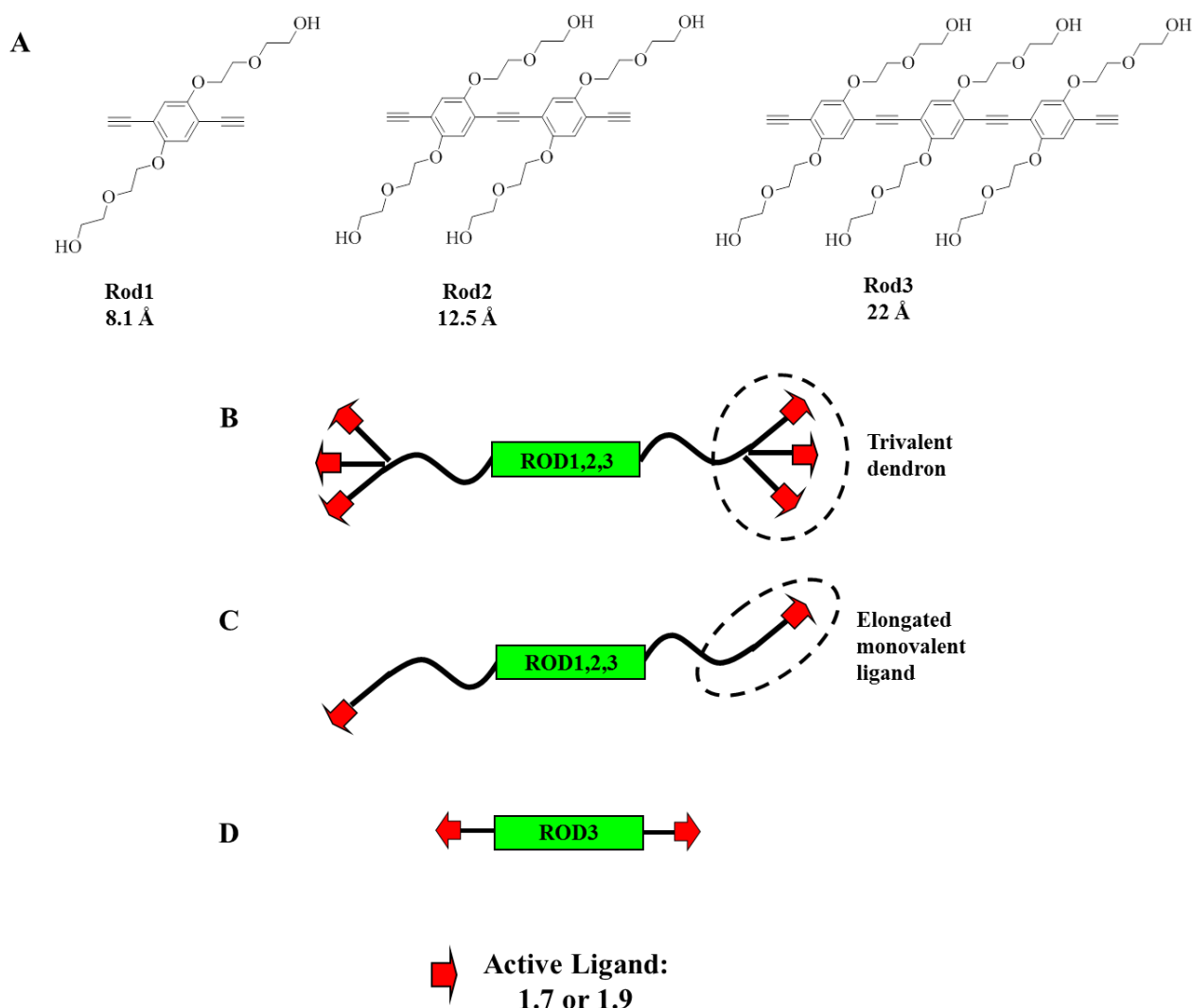
A

Rod1
8.1 Å

Rod2
12.5 Å

Rod3
22 Å

B
ROD1,2,3
Trivalent dendron

C
ROD1,2,3
Elongated monovalent ligand

D
ROD3

Active Ligand:
1.7 or 1.9

Figure 6.3 Structures of the elongated dendrimers described in this thesis. A) Rod1, Rod2 and Rod3 are molecular cores used to control the overall length of final molecules: B) hexavalent ones, C) divalent ones with a long and flexible linker, C) divalent ones with a shirt linker.

The possibility that these artificial compounds can act as DC-SIGN chelating agents was assessed through computational modelling, demonstrating that they can all span a distance higher than 4 nm. Compounds were tested through SPR inhibition assays, evaluating their ability to inhibit DC-SIGN anchoring to a highly mannosylated surface (Man α1-3[Manα1-6]Man-BSA, 15 trimannose residues, on average) and through a *trans*-infection inhibitions assays, using a cellular model HIV infection. First of all, the importance of the ligand in the overall activity was confirmed. Indeed, compounds based on **1.9** were always more active than those carrying **1.7**, as expected. The effect of the Rod length clearly emerged from SPR inhibition experiments conducted on **1.7** derivatives and for *trans*-infection assays conducted on **1.9** derivatives. Indeed, compounds bearing the longest Rod3, displayed the highest activity in each series. Moreover, the efficient role of the statistical rebinding effect was demonstrated, since hexavalent compounds had higher activities than

corresponding divalent compounds, based on monovalent ligand concentrations. Finally, divalent molecules having the short linker were two times more active than the corresponding ones including the flexible, long linker; too flexible linkers were therefore demonstrated to have a negative effect, probably because of the enthalpic and entropic penalties that they have to pay to match receptor binding sites and to decrease their degrees of freedom. The optimal combination of compound **1.9**, Rod3 and trivalent dendrimers led to compound **PM26** (Figure **6.4**); its IC_{50} = 24 nM in the *trans*-infection inhibition assay made it one of the most powerful inhibitors of DC-SIGN mediated HIV adhesion on cells, relative to other constructs of much higher valency. These results therefore highlight that a rational design can lead to efficient binders of target proteins, even with a relatively low valency.
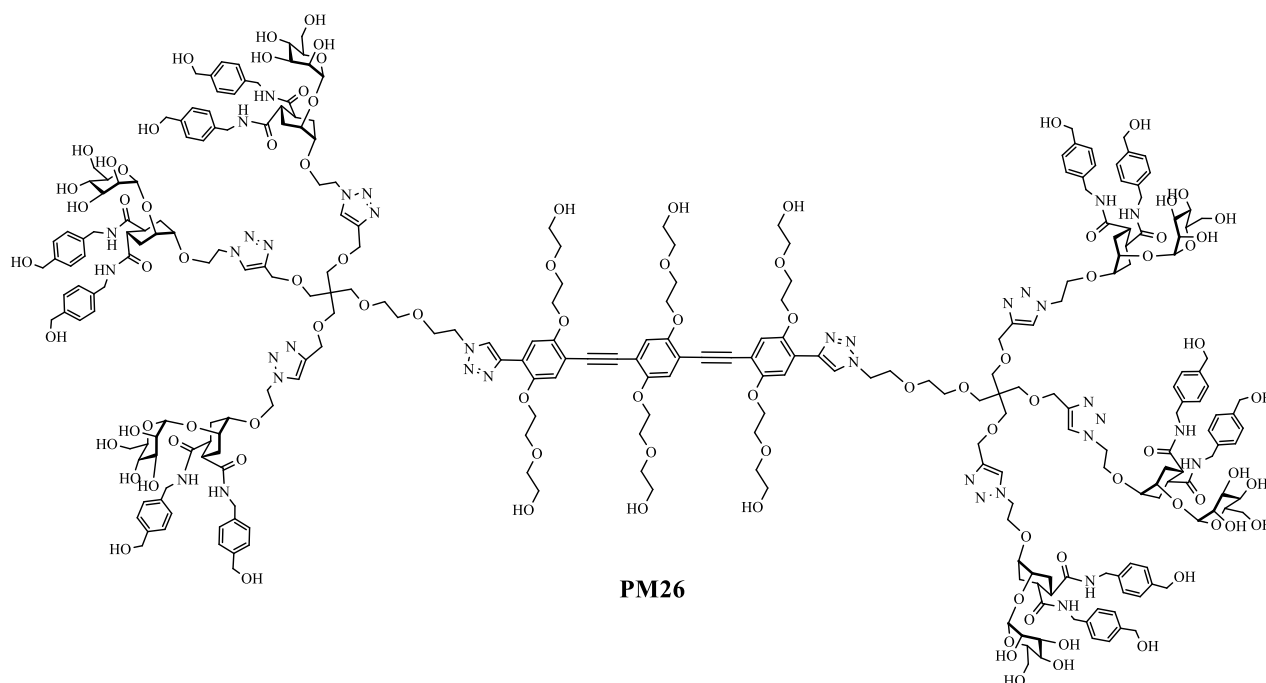

Figure 6.4 Structure of hexavalent compound **PM26**, which is the hexavalent presentation of the disaccharide **1.9** using Rod3. It is able to inhibit the DC-SIGN-mediated HIV infection with IC_{50} = 24 nM.

Results obtained from the SPR and the *trans*-infection inhibition campaign didn't always give to comparable results in terms of IC_{50} values. Besides the different experimental set up (i.e. DC-SIGN is soluble in the SPR assay, whilst embedded in the membrane in the infection experiment), this may be due to internalization processes happening in the cellular model. Internalization of **PM26** in Dendritic Cells was confirmed by confocal microscopy experiments, whose feasibility was linked to the intrinsic fluorescence behaviour of Rod3. Co-localization experiments established that, once internalized, **PM26** is routed to lysosomes. These results make **PM26** also a possible stimulator of the immune response.

The morphological behaviour of synthesised compounds, which have a clear amphiphilic structure (i.e. a hydrophobic core connected to hydrophilic heads and hydrophilic chains), was investigated in aqueous solution. The scope of this investigation was understanding if their biological performances depended on monomers or on aggregates self-assembled in water. Through DOSY NMR and AUC experiments we established that compounds are mainly monomers in solution. Nevertheless, large species were observed through DLS and TEM analysis; they have a $R_H \approx$ 100-200 nm, whereas the one associated to monomers is $\approx$ 1 nm (computational studies and DOSY NMR). Since aggregates don't seem to depend on temperature nor concentration, and since they can be removed through centrifugation without re-forming, we postulated that they are pelleting molecular nucleus that failed to dissolve. Performing UV-Vis spectroscopy on two selected samples before and after centrifugation (4000 rpm, 1-40 h), we concluded that aggregates are only a small percentage (< 10 %) of the totality of the sample. Since SPR analysis are conducted on centrifuged samples, obtained results should derive mainly from monomers. *Trans*-infection inhibition assays, on the contrary, are performed solubilizing the compound first in DMSO and then diluting it in the biological buffer; given the good solubilizing properties of DMSO, this procedure should in principle improve the dissolution of samples, thus reducing the amount of formed aggregates. Further experiments will be conducted to evaluate the morphology of aggregates.

Future studies will be dedicated to evaluate the immunological properties of these compounds, especially the most active one, **PM26**. They will be investigated as stimulators of cytokines, chemokines and other co-stimulatory molecules released in the body as a response against infections.

Selectivity was an important topic that I've pursued during my project. DC-SIGN is not the only mannose-binding lectin expressed by DCs. Langerin is another receptor able to recognize HIV; still, unlike DC-SIGN, it is able to promote virus degradations. Therefore, artificial DC-SIGN ligands not targeting Langerin have to be produced in order not to contrast the efficient anti-pathogenic activity of the human body. The synthesis of cationic constructs can be a way to produce selective DC-SIGN ligands. Indeed, Langerin has two Lysine residues in its binding site that can establish electrostatic repulsions with positively-charged groups. We therefore envisaged to modify compounds **1.7** and **1.9** by replacing the –OH group in the 6-position of the mannose residue with an amino group, which should be protonated at physiological pH. For this reason, compounds **5.1** and **5.2** (Figure **6.5**) were synthesised. The selectivity of compounds **5.1** and **5.2** *vs* Langerin compared to **1.7** and **1.9** was confirmed through SPR competition assays. Compound **5.2** was totally unable to bind to Langerin, even at a concentration $\approx$ 5 mM.
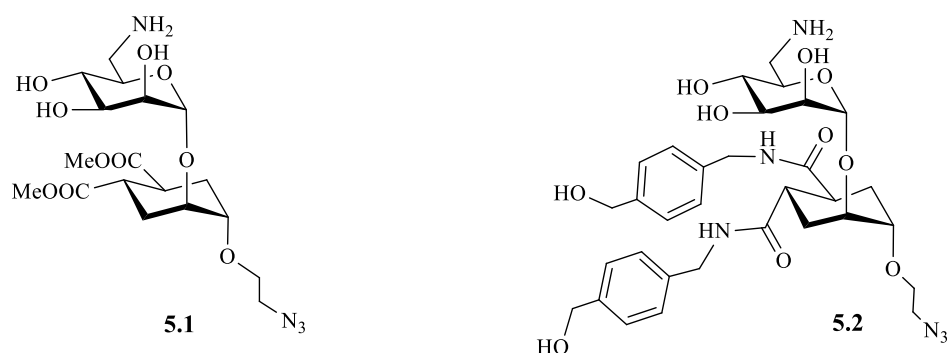
Figure 6.5 Structure of compounds **5.1** and **5.2** with an improved selectivity for DC-SIGN *vs* Langerin.

Compounds **5.1** and **5.2** were used to decorate multivalent scaffolds, thus potentially increasing their overall affinity for DC-SIGN. In principle, they should lead to polycationic species with a high selectivity *vs* Langerin. Since polycationic are known to be potentially toxic for cells, we investigated the cytotoxic behaviour of one selected multivalent compound based on **5.1**. After 24 h of incubation, the tested compound was found to be cytotoxic only at concentration > 50 μM. These negative behaviour could therefore be overcome, assuming that all multivalent compounds based on **5.1** and **5.2** will be active already at a concentration $\ll 50$ μM. Future studies will characterize their biological activity as DC-SIGN ligands and HIV-adhesion inhibitors.

The results of Chapter 2 were recently published:
S. Ordanini; N. Varga; V. Porkolab; M. Thépaut; L. Belvisi; A. Bertaglia; A. Palmioli; A. Berzi; D. Trabattoni; M. Clerici; F. Fieschi; A. Bernardi, Designing nanomolar antagonists of DC-SIGN-mediated HIV infection: ligand presentation using molecular rods, *Chem. Commun.* **2015**, 3816.

Manuscripts related to the results of Chapter 3 and 4 are under preparation.